iScience

CellPress

Article

Suzuki-Miyaura Coupling Enabled by Aryl to Vinyl 1,4-Palladium Migration

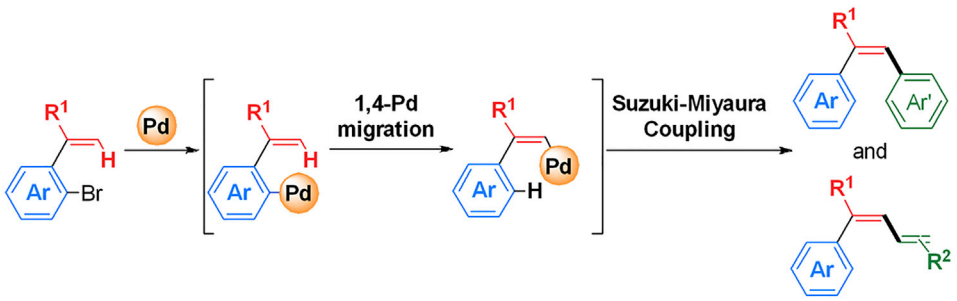

- >90 successful examples with up to 99% yield
- Efficient transformation with excellent regio- and stereoselectivity
- Excellent compatibility toward functional groups and heteroaryl rings
- Versatile transformations for the synthesis of potential material molecules

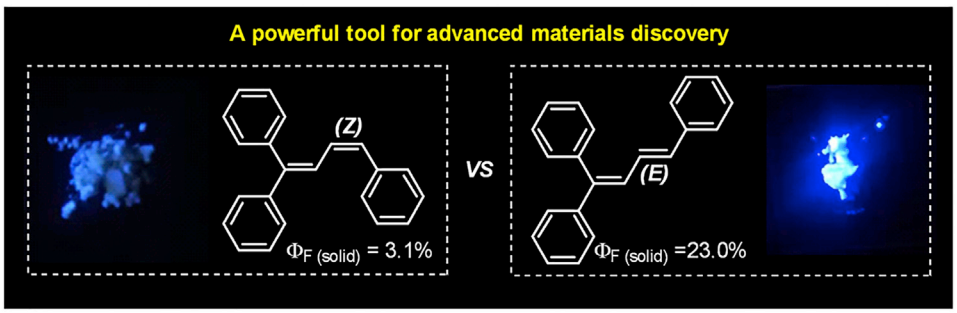

Meng-Yao Li, Pengbo Han, Tian-Jiao Hu, ..., Chen-Guo Feng, Ben Zhong Tang, Guo-Qiang Lin

fengcg@sioc.ac.cn (C.-G.F.)
lingq@sioc.ac.cn (G.-Q.L.)

HIGHLIGHTS

Suzuki-Miyaura coupling via controllable aryl to vinyl 1,4-palladium migration

Synthesis of multisubstituted olefins and 1,3-dienes in stereo-specific way

Wide substrate scope and excellent functional-group tolerance

A powerful tool for the studies on geometric isomers in material science

DATA AND CODE AVAILABILITY

www.ccdc.cam.ac.uk/data_request/cif

Li et al., iScience *23*, 100966
March 27, 2020 © 2020 The Author(s).
https://doi.org/10.1016/j.isci.2020.100966

iScience

CellPress

Article

Suzuki-Miyaura Coupling Enabled by Aryl to Vinyl 1,4-Palladium Migration

Meng-Yao Li,[1] Pengbo Han,[3] Tian-Jiao Hu,[1] Dong Wei,[1] Ge Zhang,[1] Anjun Qin,[3] Chen-Guo Feng,[1,2,4,*] Ben Zhong Tang,[3] and Guo-Qiang Lin[1,2,*]

SUMMARY

The Suzuki-Miyaura coupling is a fundamentally important transformation in modern organic synthesis. The development of new reaction modes for new chemical accessibility and higher synthetic efficiency is still the consistent pursuance in this field. An efficient Suzuki-Miyaura coupling enabled by a controllable 1,4-palladium migration was realized to afford stereodefined multisubstituted olefins and 1,3-dienes. The reaction exhibits remarkable broad substrate scope, excellent functional-group tolerance, versatile conversion with obtained products, and easy scalability. The practicality of this method is highlighted by the aggregation-induced emission feature of the produced olefins and 1,3-dienes, as well as the capability of affording geometric isomer pairs with a marked difference on photoluminescent quantum yield values.

INTRODUCTION

Since the introduction of the Suzuki-Miyaura coupling in 1979 (Miyaura et al., 1979), this Nobel Prize winning chemistry has developed into one of the most synthetically valuable processes for the construction of carbon-carbon bonds and been widely applied in both academia and industry (Beletskaya et al., 2019; Maluenda and Navarro, 2015; Miyaura and Suzuki, 1995). For example, according to statistics, over 60% of the carbon-carbon bond-forming processes in medicinal chemistry now are accomplished through this reaction (Schneider et al., 2016). Despite brilliant achievements, the continuing efforts for broader reaction scope and higher efficiency have never ceased.

Mechanistically, this reaction is initiated by the generation of a key organopalladium(II) intermediate, normally a result of direct oxidative addition of palladium(0) to a carbon-heteroatom bond. Later, direct C-H bond activation by palladium(II) becomes a second important route (Chen et al., 2006; Giri et al., 2007; Shi et al., 2007; Wang et al., 2008; Yang et al., 2008). Compared with these direct generation modes, the organopalladium(II) intermediate can also be produced via an indirect manner, which has been far less developed and mainly focused on the generation via a migratory insertion of organopalladium to olefins (Grigg et al., 1997; Schempp et al., 2017; Zhang et al., 2019) or alkynes (Couty et al., 2004; Monks and Cook, 2012) (Figure 1A).

Palladium migration, which can relay the palladium from the original place to a remote position, is a novel strategy for the indirect generation of the desired palladium(II) intermediate and has been applied in several efficient organic transformations (Ma and Gu, 2005; Shi and Larock, 2010; Rahim et al., 2019). Early attempts to execute Suzuki-Miyaura coupling via palladium migration were made, but only limited success has been achieved.

Buchwald and co-workers realized a Suzuki-Miyaura coupling through a complete aryl to alky 1,4-palladium migration (Barder et al., 2005). However, only a single arylbromide with two neighboring positions blocked by *tert*-butyl groups was tested. Later, Larock and co-workers tried Suzuki-Miyaura coupling via aryl to aryl 1,4-palladium migration and found it was hard to control this migration process efficiently (Campo et al., 2007). Usually, a significant amount of non-migrated product was generated. Therefore, Suzuki-Miyaura coupling enabled by controllable palladium migration, further expanding this important transformation and affording new chemical accessibility, is highly desirable. As a continuing effort on developing reactions via palladium migration (Hu et al., 2016, 2018), herein we present the first Suzuki-Miyaura coupling enabled by aryl to vinyl 1,4-palladium migration (Figure 1B), which offered an efficient way to synthesize stereodefined, multisubstituted olefins (Gao et al., 2010; Wang, 2012; Wencel-Delord et al., 2012; Zhang et al., 2016a; Li et al., 2017; Li and Duan, 2018; Lin et al., 2019) and 1,3-dienes (Besset et al., 2011; Boultadakis-Arapinis et al., 2014; De Paolis et al., 2012; Hu et

[1]CAS Key Laboratory of Synthetic Chemistry of Natural Substances, Center for Excellence in Molecular Synthesis, Shanghai Institute of Organic Chemistry, University of Chinese Academy of Sciences, Chinese Academy of Sciences, Shanghai 200032, China

[2]The Research Center of Chiral Drugs, Innovation Research Institute of Traditional Chinese Medicine, Shanghai University of Traditional Chinese Medicine, Shanghai 201203, China

[3]State Key Laboratory of Luminescent Materials and Devices, Key Laboratory of Luminescence from Molecular Aggregates of Guangdong Province, Center for Aggregation-Induced Emission, South China University of Technology, Guangzhou 510640, China

[4]Lead Contact

*Correspondence: fengcg@sioc.ac.cn (C.-G.F.), lingq@sioc.ac.cn (G.-Q.L.)

https://doi.org/10.1016/j.isci.2020.100966

This is an open access article under the CC BY-NC-ND license (http://creativecommons.org/licenses/by-nc-nd/4.0/).

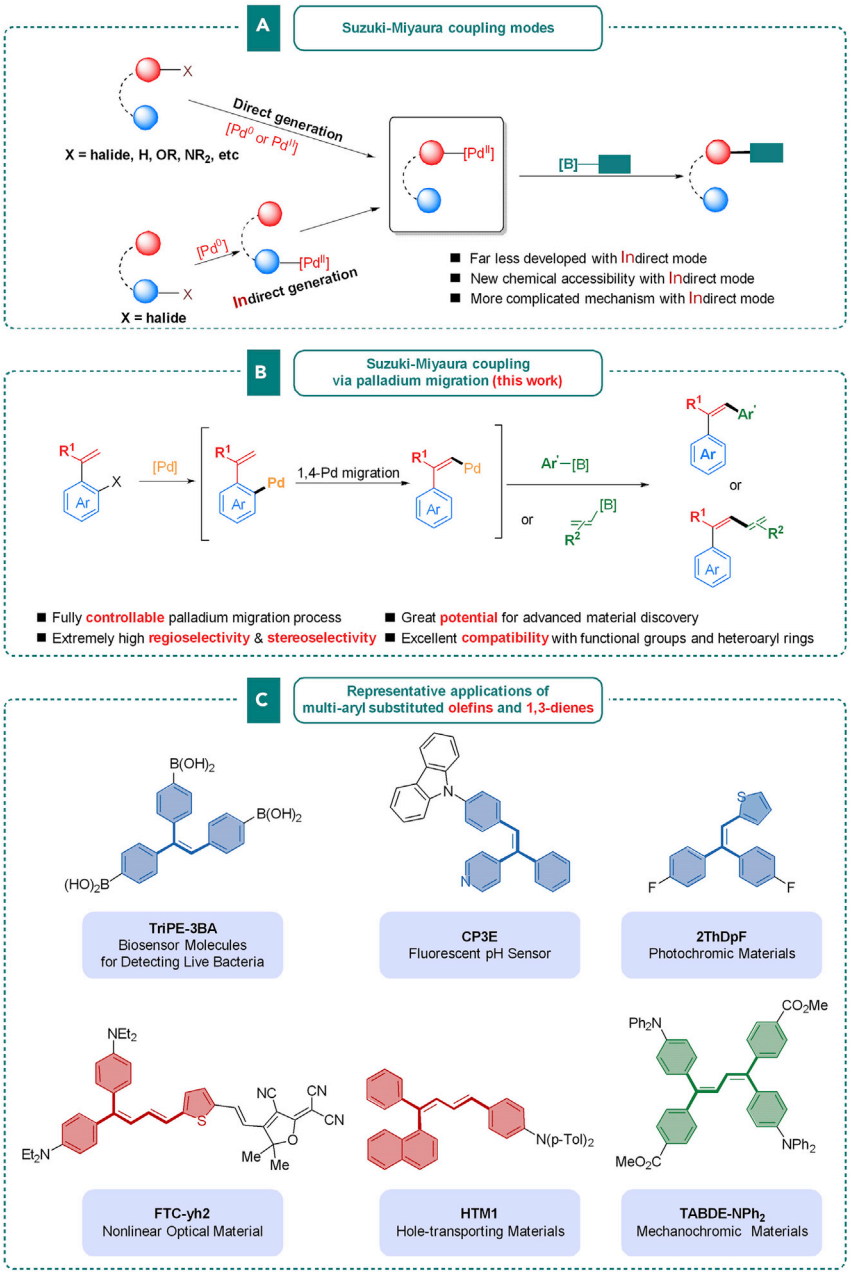

Figure 1. Suzuki-Miyaura Coupling Enabled by Aryl to Vinyl 1,4-Palladium Migration

(A) Two Suzuki-Miyaura coupling modes.

(B) Aryl to vinyl 1,4-palladium migration/Suzuki-Miyaura coupling sequence.

(C) Possible applications in material science.

al., 2015; Liang et al., 2017; Liu et al., 2019; Šiaučiulis et al., 2019). Notably, multi-aryl substituted olefins and 1,3-dienes may display interesting electronic and photonic properties owing to their π-extended systems and have been widely applied in many diverse fields, such as chemical or biological sensors, stimuli response material, and fluorescent materials (Figure 1C) (Kong et al., 2018; Yang et al., 2014; He et al., 2019). Despite the fact that the geometry of double bonds in these molecules has great influence on the material performance, effective synthetic approaches toward these structures remain to be limited, in which the application of symmetric starting material or a homo-coupling reaction is often necessary to overcome the geometric problem (Xie and Li, 2019; Zhang et al., 2016b).

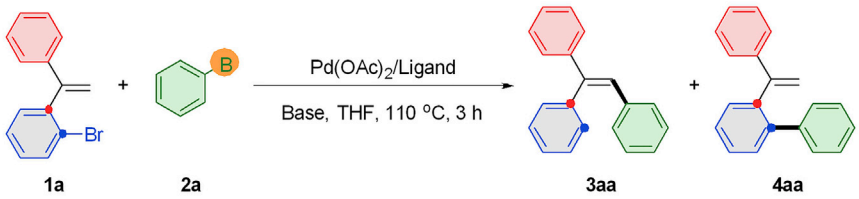

1a 2a 3aa 4aa

Entry[a]	Ligand	Base	Phenylboron	Yield of 3aa (%)[b]	Ratio of 3aa/4aa[b]
1	L1	CsOAc	$2a_1$	56	62:38
2	L1	CsOAc	$2a_2$	55	58:42
3	L1	CsOAc	$2a_3$	8	nd
4	L1	CsOAc	$2a_4$	29	97:3
5	L1	CsOAc	$2a_5$	64	94:6
6	L1	CsOAc	$2a_6$	79	93:7
7	L1	CsOAc	$2a_7$	28	33:67
8	L1	CsOAc	$2a_8$	69	91:9
9	L1	CsOAc	$2a_9$	66	90:10
10	L2	CsOAc	$2a_6$	33	60:40
11	L3	CsOAc	$2a_6$	15	nd
12	L4	CsOAc	$2a_6$	35	50:50
13	L5	CsOAc	$2a_6$	56	67:33
14	L6	CsOAc	$2a_6$	56	94:6
15	L7	CsOAc	$2a_6$	37	50:50
16	L8	CsOAc	$2a_6$	32	60:40
17	L1	KOAc	$2a_6$	41	89:11
18	L1	CsOPiv	$2a_6$	94	95:5

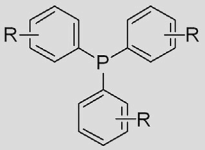

L1 R = 2-MeO
L2 R = H
L3 R = 2-Me
L4 R = 3-MeO
L5 R = 4-MeO

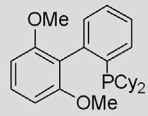

L6

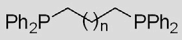

L7 n = 0
L8 n = 1

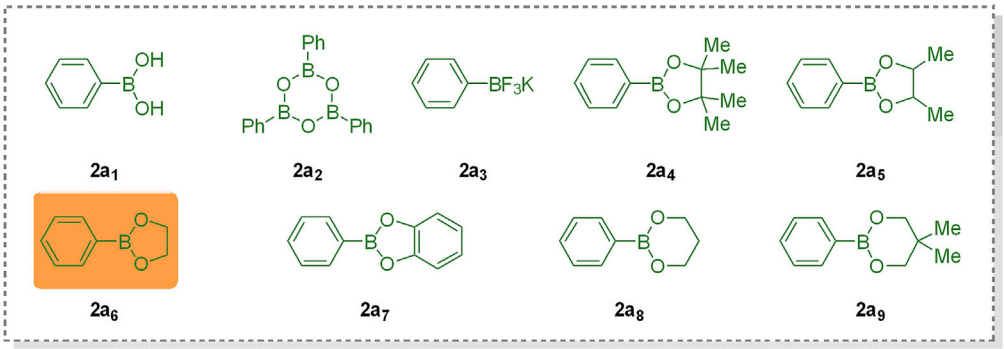

$2a_1$ $2a_2$ $2a_3$ $2a_4$ $2a_5$

$2a_6$ $2a_7$ $2a_8$ $2a_9$

Scheme 1. Reaction Conditions Optimization

[a]All reactions were conducted with **1a** (1.0 equiv, 0.2 mmol), phenylboron **2** (3.0 equiv, 0.6 mmol), $Pd(OAc)_2$ (5 mol %), **L1-L6** (10 mol %), or **L7-L8** (5 mol %) and base (2.0 equiv, 0.4 mmol) in THF (2.0 mL) at 110°C for 3 h. [b]Determined by GC analysis using dodecane as an internal standard.

RESULTS AND DISCUSSION

Reaction Conditions Development

We began our investigation by studying the coupling of *ortho*-vinyl bromobenzene **1a** and various phenylboron reagents **2a**, and some representative results are listed in Scheme 1. With phenylboronic acid $2a_1$ as the coupling partner, the expected triphenyl substituted olefin **3aa** was obtained in 56% reaction yield, but a significant amount of the direct coupling product **4aa** was formed, along with some side products from the dimerization of **1a** (entry 1). Screening of ligands, solvents, or bases failed to improve the migration efficiency. We speculated

that the arylboron reagent should have its reactivity in a reasonable zone (Lennox and Lloyd-Jones, 2014; Tobisu and Chatani, 2009), allowing for the completion of the palladium migration process prior to the subsequent coupling step, meantime keeping a faster Suzuki-Miyaura coupling with the generated alkenylpalladium species over the self-Heck reaction. Therefore, a variety of other organoboron types were evaluated (entries 2–9), including triphenylboroxine (**2a$_2$**), potassium trifluoroborate salt (**2a$_3$**), and different boronate esters (**2a$_4$**-**2a$_9$**). Triphenylboroxine **2a$_2$** gave a comparable result, but the coupling reaction was almost shut down with potassium trifluoroborate **2a$_3$** where the dimerization of **1a** became the major reaction pathway. Pinacol boronate ester **2a$_4$** gave excellent regioselectivity (**3aa/4aa** = 97:3) albeit in a low reaction yield, possibly due to its low reactivity. Slightly more reactive boronate esters with less sterically hindered protection could improve reaction yields with maintained high regioselectivities. However, catechol boronate ester **2a$_7$** was too reactive, thus affording the direct coupling product **4aa** as the major product. Six-membered boronate esters (**2a$_8$** and **2a$_9$**) could also give product **3aa** in moderate yields and with high regioselectivities but failed to offer better results compared with the best five-membered one **2a$_6$**.

With boronate ester **2a$_6$** as the coupling partner, further screening of different ligands (entries 10–16, and Table S1 for details) was carried out. Slight modifications by removing *o*-MeO substituents (**L2**), replacing them with Me substituents (**L3**), or moving them to the other positions (**L4** and **L5**) led to a sever loss of catalyst activity, as well as the capability to control regioselectivity, further demonstrating the important beneficial effect enabled by the hemilabile *o*-MeO coordination (Wakioka et al., 2014). Other types of ligands could not improve this transformation, either. Bulky electron-rich dialkylbiaryl phosphine **L6** gave a higher regioselectivity but a reduced yield of **3aa**. The open-chain bisphosphine ligands (**L7** and **L8**) afforded low yield of **3aa** and poor regioselectivity. Base also played an important role in this reaction. Both yield of **3aa** and regioselectivity were further enhanced by switching CsOAc to CsOPiv (entry 18, and Table S2 for details). A more thorough list of variable screening is given in the Supplemental Information (Tables S1–S3).

Substrate Scope

Synthesis of Trisubstituted Olefins

With the optimal reaction conditions identified, the generality of this reaction was then investigated. First, the coupling of various *ortho*-vinyl aromatic bromides **1** with aryl boronate esters **2a** was carried out (Scheme 2). In general, very good reaction yields were observed for the substrates bearing substituents with different electronic and steric properties at the phenyl ring **A**. Replacement of the phenyl ring with a naphthyl (**3ia**) or pyridyl (**3ja**) group was also well accommodated. It is worth mentioning that the possible coordination of pyridine moiety with palladium catalyst did not affect this catalytic process, and an excellent reaction yield of **3ja** (91%) was achieved.

Variation of the phenyl ring **B** was also examined. Methyl substitution at different positions of the phenyl ring was tested to explore the spatial effect on this reaction. *Ortho*-methyl substitution gave the best reaction yield, suggesting the steric hindrance from this methyl group prohibited the potential dimerization of **1**. Electronic effect at this phenyl ring **B** was also evaluated with different substitutions installed to its *para*-position, and the electron-withdrawing groups showed a beneficial effect on the reaction. When the phenyl ring **B** was replaced by naphthyl group, sterically more hindered 1-naphthyl (**3ta**) substitution showed a higher reaction yield than 2-naphthyl (**3sa**) one, which was consistent with the above observations. Switching the phenyl group to heteroaromatic rings, like substituted pyridyl (**3ua**) and 2-thienyl (**3va**) groups, was also compatible for this reaction, giving 92% and 67% reaction yields, respectively. The aryl ring can also be replaced by alkyl (**3wa** and **3xa**), cyano (**3ya**), and ester (**3za**) groups, affording the products in high reaction yields.

Next, the scope of arylboronates was examined. When *ortho*-methyl phenylboronate ester was applied, the reaction yield decreased a little to 60% due to steric effect (**3ab**). However, more sterically congested 2,6-dimethyl one could still offer a decent yield of **3ac** (44%). Good to excellent reaction yields were obtained with boronate esters bearing an electron-withdrawing or electron-donating substitution at its *para*-position of the phenyl ring. Chemically reactive functional groups, such as aldehyde (**3al**), ketone (**3am**), and ester (**3an**), were well tolerated. Free amino group (**3ao**) and thioether (**3ap**), which can frequently deactivate palladium catalyst owing to their strong coordination with palladium, were also compatible. In search for wide application of our palladium-catalyzed transformation in material science, the examples with Cl (**3aq**) and TMS (**3ar**) substitutions offered useful handles for their future incorporation to functional material molecules (Siamaki et al., 2011; Carsten et al., 2011).

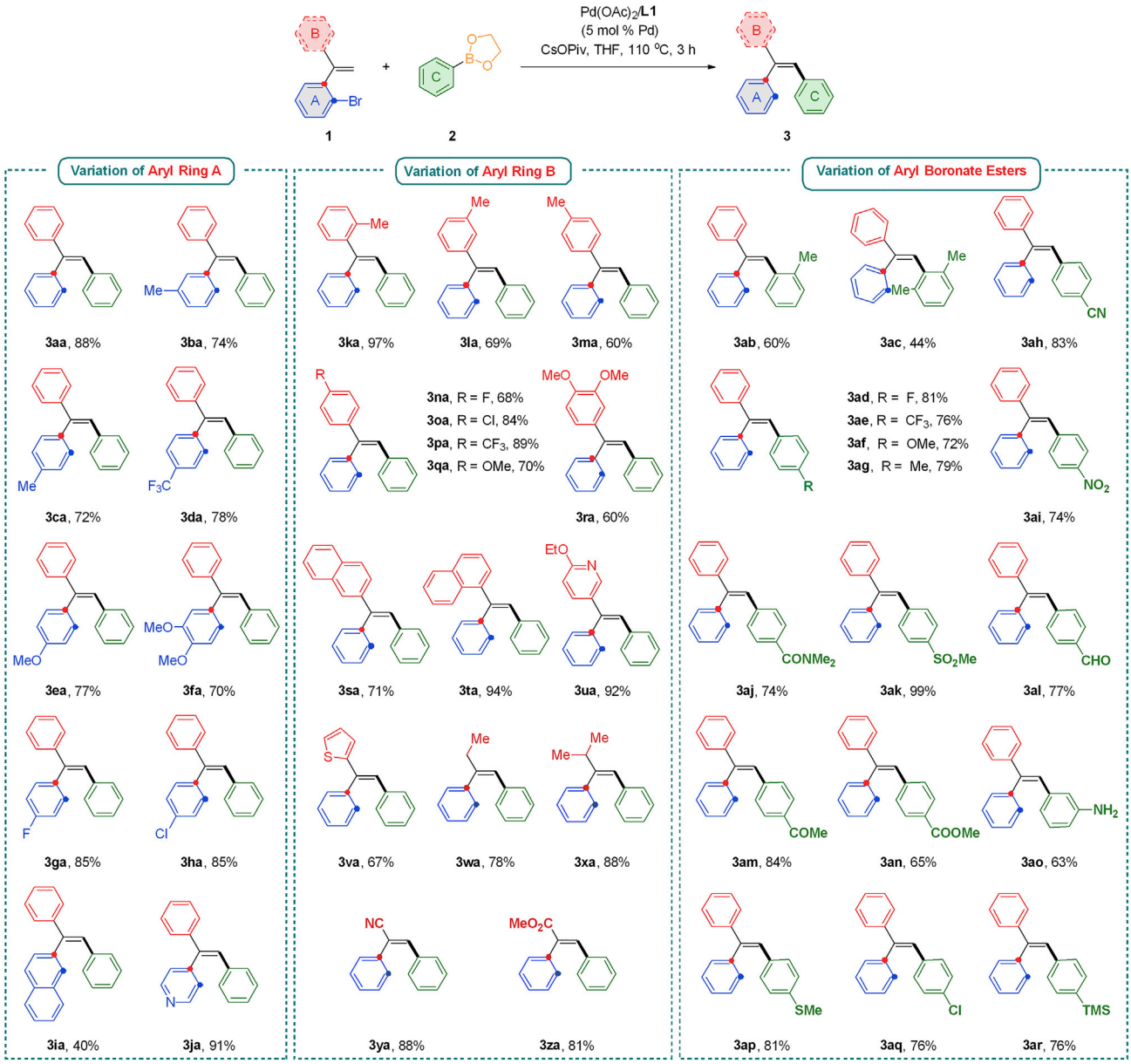

Scheme 2. Coupling of *ortho*-Vinyl Aromatic Bromides with Aryl Boronate Esters

All reactions were conducted with substrate **1** (1.0 equiv, 0.3 mmol), phenylboronate ester **2a**$_6$ (3.0 equiv, 0.9 mmol), $Pd(OAc)_2$ (5 mol %), **L1** (10 mol %), and CsOPiv (2.0 equiv, 0.6 mmol) in THF (3 mL) at 110°C for 3 h.

The introduction of polycyclic aromatic moiety to a molecule can quickly expand the existing π-extended system, which is often of great importance for enhanced electronic and photonic performance (Itami et al., 2005). Therefore, a variety of aryl boronate esters bearing commonly used polycyclic aromatic rings (Scheme 3), including naphthyl (**6aa**, **6ab**), phenanthryl (**6ac**), anthryl (**6ad**), triphenylenyl (**6ae**), and pyrenyl (**6af**) groups, were examined in the coupling with *ortho*-vinyl bromobenzene **1a**. All reactions proceeded quite well with good to excellent isolated yields. The structure of **6af** was further confirmed by X-ray crystallography.

Heteroaromatic rings are another family of substructures with wide existence in material molecules (Li et al., 2010). Although the coupling with heteroarylboron reagents is a straightforward way to install these important subunits, the strong coordinating capability of hetero atoms to palladium center may raise potential

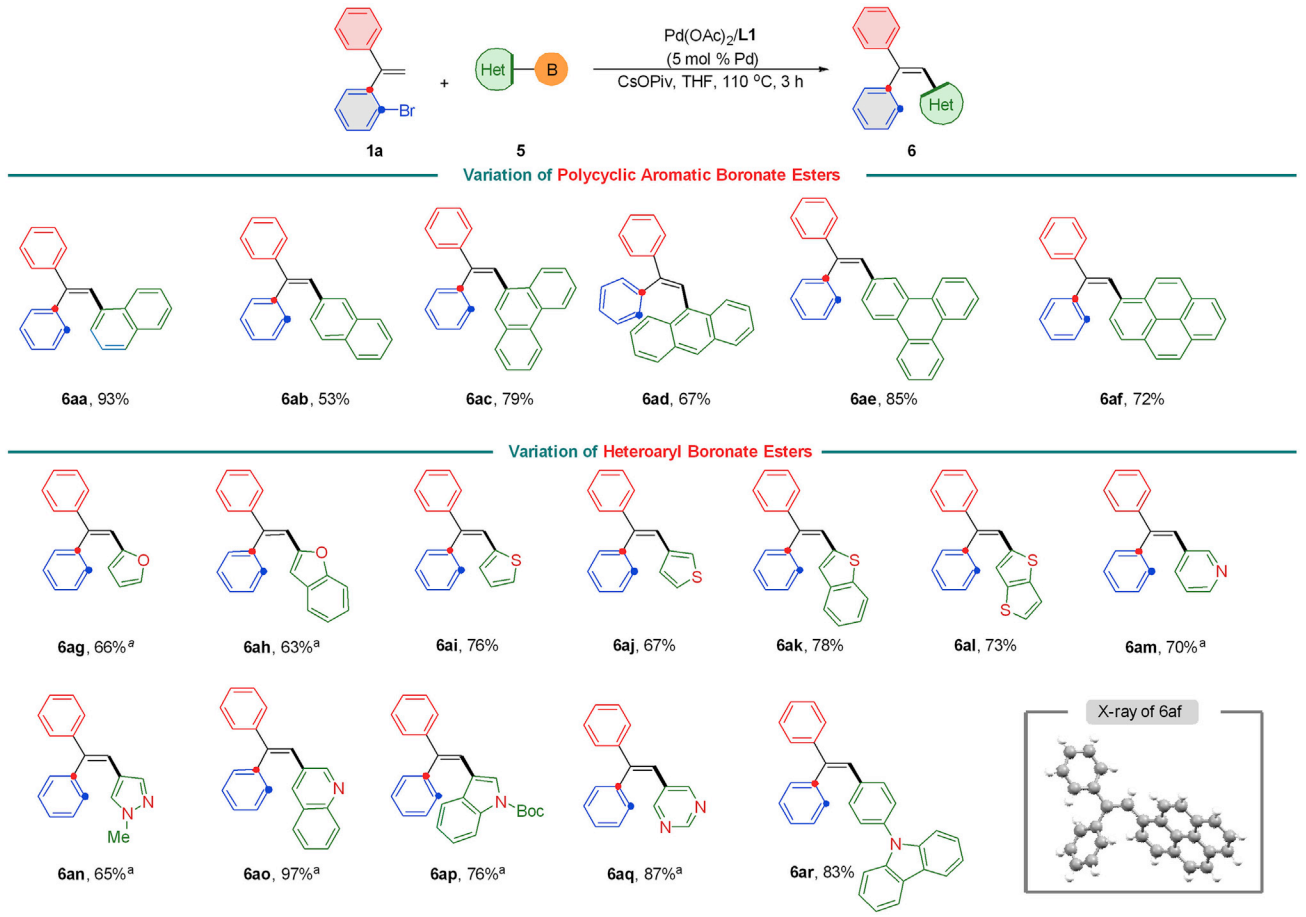

Scheme 3. Coupling of *ortho*-Vinyl Bromobenzene 1a with Polycyclic Aromatic and Heteroaryl Boronate Esters

All reactions were conducted with substrate **1a** (1.0 equiv, 0.3 mmol), (hetero)arylboronate **5** (3.0 equiv, 0.9 mmol), $Pd(OAc)_2$ (5 mol %), $P(2\text{-MeO-Ph})_3$ (10 mol %), and CsOPiv (2.0 equiv, 0.6 mmol) in THF (3 mL) at 110°C for 3 h (unless otherwise noted). [a]Pinacol esters were used instead of glycol ester.

concerns (Billingsley et al., 2006; Billingsley and Buchwald, 2007). To our delight, a wide range of heteroaromatic rings (Scheme 3), including furyl (**6ag**), benzofuryl (**6ah**), thienyl (**6ai**, **6aj**), benzothiophenyl (**6ak**), thieno[3,2-*b*]thienyl (**6al**), pyridyl (**6am**), pyrazolyl (**6an**), quinolyl (**6ao**), indolyl (**6ap**), pyrimidyl (**6aq**), and carbazolyl (**6ar**), were successfully assembled in good to excellent yields, further demonstrating the potential of this method for material science.

Synthesis of Multisubstituted 1,3-Dienes

Encouraged by the above success in preparing trisubstituted olefins, we envision that the coupling reaction with arylethenyl boron reagents would lead to the generation of stereodefined multisubstituted 1,3-dienes. A number of arylethenyl boron reagents are commercially available, and several stereoselective synthetic methods were developed, which laid a firm base for this strategy (Yoshii et al., 2019). The optimized conditions used in the above coupling with arylboronate esters were also suitable for the arylethenyl boron esters. Further screening of the reaction conditions led to the use of boronate pinacol ester as the best choice. In addition, the reaction could go to completion with a decreased catalyst loading (2.5 mol %), a lower reaction temperature (70°C), and a shorter reaction time (1 h).

By employing the above newly optimized reactions, the reaction scope was examined (Scheme 4). Unlike the reactions with arylboronate esters, variation on *ortho*-vinyl arylbromides **1** showed marginal effect on the couplings with phenylethenyl boronate pinacol ester. Excellent yields were achieved in all cases when substitutions with different steric and electronic profiles were introduced to either phenyl ring **A** or **B**. Replacement of phenyl ring **B** with 1-naphthenyl (**8ta**), 2-naphthenyl (**8sa**), or 2-thienyl (**8va**) group still maintained high reaction yield.

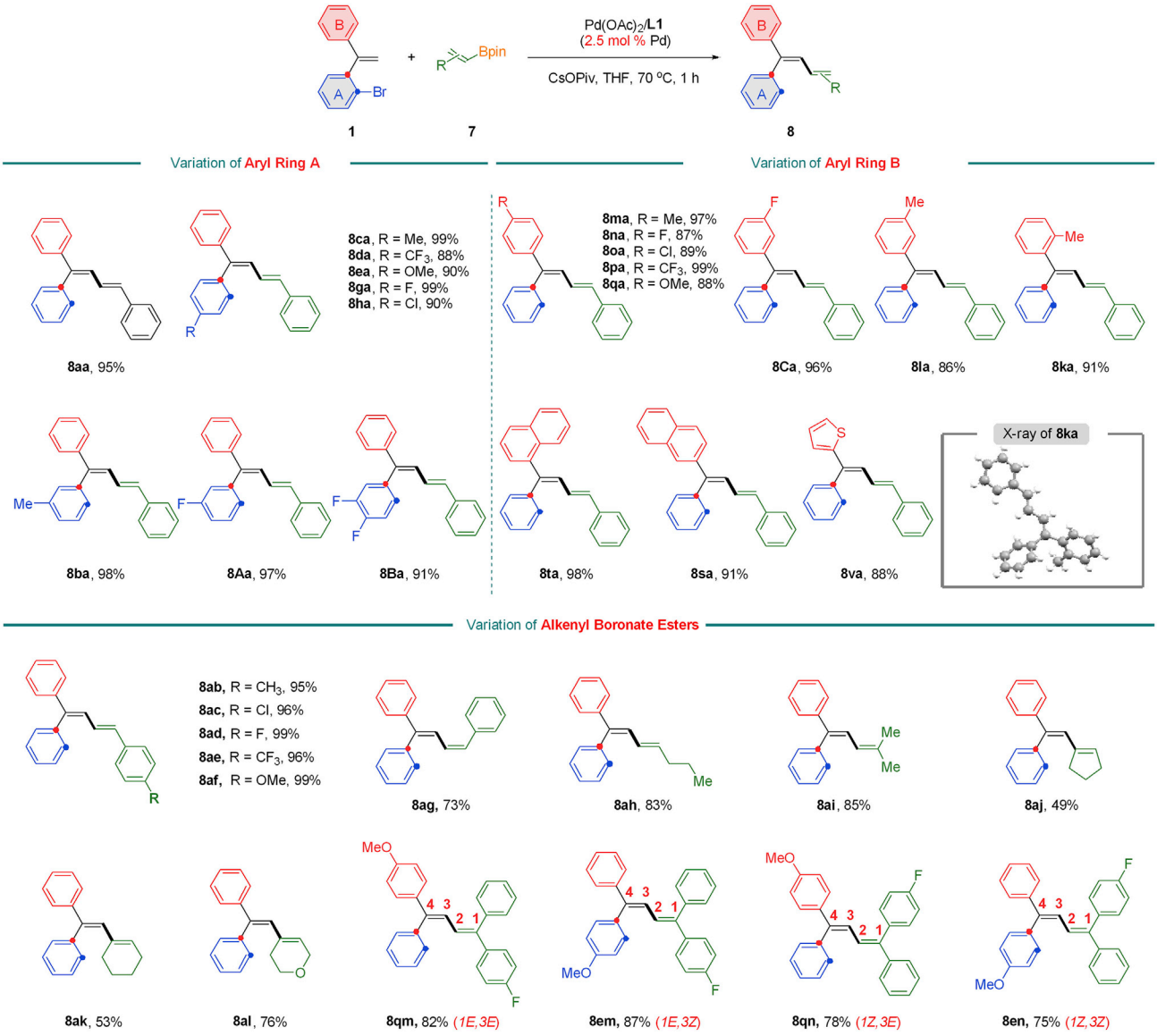

Scheme 4. Coupling of *ortho*-Vinyl Aromatic Bromides with Alkenylboronate Esters

All reactions were conducted with substrate **1** (1.0 equiv, 0.3 mmol), arylethenyl boronate ester **7** (2.0 equiv, 0.6 mmol), $Pd(OAc)_2$ (2.5 mol %), **L1** (5 mol %), and CsOPiv (2.0 equiv, 0.6 mmol) in THF (3 mL) at 70°C.

A variety of *E*-arylethenyl boronates with different substitutions at the *para*-position of the phenyl ring were evaluated. Both electron-withdrawing and -donating groups gave the desired (*E*)-1,3-dienes in excellent yields (**8ab–8af**). (*Z*)-phenylethenyl boronate pinacol ester led to (*Z*)-1,3-diene as the predominant product (**8ag**), along with some (*E*)-1,3-diene due to the partial isomerization of its double bond during the reaction process. Aryl substitutions can also be replaced by various alkyl groups (**8ah** and **8ai**), and slightly lower yields were observed with sterically more hindered cyclic alkenyl boronates (**8aj-8al**). The use of β,β-diaryl-substituted vinyl boronates can potentially generate stereodefined tetra-aryl substituted 1,3-dienes. Therefore, several stereodefined vinyl boronates, which were prepared according to our previous results (Hu et al., 2016), were applied in this transformation. Despite slightly decreased yields, likely due to the increased steric hindrance, the desired tetra-aryl substituted 1,3-dienes were produced in geometrically pure form (**8qm**, **8em**, **8qn**, and **8en**), overcoming the synthetic challenges in the preparation of such single stereoisomers by traditional methods. The stereochemistry of the obtained products was further confirmed by the X-ray crystallography of diene **8ka**.

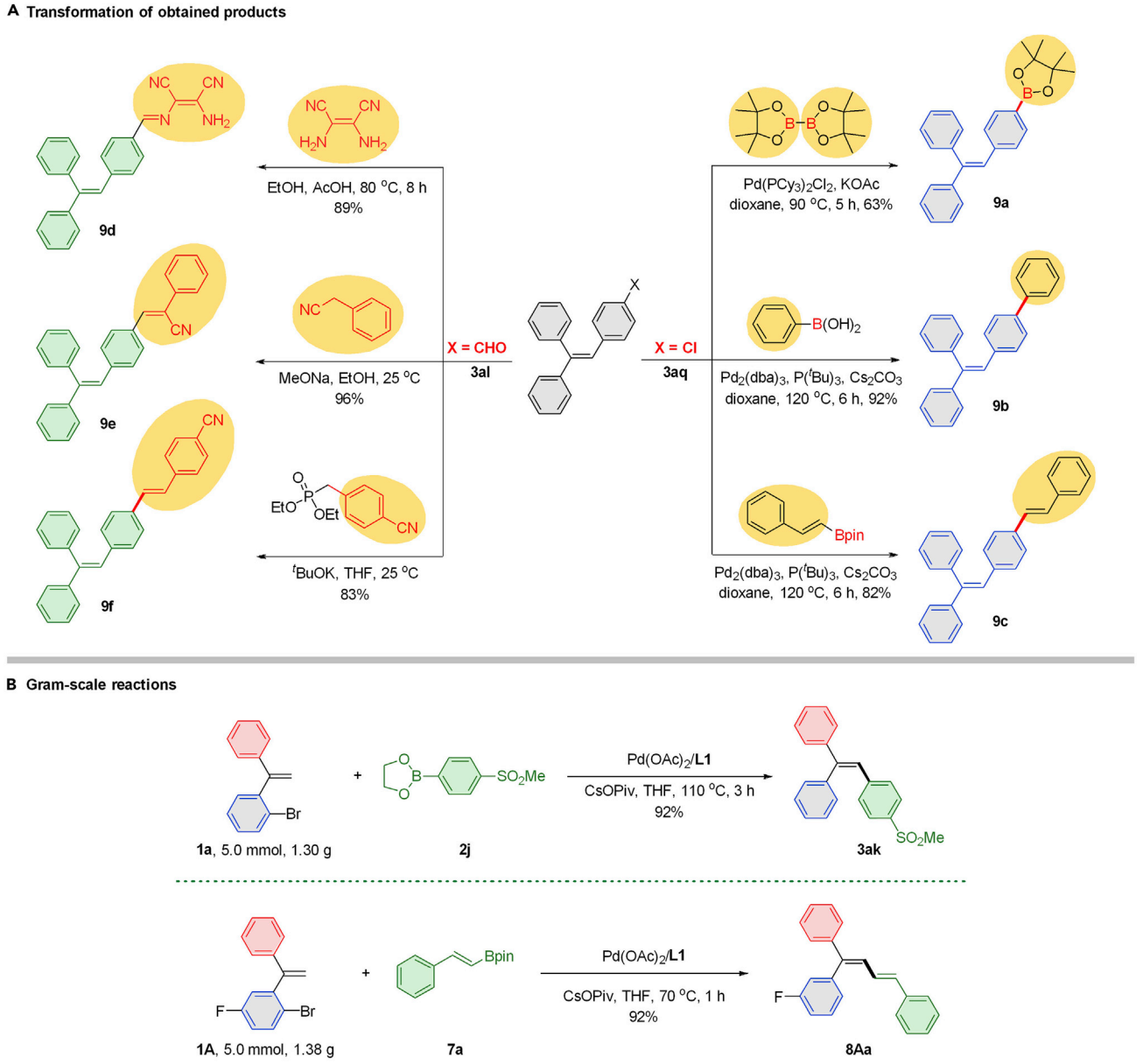

Scheme 5. Practicality Demonstrations

(A) Transformations of the obtained products.

(B) Gram-scale reactions.

Transformation of the Products and Gram Scale Synthesis

To demonstrate the practicality of this method, we illustrated some chemical transformations of the produced trisubstituted olefins, providing potentials to embody these subunits to the designed material molecules (Scheme 5A). The chloride in olefin **3aq** offered a handle for versatile derivatization using palladium-catalyzed coupling reactions, like Miyaura borylation with $(Bpin)_2$ and Suzuki-Miyaura coupling with aryl- or alkenylboronates, which are widely used transformations in material science (Yu et al., 2017; Li et al., 2018; Wang et al., 2020). The CHO group also offers potential use in versatile functionalization. The aldehyde **3al** could be converted to diaminomaleonitrile-modified olefin **9d** (Huang et al., 2017). Such a special imine derivative displayed photo- and mechano-responsive properties, further expanding the application of this method in the field of multi-responsive material. In addition, the compounds **9e** and **9f** with triphenylethylene skeleton, a kind of donor-π-acceptor fluorophores with color-tunable aggregation-induced

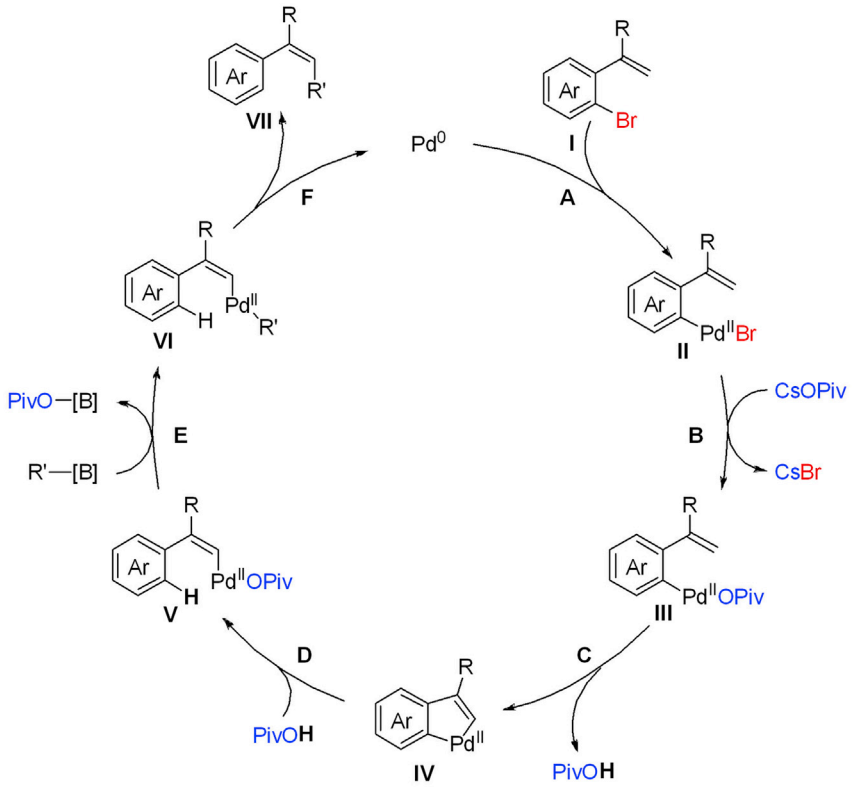

Scheme 6. Plausible Catalytic Cycle

emission (AIE) behaviors (Wen et al., 2016), were prepared from aldehyde **3al** through Knoevenagel condensation and HWE olefination reaction, respectively. All these high-yielding transformations provide infinite potentials in commercial application for full-color displays.

The scalability of the reaction was also investigated with two representative examples (Scheme 5B). The coupling of *ortho*-vinyl bromobenzene **1a** with arylboronate **2j** produced the desired olefin **3ak** in excellent yield (92%), similar to the small trial. It is also the case for the coupling of *ortho*-vinyl bromobenzene **1A** with phenylethenylboronate **7a**.

Proposed Reaction Mechanism

Although the mechanism of this reaction is not clear at this stage, a tentative catalytic cycle is proposed in Scheme 6. Initial oxidative addition of arylbromide to palladium(0) generates the intermediate **II** (step **A**), which may exchange its bromide anion with $PivO^-$ (step **B**) to facilitate the following C-H activation step (step **C**). Instead of a second oxidative addition to form a palladium(**IV**) species, theoretical studies have revealed that a concerted metalation-deprotonation (CMD) mechanism would be energetically favored, in which carboxylates were often needed to act as an inner base (Cheng et al., 2014; Gorelsky et al., 2008). The generated five-membered palladacycle **IV** undergoes a formal proton transfer to render a net 1,4-palladium shift from the aryl to alkenyl position (step **D**) and then proceeds through the following Suzuki coupling sequences to afford the desired product **VII** (step **E** and **F**).

Application in Aggregation-Induced Emission Materials

AIE Characteristics

To shed light on the potential application of our methodology in material science, some obtained products with rotatable aryl rings were subjected to the AIE properties test according to the restriction of intramolecular motion (Mei et al., 2014, 2015). Since the first report by Tang and co-workers in 2001, AIE concept and phenomenon have attracted considerable research attention and created a variety of potential applications in various fields (Luo et al., 2001; An et al., 2002). Several AIE systems have been elaborately

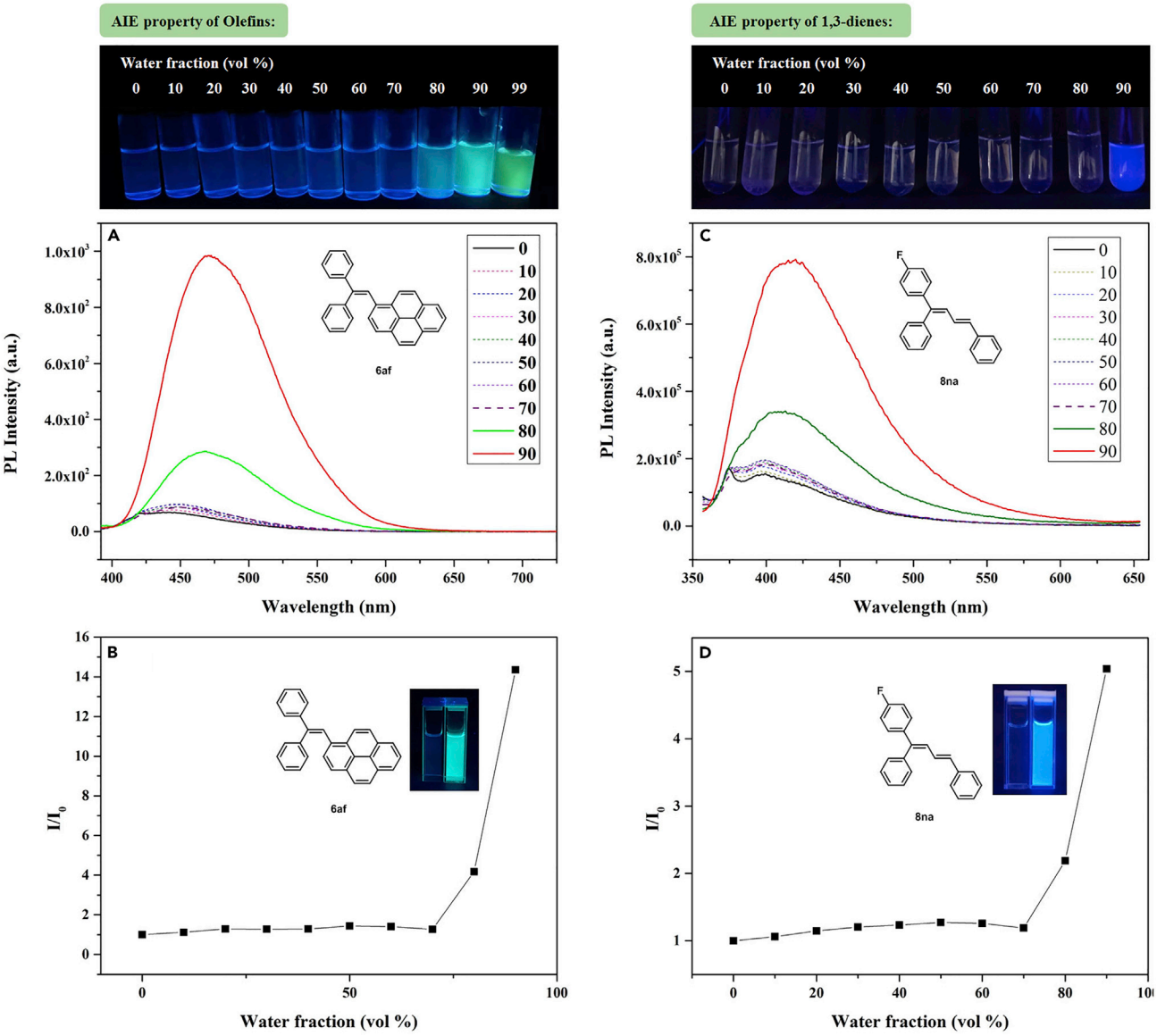

Figure 2. AIE Activity of Products

(A) PL spectra of **6af** in THF/water mixtures with different water fractions.

(B) Plots of relative PL intensity versus the composition of THF/water mixtures of **6af**.

(C) PL spectra of **8na** in THF/water mixtures with different water fractions.

(D) Plots of relative PL intensity versus the composition of THF/water mixtures of **8na**.

designed and well studied, where multi-aryl-substituted olefins and 1,3-dienes represent two of the most effective structures (Kong et al., 2018; Yang et al., 2014; He et al., 2019).

Some of the obtained products exhibited a distinct AIE effect. Non-emission was observed in dilute solutions, whereas the solid states gave strong emission. To further confirm the AIE feature of these compounds, the photoluminescence (PL) was studied in THF and THF/water mixtures with varying water fractions (f_w). As shown in Figure 2, olefin **6af** was negligibly emissive in dilute THF solution. However, the PL intensity was greatly enhanced in THF/water mixtures with f_w >70%, probably due to the formation of nanoaggregate, exhibiting typical AIE characteristics. Notably, the luminescence intensity achieved a maximum at 469 nm when water fraction reached 90%. 1,3-Dienes also showed similar AIE behavior. The fluorescence intensity of **8na** was about 5.0-fold higher in THF/water mixtures with f_w >90% than in pure THF.

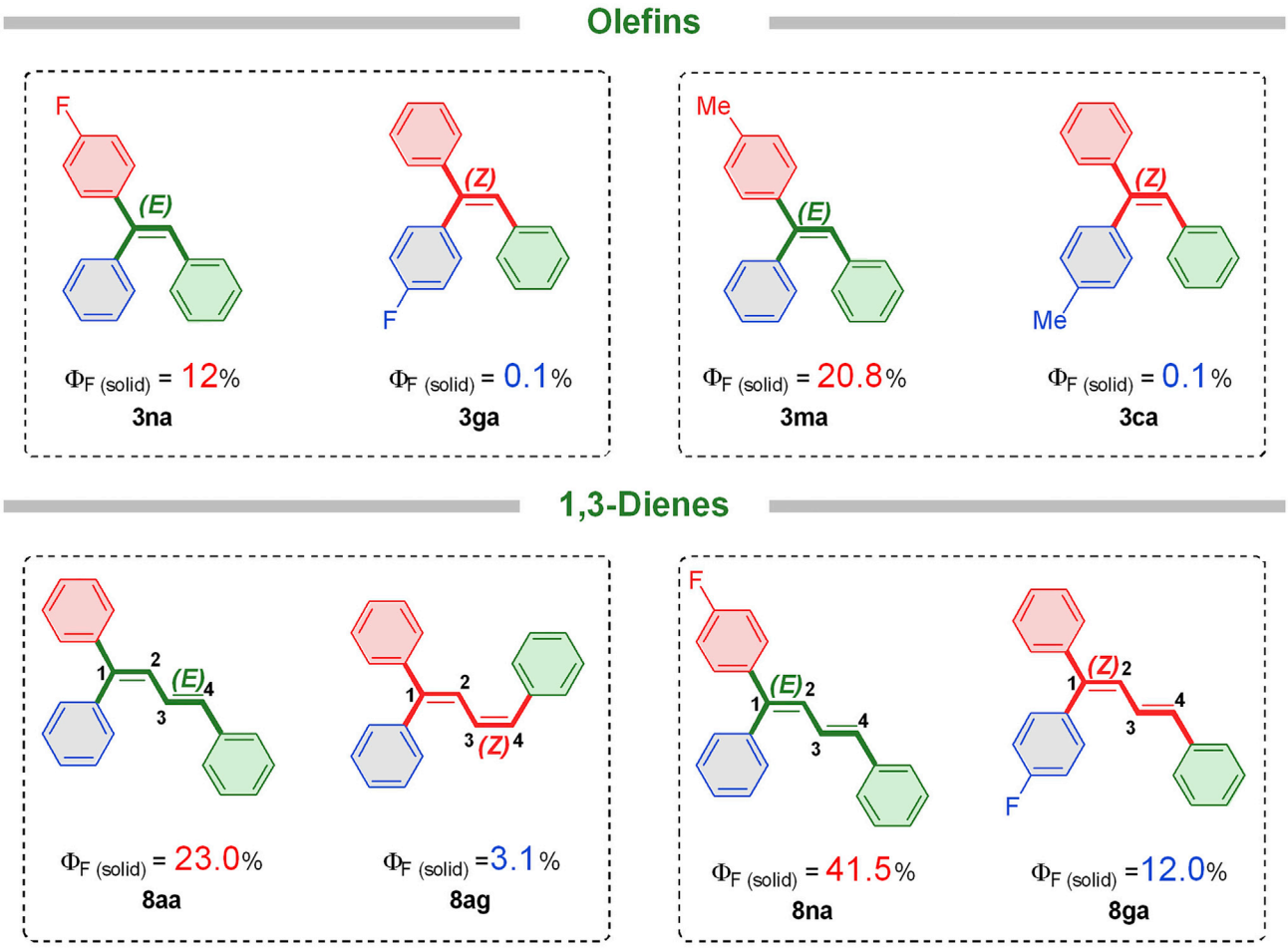

Figure 3. Comparison of PL Quantum Yields of Geometric Isomers

PL Quantum Yields of Geometric Isomers

It is well known that structurally similar geometric isomers may exhibit different AIE properties. However, the accessibility of all corresponding isomers in pure form restricted such systematic studies.

Our new method allowed for the convenient generation of various pure geometric isomers, and several pairs of multi-aryl substituted olefins and 1,3-dienes were prepared. Figure 3 listed the PL quantum yields (PLQY, Φ_F) of these geometric isomers in solid states (for further details, see Table S4). *E*-TriPE-F (**3na**) and *E*-TriPE-Me (**3ma**) showed higher Φ_F (12.0% and 20.8%, respectively) than those of *Z*-TriPE-F (**3ga**, Φ_F = 0.1%) and *Z*-TriPE-Me (**3ca**, Φ_F = 0.1%). These results suggest that rigidification of the *E*-isomers is higher than that of *Z*-ones (Mei et al., 2014). Similar phenomena were also observed for 1,3-dienes. Compared with *3Z*-TPBDE (**8ag**, Φ_F = 3.1%) and *1Z*-TPBDE-F (**8ga**, Φ_F = 12.0%), *3E*-TPBDE (**8aa**, Φ_F = 23.0%) and *1E*-TPBDE-F (**8na**, Φ_F = 41.5%) exhibited significantly enhanced Φ_F. These results indicated that the geometry of double bond significantly affects the photophysical properties in solid state. Therefore, our synthetic methodology provided a powerful tool for the discovery of advanced material through precise control of the double bond geometry.

Conclusion

We have developed an efficient Suzuki-Miyaura coupling through a controllable 1,4-palladium migration process for the stereospecific synthesis of multisubstituted olefins and 1,3-dienes. A precise reactivity balance of the used organoboronates played a vital role in this process. The practicality of this method was demonstrated by the excellent capability and flexibility in stereochemical control, broad substrate scope, excellent functional

group tolerance, as well as versatile conversion with obtained products and easy scalability. The power of this method is also highlighted by the AIE feature studies of some obtained products. Several pairs of pure geometrical isomers were prepared and showed significant differences in photoluminescent quantum yield values.

Limitations of the Study

All *ortho*-vinyl aromatic bromides used in the current 1,4-palladium migration/Suzuki-Miyaura coupling sequence were terminal alkenes. Effort to use trisubstituted olefins as starting material is unsuccessful, and only a trace amount of desired product can be observed.

METHODS

All methods can be found in the accompanying Transparent Methods supplemental file.

DATA AND CODE AVAILABILITY

The X-ray crystallographic coordinates for structures reported in this study have been deposited at the Cambridge Crystallographic Data Centre (CCDC) under accession number CCDC: 1965806 (**6af**) and 1965685 (**8ka**). These data can be obtained free of charge from The Cambridge Crystallographic Data Centre via www.ccdc.cam.ac.uk/data_request/cif.

SUPPLEMENTAL INFORMATION

Supplemental Information can be found online at https://doi.org/10.1016/j.isci.2020.100966.

ACKNOWLEDGMENTS

This work was supported by The National Natural Science Foundation of China (21772216, 21871284, 91956113), The Strategic Priority Research Program of the Chinese Academy of Sciences (XDB 20020100), The Key Research Program of Frontier Science (QYZDY-SSWSLH026), the STCSM (18401933500), and the SMEC (2019-01-07-00-10-E00072) for financial support. We thank Dr. Han-Qing Dong (Arvinas, Inc.) for his help in the preparation of this manuscript.

AUTHOR CONTRIBUTIONS

M.-Y.L. and T.-J.H. performed the reaction optimization. M.-Y.L. investigated the scope of the substrate. P.H. invested the AIE behavior of the obtained products. D.W. and G.Z. prepared some starting materials. A.Q. and B.Z.T. directed the AIE studies. G.-Q.L. and C.-G.F. directed the project and wrote the manuscript with input from all authors. All authors analyzed the results and commented on the manuscript.

DECLARATION OF INTERESTS

The authors declare no competing interests.

Received: January 15, 2020
Revised: February 20, 2020
Accepted: March 3, 2020
Published: March 27, 2020

REFERENCES

An, B.K., Kwon, S.K., Jung, S.D., and Park, S.Y. (2002). Enhanced emission and its switching in fluorescent organic nanoparticles. J. Am. Chem. Soc. *124*, 14410–14415.

Barder, T.E., Walker, S.D., Martinelli, J.R., and Buchwald, S.L. (2005). Catalysts for Suzuki-Miyaura coupling processes: scope and studies of the effect of ligand structure. J. Am. Chem. Soc. *127*, 4685–4696.

Beletskaya, I.P., Alonso, F., and Tyurin, V. (2019). The Suzuki-Miyaura reaction after the Nobel prize. Coord. Chem. Rev. *385*, 137–173.

Besset, T., Kuhl, N., Patureau, F.W., and Glorius, F. (2011). Rh(III)-catalyzed oxidative olefination of vinylic C-H bonds: efficient and selective access to di-unsaturated alpha-amino acid derivatives and other linear 1,3-butadienes. Chem. Eur. J. *17*, 7167–7171.

Billingsley, K., and Buchwald, S.L. (2007). Highly efficient monophosphine-based catalyst for the palladium-catalyzed Suzuki-Miyaura reaction of heteroaryl halides and heteroaryl boronic acids and esters. J. Am. Chem. Soc. *129*, 3358–3366.

Billingsley, K.L., Anderson, K.W., and Buchwald, S.L. (2006). A highly active catalyst for Suzuki-Miyaura cross-coupling reactions of heteroaryl compounds. Angew. Chem. Int. Ed. *45*, 3484–3488.

Boultadakis-Arapinis, M., Hopkinson, M.N., and Glorius, F. (2014). Using Rh(III)-catalyzed C-H activation as a tool for the selective functionalization of ketone-containing molecules. Org. Lett. *16*, 1630–1633.

Campo, M.A., Zhang, H., Yao, T., Ibdah, A., McCulla, R.D., Huang, Q., Zhao, J., Jenks, W.S., and Larock, R.C. (2007). Aryl to aryl palladium migration in the Heck and Suzuki coupling of o-halobiaryls. J. Am. Chem. Soc. *129*, 6298–6307.

Carsten, B., He, F., Son, H.J., Xu, T., and Yu, L. (2011). Stille polycondensation for synthesis of functional materials. Chem. Rev. *111*, 1493–1528.

Chen, X., Goodhue, C.E., and Yu, J.-Q. (2006). Palladium-catalyzed alkylation of sp(2) and sp(3) C-H bonds with methylboroxine and alkylboronic acids: two distinct C-H activation pathways. J. Am. Chem. Soc. *128*, 12634–12635.

Cheng, G.J., Yang, Y.F., Liu, P., Chen, P., Sun, T.Y., Li, G., Zhang, X., Houk, K.N., Yu, J.Q., and Wu, Y.D. (2014). Role of N-acyl amino acid ligands in Pd(II)-catalyzed remote C-H activation of tethered arenes. J. Am. Chem. Soc. *136*, 894–897.

Couty, S., Liégault, B., Meyer, C., and Cossy, J. (2004). Heck-Suzuki-Miyaura domino reactions involving ynamides. An efficient access to 3-(Arylmethylene)isoindolinones. Org. Lett. *6*, 2511–2514.

De Paolis, M., Chataigner, I., and Maddaluno, J. (2012). Recent advances in stereoselective synthesis of 1,3-dienes. In Stereoselective Alkene Synthesis, J. Wang, ed. (Springer-Verlag), pp. 87–146.

Gao, K., Lee, P.-S., Fujita, T., and Yoshikai, N. (2010). Cobalt-catalyzed hydroarylation of alkynes through chelation-assisted C-H bond activation. J. Am. Chem. Soc. *132*, 12249–12251.

Giri, R., Maugel, N., Li, J.-J., Wang, D.-H., Breazzano, S.P., Saunders, L.B., and Yu, J.-Q. (2007). Palladium-catalyzed methylation and arylation of sp(2) and sp(3) C-H bonds in simple carboxylic acids. J. Am. Chem. Soc. *129*, 3510–3511.

Gorelsky, S.I., Lapointe, D., and Fagnou, K. (2008). Analysis of the concerted metalation-deprotonation mechanism in palladium-catalyzed direct arylation across a broad range of aromatic substrates. J. Am. Chem. Soc. *130*, 10848–10849.

Grigg, R., Sansano, J.M., Santhakumar, V., Sridharan, V., Thangavelanthum, R., Thornton-Pett, M., and Wilson, D. (1997). Palladium catalysed tandem cyclisation-anion capture processes .3. Organoboron anion transfer agents. Tetrahedron *53*, 11803–11826.

He, Z., Liu, P., Zhang, S., Yan, J., Wang, M., Cai, Z., Wang, J., and Dong, Y. (2019). A freezing-induced turn-on imaging modality for real-time monitoring of cancer cells in cryosurgery. Angew. Chem. Int. Ed. *58*, 3834–3837.

Hu, X.H., Zhang, J., Yang, X.F., Xu, Y.H., and Loh, T.P. (2015). Stereo- and chemoselective cross-coupling between two electron-deficient acrylates: an efficient route to (Z,E)-muconate derivatives. J. Am. Chem. Soc. *137*, 3169–3172.

Hu, T.J., Zhang, G., Chen, Y.H., Feng, C.G., and Lin, G.Q. (2016). Borylation of olefin C-H bond via aryl to vinyl palladium 1,4-migration. J. Am. Chem. Soc. *138*, 2897–2900.

Hu, T.J., Li, M.Y., Zhao, Q., Feng, C.G., and Lin, G.Q. (2018). Highly stereoselective synthesis of 1,3-dienes through an aryl to vinyl 1,4-palladium migration/heck sequence. Angew. Chem. Int. Ed. *57*, 5871–5875.

Huang, Q., Yu, T., Xie, Z., Li, W., Wang, L., Liu, S., Zhang, Y., Chi, Z., Xu, J., and Aldred, M.P. (2017). Hydrogen bonding-assisted loosely packed crystals of a diaminomaleonitrile-modified tetraphenylethene compound and their photo- and mechano-responsive properties. J. Mater. Chem. C *5*, 11867–11872.

Itami, K., Ohashi, Y., and Yoshida, J. (2005). Triarylethene-based extended pi-systems: programmable synthesis and photophysical properties. J. Org. Chem. *70*, 2778–2792.

Kong, T.T., Zhao, Z., Li, Y., Wu, F., Jin, T., and Tang, B.Z. (2018). Detecting live bacteria instantly utilizing AIE strategies. J. Mater. Chem. B *6*, 5986–5991.

Lennox, A.J., and Lloyd-Jones, G.C. (2014). Selection of boron reagents for Suzuki-Miyaura coupling. Chem. Soc. Rev. *43*, 412–443.

Li, Z., and Duan, W.L. (2018). Palladium-catalyzed C-H alkenylation of arenes with alkynes: stereoselective synthesis of vinyl chlorides via a 1,4-chlorine migration. Angew. Chem. Int. Ed. *57*, 16041–16045.

Li, H., Chi, Z., Xu, B., Zhang, X., Yang, Z., Li, X., Liu, S., Zhang, Y., and Xu, J. (2010). New aggregation-induced emission enhancement materials combined triarylamine and dicarbazolyl triphenylethylene moieties. J. Mater. Chem. *20*, 6103–6110.

Li, B.X., Le, D.N., Mack, K.A., McClory, A., Lim, N.-K., Cravillion, T., Savage, S., Han, C., Collum, D.B., Zhang, H., and Gosselin, F. (2017). Highly stereoselective synthesis of tetrasubstituted acyclic all-carbon olefins via Enol tosylation and Suzuki-Miyaura coupling. J. Am. Chem. Soc. *139*, 10777–10783.

Li, Y., Zhao, Z., Zhang, J., Kwok, R.T.K., Xie, S., Tang, R., Jia, Y., Yang, J., Wang, L., Lam, J.W.Y., et al. (2018). A bifunctional aggregation-induced emission luminogen for monitoring and killing of multidrug-resistant bacteria. Adv. Funct. Mater. *28*, 1804632.

Liang, Q.J., Yang, C., Meng, F.F., Jiang, B., Xu, Y.H., and Loh, T.P. (2017). Chelation versus non-chelation control in the stereoselective alkenyl sp(2) C-H bond functionalization reaction. Angew. Chem. Int. Ed. *56*, 5091–5095.

Lin, E.E., Wu, J.-Q., Schäfers, F., Su, X.-X., Wang, K.-F., Li, J.-L., Chen, Y., Zhao, X., Ti, H., Li, Q., et al. (2019). Regio- and stereoselective synthesis of tetra- and triarylethenes by N-methylimidodiacetyl boron-directed palladium-catalysed three-component coupling. Commun. Chem. (Camb.) *2*, 49.

Liu, J., Yang, J., Baumann, W., Jackstell, R., and Beller, M. (2019). Stereoselective synthesis of highly substituted conjugated dienes via Pd-catalyzed carbonylation of 1,3-diynes. Angew. Chem. Int. Ed. *58*, 10683–10687.

Luo, J.D., Xie, Z.L., Lam, J.W.Y., Cheng, L., Chen, H.Y., Qiu, C.F., Kwok, H.S., Zhan, X.W., Liu, Y.Q., Zhu, D.B., and Tang, B.Z. (2001). Aggregation-induced emission of 1-methyl-1,2,3,4,5-pentaphenylsilole. Commun. Chem. (Camb.) *18*, 1740–1741.

Ma, S.M., and Gu, Z.H. (2005). 1,4-Migration of rhodium and palladium in catalytic organometallic reactions. Angew. Chem. Int. Ed. *44*, 7512–7517.

Maluenda, I., and Navarro, O. (2015). Recent developments in the Suzuki-Miyaura reaction: 2010-2014. Molecule *20*, 7528–7557.

Mei, J., Hong, Y., Lam, J.W.Y., Qin, A., Tang, Y., and Tang, B.Z. (2014). Aggregation-induced emission: the whole is more brilliant than the parts. Adv. Mater. *26*, 5429–5479.

Mei, J., Leung, N.L.C., Kwok, R.T.K., Lam, J.W.Y., and Tang, B.Z. (2015). Aggregation-induced emission: together we shine, united we soar! Chem. Rev. *115*, 11718–11940.

Miyaura, N., and Suzuki, A. (1995). Palladium-catalyzed cross-coupling reactions of organoboron compounds. Chem. Rev. *95*, 2457–2483.

Miyaura, N., Yamada, K., and Suzuki, A. (1979). New stereospecific cross-coupling by the palladium-catalyzed reaction of 1-alkenylboranes with 1-alkenyl or 1-alkynyl halides. Tetrahedron Lett. *20*, 3437–3440.

Monks, B.M., and Cook, S.P. (2012). Palladium-catalyzed alkyne insertion/Suzuki reaction of alkyl iodides. J. Am. Chem. Soc. *134*, 15297–15300.

Rahim, A., Feng, J., and Gu, Z. (2019). 1,4-Migration of transition metals in organic synthesis. Chin. J. Chem. *37*, 929–945.

Schempp, T.T., Daniels, B.E., Staben, S.T., and Stivala, C.E. (2017). A general strategy for the construction of functionalized azaindolines via domino palladium-catalyzed heck cyclization/Suzuki coupling. Org. Lett. *19*, 3616–3619.

Schneider, N., Lowe, D.M., Sayle, R.A., Tarselli, M.A., and Landrum, G.A. (2016). Big data from pharmaceutical patents: a computational analysis of medicinal chemists' bread and butter. J. Med. Chem. *59*, 4385–4402.

Shi, F., and Larock, R.C. (2010). Remote C-H activation via through-space palladium and rhodium migrations. Top. Curr. Chem. *292*, 123–164.

Shi, Z., Li, B., Wan, X., Cheng, J., Fang, Z., Cao, B., Qin, C., and Wang, Y. (2007). Suzuki-Miyaura coupling reaction by Pd-II-catalyzed aromatic C-H bond activation directed by an N-alkyl acetamino group. Angew. Chem. Int. Ed. *46*, 5554–5558.

Siamaki, A.R., Sakalauskas, M., and Arndtsen, B.A. (2011). A palladium-catalyzed multicomponent coupling approach to pi-conjugated oligomers: assembling imidazole-based materials from imines and acyl chlorides. Angew. Chem. Int. Ed. *50*, 6552–6556.

Šiaučiulis, M., Ahlsten, N., Pulis, A.P., and Procter, D.J. (2019). Transition-metal-free cross-coupling of benzothiophenes and styrenes in a stereoselective synthesis of substituted (E,Z)-1,3-Dienes. Angew. Chem. Int. Ed. *58*, 8779–8783.

Tobisu, M., and Chatani, N. (2009). Devising boron reagents for orthogonal functionalization through Suzuki-Miyaura cross-coupling. Angew. Chem. Int. Ed. *48*, 3565–3568.

Wakioka, M., Nakamura, Y., Montgomery, M., and Ozawa, F. (2014). Remarkable ligand effect of P(2-MeOC6H4)3 on palladium-catalyzed direct arylation. Organometallics *34*, 198–205.

Wang, J. (2012). Stereoselective Alkene Synthesis (Springer-Verlag).

Wang, D.-H., Wasa, M., Giri, R., and Yu, J.-Q. (2008). Pd(II)-catalyzed cross-coupling of sp(3) C-H bonds with sp(2) and sp(3) boronic acids using air as the oxidant. J. Am. Chem. Soc. *130*, 7190–7191.

Wang, C., Yu, Y., Yuan, Y., Ren, C., Liao, Q., Wang, J., Chai, Z., Li, Q., and Li, Z. (2020). Heartbeat-sensing mechanoluminescent device based on a quantitative relationship between pressure and emissive intensity. Matter *2*, 181–193.

Wen, W., Shi, Z.-F., Cao, X.-P., and Xu, N.-S. (2016). Triphenylethylene-based fluorophores: facile preparation and full-color emission in both solution and solid states. Dyes Pigm. *132*, 282–290.

Wencel-Delord, J., Nimphius, C., Patureau, F.W., and Glorius, F. (2012). Undirected arene and chelate-assisted olefin C-H bond activation: RhIIICp* -catalyzed dehydrogenative alkene-arene coupling as a new pathway for the selective synthesis of highly substituted Z olefins. Chem. Asian J. *7*, 1208–1212.

Xie, Y., and Li, Z. (2019). Recent advances in the Z/E isomers of tetraphenylethene derivatives: stereoselective synthesis, AIE mechanism, photophysical properties, and application as chemical probes. Chem. Asian J. *14*, 2524–2541.

Yang, S.-D., Sun, C.-L., Fang, Z., Li, B.-H., Li, Y.-Z., and Shi, Z.-J. (2008). Palladium-catalyzed direct arylation of (hetero)arenes with aryl boronic acids. Angew. Chem. Int. Ed. *47*, 1473–1476.

Yang, Y., Xu, H., Liu, F., Wang, H., Deng, G., Si, P., Huang, H., Bo, S., Liu, J., Qiu, L., et al. (2014). Synthesis and optical nonlinear property of Y-type chromophores based on double-donor structures with excellent electro-optic activity. J. Mater. Chem. C *2*, 5124–5132.

Yoshii, D., Jin, X.J., Mizuno, N., and Yamaguchi, K. (2019). Selective dehydrogenative mono- or diborylation of styrenes by supported copper catalysts. ACS Catal. *9*, 3011–3016.

Yu, T., Ou, D., Wang, L., Zheng, S., Yang, Z., Zhang, Y., Chi, Z., Liu, S., Xu, J., and Aldred, M.P. (2017). A new approach to switchable photochromic materials by combining photochromism and piezochromism together in an AIE-active molecule. Mater. Chem. Front. *1*, 1900–1904.

Zhang, J., Shrestha, R., Hartwig, J.F., and Zhao, P. (2016a). A decarboxylative approach for regioselective hydroarylation of alkynes. Nat. Chem. *8*, 1144–1151.

Zhang, Y., Mao, H., Kong, L., Tian, Y., Tian, Z., Zeng, X., Zhi, J., Shi, J., Tong, B., and Dong, Y. (2016b). Effect of E/Z isomerization on the aggregation-induced emission features and mechanochromic performance of dialdehyde-substituted hexaphenyl-1,3-butadiene. Dyes Pigm. *133*, 354–362.

Zhang, Z.-M., Xu, B., Wu, L., Wu, Y., Qian, Y., Zhou, L., Liu, Y., and Zhang, J. (2019). Enantioselective dicarbofunctionalization of unactivated alkenes by palladium-catalyzed tandem heck/Suzuki coupling reaction. Angew. Chem. Int. Ed. *58*, 14653–14659.

iScience, Volume *23*

Supplemental Information

Suzuki-Miyaura Coupling Enabled by Aryl to Vinyl 1,4-Palladium Migration

Meng-Yao Li, Pengbo Han, Tian-Jiao Hu, Dong Wei, Ge Zhang, Anjun Qin, Chen-Guo Feng, Ben Zhong Tang, and Guo-Qiang Lin

More reaction condition optimization details:

Table S1. The effect of ligand, related to **Scheme 1**.

Entry[a]	Ligand	Yield of **3aa** (%)[b]	Ratio of **3aa/4aa**[c]	Entry[a]	Ligand	Yield of **3aa** (%)[b]	Ratio of **3aa/4aa**[c]
1	**L1**	45	60:40	10	**L7**	39	90:10
2	**L2**	35	60:40	11	**L8**	40	50:50
3	**L3**	25	50:50	12	**L9**	36	50:50
4	**L4**	65	93:7	13	**L10**	29	50:50
5	**L5**	27	96:4	14	**L11**	79	75:25
6	**L6**	75	84:16	15	**L12**	54	83:17

[a] Reactions conditions: **1a** (1.0 equiv, 0.2 mmol), phenylboron **2a$_6$** (3.0 equiv, 0.6 mmol) $Pd(OAc)_2$ (5 mol %), **L1-L7** (10 mol %) or **L8-L12** (5 mol %), and CsOAc (2.0 equiv, 0.4 mmol in THF (2.0 mL) at 110 °C for 3 h. [b, c] Determined by GC analysis using dodecane as an internal standard.

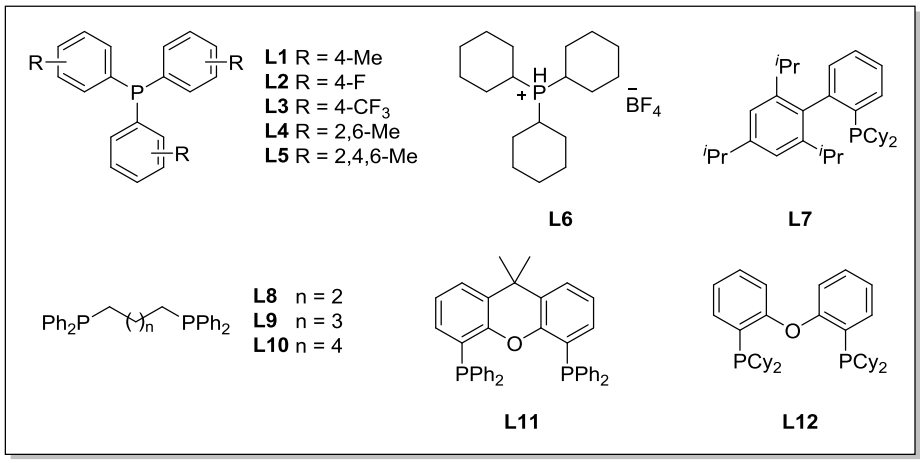

Table S2. The effect of solvent, related to **Scheme 1**.

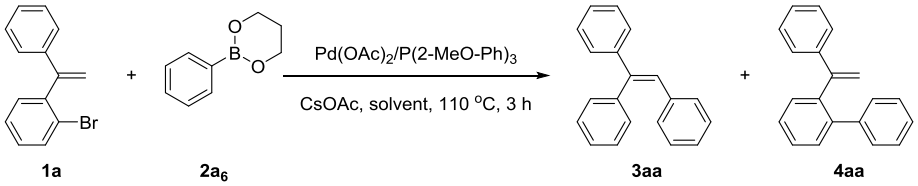

1a **2a$_6$** **3aa** **4aa**

Entry[a]	Solvent	Yield of **3aa** (%)[b]	Ratio of **3aa/4aa**[c]	Entry[a]	Solvent	Yield of **3aa** (%)[b]	Ratio of **3aa/4aa**[c]
1	THF	79	93:7	8	DMF	46	92:8
2	2-Me-THF	40	89:11	9	CH_3CN	66	86:14
3	Dioxane	45	90:10	10	DCE	21	75:25
4	DME	14	66:34	11	EA	66	90:10
5	TBME	51	50:50	12	Toluene	14	80:20
6	PhOMe	47	50:50	13	Hexane	45	80:20
7	Et_2O	67	80:20	14	EtOH	31	83:17

[a] Reactions conditions: **1a** (1.0 equiv, 0.2 mmol), phenylboron **2a$_6$** (3.0 equiv, 0.6 mmol), $Pd(OAc)_2$ (5 mol %), P(2-MeO-$C_6H_5)_3$ (10 mol %) and CsOAc (2.0 equiv, 0.4 mmol) in solvent (2.0 mL) at 110 °C for 3 h unless otherwise noted. [b, c] Determined by GC analysis using dodecane as an internal standard.

Table S3. The effect of base, related to **Scheme 1**.

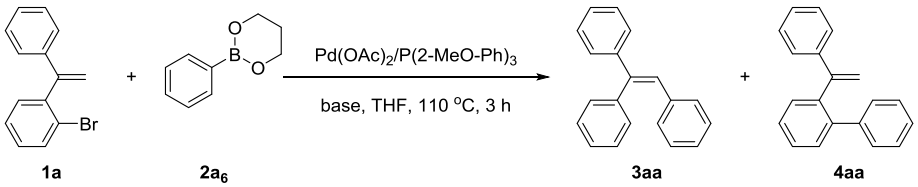

1a **2a$_6$** **3aa** **4aa**

Entry[a]	Base	Yield of **3aa** (%)[b]	Ratio of **3aa/4aa**[c]	Entry[a]	Base	Yield of **3aa** (%)[b]	Ratio of **3aa/4aa**[c]
1	LiOAc	3	nd	10	KF	38	66:34
2	NH_4OAc	3	nd	11	Na_2CO_3	20	66:34
3	KOAc	41	89:11	12	K_2CO_3	30	50:50
4	CsOAc	79	93:7	13	$BaCO_3$	Trace	nd
5	AgOAc	Trace	nd	14	$NaHCO_3$	3	nd
6	Cs_2CO_3	Trace	nd	15	KOH	Trace	nd
7	CsF	32	50:50	16	KO^{t}Bu	Trace	nd
8	CsOPiv	94	95:5	17	K_3PO_4	6	14:86
9	CF_3COOCs	Trace	nd	18	LiOH	14	17:83

[a] Reactions conditions: **1a** (1.0 equiv, 0.2 mmol), phenylboron **2a$_6$** (3.0 equiv, 0.6 mmol), $Pd(OAc)_2$ (5 mol %), P(2-MeO-$C_6H_5)_3$ (10 mol %) and base (2.0 equiv, 0.4 mmol) in THF (2.0 mL) at 110 °C for 3 h unless otherwise noted. [b, c] Determined by GC analysis using dodecane as an internal standard.

Supplemental Figures for NMR spectrums:

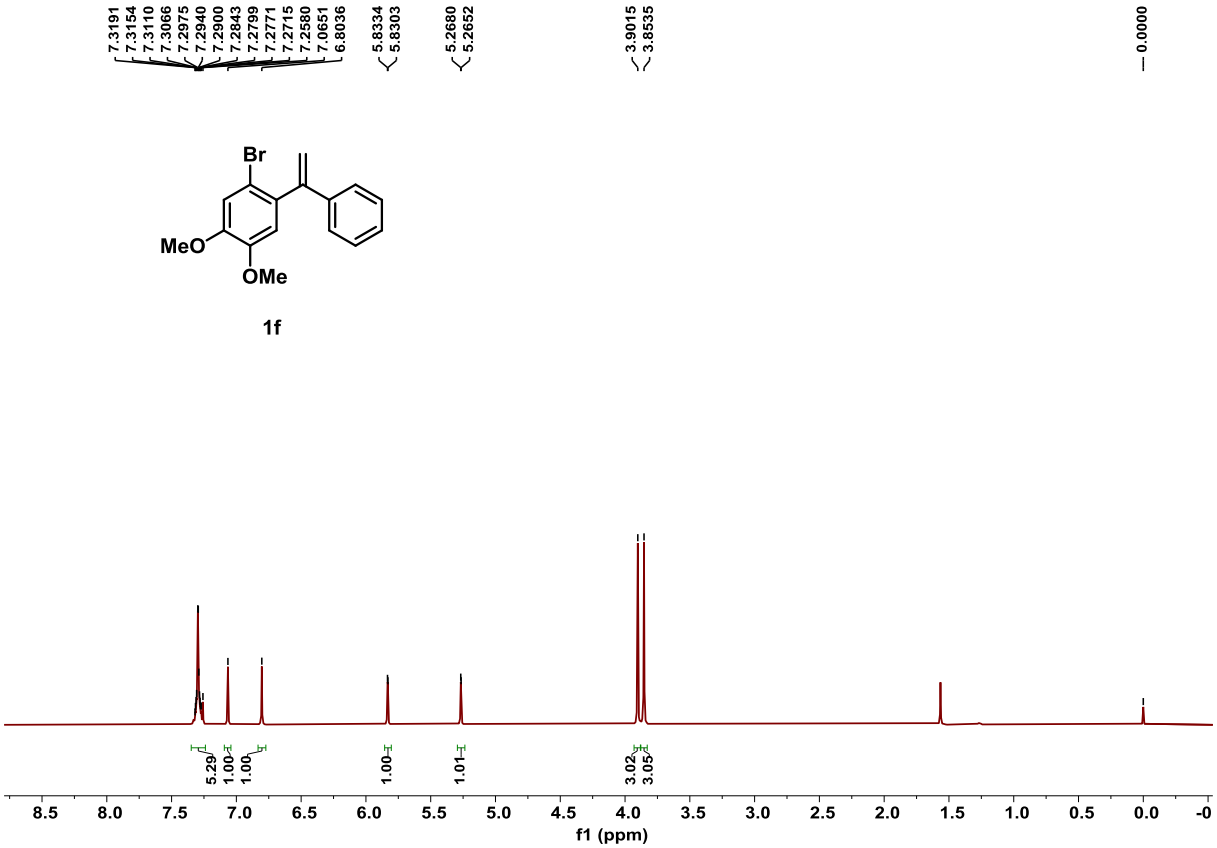

Figure S1. ^{1}H NMR spectrum of substrate **1f**, related to **Scheme 2**.

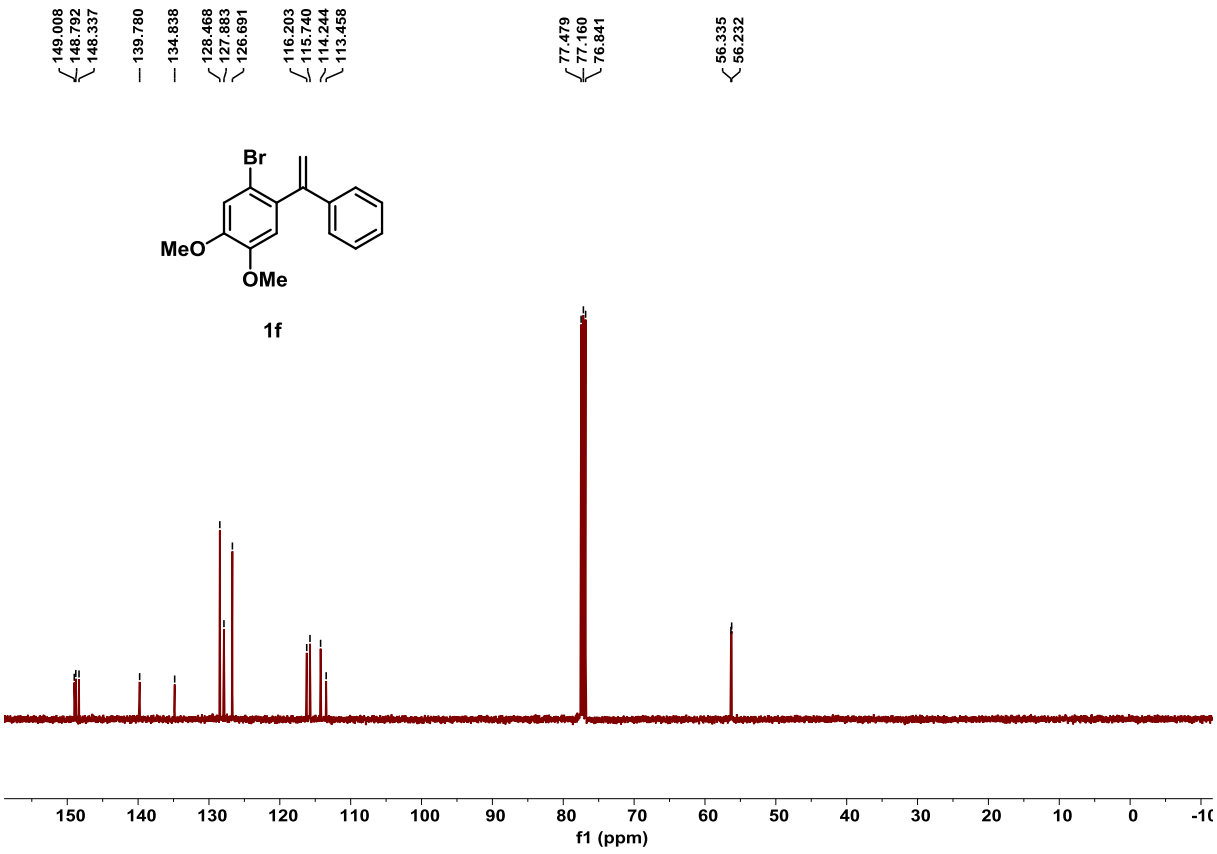

Figure S2. ^{13}C NMR spectrum of substrate **1f**, related to **Scheme 2**.

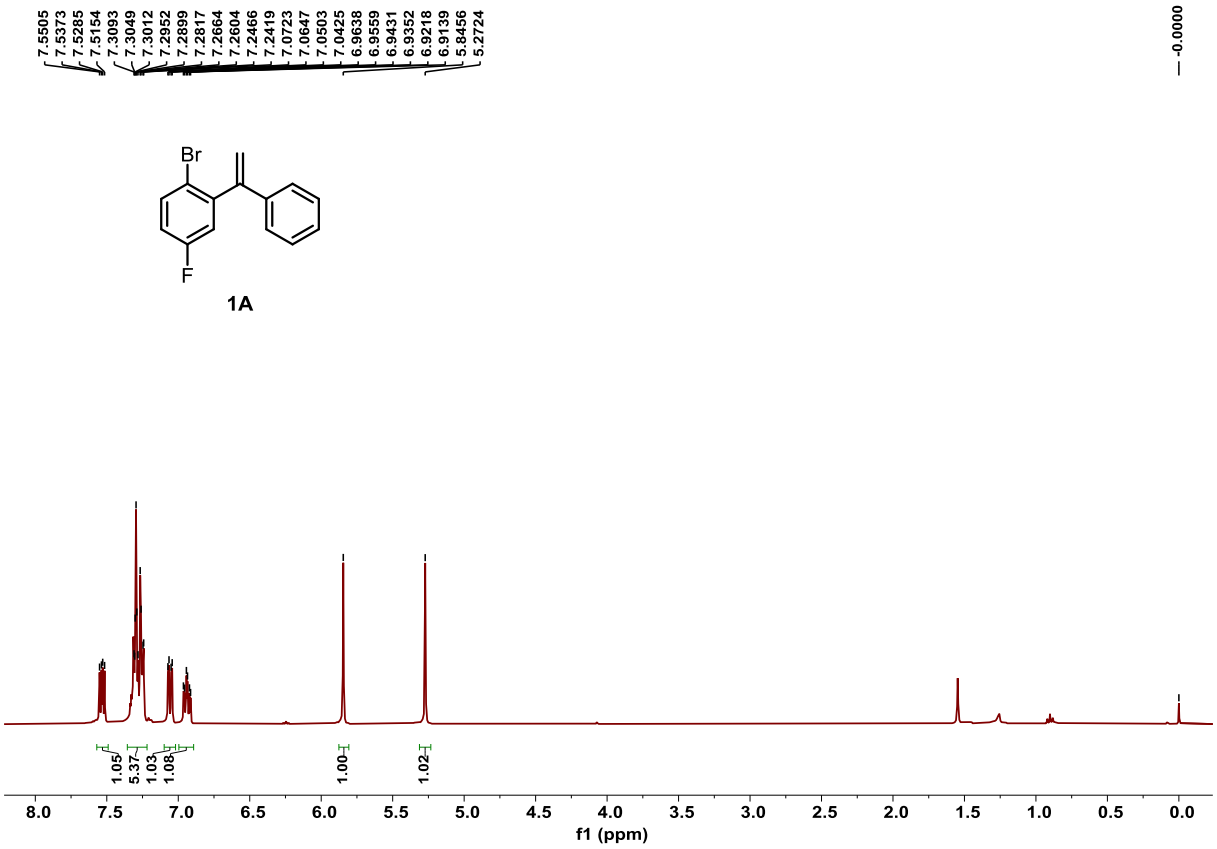

Figure S3. ^{1}H NMR spectrum of substrate **1A**, related to **Scheme 2**.

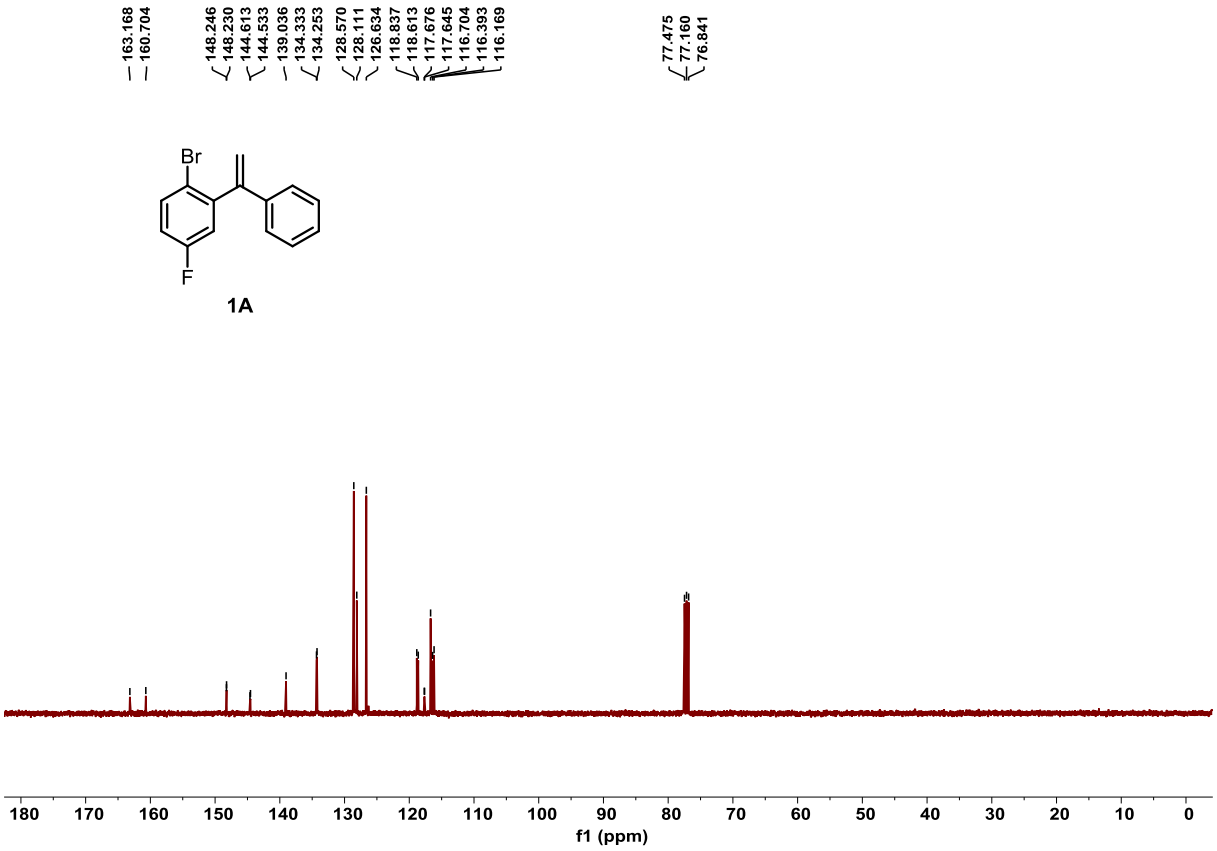

Figure S4. ^{13}C NMR spectrum of substrate **1A**, related to **Scheme 2**.

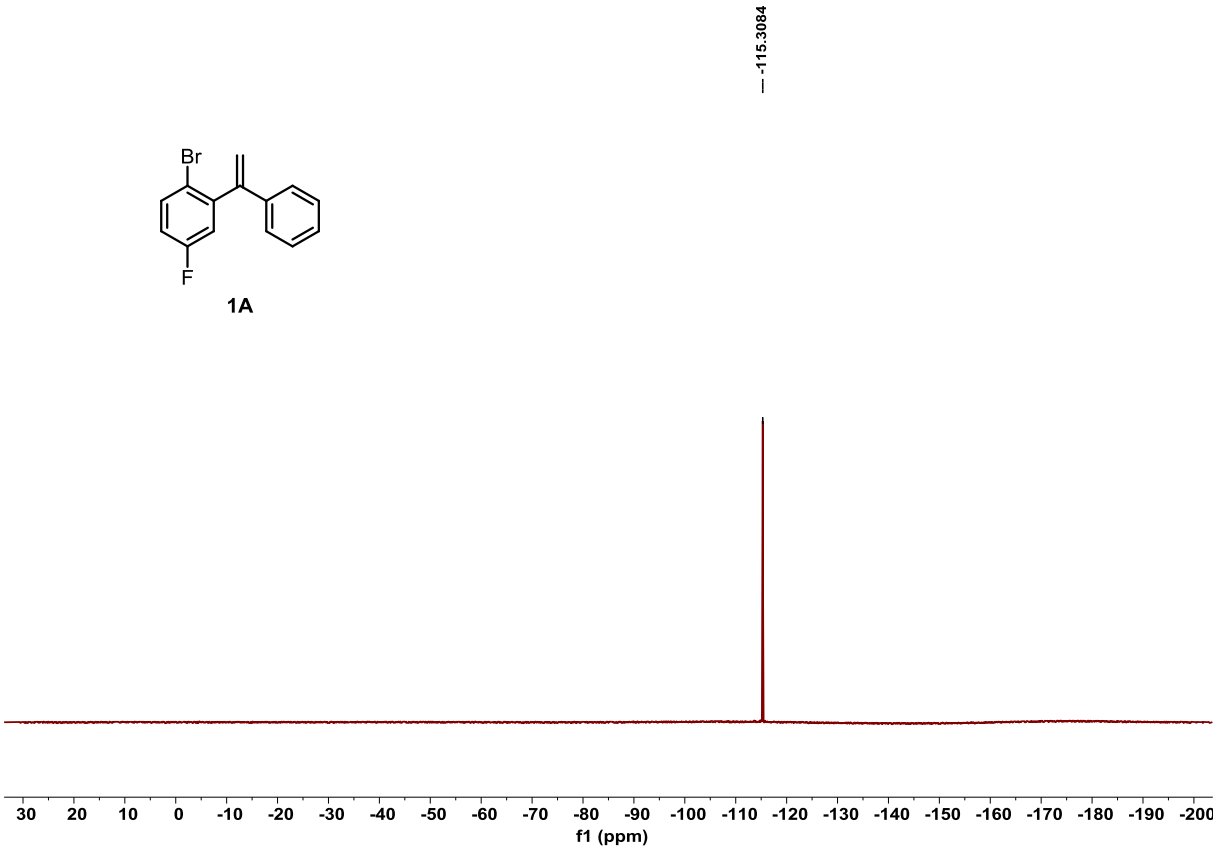

Figure S5. ^{19}F NMR spectrum of substrate **1A**, related to **Scheme 2**.

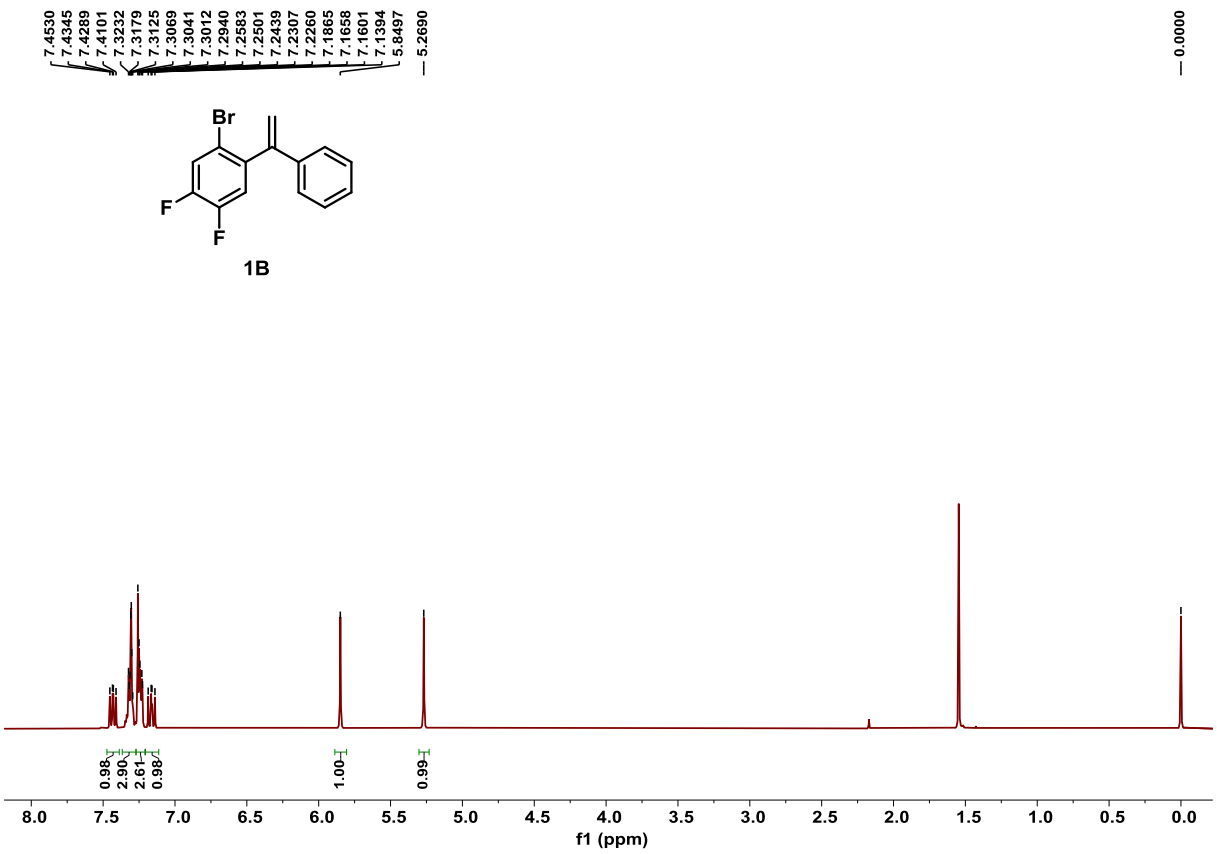

Figure S6. ^{1}H NMR spectrum of substrate **1B**, related to **Scheme 2**.

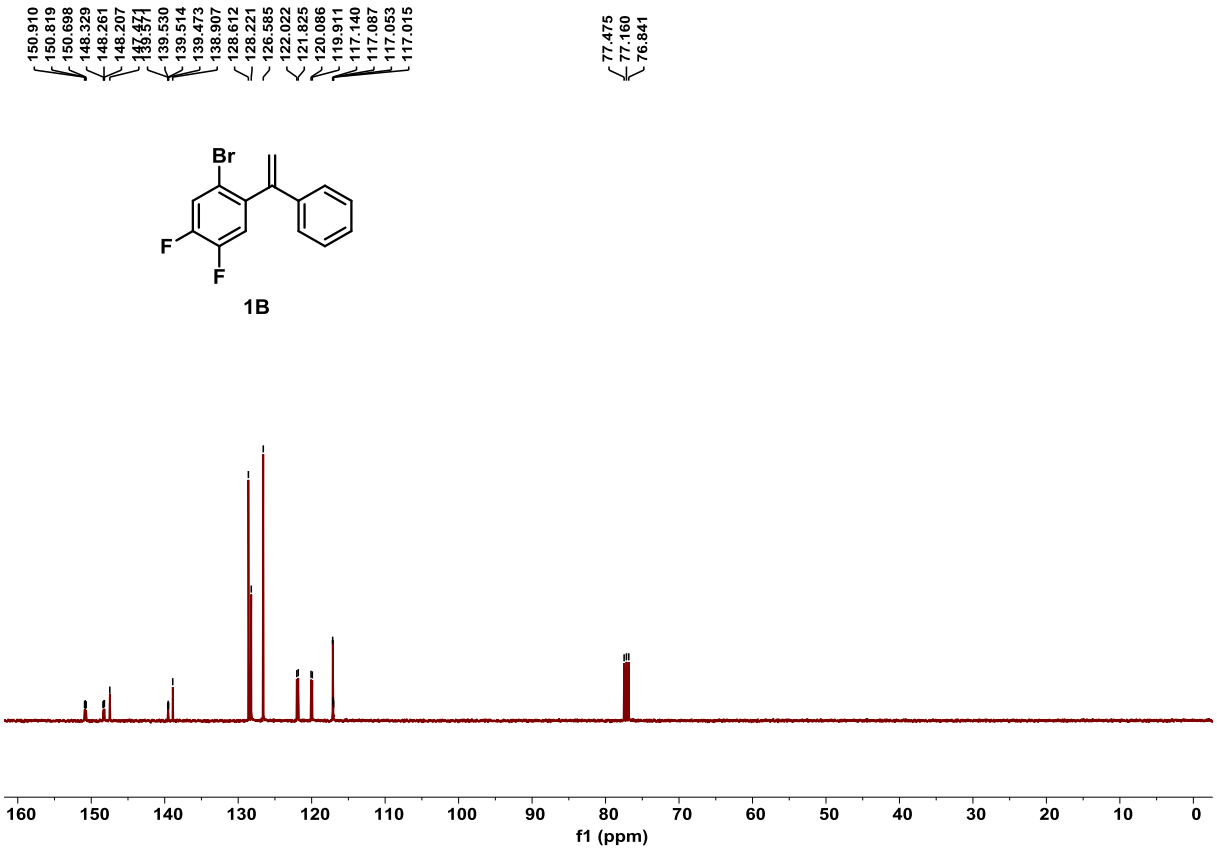

Figure S7. ^{13}C NMR spectrum of substrate **1B**, related to **Scheme 2**.

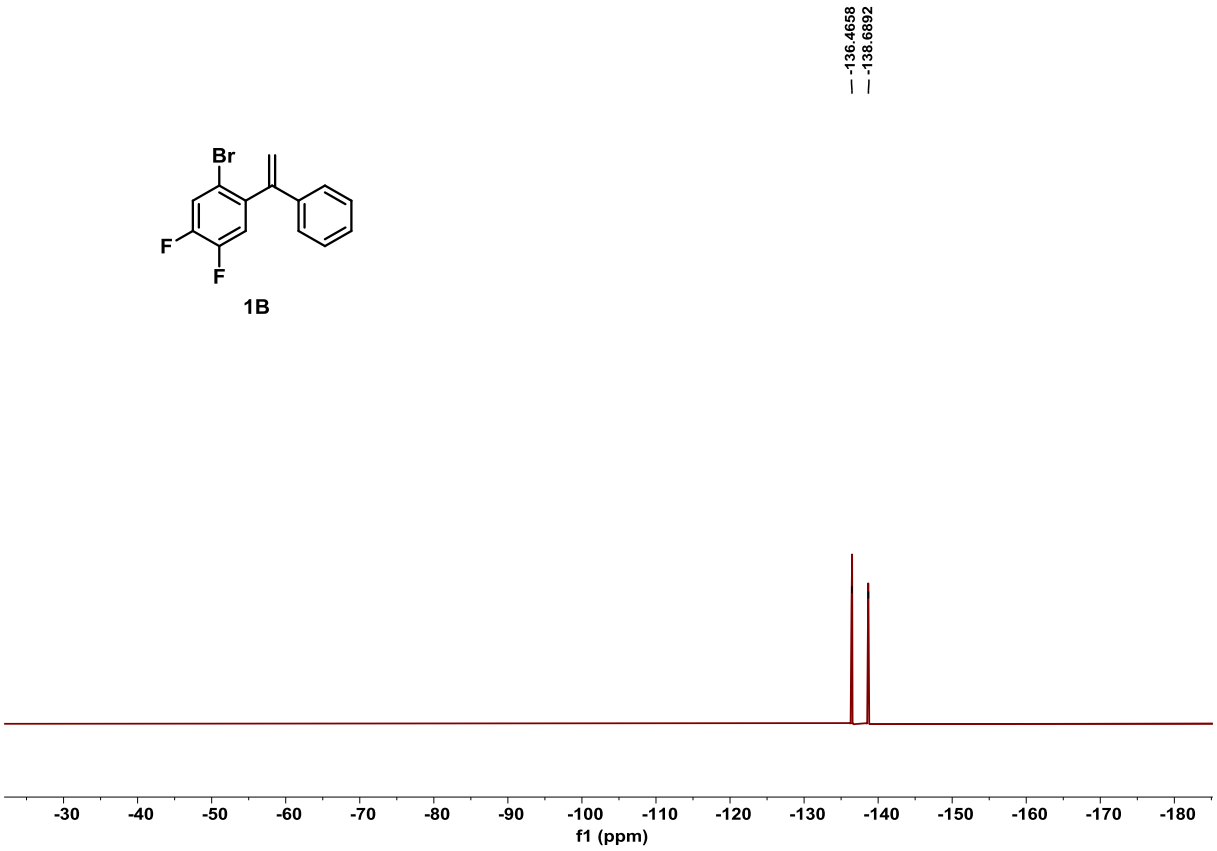

Figure S8. ^{19}F NMR spectrum of substrate **1B**, related to **Scheme 2**.

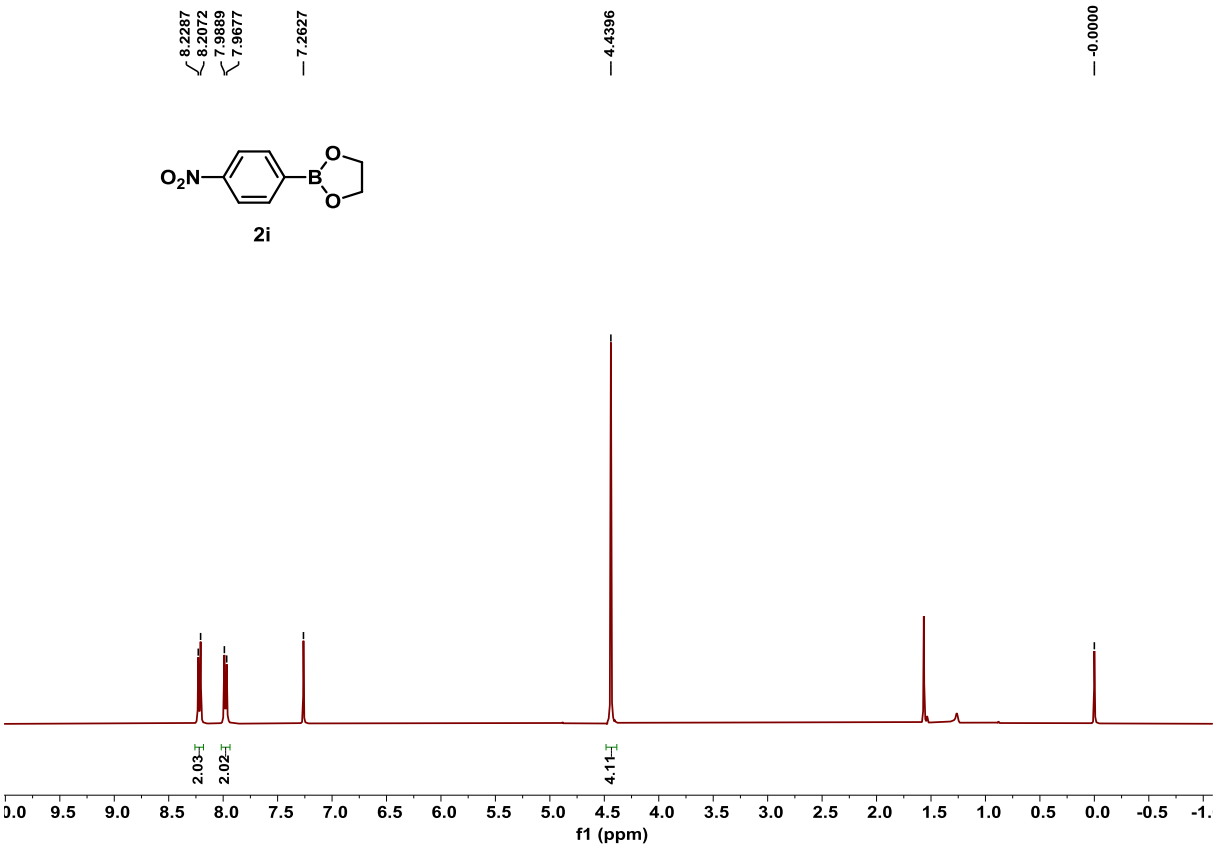

Figure S9. ^{1}H NMR spectrum of substrate **2i**, related to **Scheme 2**.

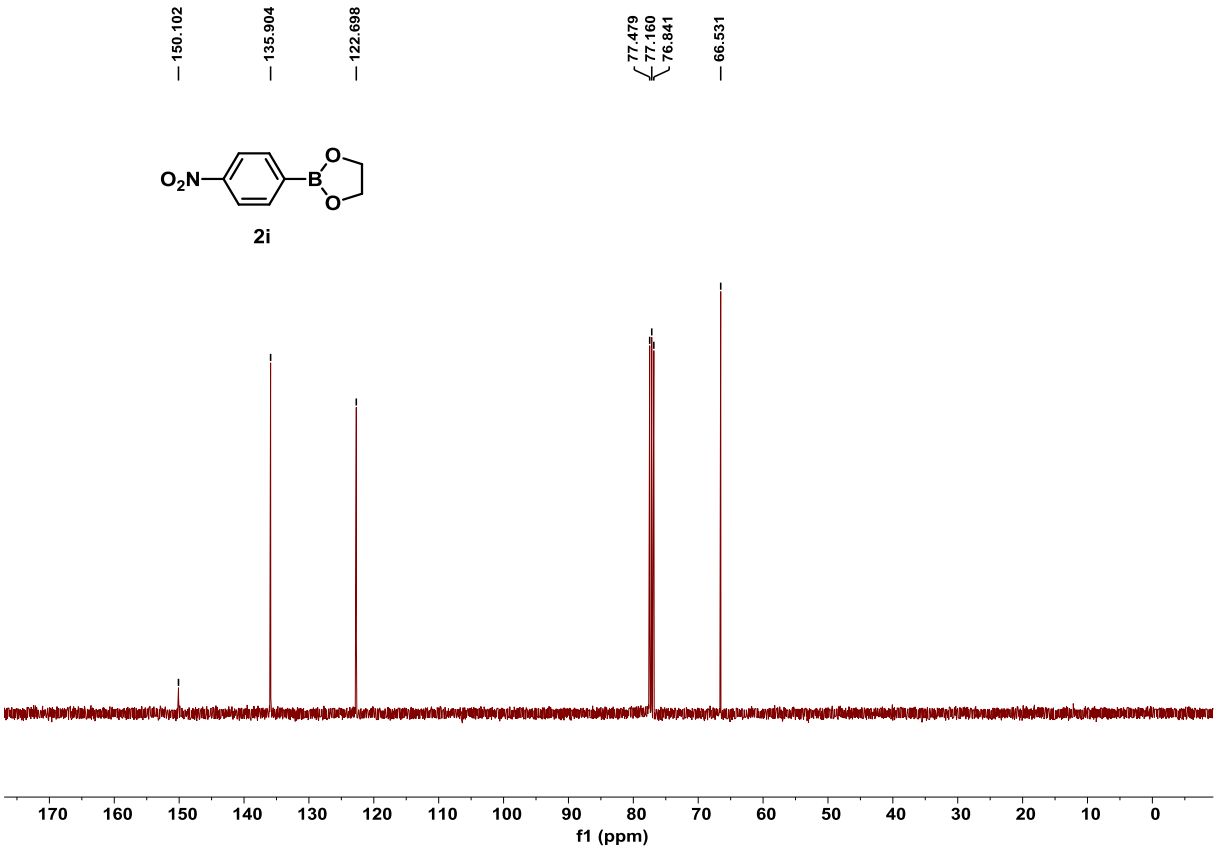

Figure S10. ^{13}C NMR spectrum of substrate **2i**, related to **Scheme 2**.

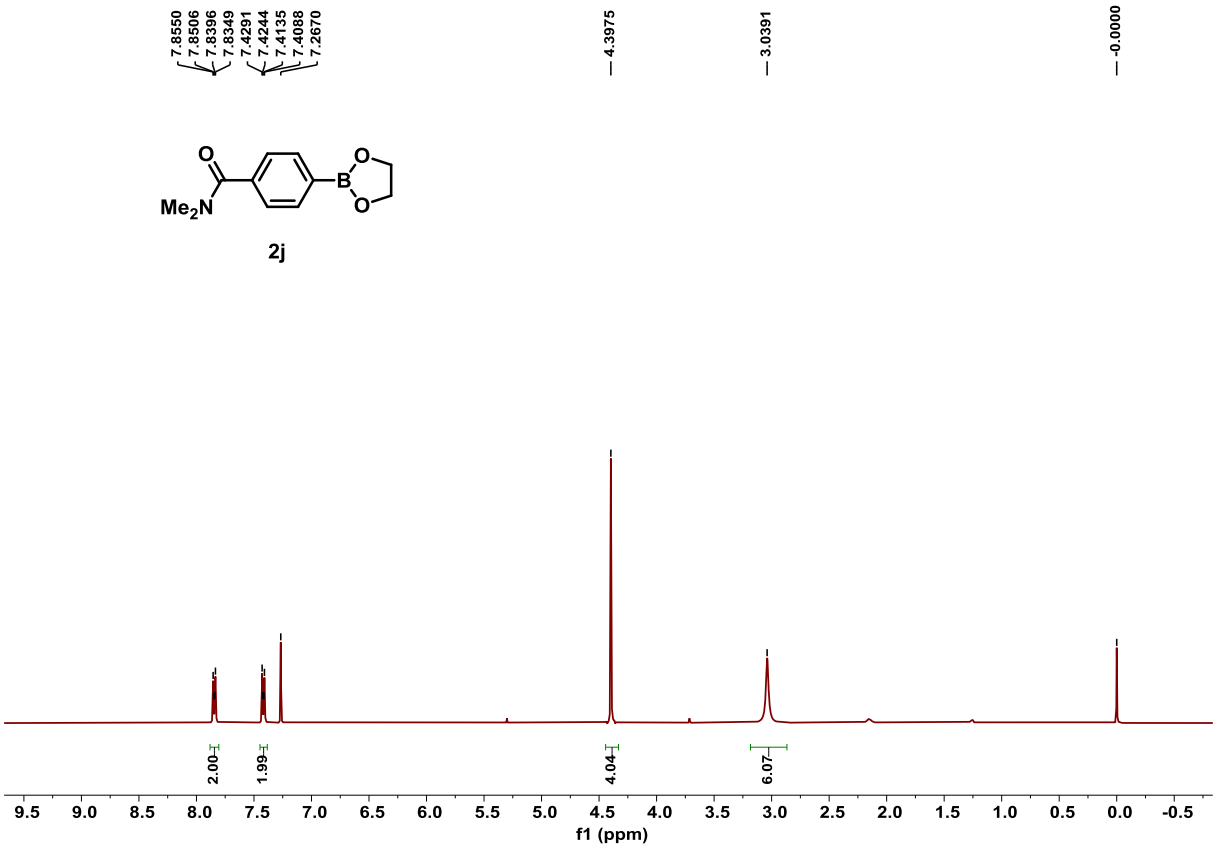

Figure S11. ^{1}**H NMR** spectrum of substrate **2j**, related to **Scheme 2**.

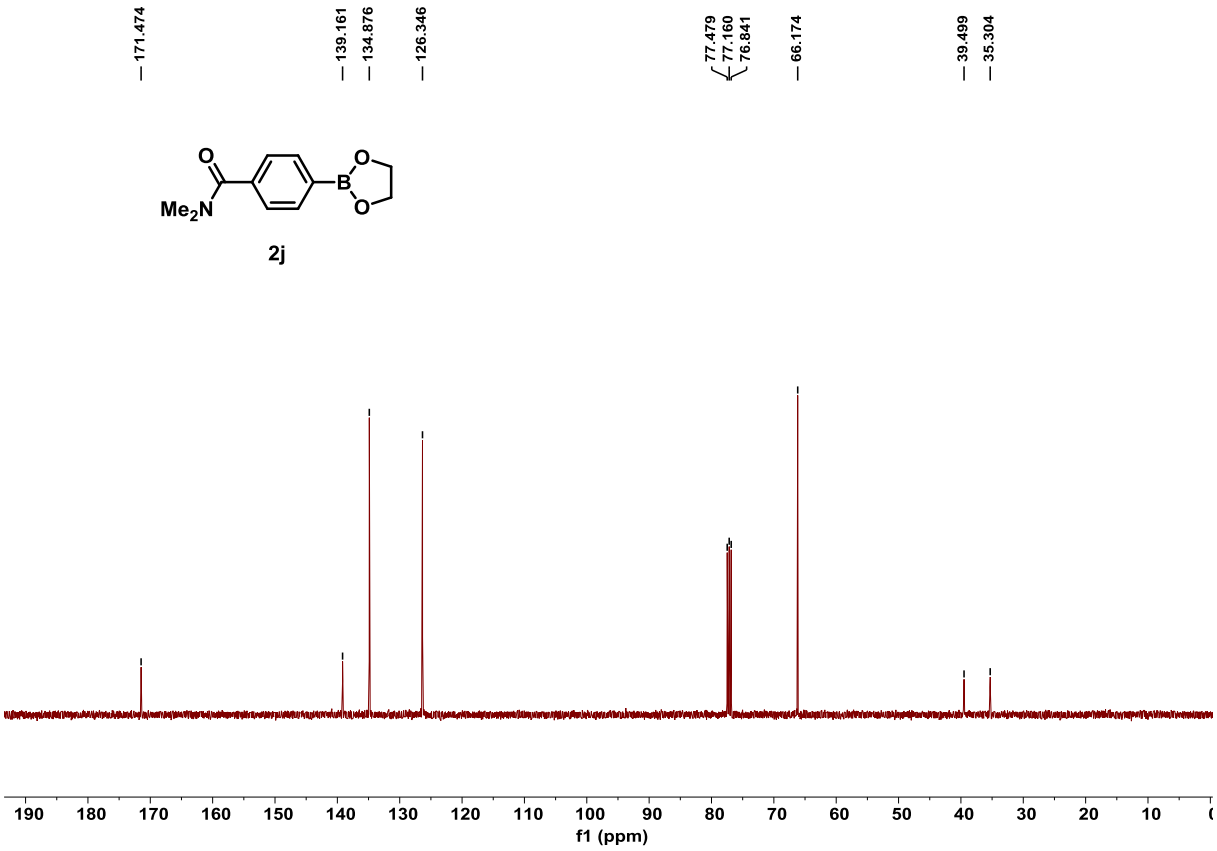

Figure S12. ^{13}**C NMR** spectrum of substrate **2j**, related to **Scheme 2**.

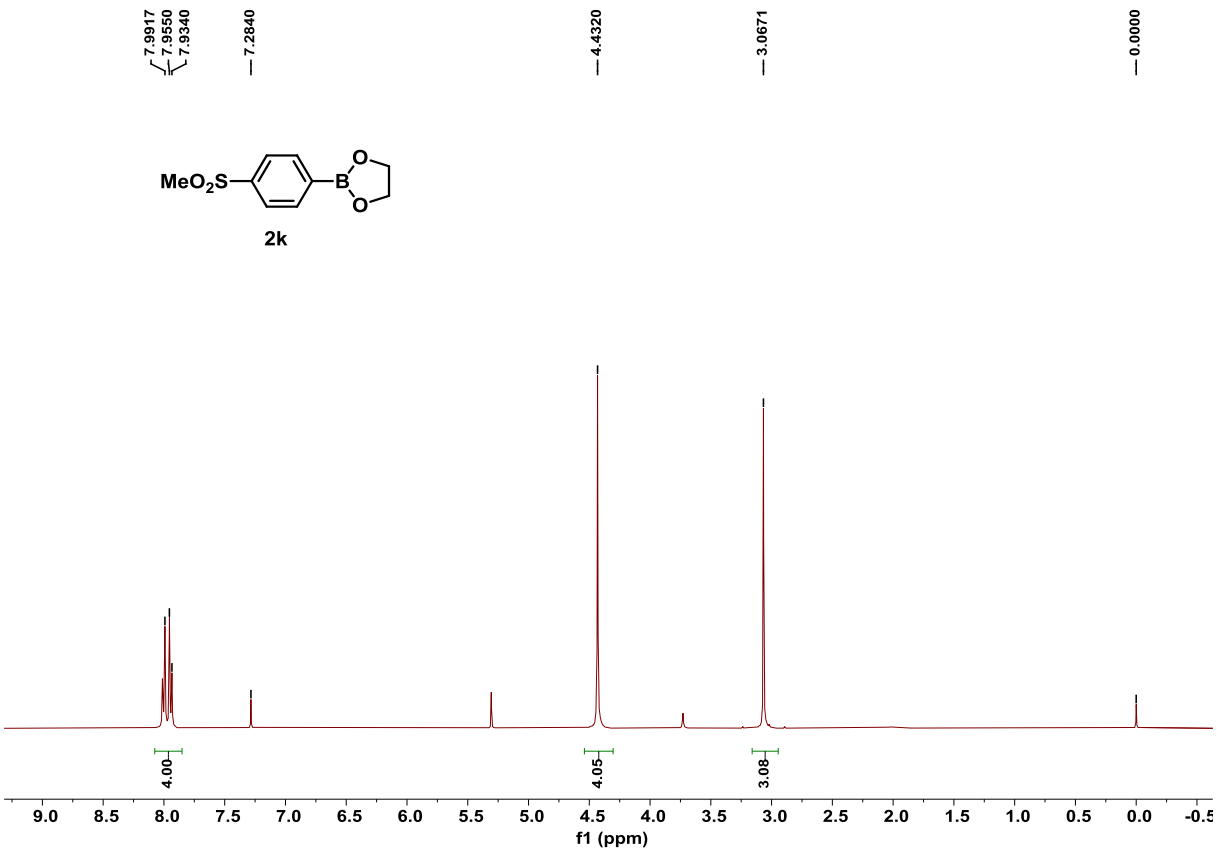

Figure S13. ^{1}H NMR spectrum of substrate **2k**, related to **Scheme 2**.

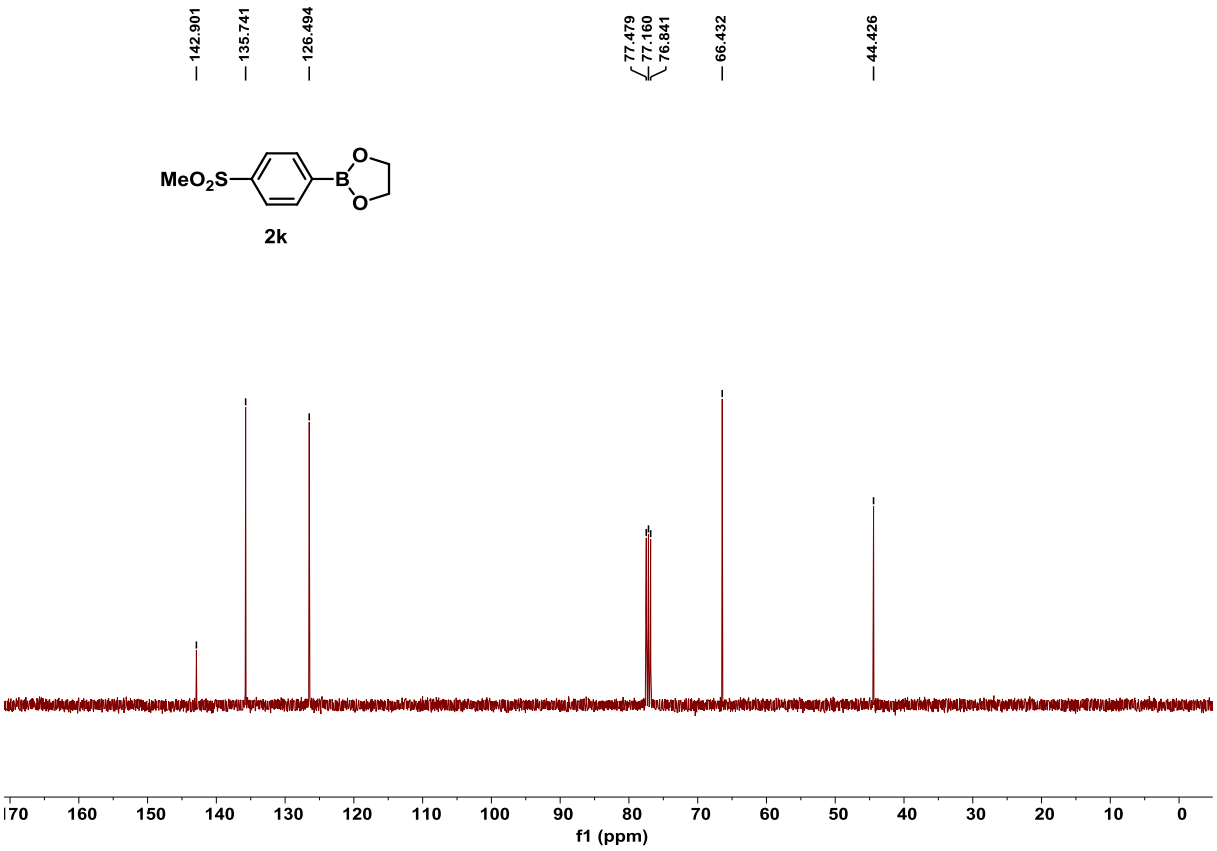

Figure S14. ^{13}C NMR spectrum of substrate **2k**, related to **Scheme 2**.

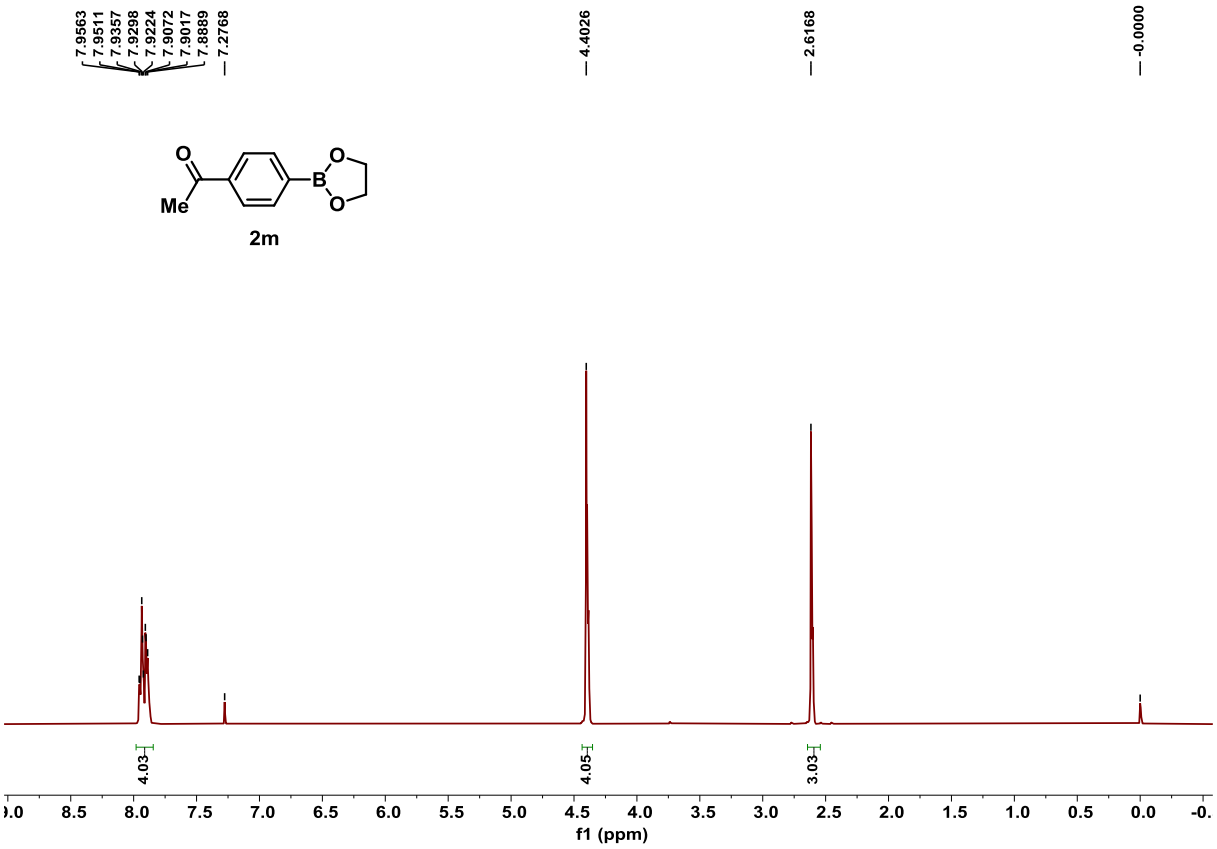

Figure S15. ^{1}H NMR spectrum of substrate **2m**, related to **Scheme 2**.

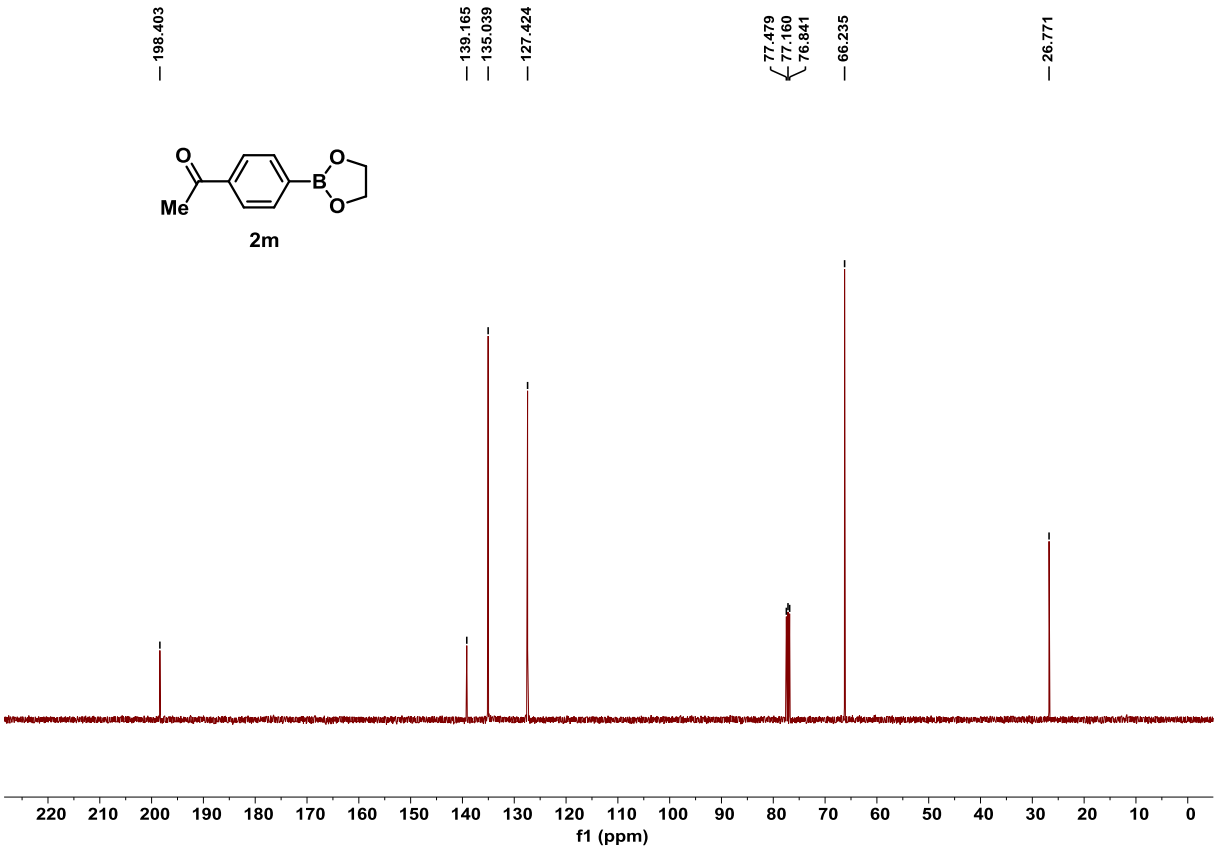

Figure S16. ^{13}C NMR spectrum of substrate **2m**, related to **Scheme 2**.

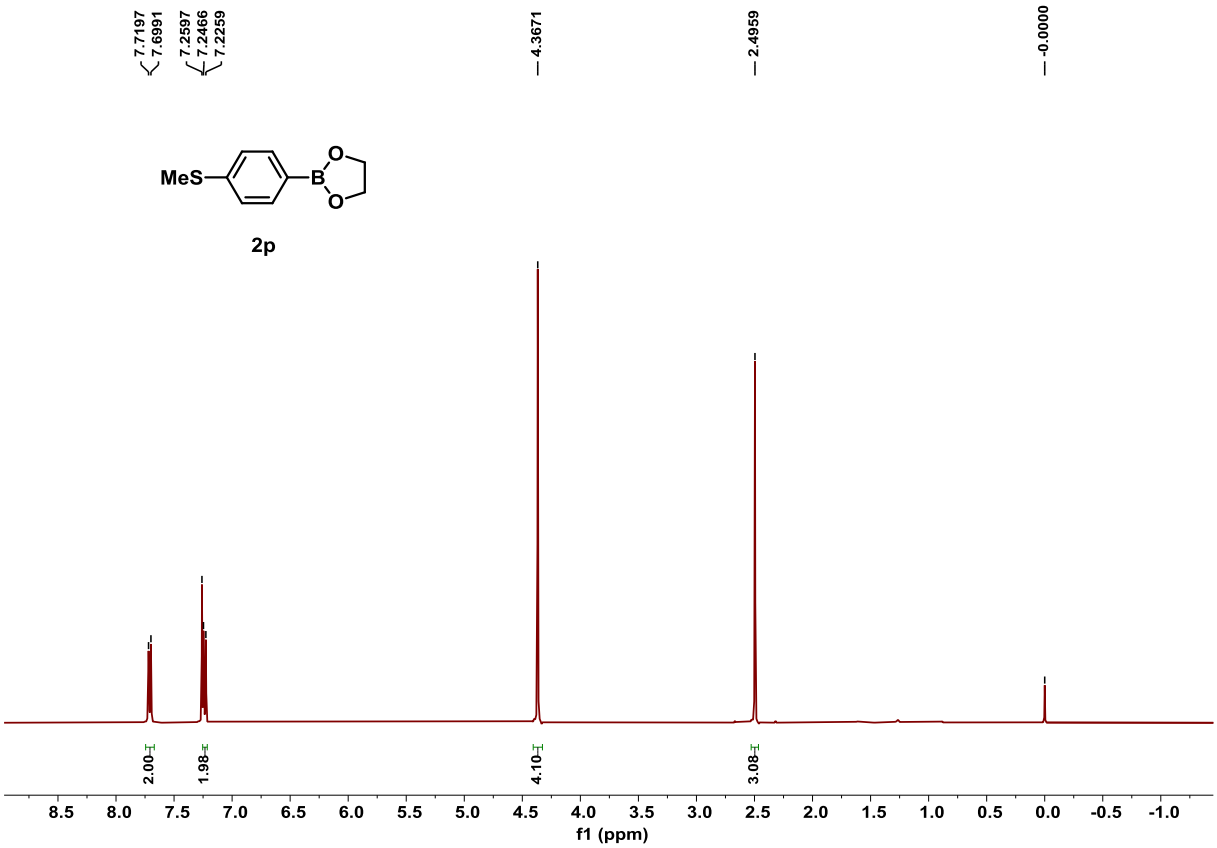

Figure S17. ^{1}H NMR spectrum of substrate **2p**, related to **Scheme 2**.

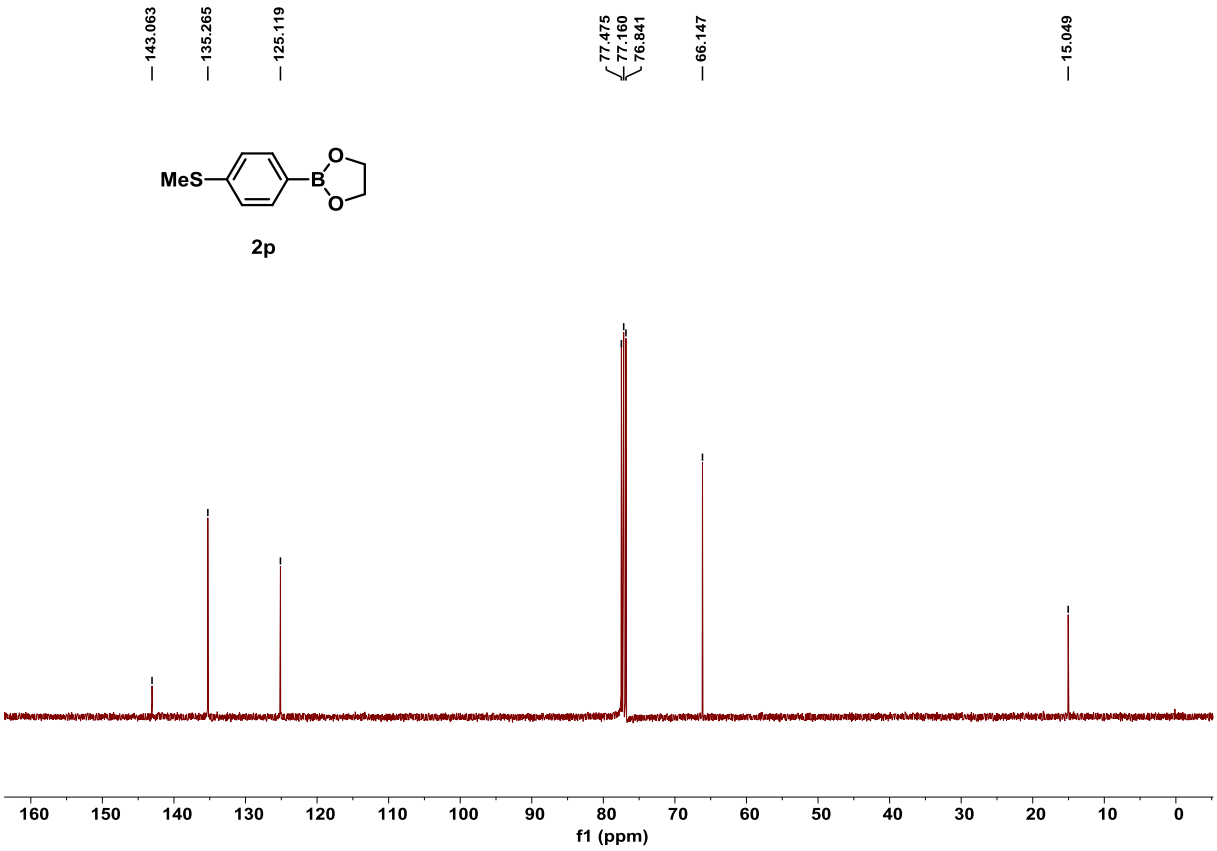

Figure S18. ^{13}C NMR spectrum of substrate **2p**, related to **Scheme 2**.

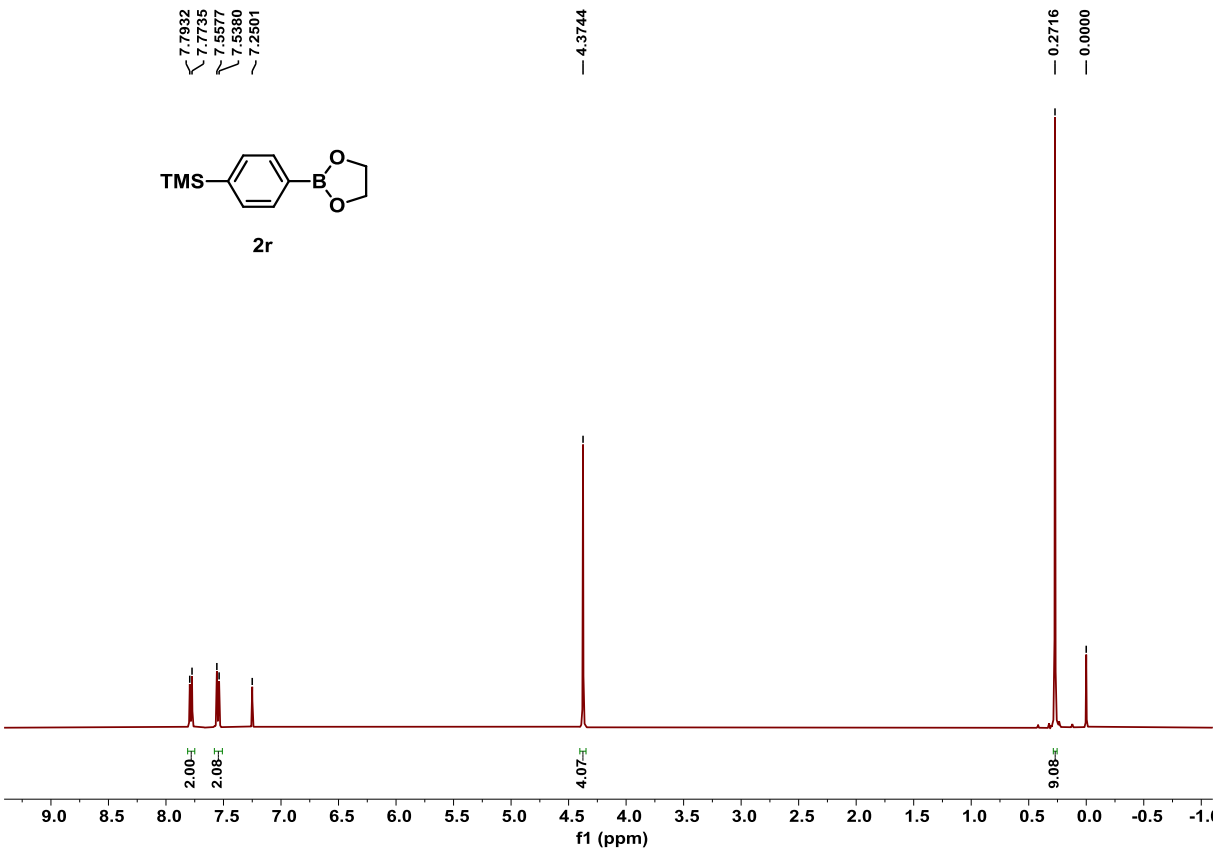

Figure S19. ^{1}H NMR spectrum of substrate **2r**, related to **Scheme 2**.

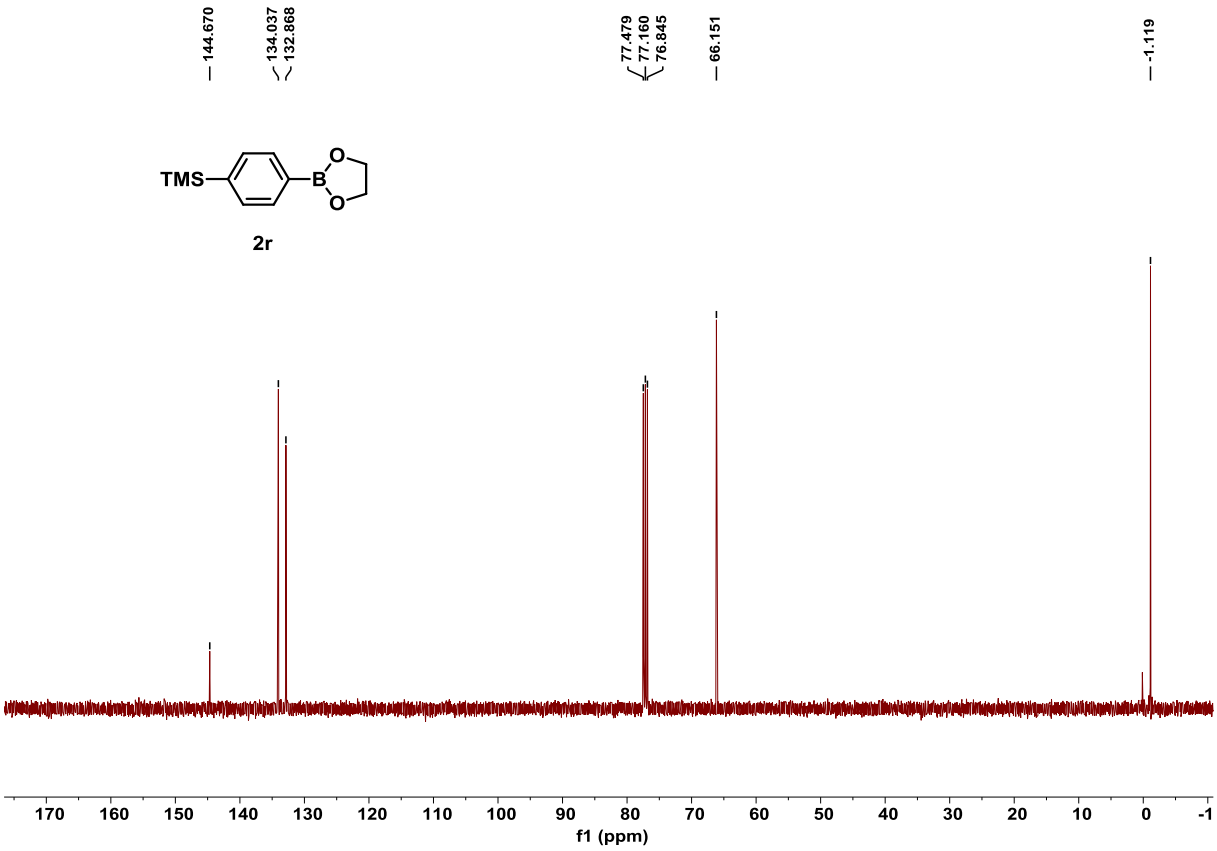

Figure S20. ^{13}C NMR spectrum of substrate **2r**, related to **Scheme 2**.

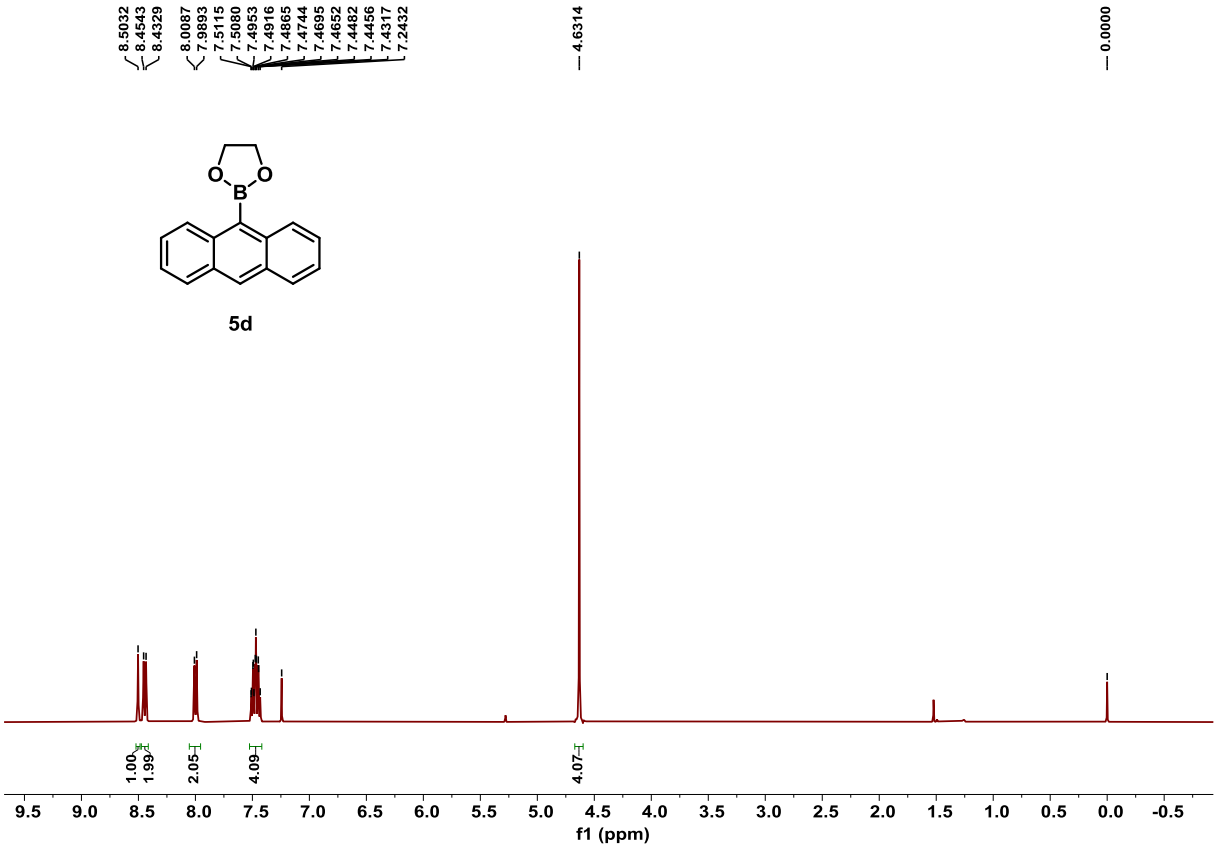

Figure S21. ^{1}H NMR spectrum of substrate **5d**, related to **Scheme 2**.

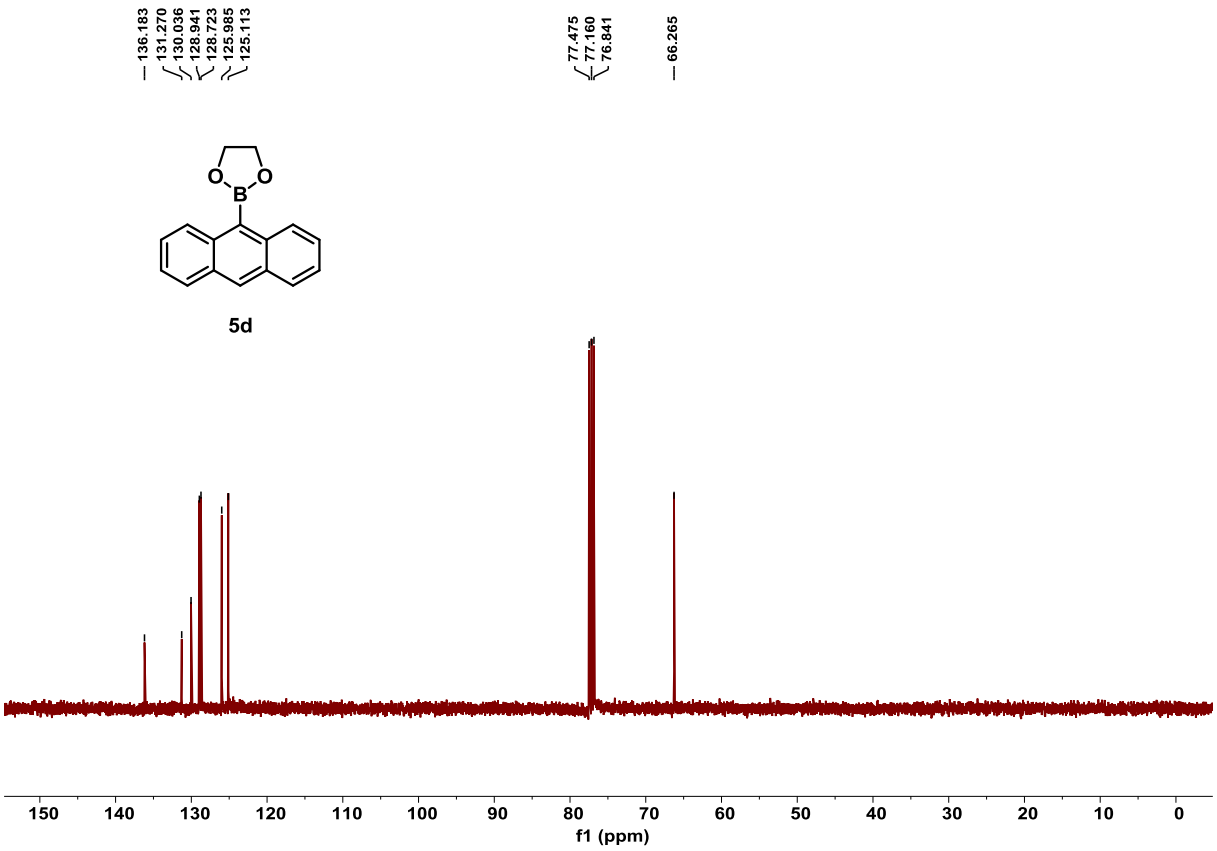

Figure S22. ^{13}C NMR spectrum of substrate **5d**, related to **Scheme 2**.

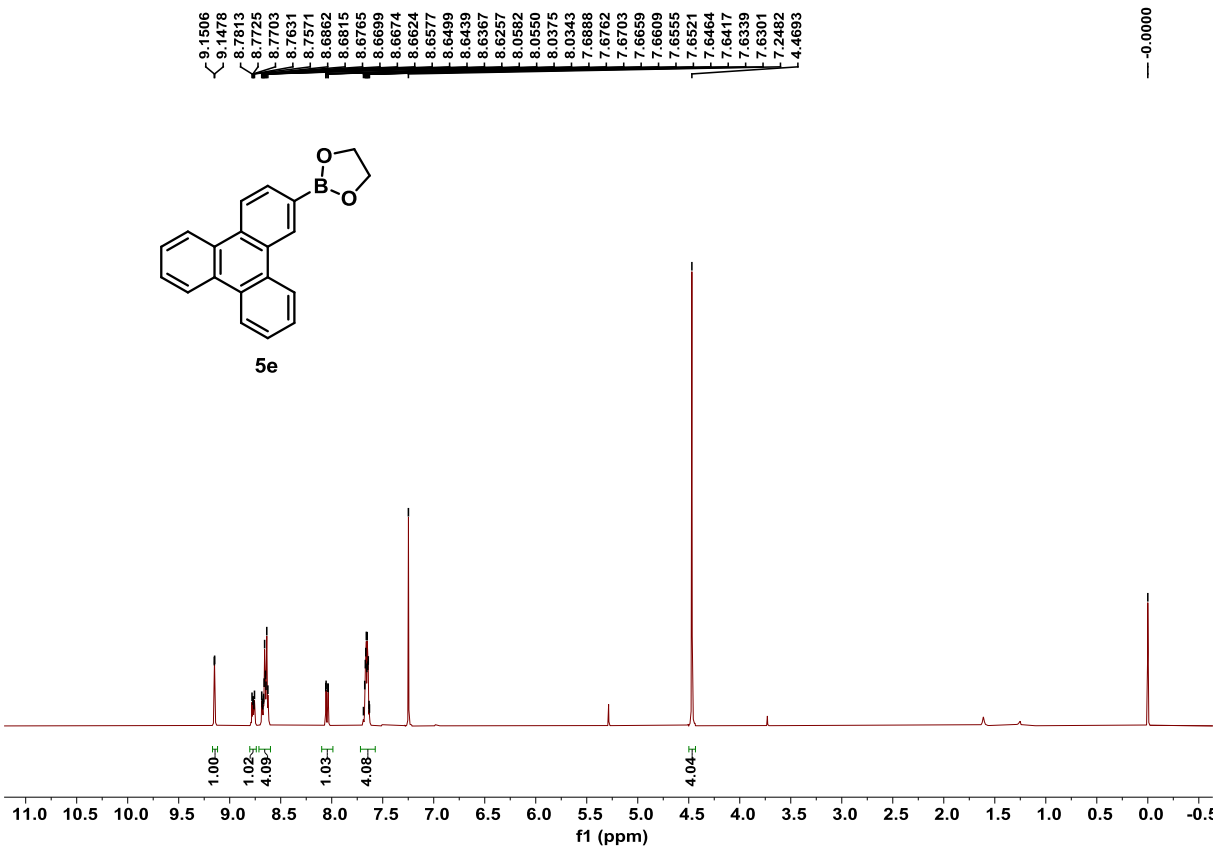

Figure S23. ^{1}H NMR spectrum of substrate **5e**, related to **Scheme 2**.

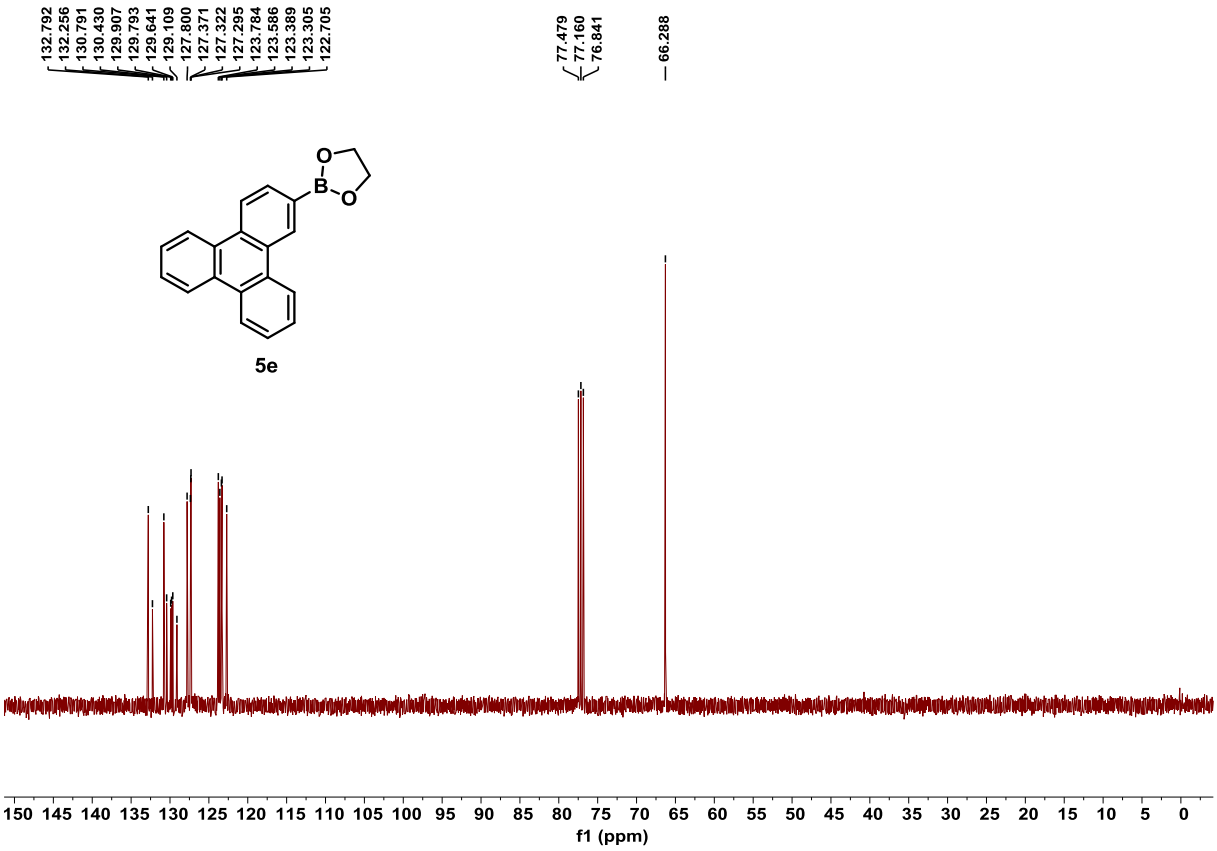

Figure S24. ^{13}C NMR spectrum of substrate **5e**, related to **Scheme 2**.

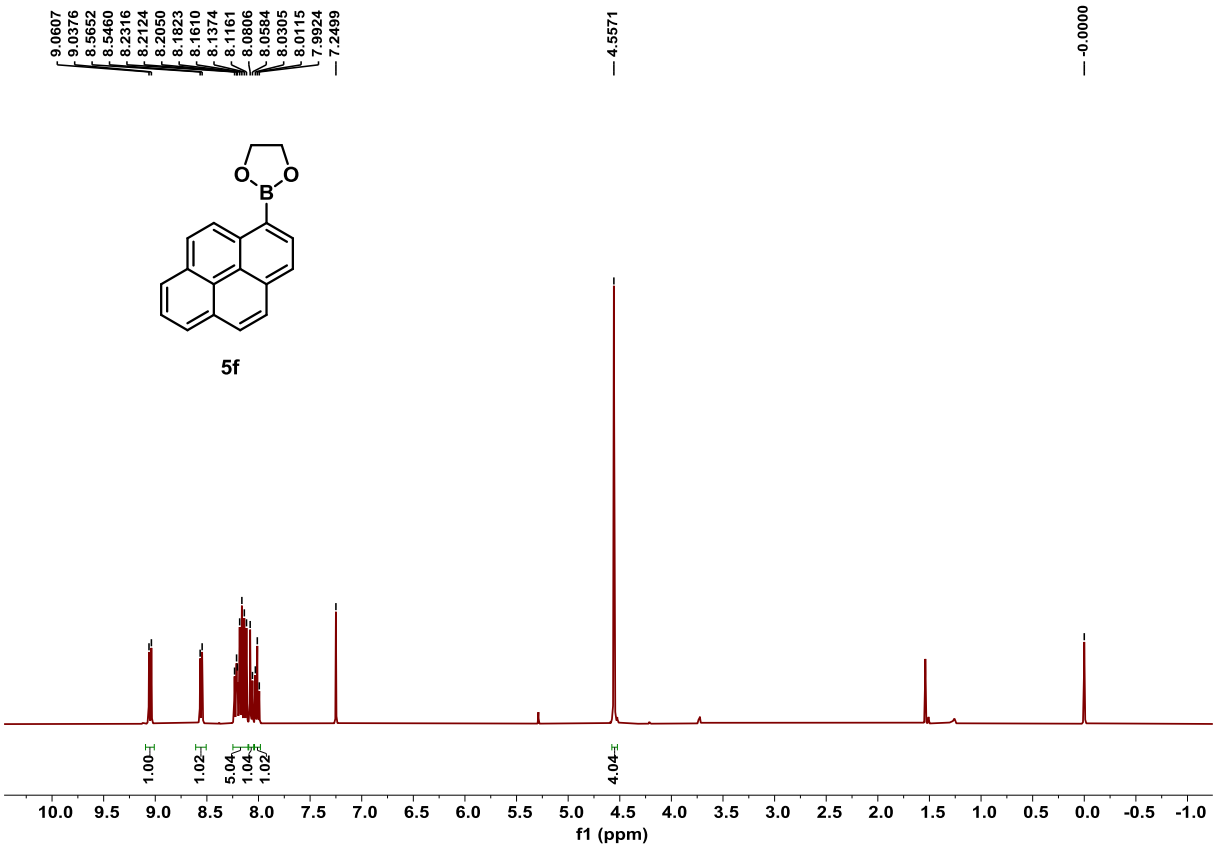

Figure S25. ^{1}H NMR spectrum of substrate **5f**, related to **Scheme 2**.

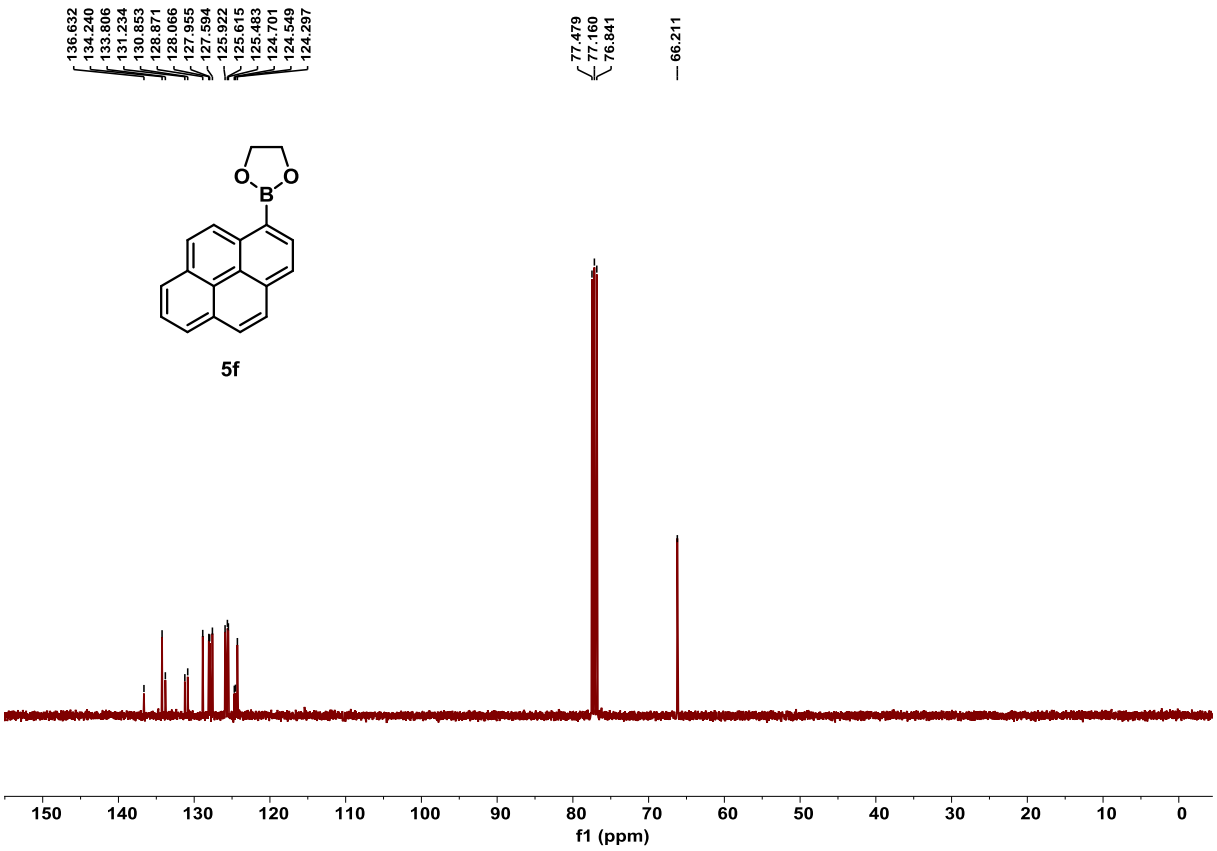

Figure S26. ^{13}C NMR spectrum of substrate **5f**, related to **Scheme 2**.

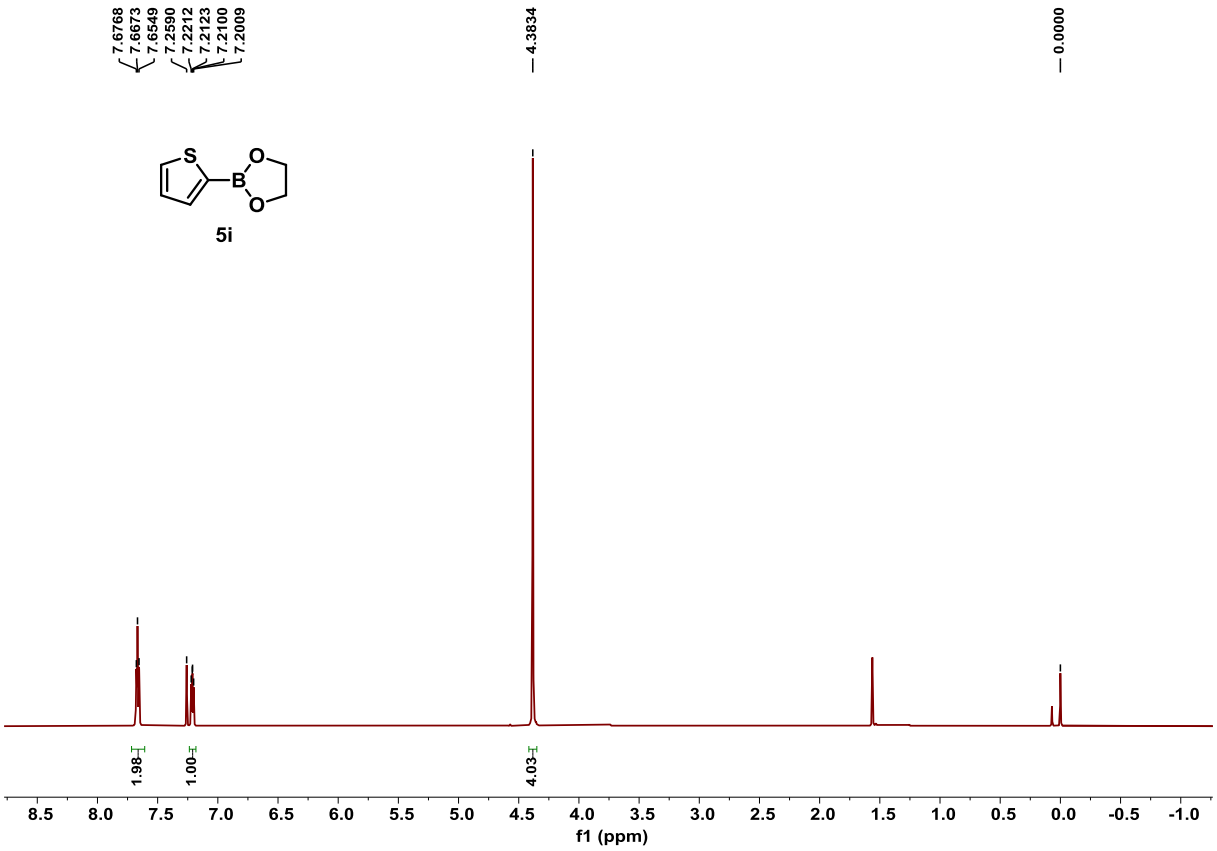

Figure S27. ^{1}H NMR spectrum of substrate **5i**, related to **Scheme 2**.

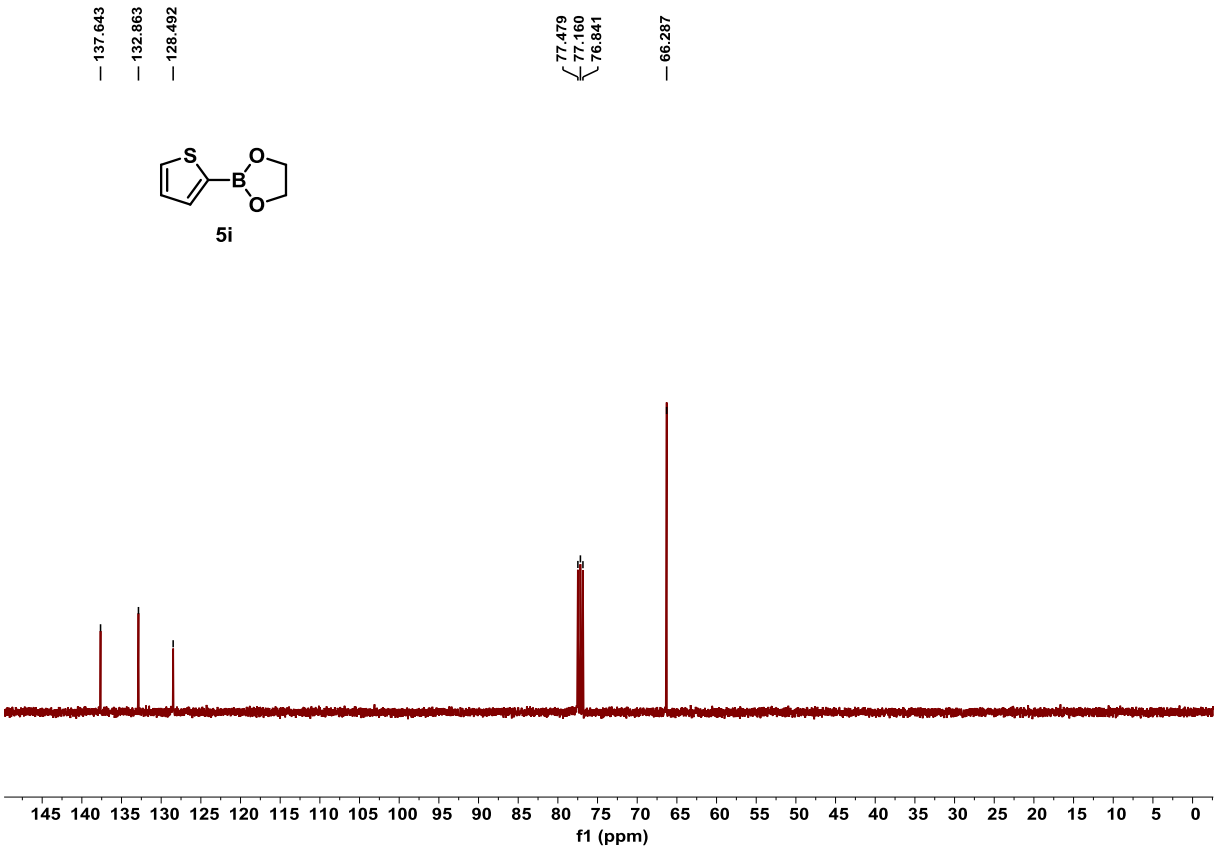

Figure S28. ^{13}C NMR spectrum of substrate **5i**, related to **Scheme 2**.

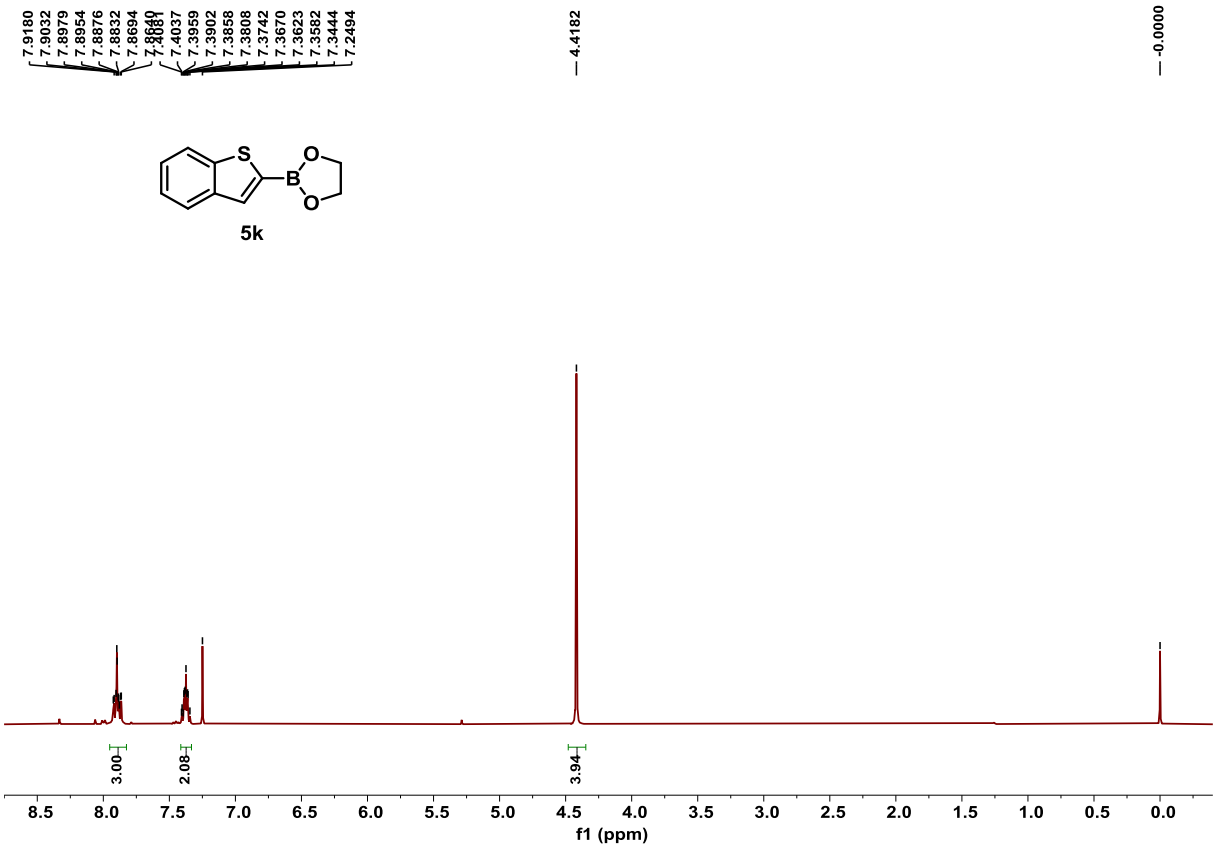

Figure S29. ^{1}**H NMR** spectrum of substrate **5k**, related to **Scheme 2**.

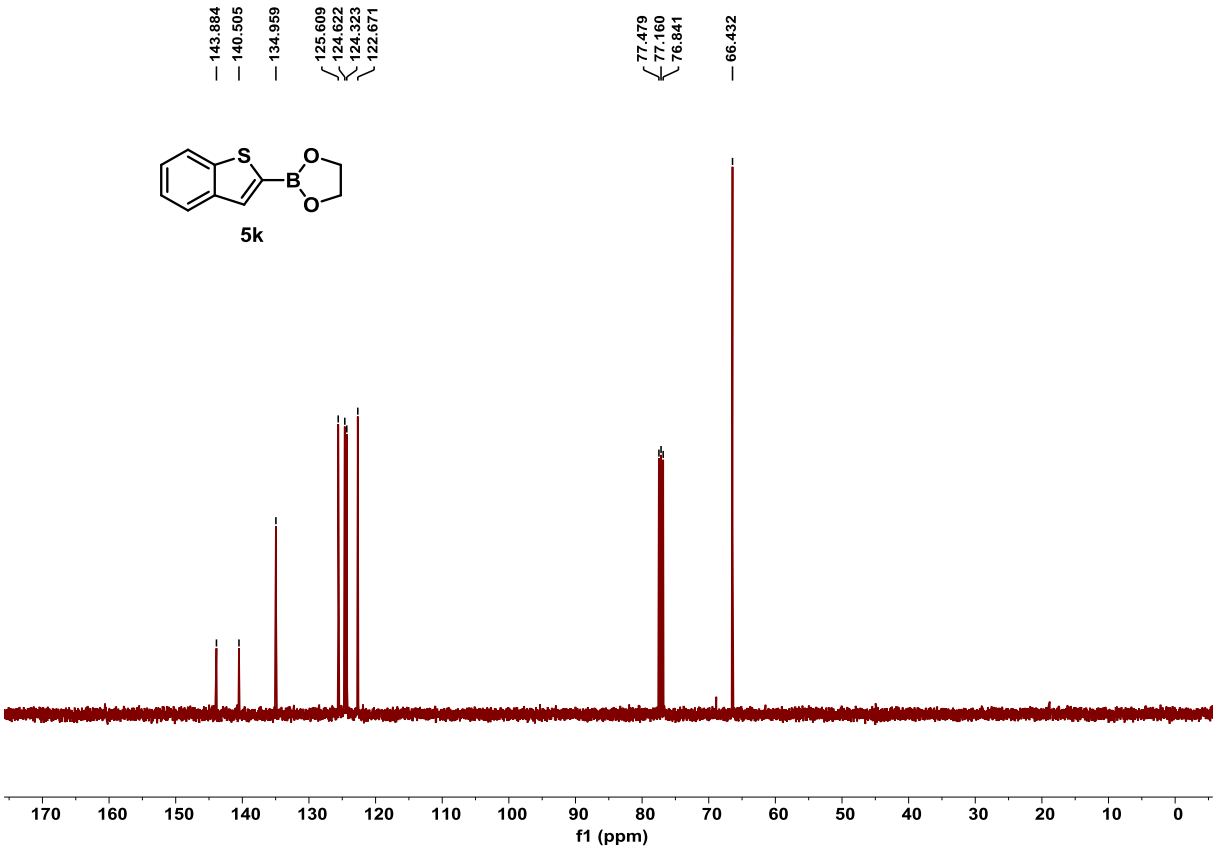

Figure S30. ^{13}**C NMR** spectrum of substrate **5k**, related to **Scheme 2**.

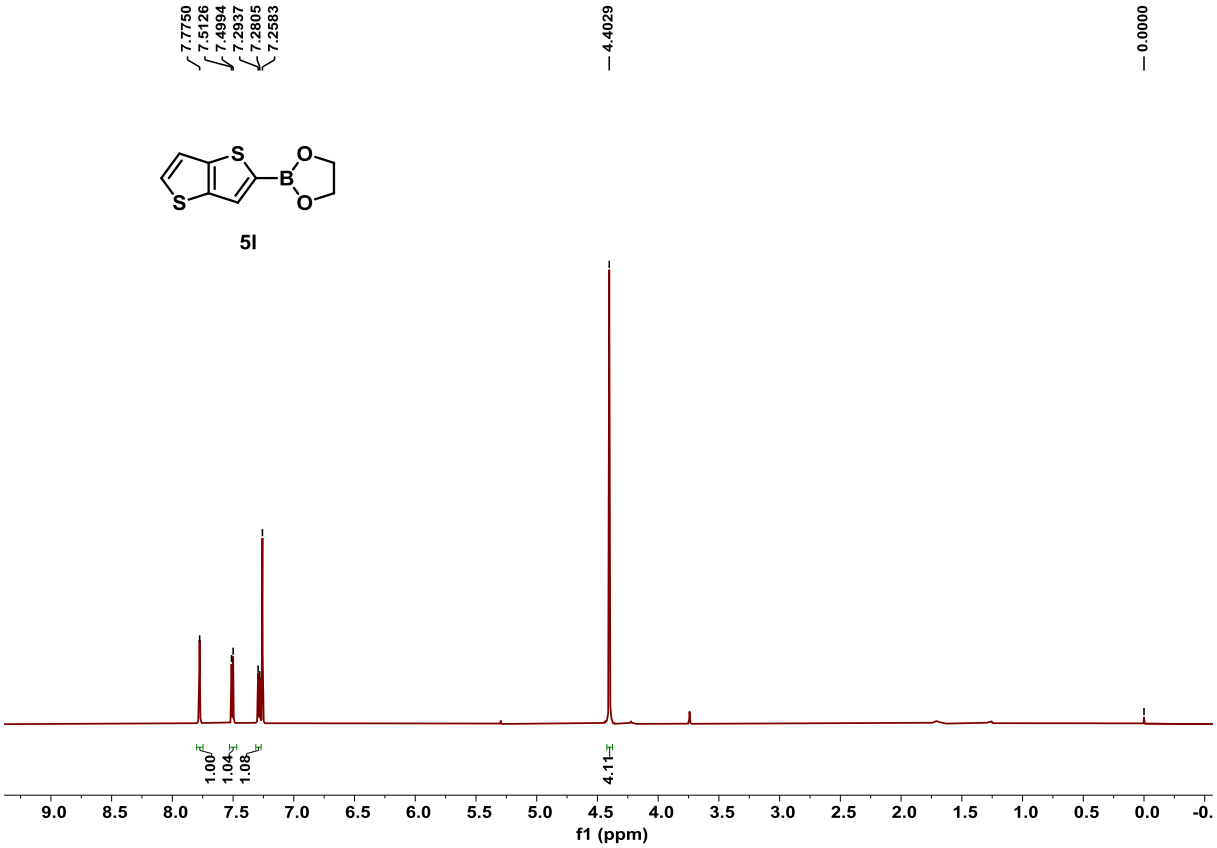

Figure S31. ^{1}H NMR spectrum of substrate **5l**, related to **Scheme 2**.

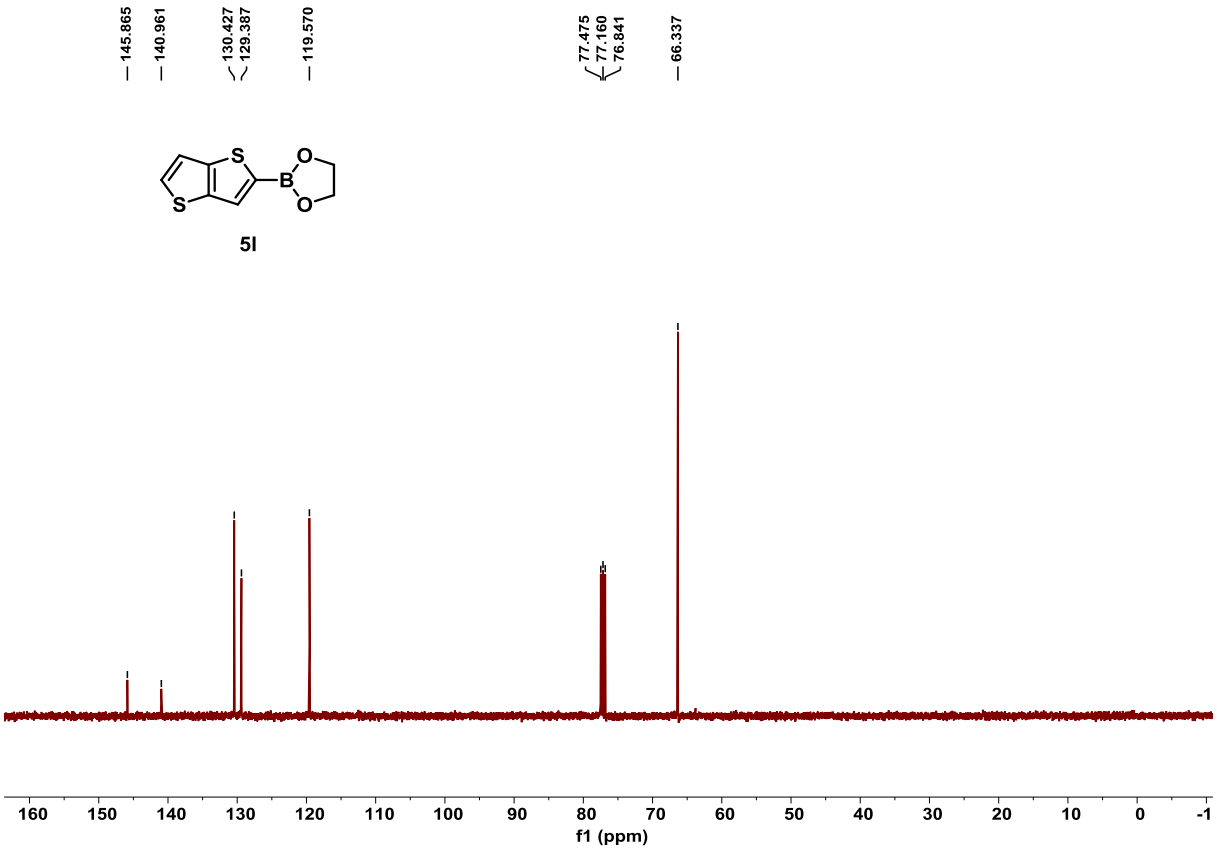

Figure S32. ^{13}C NMR spectrum of substrate **5l**, related to **Scheme 2**.

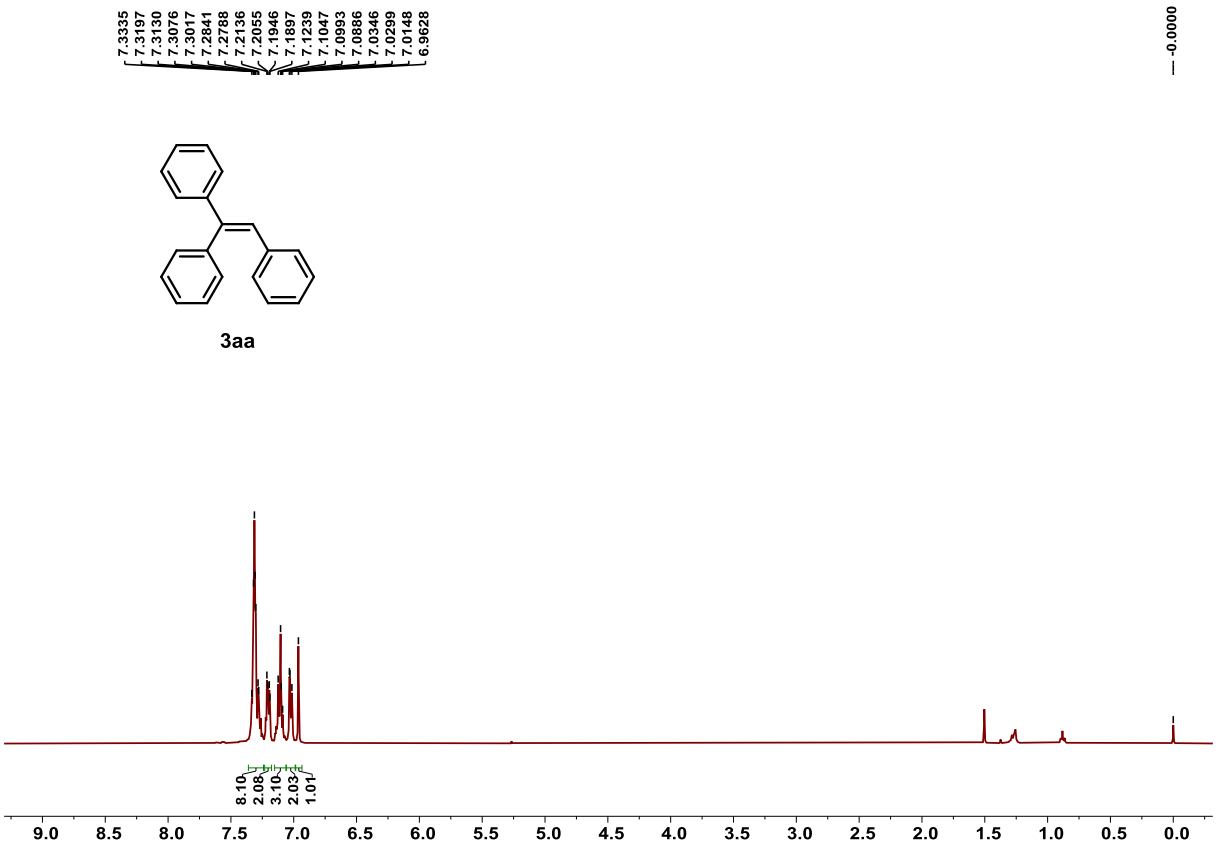

Figure S33. ^{1}**H NMR** spectrum of product **3aa**, related to **Scheme 2**.

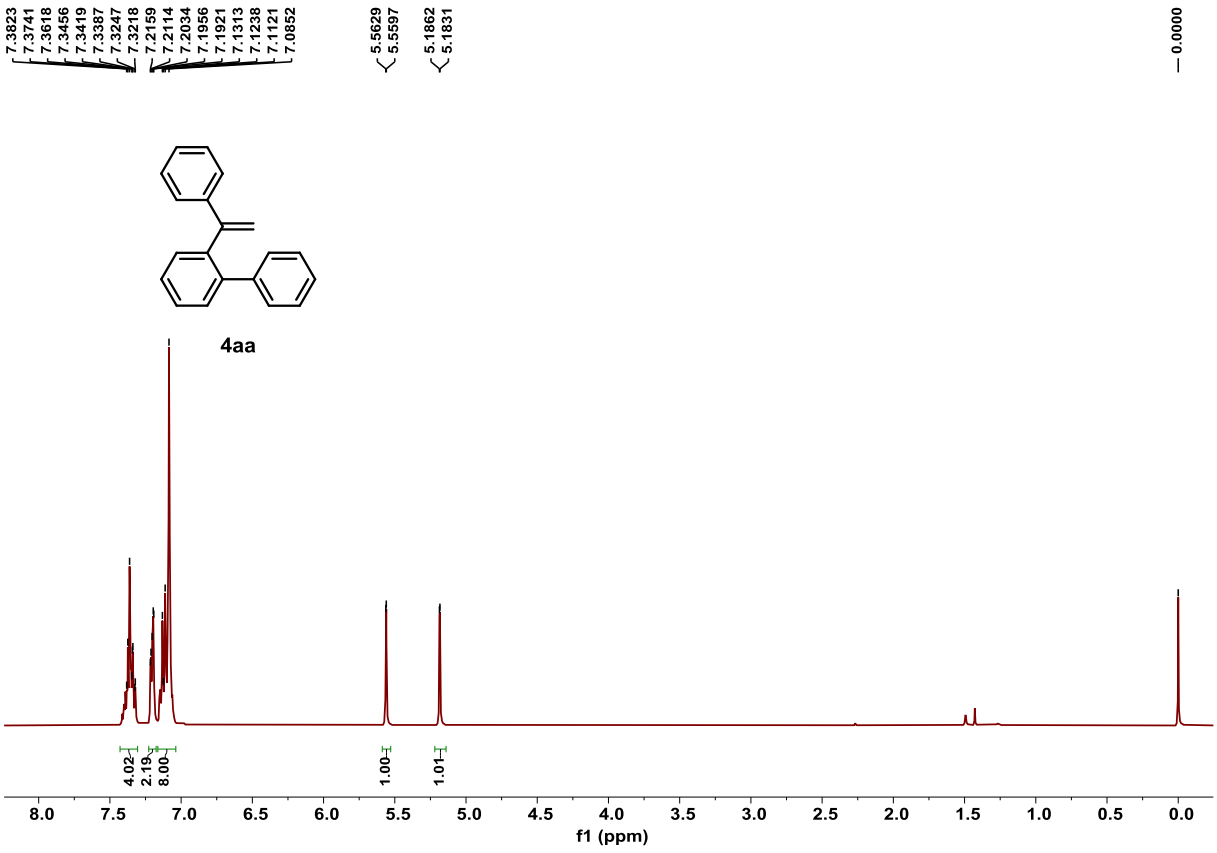

Figure S34. ^{1}**H NMR** spectrum of product **4aa**, related to **Scheme 2**.

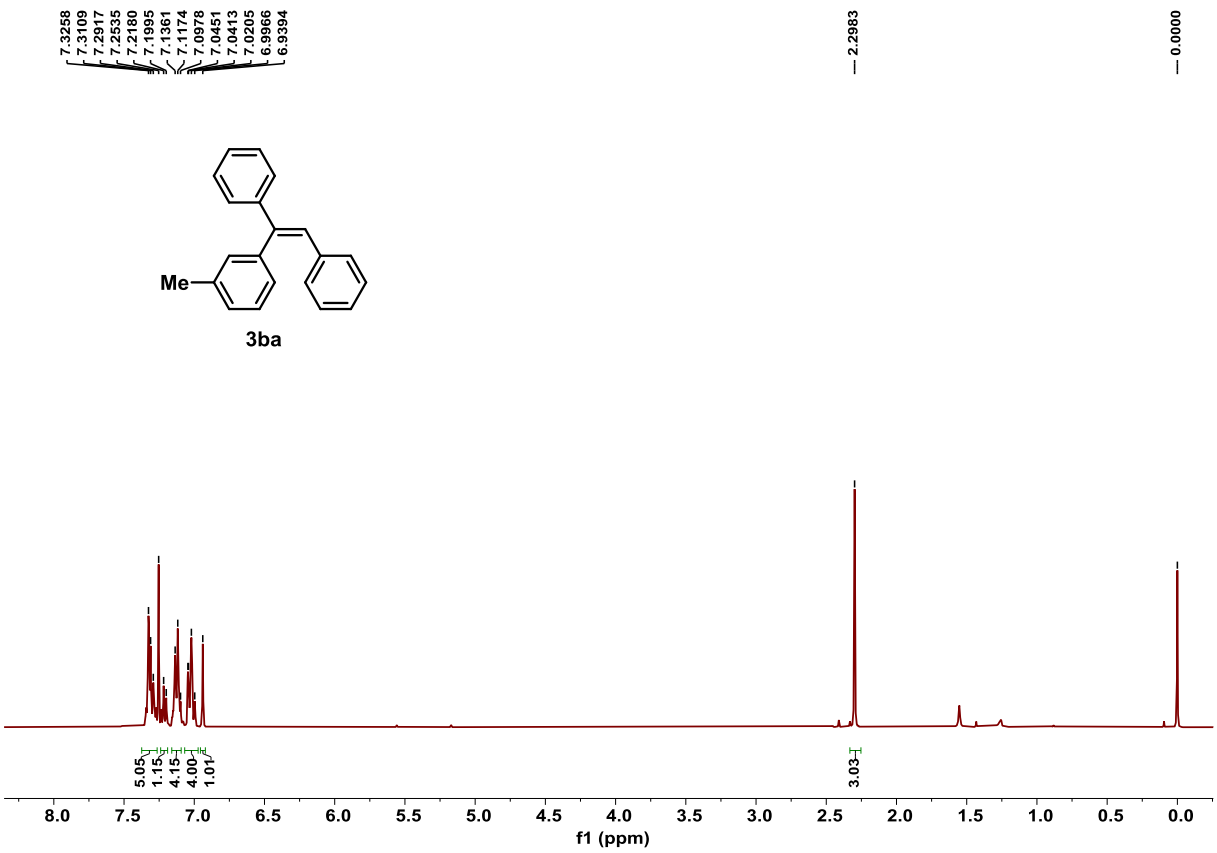

Figure S35. ^{1}**H NMR** spectrum of product **3ba**, related to **Scheme 2**.

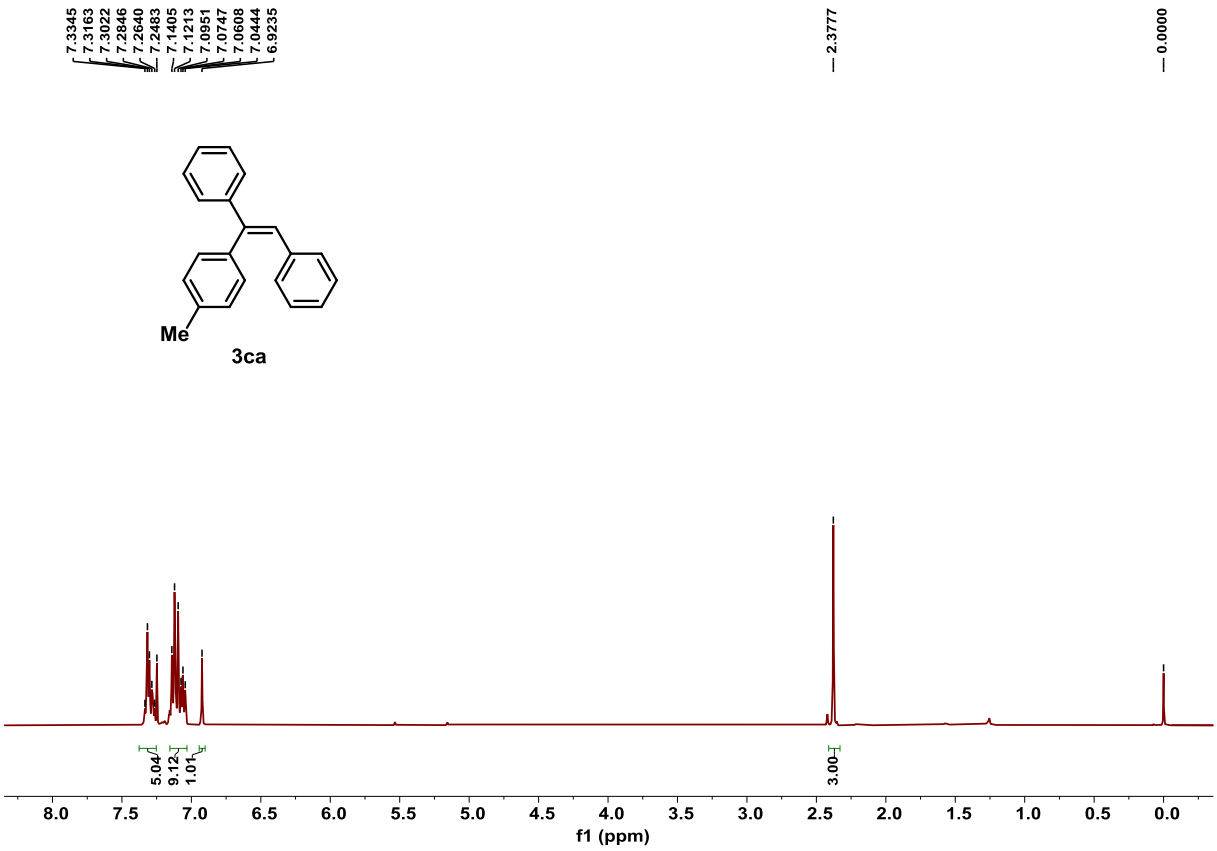

Figure S36. ^{1}**H NMR** spectrum of product **3ca**, related to **Scheme 2**.

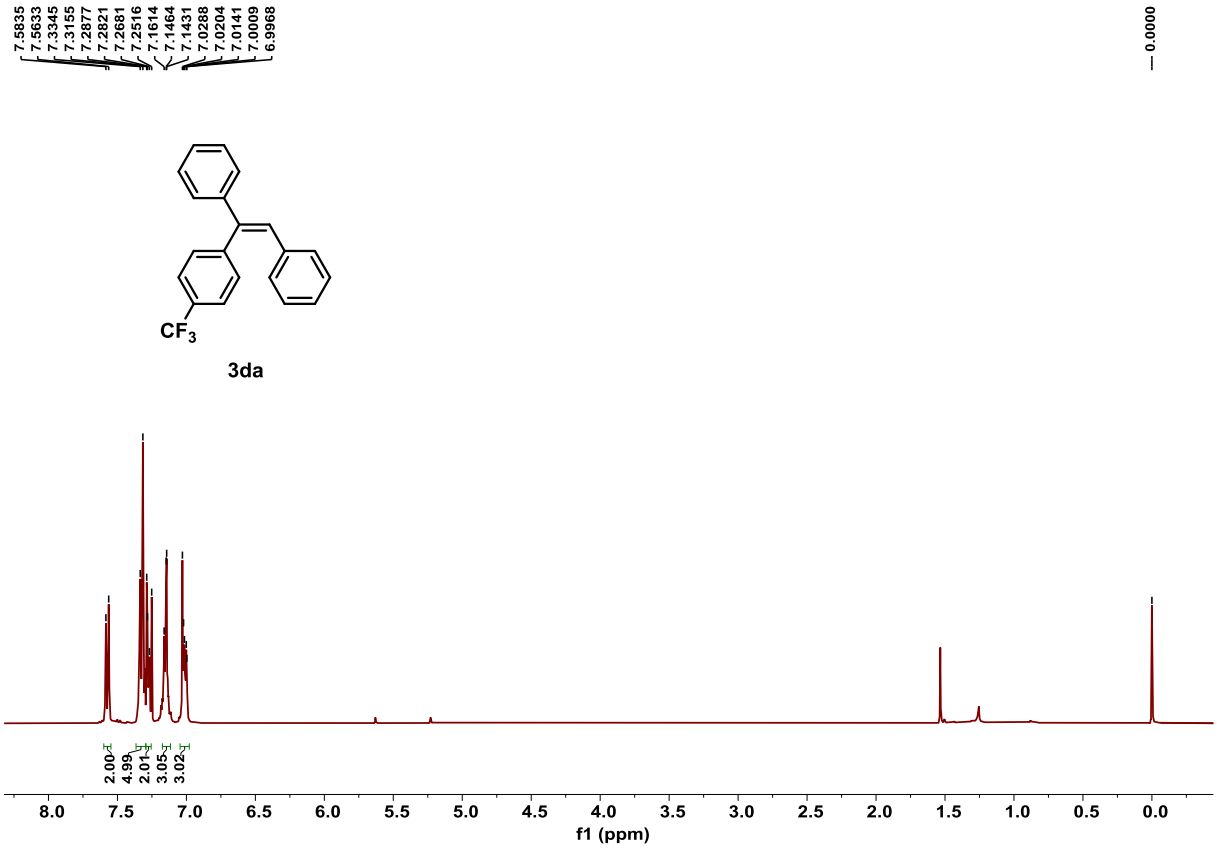

Figure S37. ^{1}**H NMR** spectrum of product **3da**, related to **Scheme 2**.

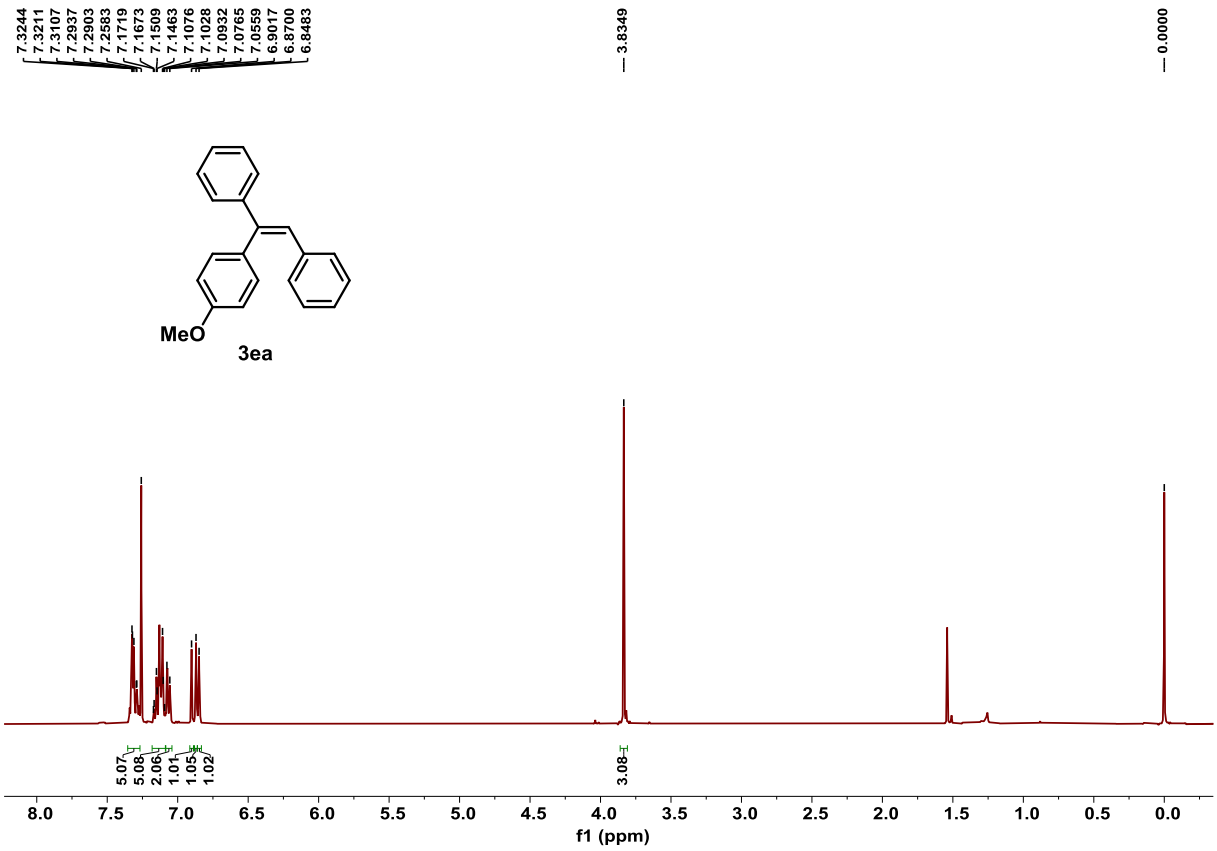

Figure S38. ^{1}**H NMR** spectrum of product **3ea**, related to **Scheme 2**.

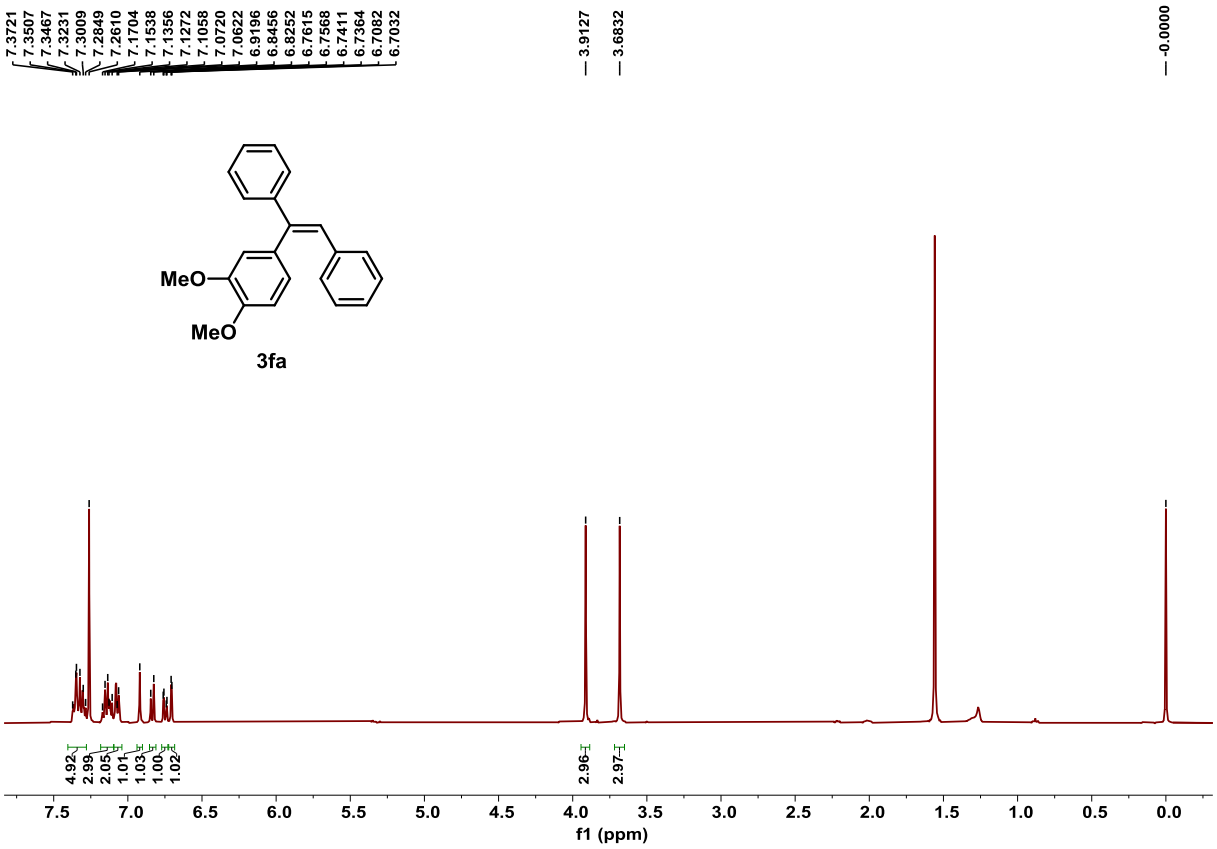

Figure S39. ^{1}H NMR spectrum of product **3fa**, related to **Scheme 2**.

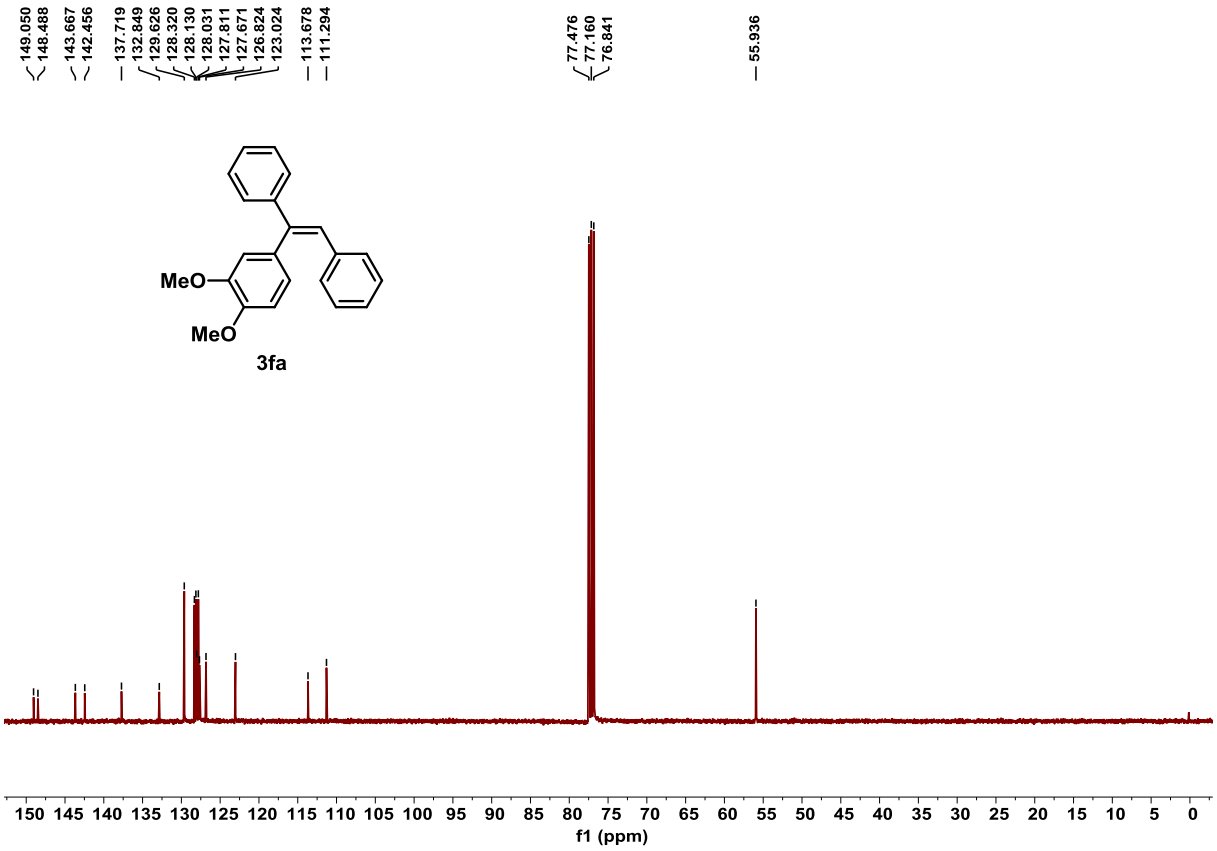

Figure S40. ^{13}C NMR spectrum of product **3fa**, related to **Scheme 2**.

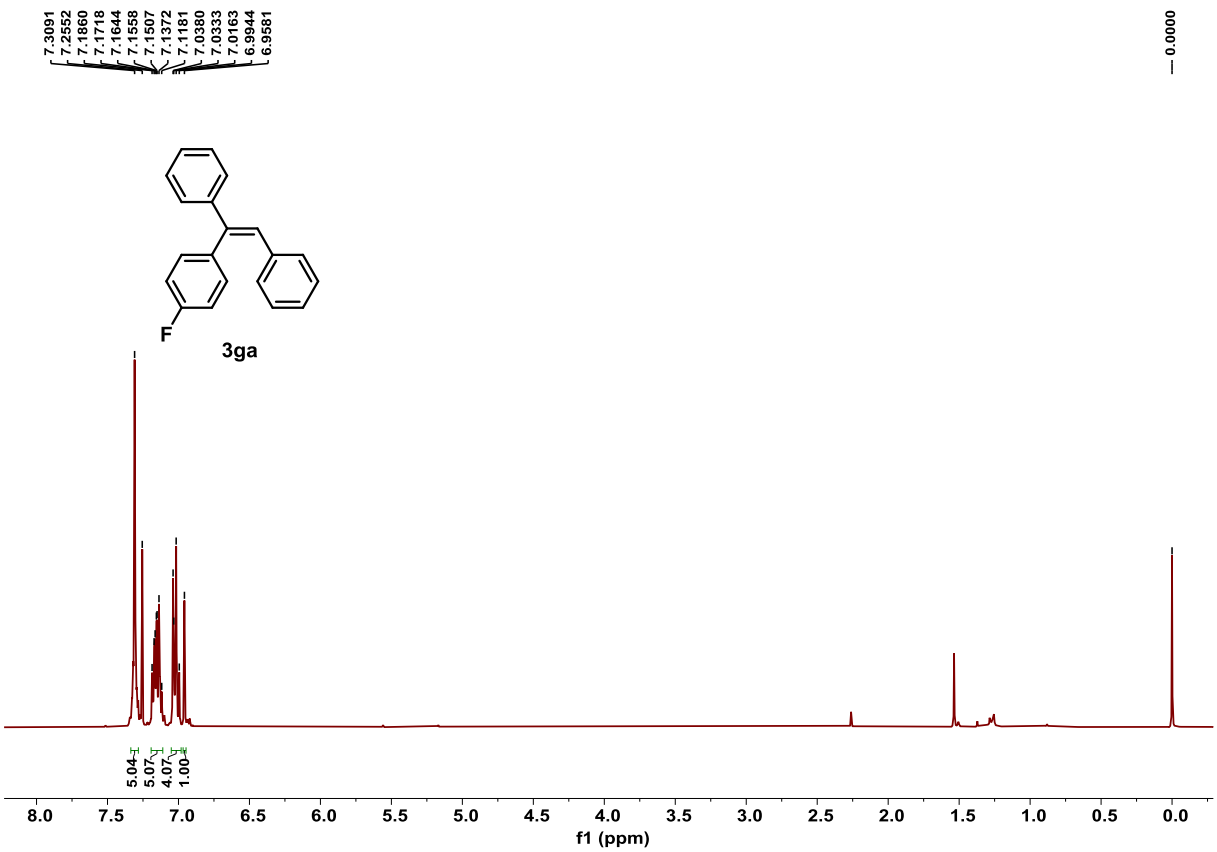

Figure S41. ^{1}**H NMR** spectrum of product **3ga**, related to **Scheme 2**.

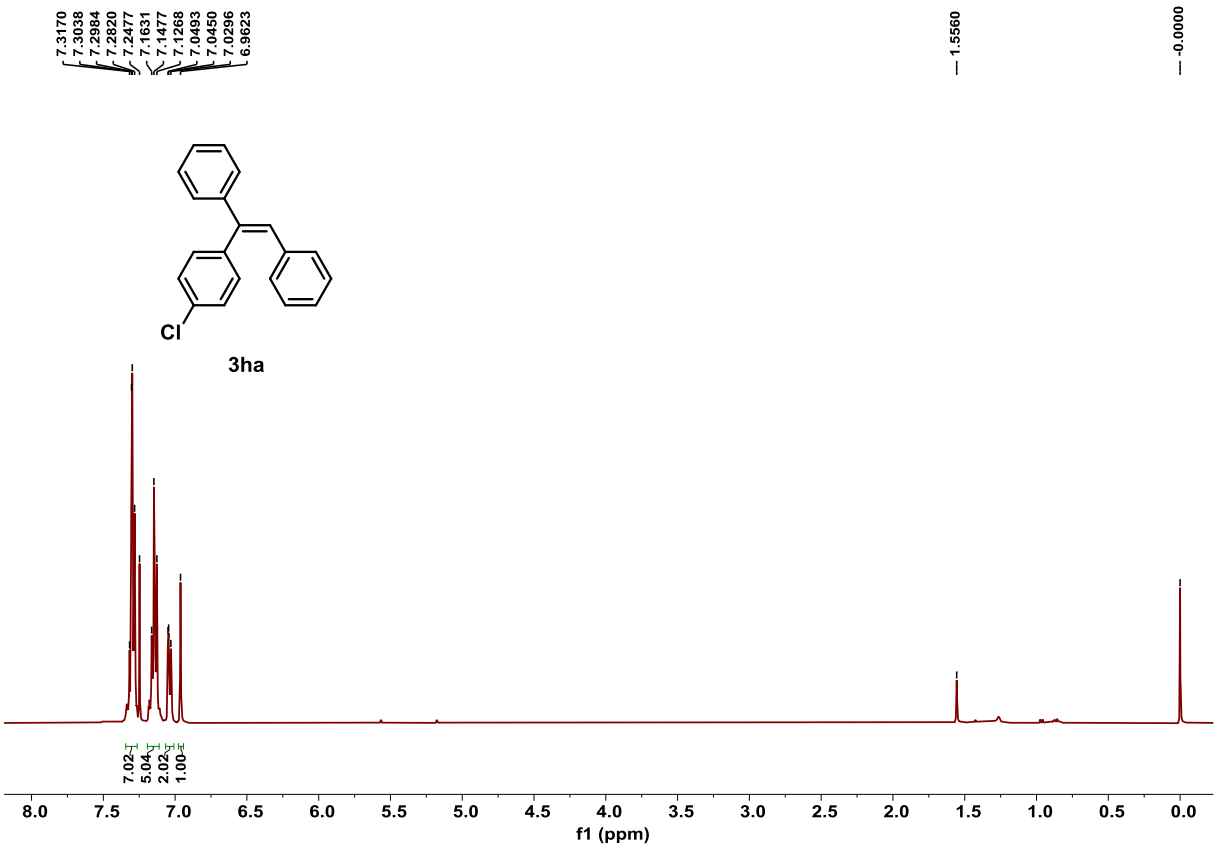

Figure S42. ^{1}**H NMR** spectrum of product **3ha**, related to **Scheme 2**.

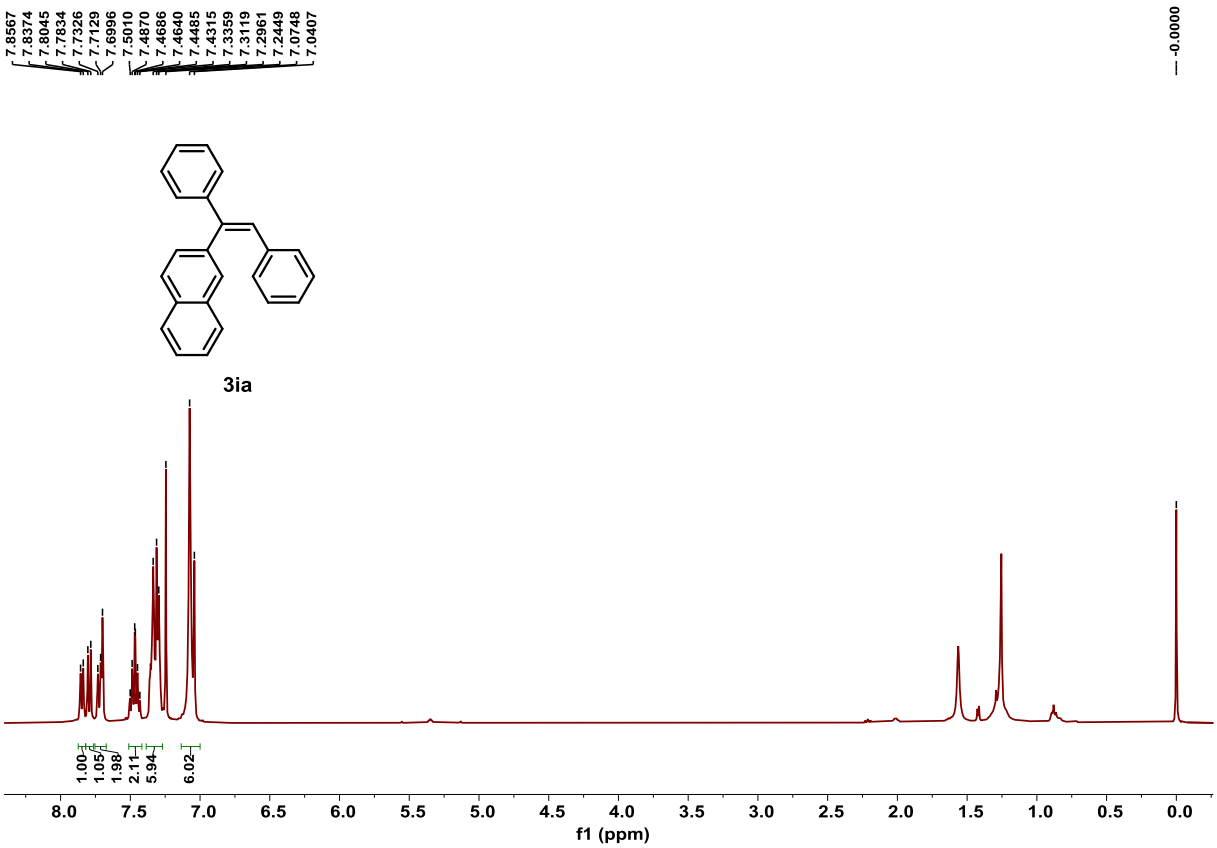

Figure S43. ^{1}H NMR spectrum of product **3ia**, related to **Scheme 2**.

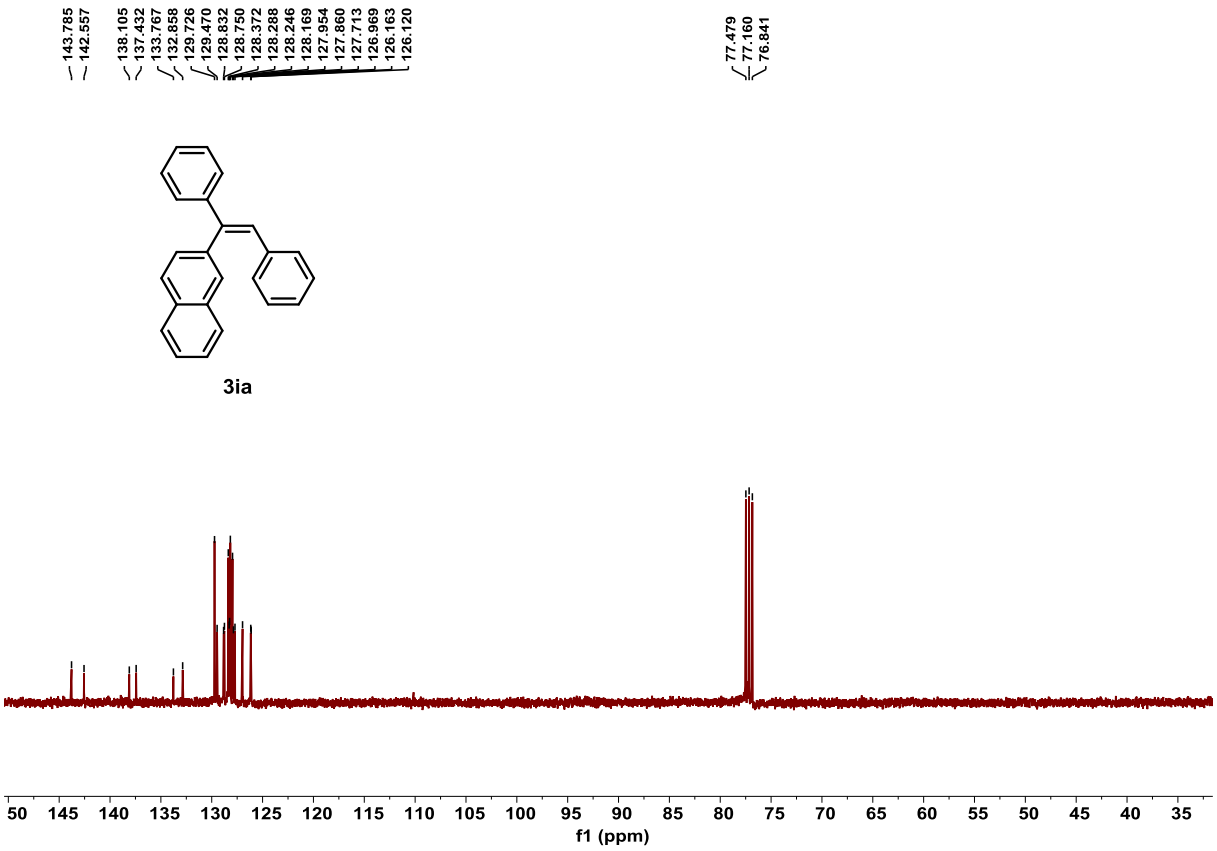

Figure S44. ^{13}C NMR spectrum of product **3ia**, related to **Scheme 2**.

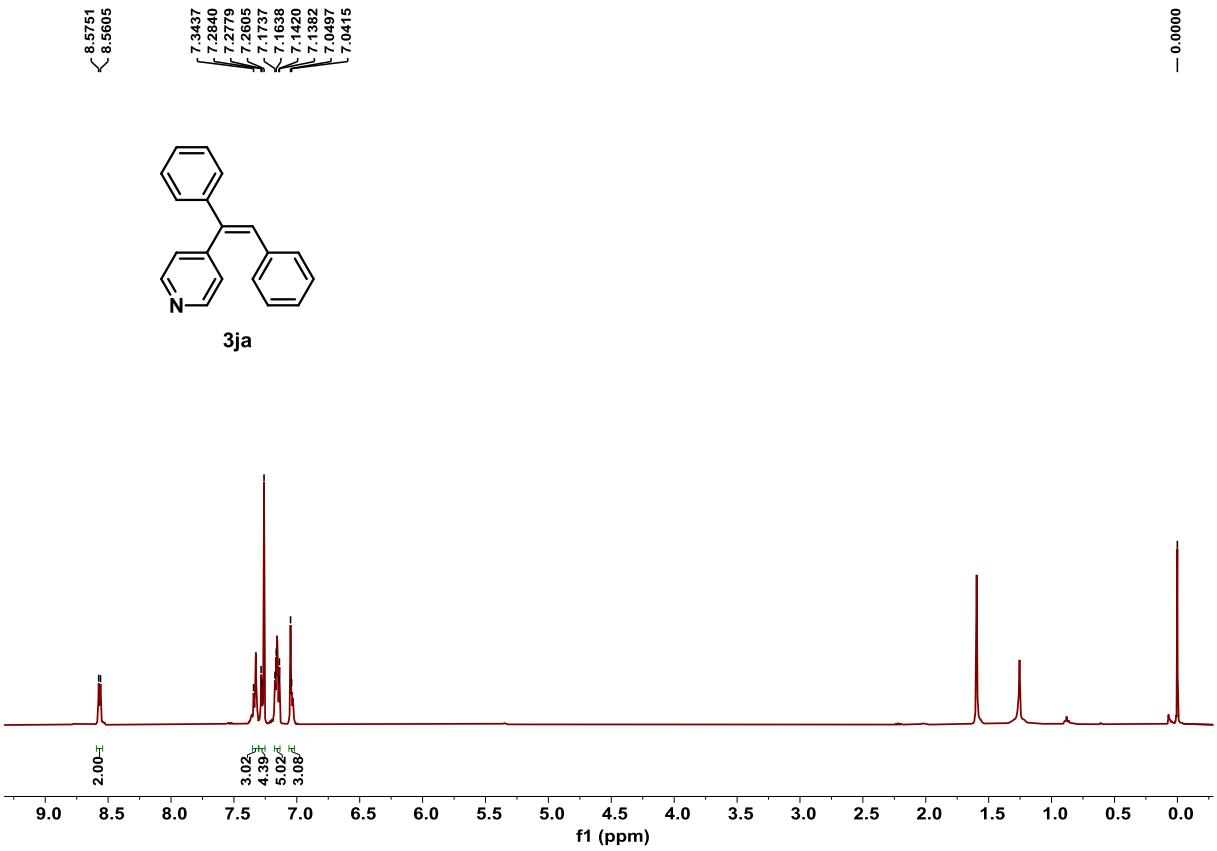

Figure S45. ^{1}H NMR spectrum of product **3ja**, related to **Scheme 2**.

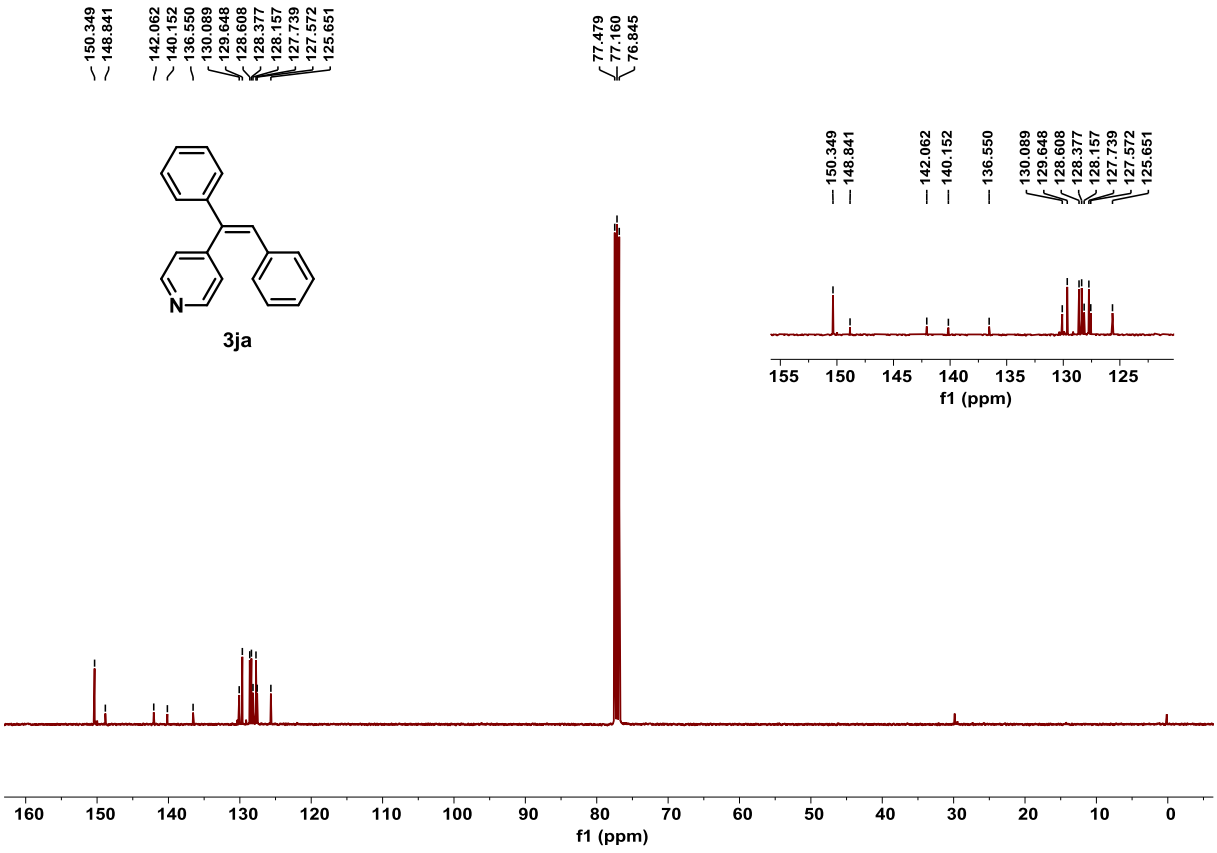

Figure S46. ^{13}C NMR spectrum of product **3ja**, related to **Scheme 2**.

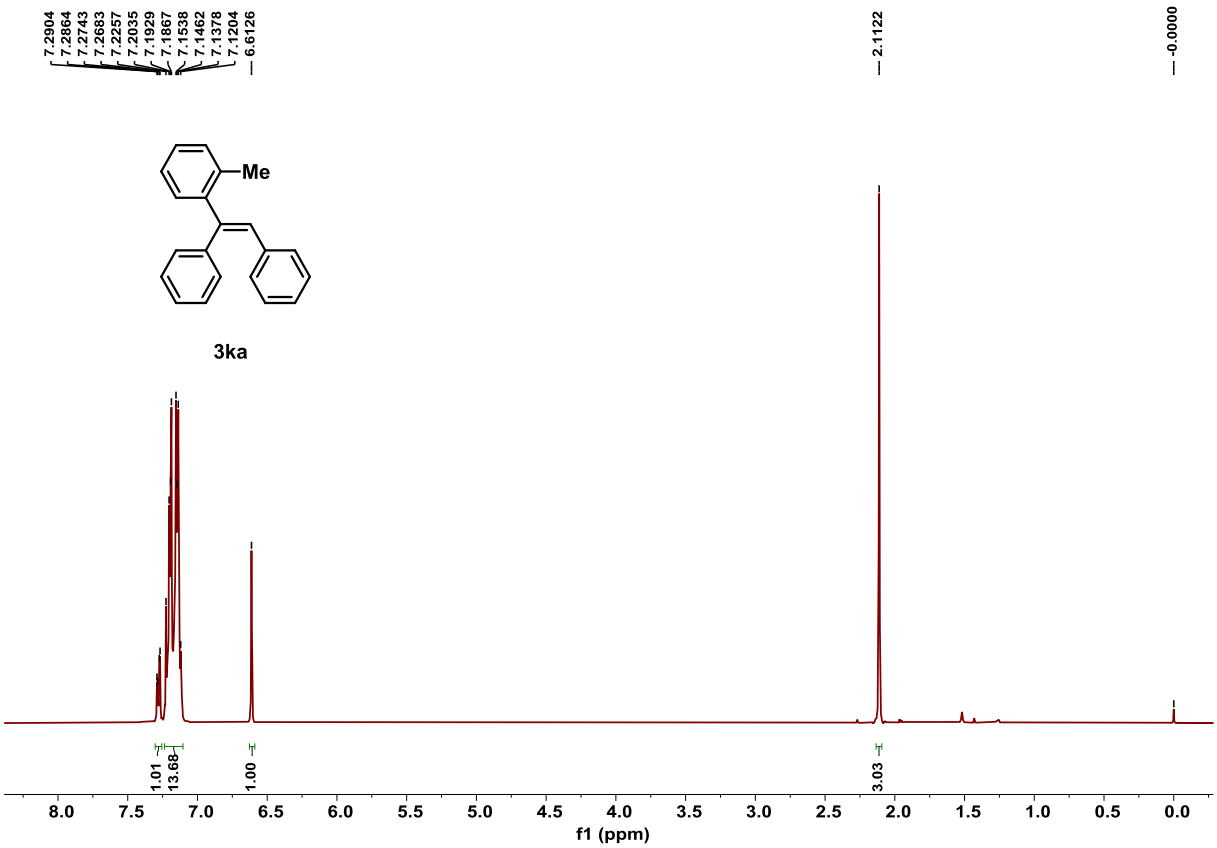

Figure S47. ^{1}H NMR spectrum of product **3ka**, related to **Scheme 2**.

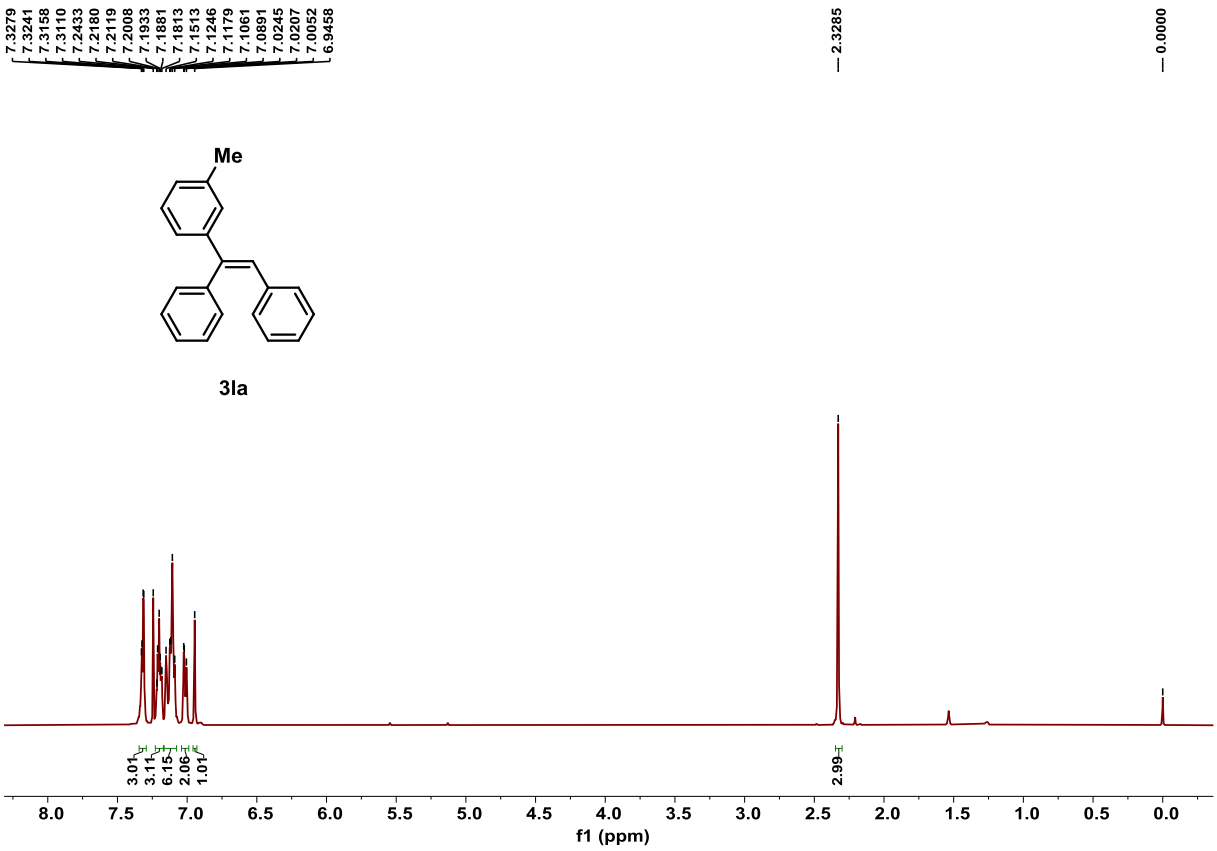

Figure S48. ^{1}H NMR spectrum of product **3la**, related to **Scheme 2**.

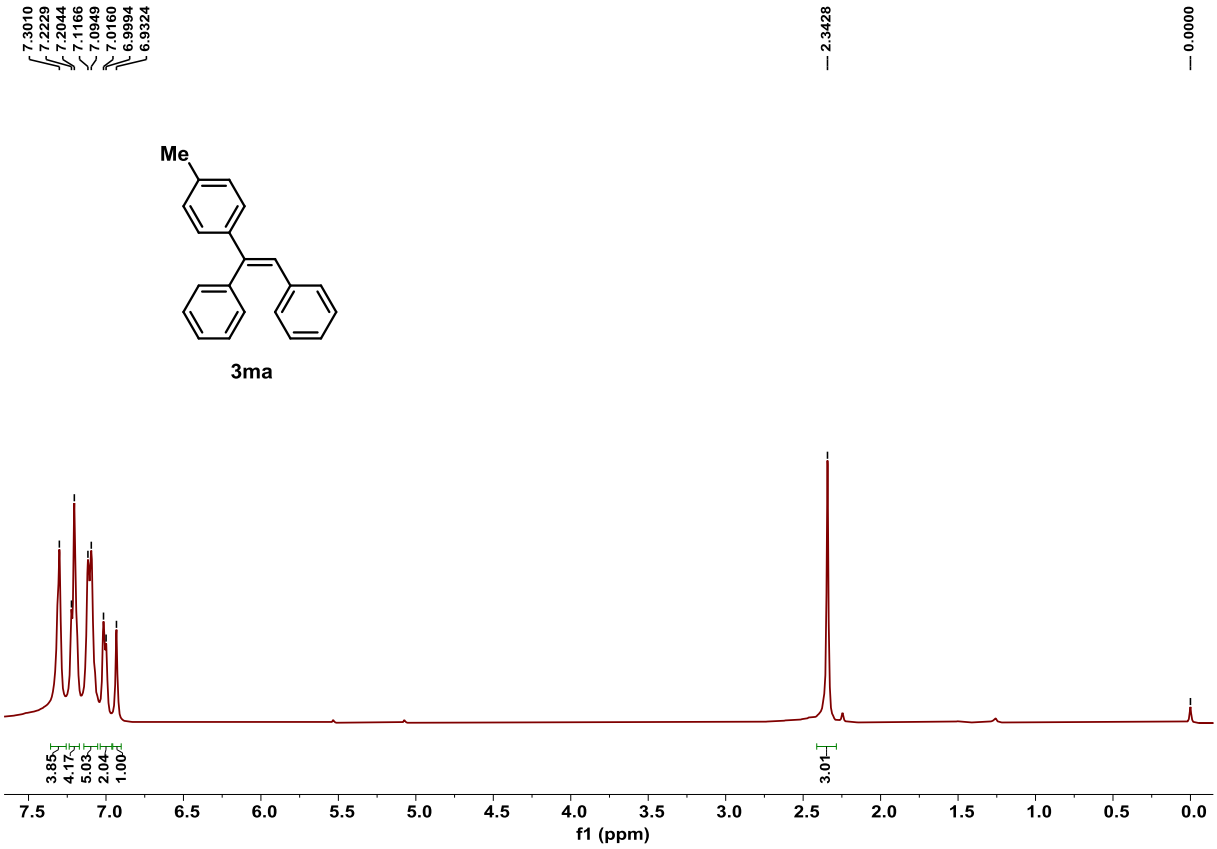

Figure S49. ^{1}**H NMR** spectrum of product **3ma**, related to **Scheme 2**.

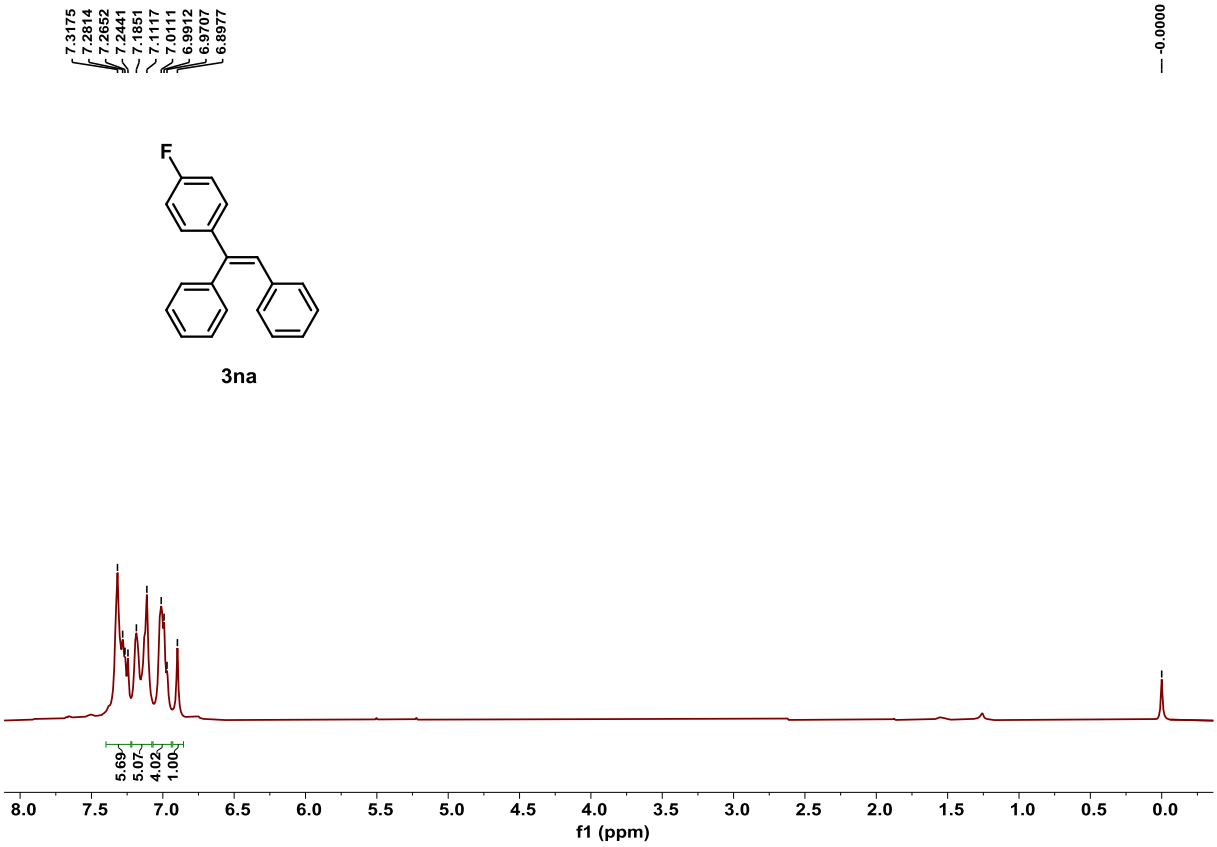

Figure S50. ^{1}**H NMR** spectrum of product **3na**, related to **Scheme 2**.

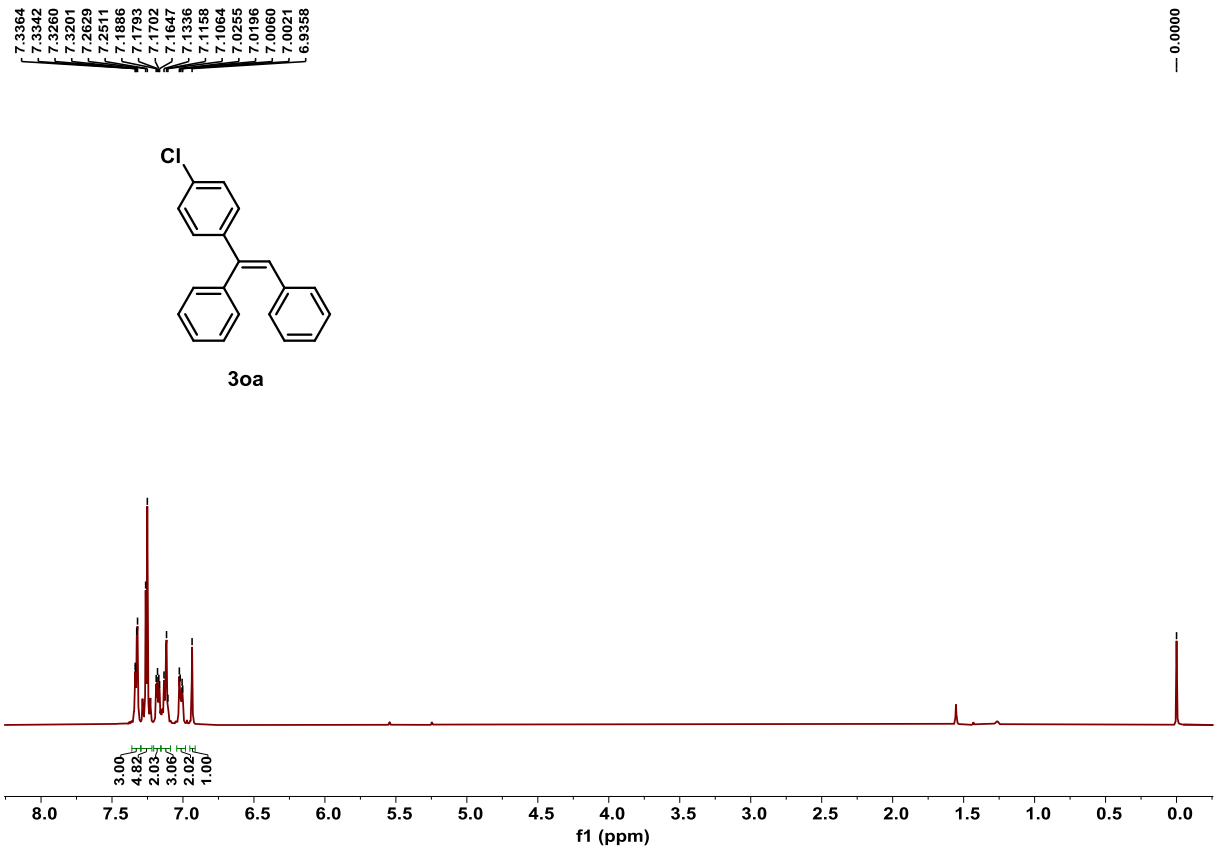

Figure S51. ^{1}**H NMR** spectrum of product **3oa**, related to **Scheme 2**.

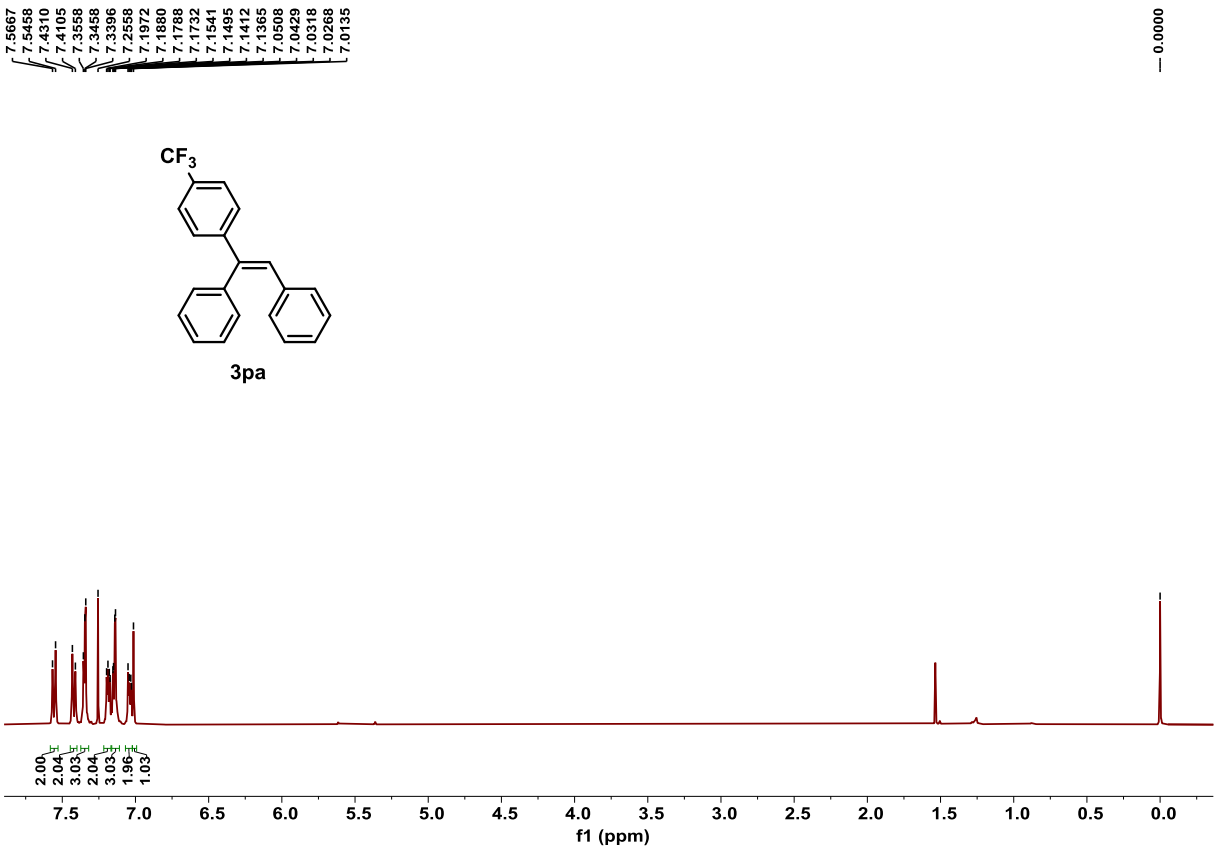

Figure S52. ^{1}**H NMR** spectrum of product **3pa**, related to **Scheme 2**.

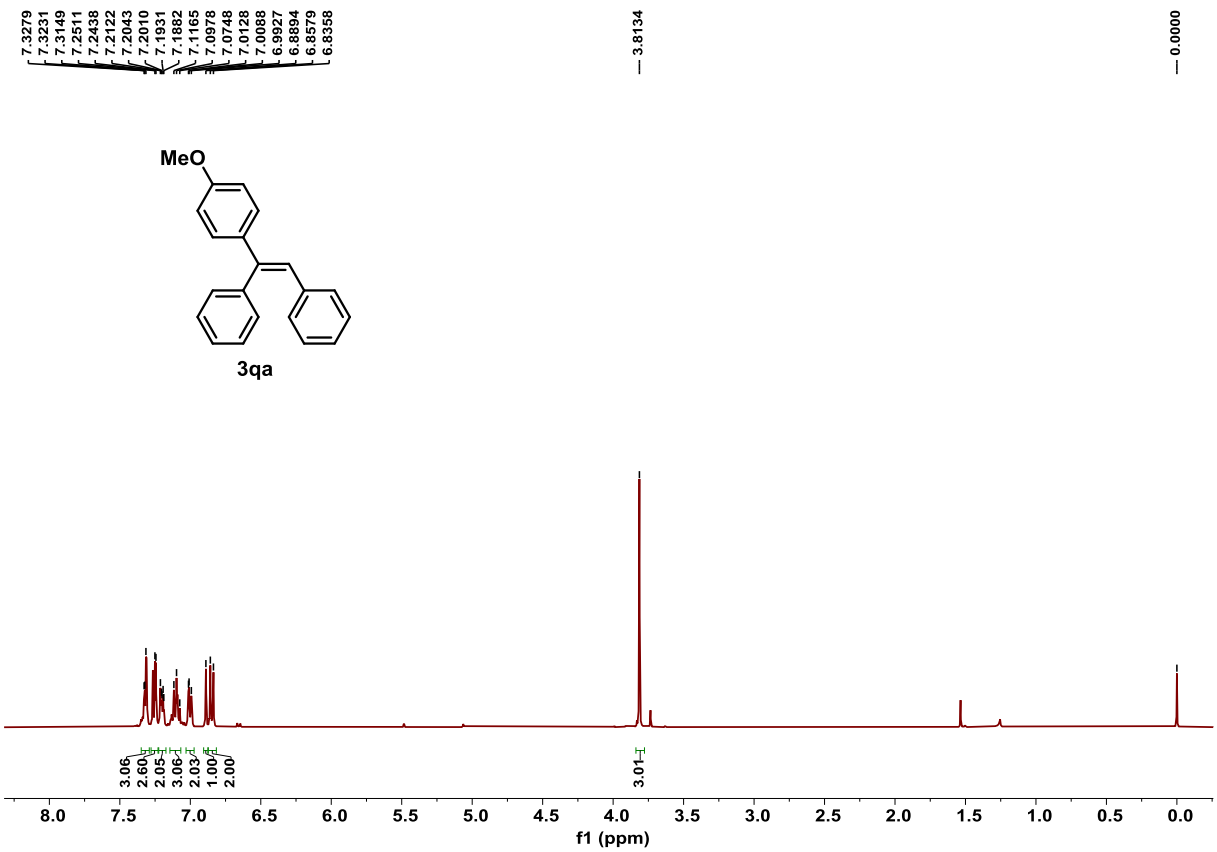

Figure S53. ^{1}H NMR spectrum of product **3qa**, related to **Scheme 2**.

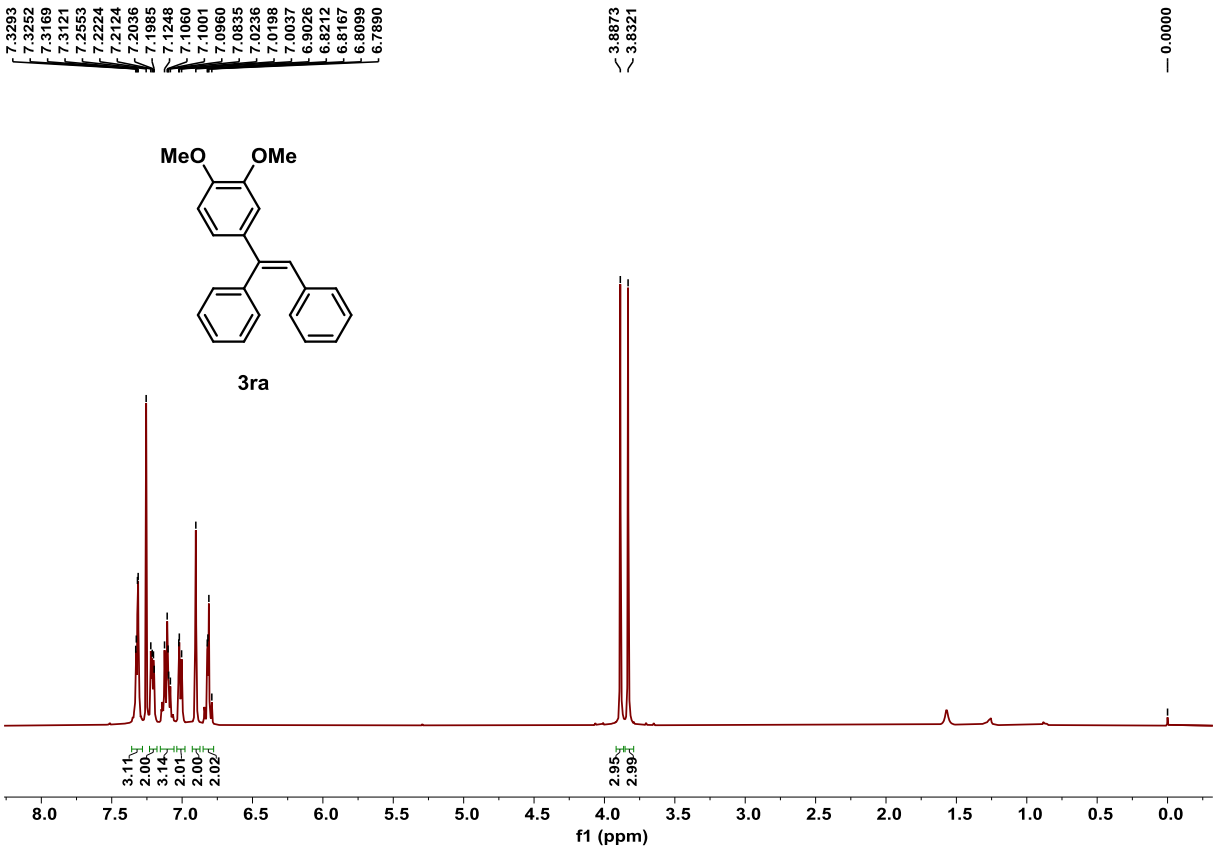

Figure S54. ^{1}H NMR spectrum of product **3ra**, related to **Scheme 2**.

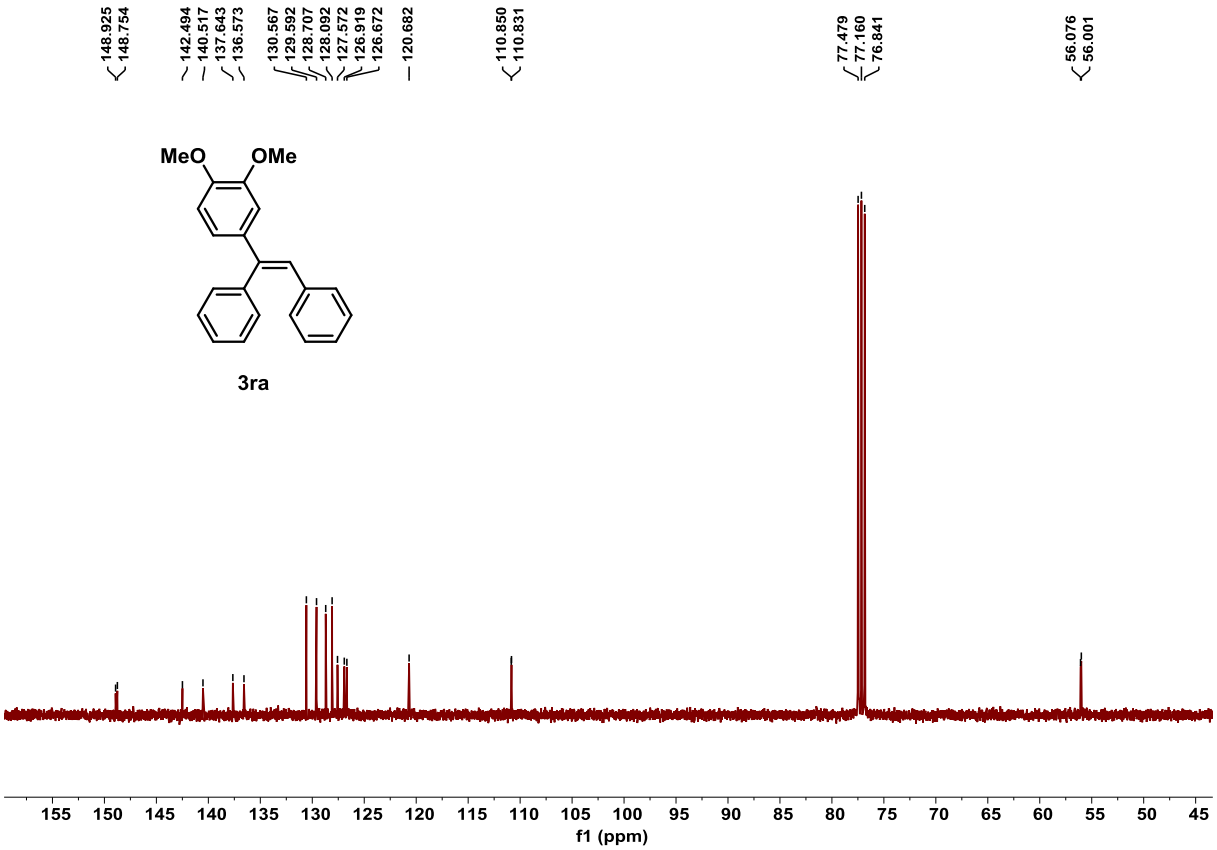

Figure S55. ^{13}**C NMR** spectrum of product **3ra**, related to **Scheme 2**.

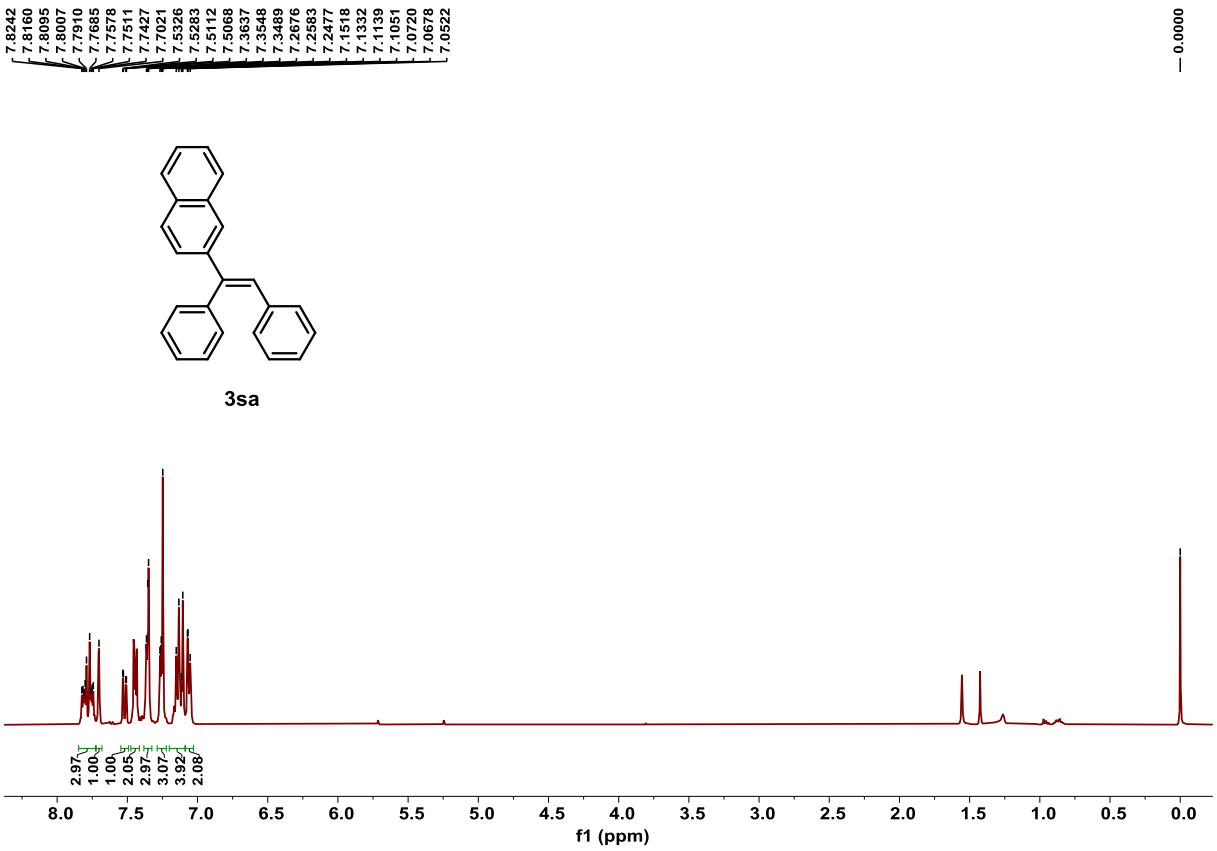

Figure S56. ^{1}**H NMR** spectrum of product **3sa**, related to **Scheme 2**.

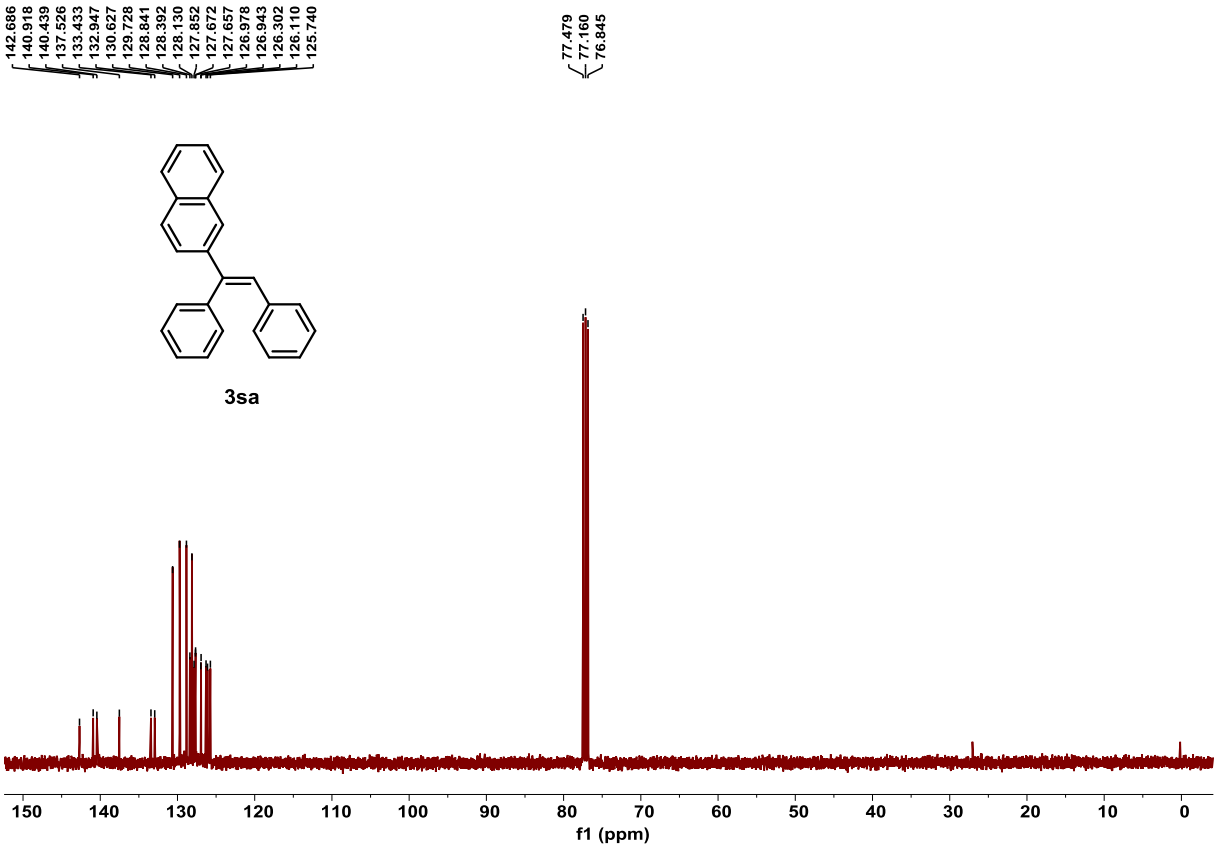

Figure S57. ^{13}C NMR spectrum of product **3sa**, related to **Scheme 2**.

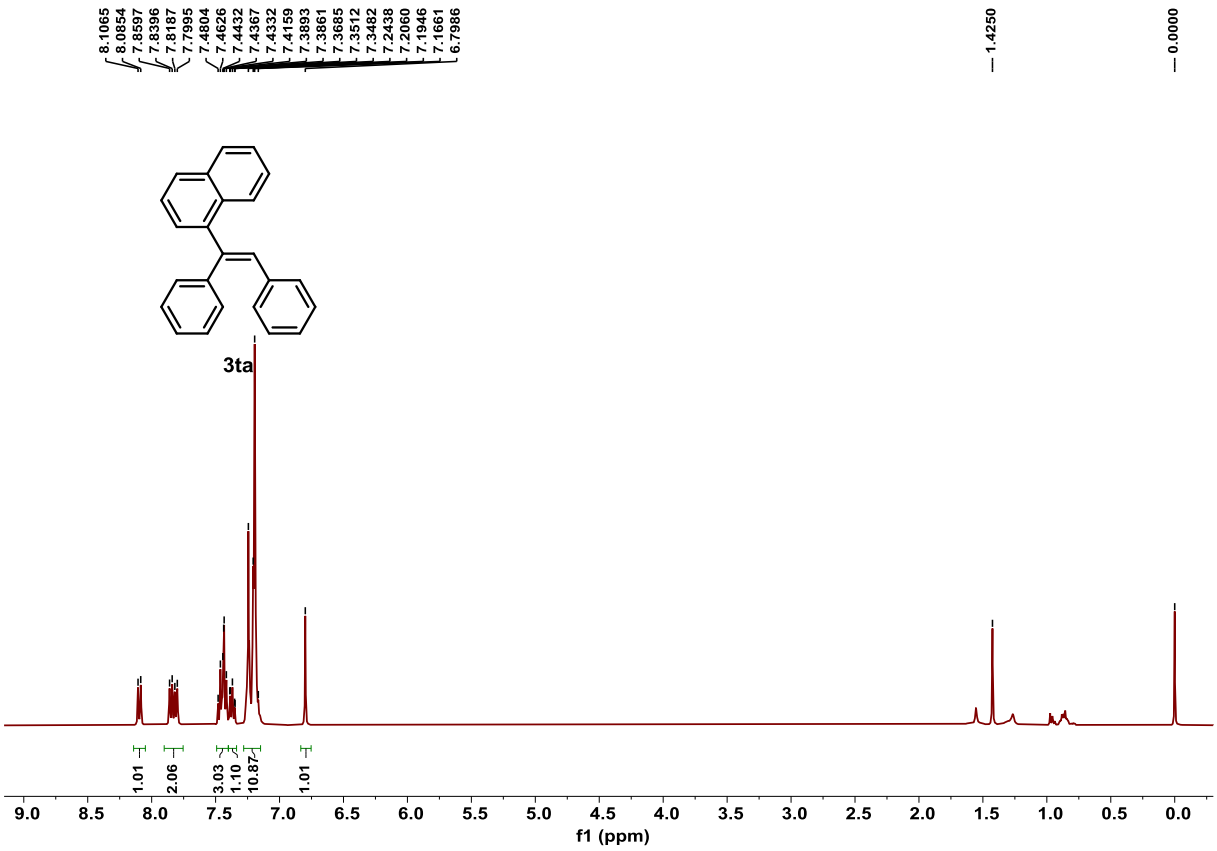

Figure S58. ^{1}H NMR spectrum of product **3ta**, related to **Scheme 2**.

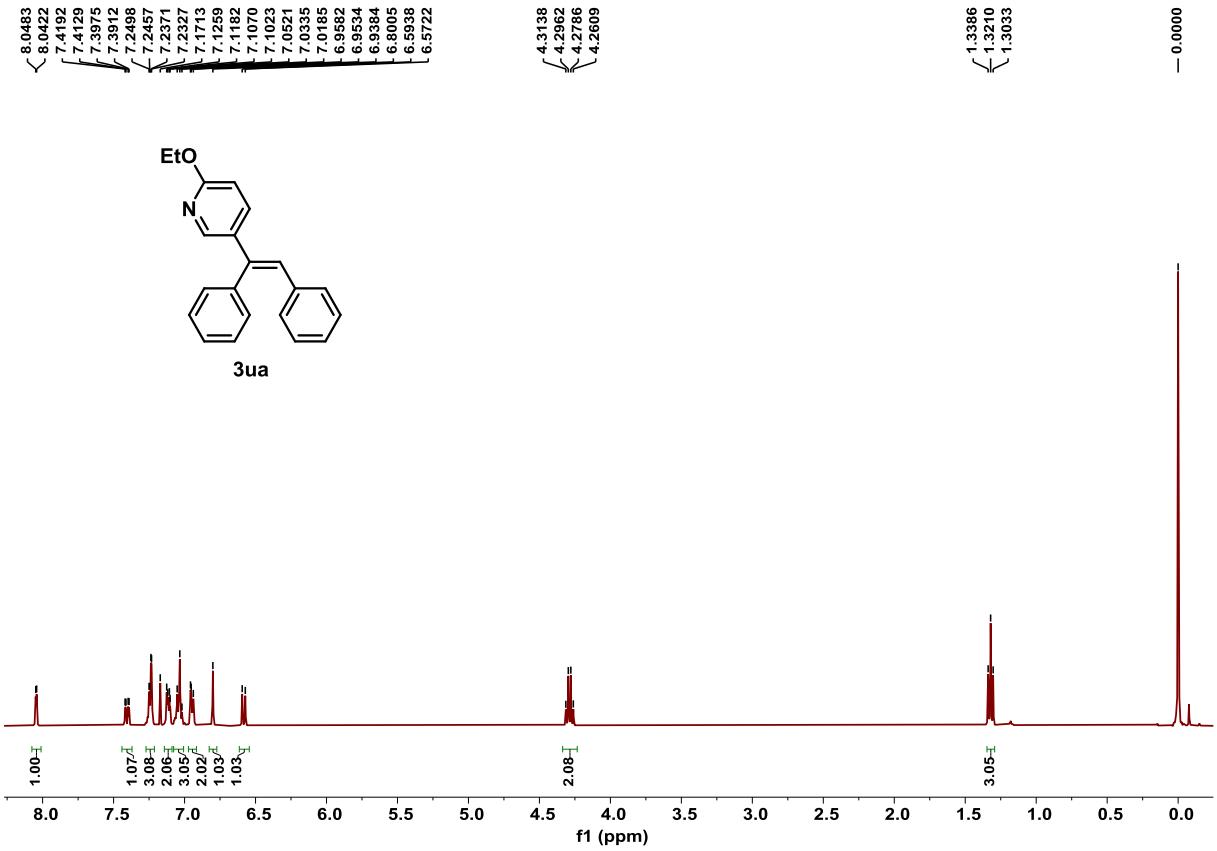

Figure S59. ^{1}H NMR spectrum of product **3ua**, related to **Scheme 2**.

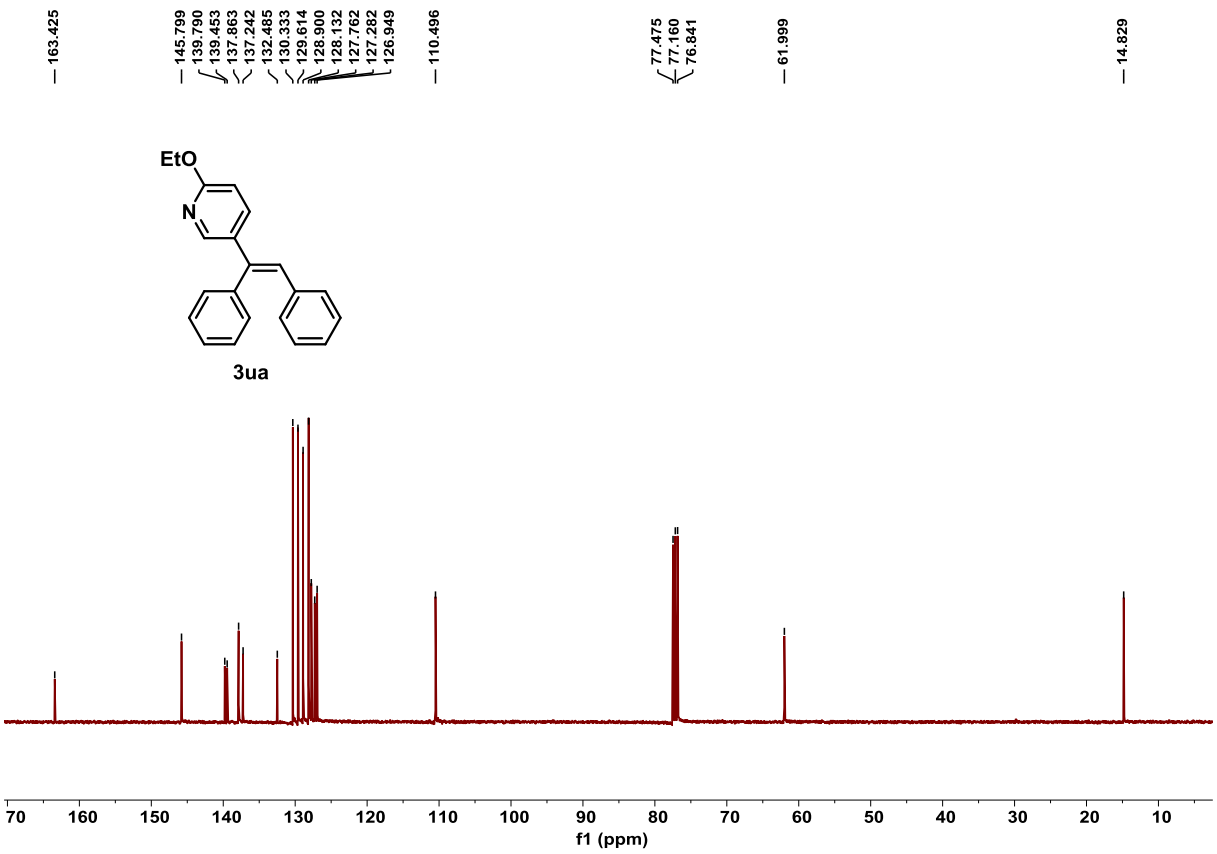

Figure S60. ^{13}C NMR spectrum of product **3ua**, related to **Scheme 2**.

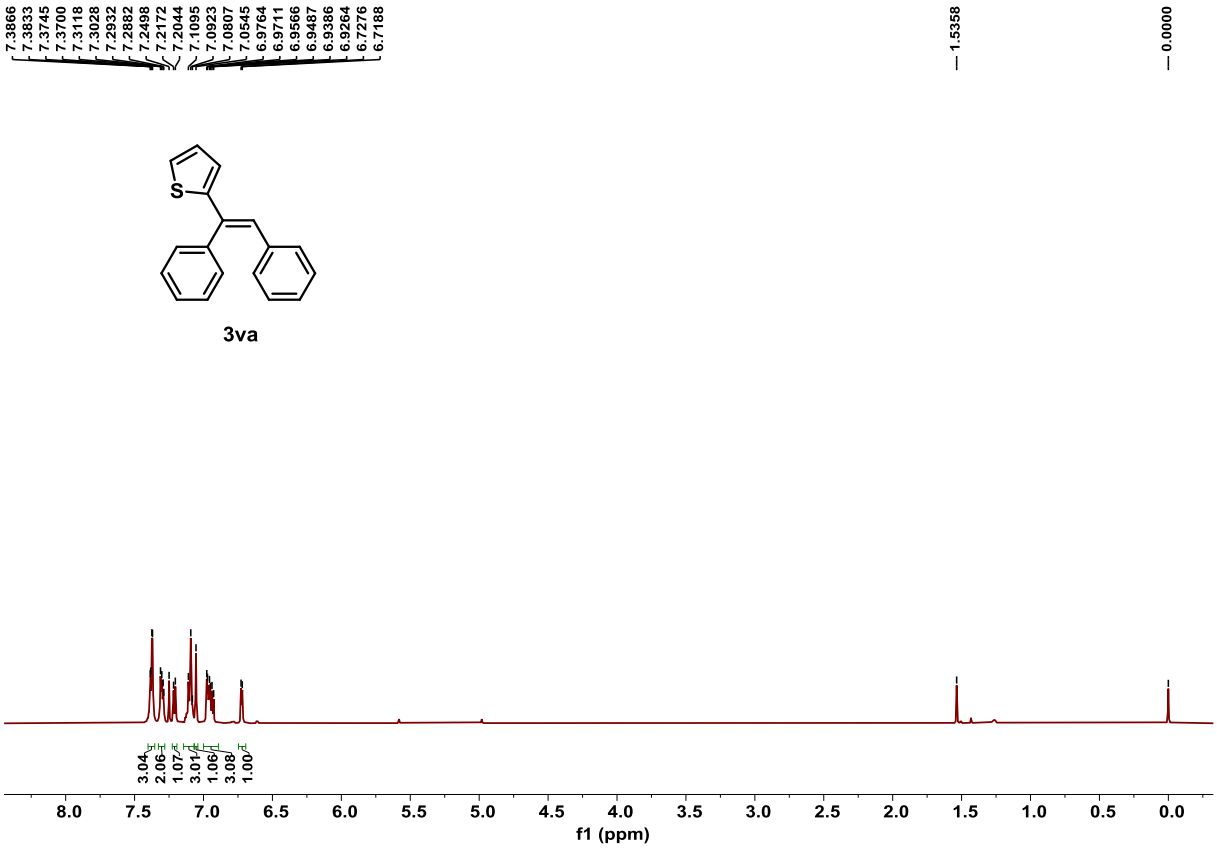

Figure S61. ^{1}H NMR spectrum of product **3va**, related to **Scheme 2**.

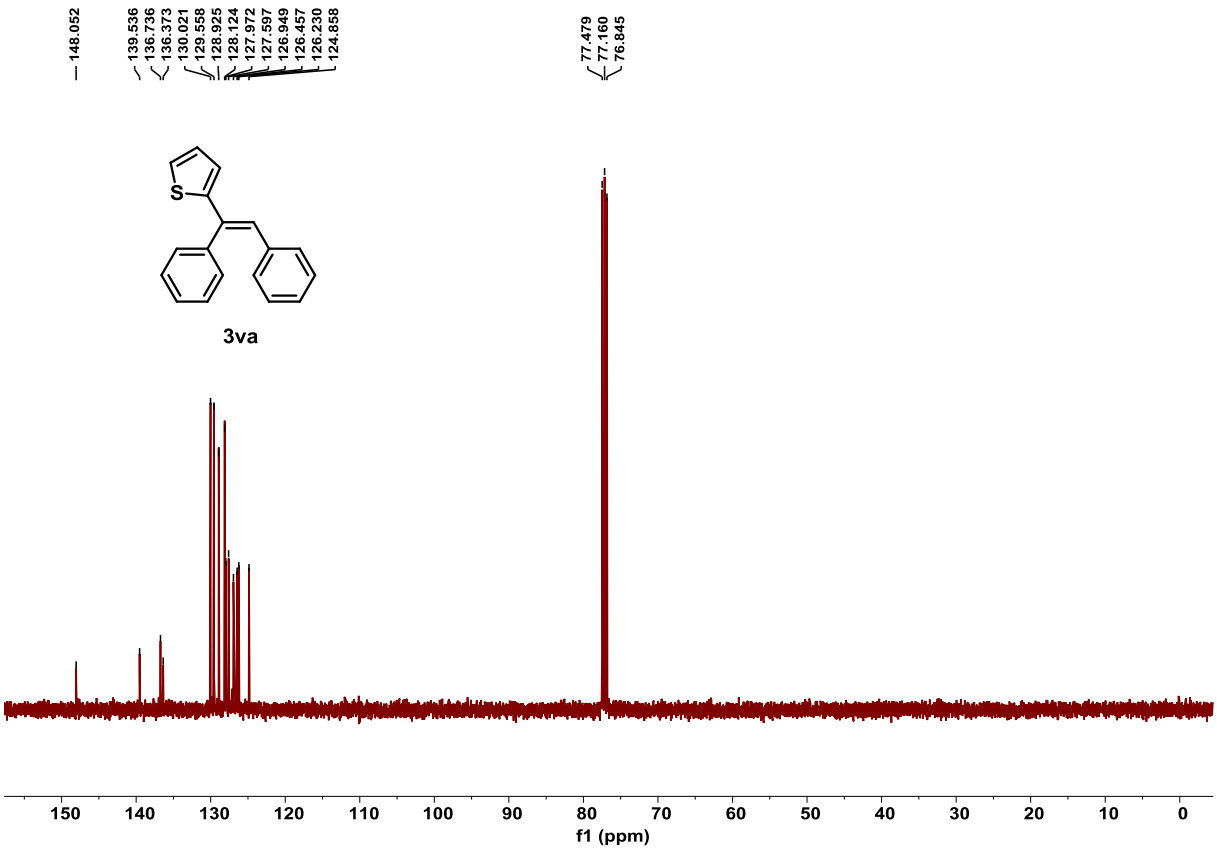

Figure S62. ^{13}C NMR spectrum of product **3va**, related to **Scheme 2**.

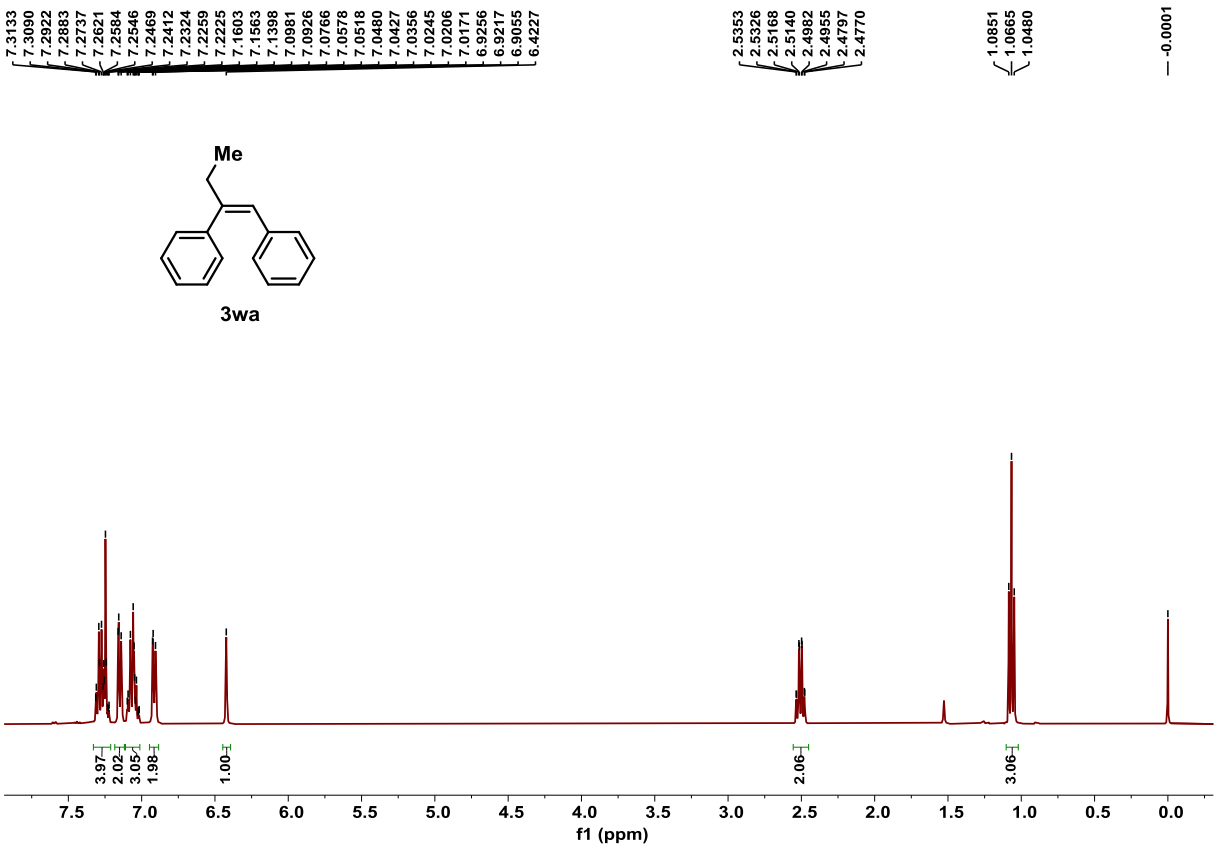

Figure S63. ^{1}**H NMR** spectrum of product **3wa**, related to **Scheme 2**.

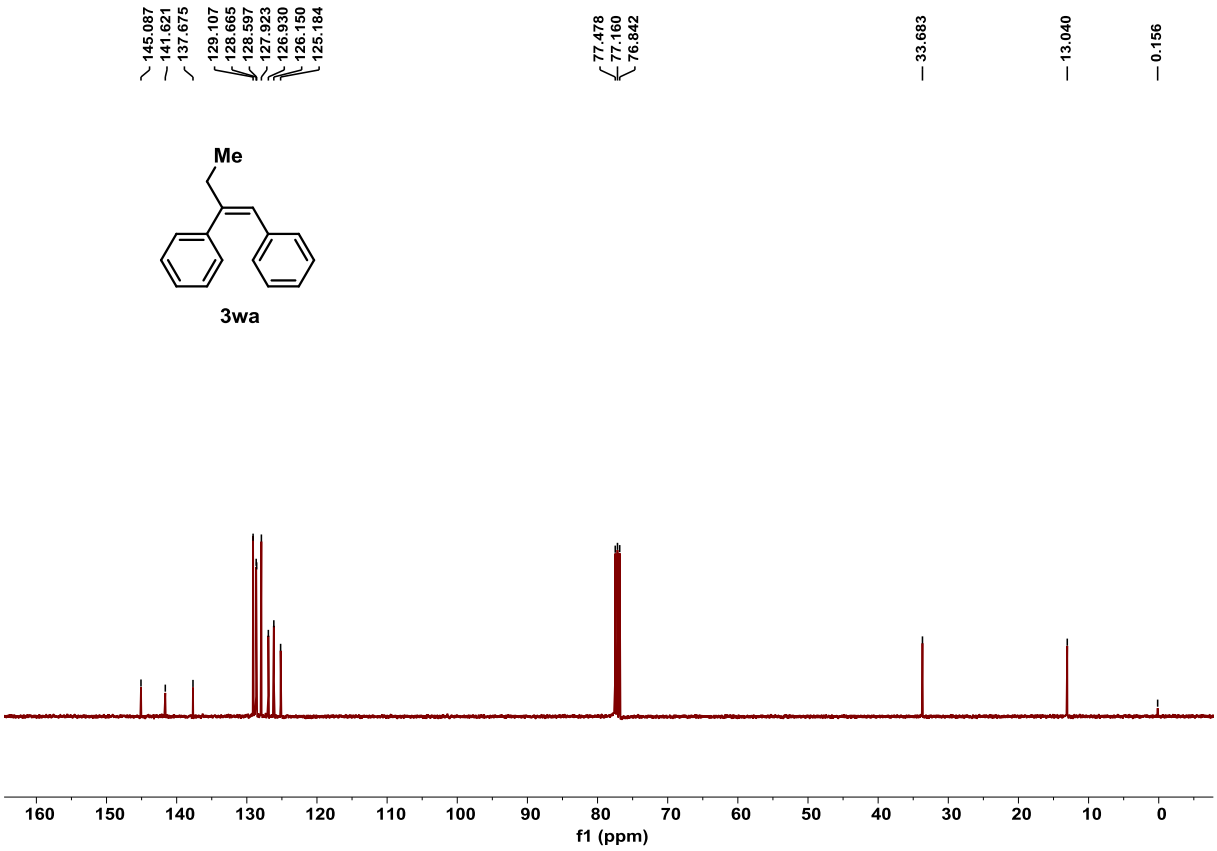

Figure S64. ^{13}**C NMR** spectrum of product **3wa**, related to **Scheme 2**.

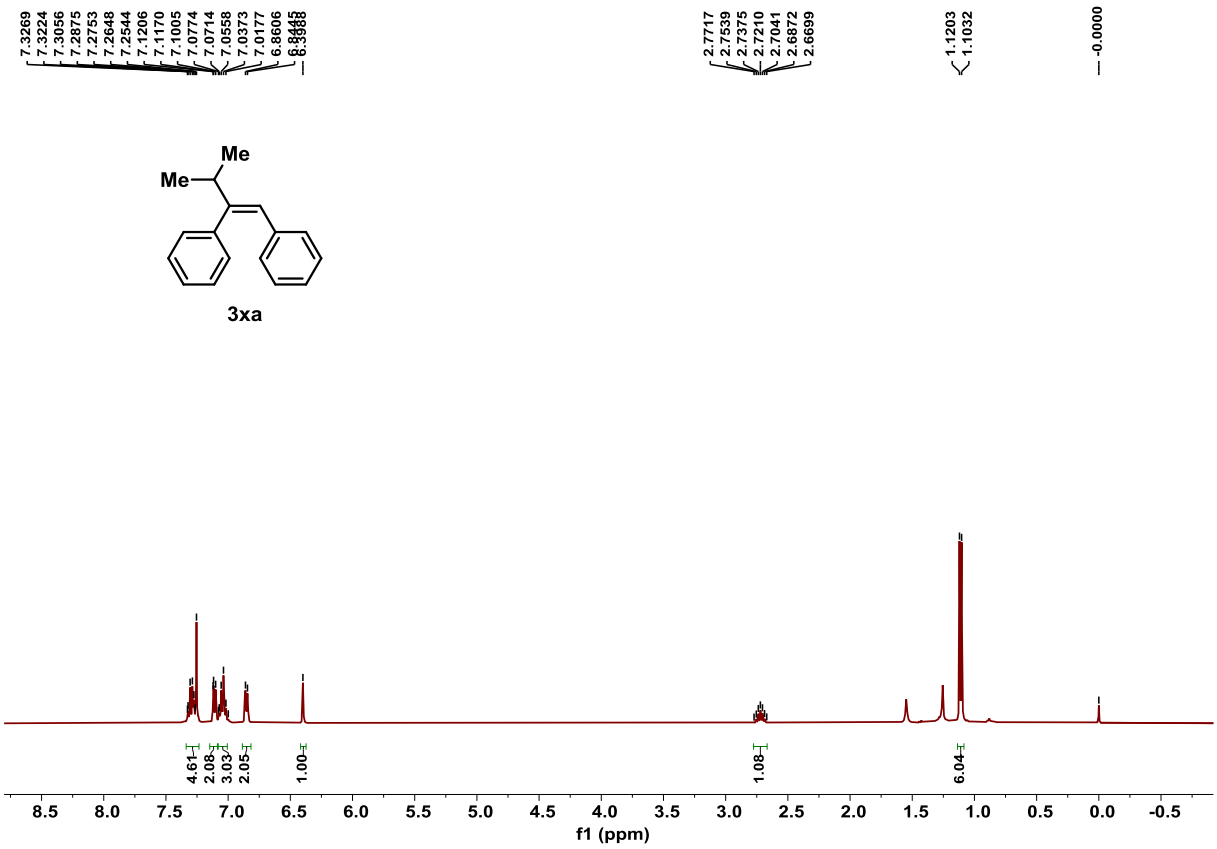

Figure S65. ^{1}H NMR spectrum of product **3xa**, related to **Scheme 2**.

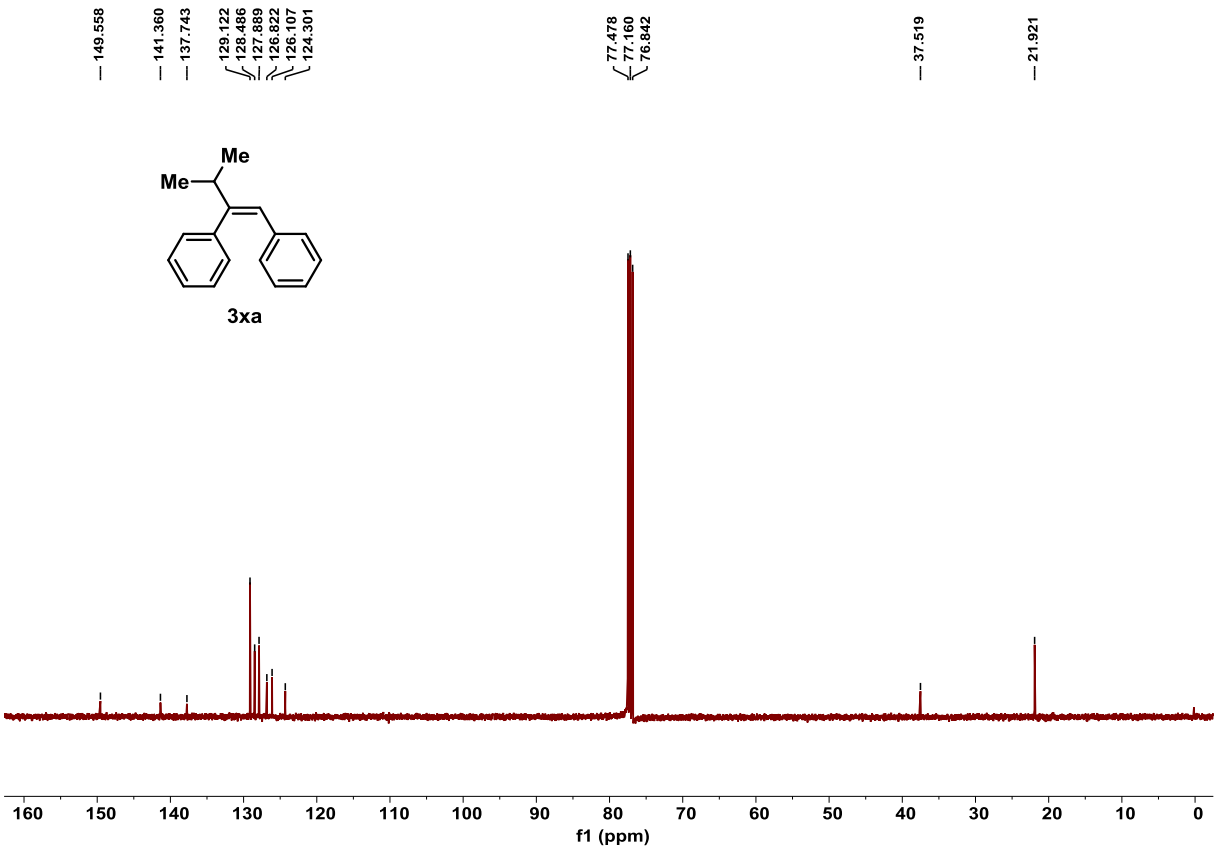

Figure S66. ^{13}C NMR spectrum of product **3xa**, related to **Scheme 2**.

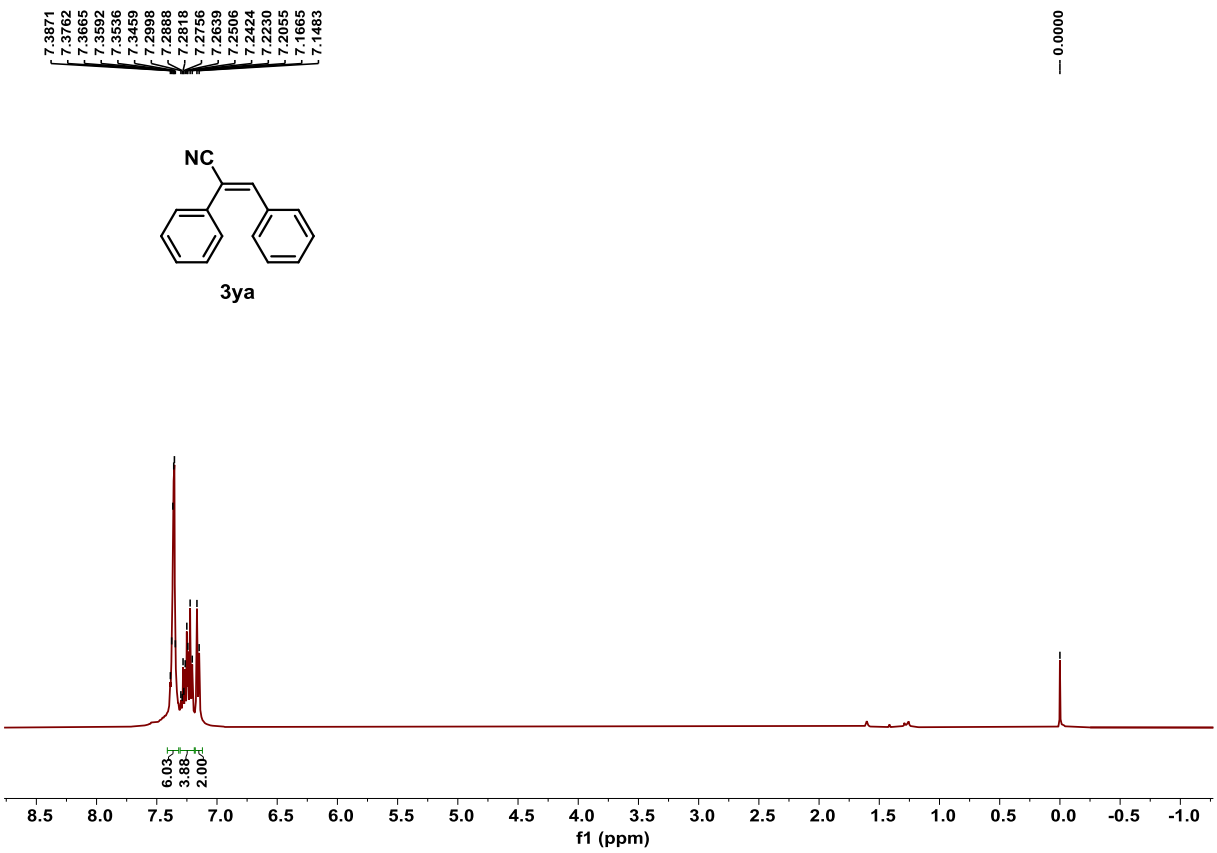

Figure S67. ^{1}**H NMR** spectrum of product **3ya**, related to **Scheme 2**.

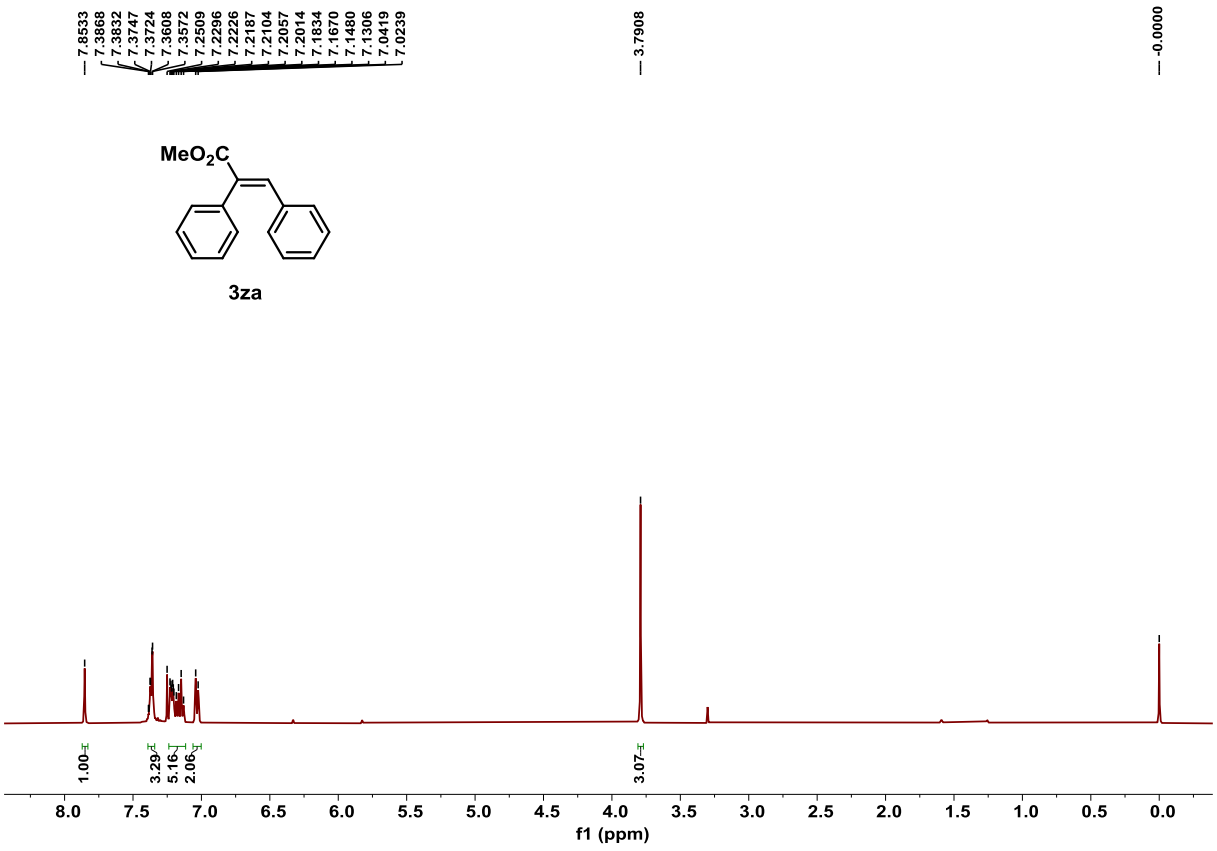

Figure S68. ^{1}**H NMR** spectrum of product **3za**, related to **Scheme 2**.

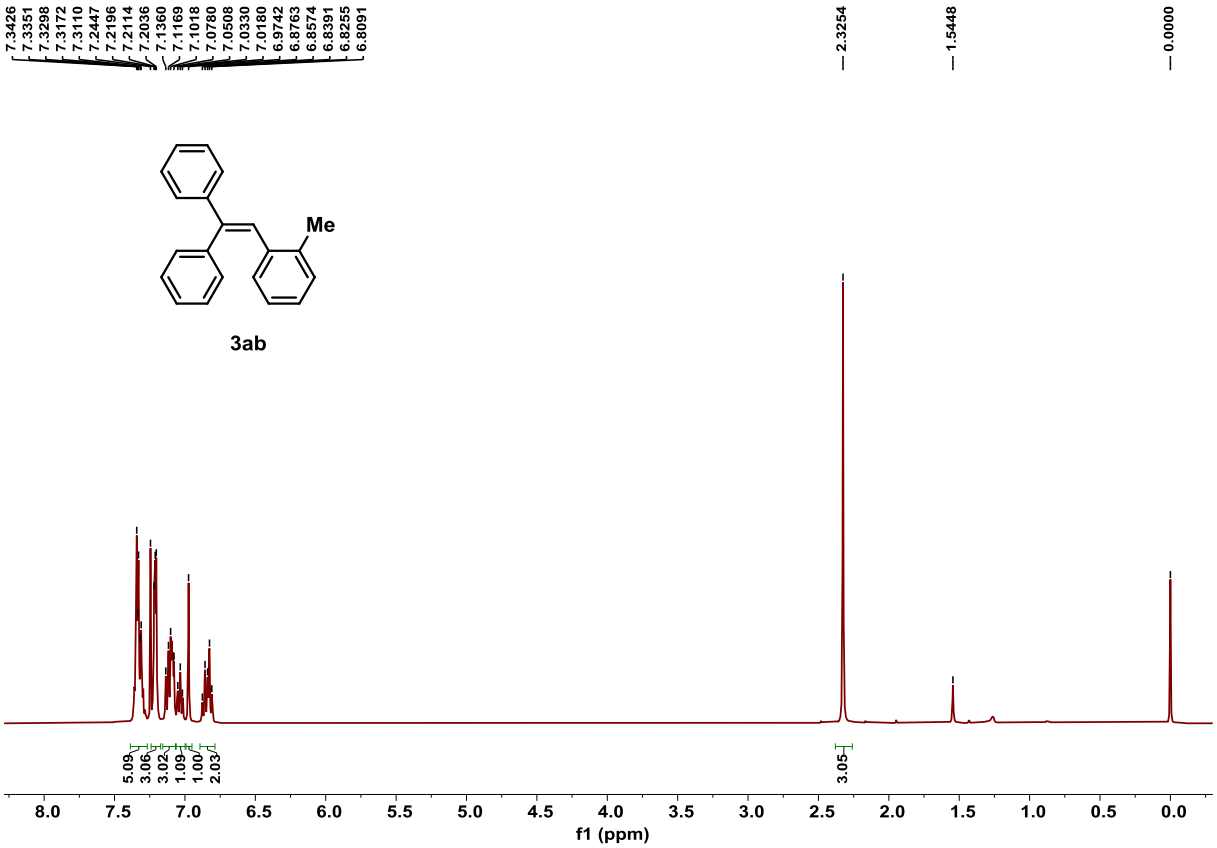

Figure S69. ^{1}H NMR spectrum of product **3ab**, related to **Scheme 2**.

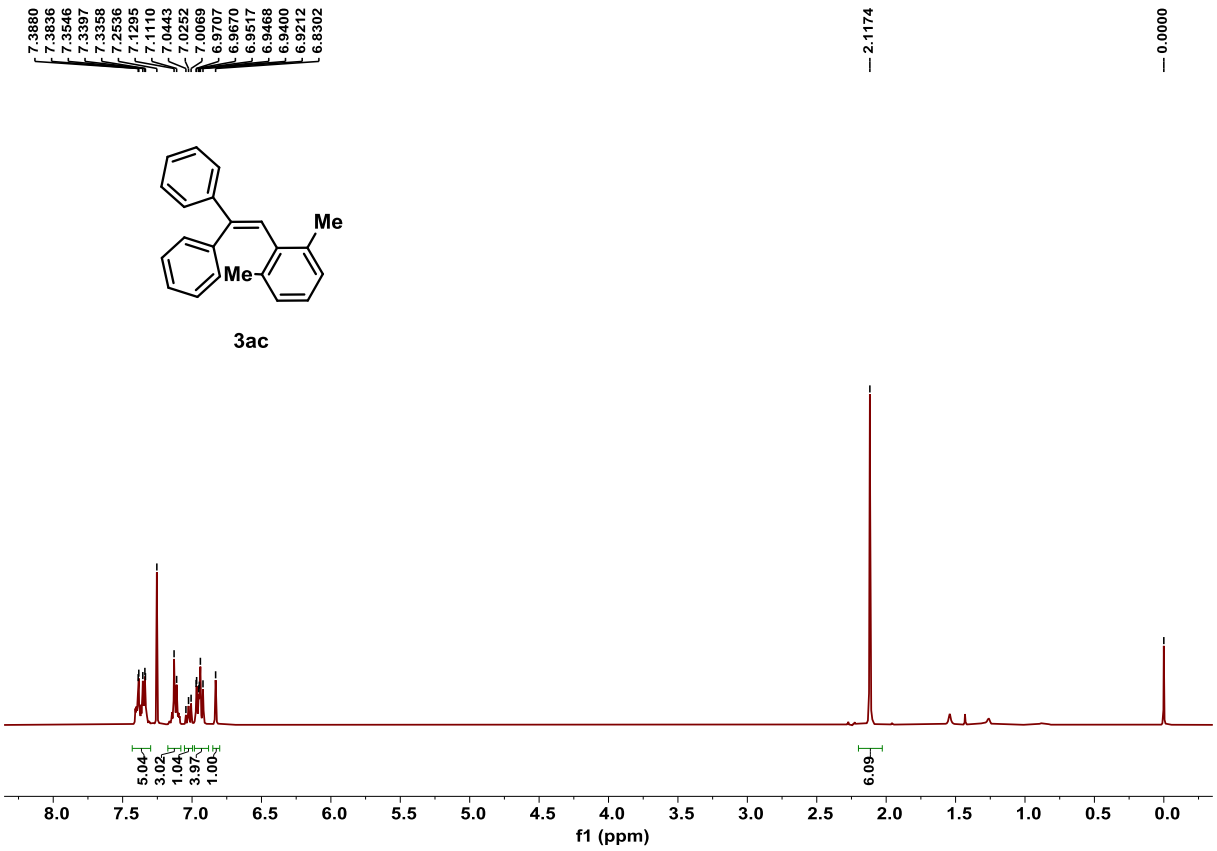

Figure S70. ^{1}H NMR spectrum of product **3ac**, related to **Scheme 2**.

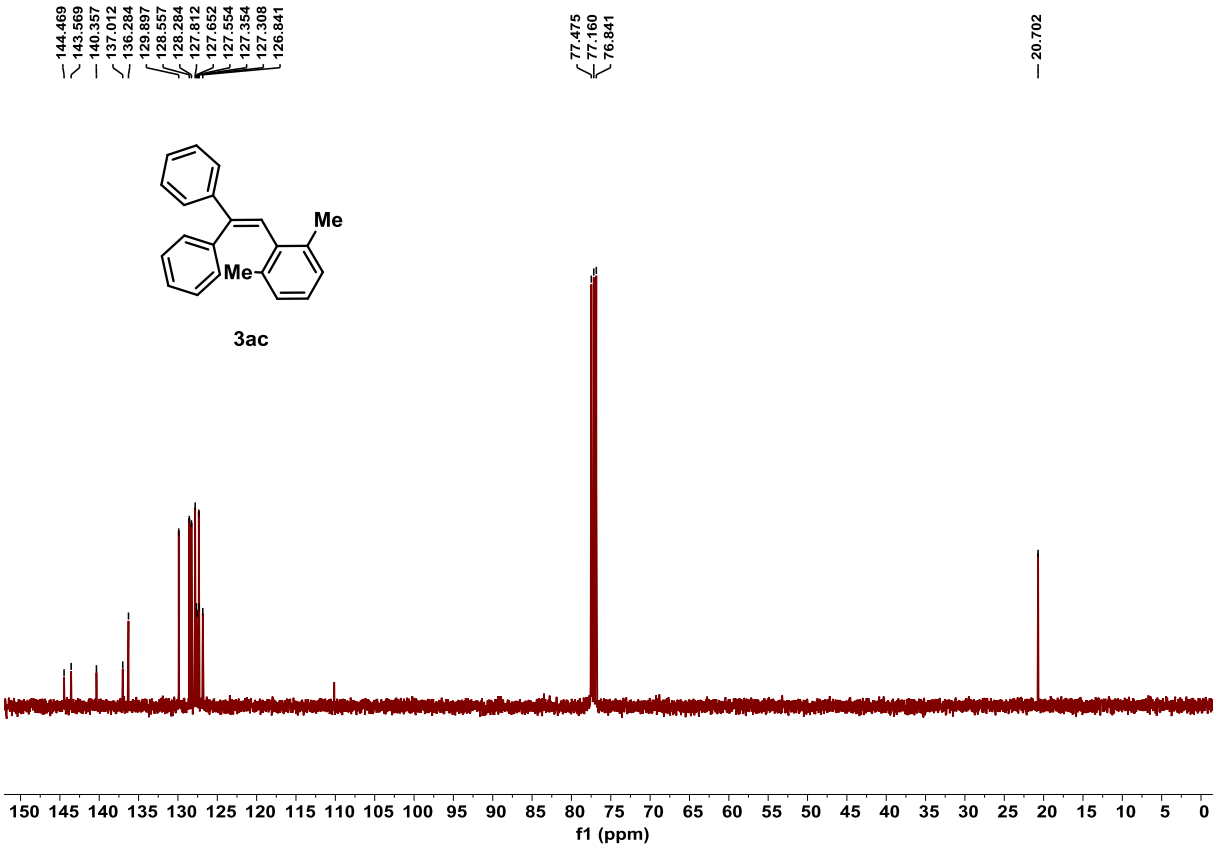

Figure S71. ^{13}**C NMR** spectrum of product **3ac**, related to **Scheme 2**.

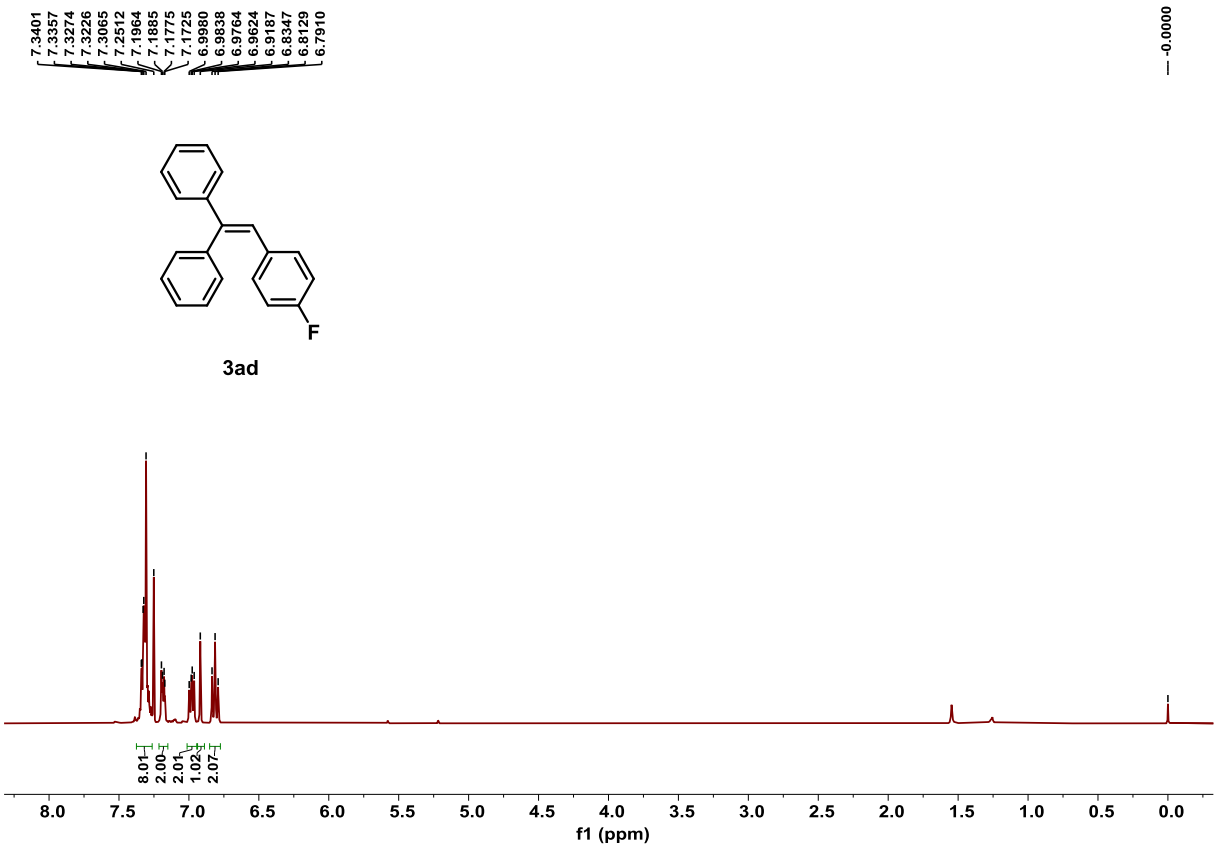

Figure S72. ^{1}**H NMR** spectrum of product **3ad**, related to **Scheme 2**.

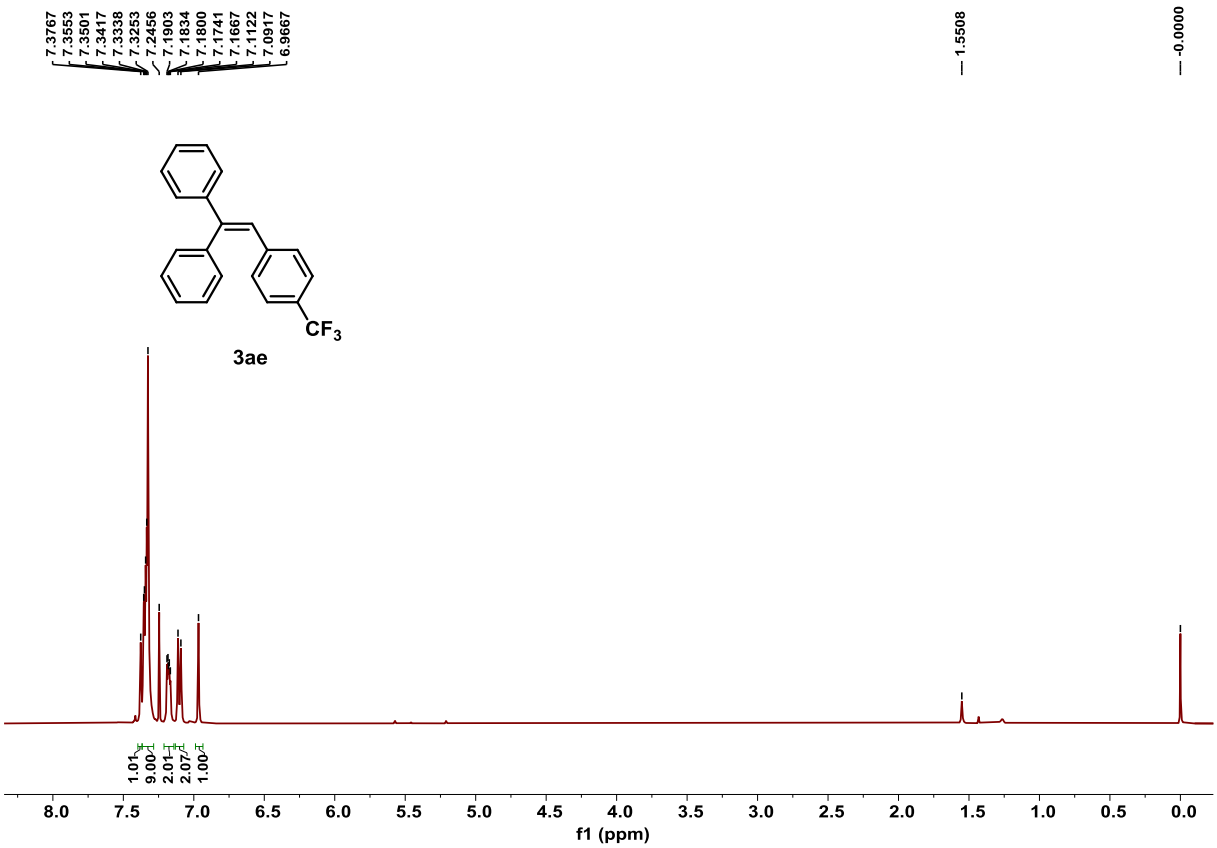

Figure S73. ^{1}**H NMR** spectrum of product **3ae**, related to **Scheme 2**.

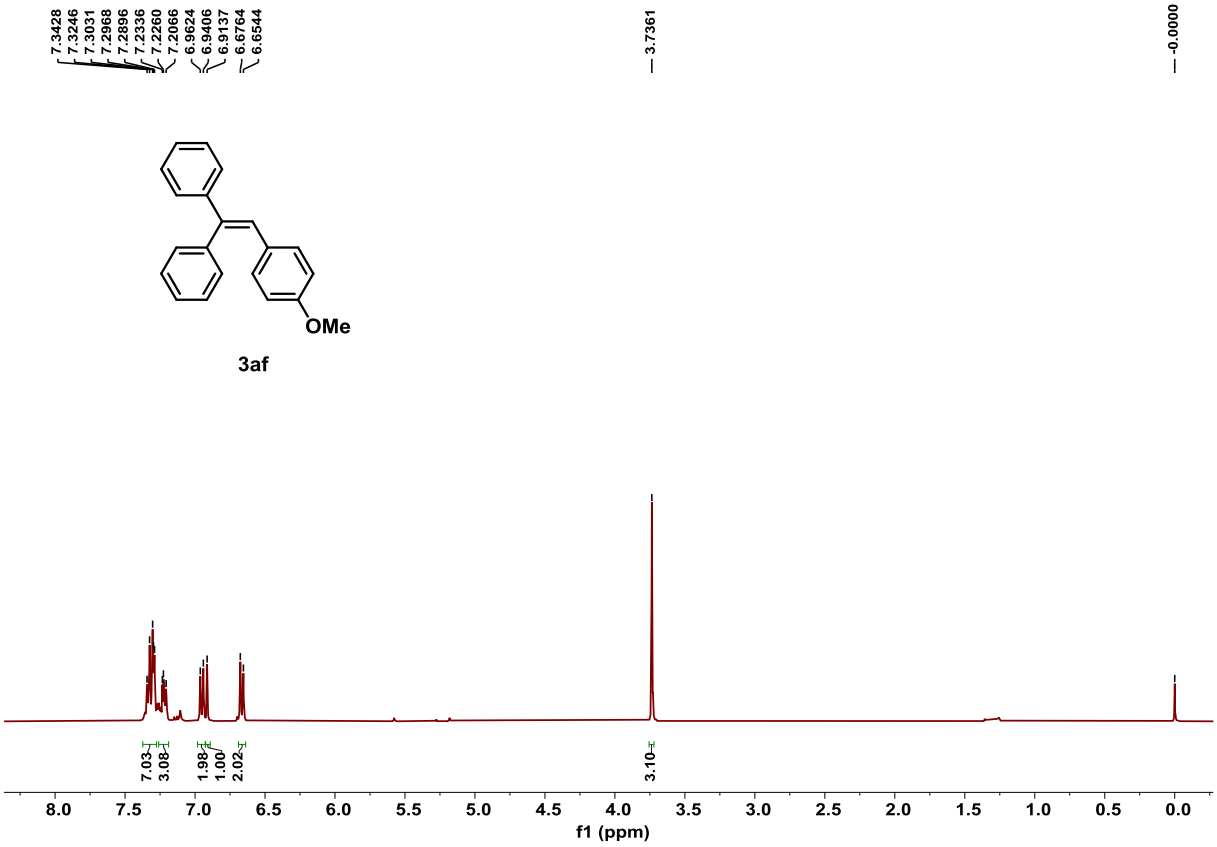

Figure S74. ^{1}**H NMR** spectrum of product **3af**, related to **Scheme 2**.

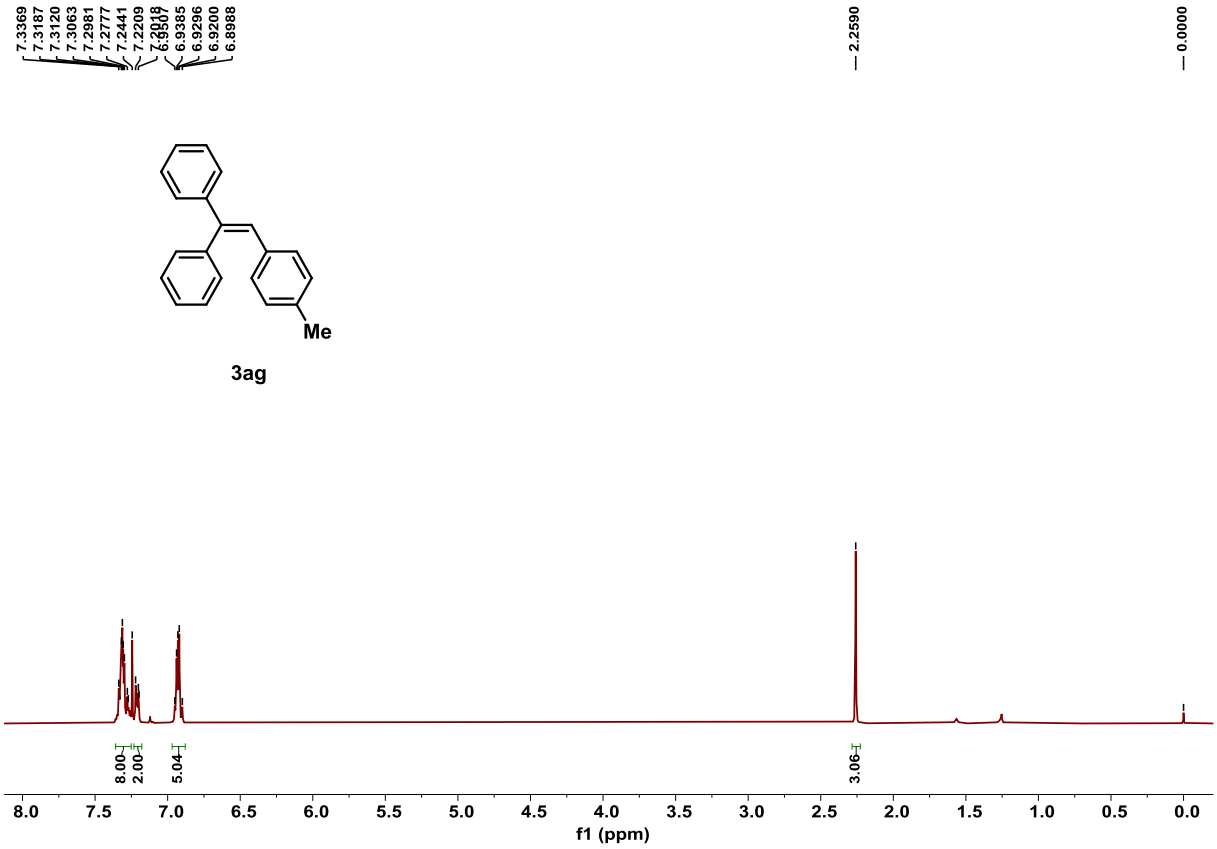

Figure S74. ^{1}**H NMR** spectrum of product **3ag**, related to **Scheme 2**.

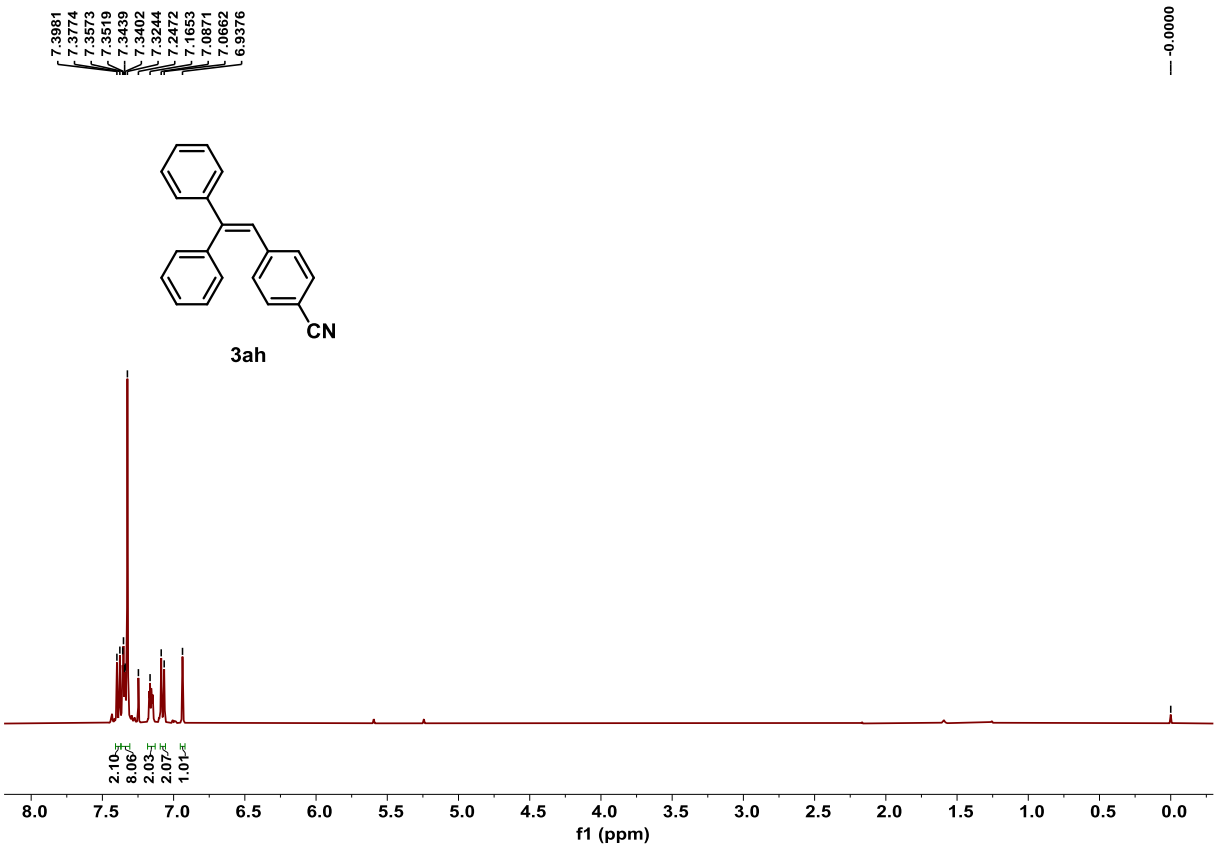

Figure S76. ^{1}**H NMR** spectrum of product **3ah**, related to **Scheme 2**.

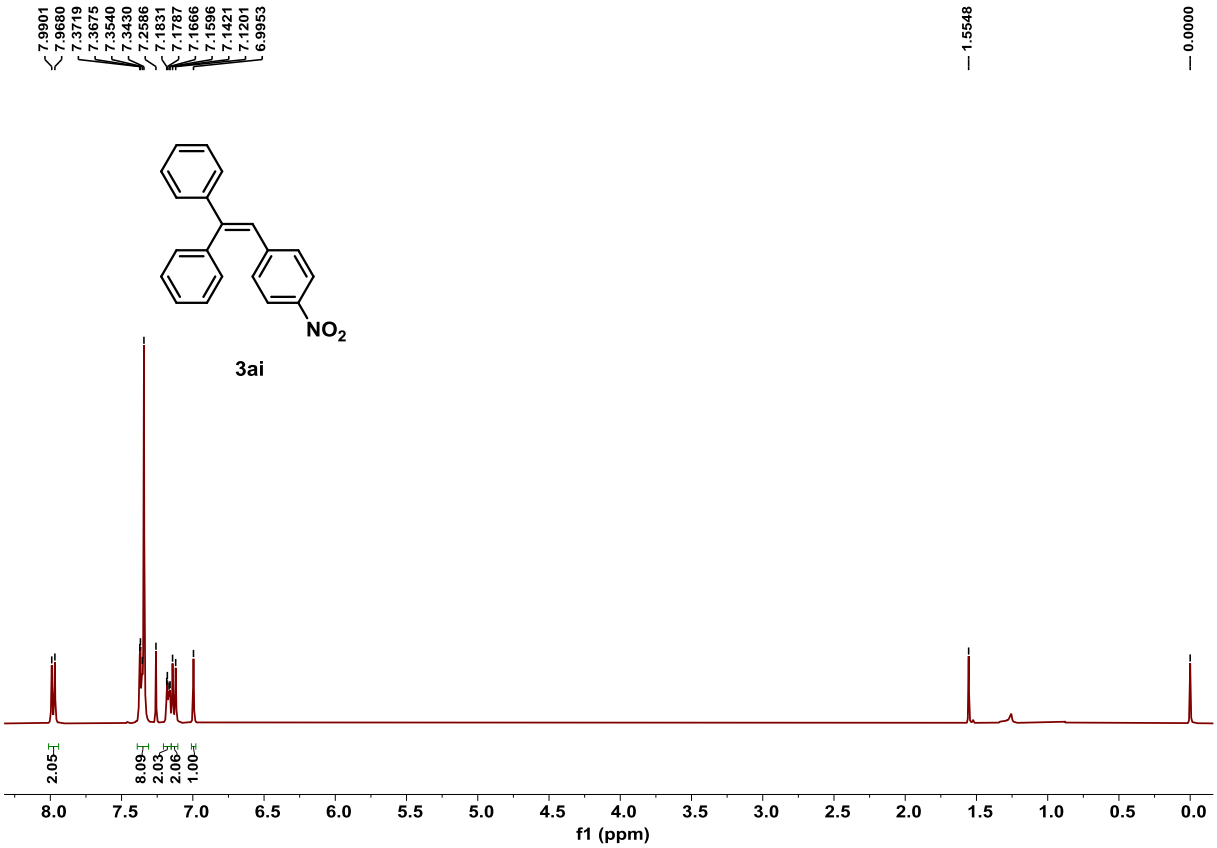

Figure S77. ^{1}H NMR spectrum of product **3ai**, related to **Scheme 2**.

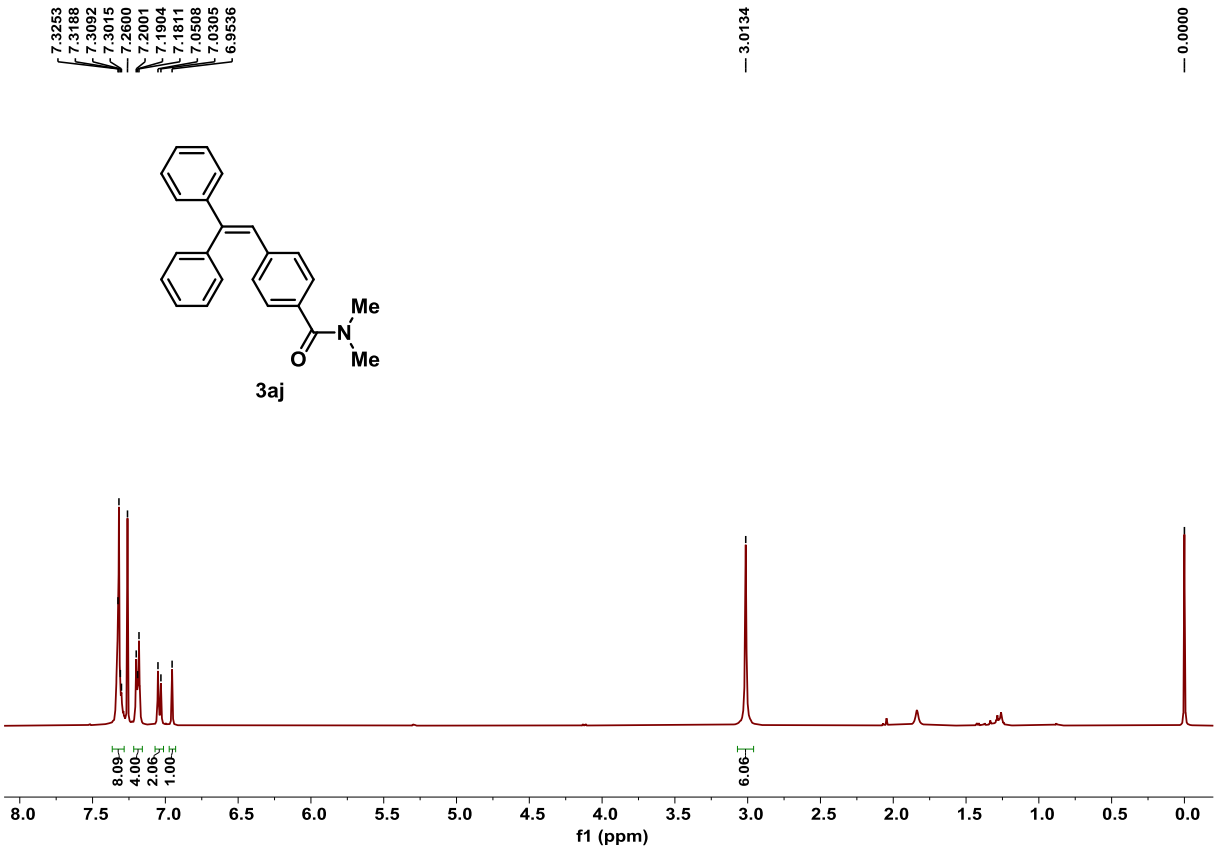

Figure S78. ^{1}H NMR spectrum of product **3aj**, related to **Scheme 2**.

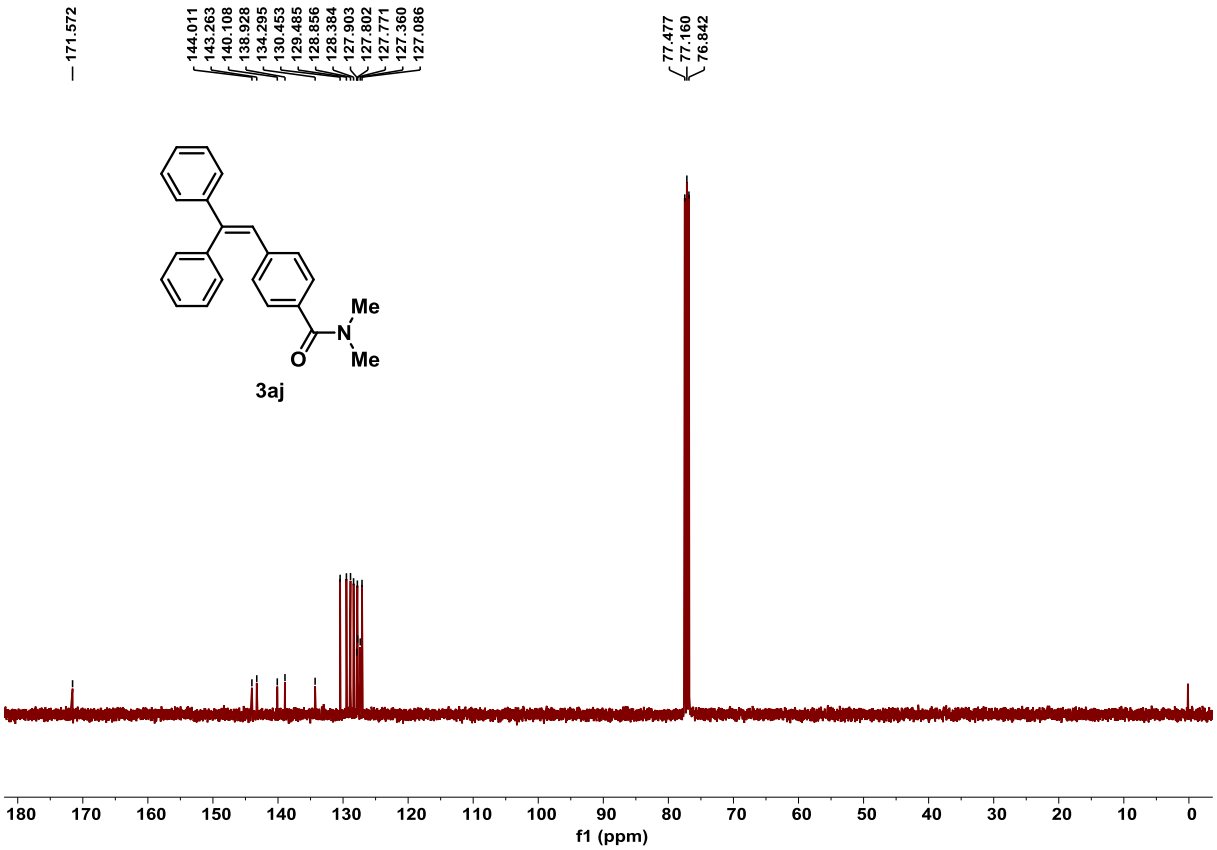

Figure S79. ^{13}**C NMR** spectrum of product **3aj**, related to **Scheme 2**.

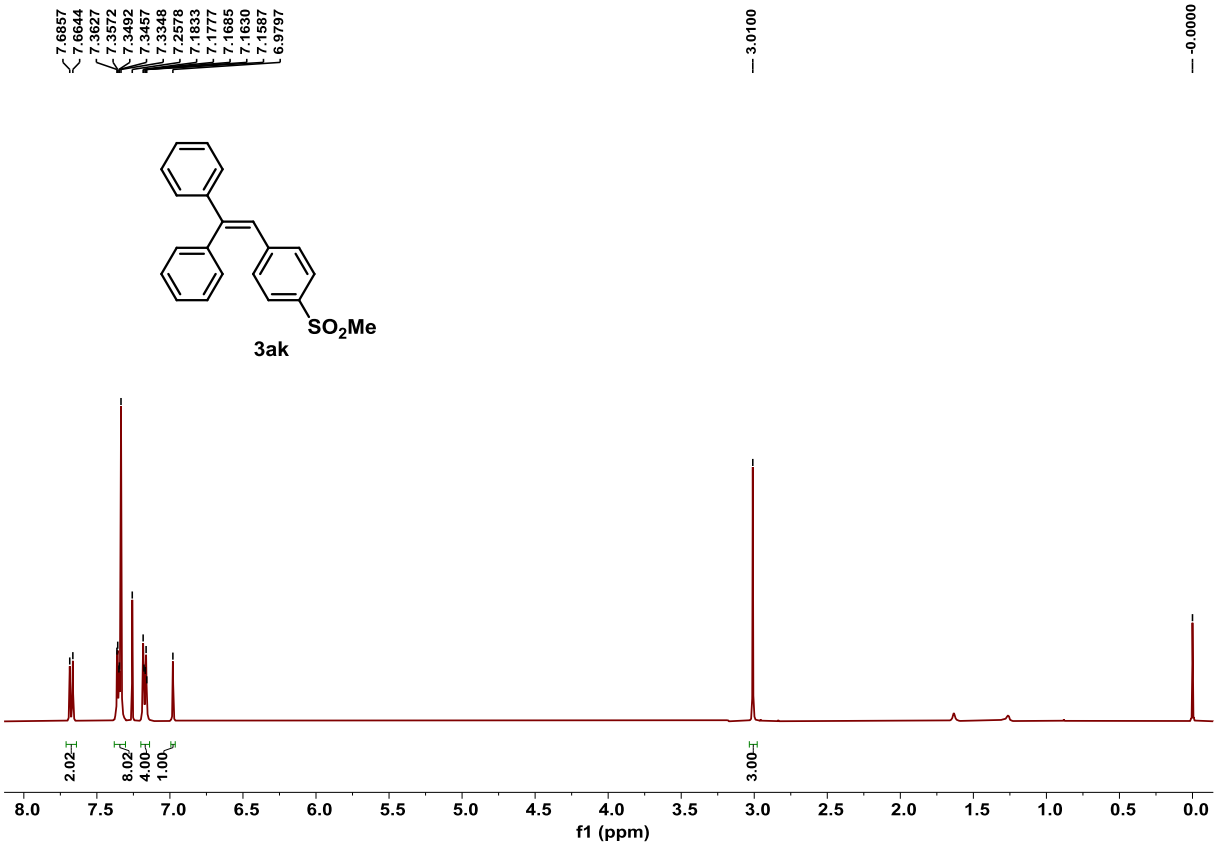

Figure S80. ^{1}**H NMR** spectrum of product **3ak**, related to **Scheme 2**.

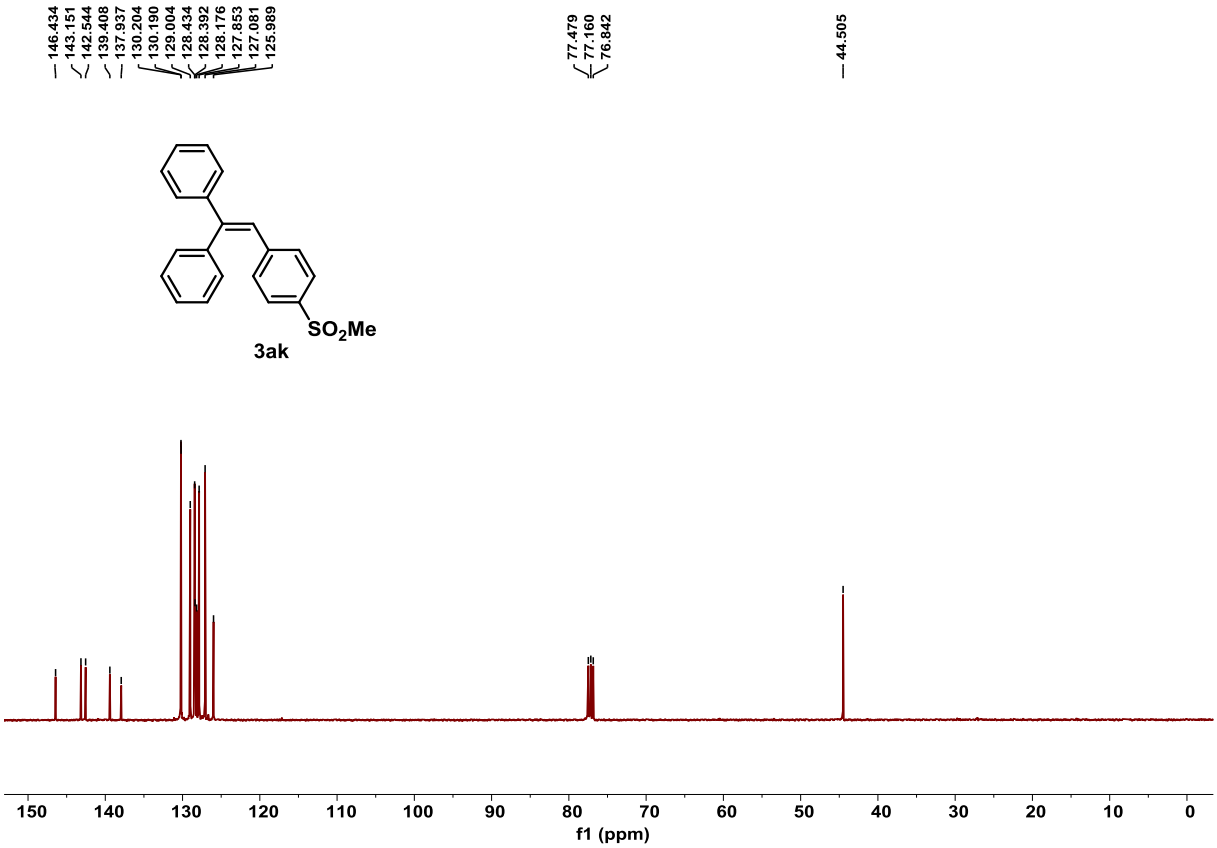

Figure S81. ^{13}**C NMR** spectrum of product **3ak**, related to **Scheme 2**.

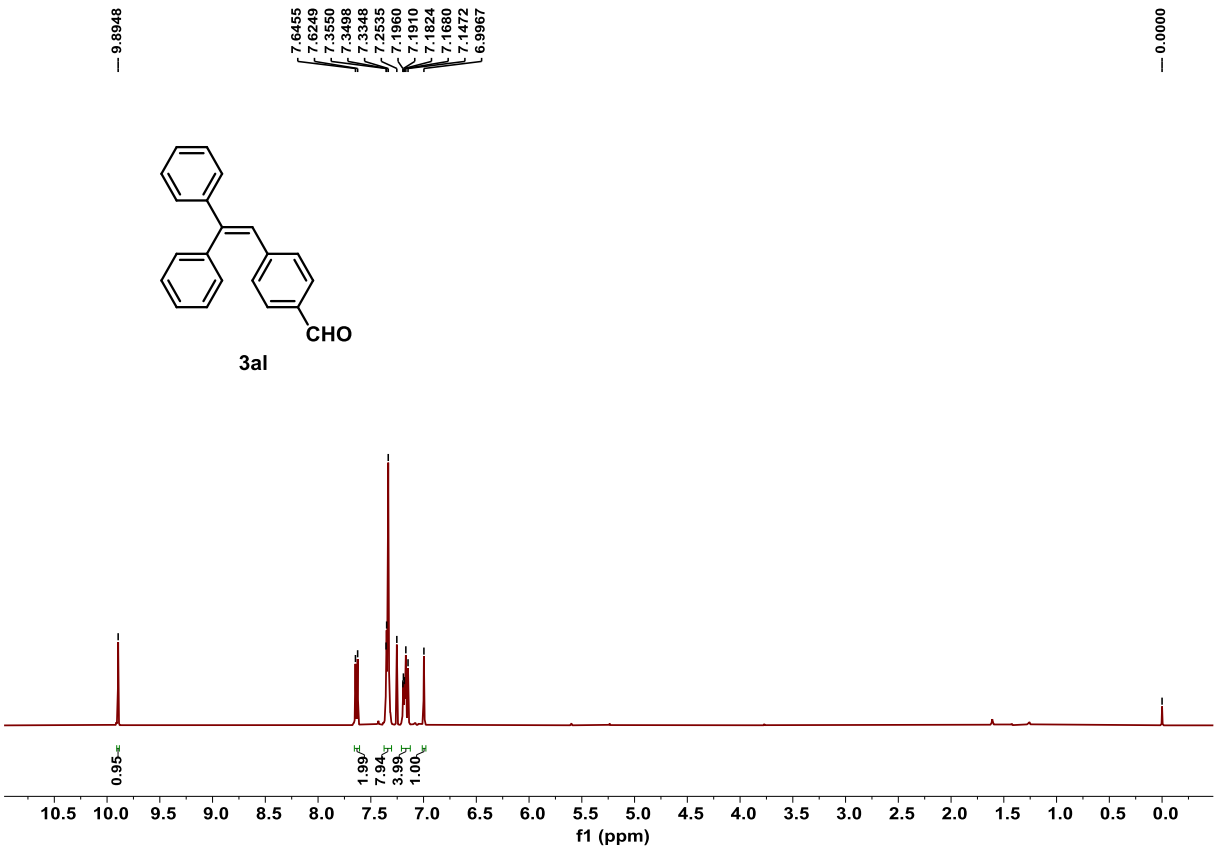

Figure S82. ^{1}**H NMR** spectrum of product **3al**, related to **Scheme 2**.

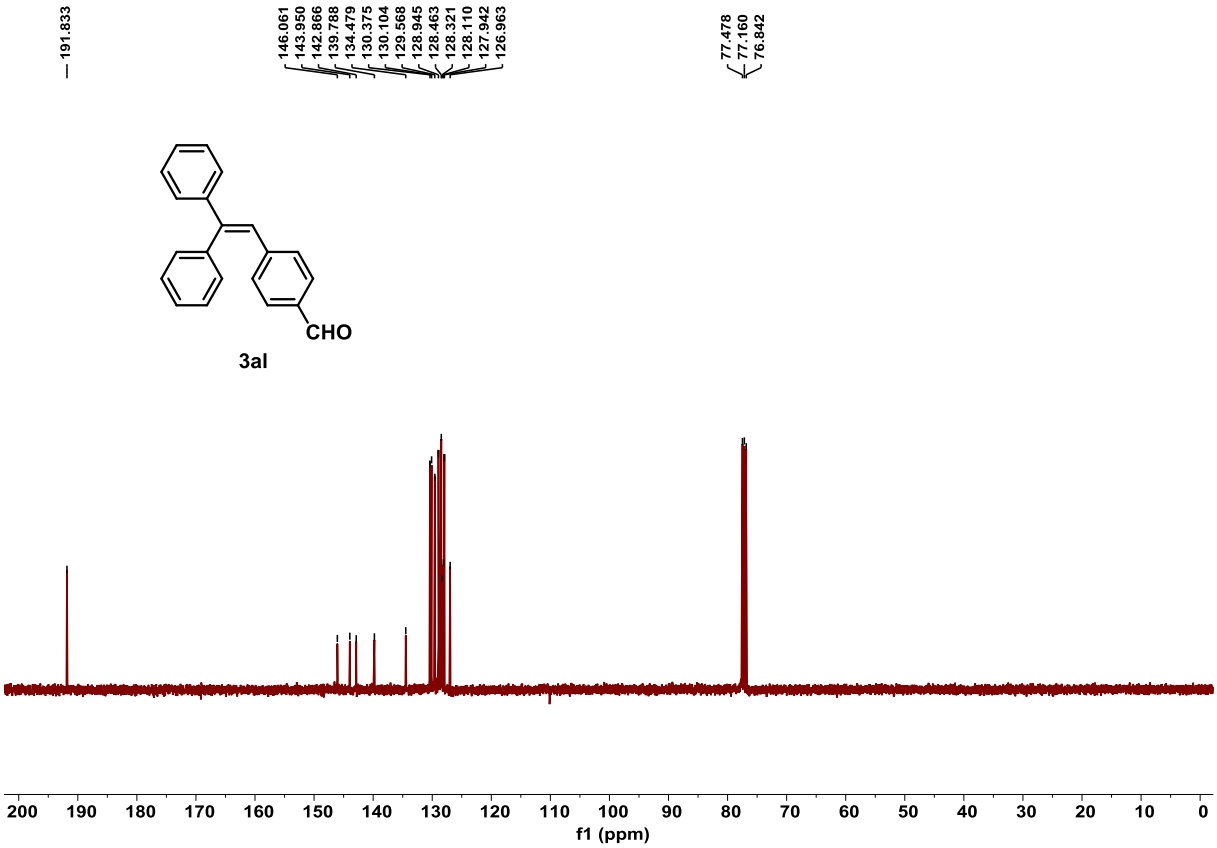

Figure S83. ^{13}**C NMR** spectrum of product **3al**, related to **Scheme 2**.

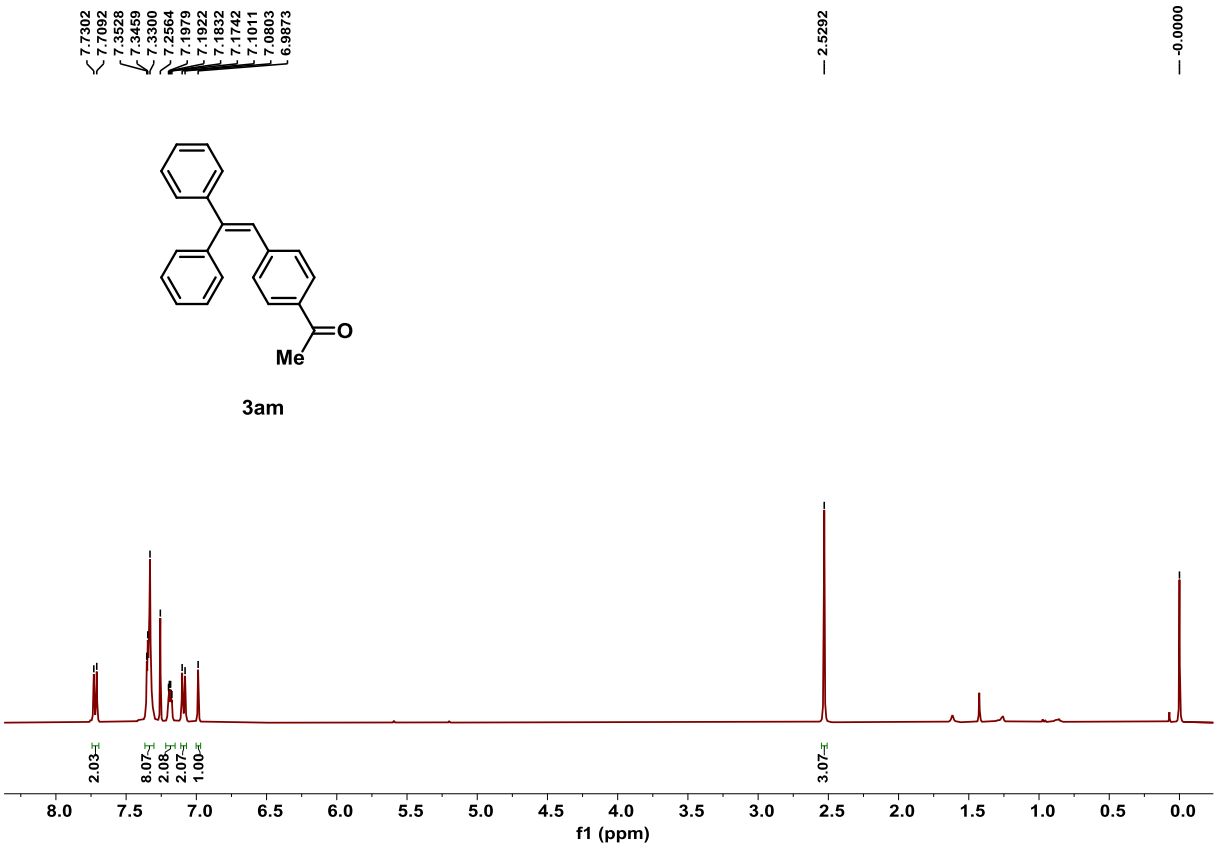

Figure S84. ^{1}**H NMR** spectrum of product **3am**, related to **Scheme 2**.

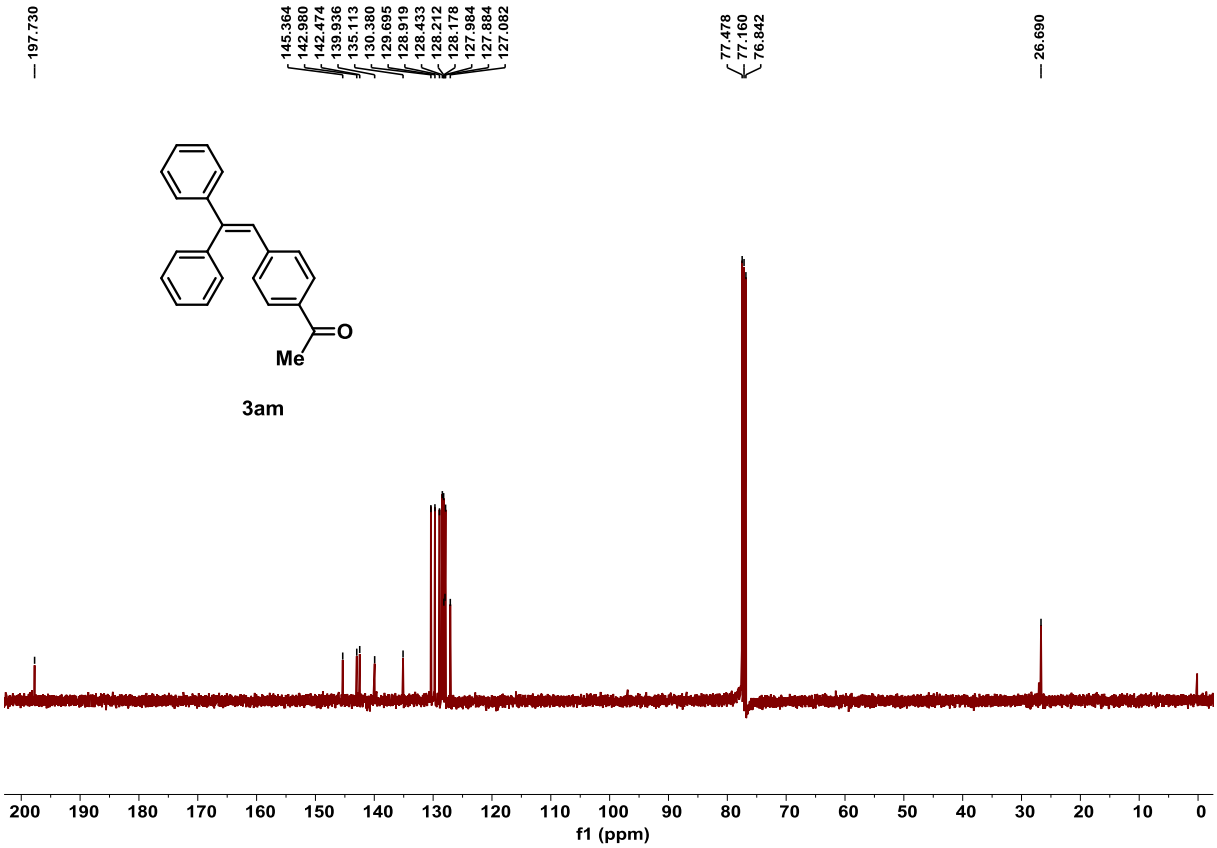

Figure S85. ^{13}**C NMR** spectrum of product **3am**, related to **Scheme 2**.

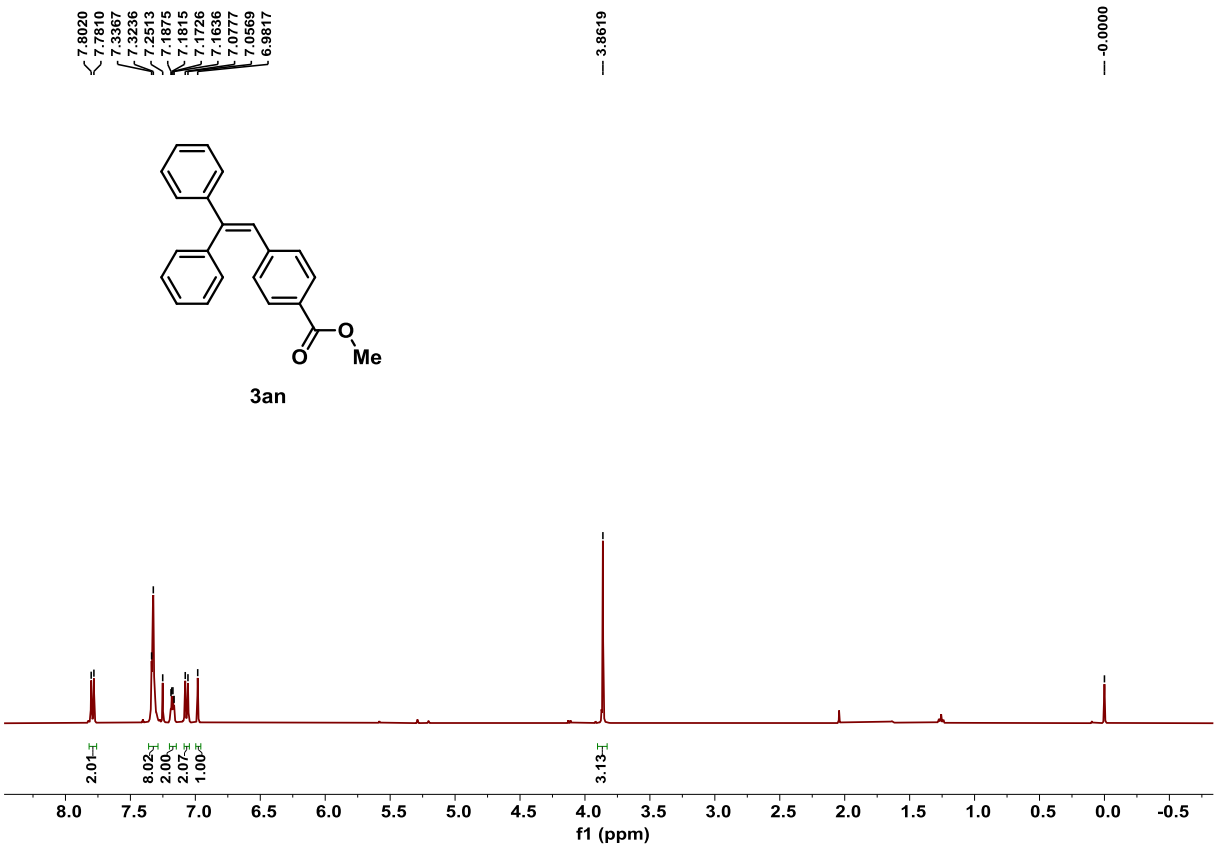

Figure S86. ^{1}**H NMR** spectrum of product **3an**, related to **Scheme 2**.

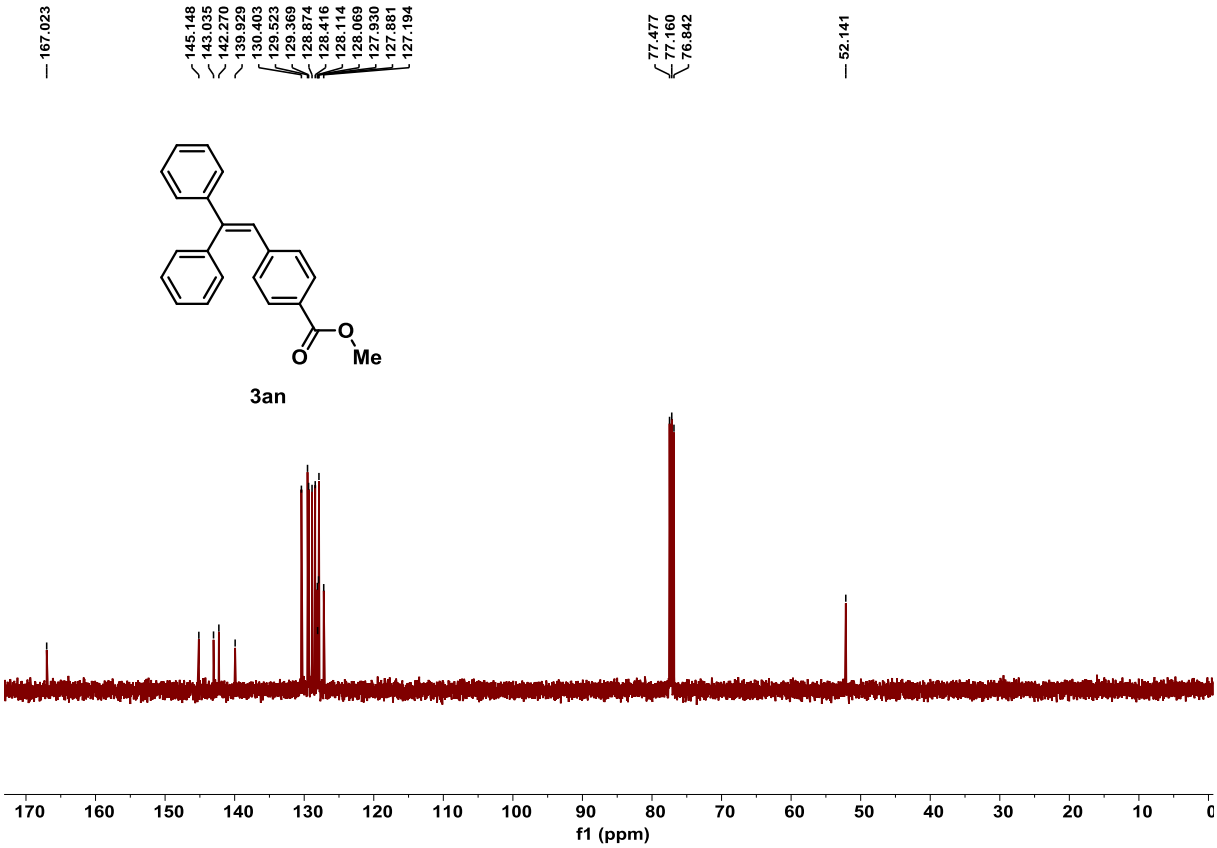

Figure S87. ^{13}**C NMR** spectrum of product **3an**, related to **Scheme 2**.

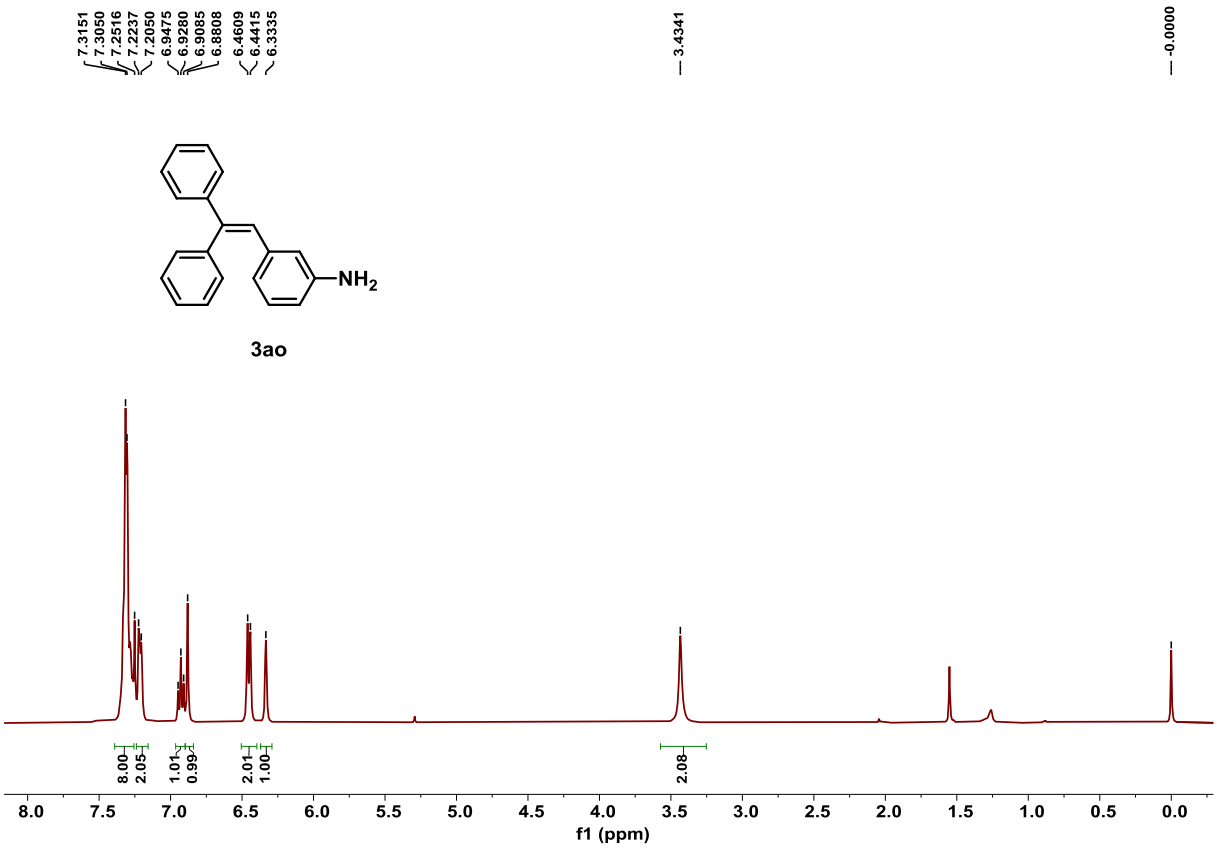

Figure S88. ^{1}**H NMR** spectrum of product **3ao**, related to **Scheme 2**.

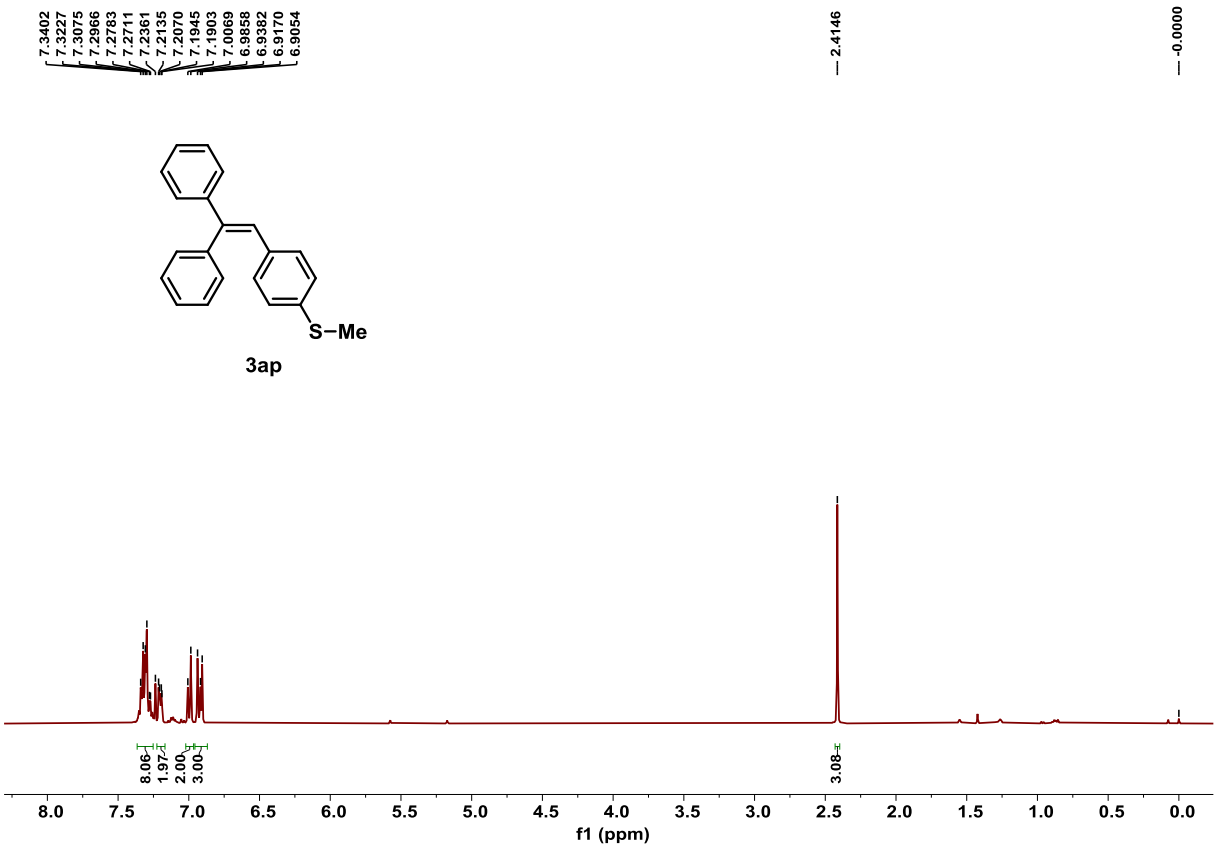

Figure S89. ^{1}**H NMR** spectrum of product **3ap**, related to **Scheme 2**.

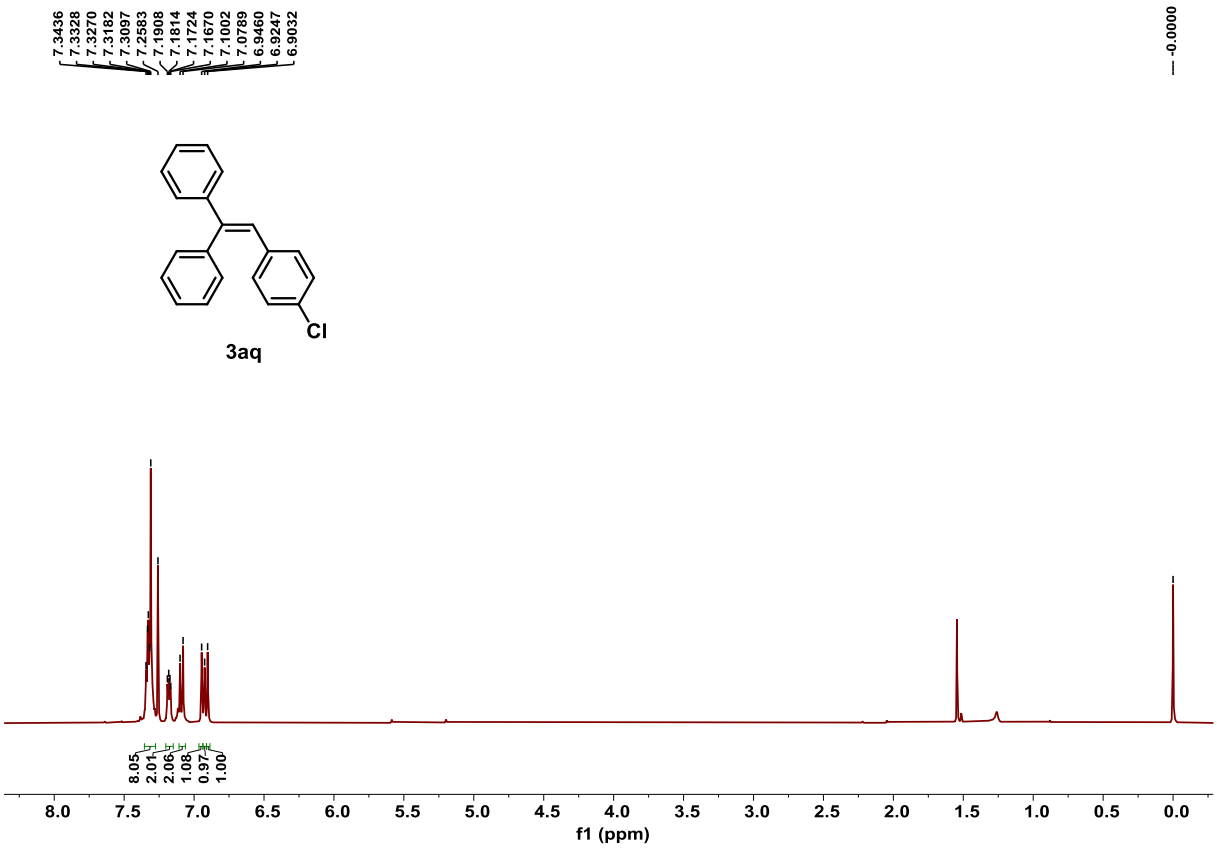

Figure S90. ^{1}**H NMR** spectrum of product **3aq**, related to **Scheme 2**.

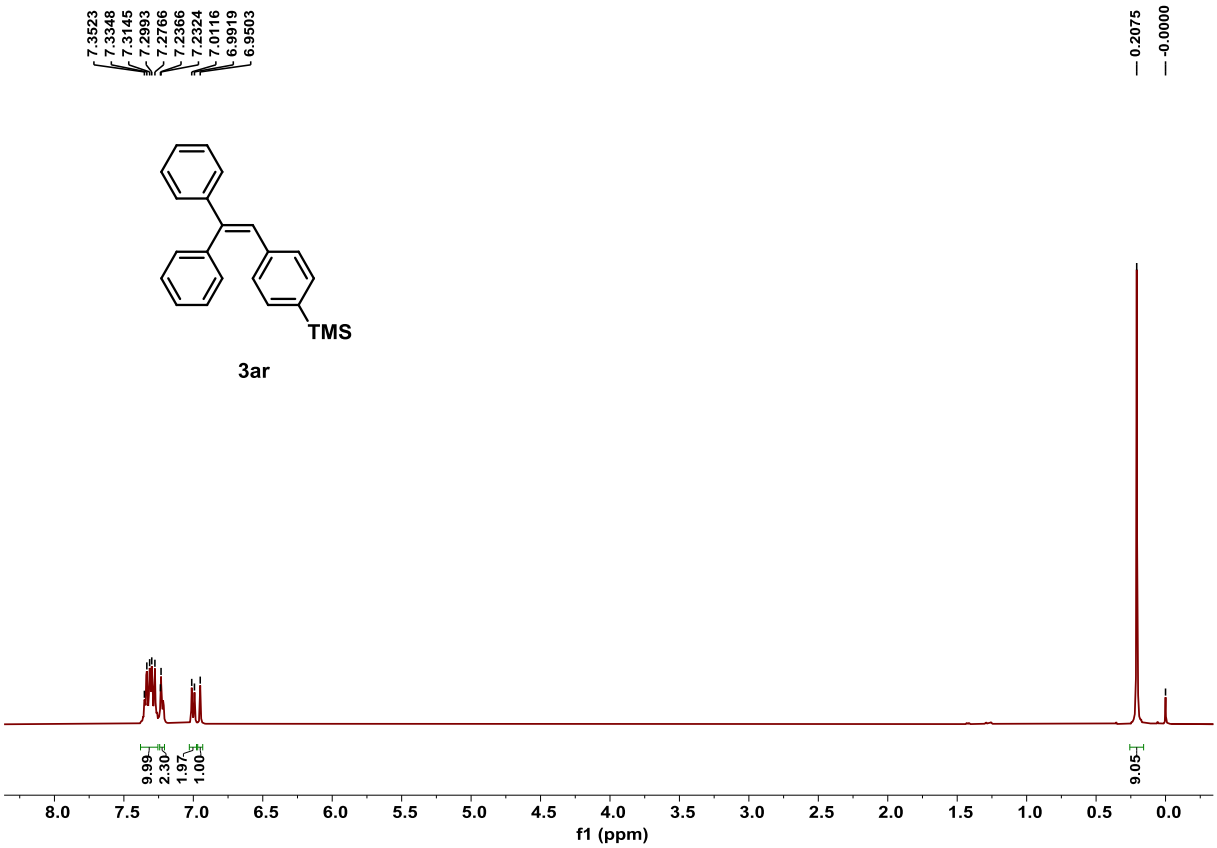

Figure S91. ^{1}H NMR spectrum of product **3ar**, related to **Scheme 2**.

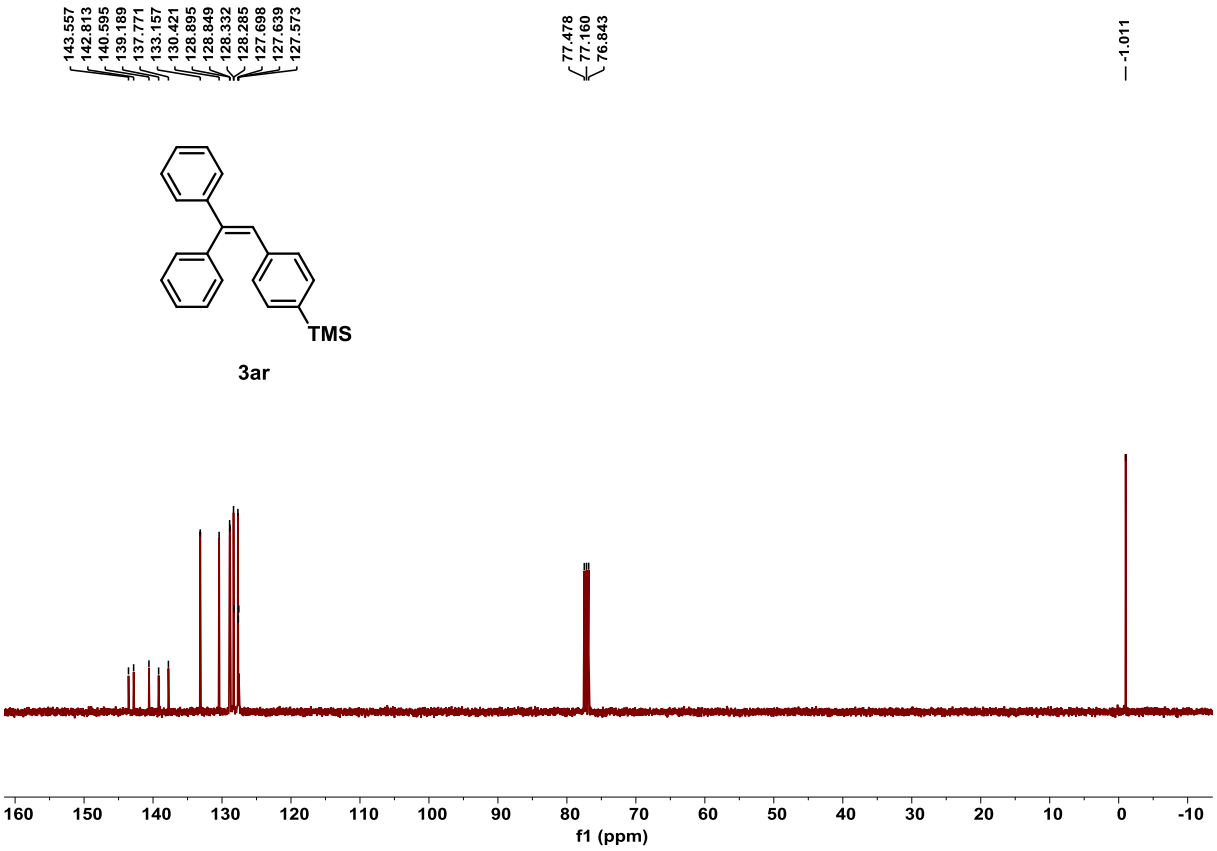

Figure S92. ^{13}C NMR spectrum of product **3ar**, related to **Scheme 2**.

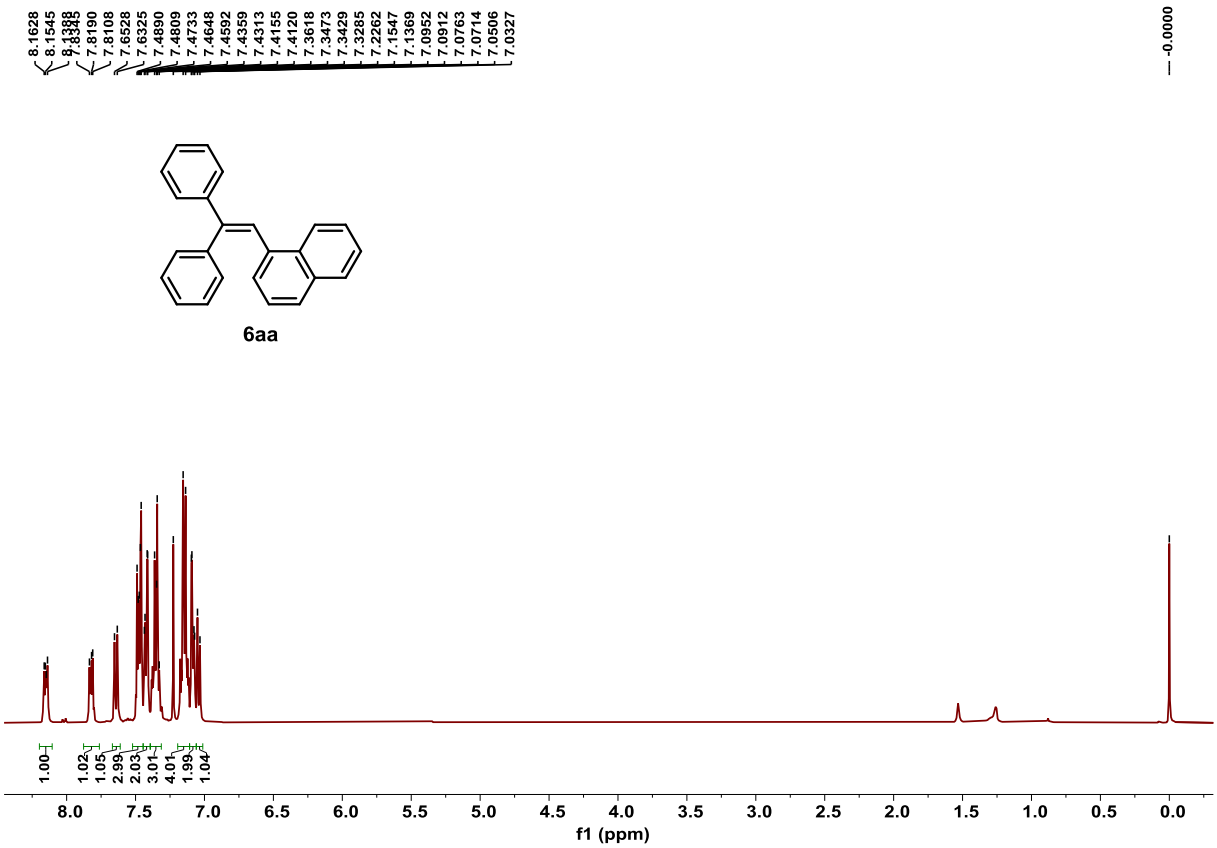

Figure S93. ^{1}H NMR spectrum of product **6aa**, related to **Scheme 3**.

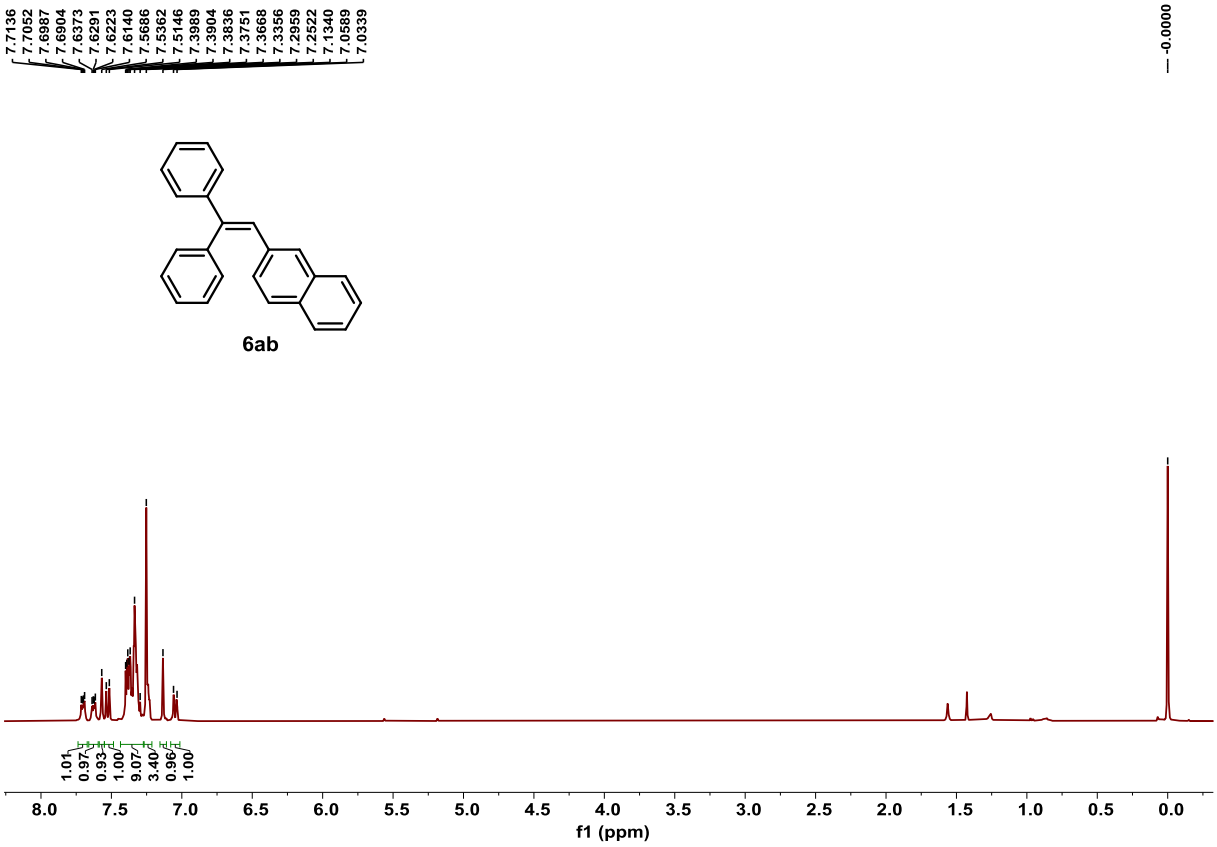

Figure S94. ^{1}H NMR spectrum of product **6ab**, related to **Scheme 3**.

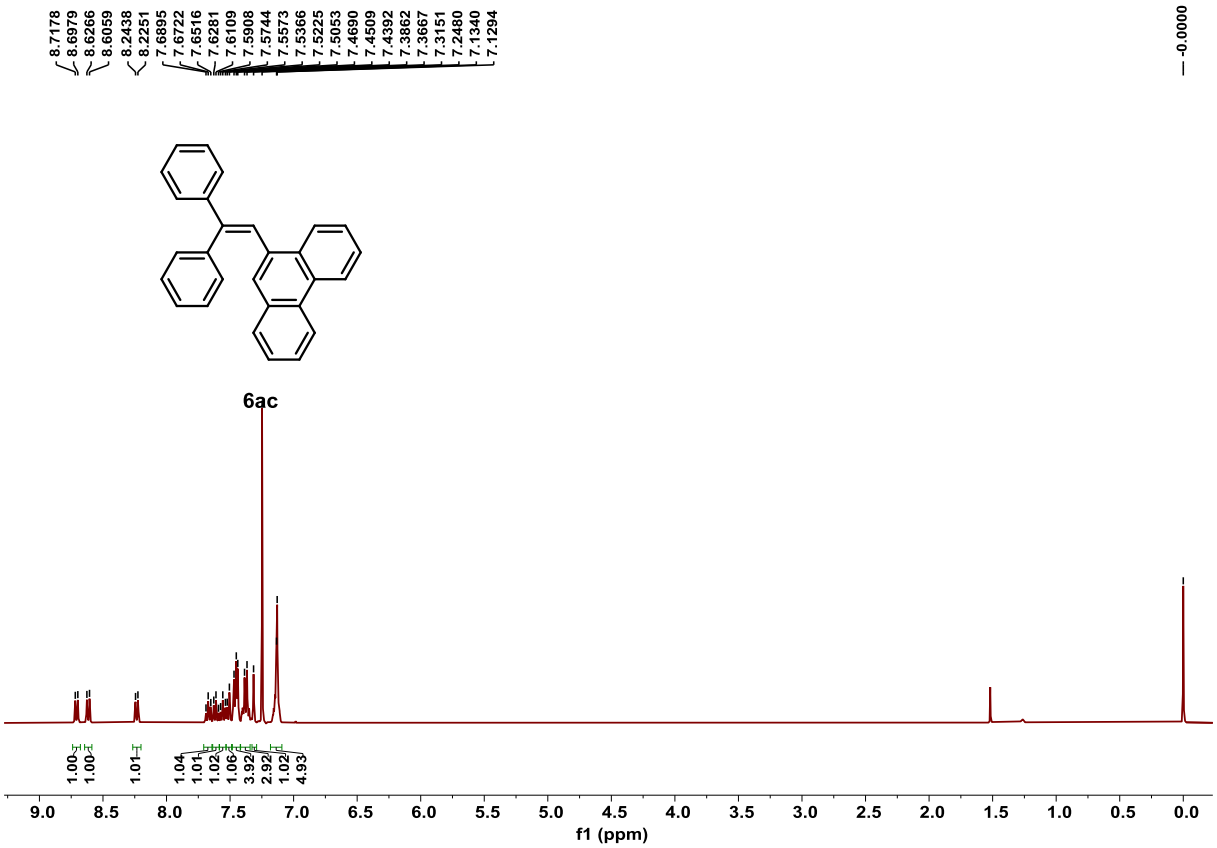

Figure S95. ^{1}**H NMR** spectrum of product **6ac**, related to **Scheme 3**.

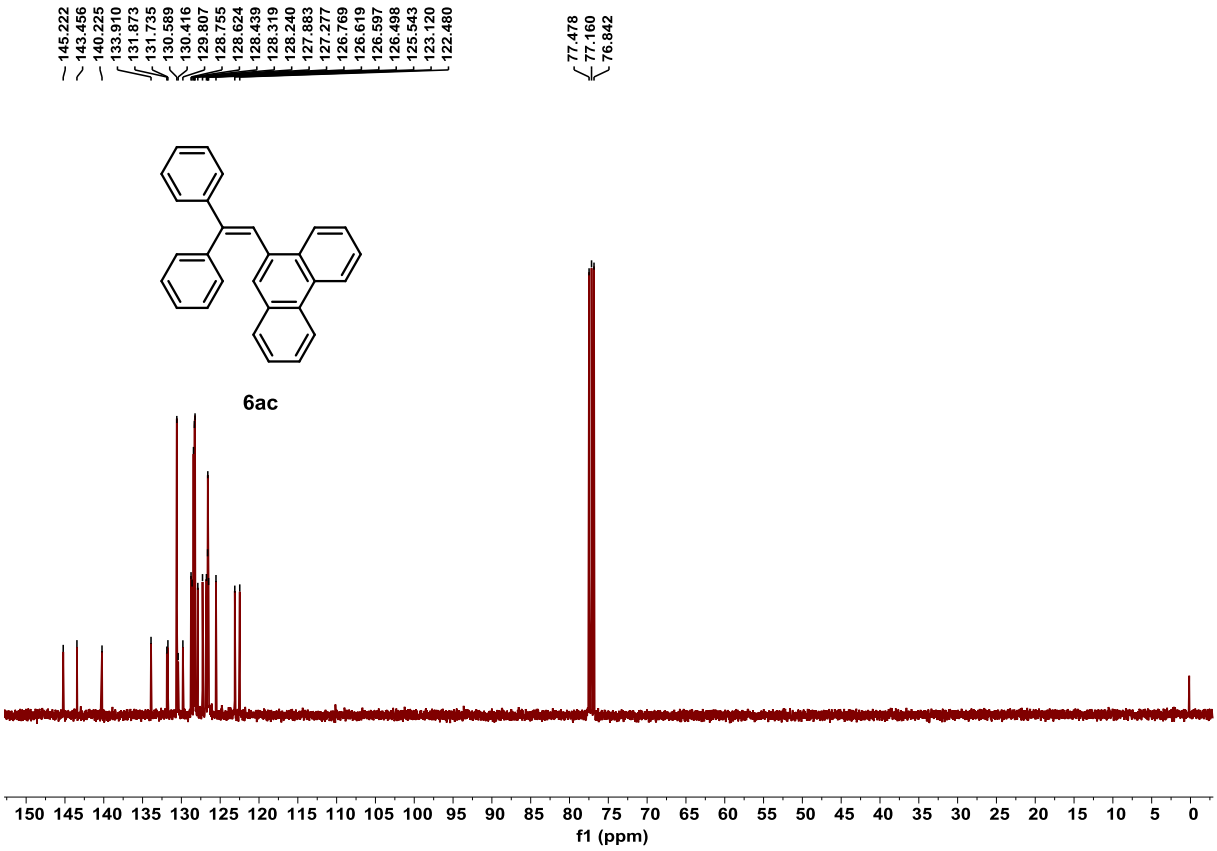

Figure S96. ^{13}**C NMR** spectrum of product **6ac**, related to **Scheme 3**.

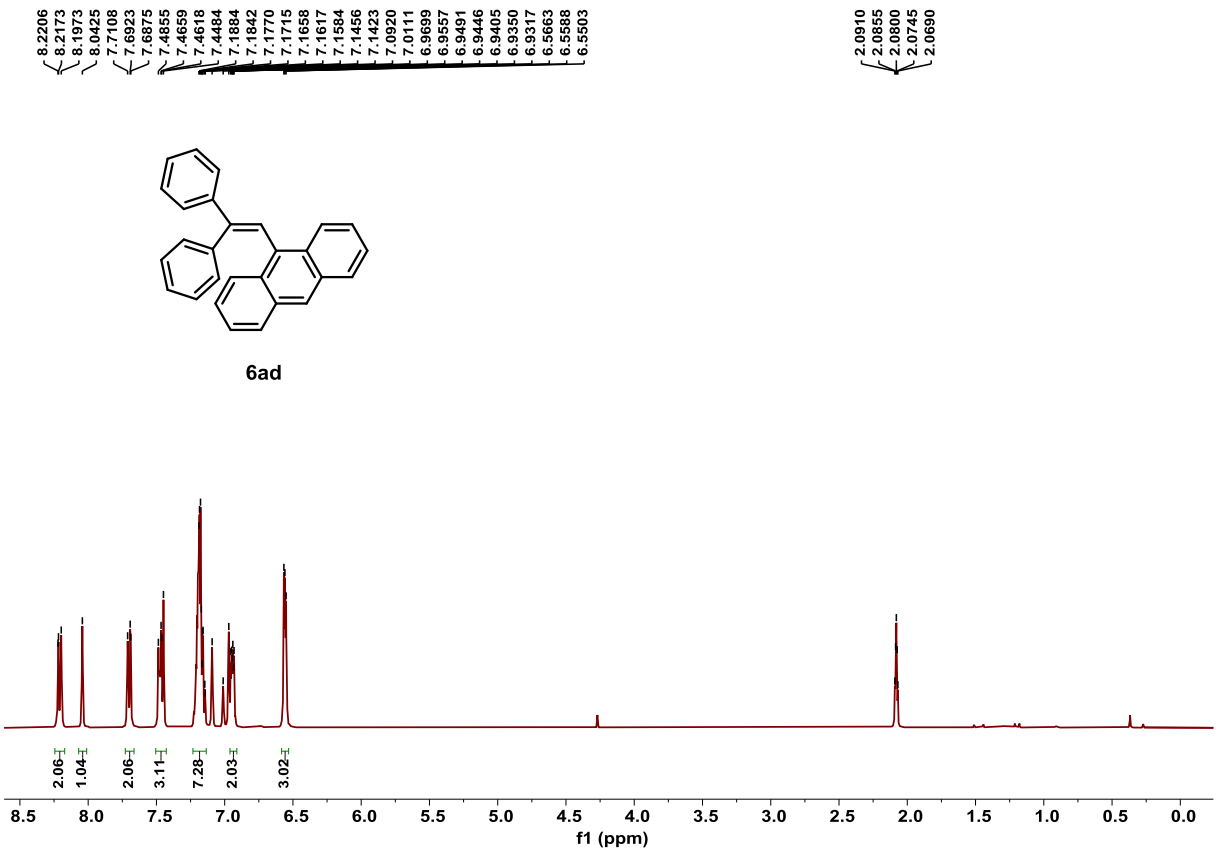

Figure S97. ^{1}H NMR spectrum of product **6ad**, related to **Scheme 3**.

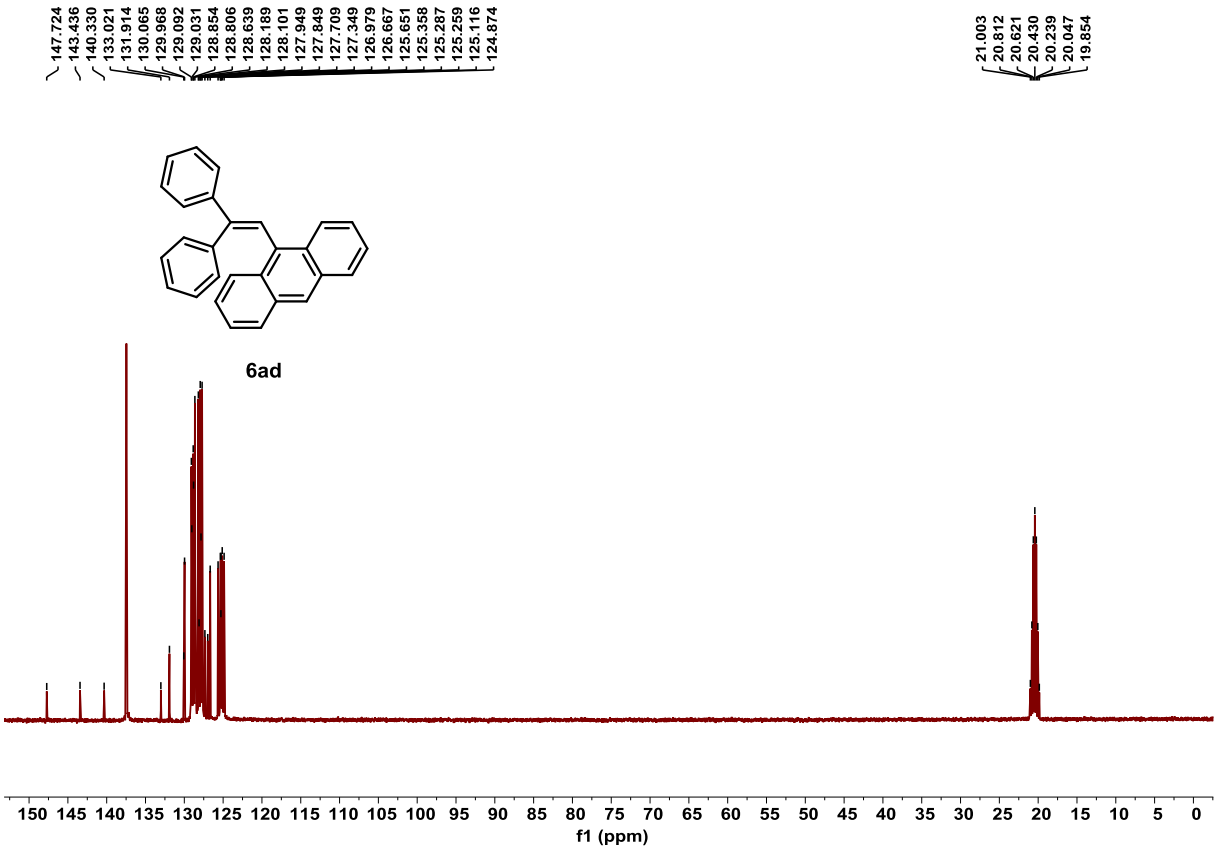

Figure S98. ^{13}C NMR spectrum of product **6ad**, related to **Scheme 3**.

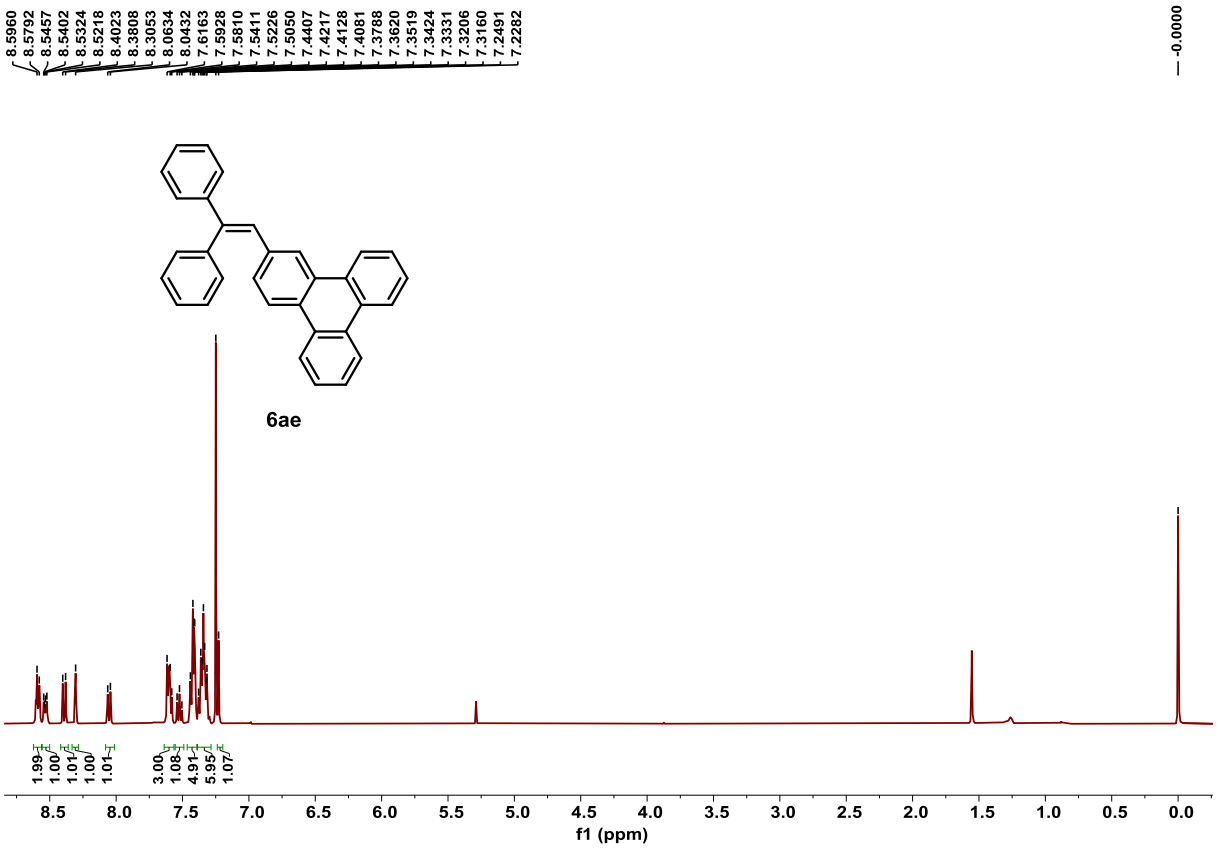

Figure S99. ^{1}H NMR spectrum of product **6ae**, related to **Scheme 3**.

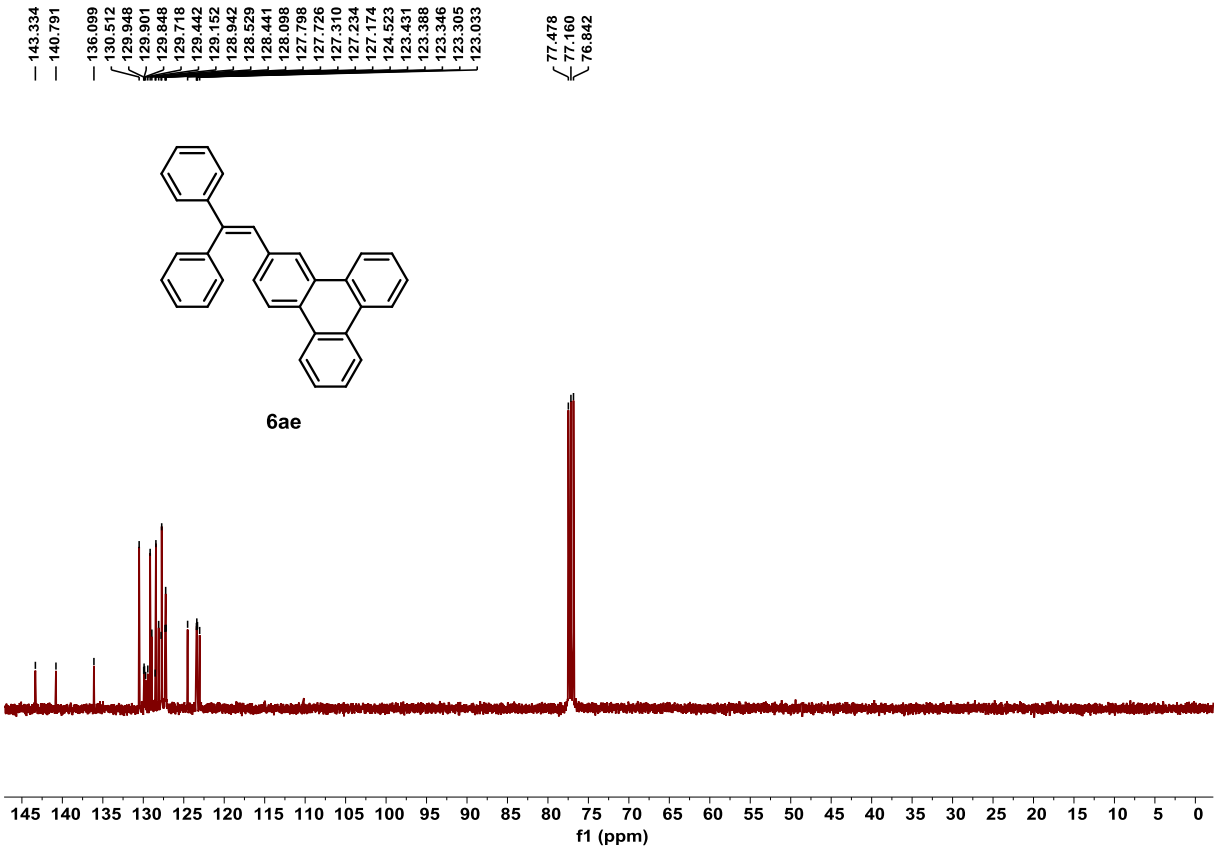

Figure S100. ^{13}C NMR spectrum of product **6ae**, related to **Scheme 3**.

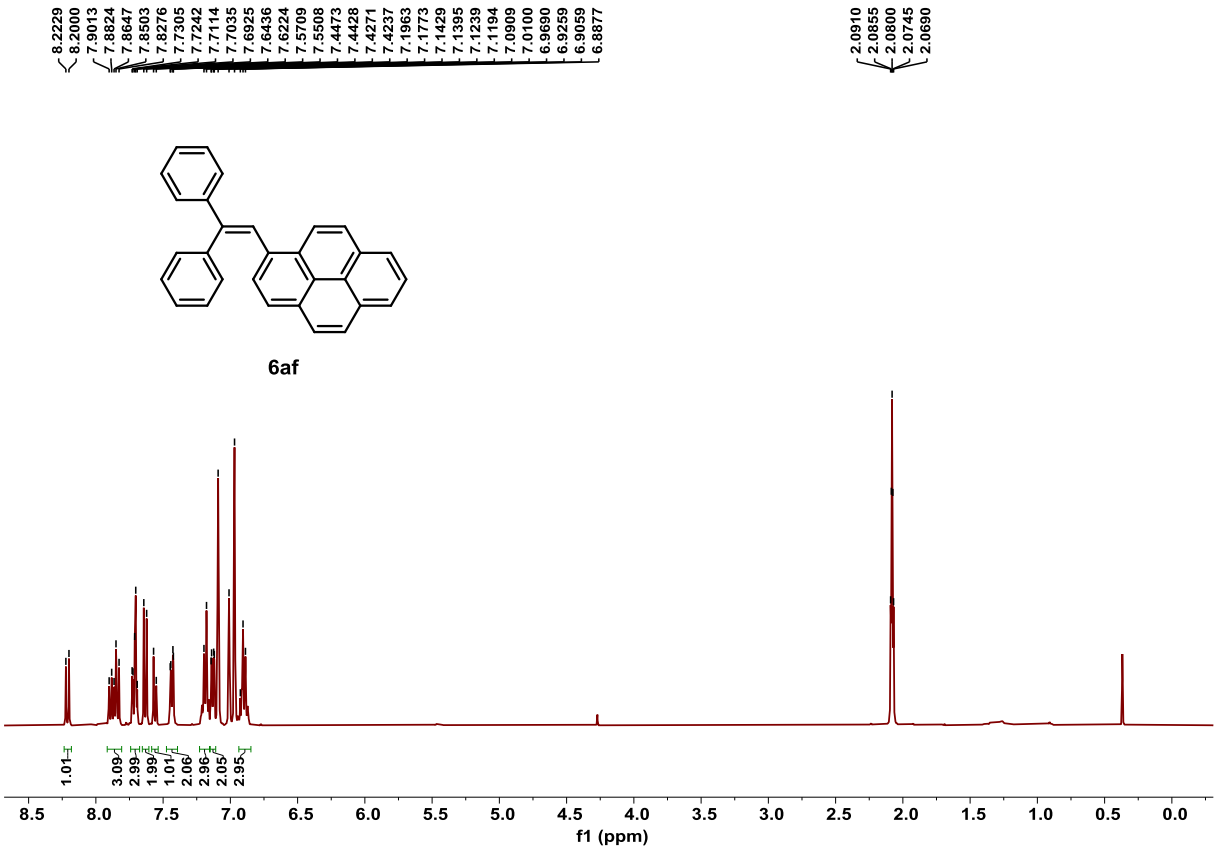

Figure S101. ^{1}**H NMR** spectrum of product **6af**, related to **Scheme 3**.

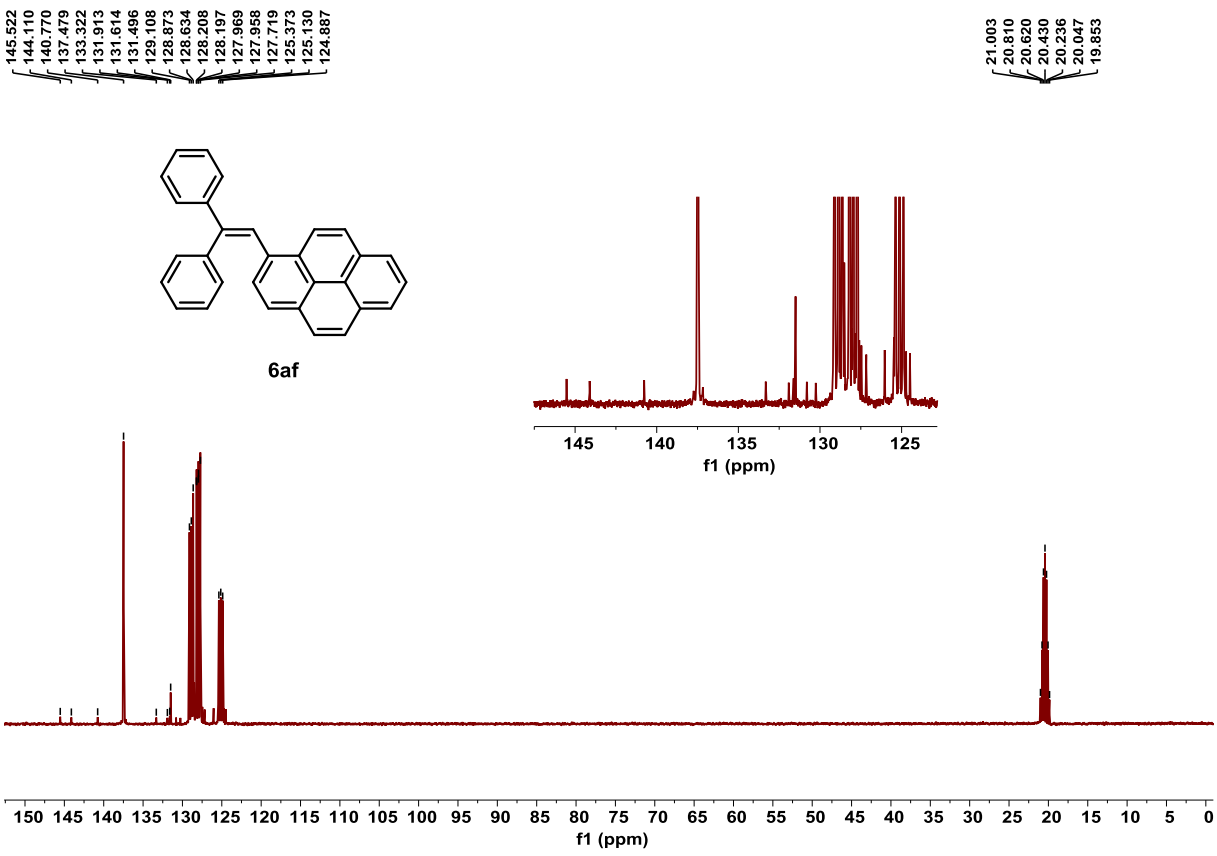

Figure S102. ^{13}**C NMR** spectrum of product **6af**, related to **Scheme 3**.

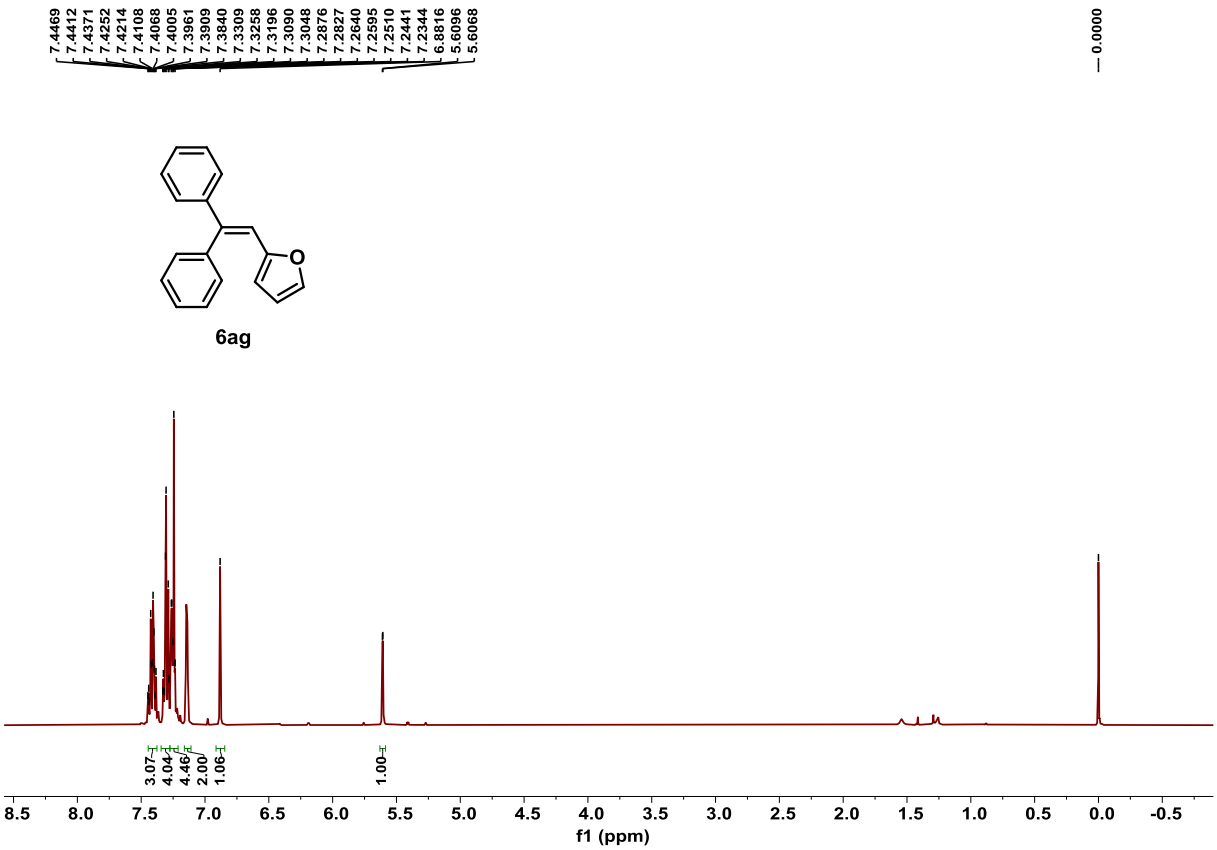

Figure S103. ^{1}**H NMR** spectrum of product **6ag**, related to **Scheme 3**.

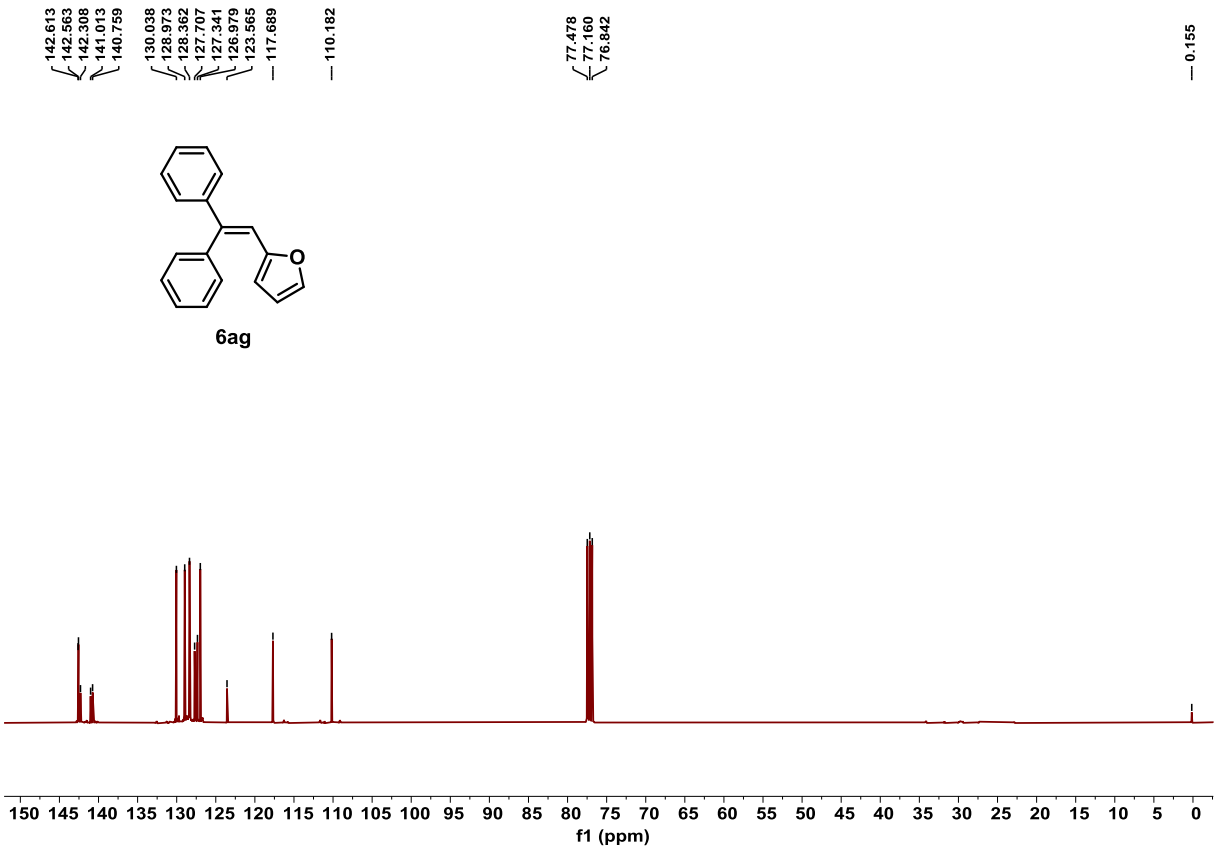

Figure S104. ^{13}**C NMR** spectrum of product **6ag**, related to **Scheme 3**.

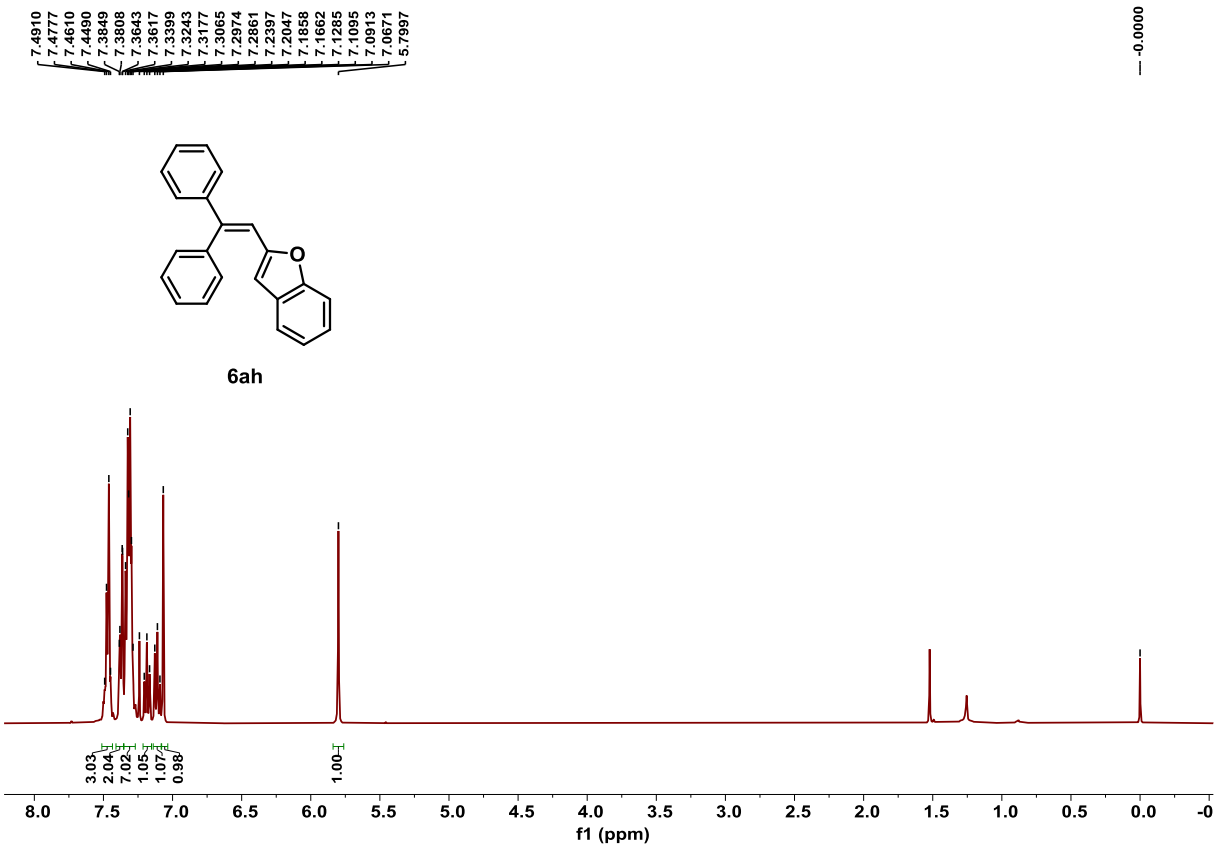

Figure S105. ^{1}**H NMR** spectrum of product **6ah**, related to **Scheme 3**.

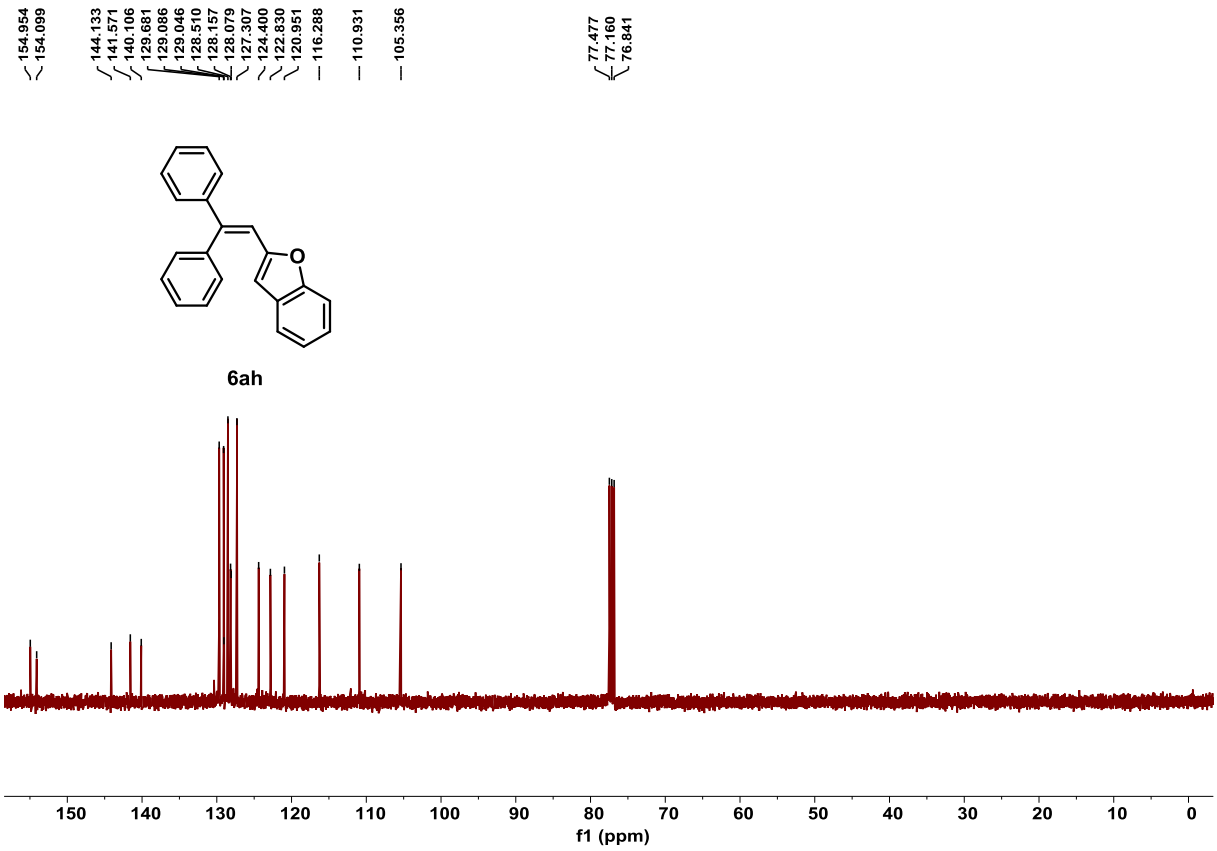

Figure S106. ^{13}**C NMR** spectrum of product **6ah**, related to **Scheme 3**.

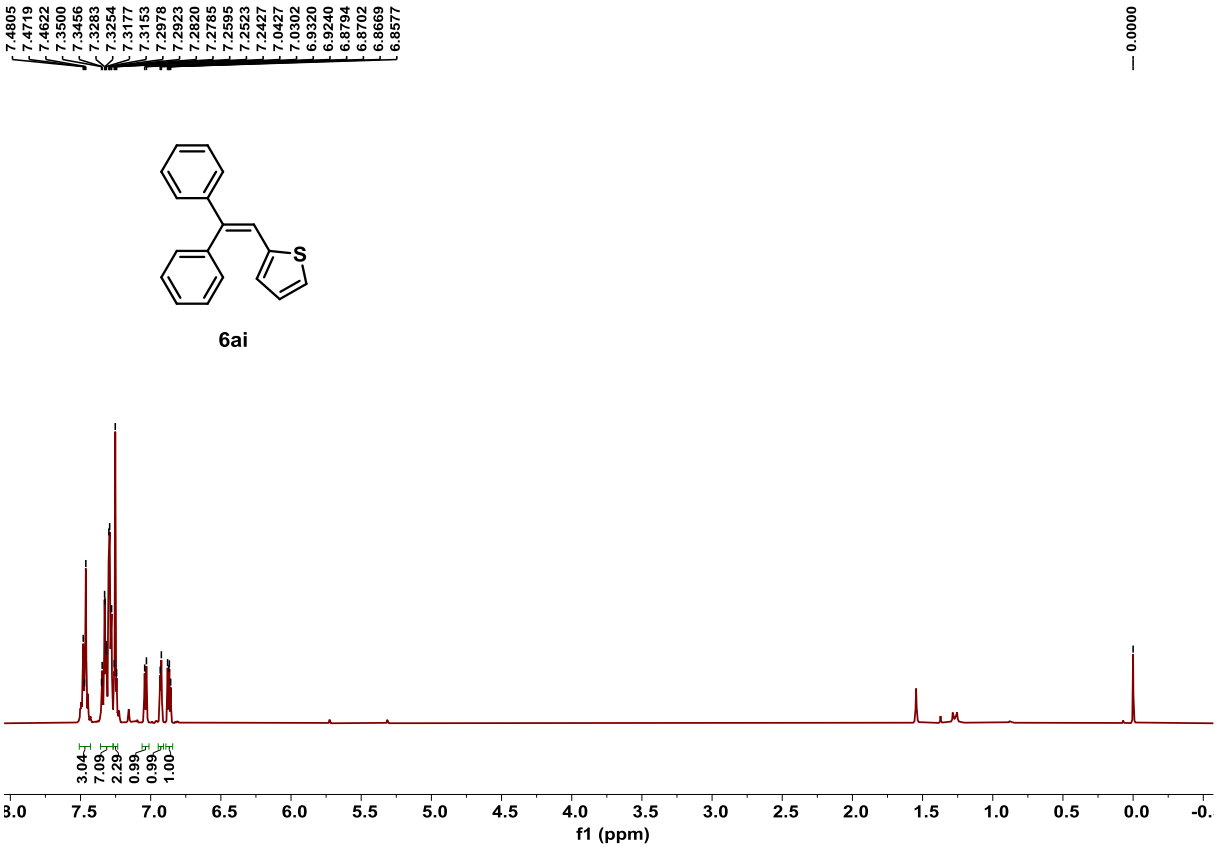

Figure S107. ^{1}H NMR spectrum of product **6ai**, related to **Scheme 3**.

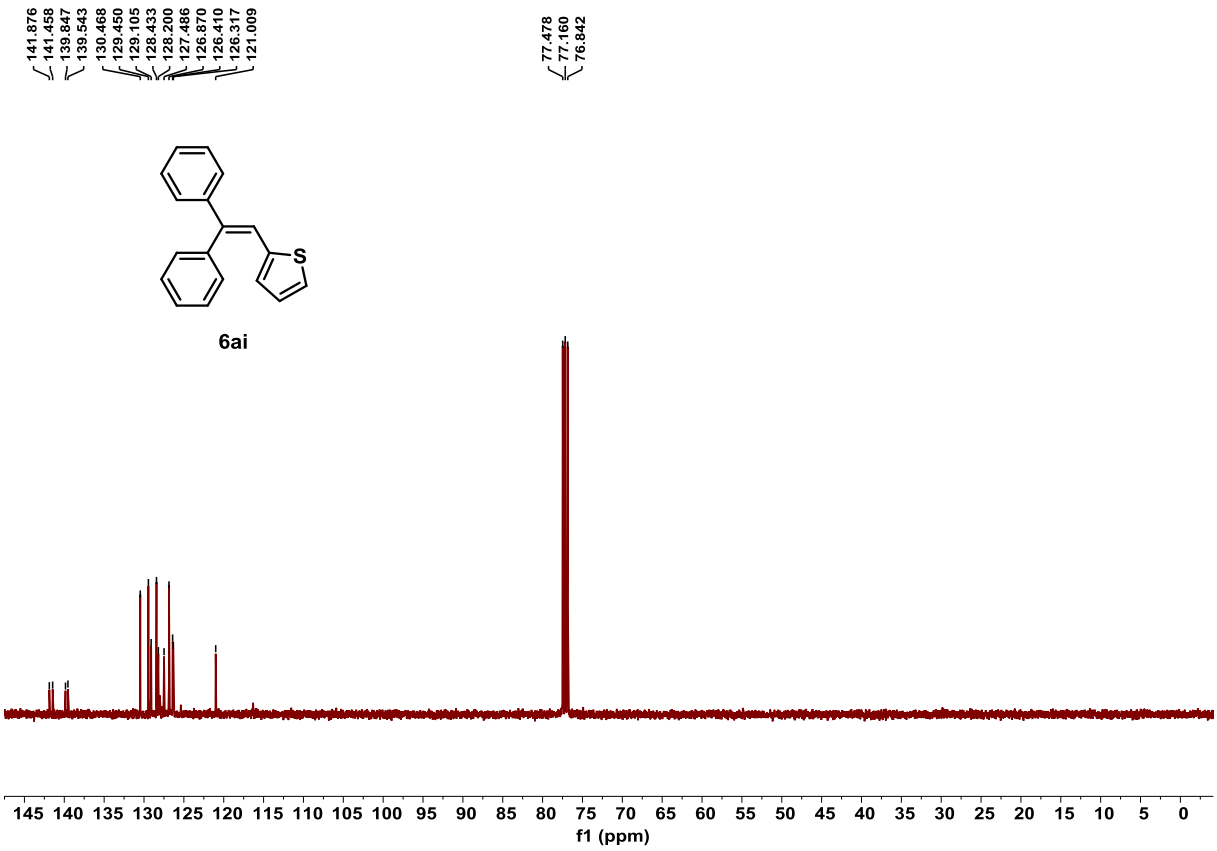

Figure S108. ^{13}C NMR spectrum of product **6ai**, related to **Scheme 3**.

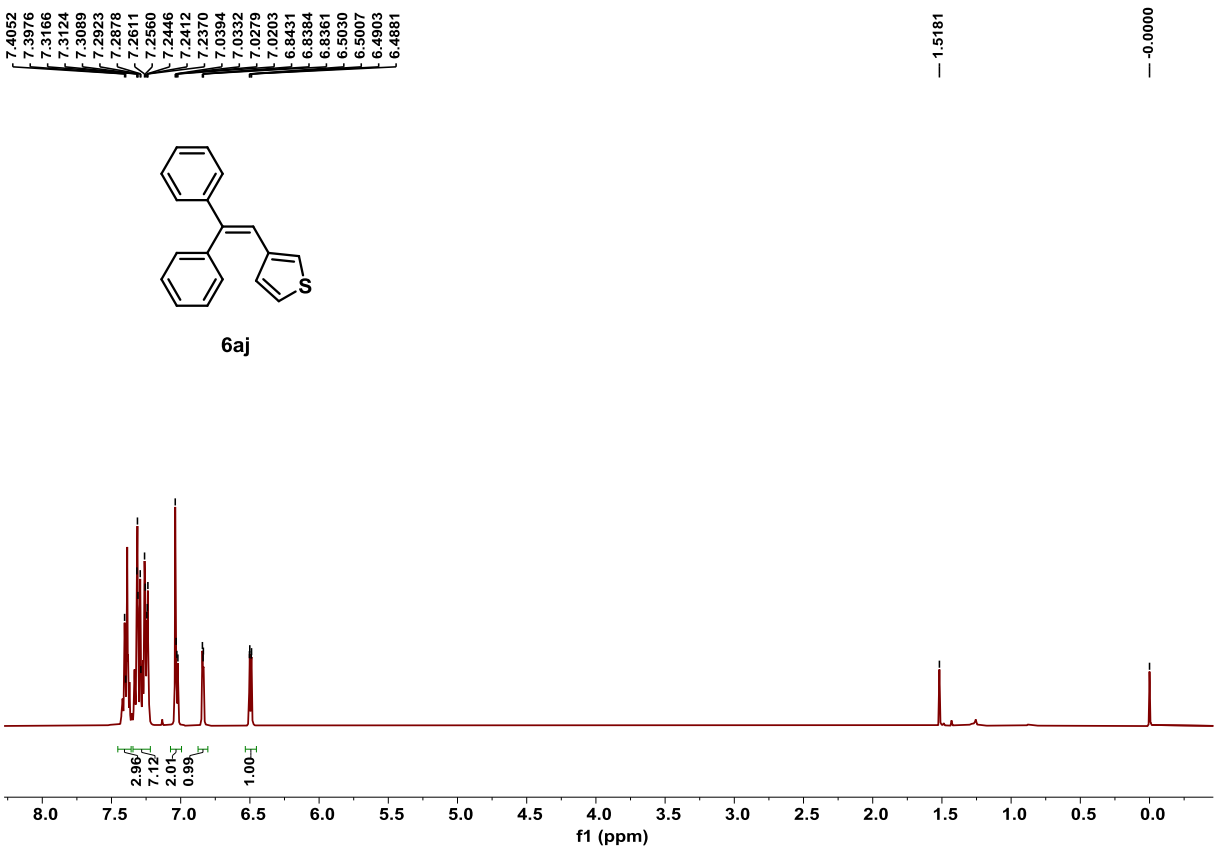

Figure S109. ^{1}H NMR spectrum of product **6aj**, related to **Scheme 3**.

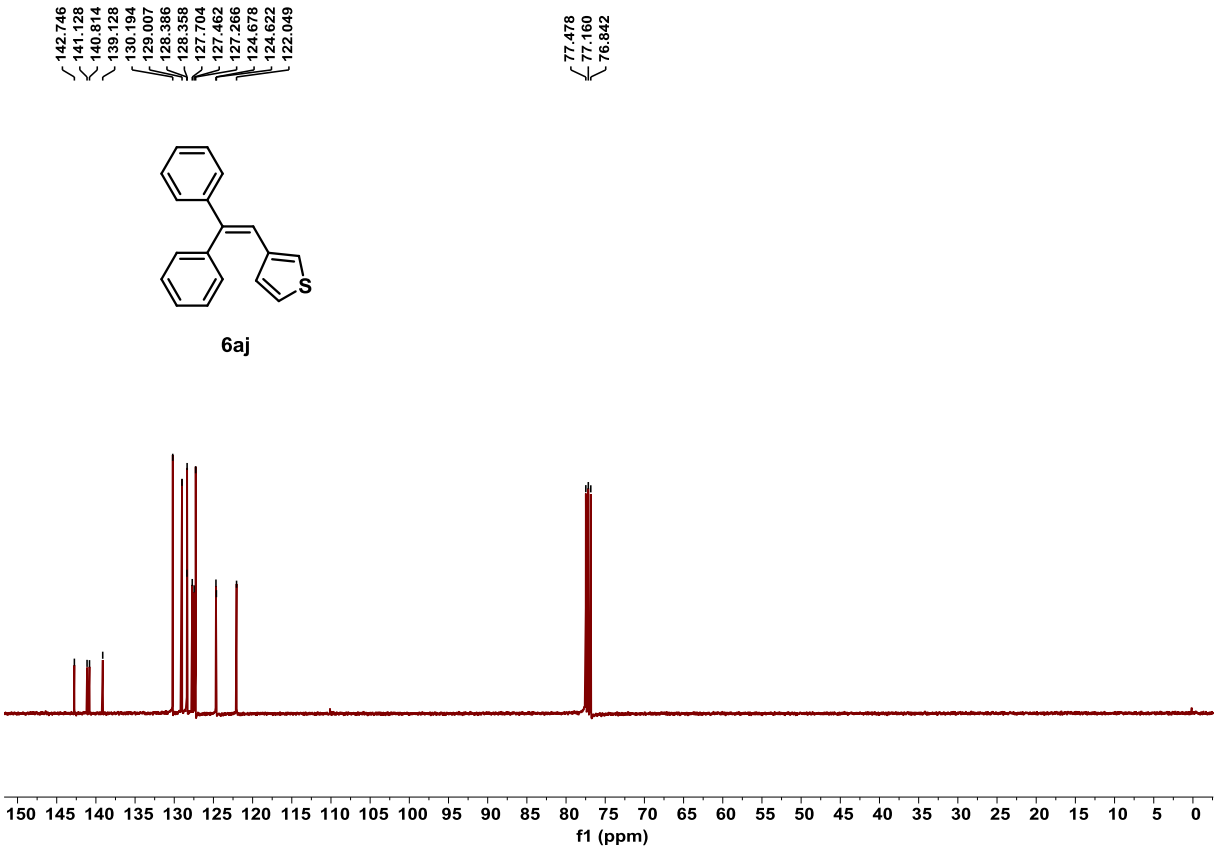

Figure S110. ^{13}C NMR spectrum of product **6aj**, related to **Scheme 3**.

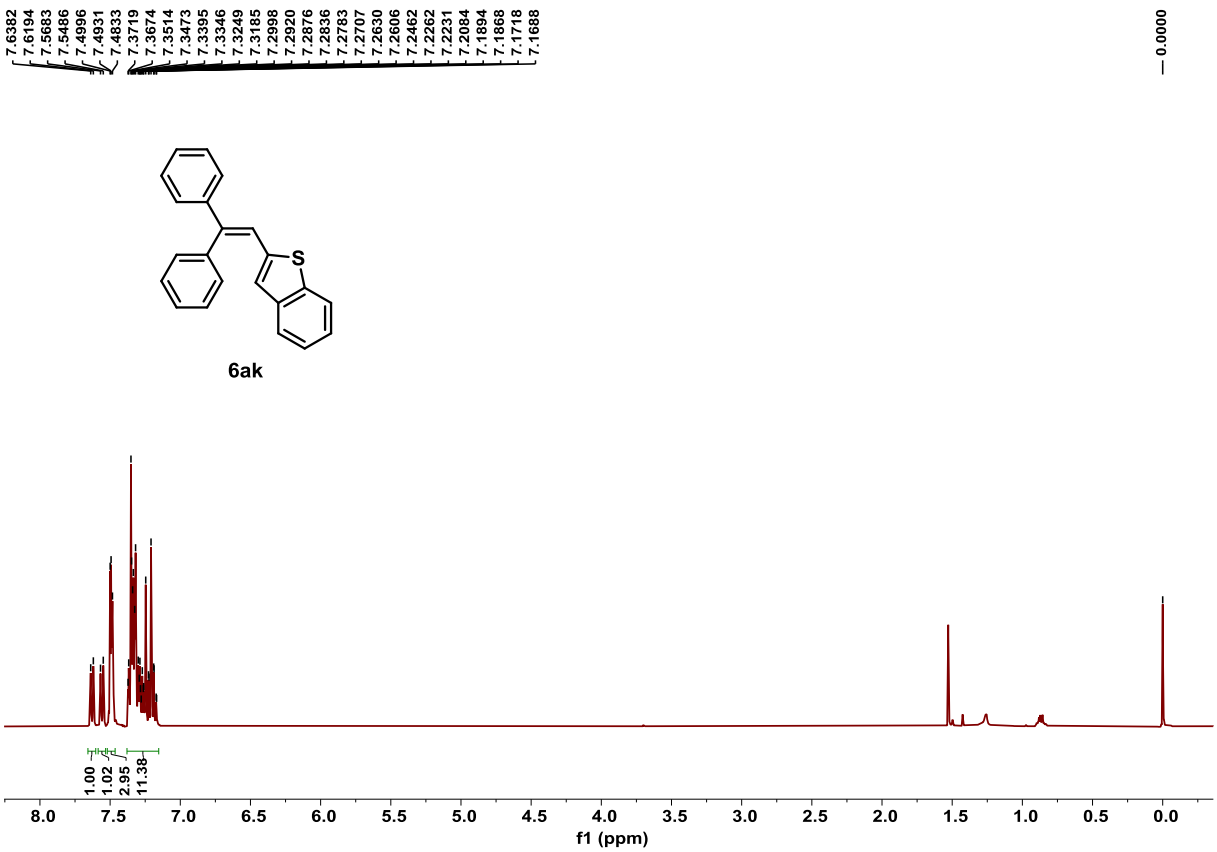

Figure S111. ^{1}**H NMR** spectrum of product **6ak**, related to **Scheme 3**.

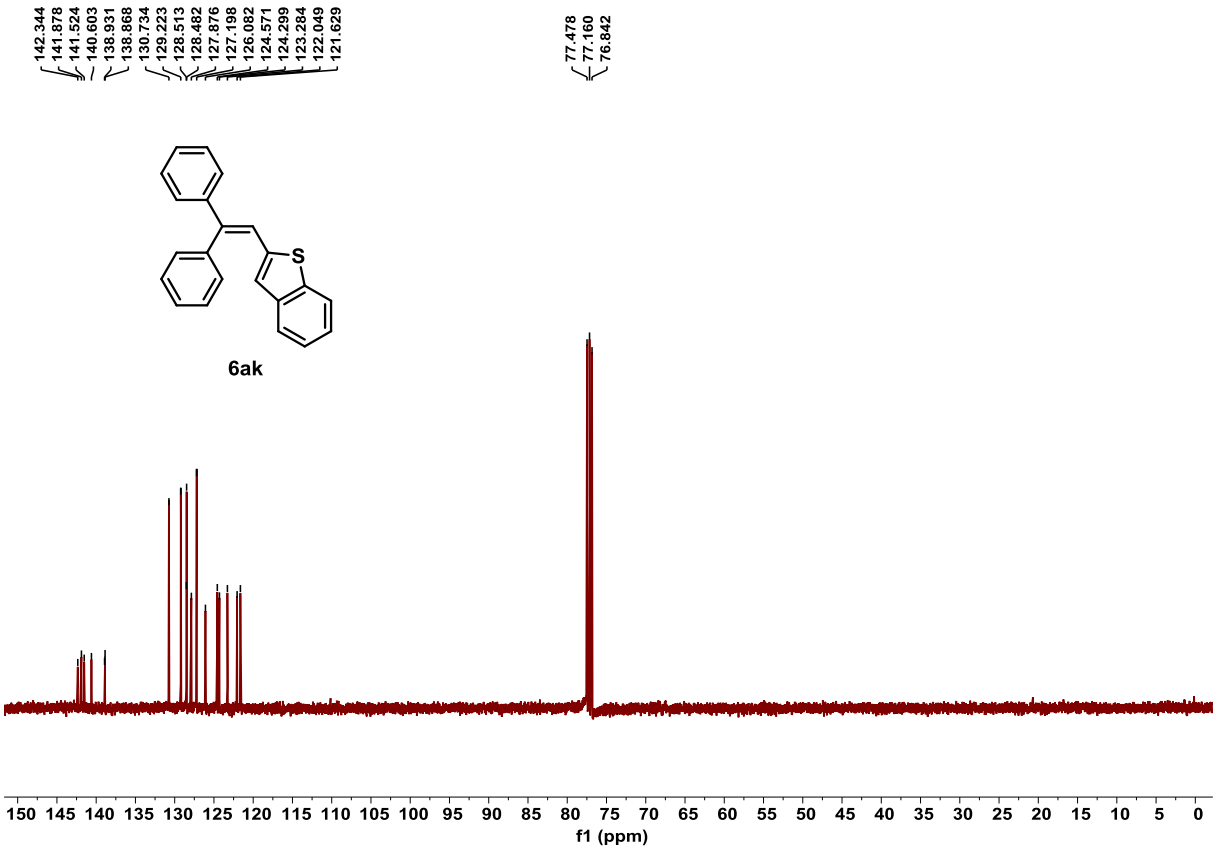

Figure S112. ^{13}**C NMR** spectrum of product **6ak**, related to **Scheme 3**.

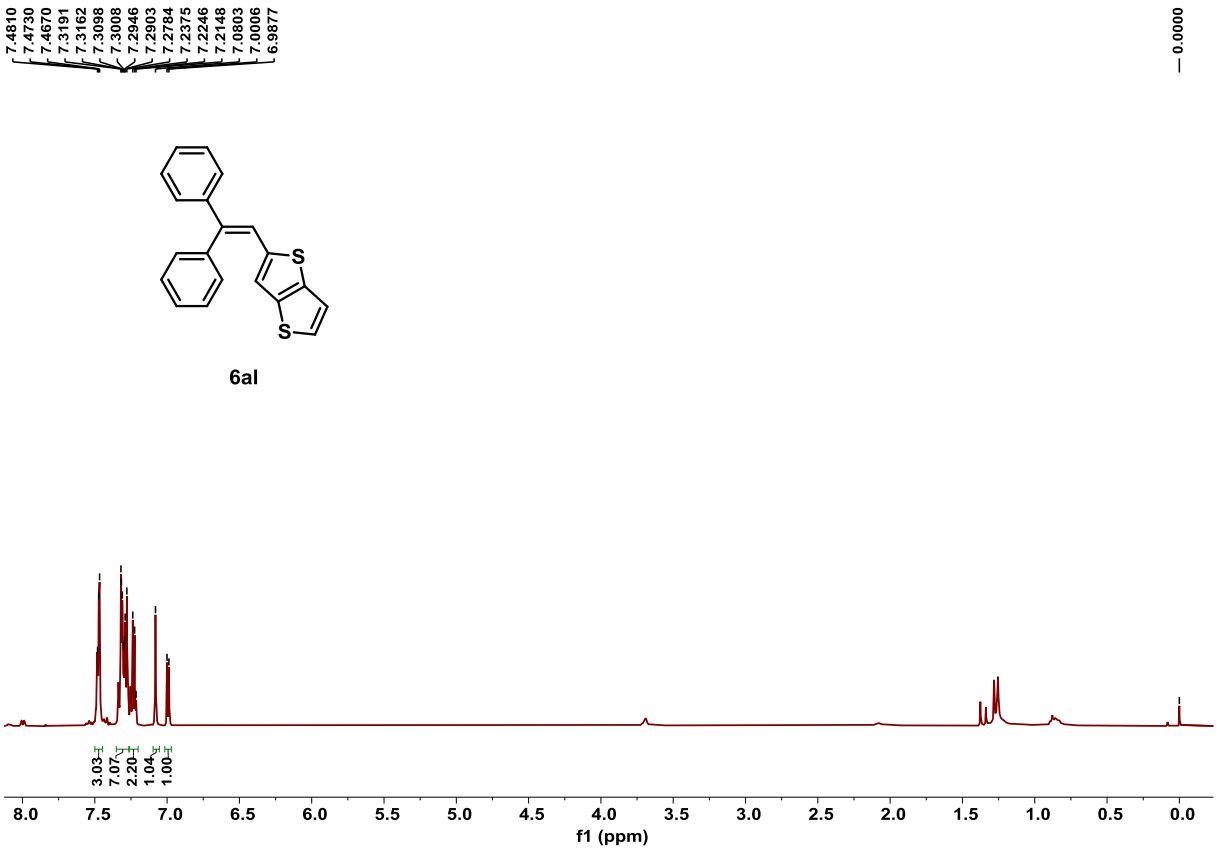

Figure S113. ^{1}H NMR spectrum of product **6al**, related to **Scheme 3**.

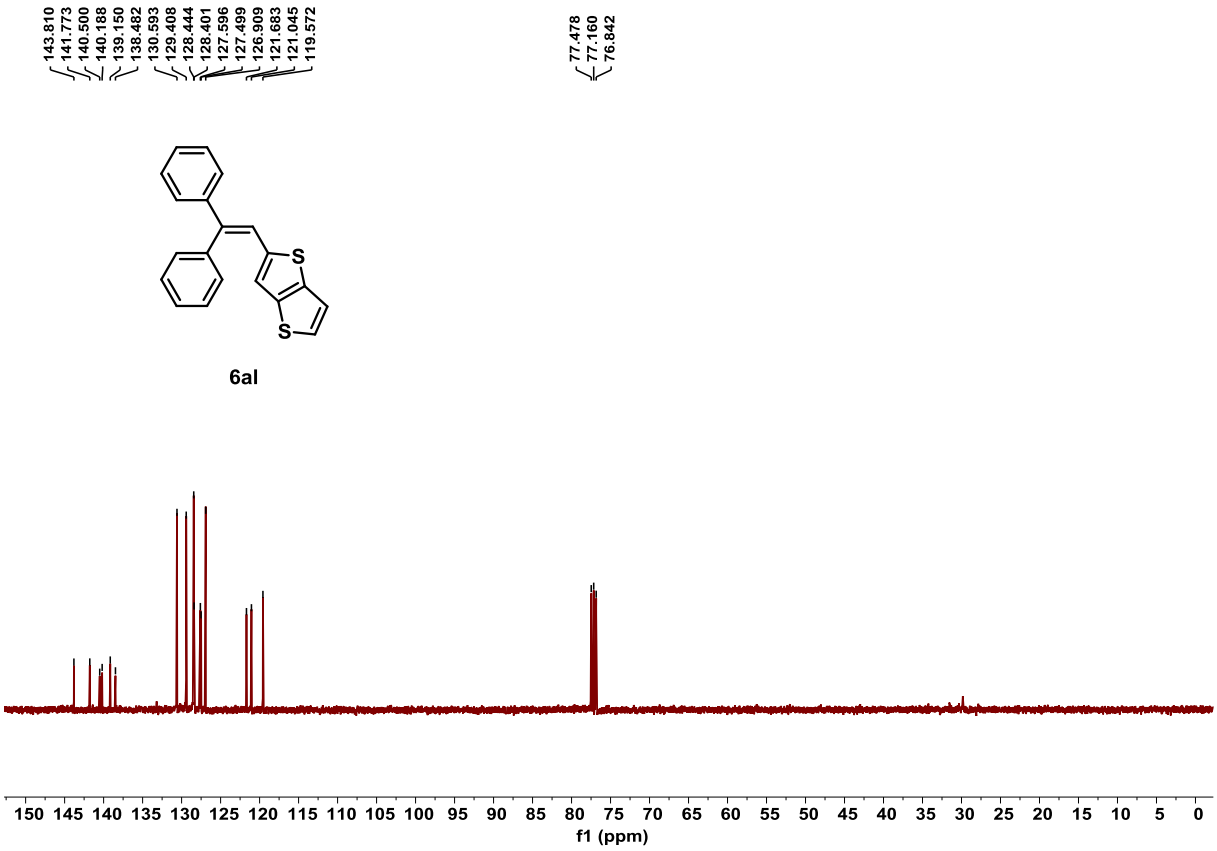

Figure S114. ^{13}C NMR spectrum of product **6al**, related to **Scheme 3**.

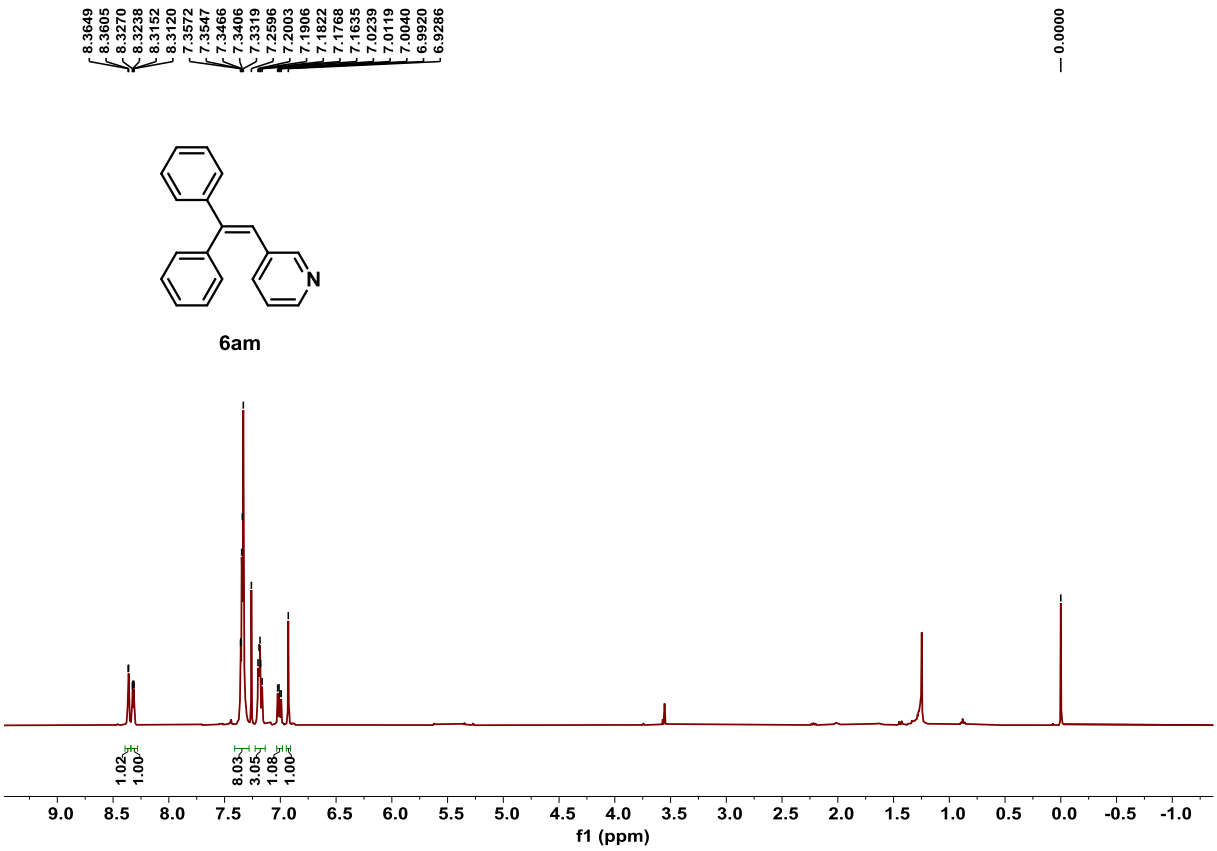

Figure S115. ^{1}**H NMR** spectrum of product **6am**, related to **Scheme 3**.

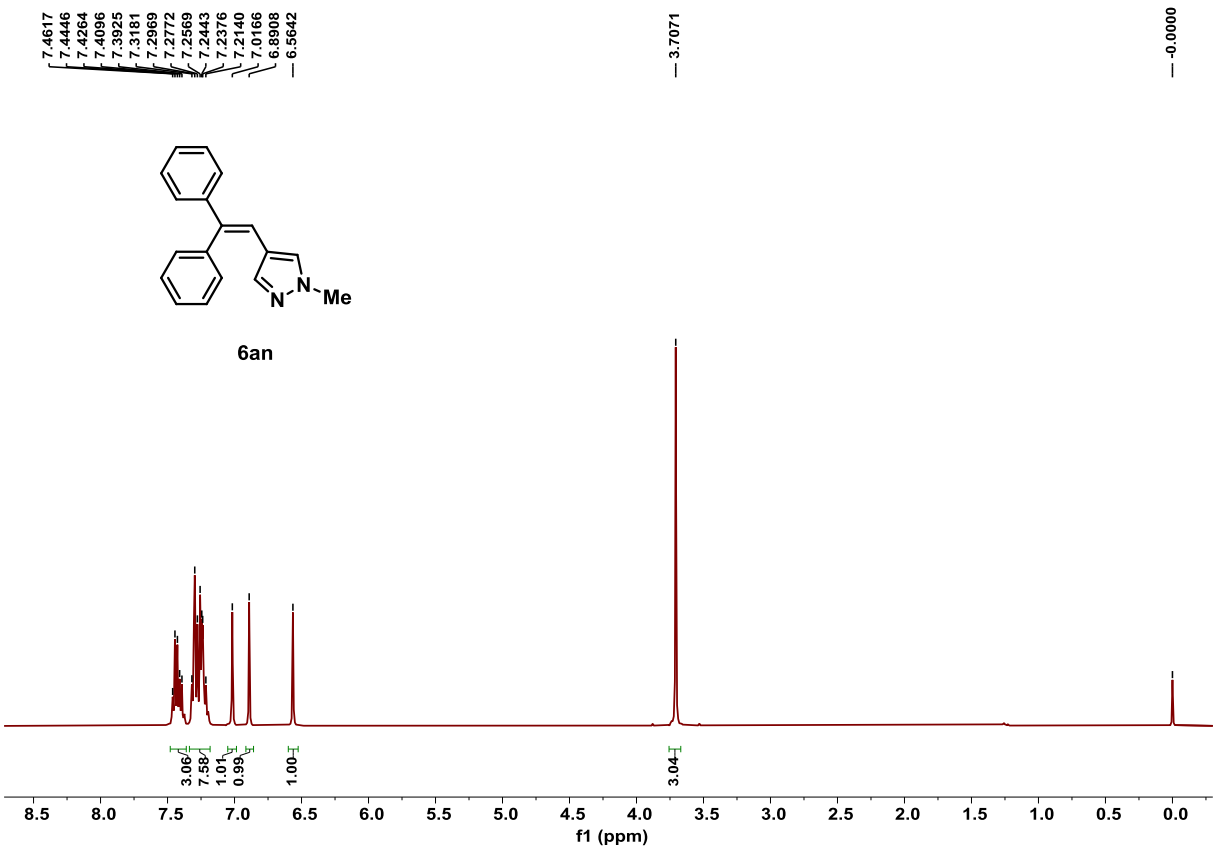

Figure S116. ^{1}**H NMR** spectrum of product **6an**, related to **Scheme 3**.

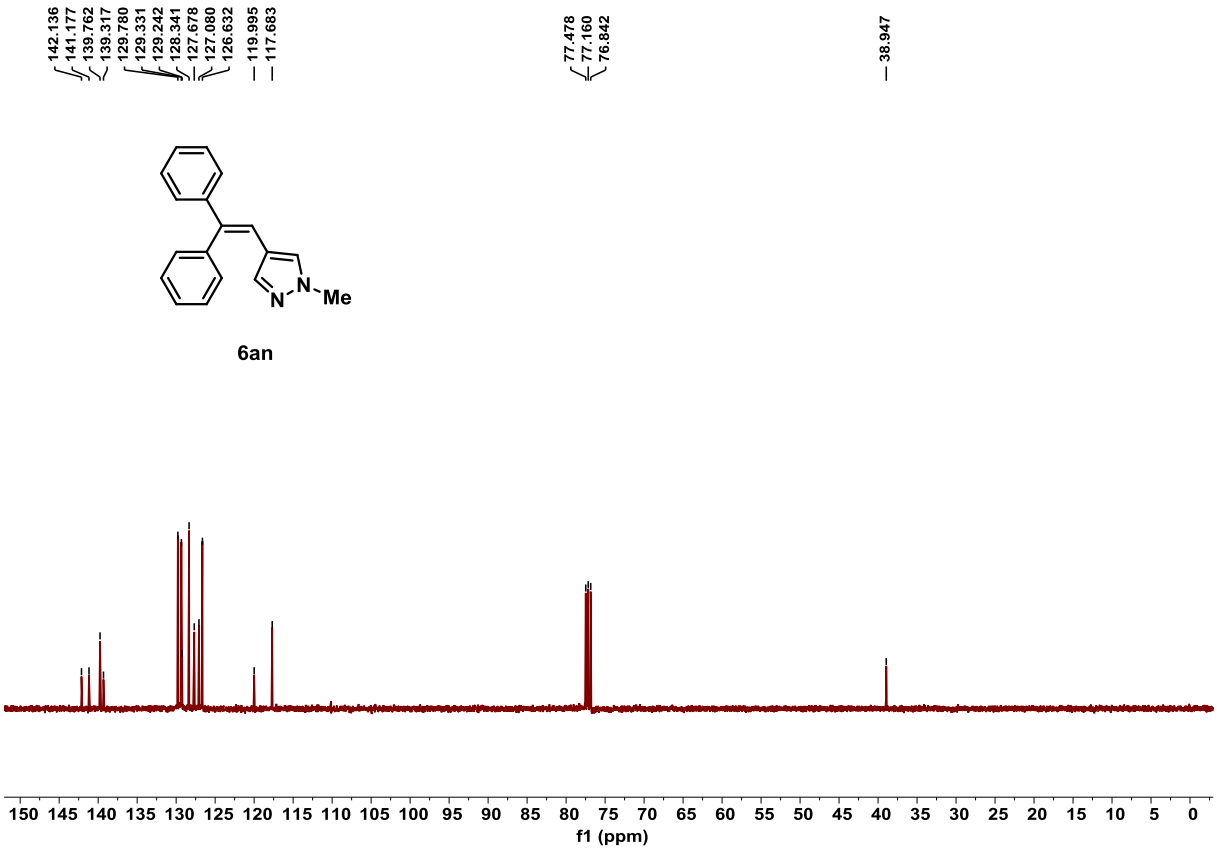

Figure S117. ^{13}**C NMR** spectrum of product **6an**, related to **Scheme 3**.

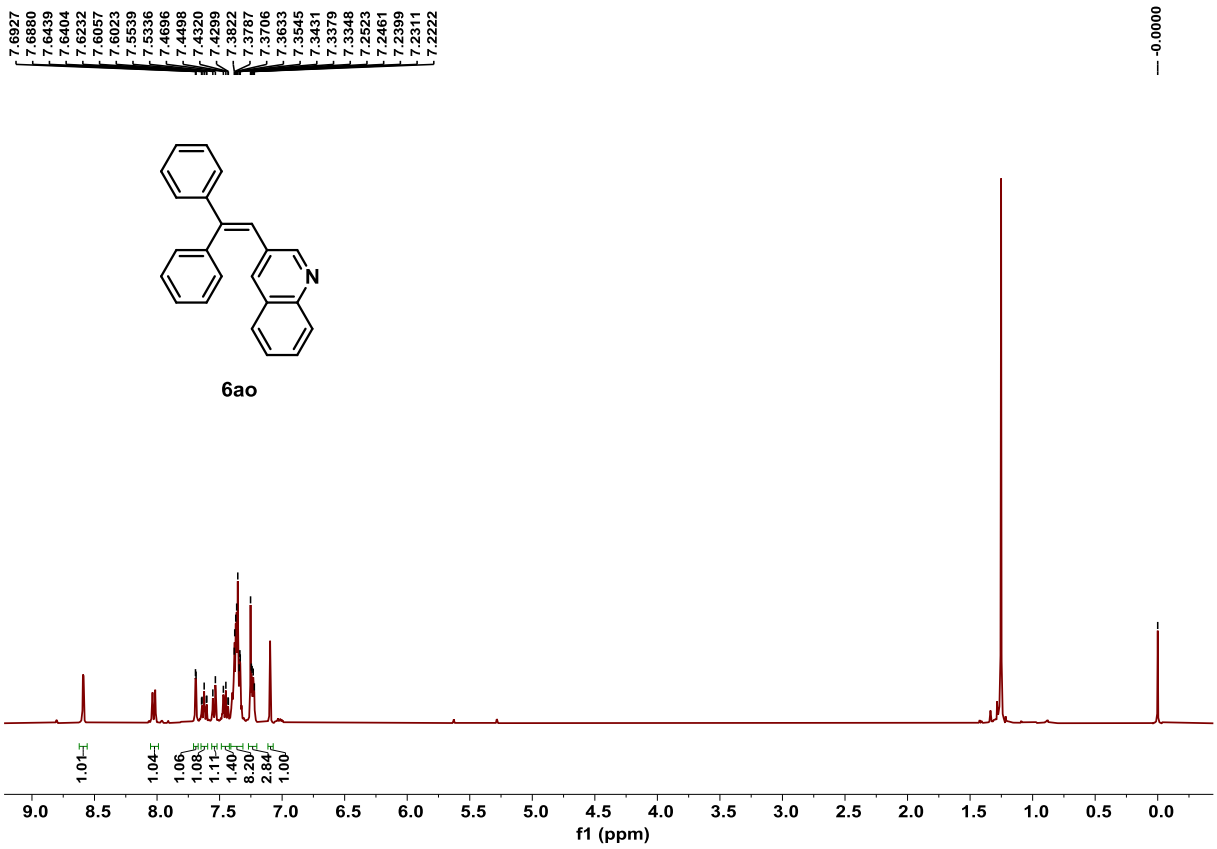

Figure S118. ^{1}**H NMR** spectrum of product **6ao**, related to **Scheme 3**.

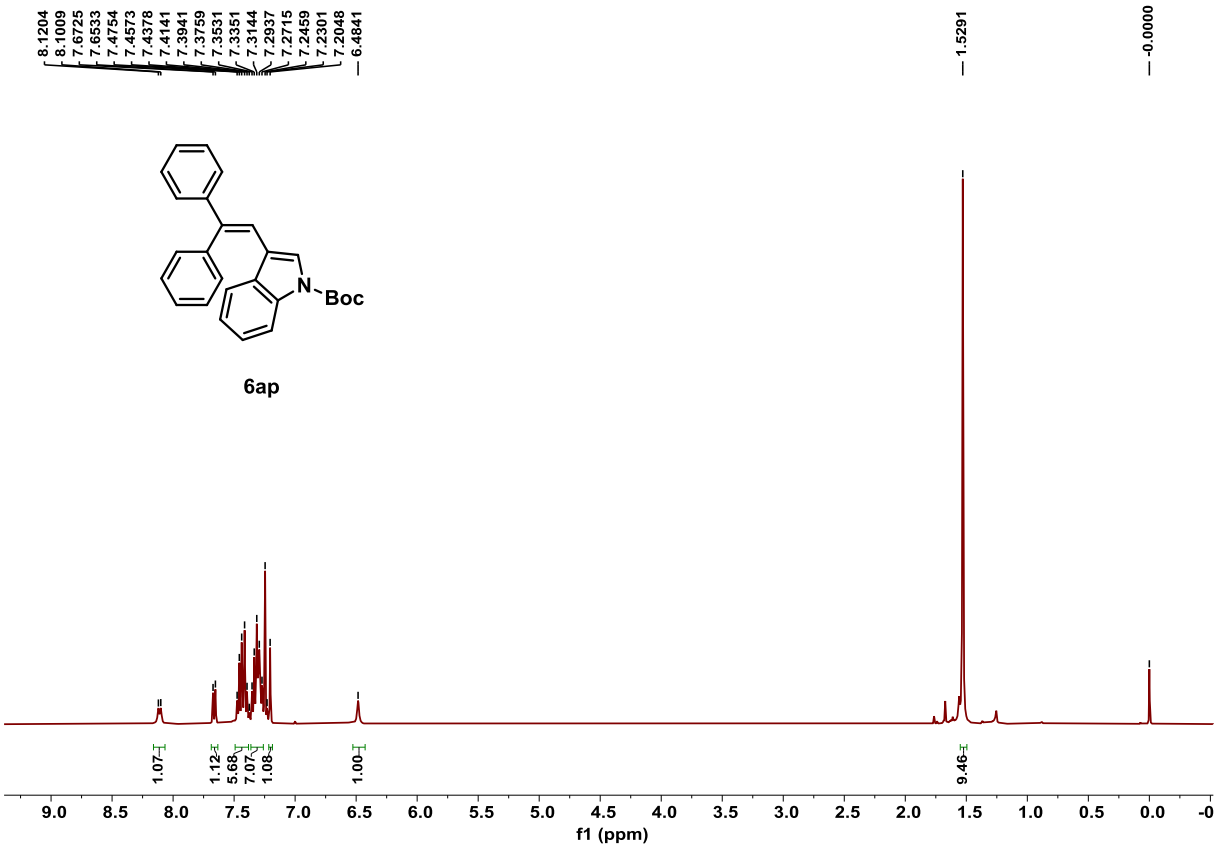

Figure S119. ^{1}**H NMR** spectrum of product **6ap**, related to **Scheme 3**.

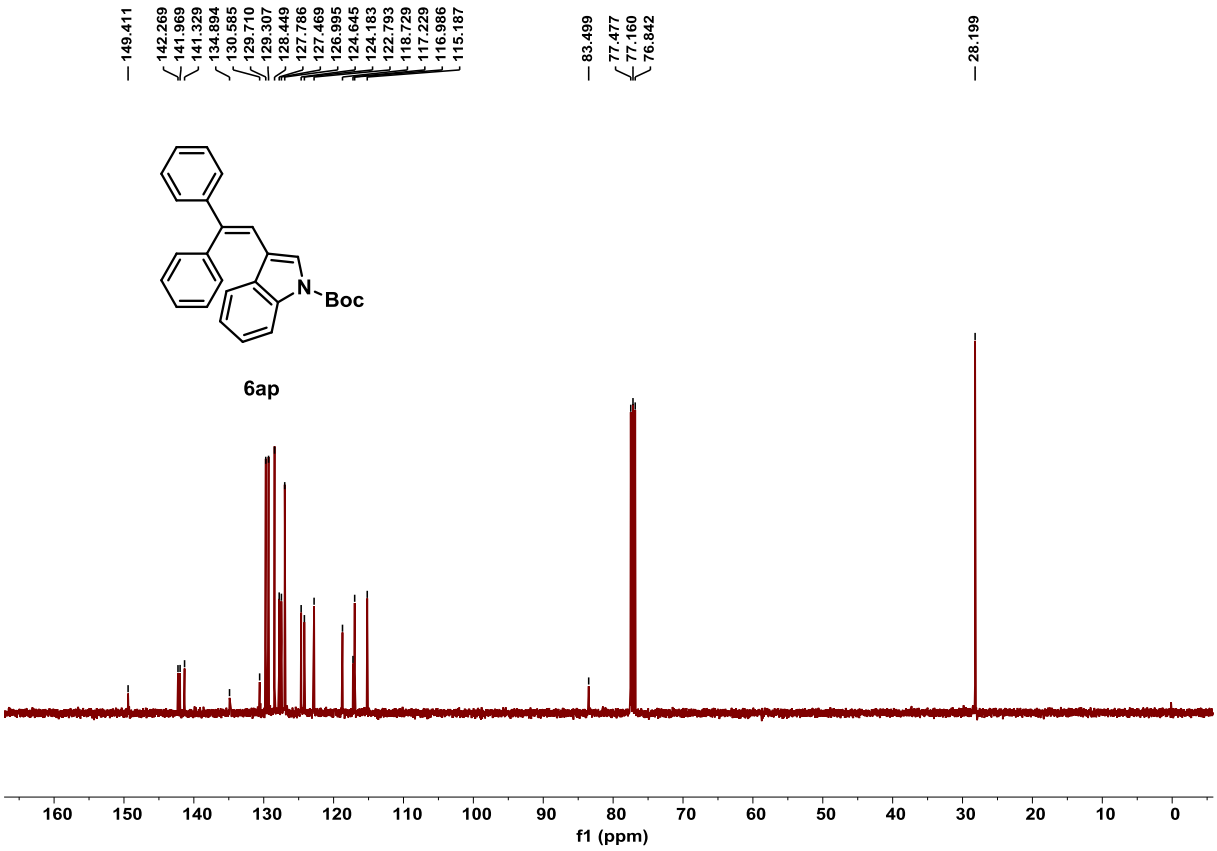

Figure S120. ^{13}**C NMR** spectrum of product **6ap**, related to **Scheme 3**.

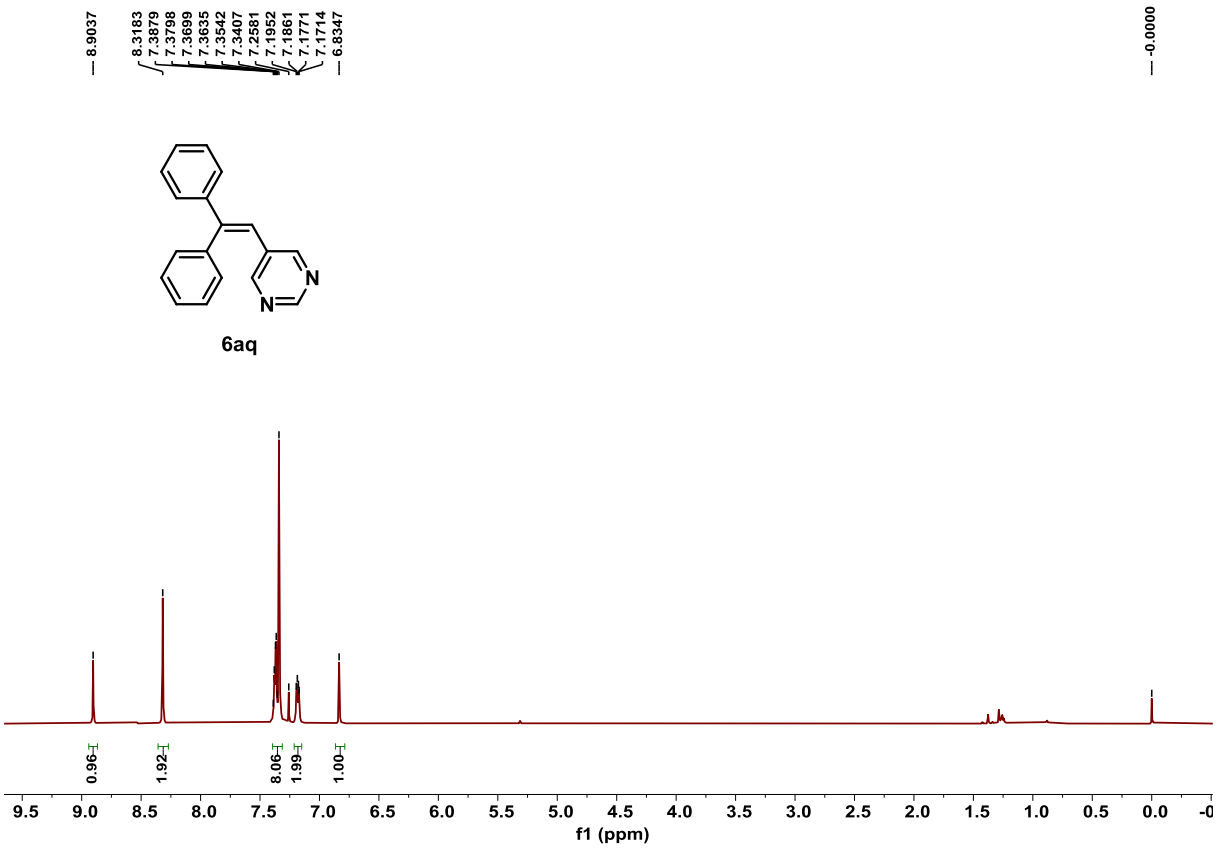

Figure S121. ^{1}**H NMR** spectrum of product **6aq**, related to **Scheme 3**.

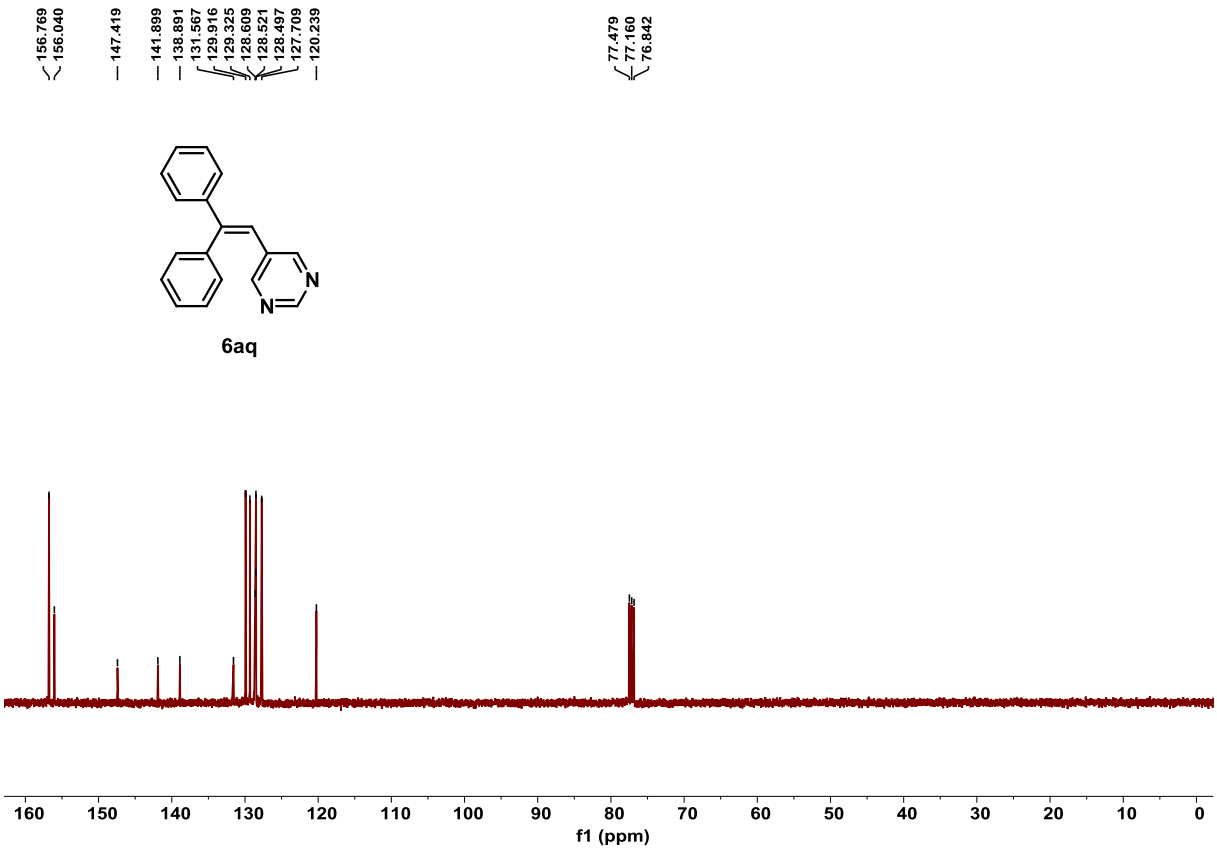

Figure S122. ^{13}**C NMR** spectrum of product **6aq**, related to **Scheme 3**.

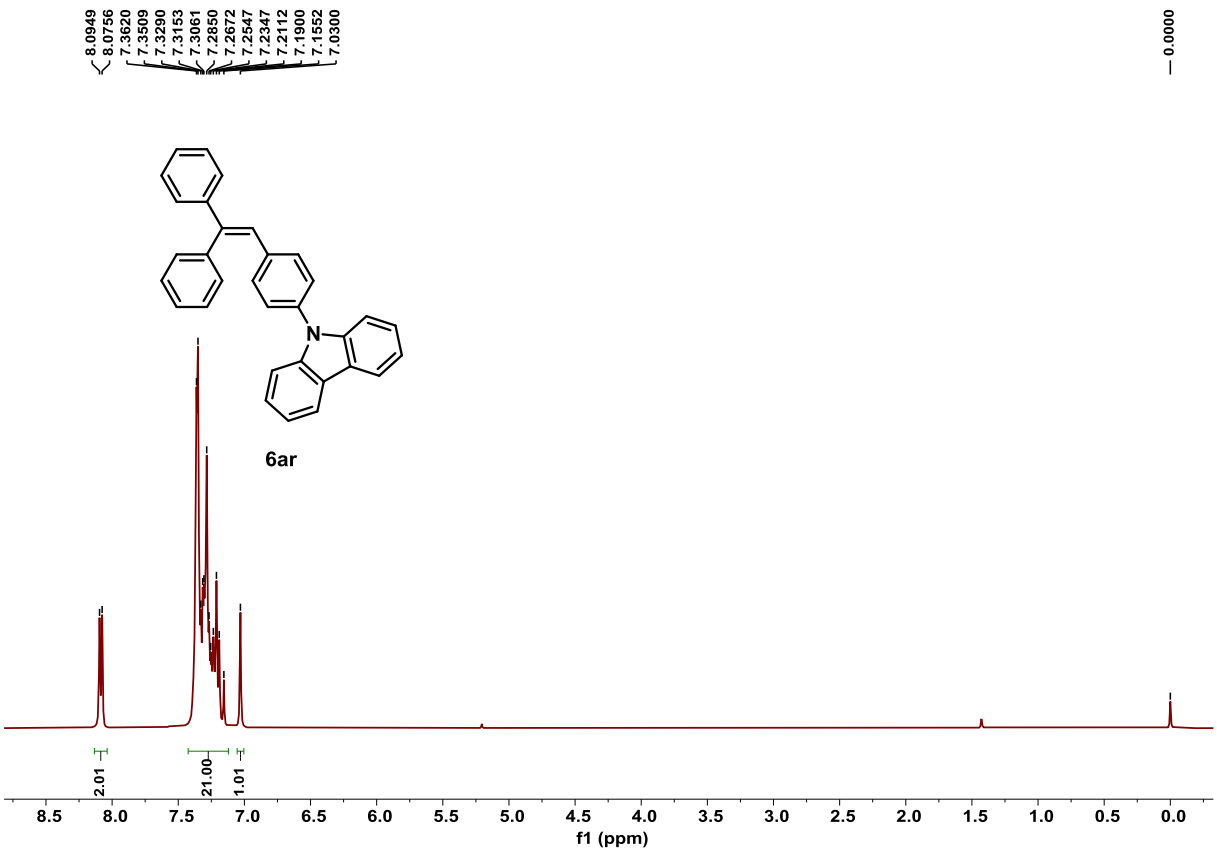

Figure S123. ^{1}H NMR spectrum of product **6ar**, related to **Scheme 3**.

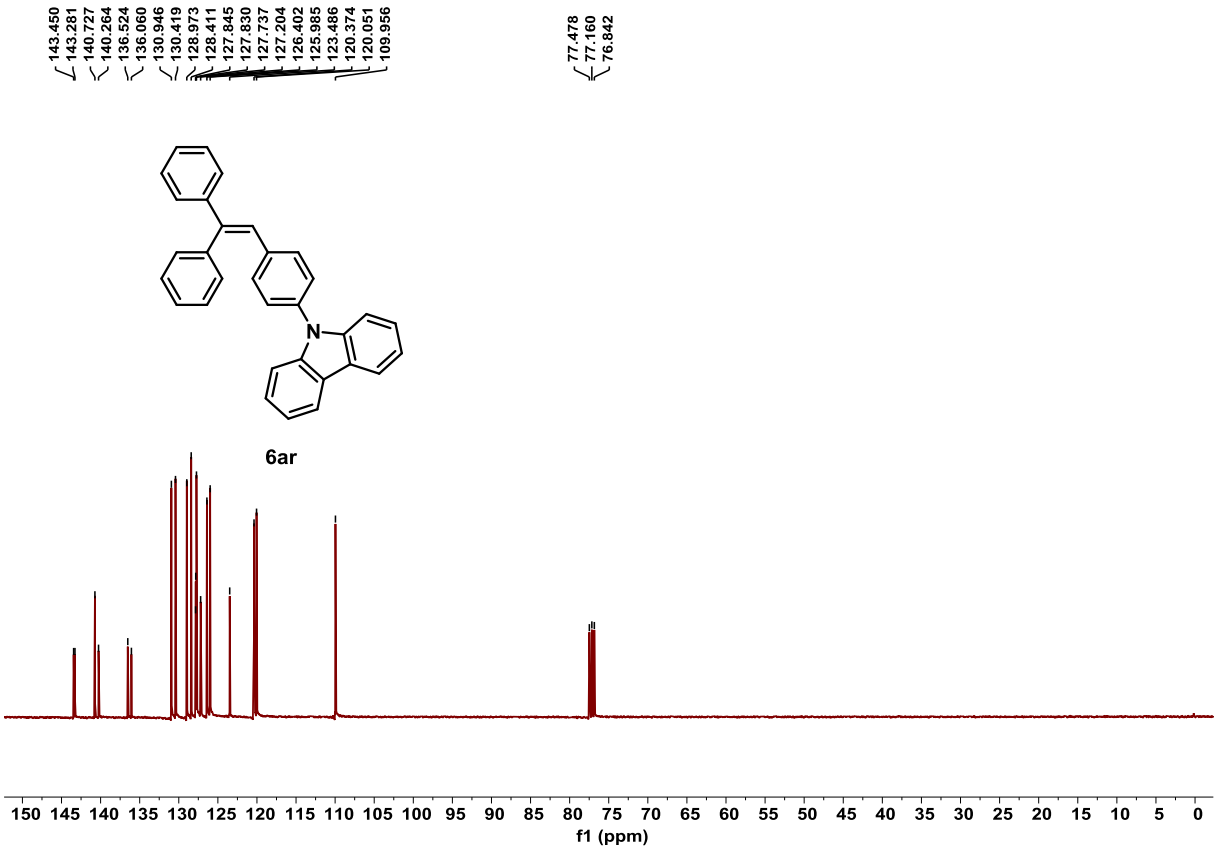

Figure S124. ^{13}C NMR spectrum of product **6ar**, related to **Scheme 3**.

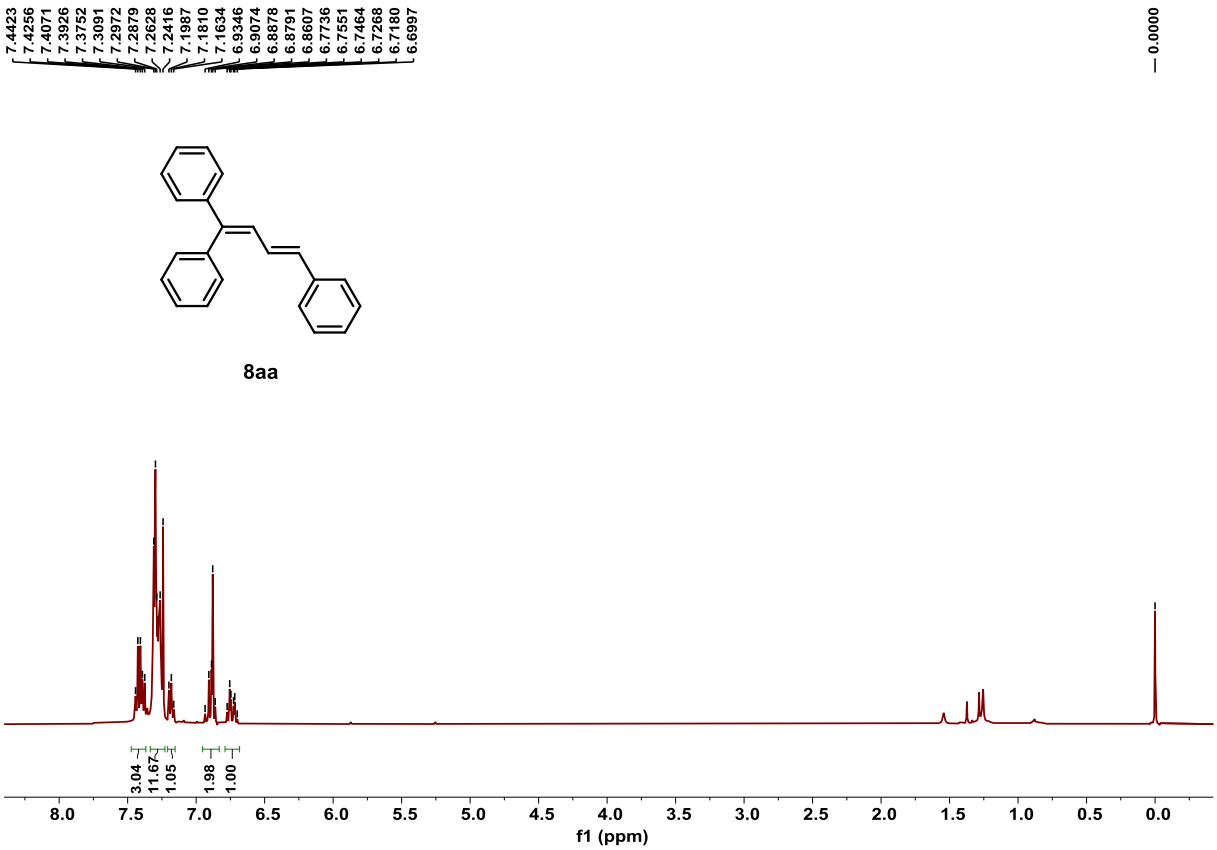

Figure S125. ^{1}**H NMR** spectrum of product **8aa**, related to **Scheme 4**.

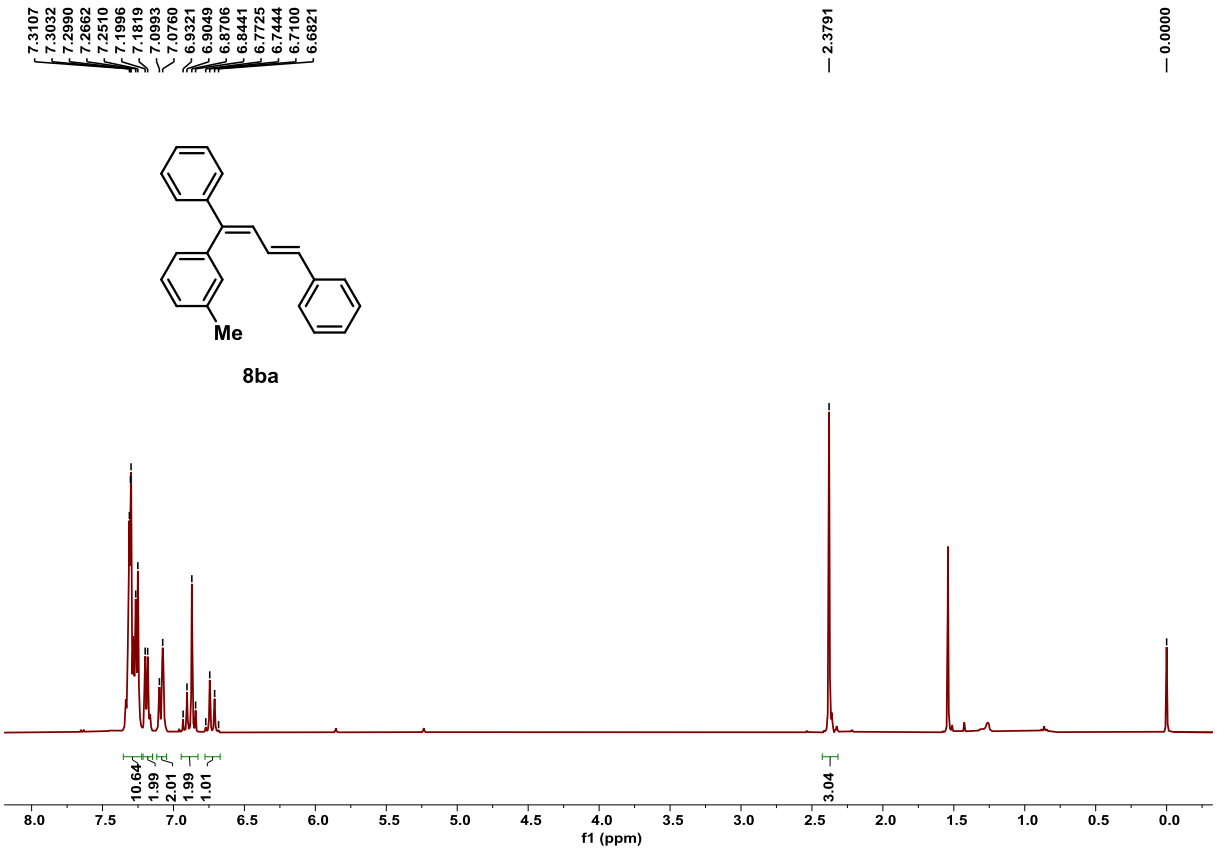

Figure S126. ^{1}**H NMR** spectrum of product **8ba**, related to **Scheme 4**.

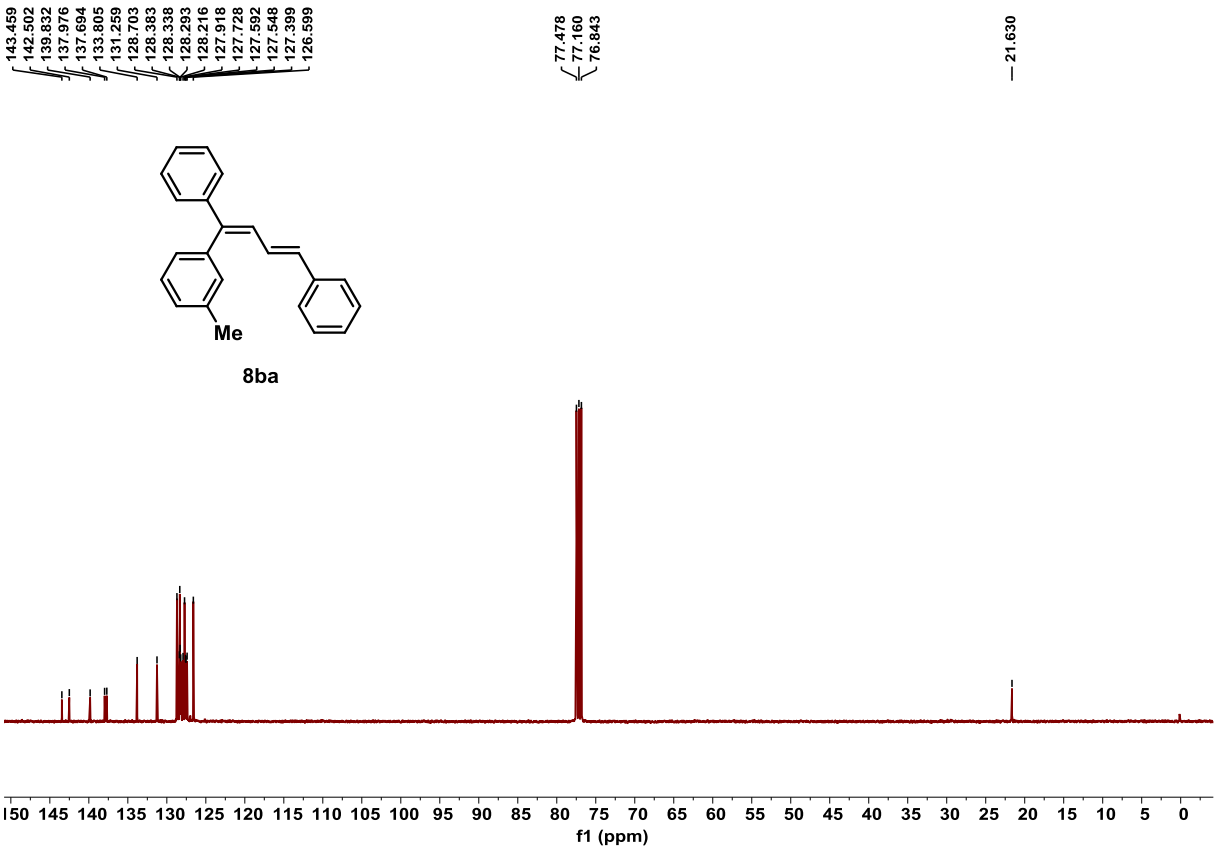

Figure S127. ^{13}**C NMR** spectrum of product **8ba**, related to **Scheme 4**.

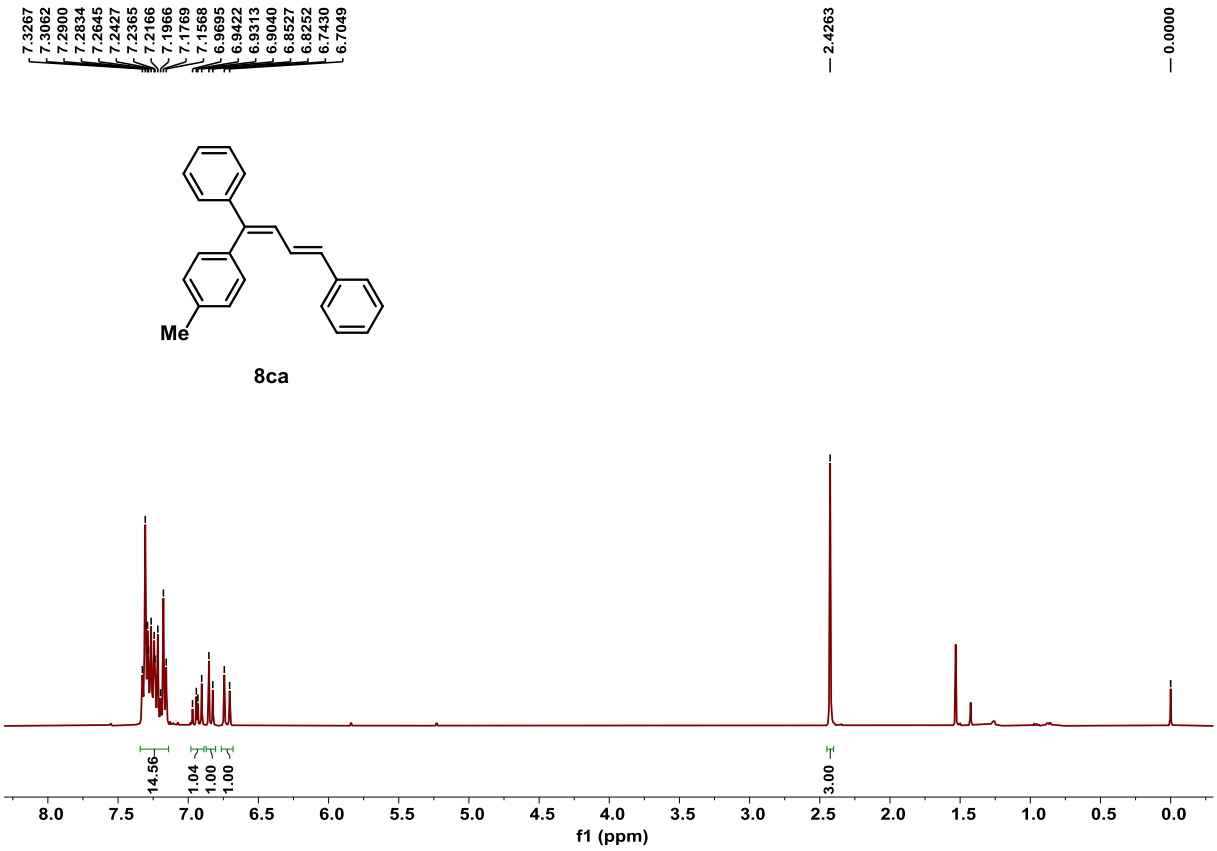

Figure S128. ^{1}**H NMR** spectrum of product **8ca**, related to **Scheme 4**.

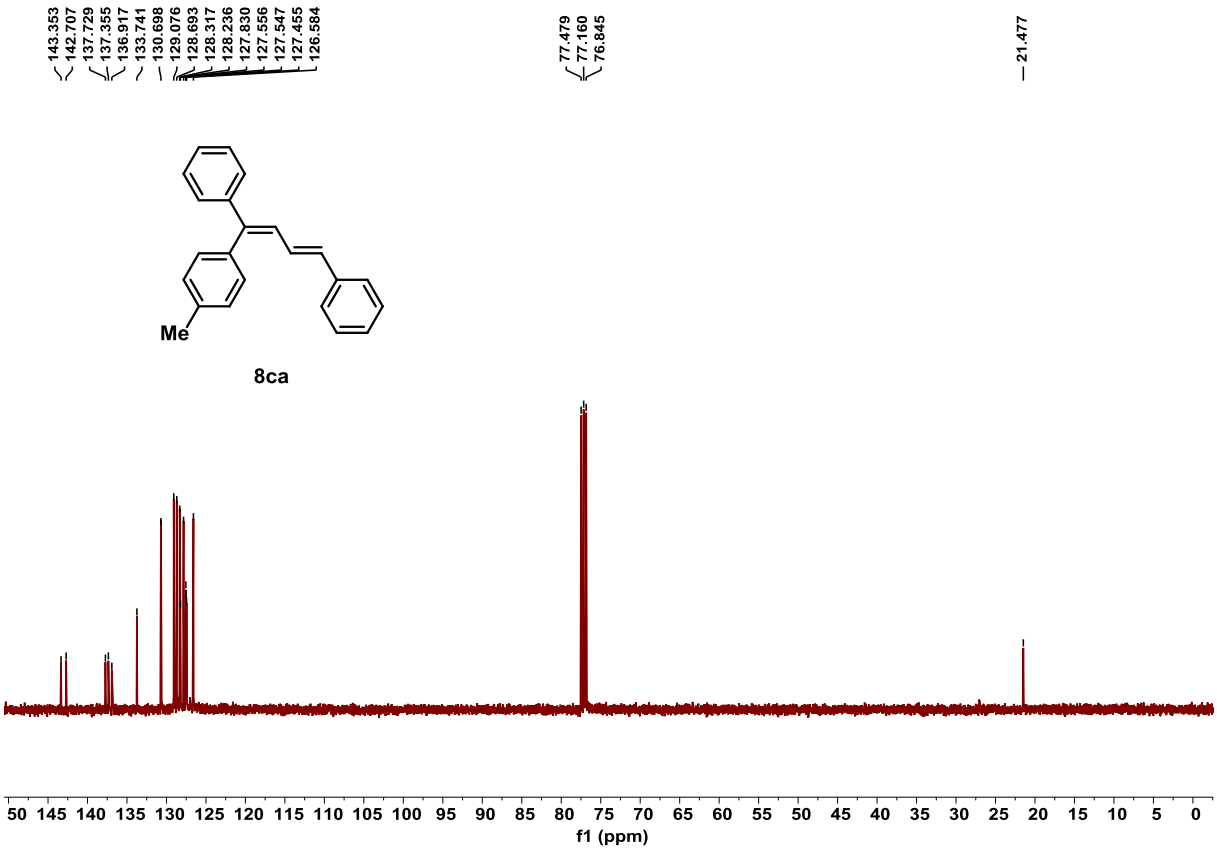

Figure S129. ^{13}**C NMR** spectrum of product **8ca**, related to **Scheme 4**.

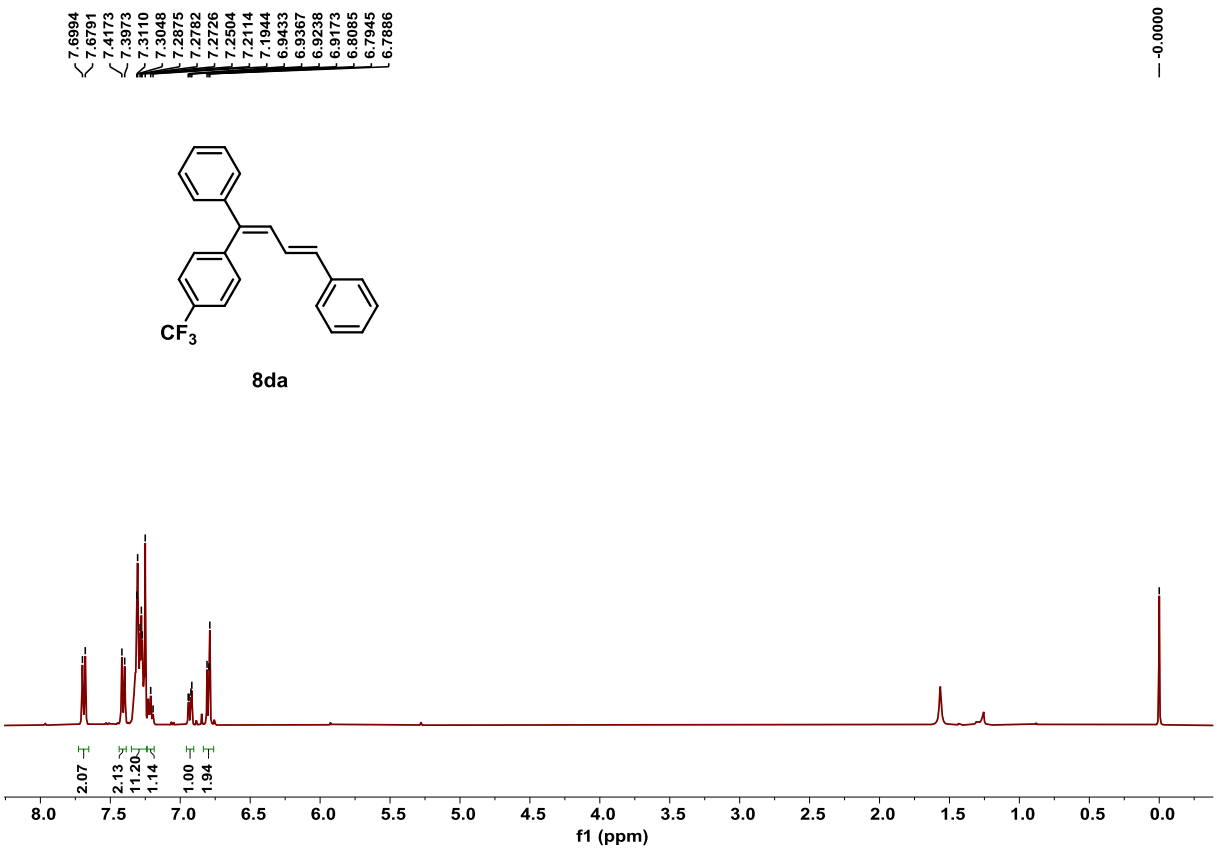

Figure S130. ^{1}**H NMR** spectrum of product **8da**, related to **Scheme 4**.

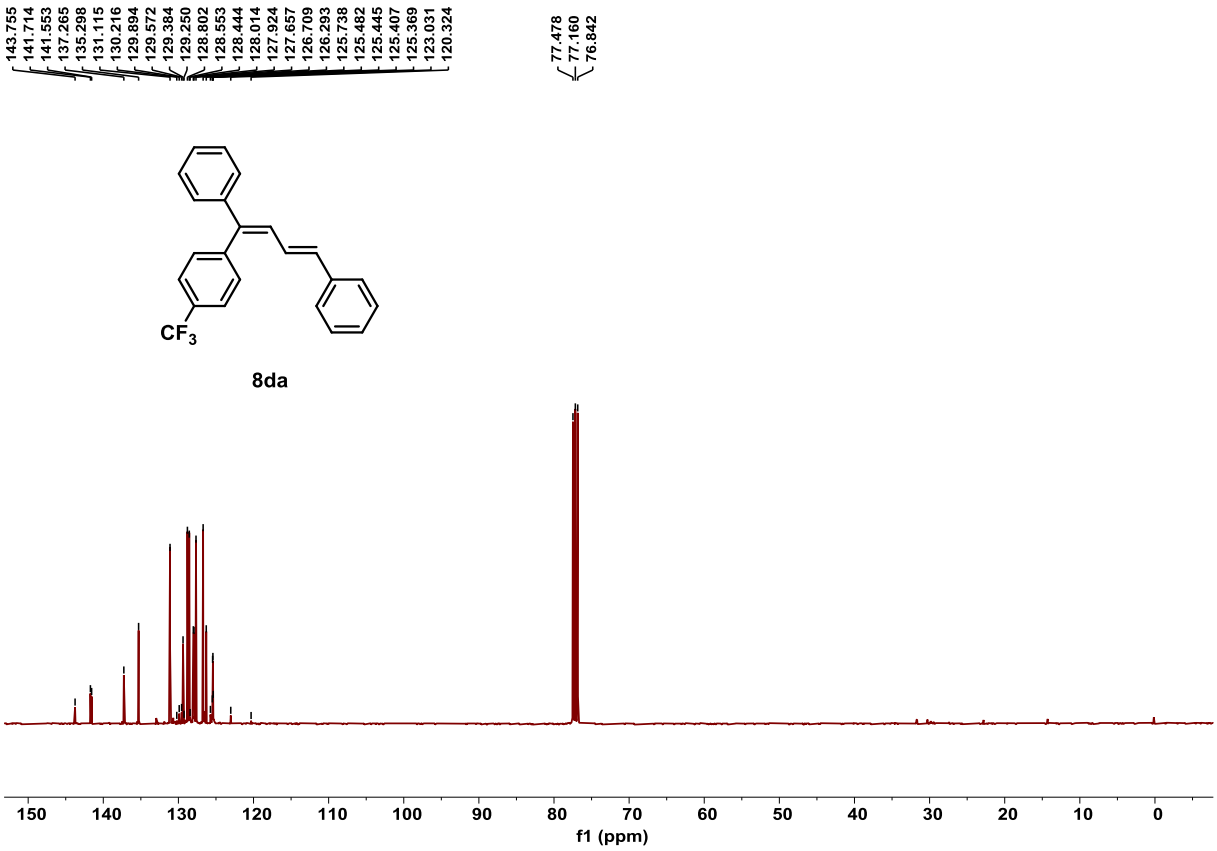

Figure S131. ^{13}**C NMR** spectrum of product **8da**, related to **Scheme 4**.

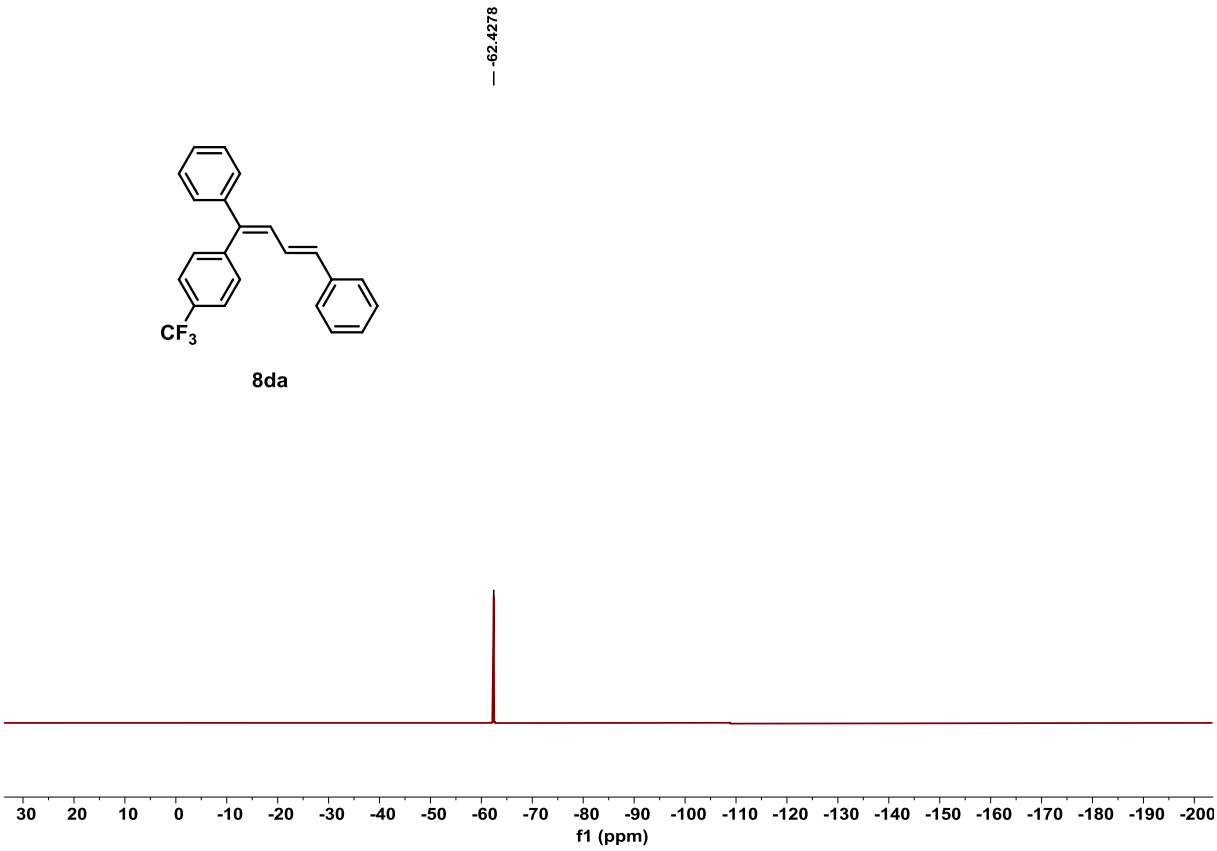

Figure S132. ^{19}**F NMR** spectrum of product **8da**, related to **Scheme 4**.

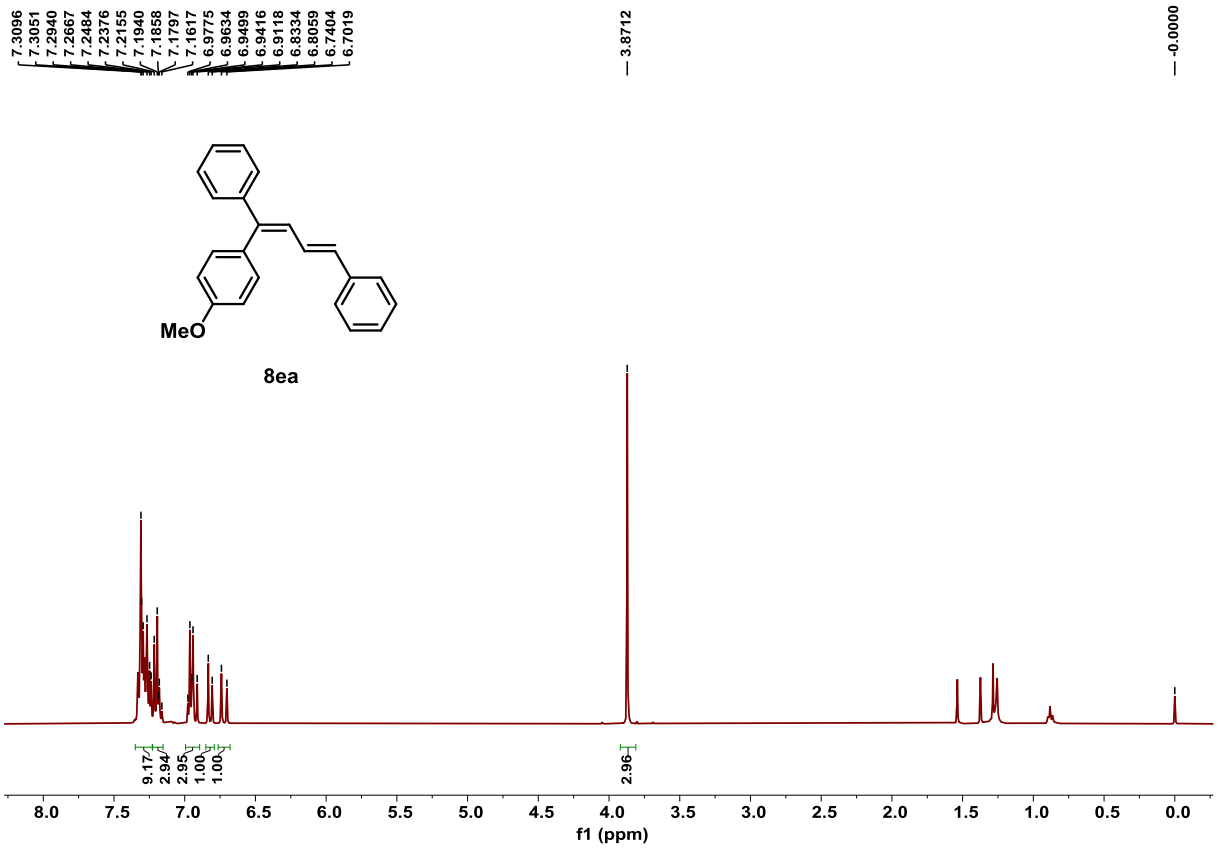

Figure S133. ^{1}**H NMR** spectrum of product **8ea**, related to **Scheme 4**.

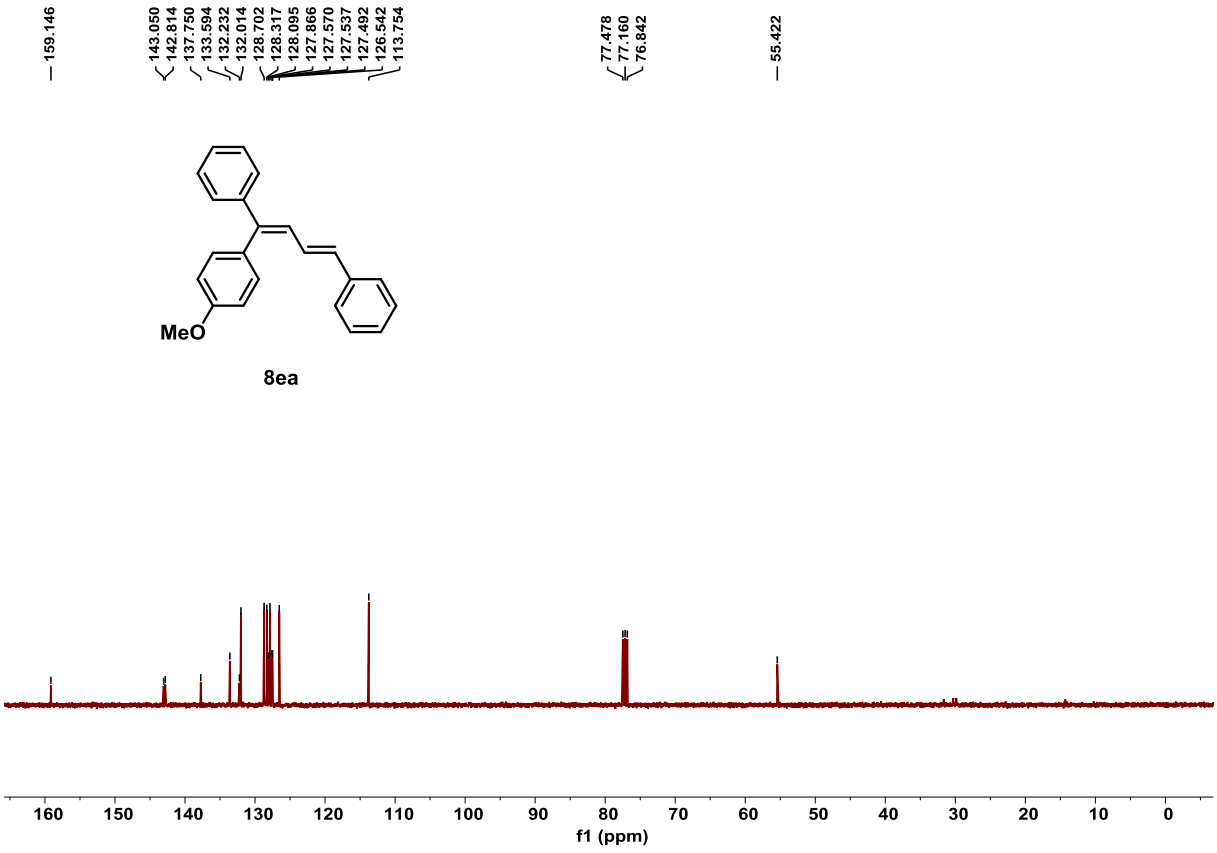

Figure S134. ^{13}**C NMR** spectrum of product **8ea**, related to **Scheme 4**.

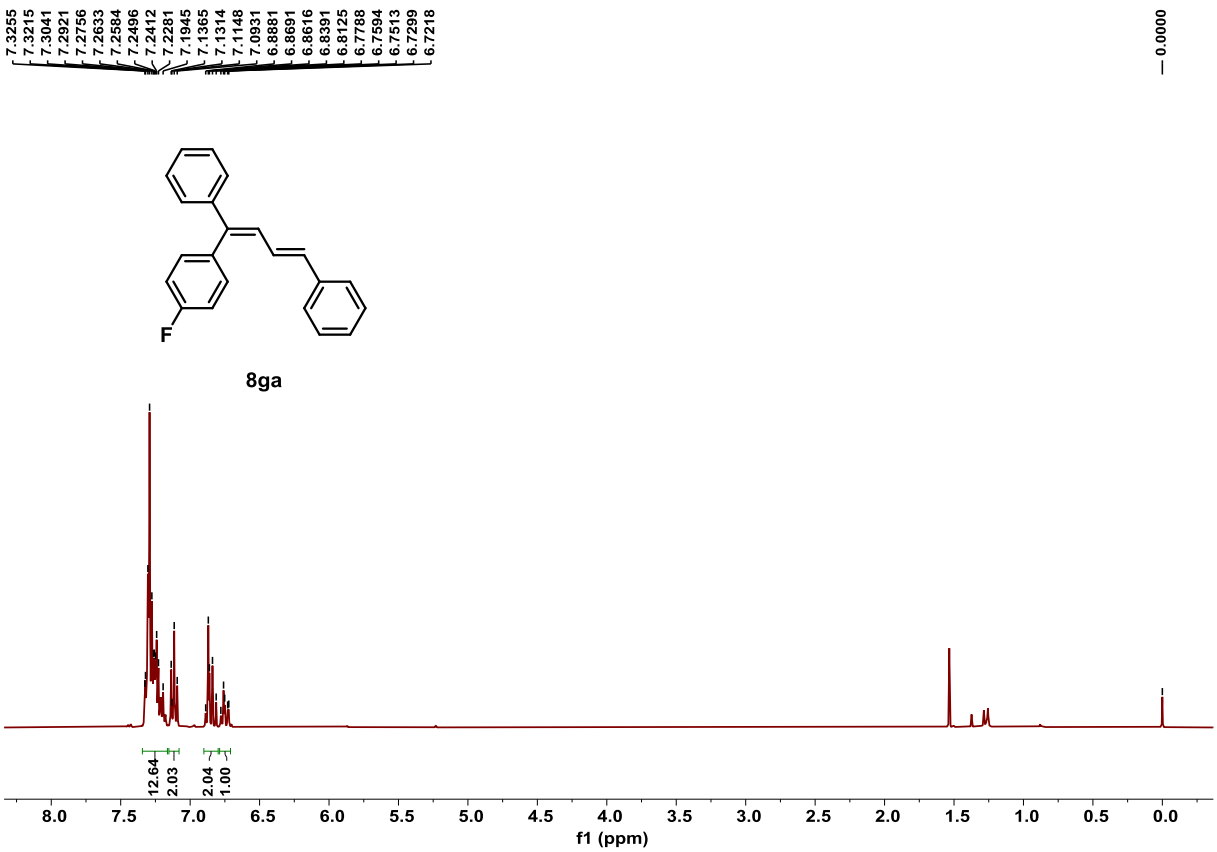

Figure S135. ^{1}**H NMR** spectrum of product **8ga**, related to **Scheme 4**.

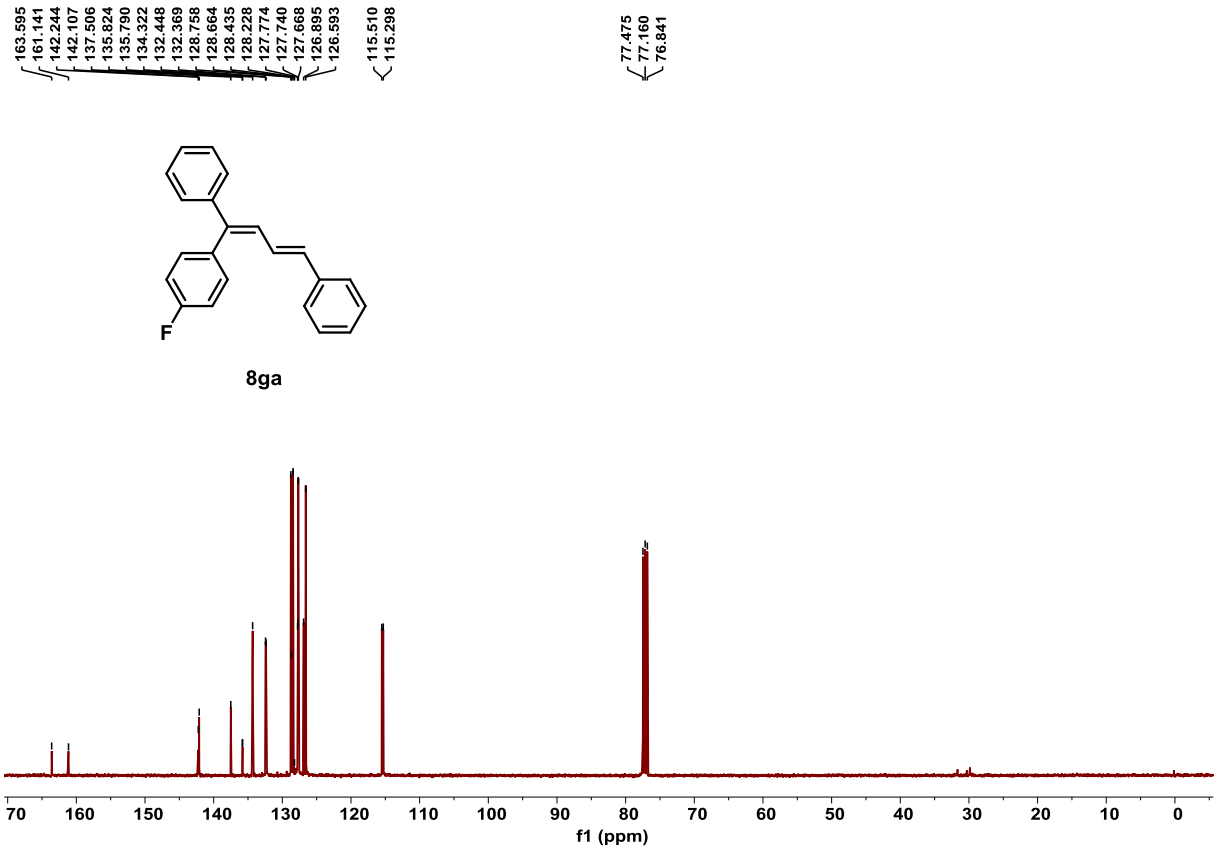

Figure S136. ^{13}**C NMR** spectrum of product **8ga**, related to **Scheme 4**.

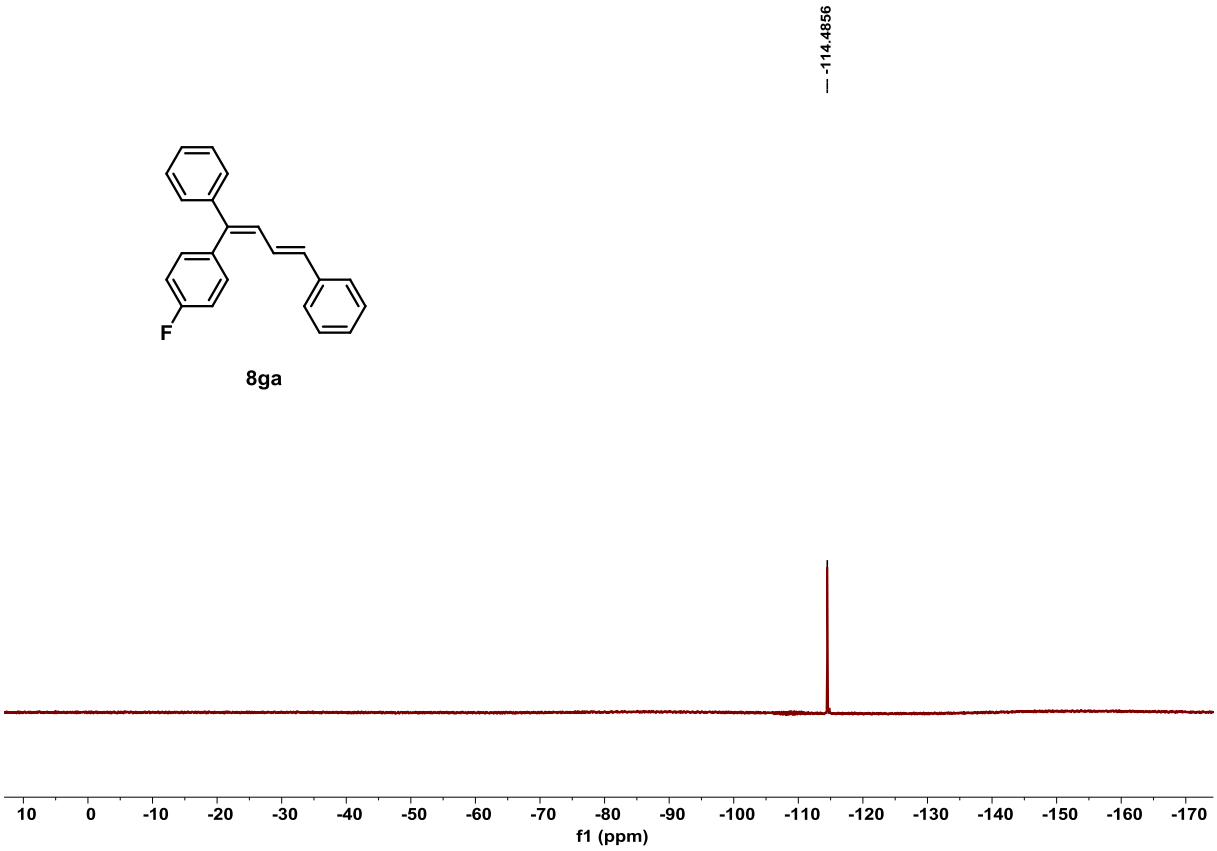

Figure S137. ^{19}**F NMR** spectrum of product **8ga**, related to **Scheme 4**.

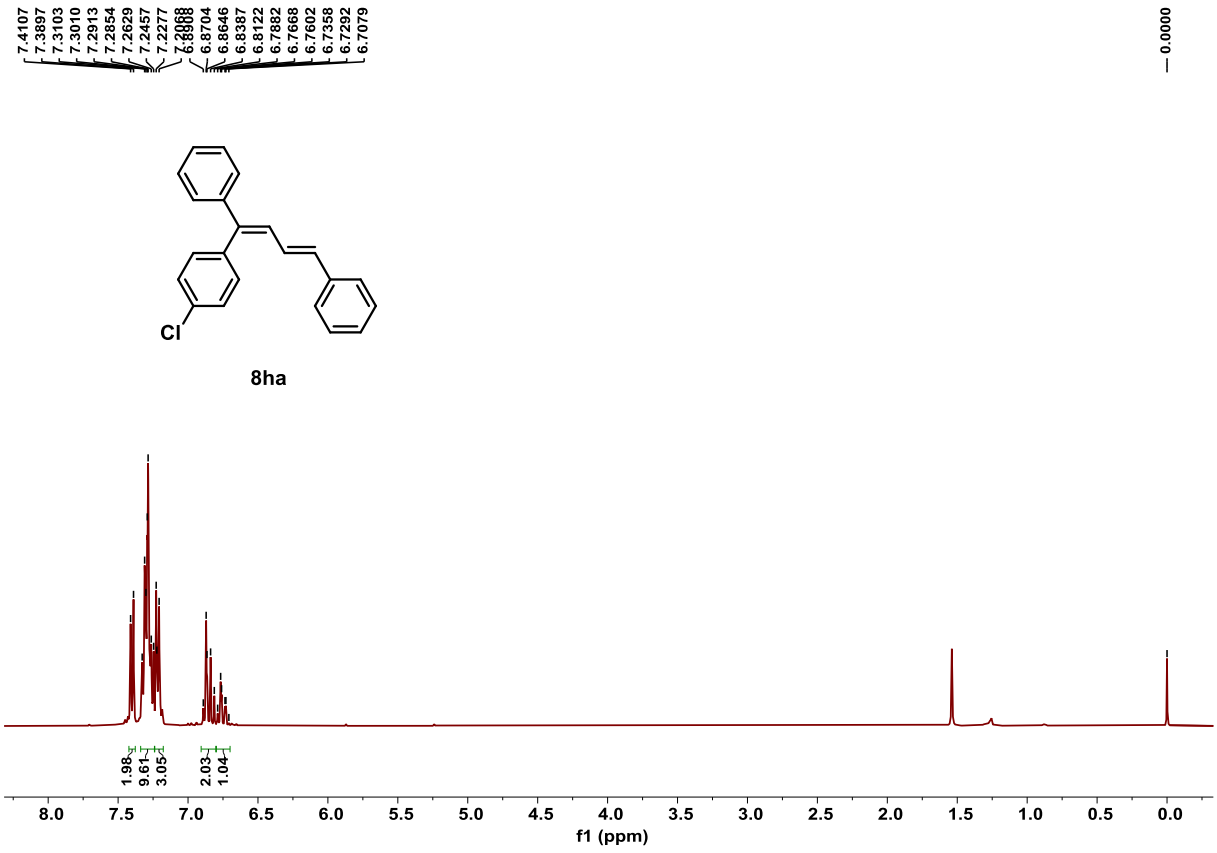

Figure S138. ^{1}**H NMR** spectrum of product **8ha**, related to **Scheme 4**.

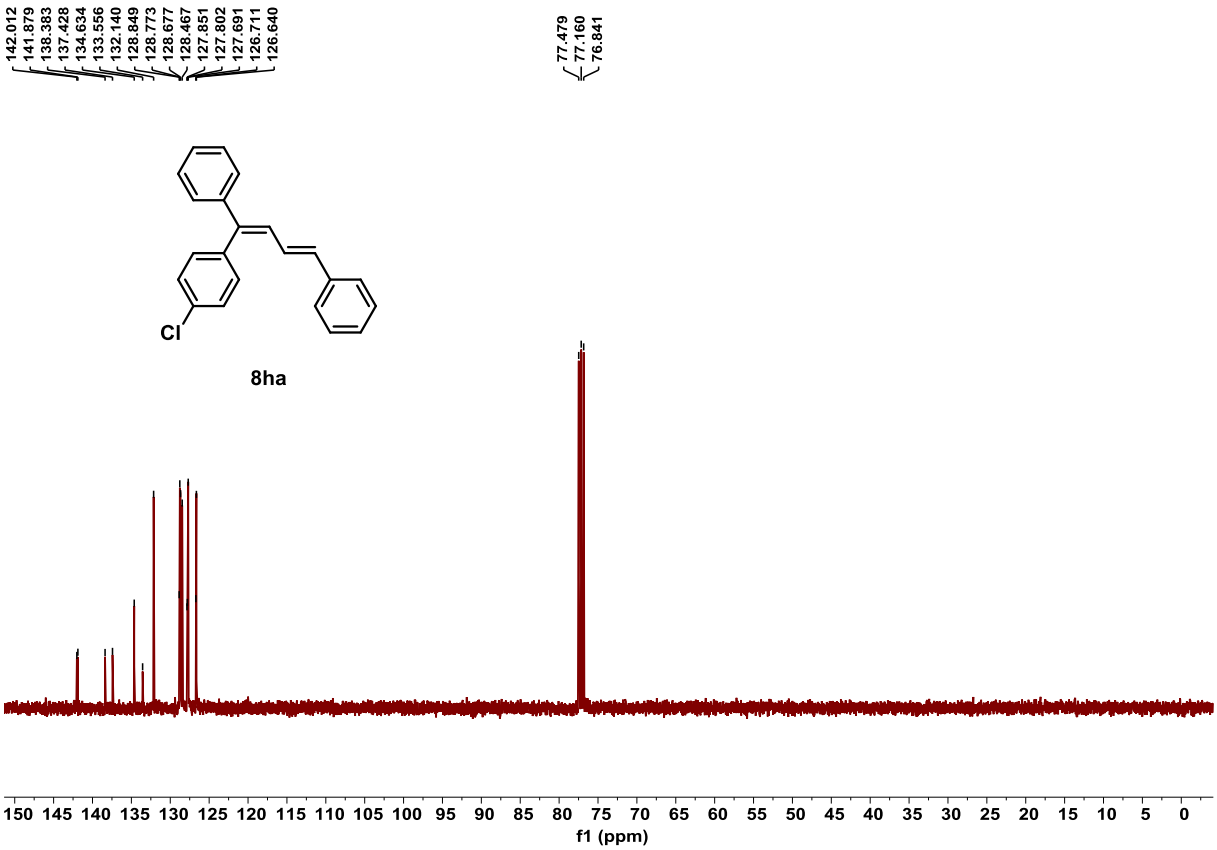

Figure S139. ^{13}**C NMR** spectrum of product **8ha**, related to **Scheme 4**.

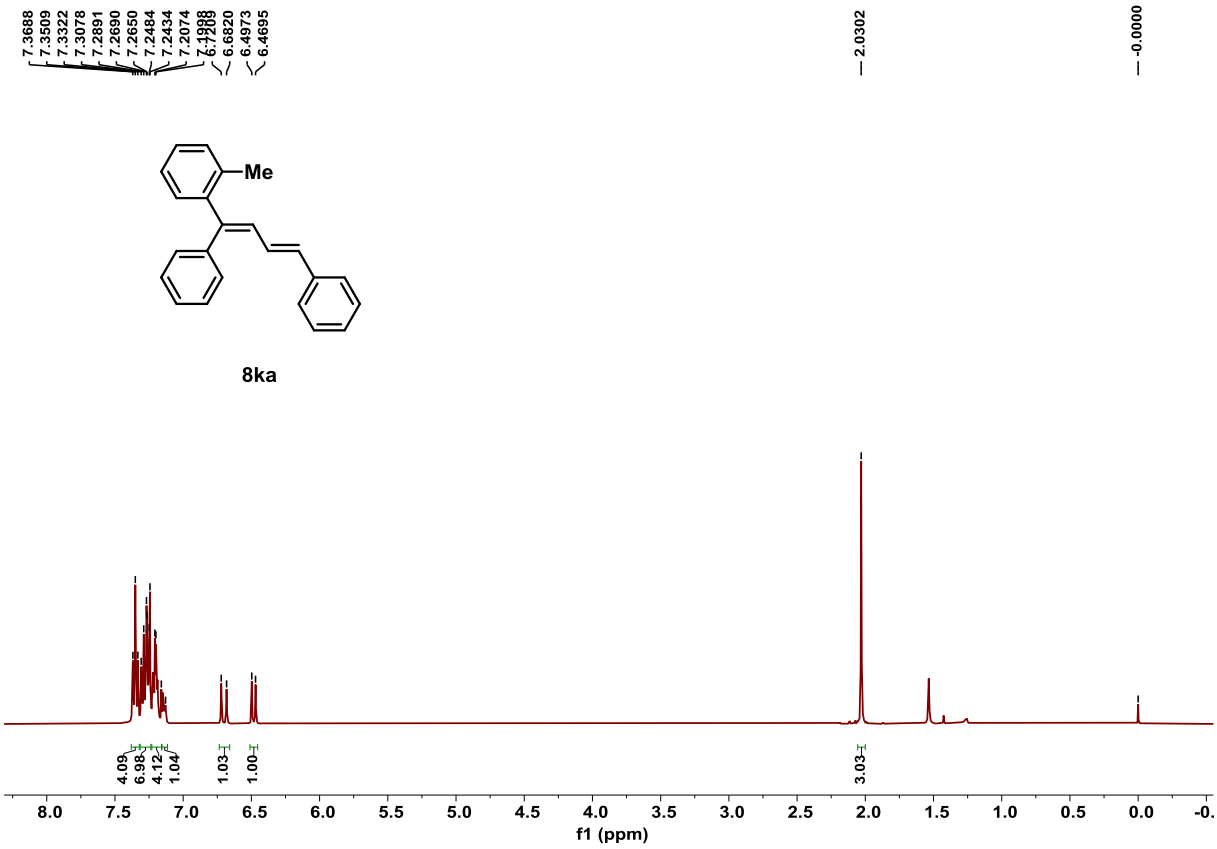

Figure S140. ^{1}**H NMR** spectrum of product **8ka**, related to **Scheme 4**.

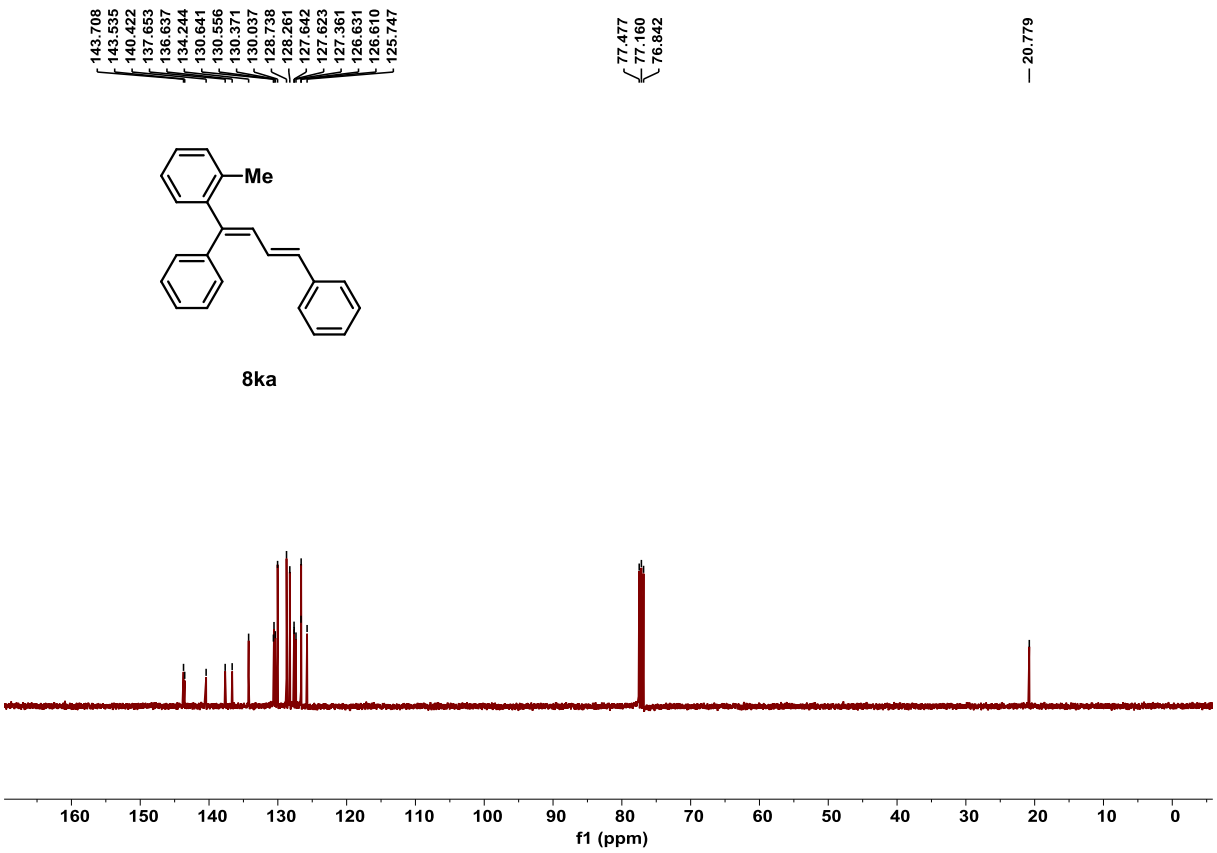

Figure S141. ^{13}**C NMR** spectrum of product **8ka**, related to **Scheme 4**.

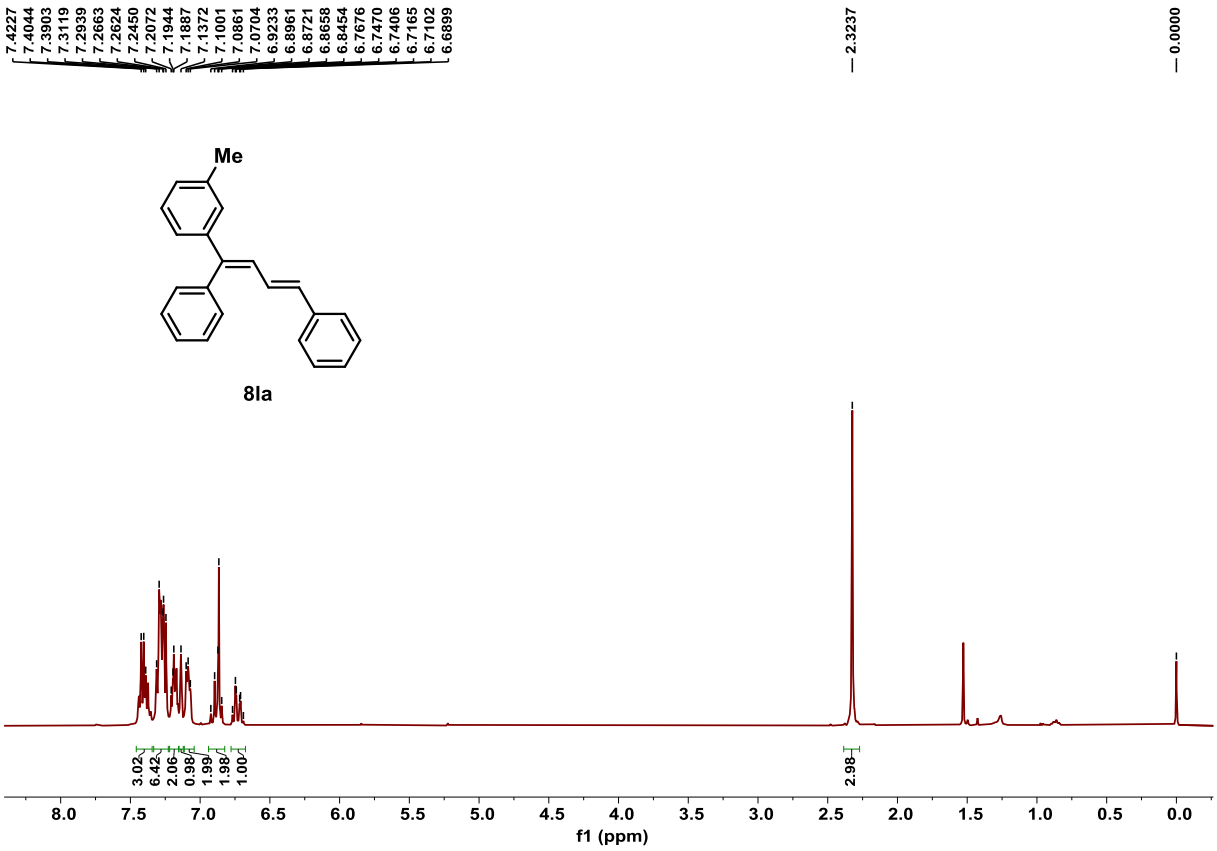

Figure S142. ^{1}**H NMR** spectrum of product **8la**, related to **Scheme 4**.

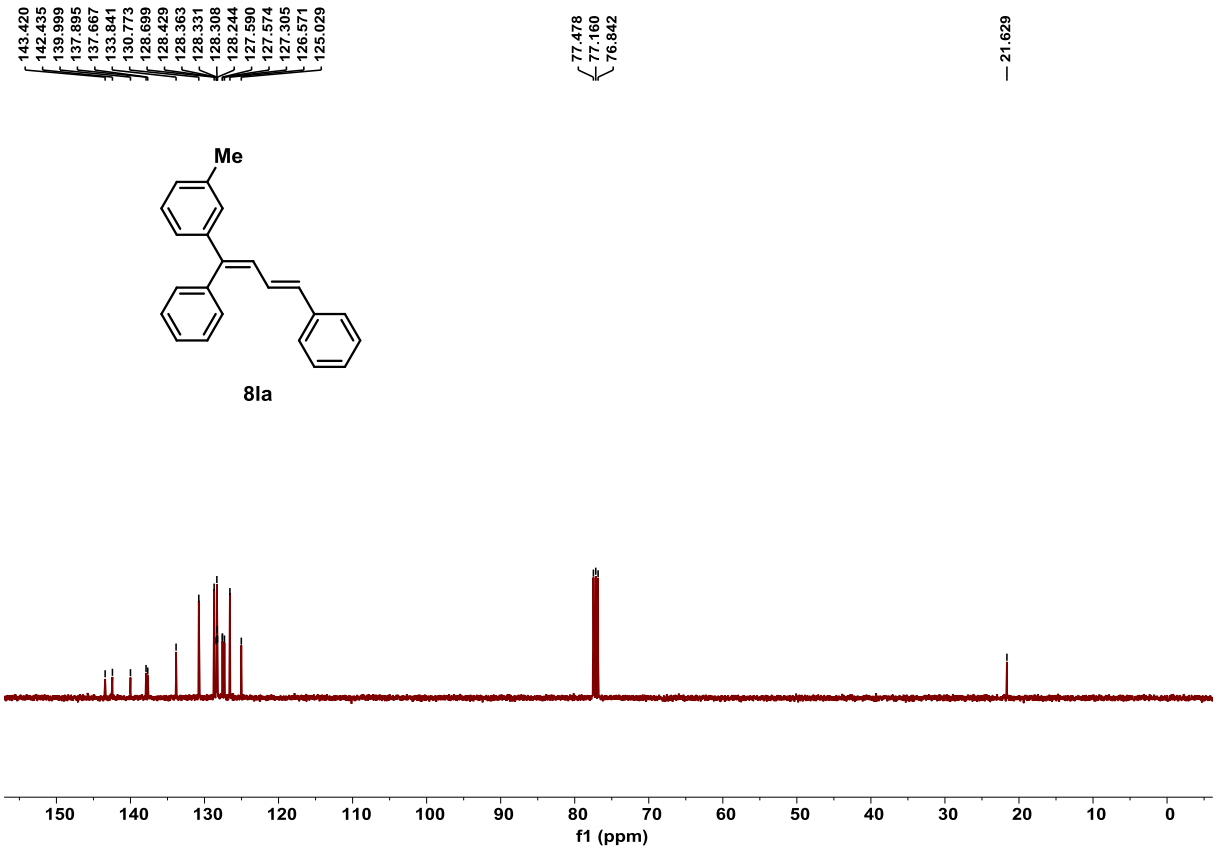

Figure S143. ^{13}**C NMR** spectrum of product **8la**, related to **Scheme 4**.

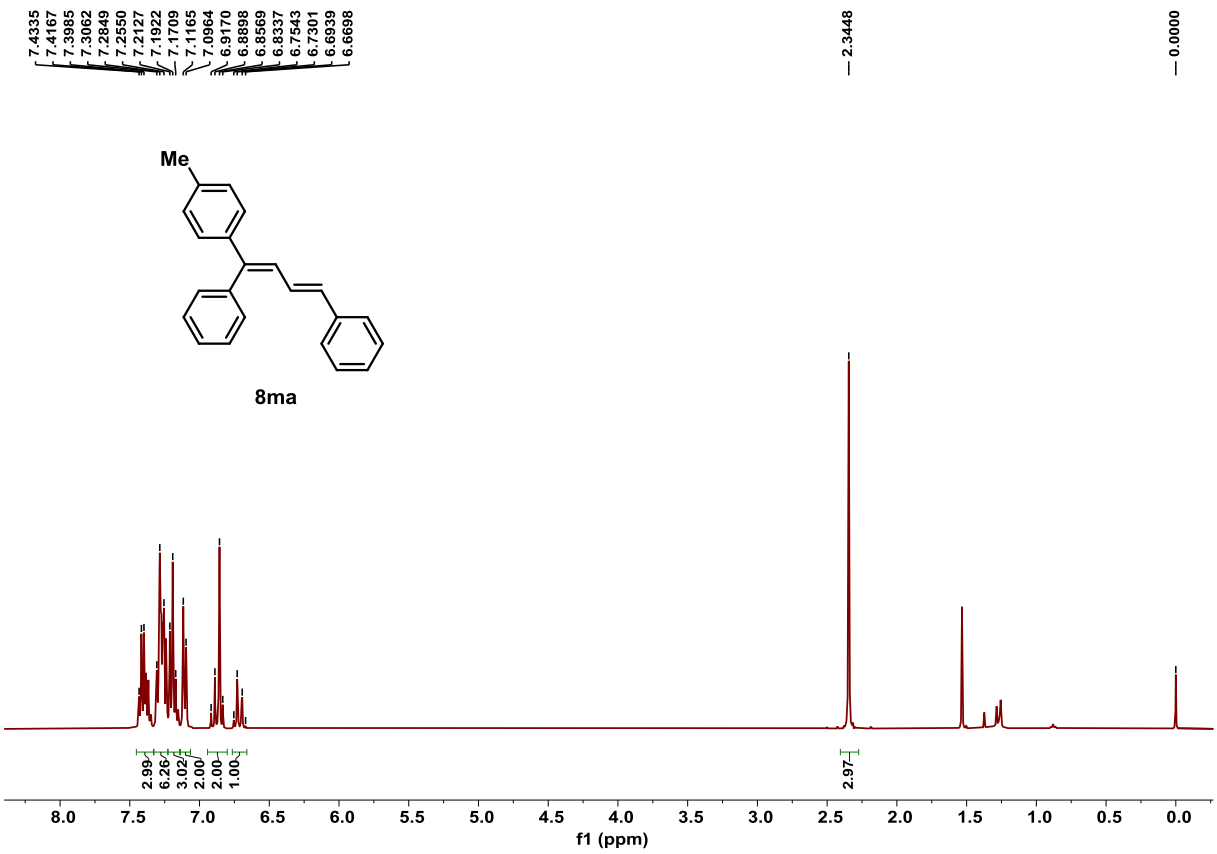

Figure S144. ^{1}**H NMR** spectrum of product **8ma**, related to **Scheme 4**.

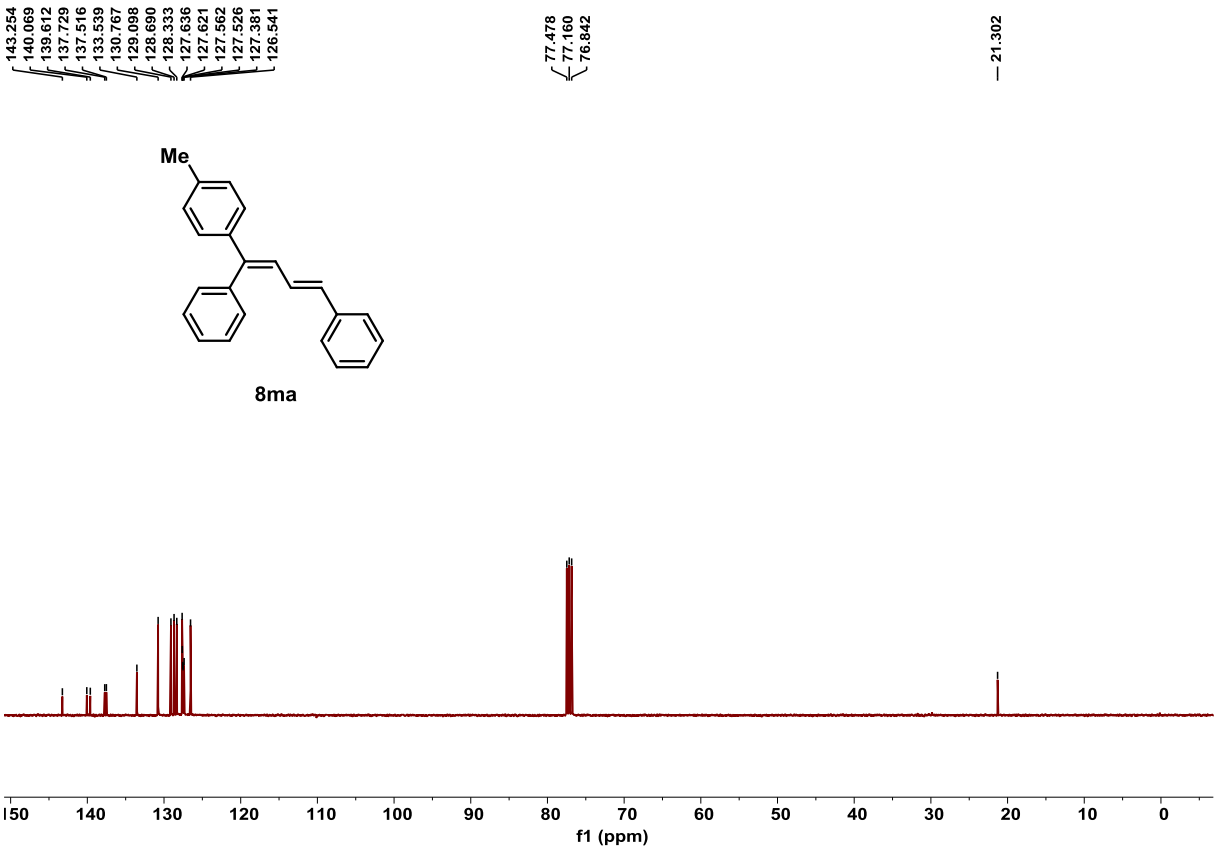

Figure S145. ^{13}**C NMR** spectrum of product **8ma**, related to **Scheme 4**.

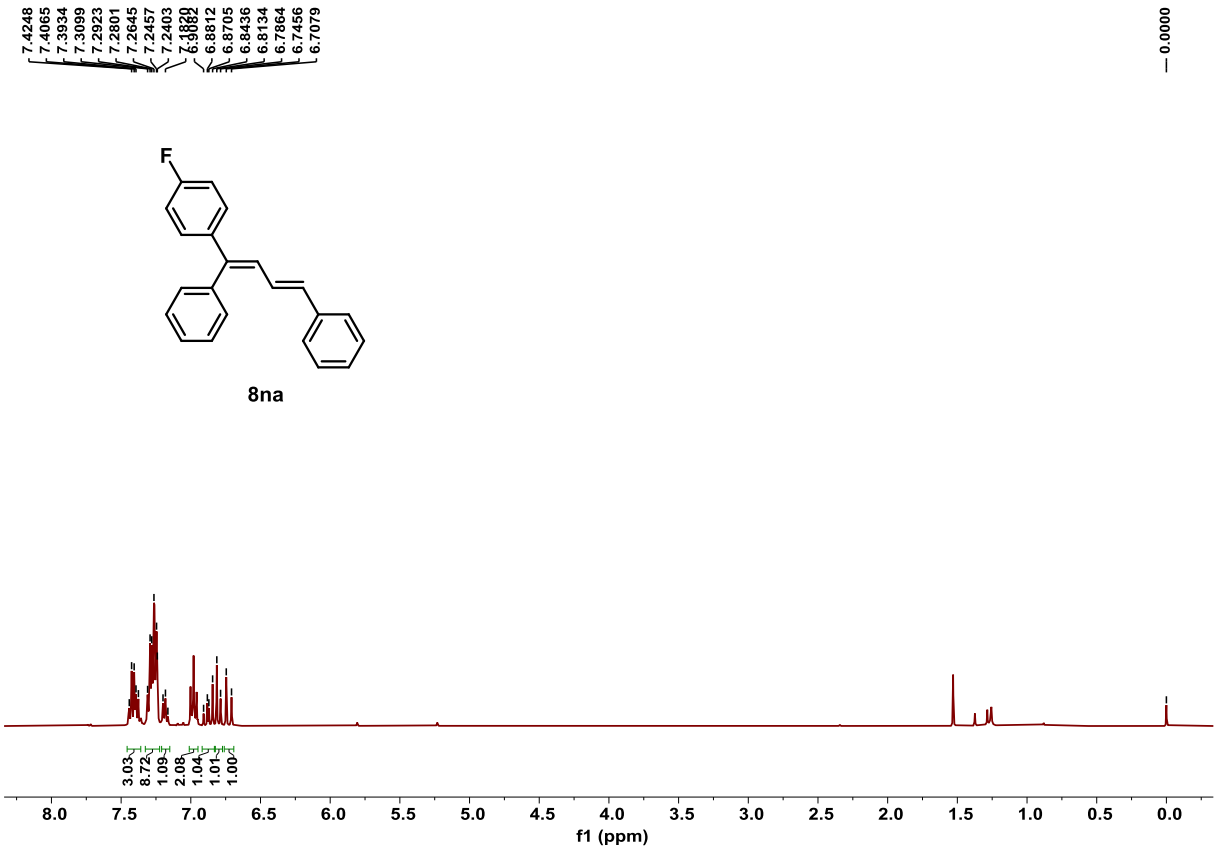

Figure S146. ^{1}**H NMR** spectrum of product **8na**, related to **Scheme 4**.

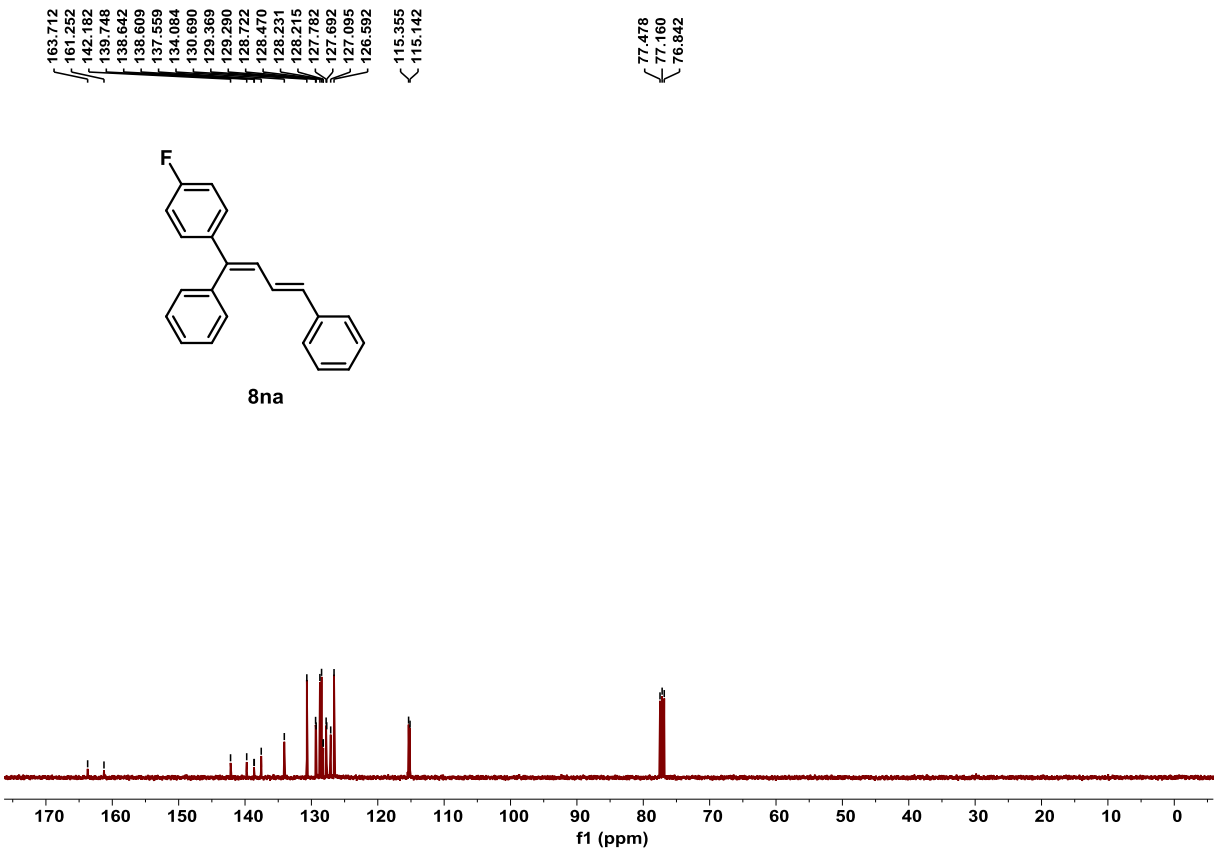

Figure S147. ^{13}**C NMR** spectrum of product **8na**, related to **Scheme 4**.

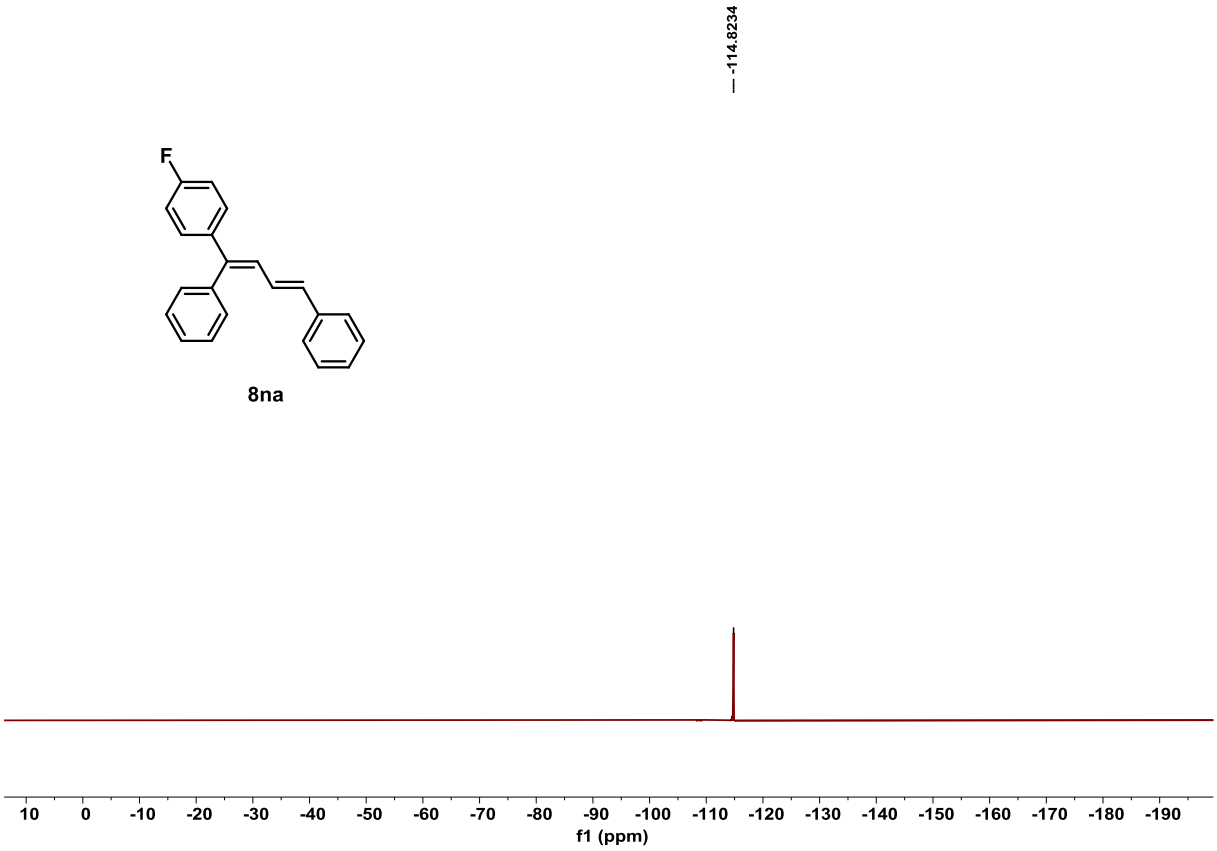

Figure S148. ^{19}**F NMR** spectrum of product **8na**, related to **Scheme 4**.

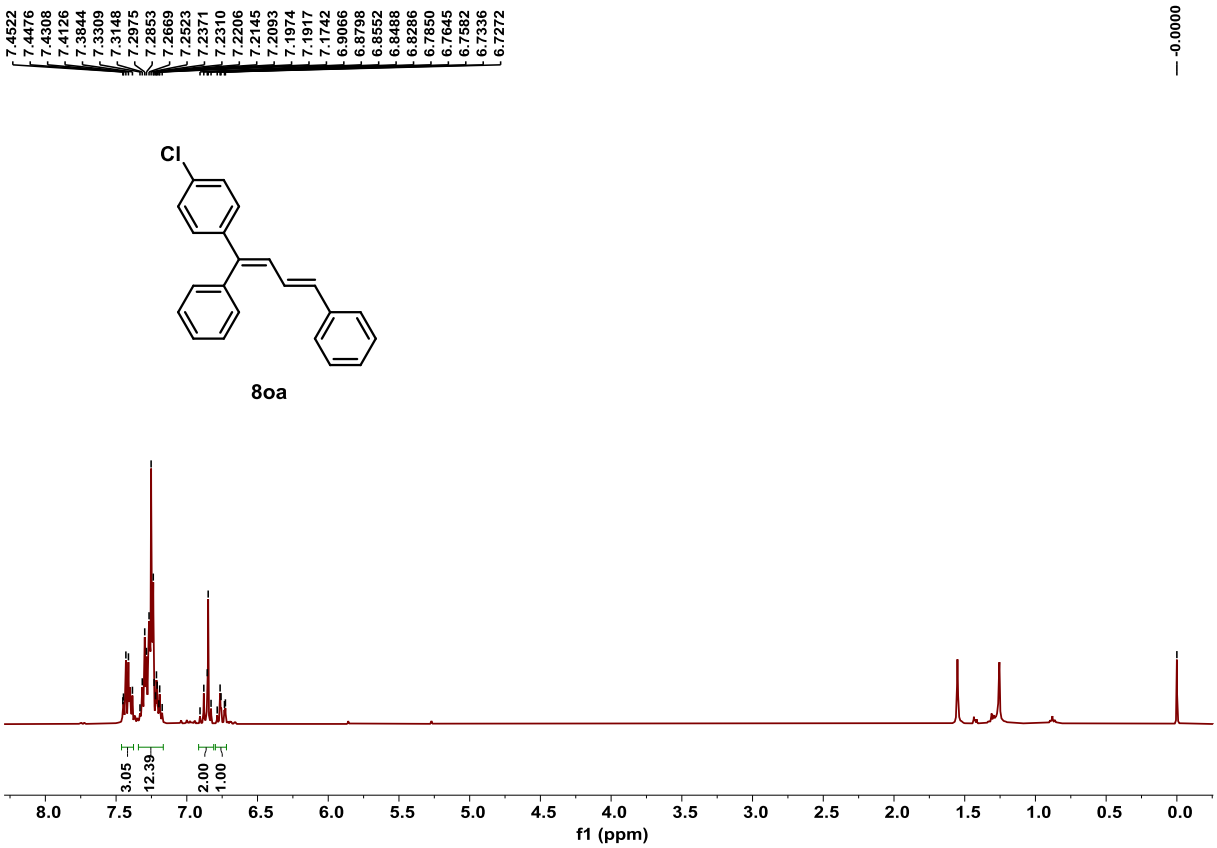

Figure S149. ^{1}H NMR spectrum of product **8oa**, related to **Scheme 4**.

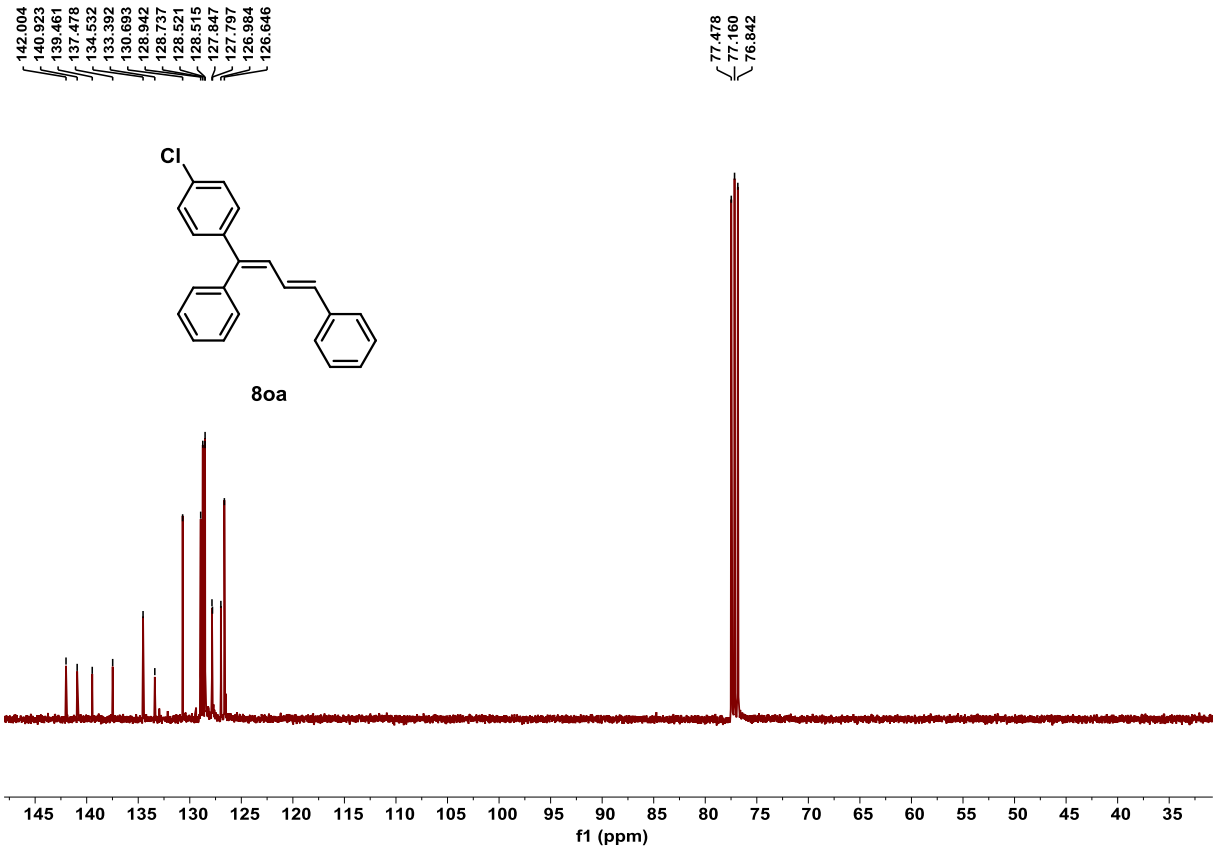

Figure S150. ^{13}C NMR spectrum of product **8oa**, related to **Scheme 4**.

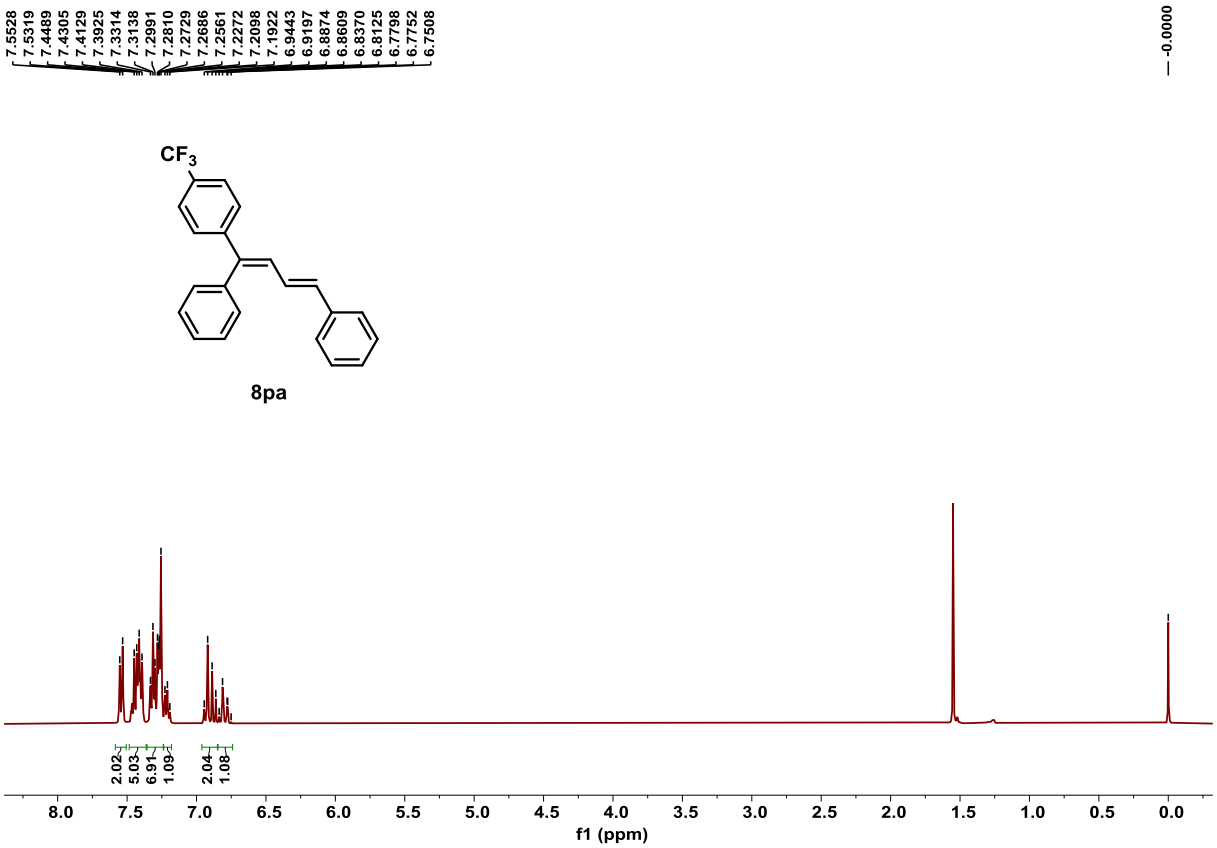

Figure S151. ^{1}H NMR spectrum of product **8pa**, related to **Scheme 4**.

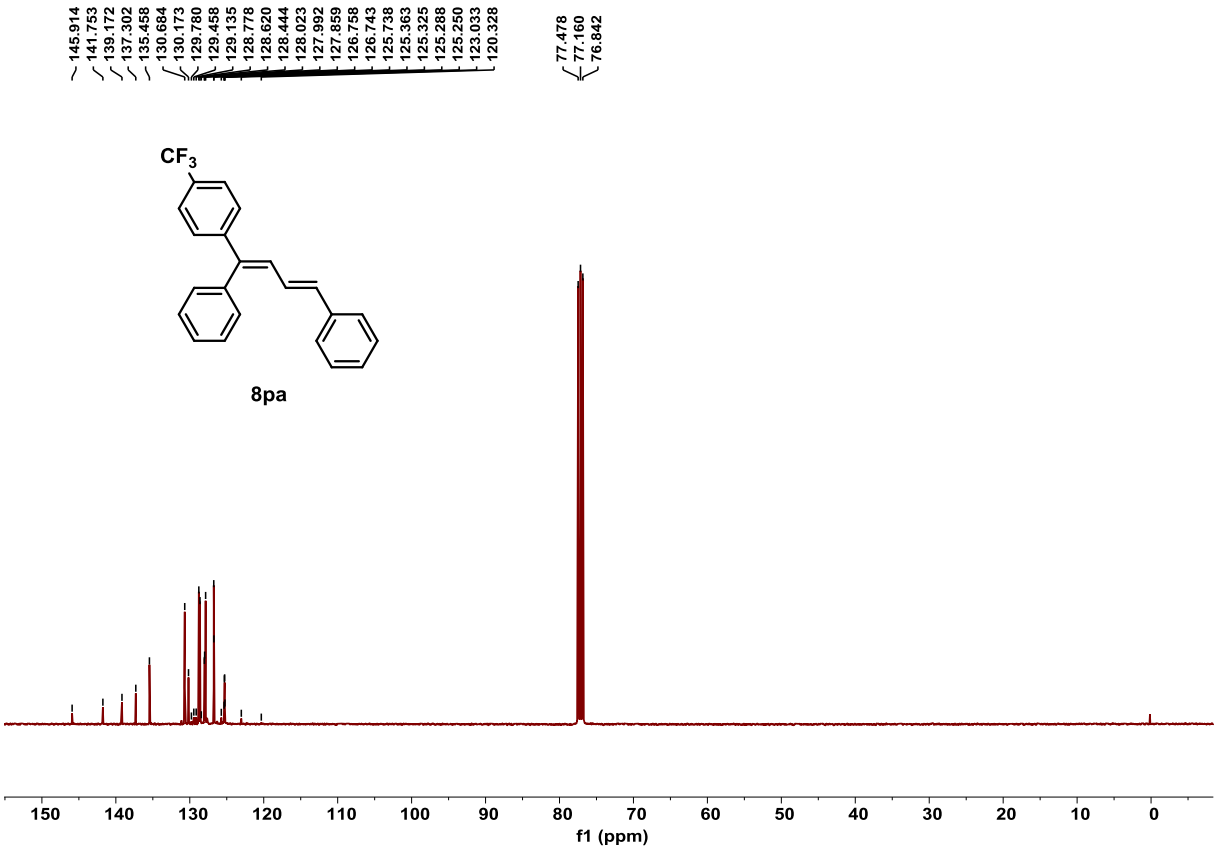

Figure S152. ^{13}C NMR spectrum of product **8pa**, related to **Scheme 4**.

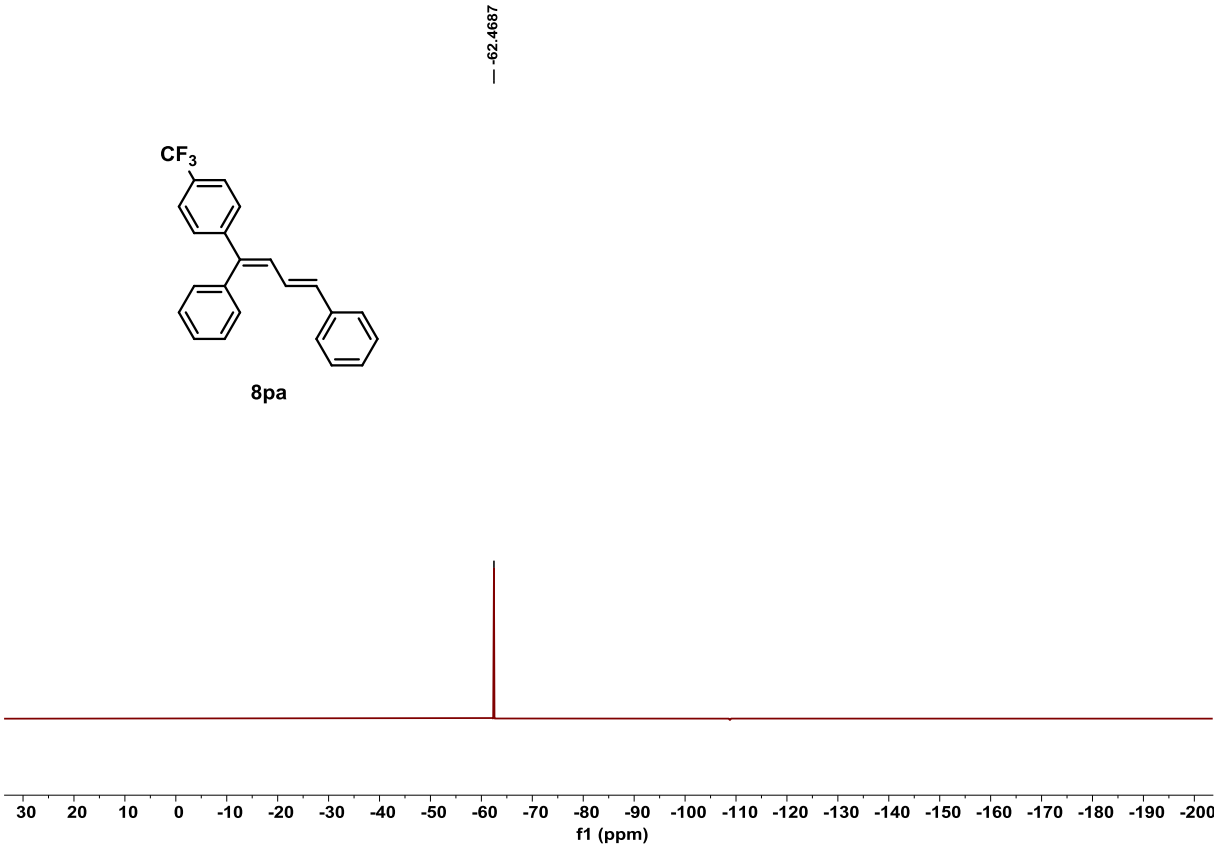

Figure S153. ^{19}F NMR spectrum of product **8pa**, related to **Scheme 4**.

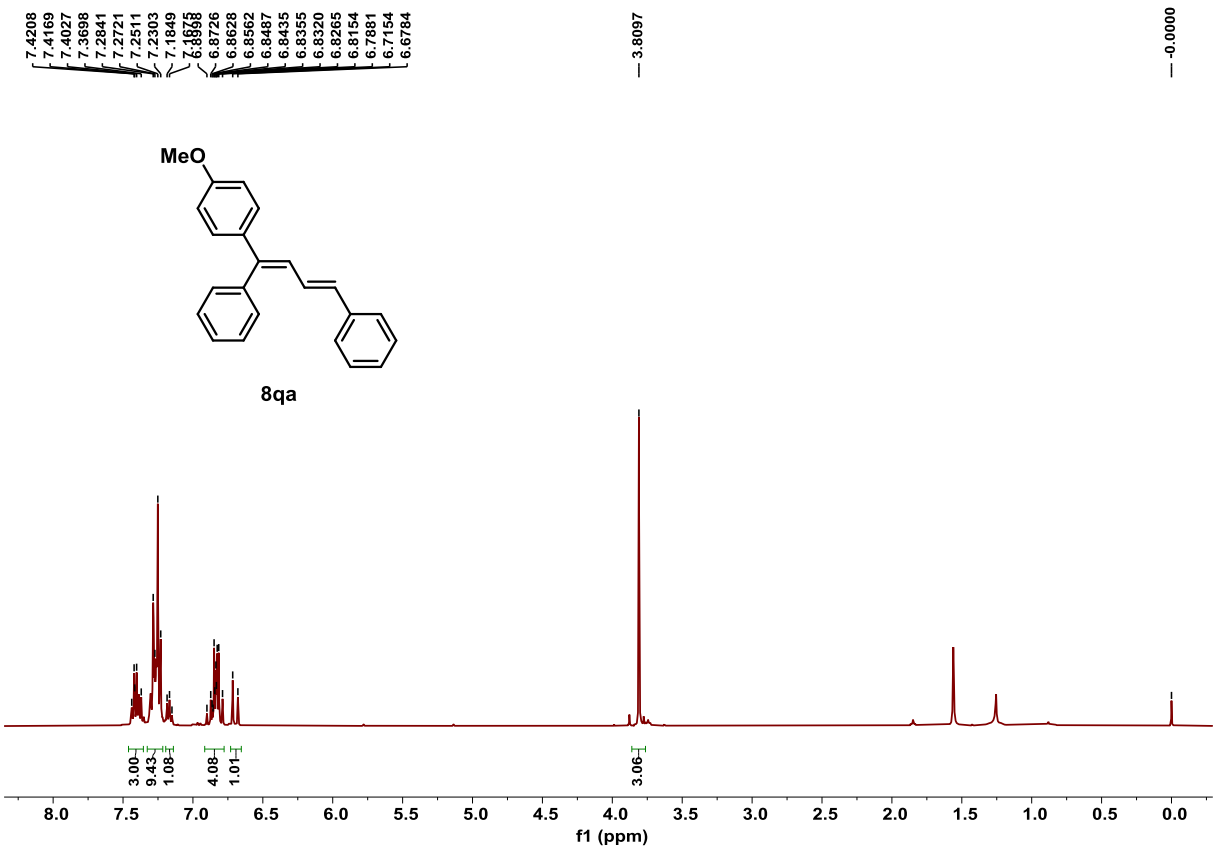

Figure S154. ^{1}H NMR spectrum of product **8qa**, related to **Scheme 4**.

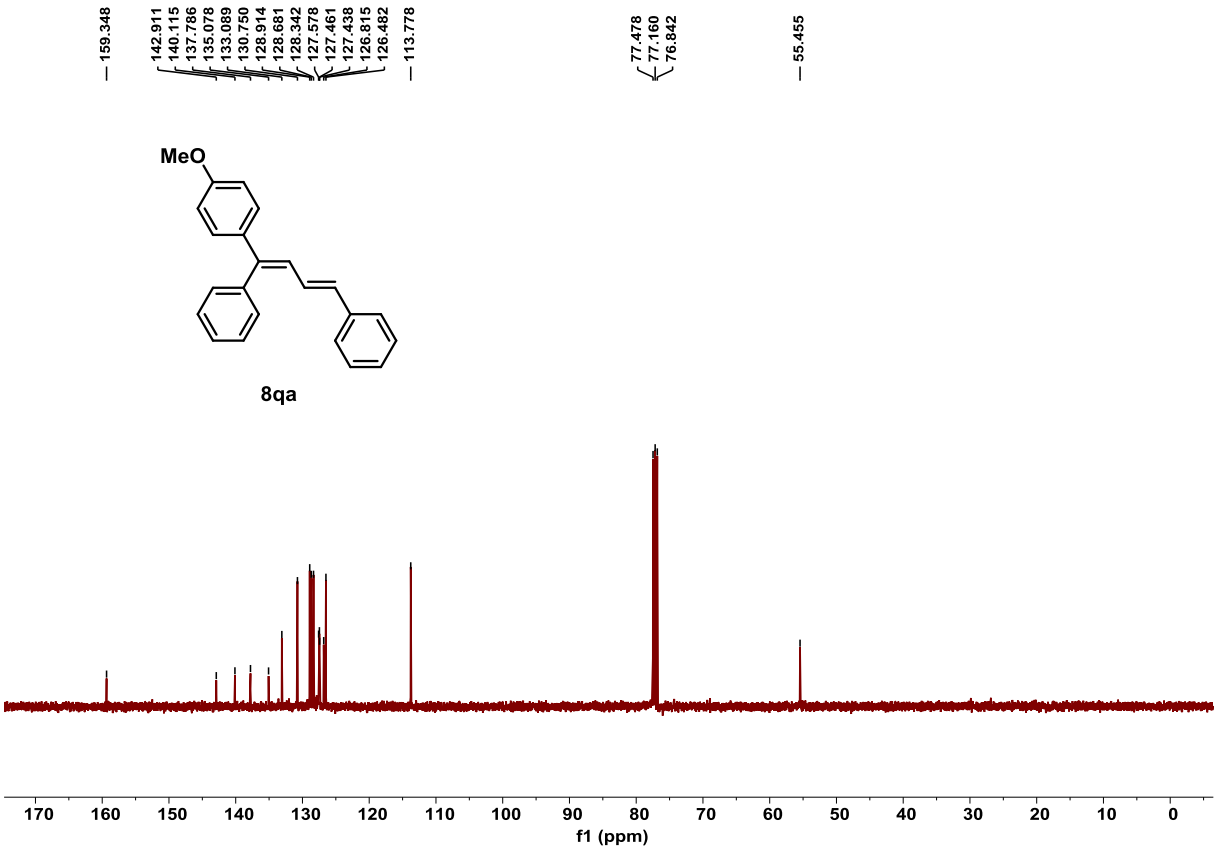

Figure S155. ^{13}**C NMR** spectrum of product **8qa**, related to **Scheme 4**.

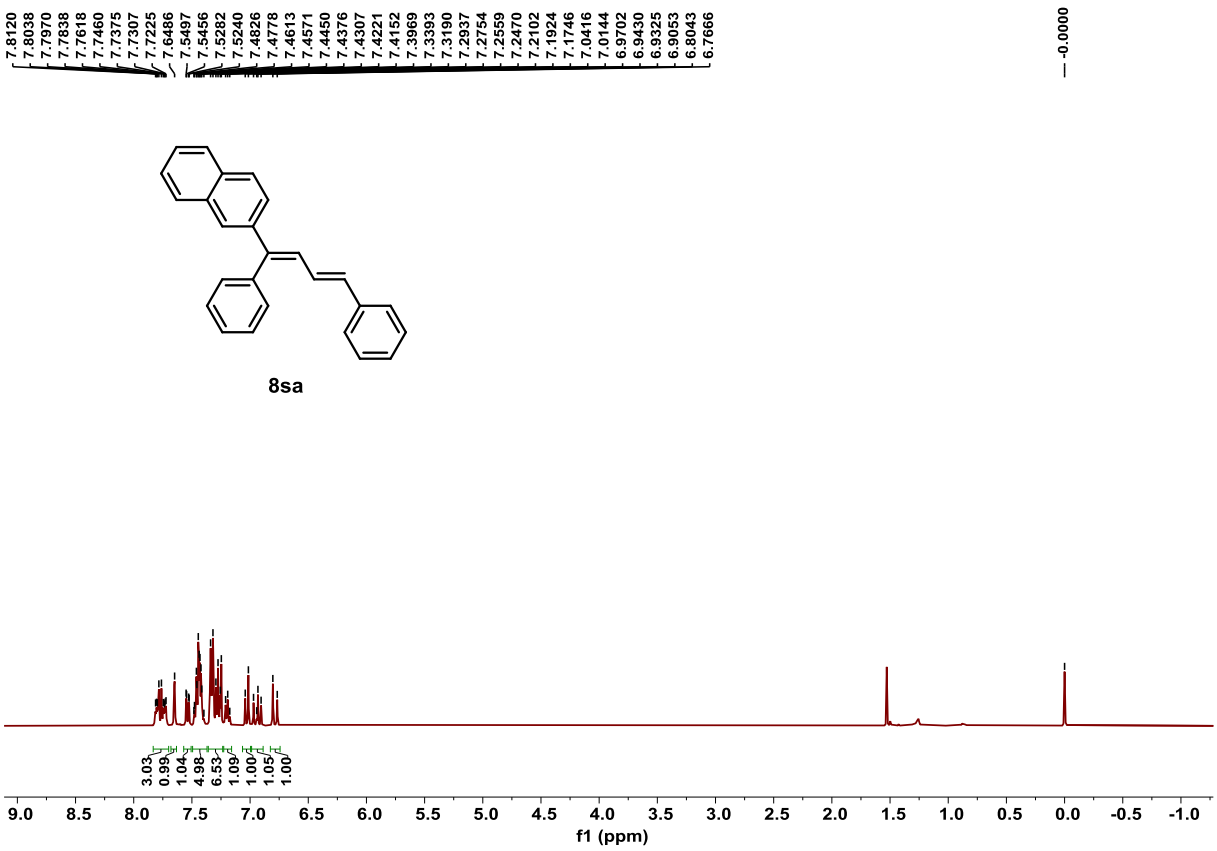

Figure S156. ^{1}**H NMR** spectrum of product **8sa**, related to **Scheme 4**.

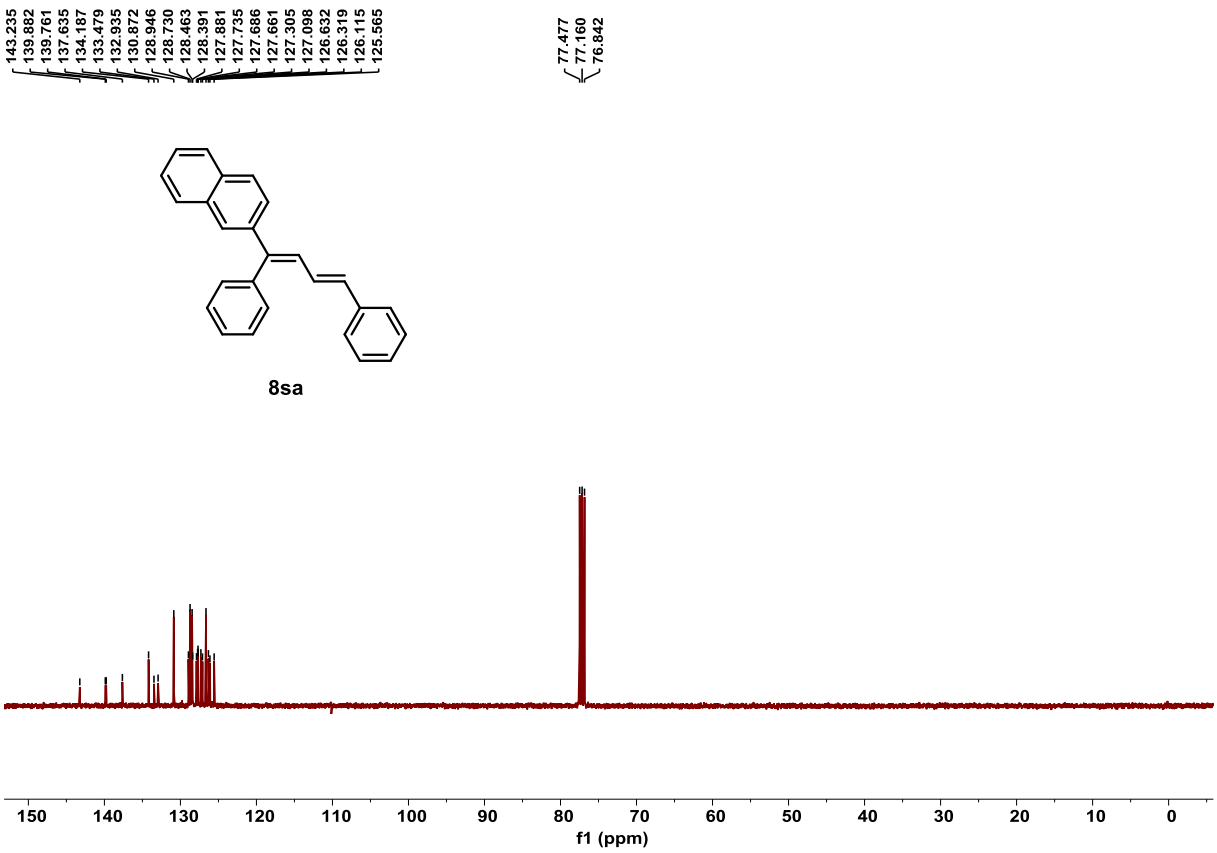

Figure S157. ^{13}C NMR spectrum of product **8sa**, related to **Scheme 4**.

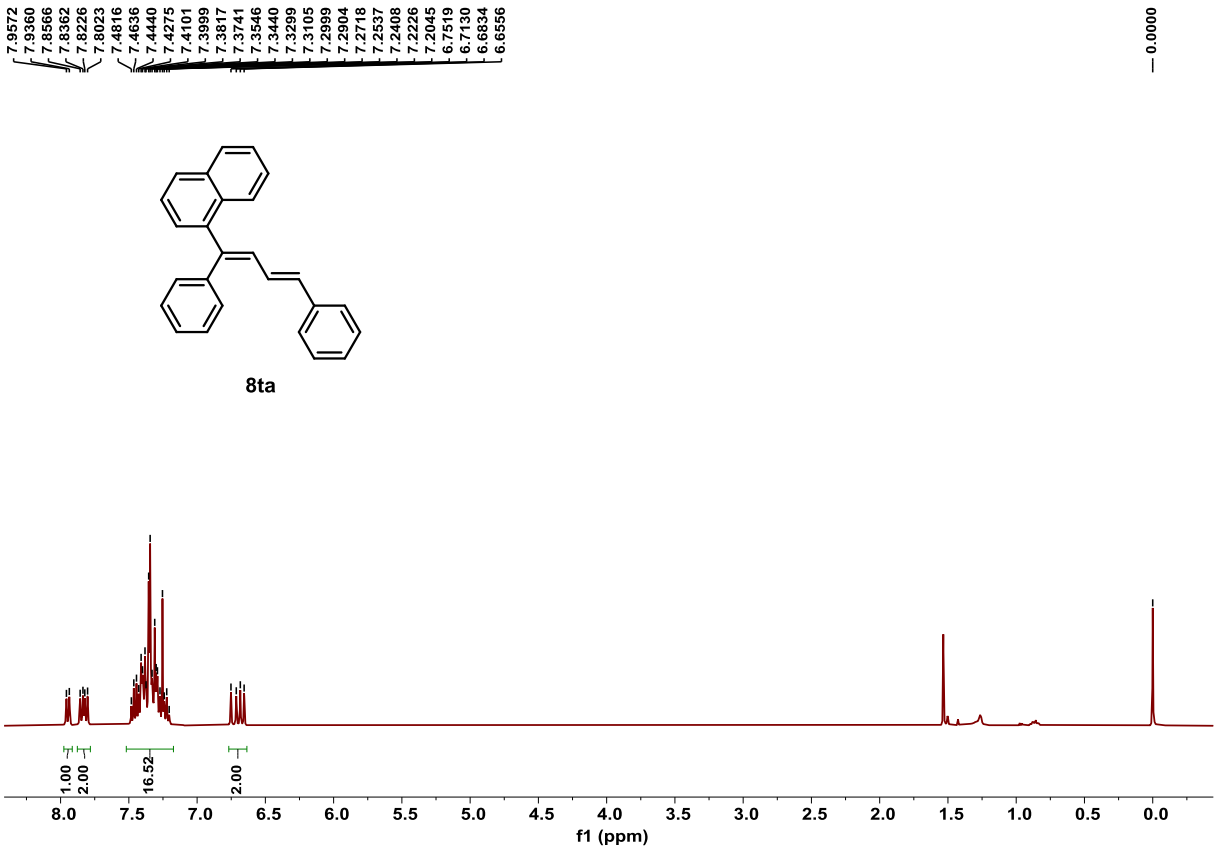

Figure S158. ^{1}H NMR spectrum of product **8ta**, related to **Scheme 4**.

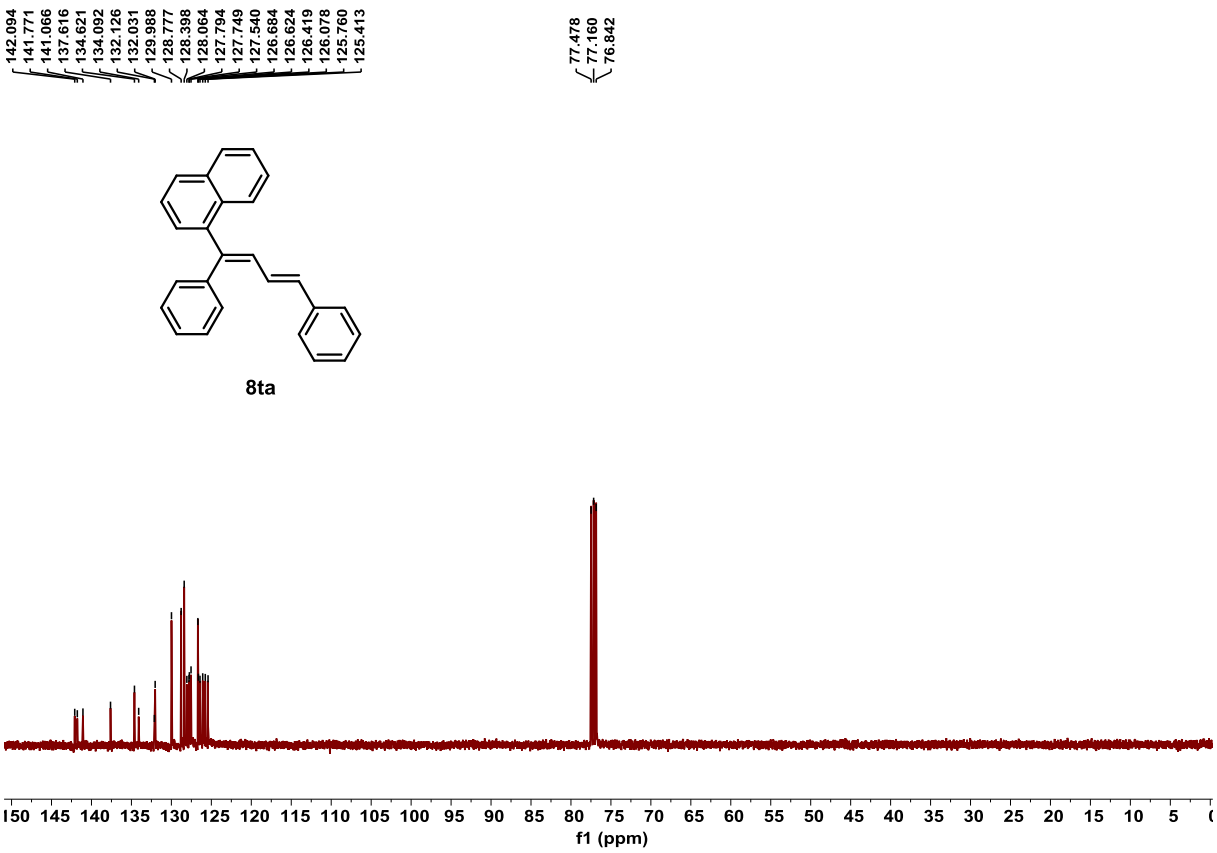

Figure S159. ^{13}**C NMR** spectrum of product **8ta**, related to **Scheme 4**.

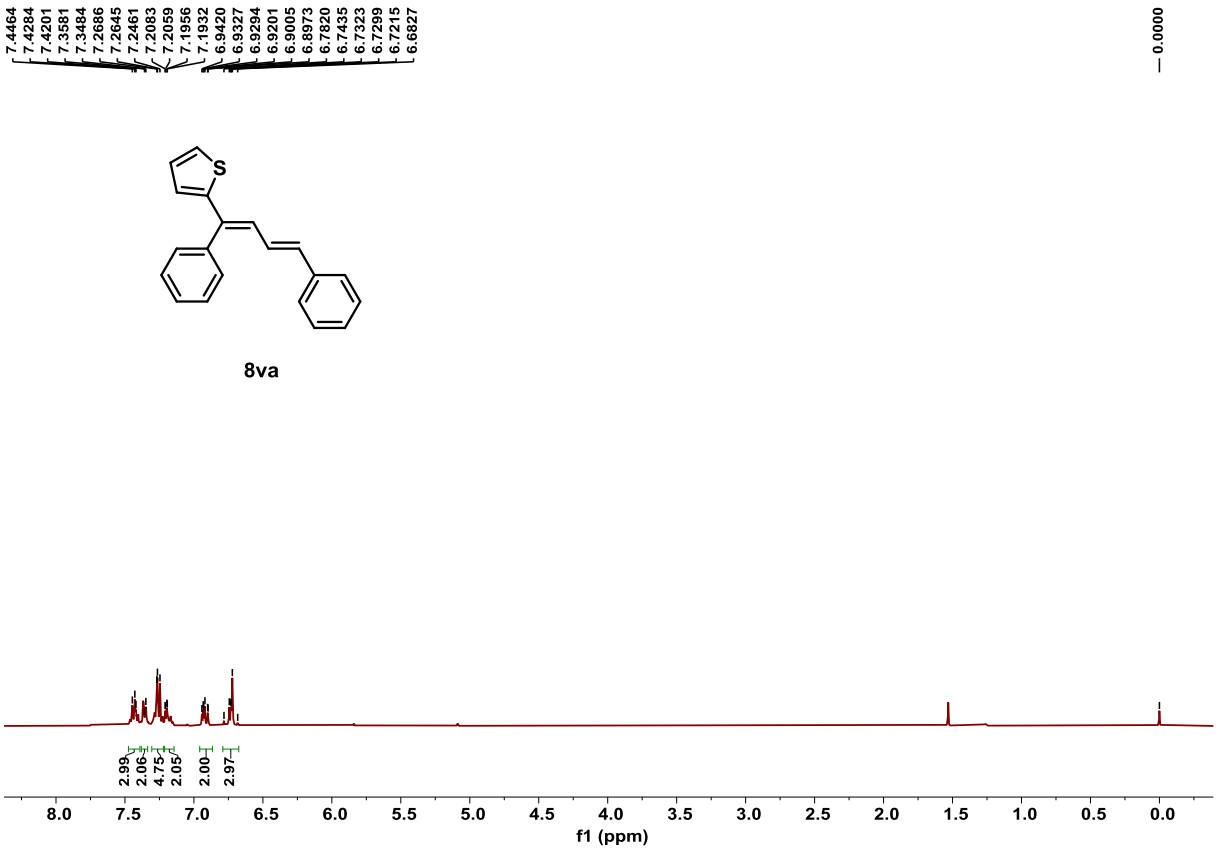

Figure S160. ^{1}**H NMR** spectrum of product **8va**, related to **Scheme 4**.

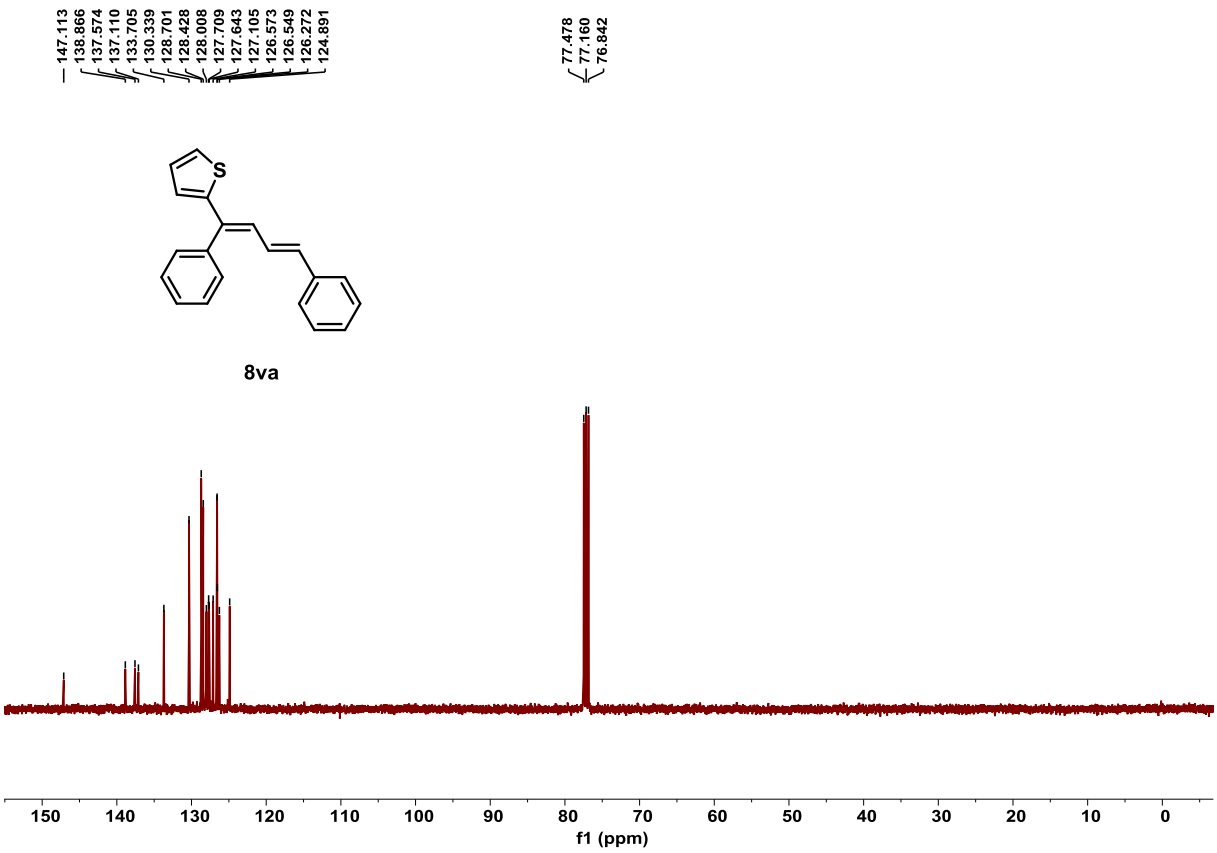

Figure S161. ^{13}**C NMR** spectrum of product **8va**, related to **Scheme 4**.

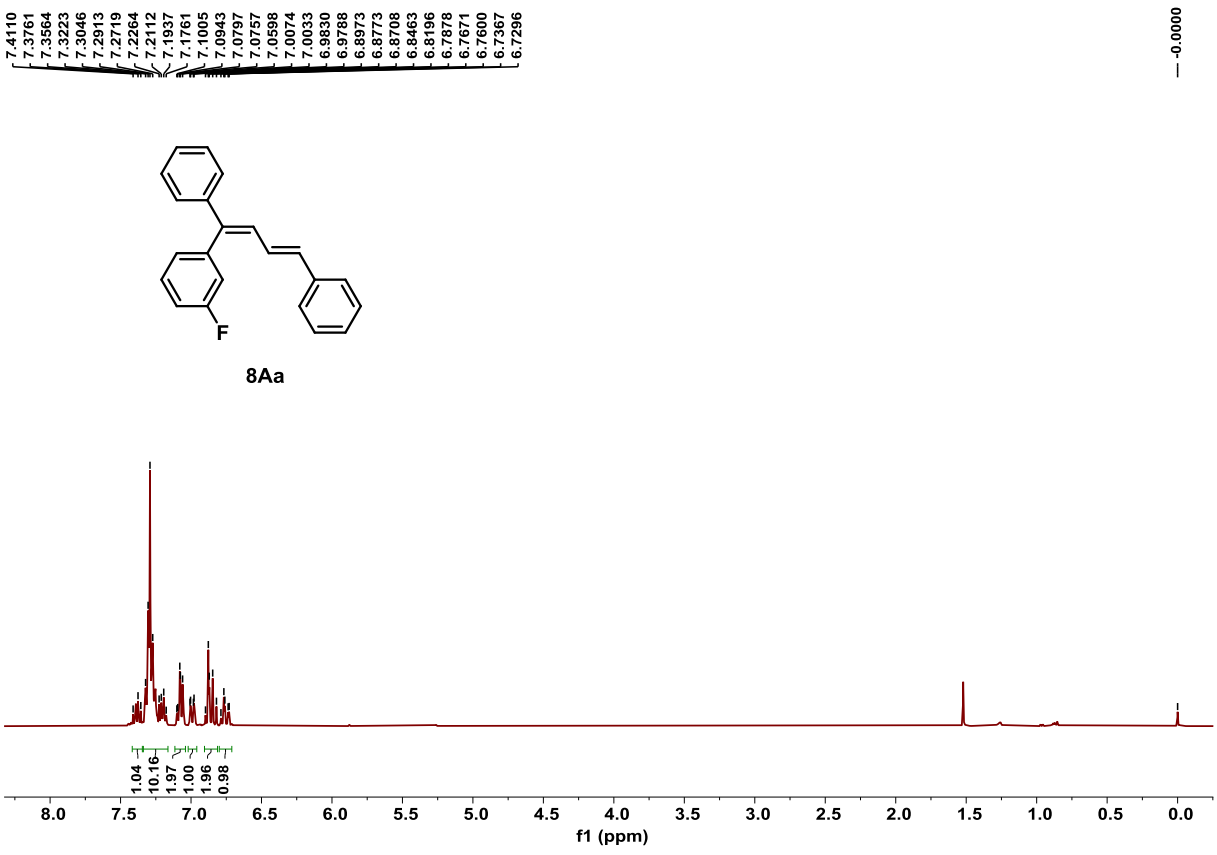

Figure S162. ^{1}**H NMR** spectrum of product **8Aa**, related to **Scheme 4**.

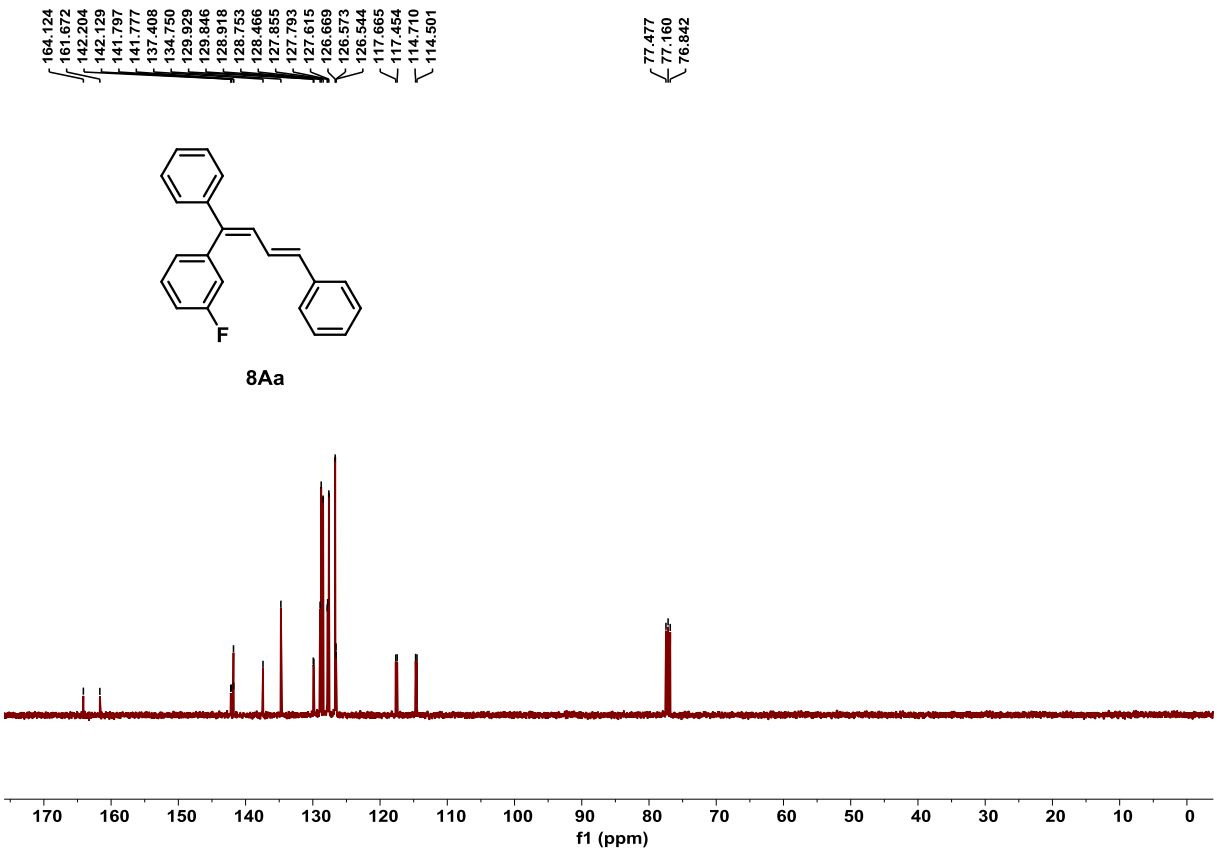

Figure S163. ^{13}**C NMR** spectrum of product **8Aa**, related to **Scheme 4**.

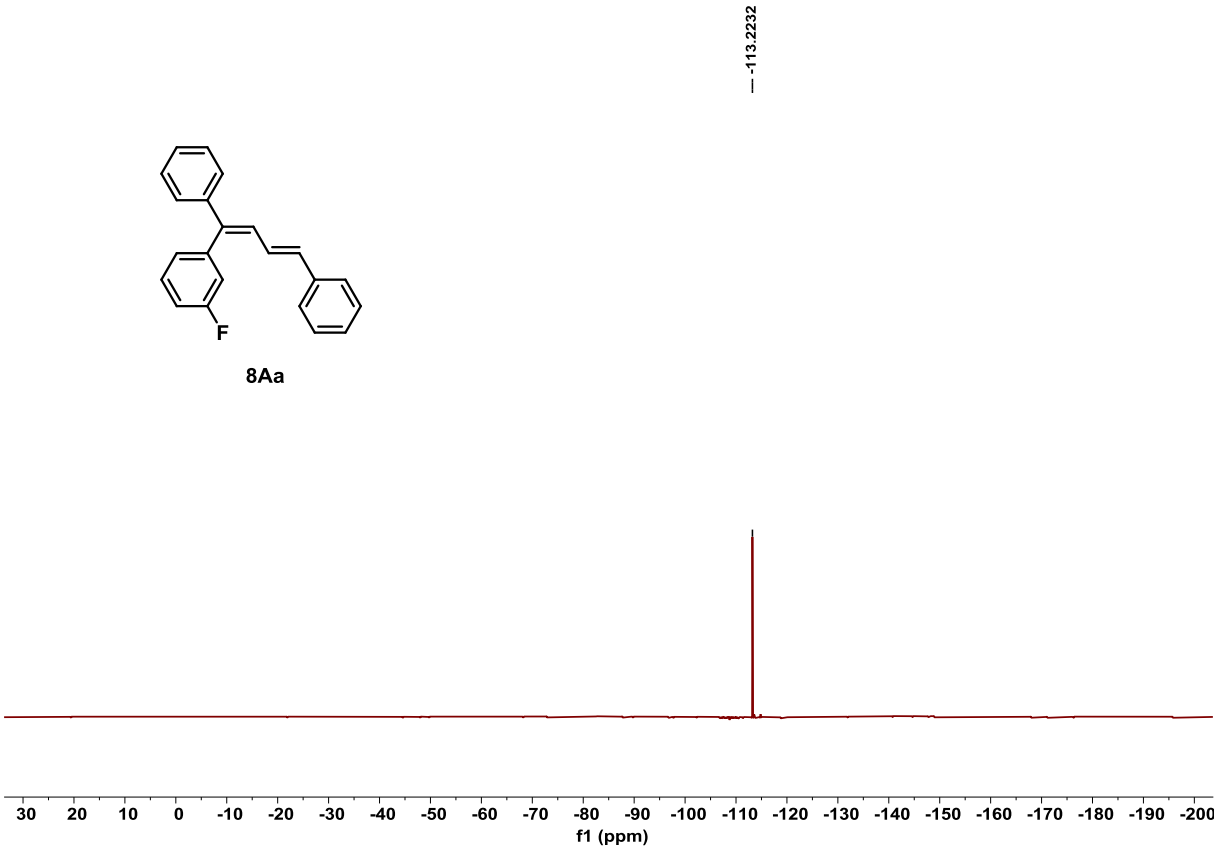

Figure S164. ^{19}**F NMR** spectrum of product **8Aa**, related to **Scheme 4**.

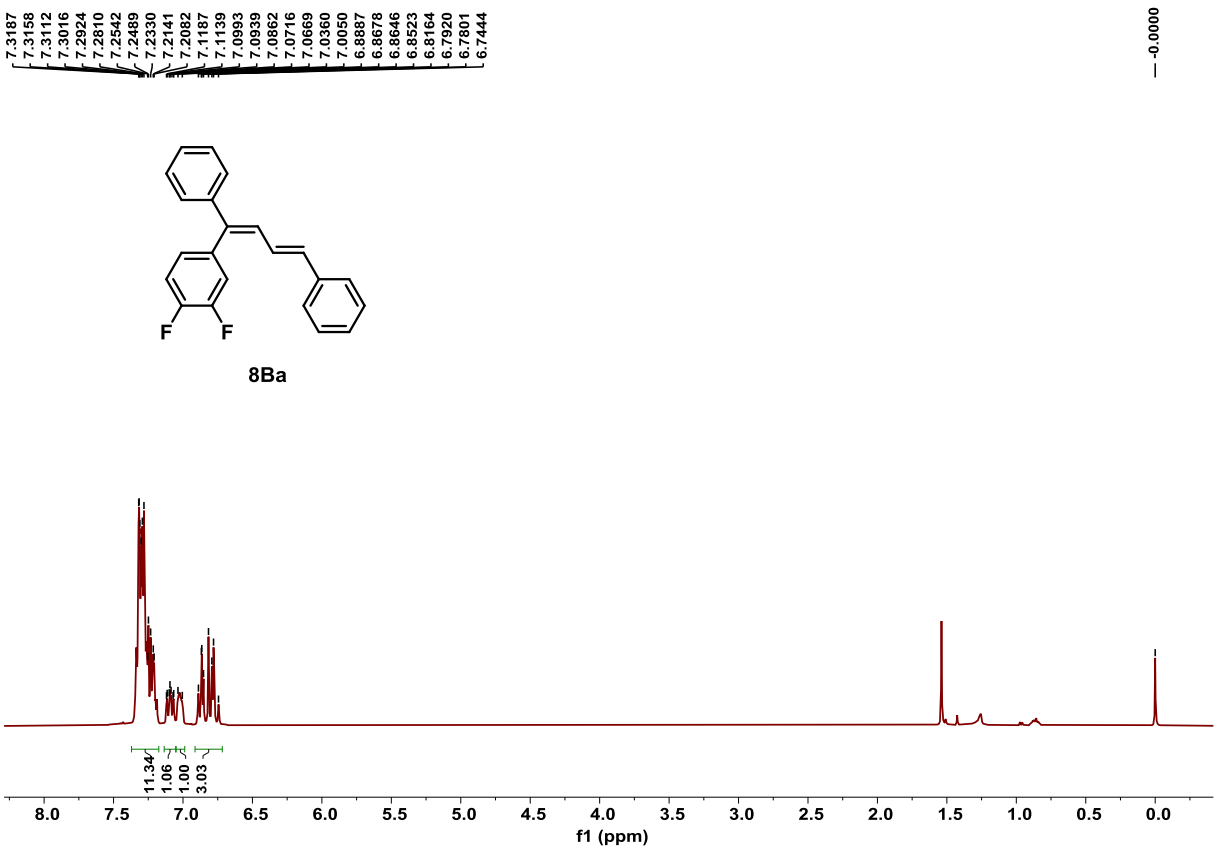

Figure S165. ^{1}H NMR spectrum of product **8Ba**, related to **Scheme 4**.

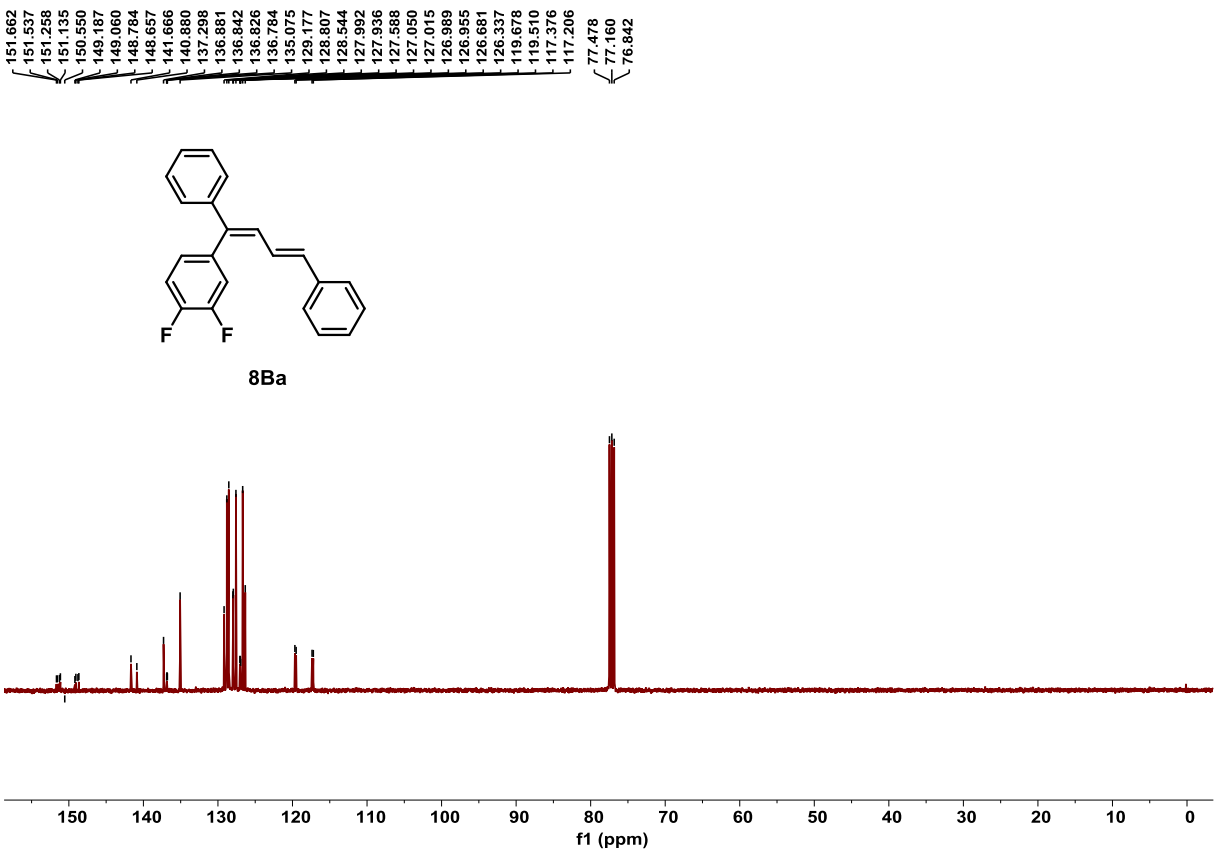

Figure S166. ^{13}C NMR spectrum of product **8Ba**, related to **Scheme 4**.

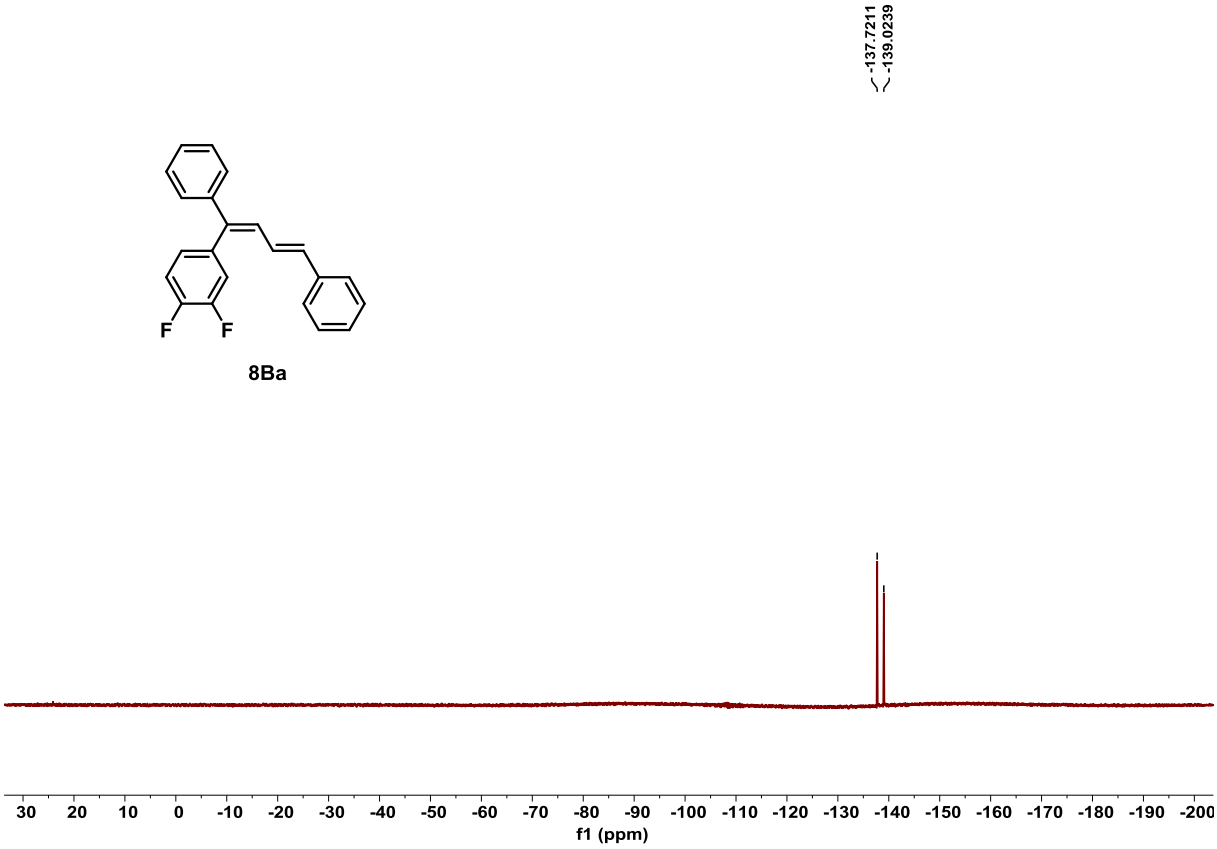

Figure S167. ^{19}**F NMR** spectrum of product **8Ba**, related to **Scheme 4**.

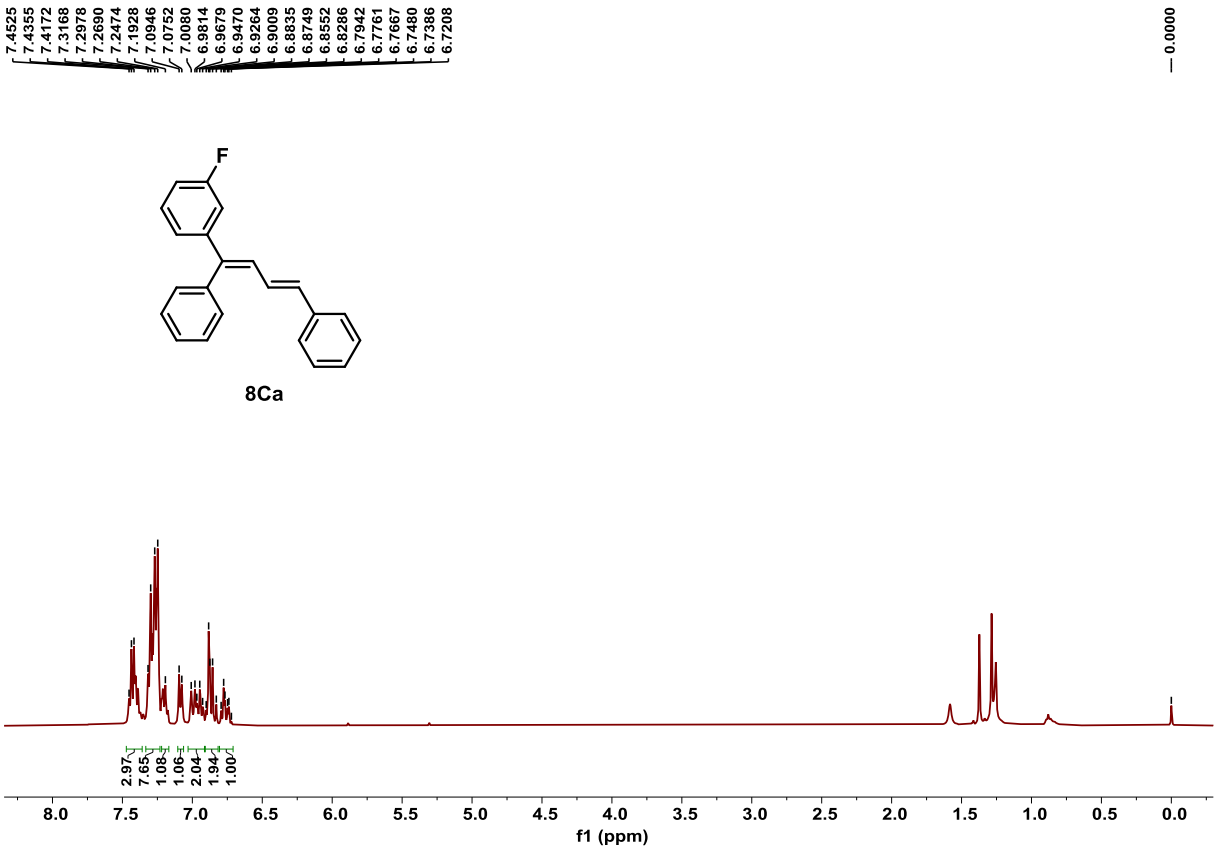

Figure S168. ^{1}**H NMR** spectrum of product **8Ca**, related to **Scheme 4**.

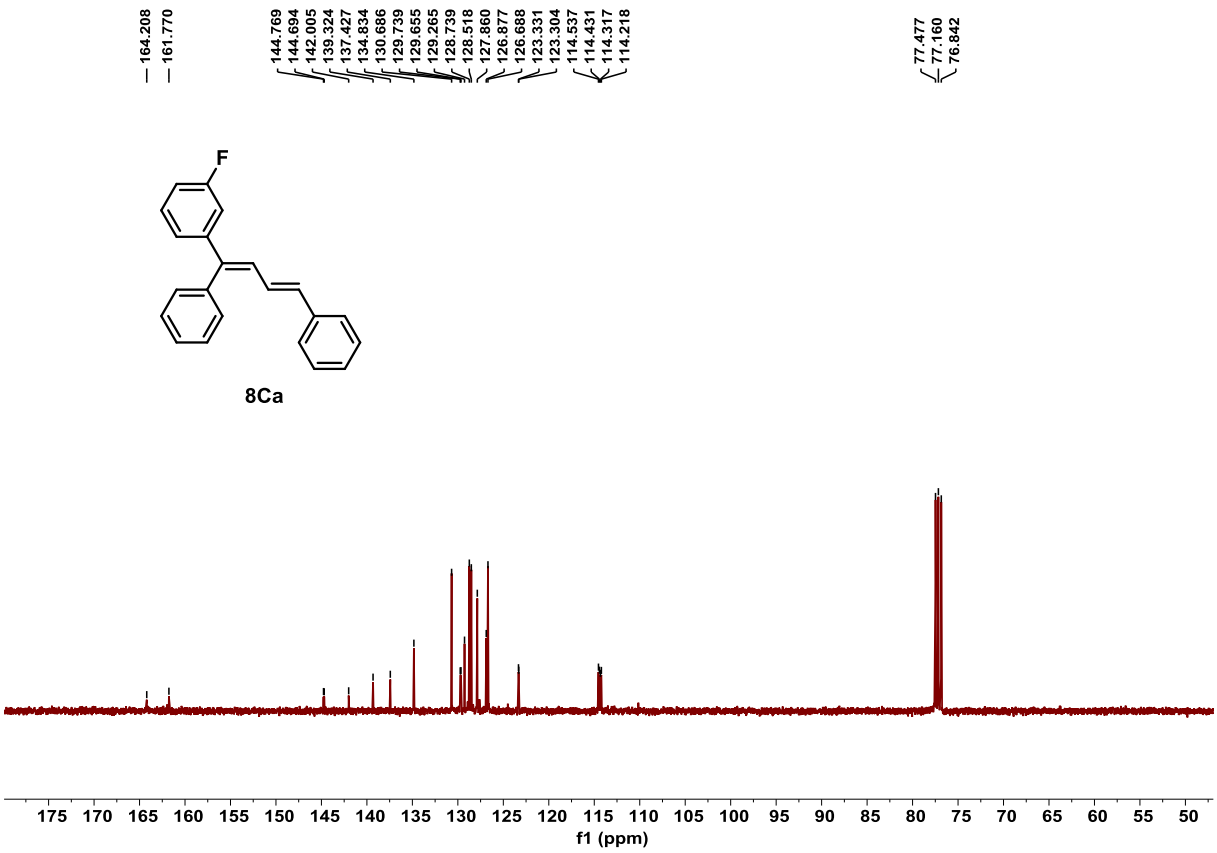

Figure S169. ^{13}**C NMR** spectrum of product **8Ca**, related to **Scheme 4**.

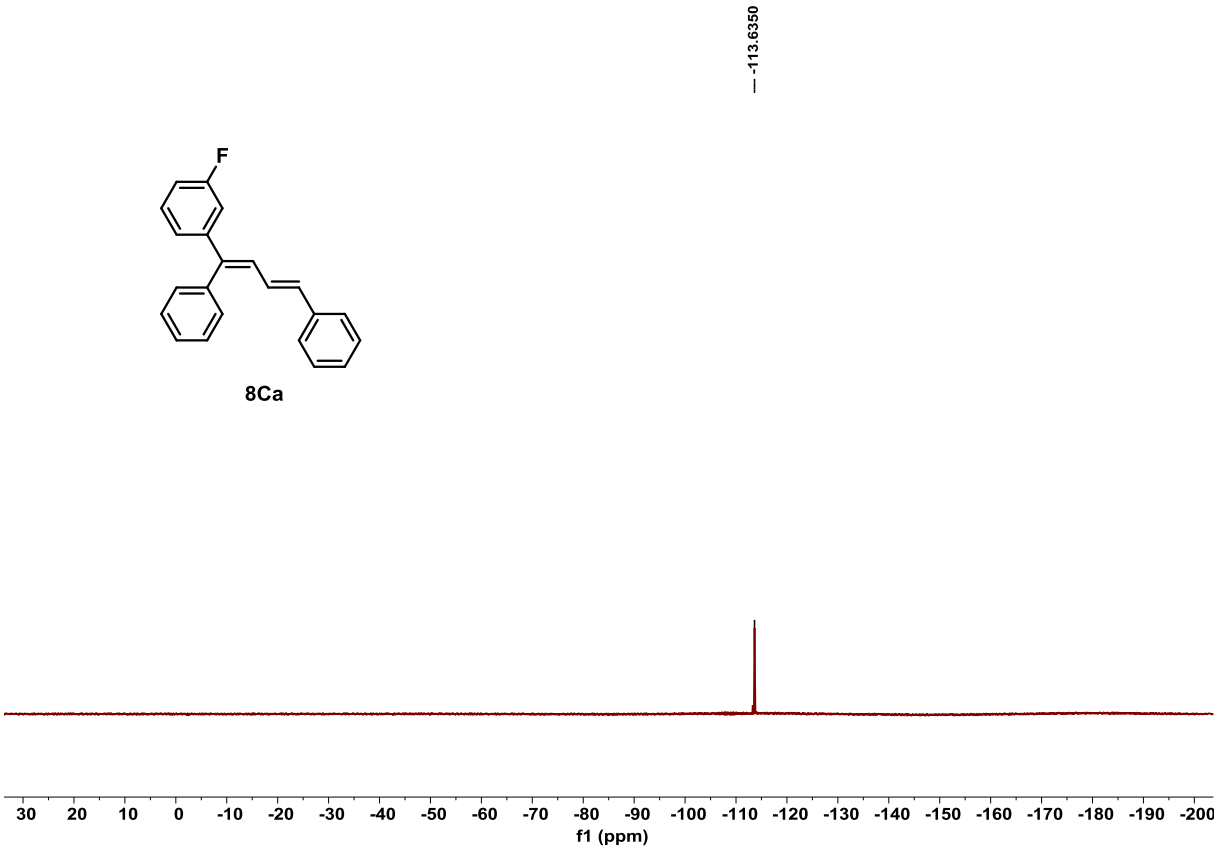

Figure S170. ^{19}**F NMR** spectrum of product **8Ca**, related to **Scheme 4**.

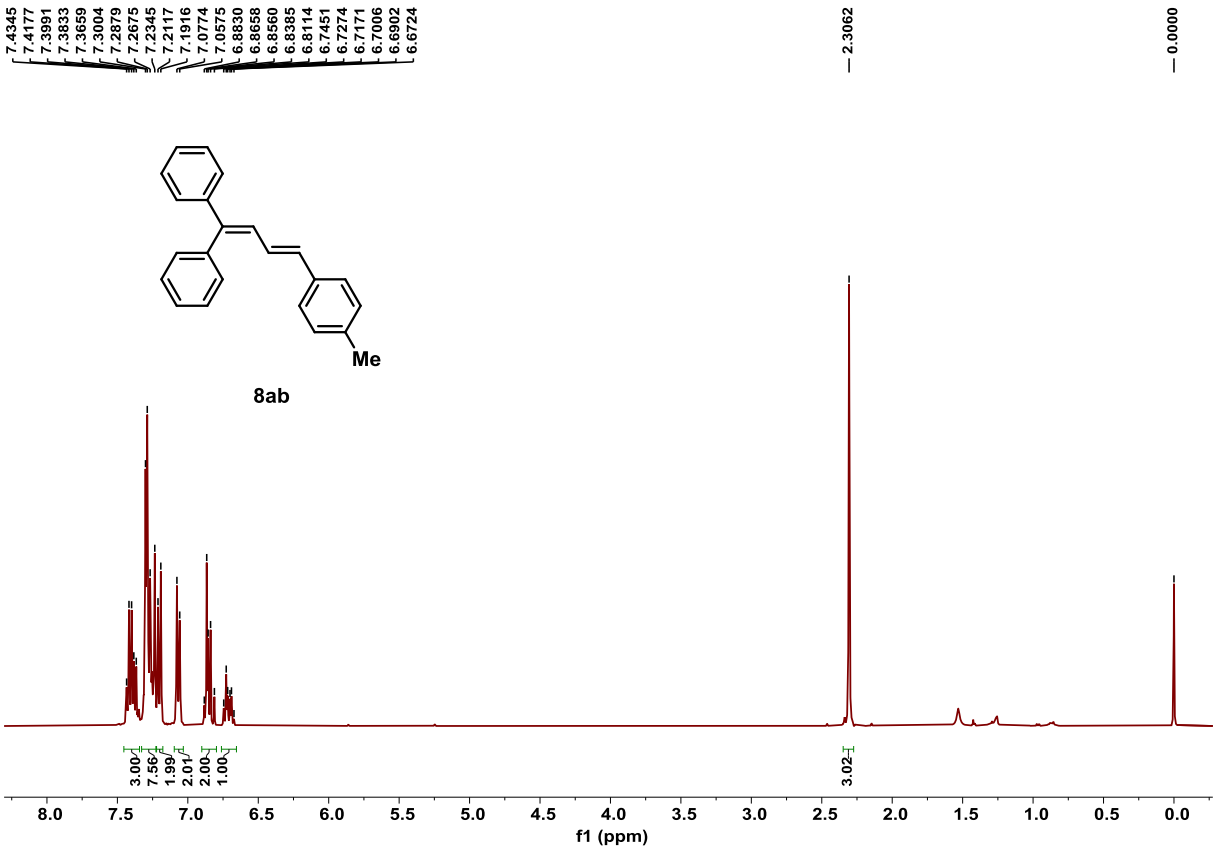

Figure S171. ^{1}**H NMR** spectrum of product **8ab**, related to **Scheme 4**.

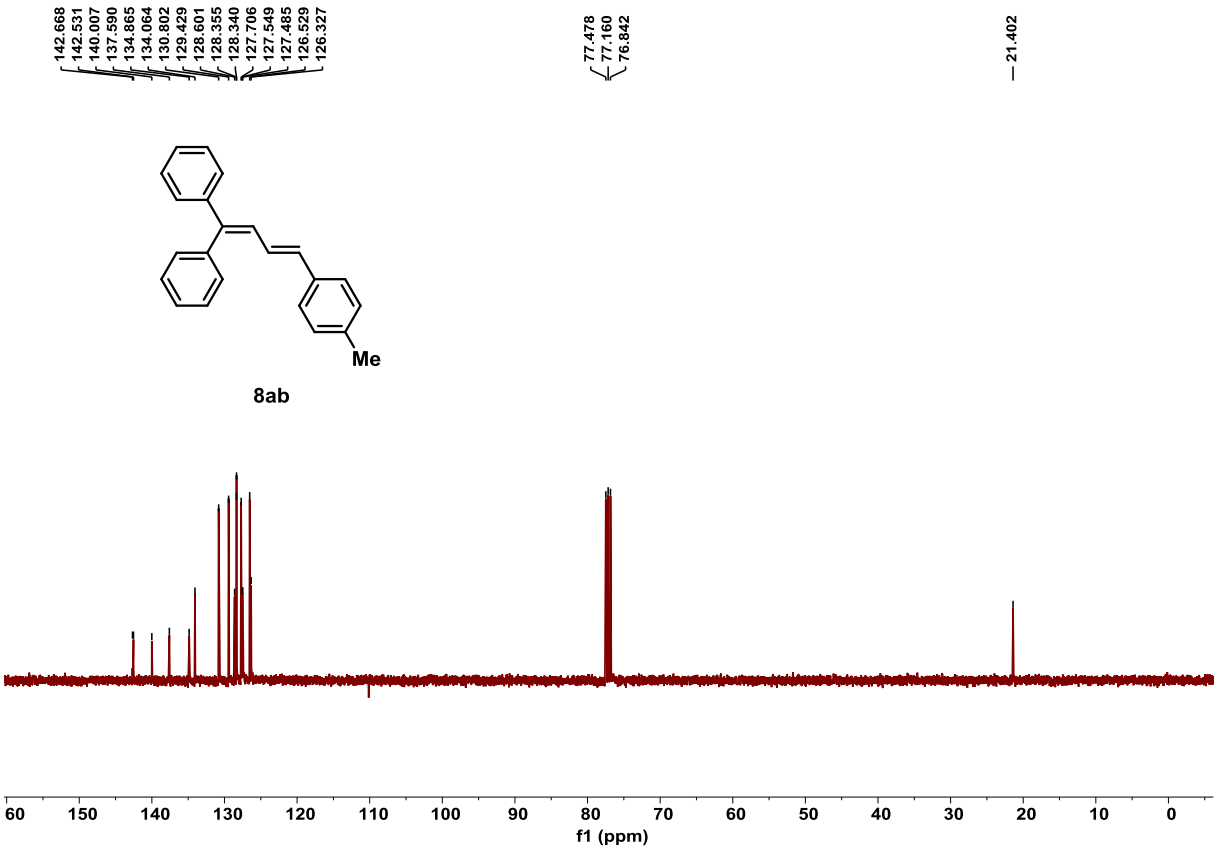

Figure S172. ^{13}**C NMR** spectrum of product **8ab**, related to **Scheme 4**.

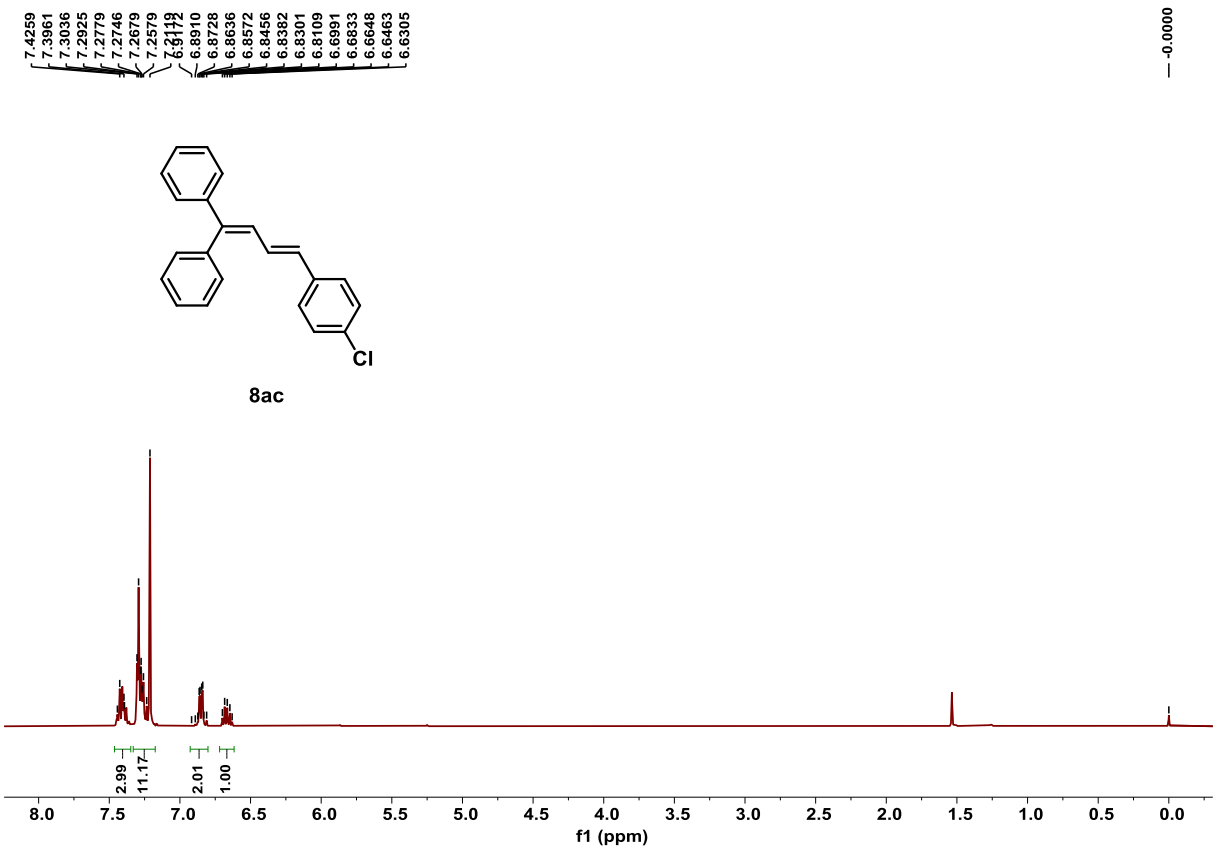

Figure S173. ^{1}**H NMR** spectrum of product **8ac**, related to **Scheme 4**.

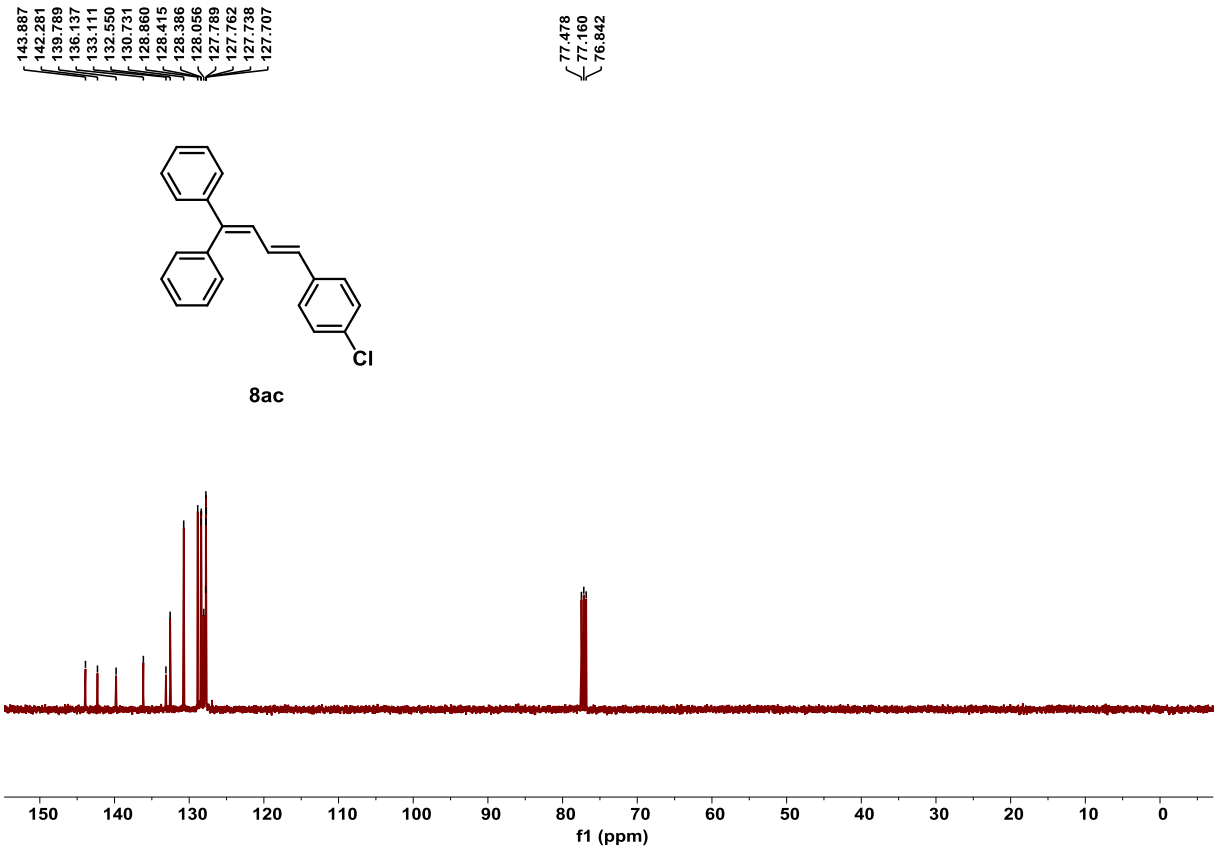

Figure S174. ^{13}**C NMR** spectrum of product **8ac**, related to **Scheme 4**.

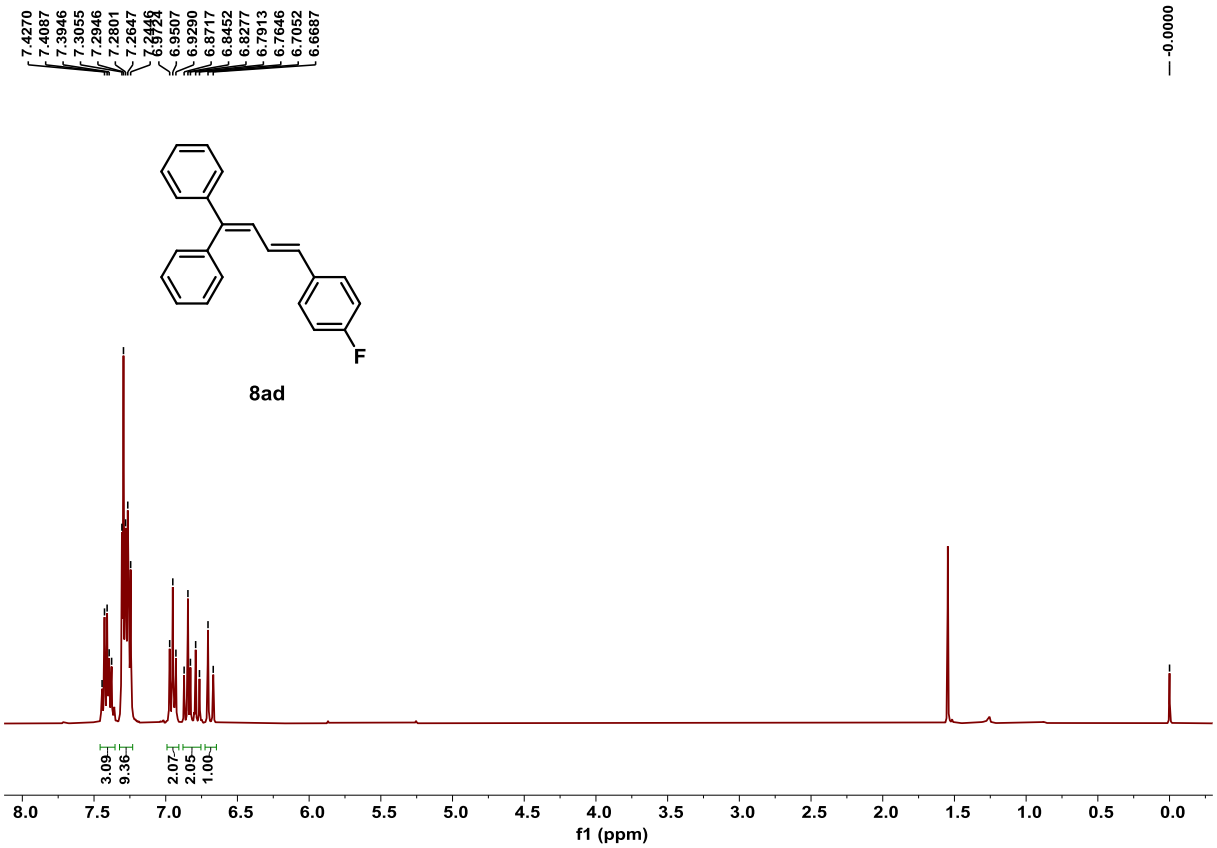

Figure S175. ^{1}H NMR spectrum of product **8ad**, related to **Scheme 4**.

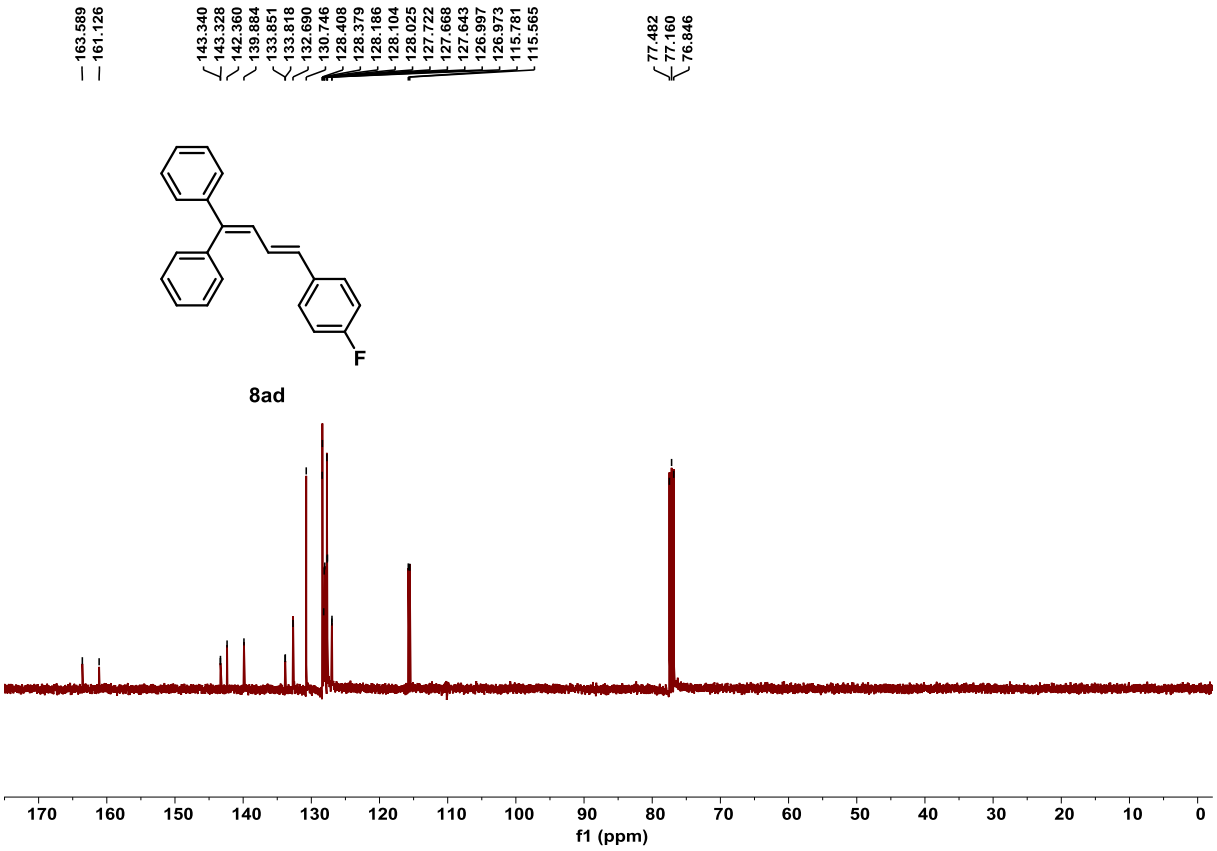

Figure S176. ^{13}C NMR spectrum of product **8ad**, related to **Scheme 4**.

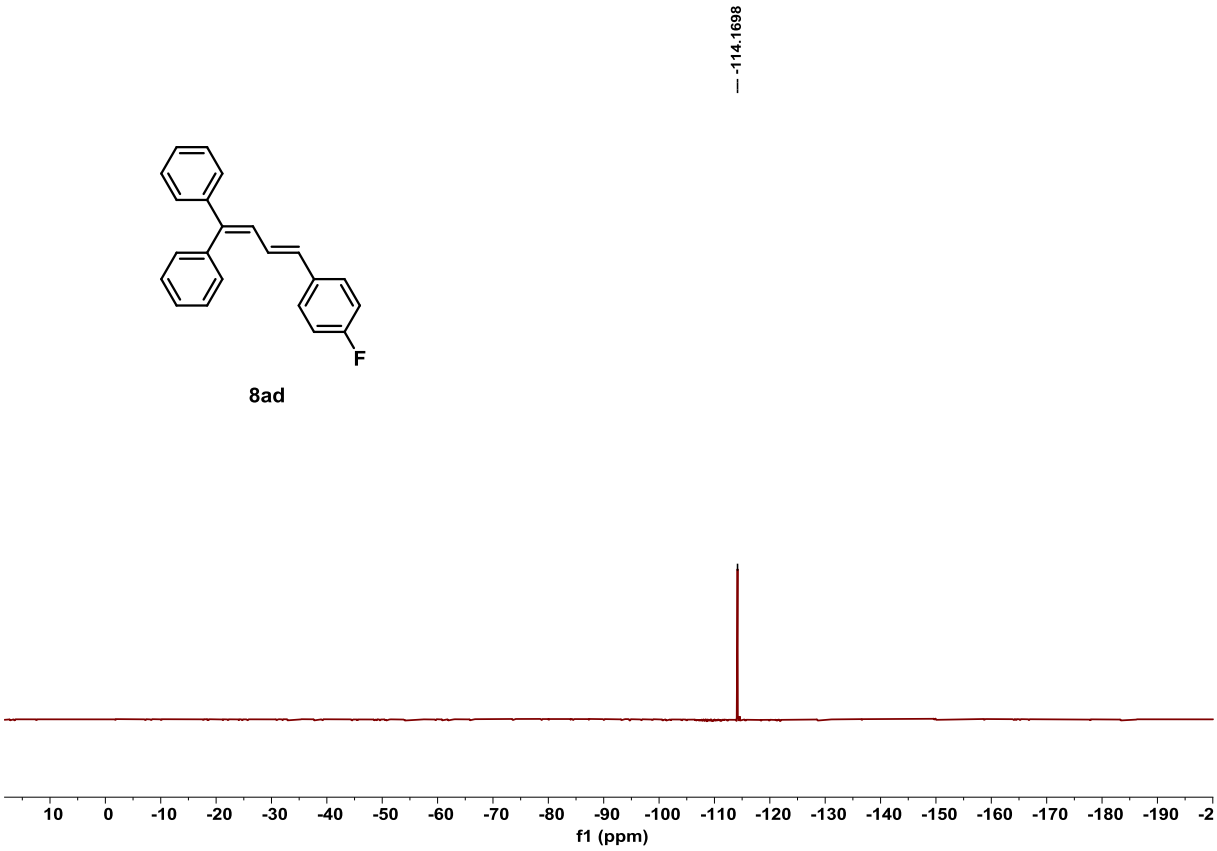

Figure S177. ^{19}**F NMR** spectrum of product **8ad**, related to **Scheme 4**.

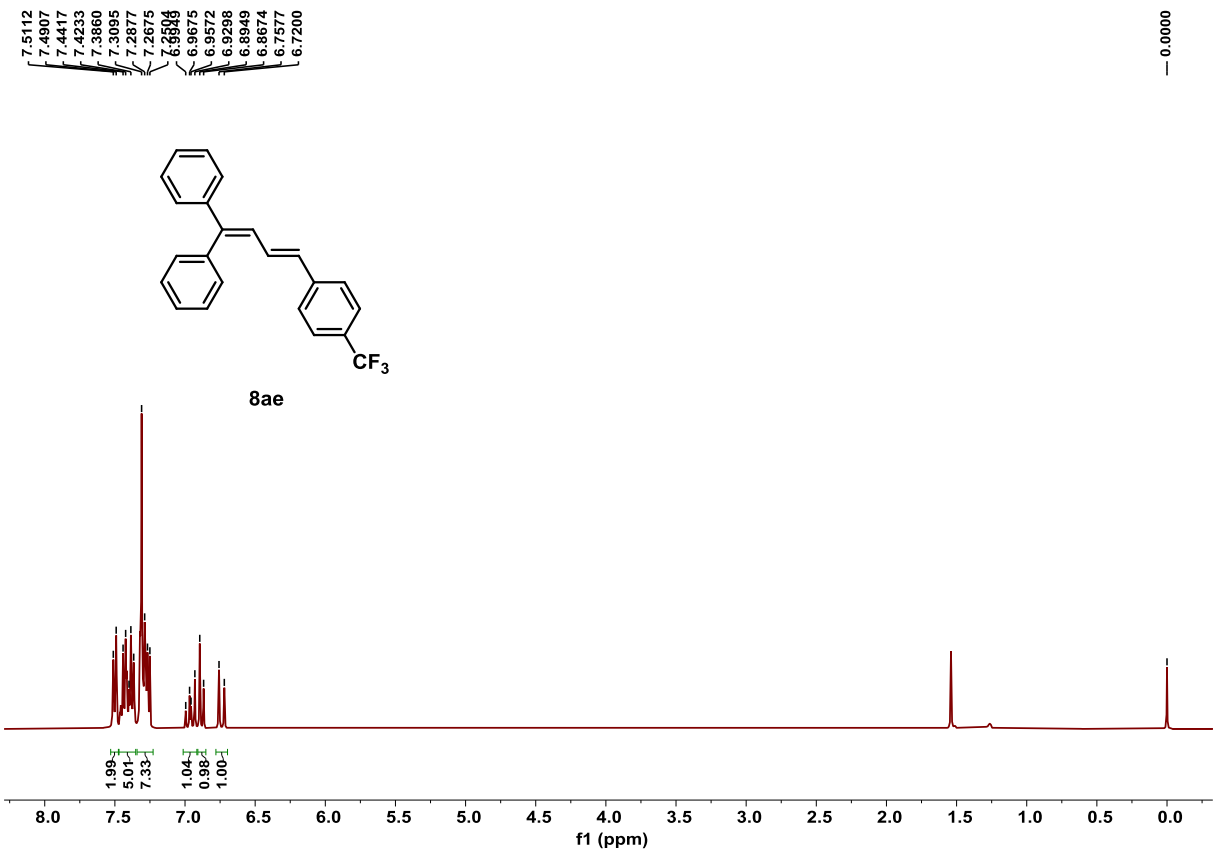

Figure S178. ^{1}**H NMR** spectrum of product **8ae**, related to **Scheme 4**.

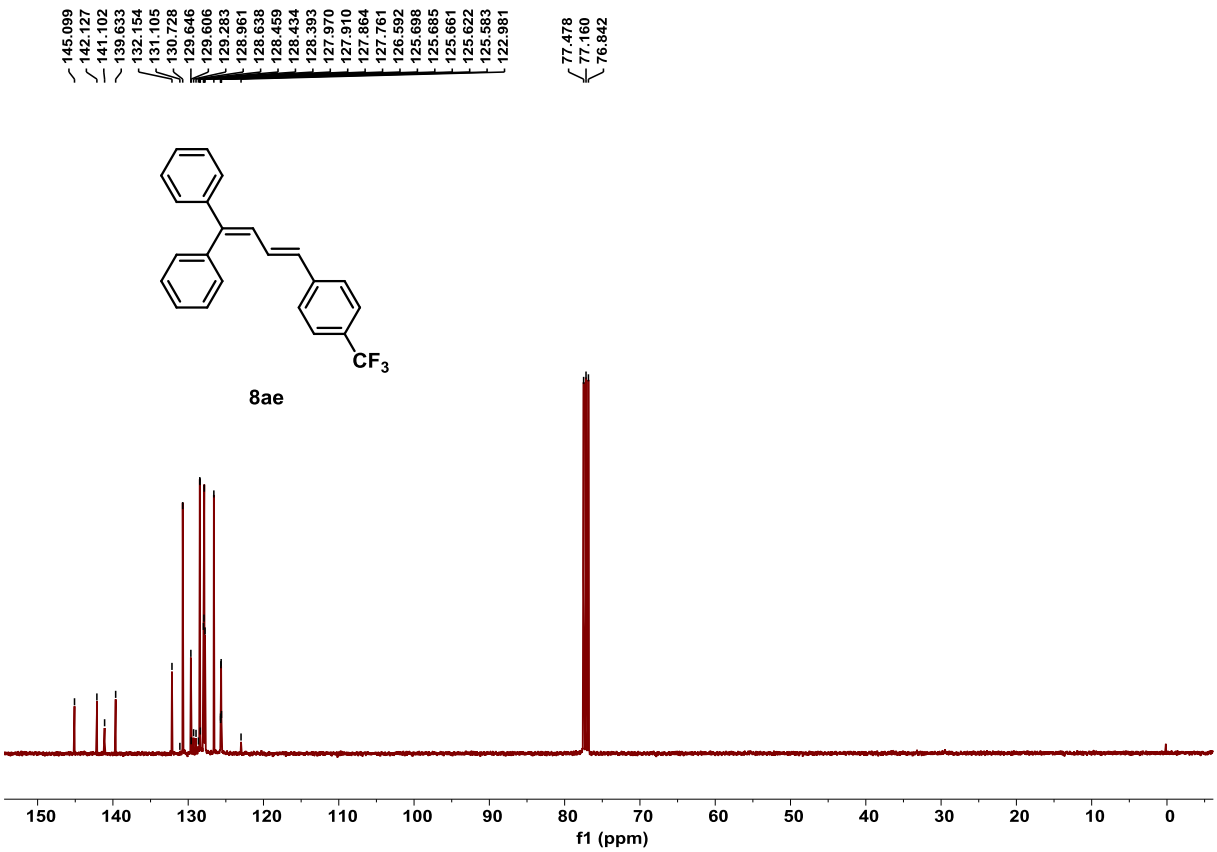

Figure S179. ^{13}**C NMR** spectrum of product **8ae**, related to **Scheme 4**.

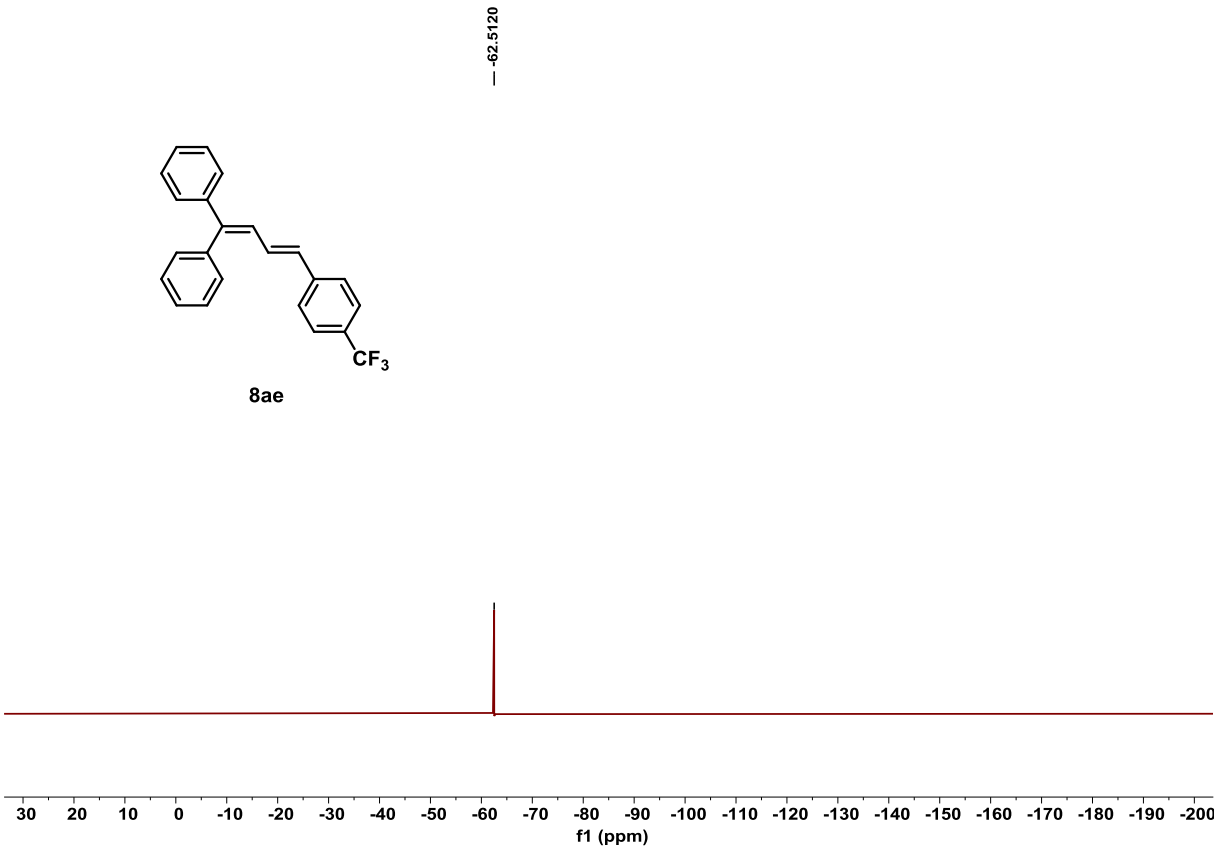

Figure S180. ^{19}**F NMR** spectrum of product **8ae**, related to **Scheme 4**.

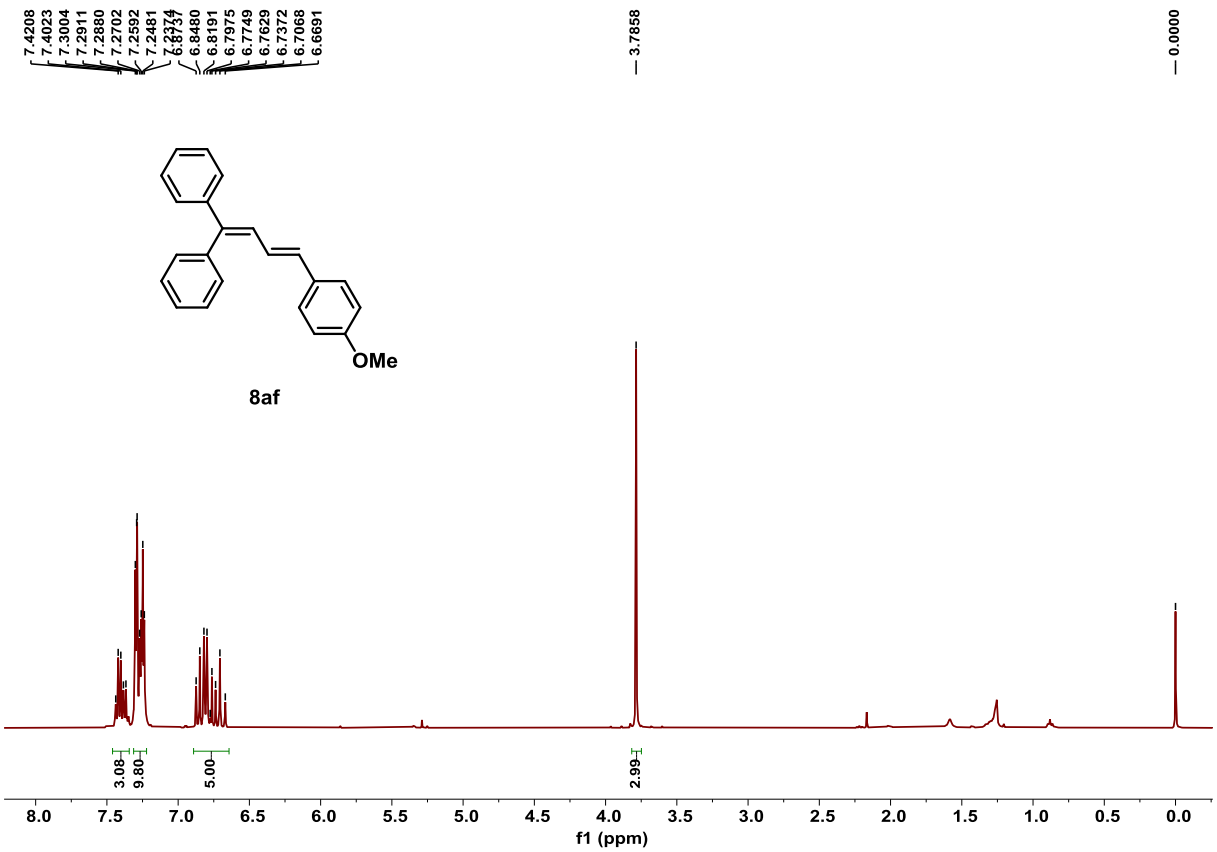

Figure S181. ^{1}**H NMR** spectrum of product **8af**, related to **Scheme 4**.

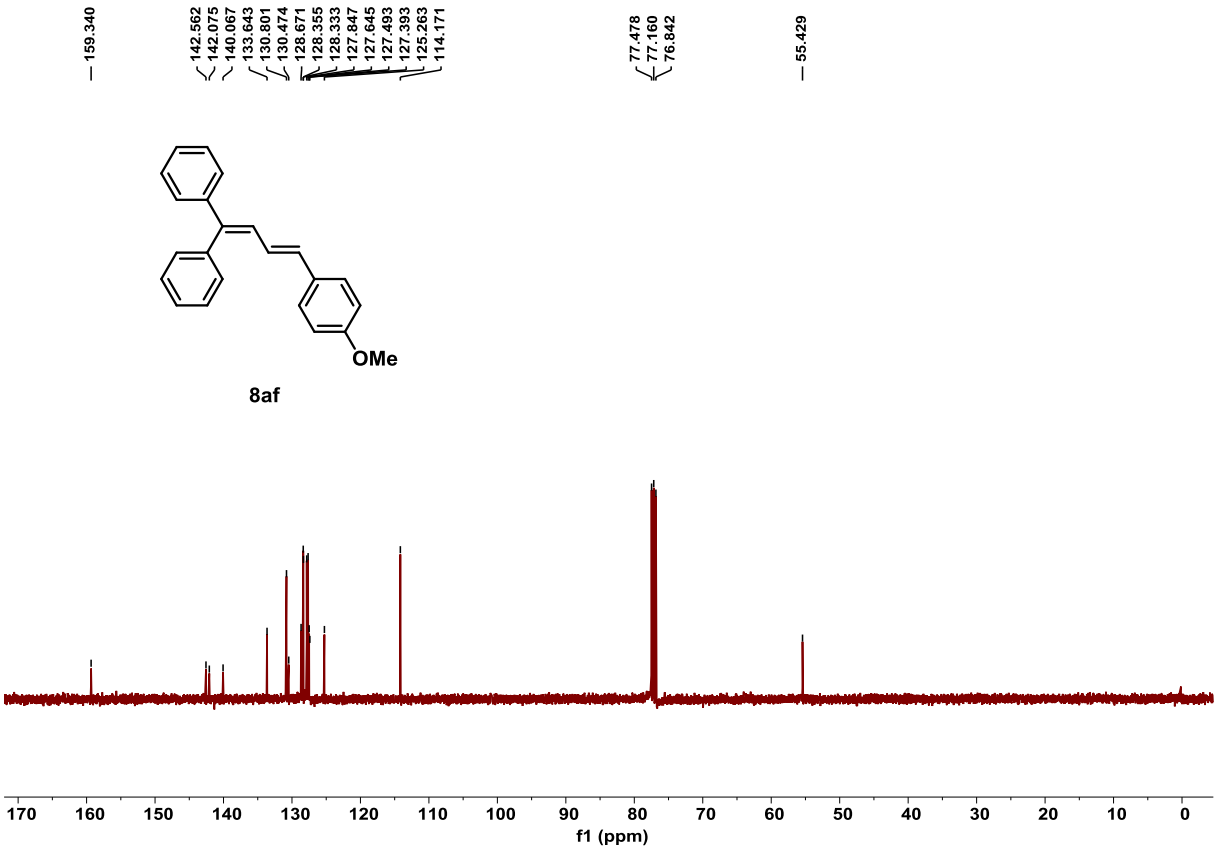

Figure S182. ^{13}**C NMR** spectrum of product **8af**, related to **Scheme 4**.

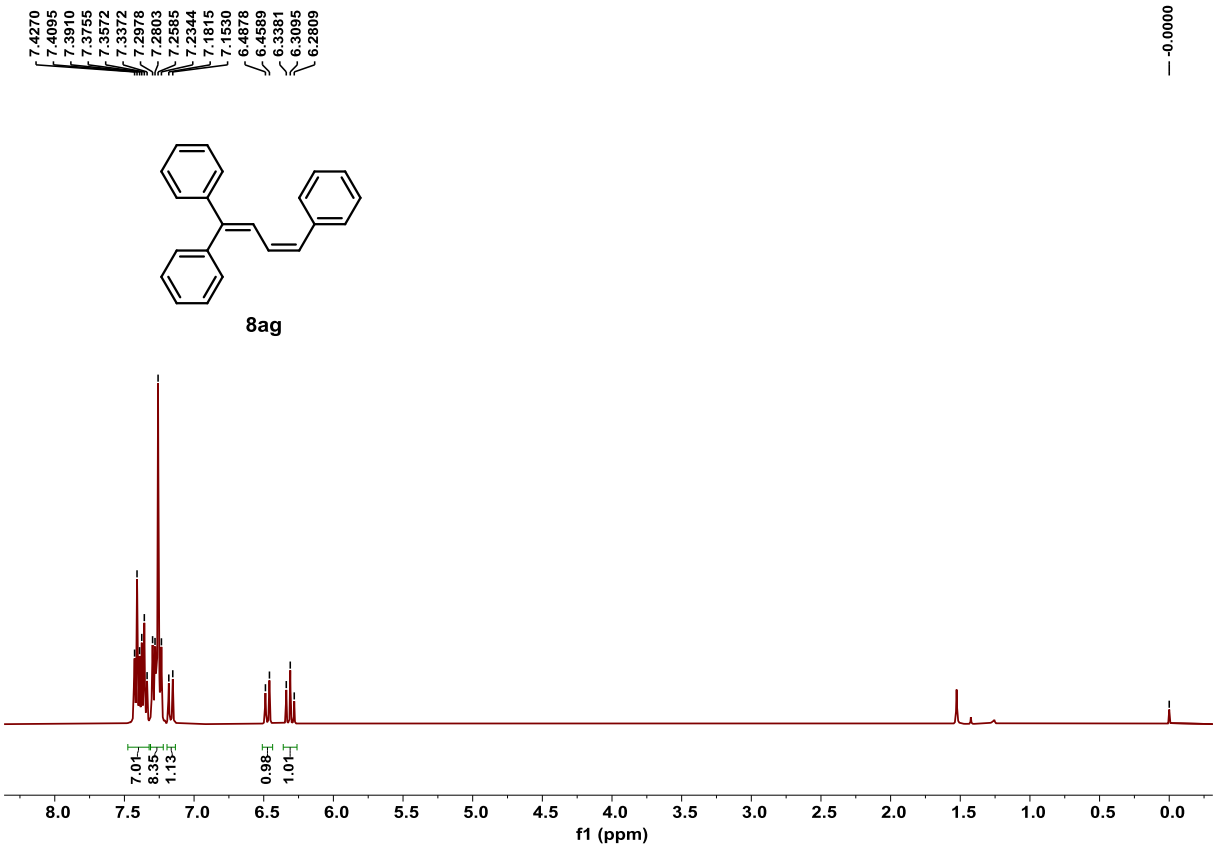

Figure S183. ^{1}**H NMR** spectrum of product **8ag**, related to **Scheme 4**.

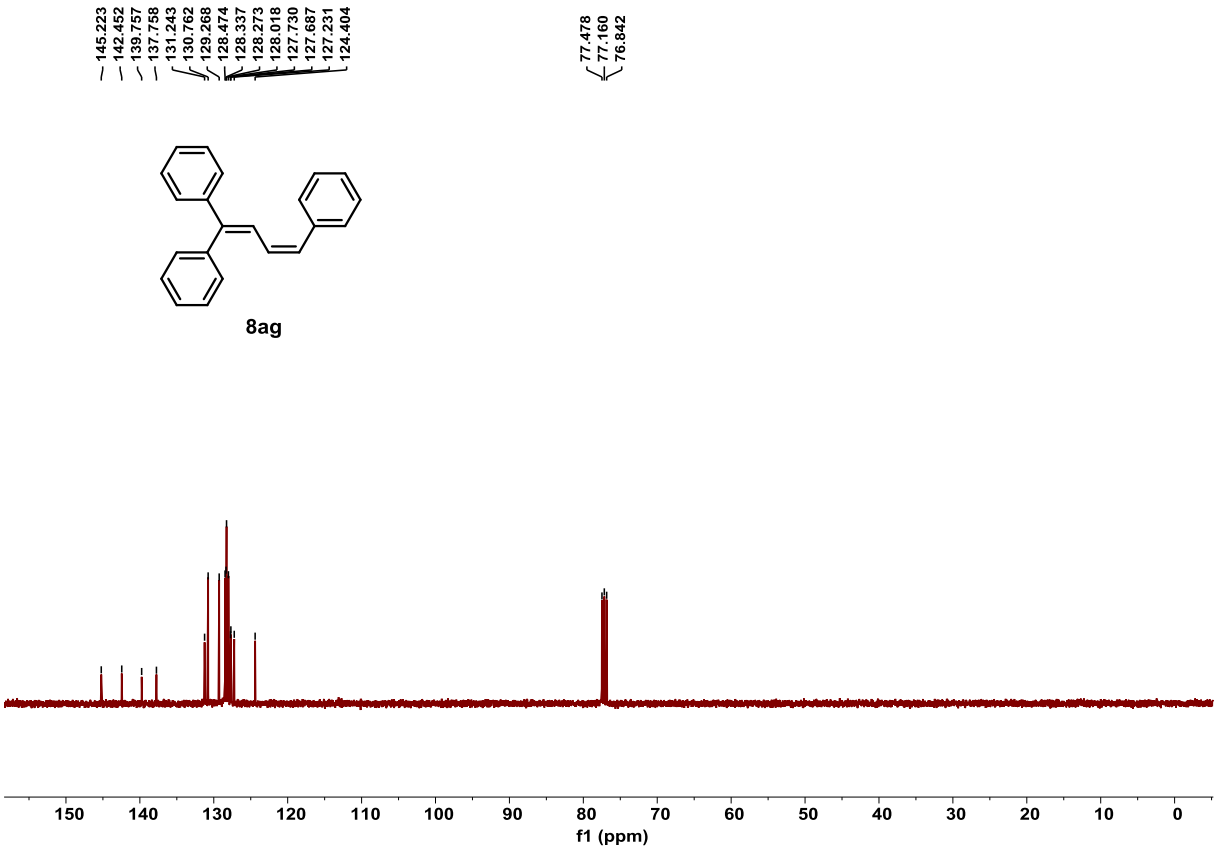

Figure S184. ^{13}**C NMR** spectrum of product **8ag**, related to **Scheme 4**.

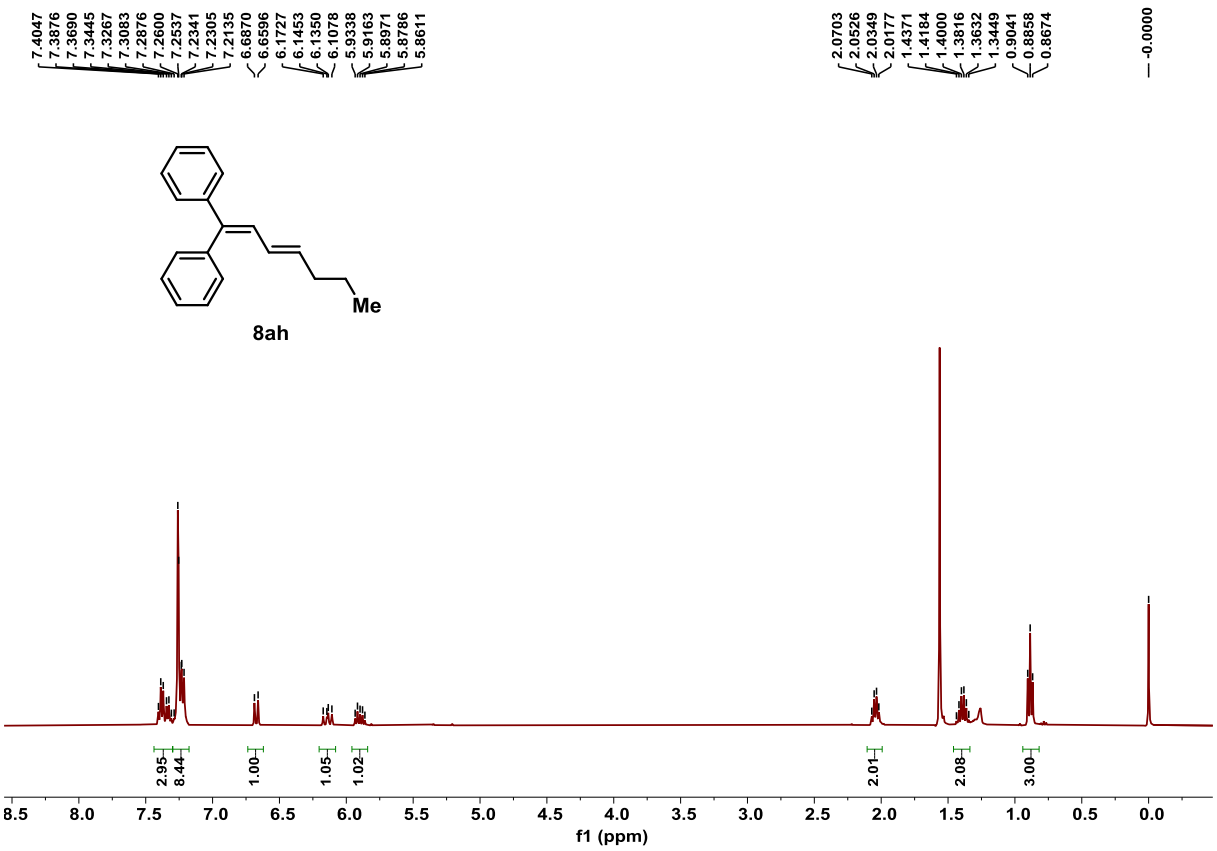

Figure S185. ^{1}**H NMR** spectrum of product **8ah**, related to **Scheme 4**.

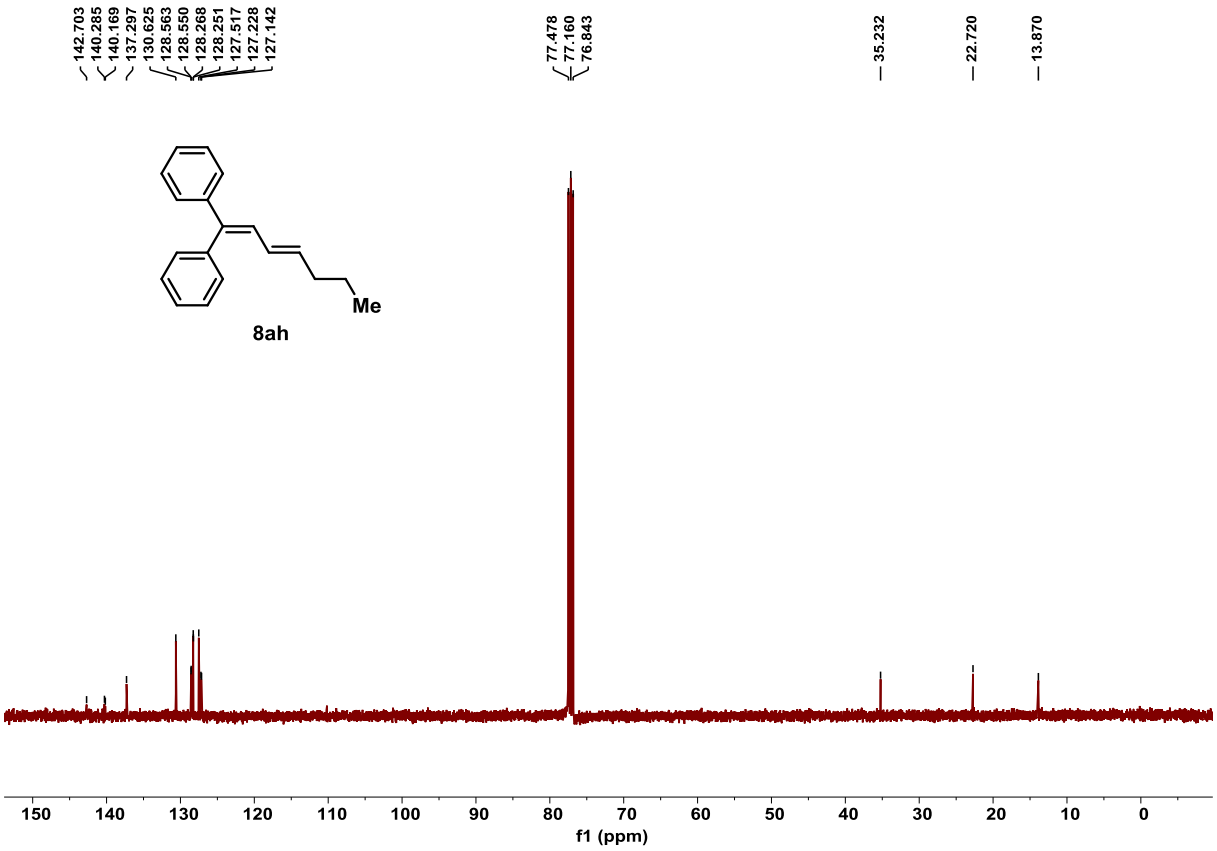

Figure S186. ^{13}**C NMR** spectrum of product **8ah**, related to **Scheme 4**.

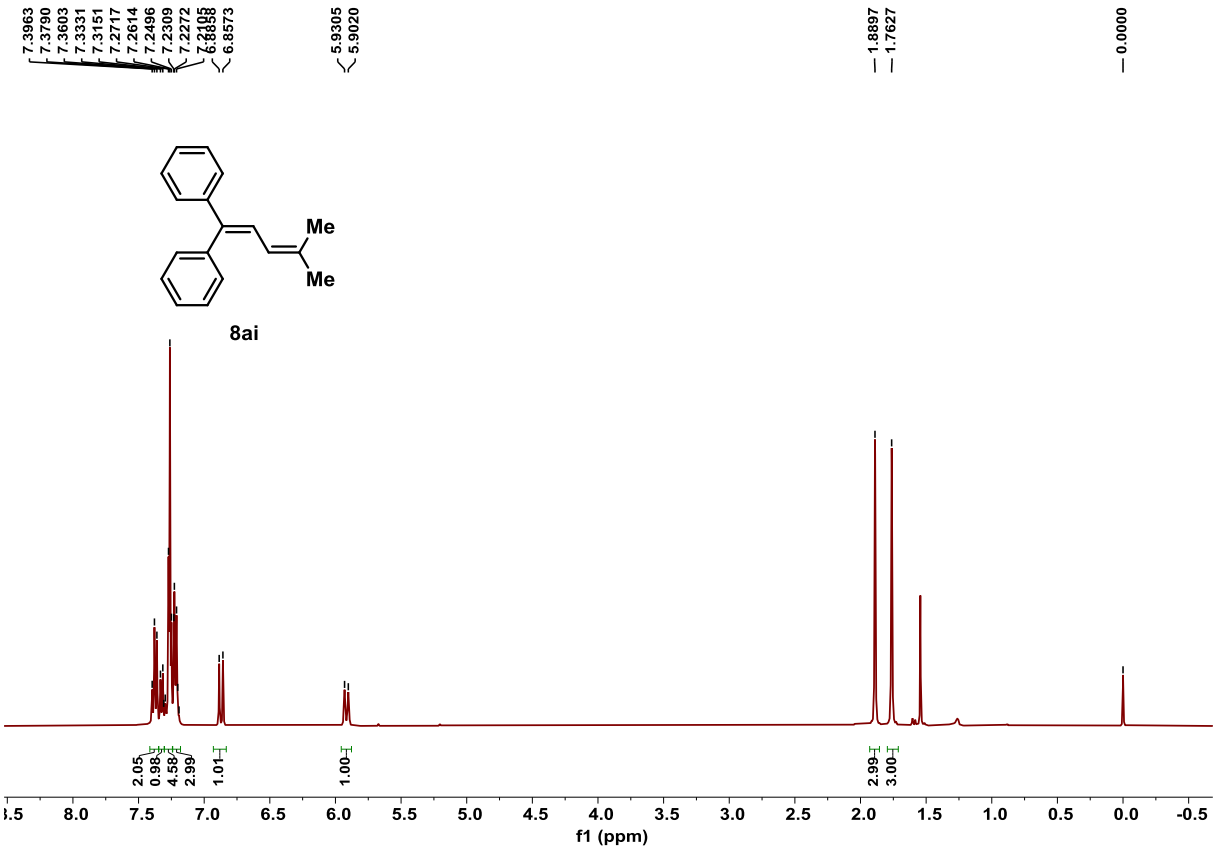

Figure S187. ^{1}**H NMR** spectrum of product **8ai**, related to **Scheme 4**.

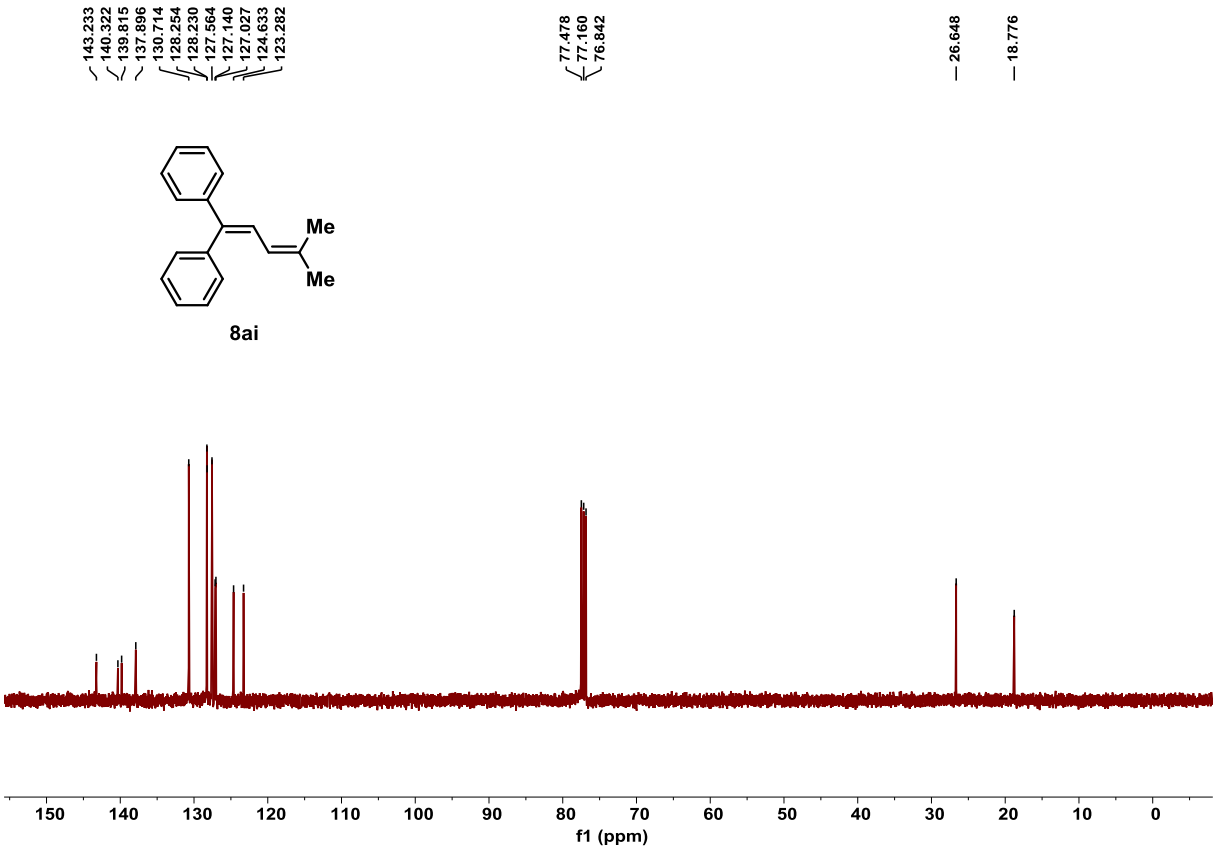

Figure S188. ^{13}**C NMR** spectrum of product **8ai**, related to **Scheme 4**.

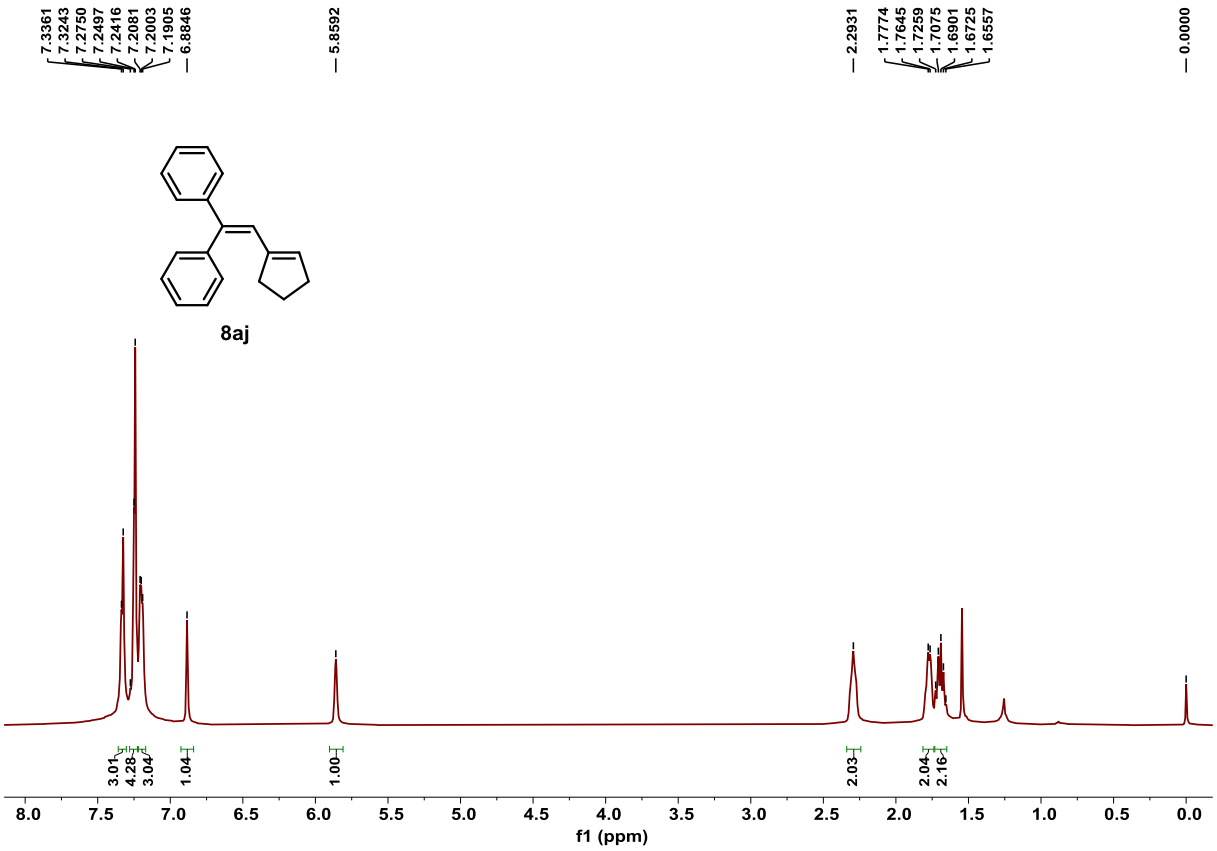

Figure S189. ^{1}H NMR spectrum of product **8aj**, related to **Scheme 4**.

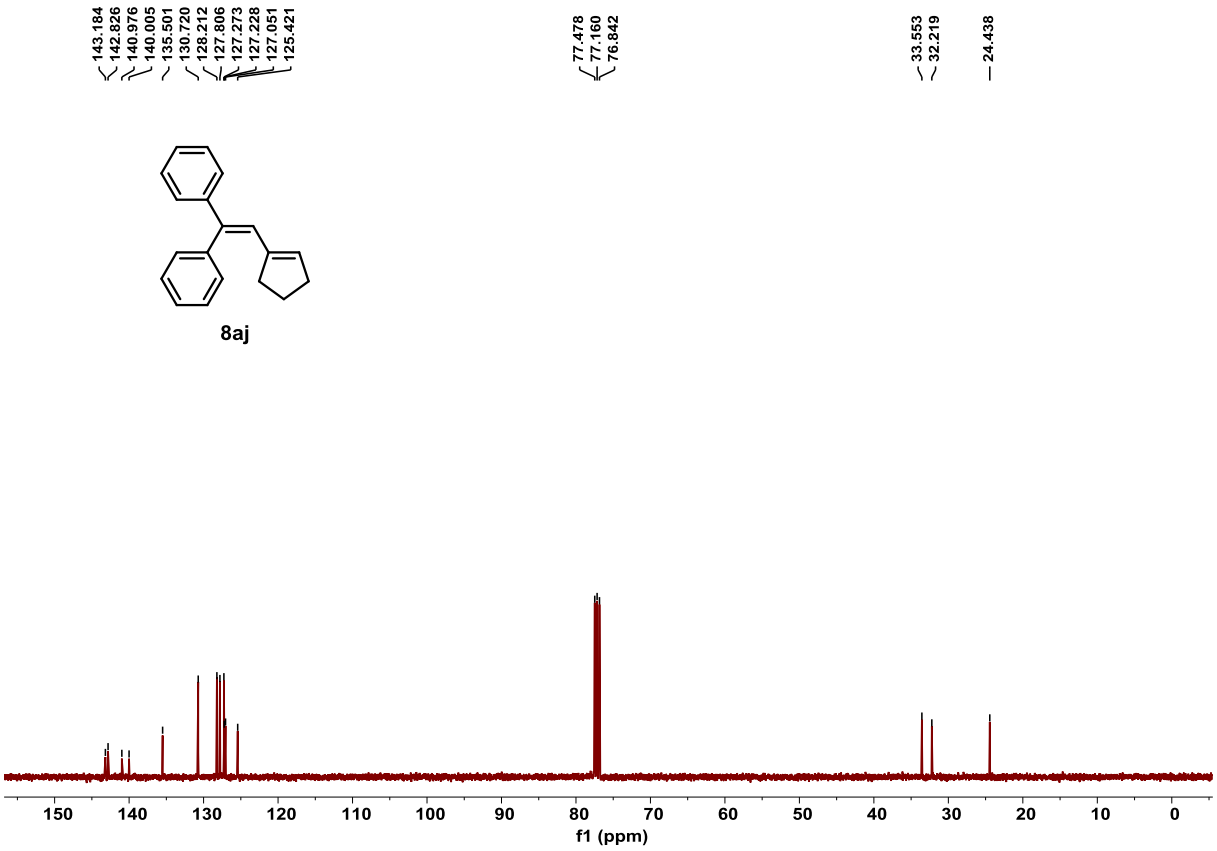

Figure S190. ^{13}C NMR spectrum of product **8aj**, related to **Scheme 4**.

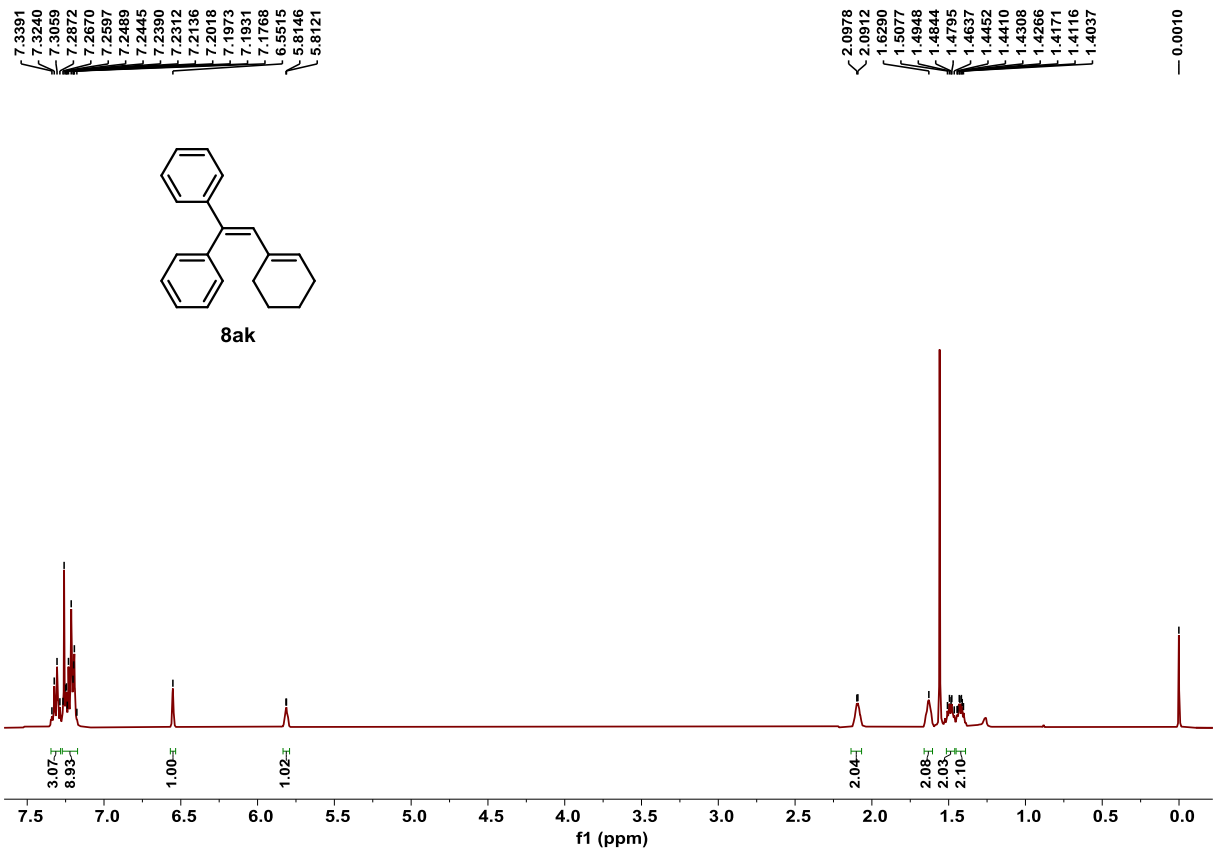

Figure S191. ^{1}**H NMR** spectrum of product **8ak**, related to **Scheme 4**.

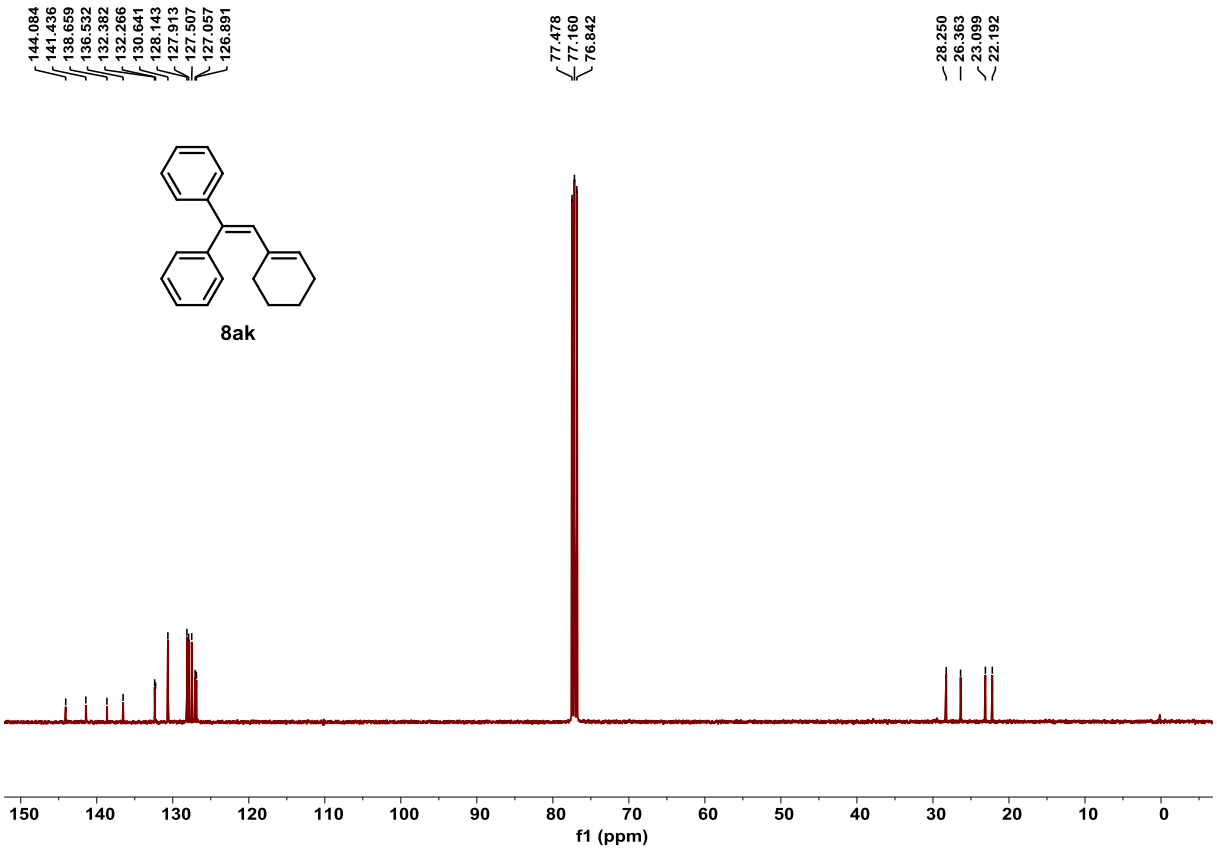

Figure S192. ^{13}**C NMR** spectrum of product **8ak**, related to **Scheme 4**.

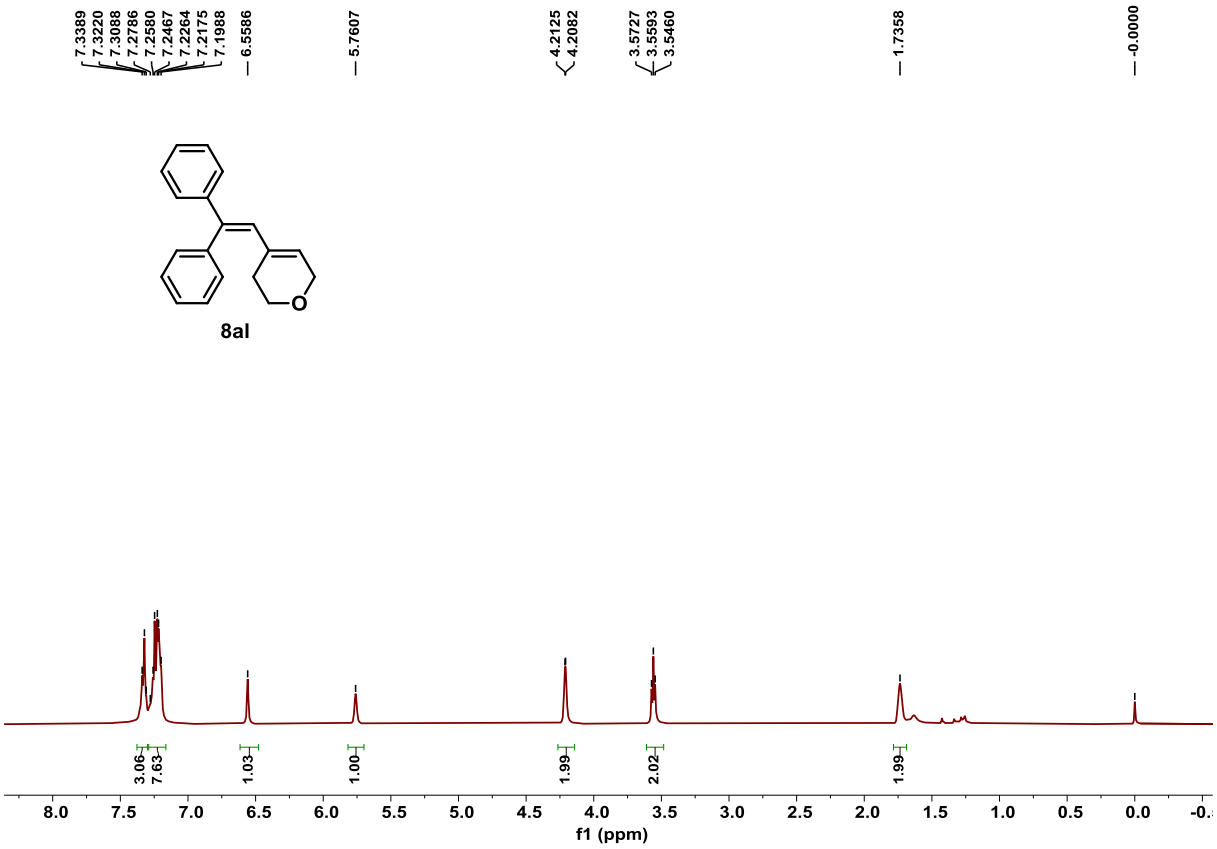

Figure S193. ^{1}H NMR spectrum of product **8al**, related to **Scheme 4**.

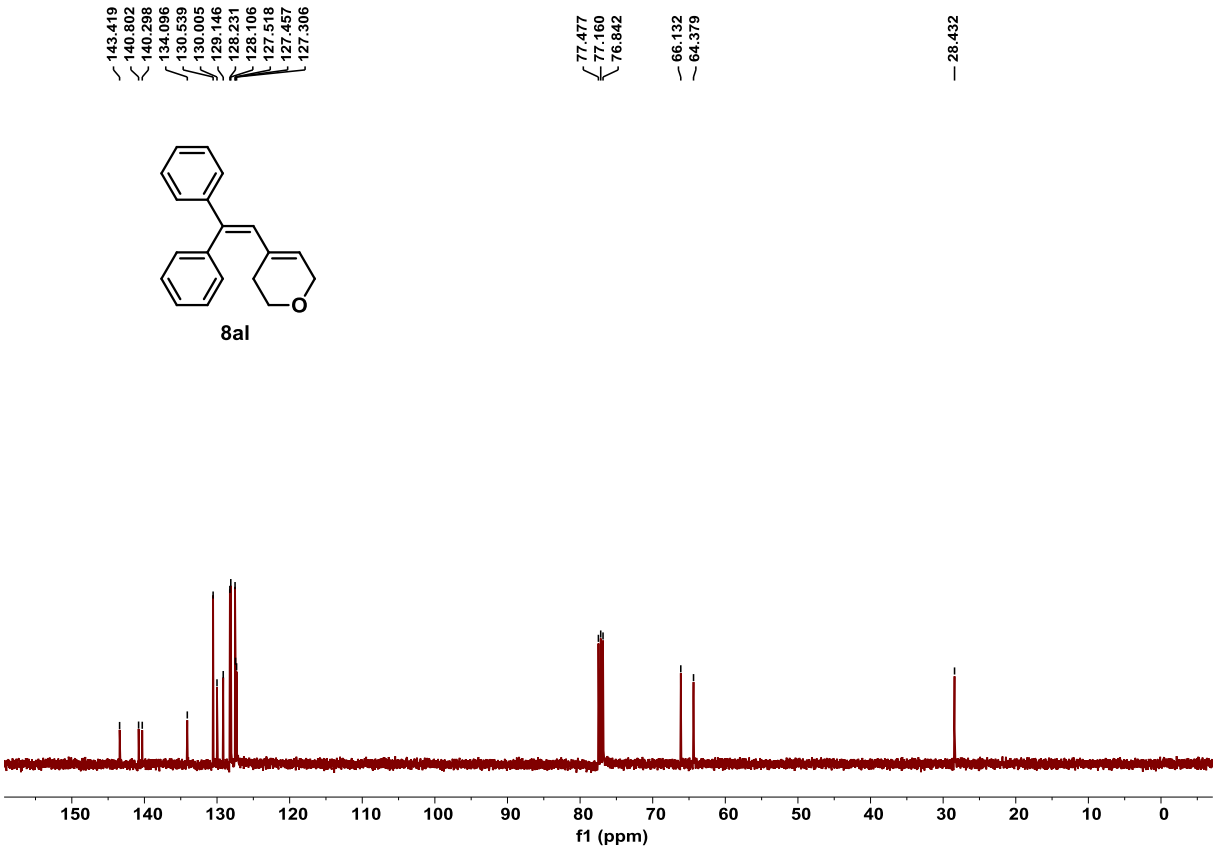

Figure S194. ^{13}C NMR spectrum of product **8al**, related to **Scheme 4**.

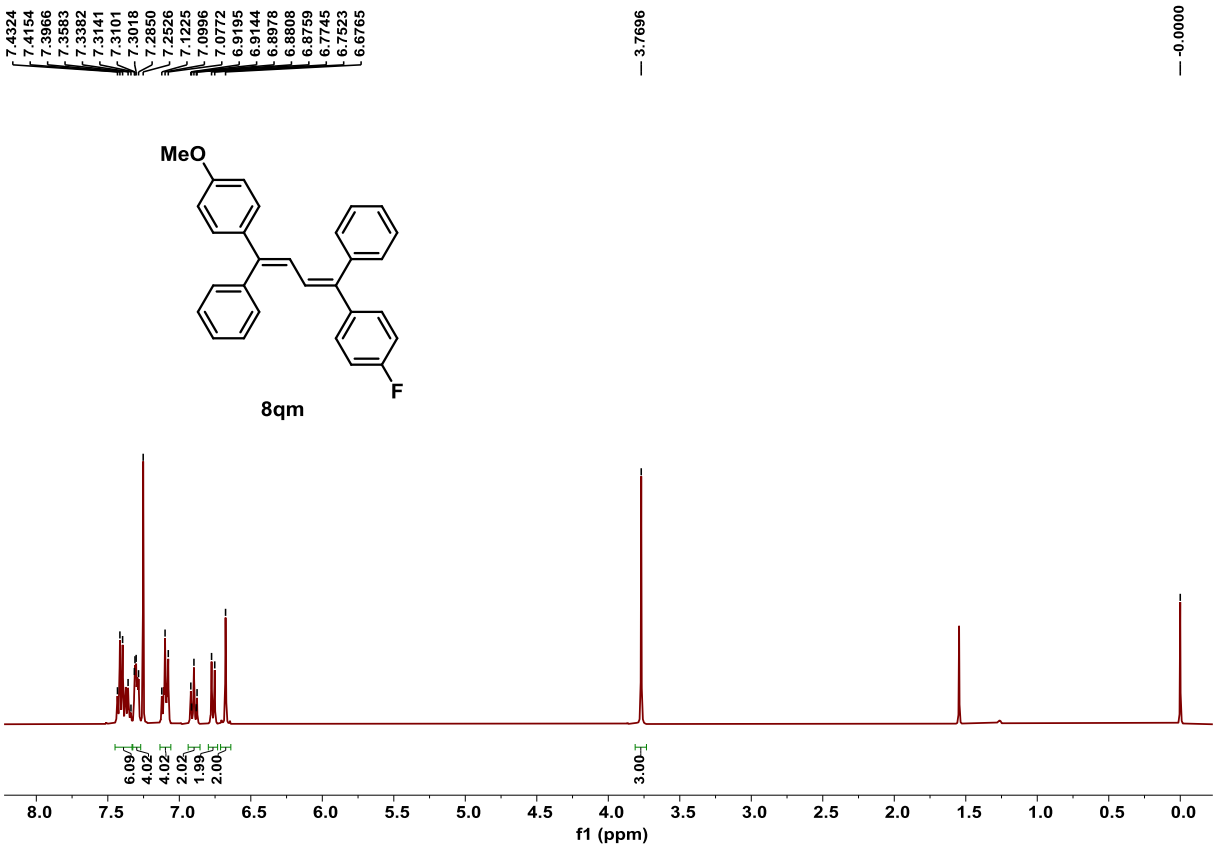

Figure S195. ^{1}**H NMR** spectrum of product **8qm**, related to **Scheme 4**.

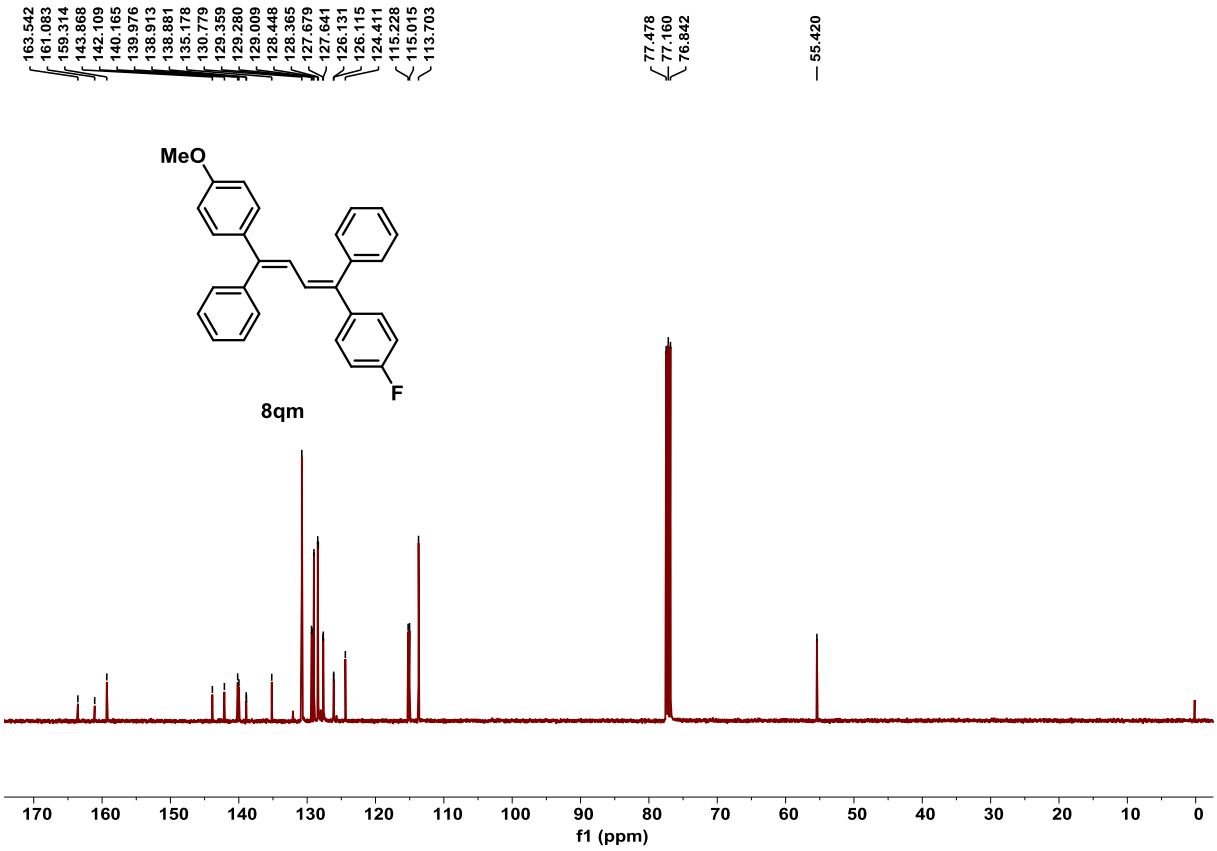

Figure S196. ^{13}**C NMR** spectrum of product **8qm**, related to **Scheme 4**.

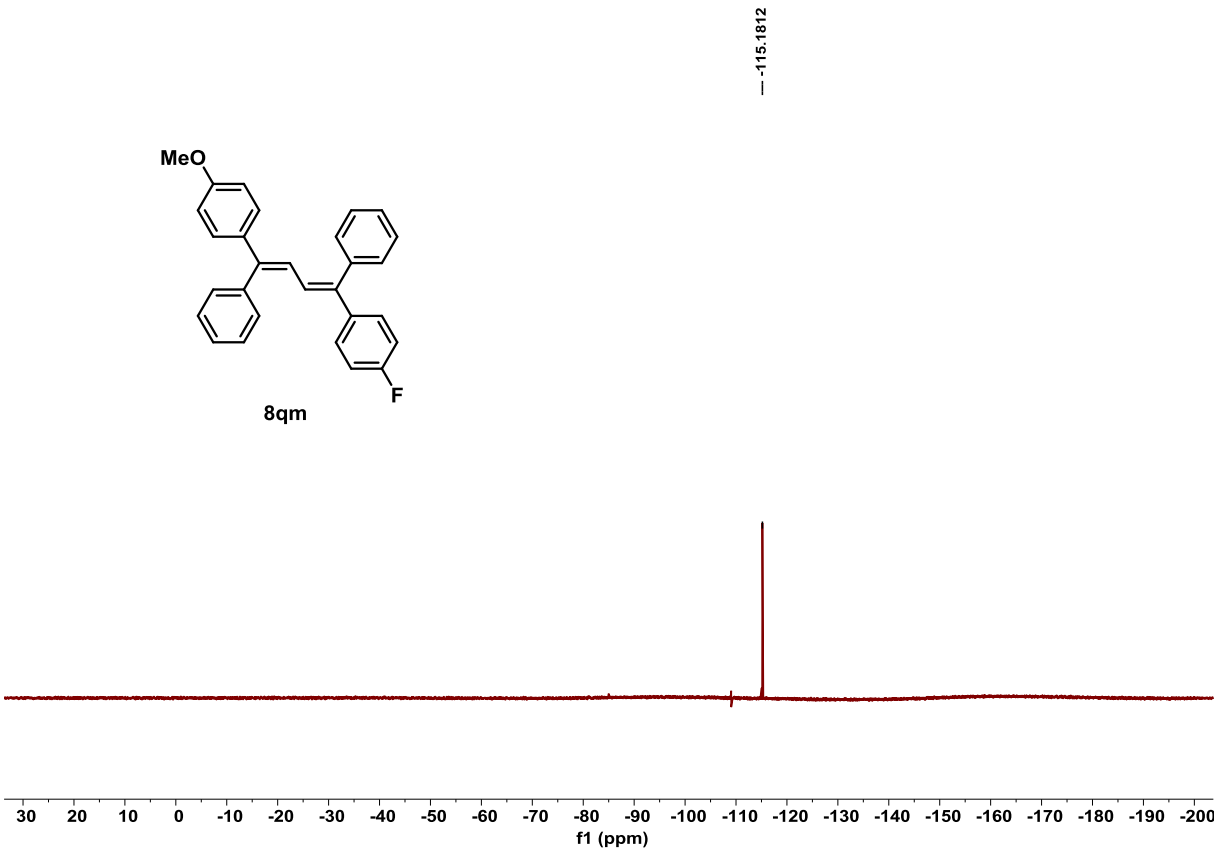

Figure S197. ^{19}F NMR spectrum of product **8qm**, related to **Scheme 4**.

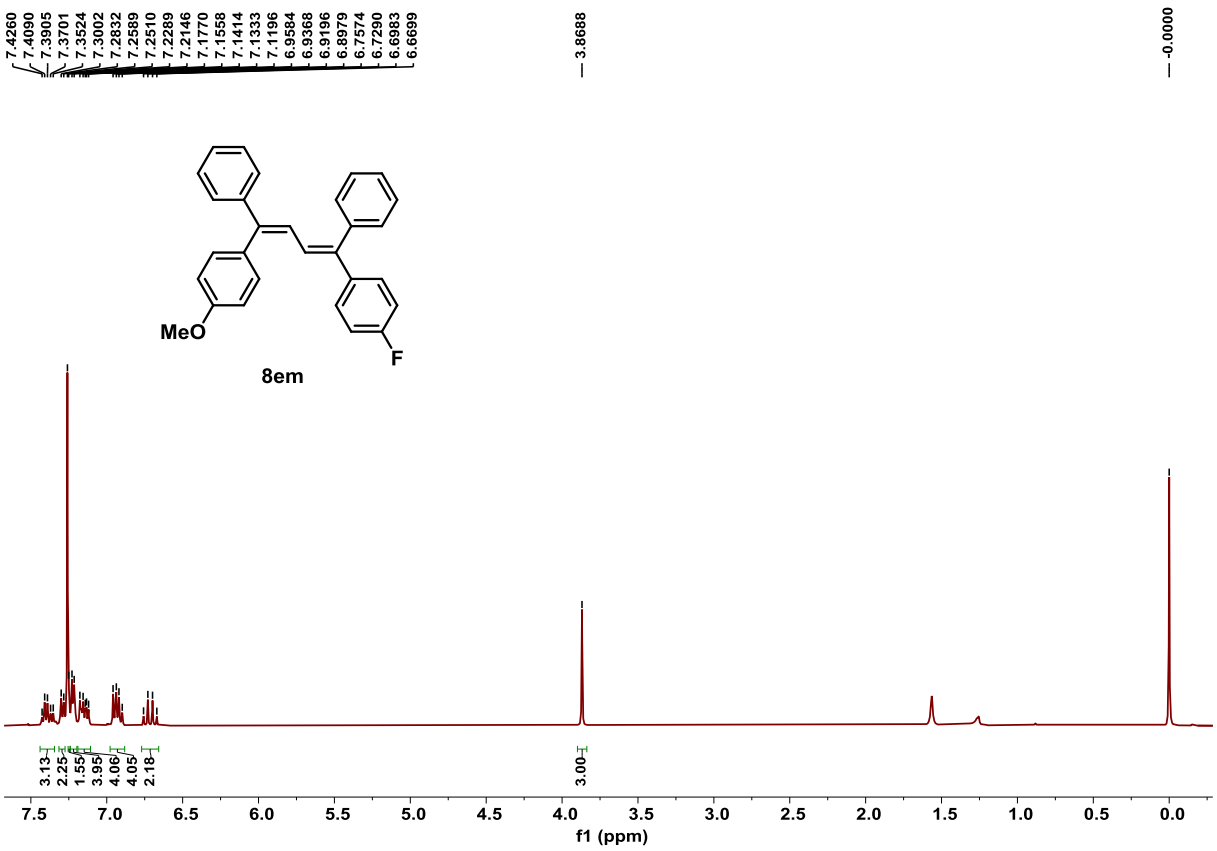

Figure S198. ^{1}H NMR spectrum of product **8em**, related to **Scheme 4**.

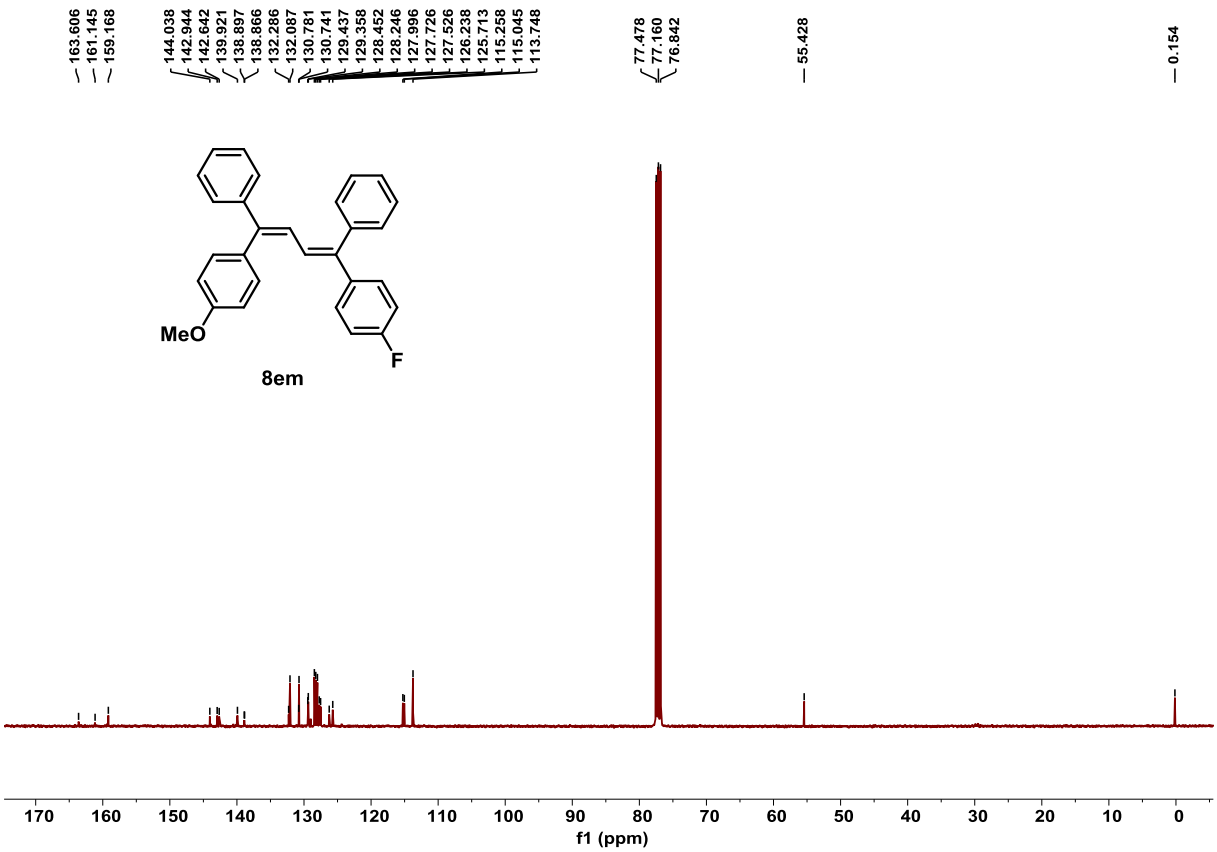

Figure S199. ^{13}**C NMR** spectrum of product **8em**, related to **Scheme 4**.

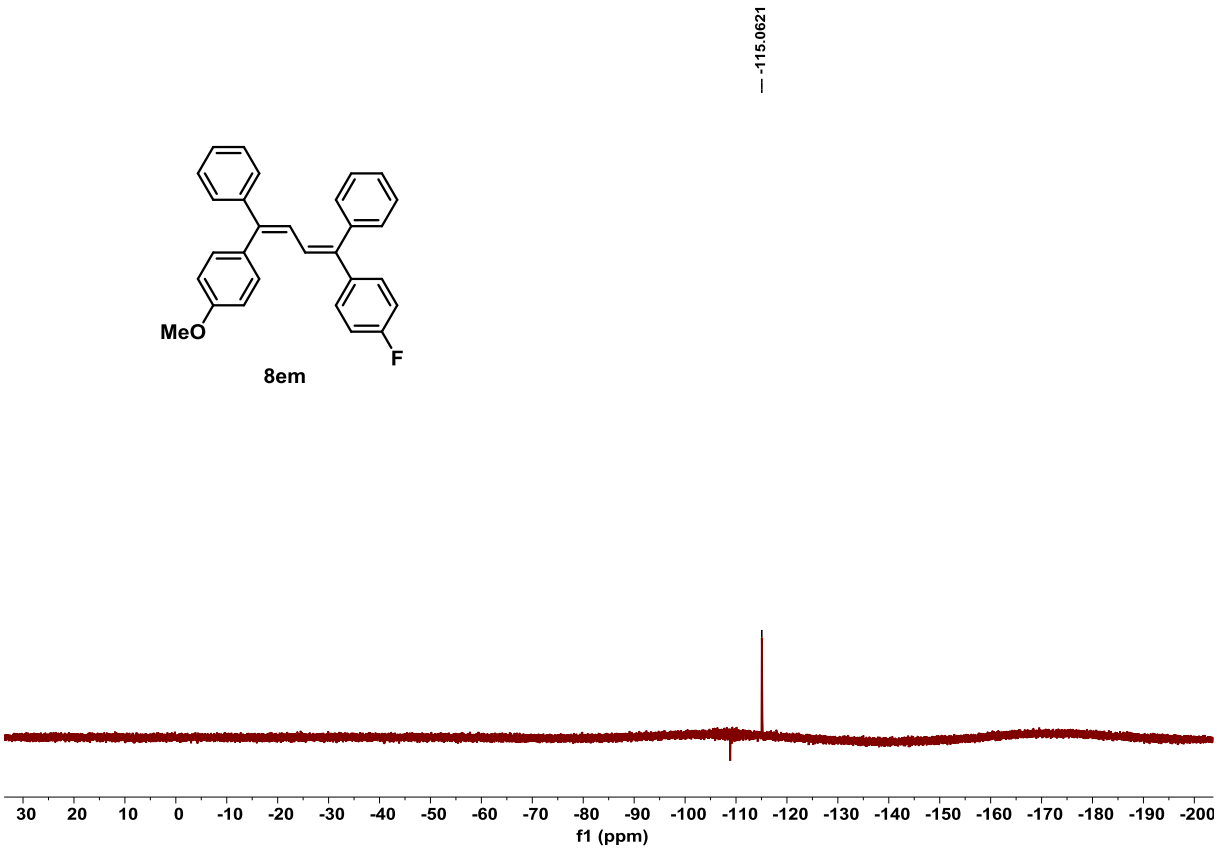

Figure S200. ^{19}**F NMR** spectrum of product **8em**, related to **Scheme 4**.

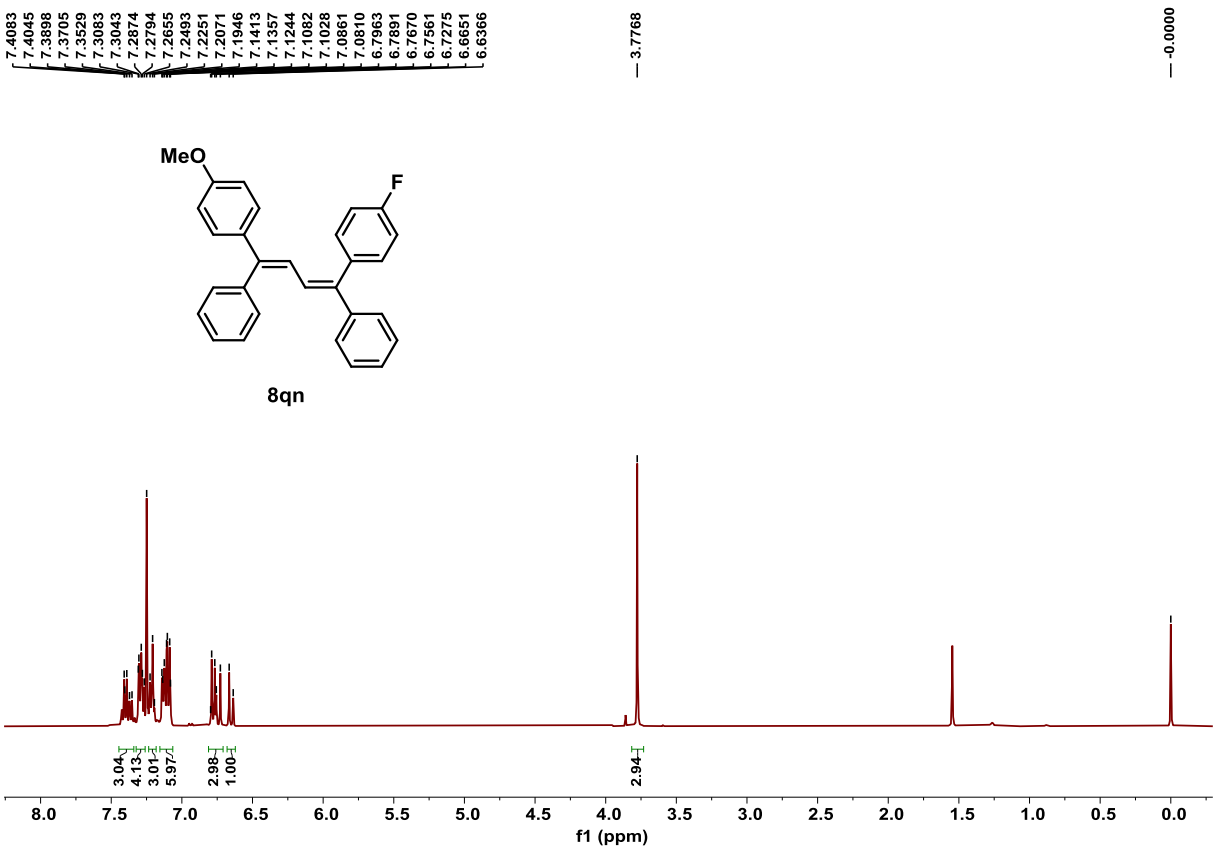

Figure S201. ^{1}H NMR spectrum of product **8qn**, related to **Scheme 4**.

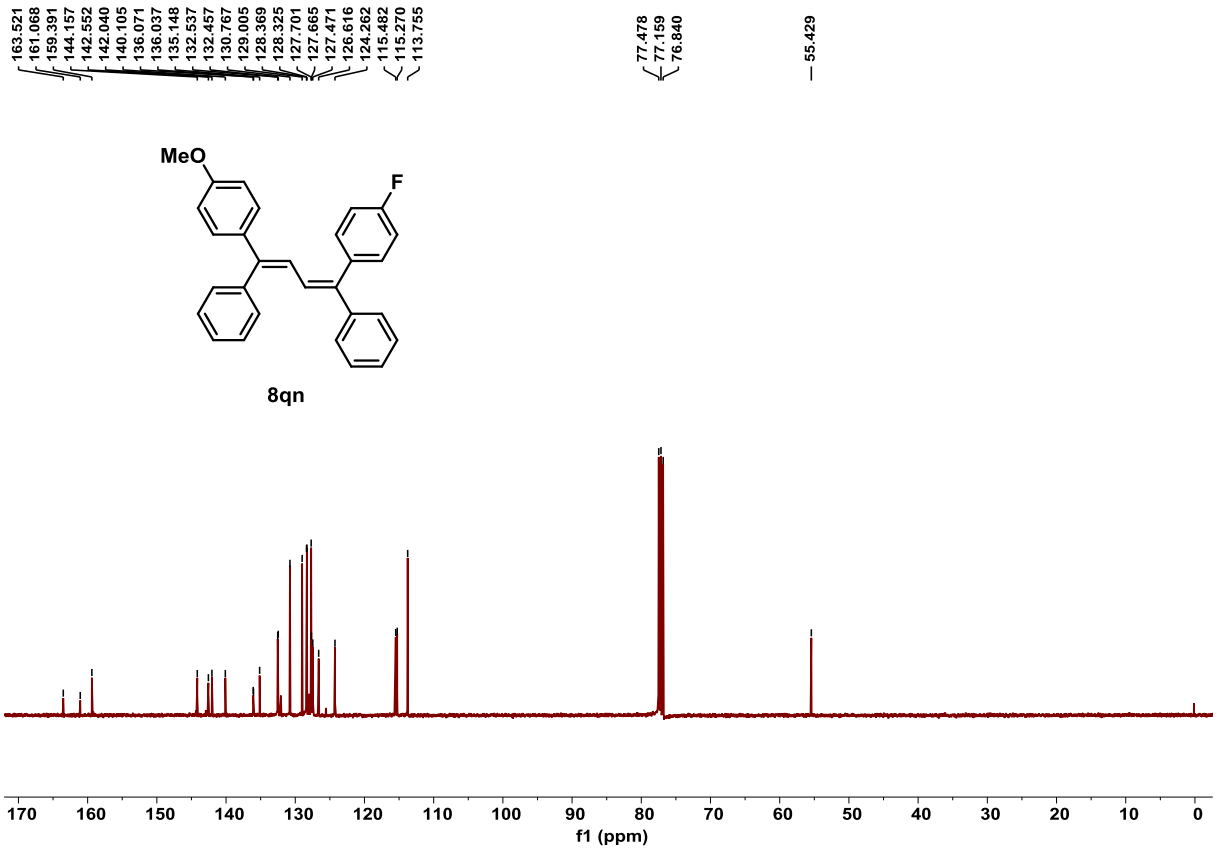

Figure S202. ^{13}C NMR spectrum of product **8qn**, related to **Scheme 4**.

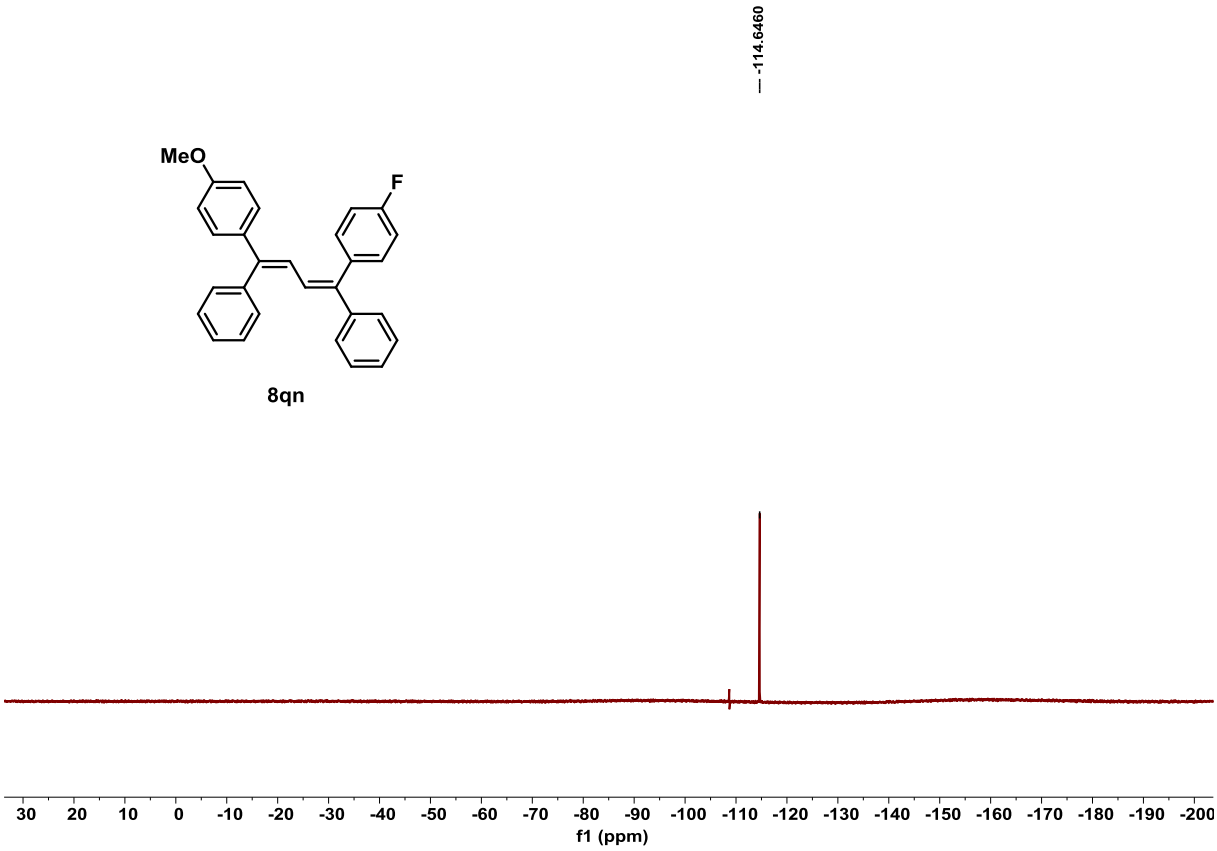

Figure S203. ^{19}F NMR spectrum of product **8qn**, related to **Scheme 4**.

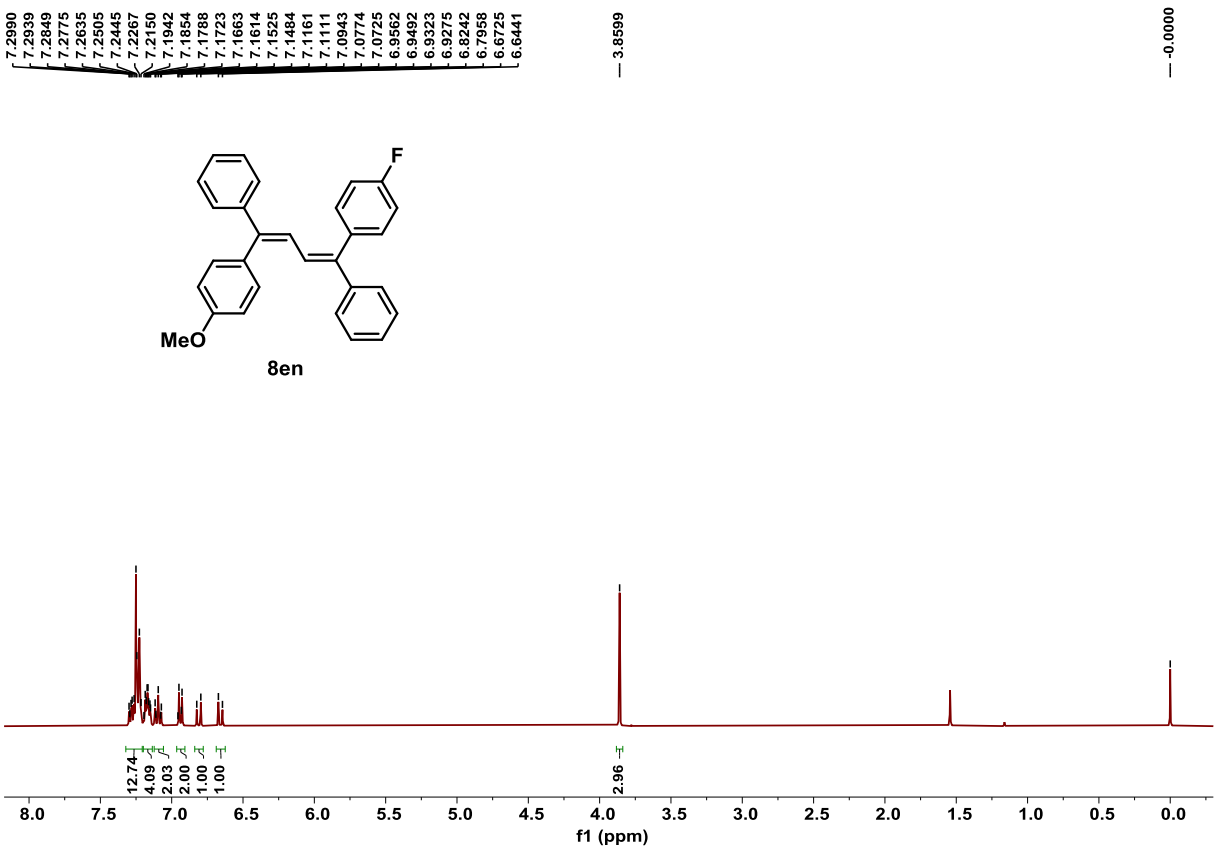

Figure S204. ^{1}H NMR spectrum of product **8en**, related to **Scheme 4**.

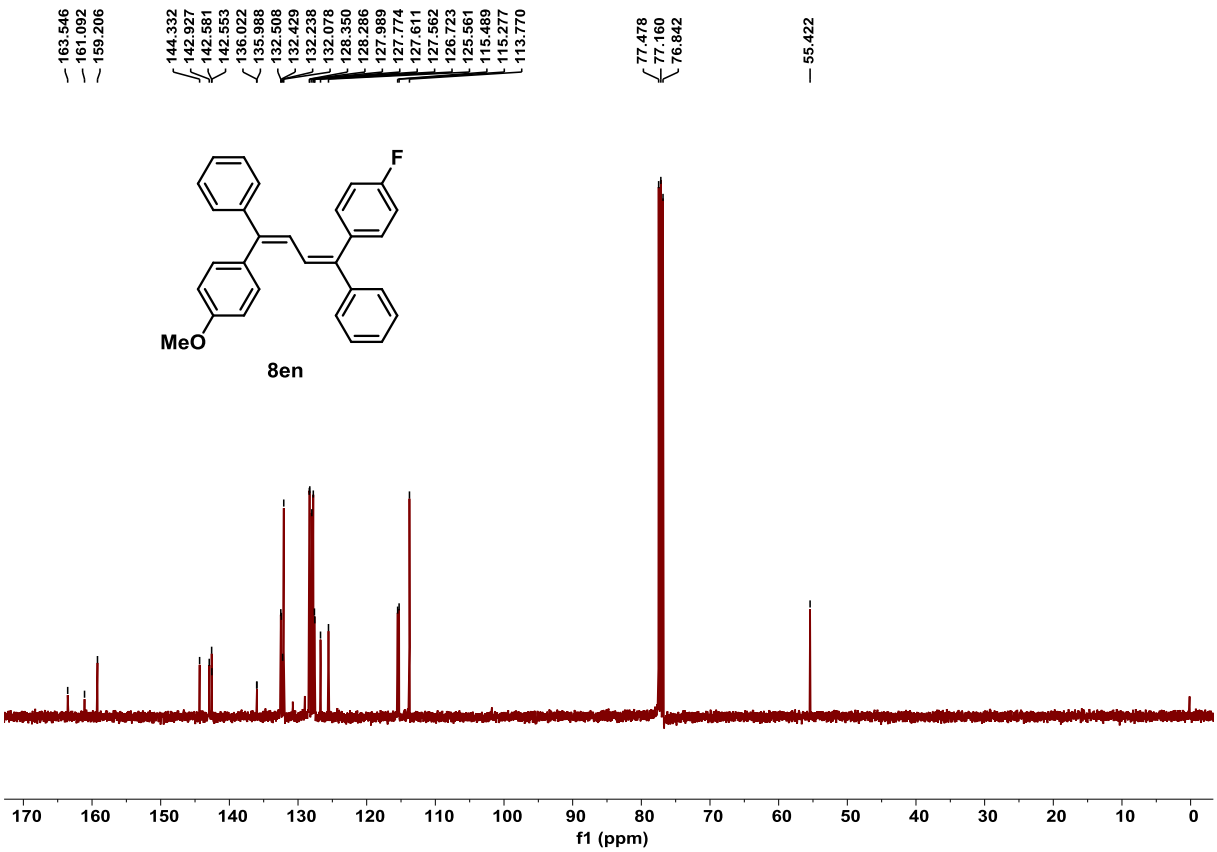

Figure S205. ^{13}**C NMR** spectrum of product **8en**, related to **Scheme 4**.

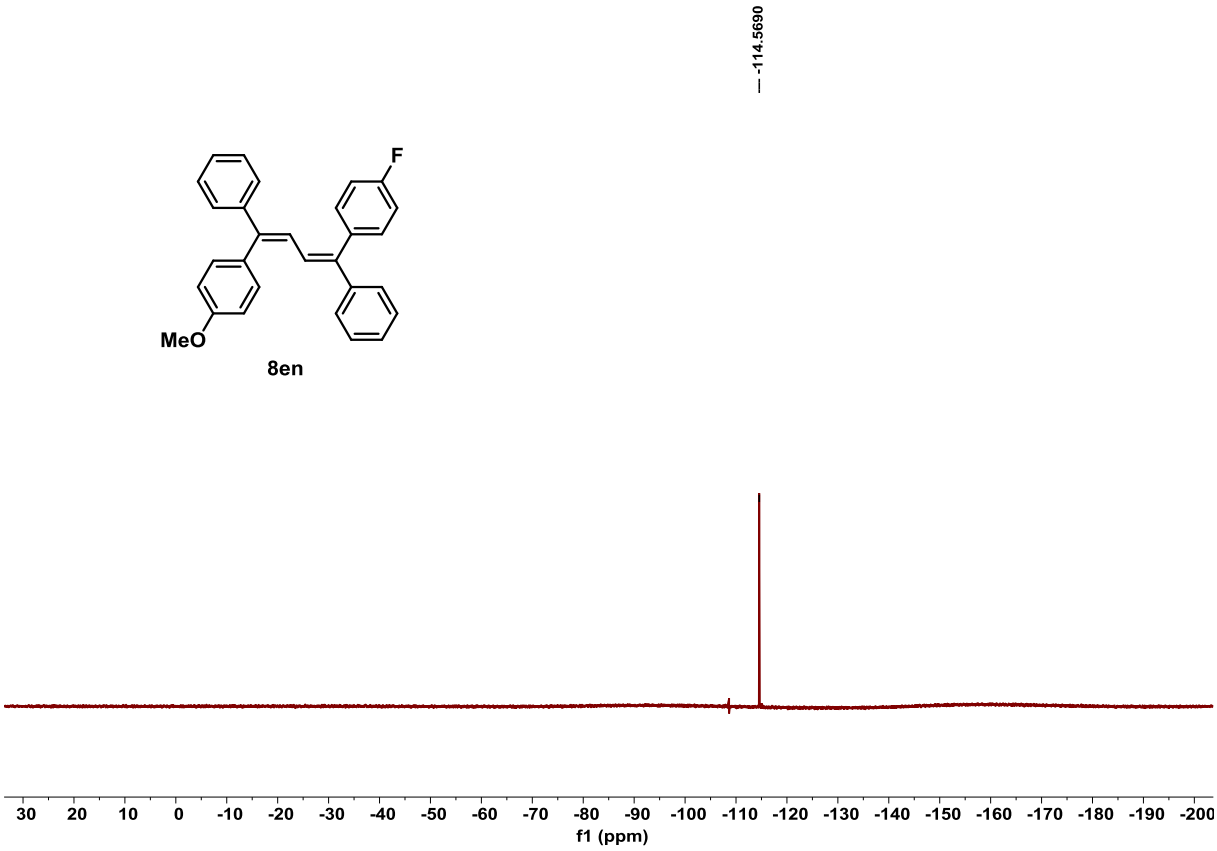

Figure S206. ^{19}**F NMR** spectrum of product **8en**, related to **Scheme 4**.

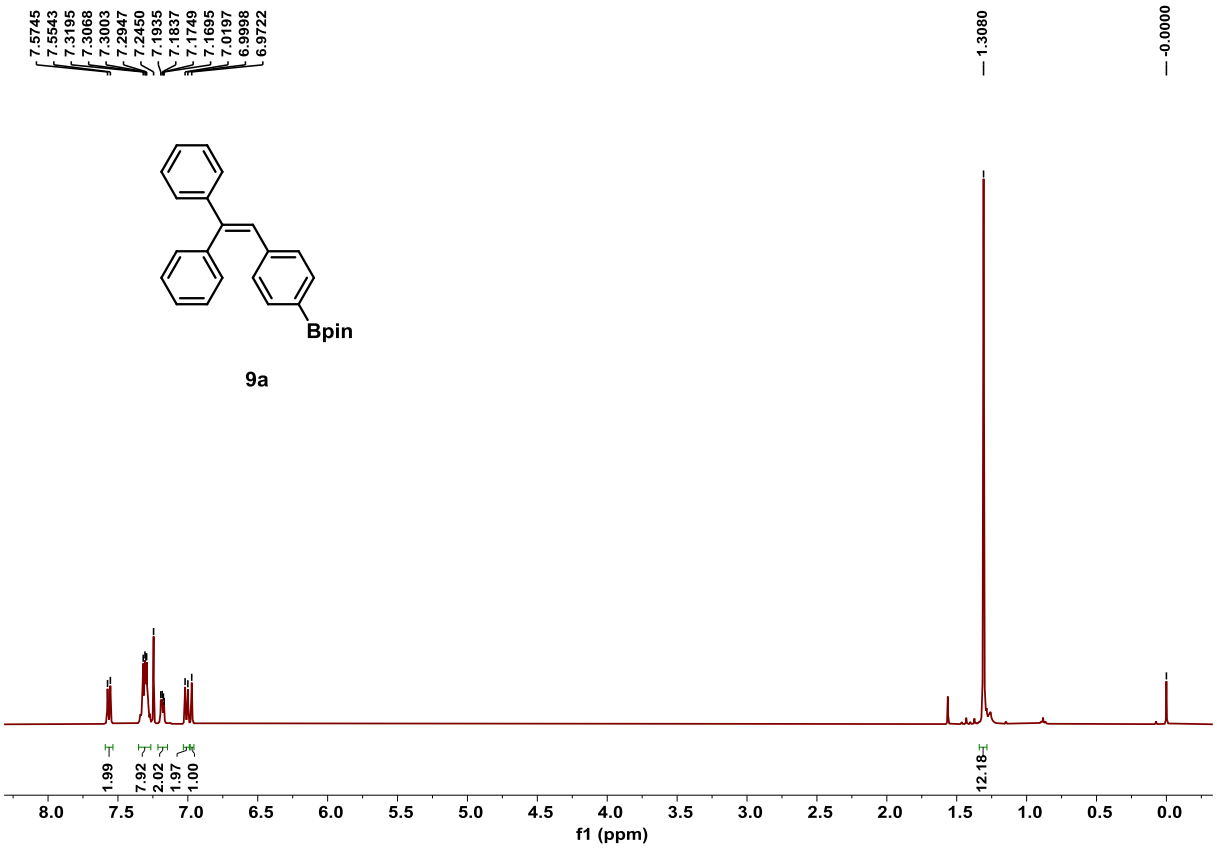

Figure S207. ^{1}**H NMR** spectrum of product **9a**, related to **Scheme 5**.

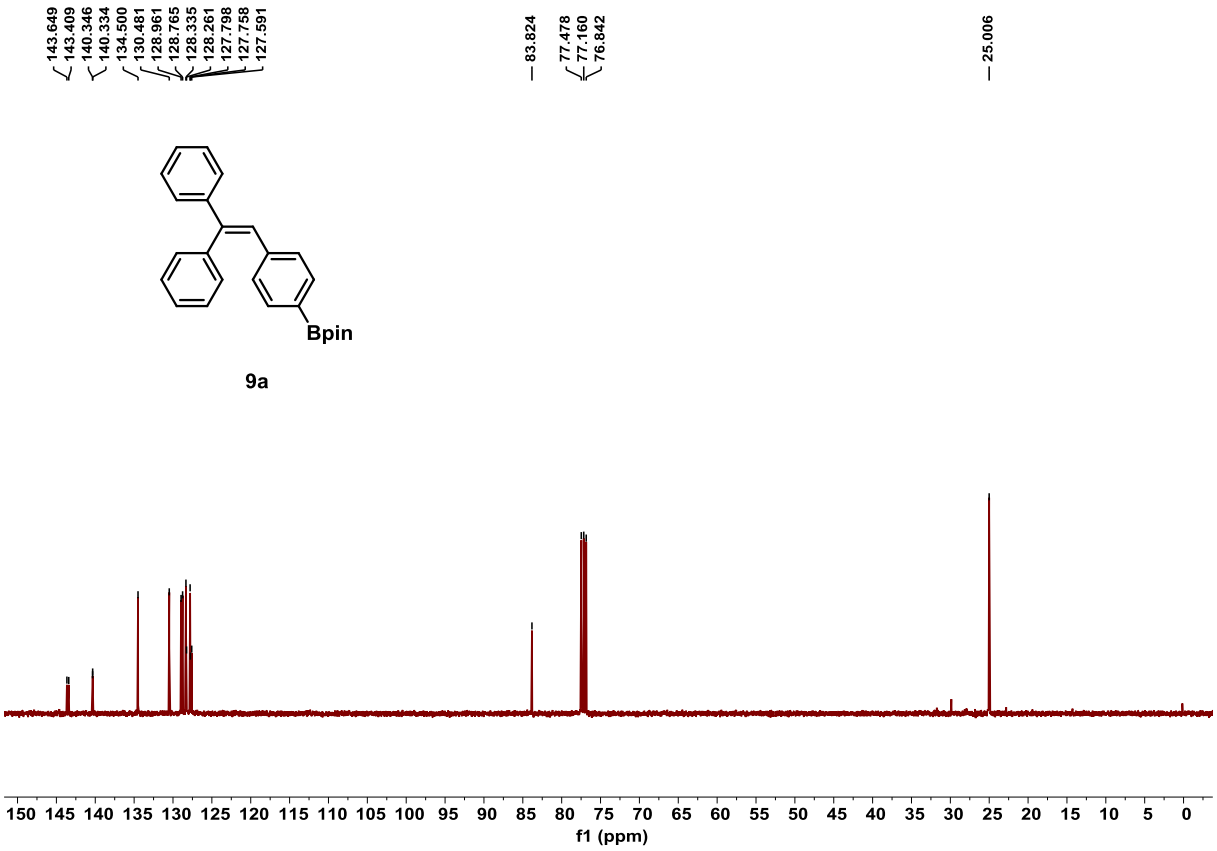

Figure S208. ^{13}**C NMR** spectrum of product **9a**, related to **Scheme 5**.

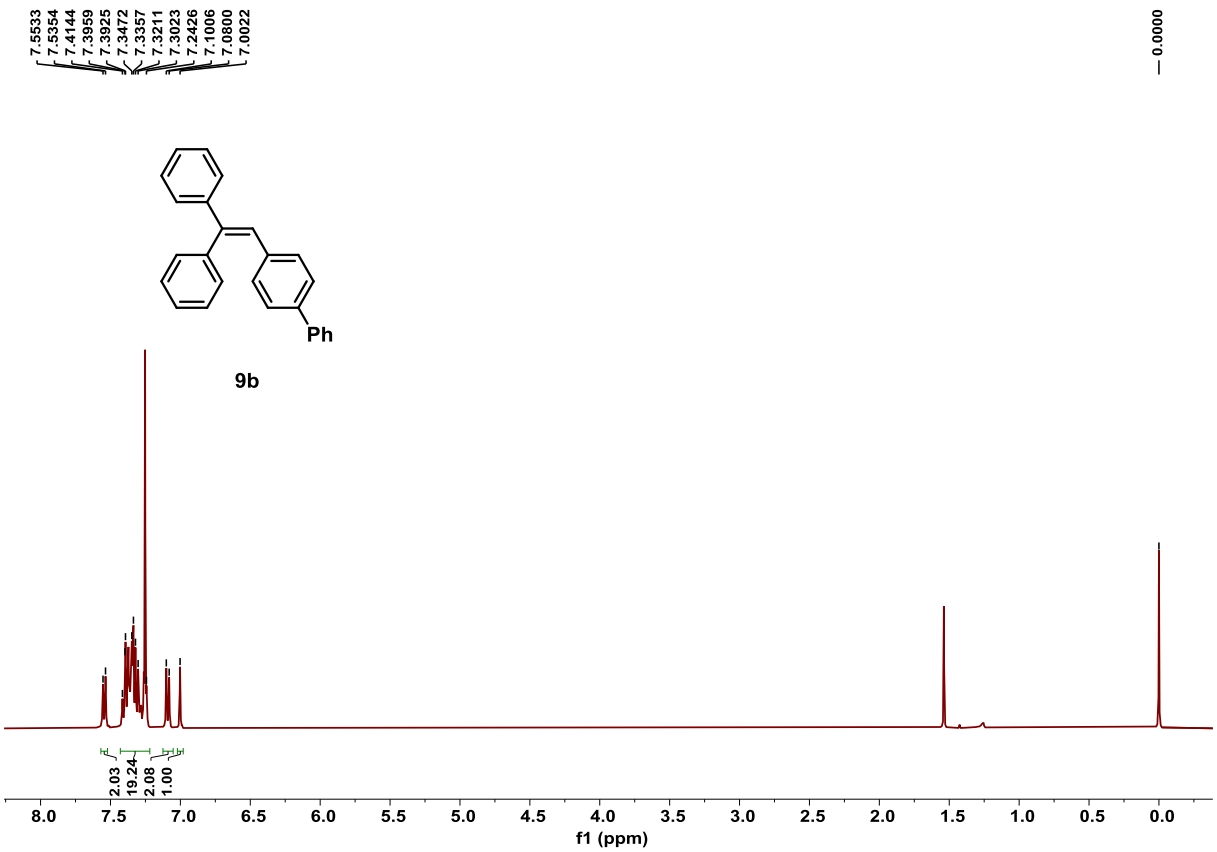

Figure S209. ^{1}**H NMR** spectrum of product **9b**, related to **Scheme 5**.

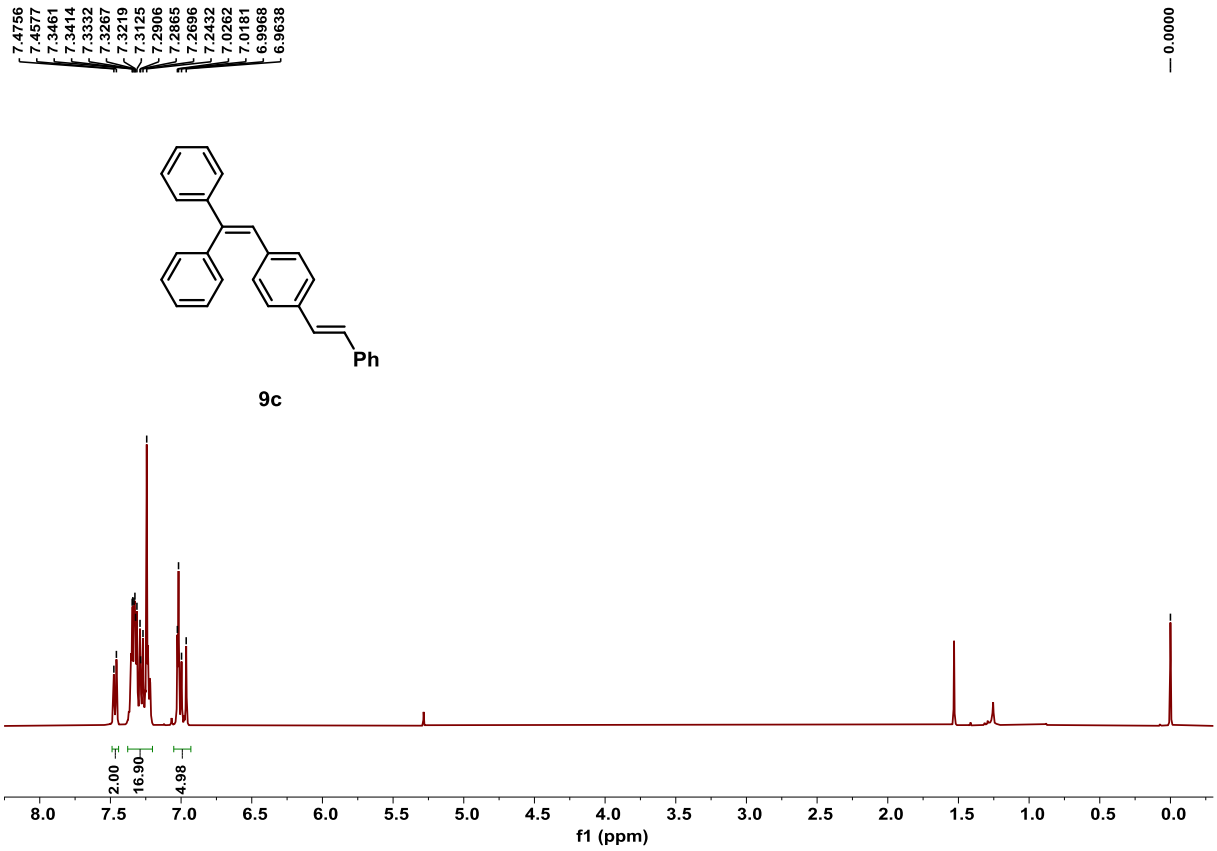

Figure S210. ^{1}**H NMR** spectrum of product **9c**, related to **Scheme 5**.

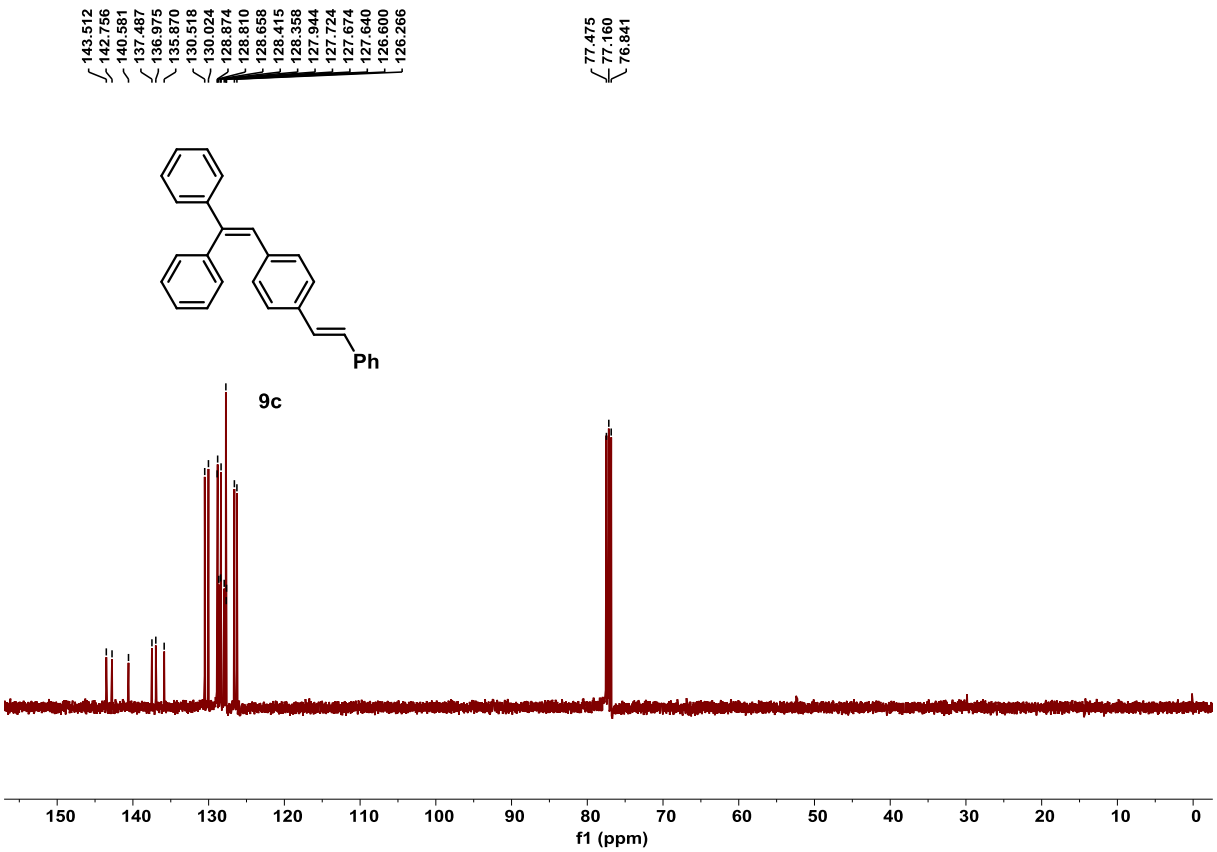

Figure S211. ^{13}C NMR spectrum of product **9c**, related to **Scheme 5**.

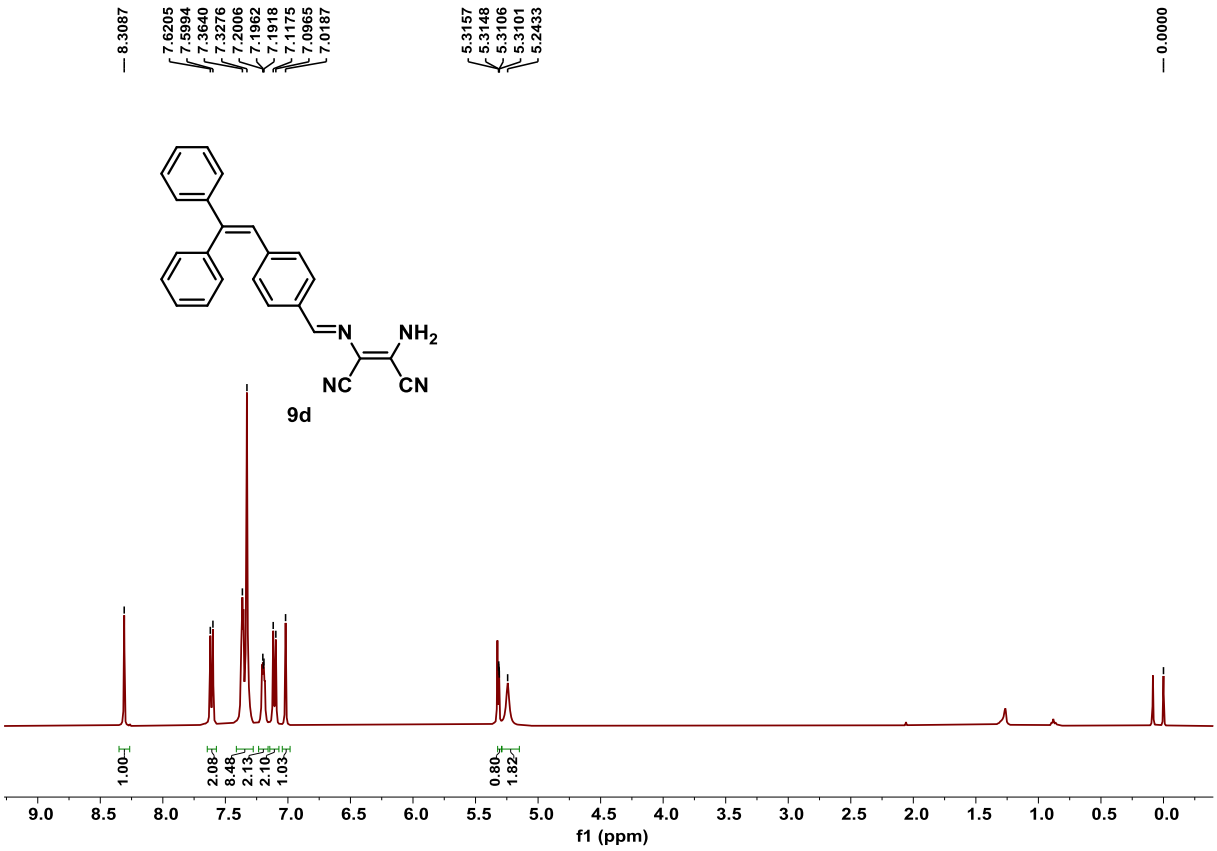

Figure S212. ^{1}H NMR spectrum of product **9d**, related to **Scheme 5**.

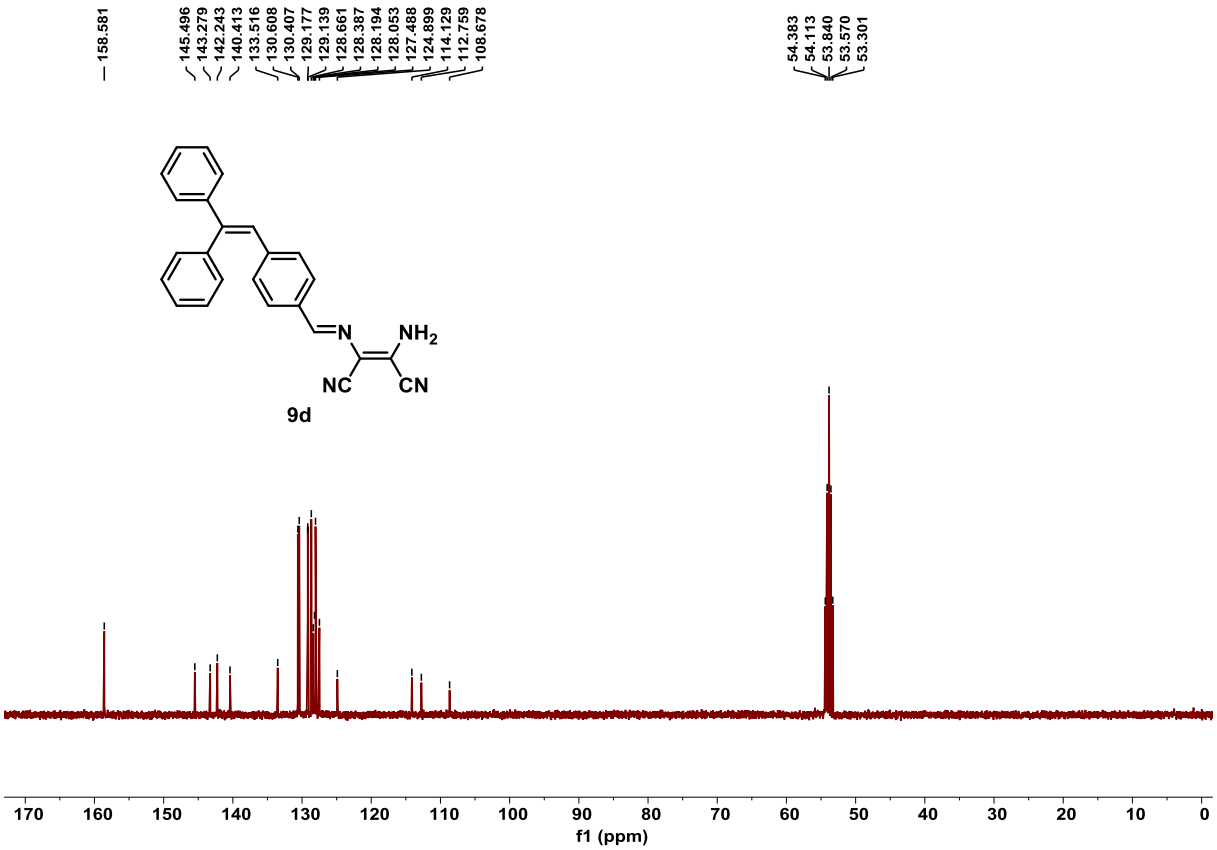

Figure S213. ^{13}**C NMR** spectrum of product **9d**, related to **Scheme 5**.

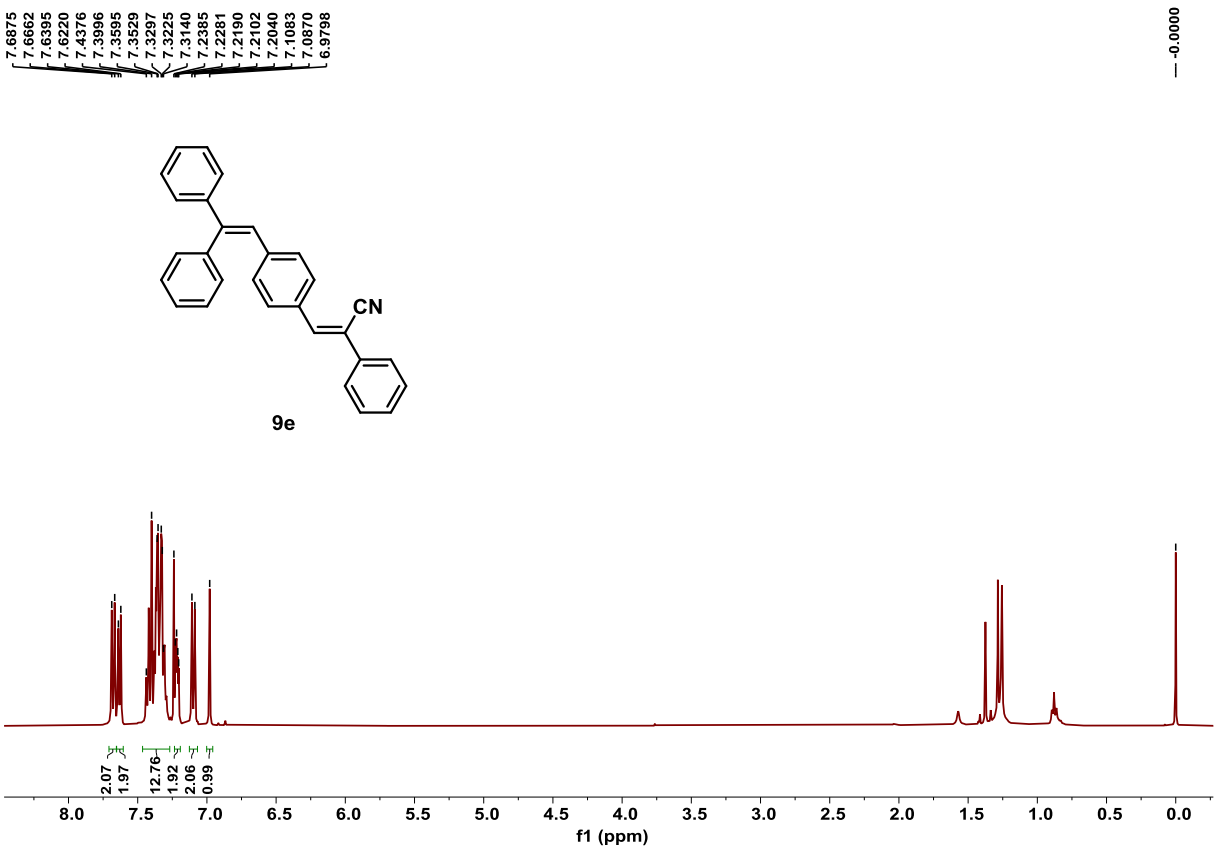

Figure S214. ^{1}**H NMR** spectrum of product **9e**, related to **Scheme 5**.

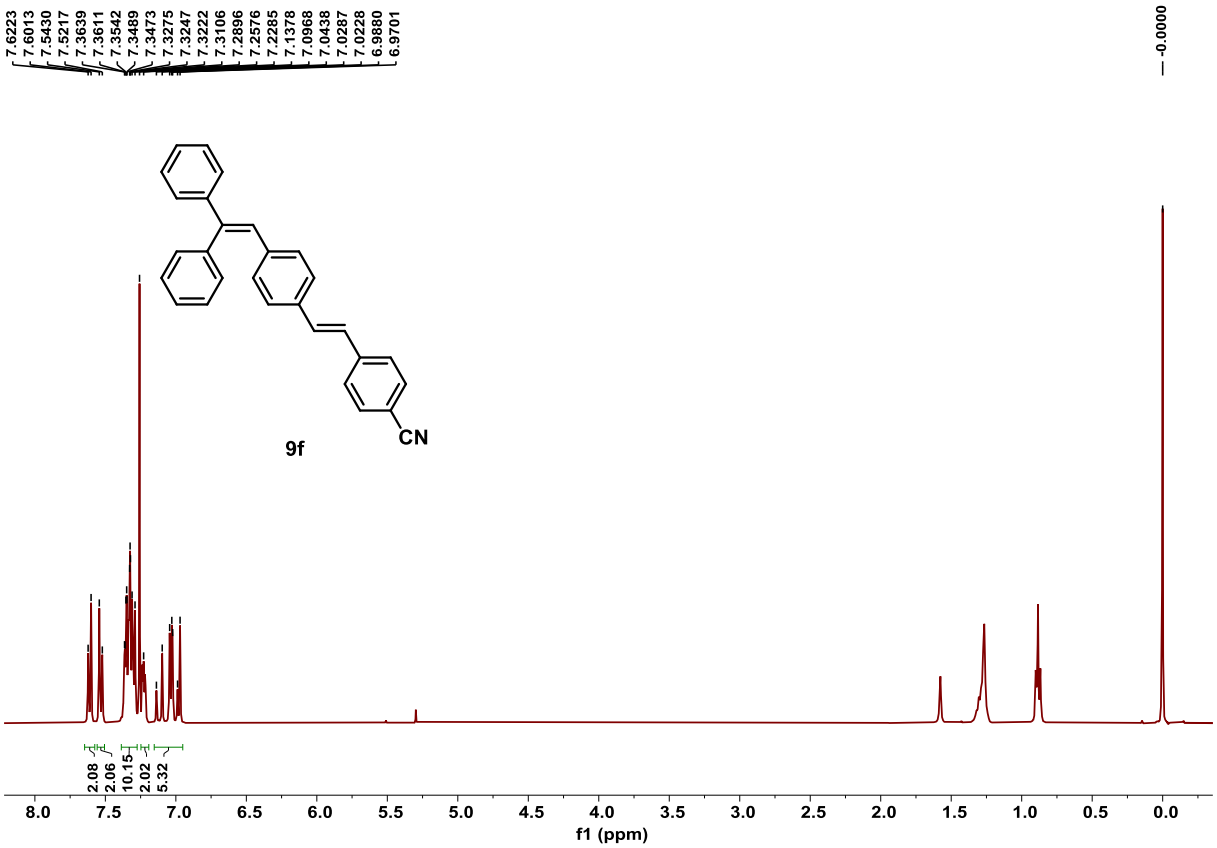

Figure S215. ^{1}**H NMR** spectrum of product **9f**, related to **Scheme 5**.

Transparent Methods

1. General information

All reactions were carried out with standard Schlenk techniques under argon atmosphere. All the solvents were dried using standard procedure and distilled before use. All commercially available chemical resources were used as received, unless otherwise stated. Reactions were monitored by thin layer chromatography (TLC) supplied by Yantai Jiangyou Silicon Material Company (China). Visualization was accomplished with UV light or basic aqueous potassium permangante ($KMnO_4$). Chromatography was achieved using forced flow (flash chromatography) of the indicated solvent system on 300-400 mesh silica gel (Silicycle flash F60) unless otherwise noted. Nuclear Magnetic Resonance (**NMR**) spectra were acquired on Agilent 400 or Bruker 400 instrument operating at 400, 100 and 376 MHz for ^{1}H, ^{13}C and ^{19}F, respectively. Chemical shifts are reported in δ ppm referenced to an internal $SiMe_4$ standard (TMS: δ 0.000 ppm) for **^{1}H NMR**, chloroform-*d* (δ 77.16) for **^{13}C NMR** unless otherwise noted. Multiplicities are reported using the following abbreviations: s = singlet, d = doublet, t = triplet, q = quartet, quintet = quint, heptet = hept, m = multiplet, br = broad resonance. High-resolution mass spectra (**HRMS**) and Low resolution mass spectra (**LRMS**) were acquired through the National Center for Organic Mass Spectrometry in Shanghai, Shanghai Institute of Organic Chemistry (CAS) and determined on a Waters Micromass GCT Premie spectrometer. Solid state luminescent quantum yield measurements for olefins and 1,3-dienes were performed with Hamamatsu absolute PL quantum yield spectrometer C11347 Quantaurus_QY. UV-vis absorption spectra were measured on a Shimadzu UV-2600 spectrophotometer and photoluminescence spectra were recorded on a Horiba Fluoromax-4 spectrofluorometer.

The *ortho*-vinyl arylbromides (**1a-1e, 1g-1v, 1B**) (Wei et al., 2019; Wei et al., 2018; Ryutaro Hayashi, 2018; Hu et al., 2018; Shen et al., 2017; Rossi et al., 2001), (hetero)aryl boronate esters (**2a-2h, 2l-2o, 2q, 5a-5c, 5j, 5r**) (Zhang et al., 2018; Carreira-Barral et al., 2018; Zhou et al., 2017; Ranjani and Nagarajan, 2017; Bello and Schmidt-Leithoff, 2012; Yu et al., 2010; Gómez-Blanco et al., 2009; Iwai et al., 2008; Stephen J. Baker, 2006; Burstein et al., 2005; Wong et al., 2002), diaryl-vinyl boronate esters (**7h, 7i**) (Hu et al., 2016) were prepared according to the literatures. Heteroaryl boronate esters (**5g-5h, 5m-5q**) and vinyl boronate esters (**7a-7g**) were purchased and used directly from commercial sources.

2. Synthesis of substrates

2.1. Preparation of *ortho*-vinyl arylbromides **1**

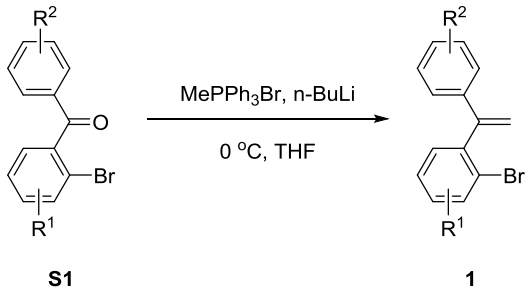

S1 **1**

Scheme S1. Synthesis of *ortho*-vinyl arylbromides **1**, related to **Scheme 2** and **Scheme 4**.

To a stirred mixture of triphenyl phosphonium salt (5.5 mmol) in THF (20 mL) was added ^{n}BuLi (2 mL, 2.5 N

in hexane, 5.0 mmol) dropwise at 0 ℃ under argon atmosphere. After 30 min, a solution of *ortho*-carbonyl arylbromides **S1** (4.0 mmol) in THF (4 mL) was added to the yellowish mixture dropwise at the same temperature. After being stirred at room temperature for further 8 h, the reaction was quenched by adding H_2O and ethyl acetate. The organic layer was separated and the aqueous layer was extracted with ethyl acetate. The combined organic phases were washed with brine, dried over anhydrous Na_2SO_4 and concentrated under reduced pressure. The residue was purified by chromatography on silica gel to afford product **1**.

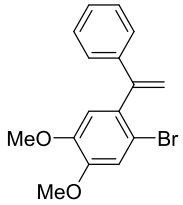

1-bromo-4,5-dimethoxy-2-(1-phenylvinyl)benzene (1f), white solid (92% yield), **^{1}H NMR** (400 MHz, $CDCl_3$) δ 7.34-7.23 (m, 5H), 7.07 (s, 1H), 6.80 (s, 1H), 5.83 (d, *J* = 1.3 Hz, 1H), 5.27 (d, *J* = 1.1 Hz, 1H), 3.90 (s, 3H), 3.85 (s, 3H) ppm; **^{13}C NMR** (100 MHz, $CDCl_3$) δ 149.01, 148.79, 148.34, 139.78, 134.84, 128.47, 127.88, 126.69, 116.20, 115.74, 114.24, 113.46, 56.33, 56.23 ppm; **EI-MS** m/z **(**%**)**: 318 (M^+); **HRMS** (EI): m/z Exact mass calcd for $C_{16}H_{15}O_2Br$ $[M]^+$: 318.0255, found: 318.0264.

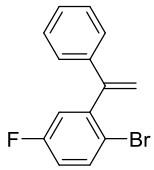

1-bromo-4-fluoro-2-(1-phenylvinyl)benzene (1A), colorless oil (95% yield), **^{1}H NMR** (400 MHz, $CDCl_3$) δ 7.54 (dd, *J* = 8.8, 5.3 Hz, 1H), 7.39-7.20 (m, 5H), 7.06 (dd, *J* = 8.9, 3.0 Hz, 1H), 6.95 (td, *J* = 8.4, 3.1 Hz, 1H), 5.85 (s, 1H), 5.28 (s, 1H) ppm; **^{13}C NMR** (100 MHz, $CDCl_3$) δ 161.94 (d, *J* = 247.6 Hz), 148.24 (d, *J* = 1.5 Hz), 144.57 (d, *J* = 8.0 Hz), 139.04, 134.29 (d, *J* = 8.0 Hz), 128.57, 128.11, 126.63, 118.73 (d, *J* = 22.5 Hz), 117.66 (d, *J* = 3.1 Hz), 116.70, 116.28 (d, *J* = 22.5 Hz) ppm; **^{19}F NMR** (376 MHz, $CDCl_3$) δ -115.31 ppm; **EI-MS** m/z (%): 276 (M^+); **HRMS** (EI): m/z Exact mass calcd for $C_{14}H_{10}FBr$ $[M]^+$: 275.9950, found: 275.9952.

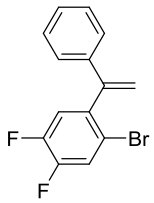

1-bromo-4,5-difluoro-2-(1-phenylvinyl)benzene (1B), white solid (89% yield), **^{1}H NMR** (400 MHz, $CDCl_3$) δ 7.43 (dd, *J* = 9.7, 7.5 Hz, 1H), 7.36-7.28 (m, 3H), 7.28-7.20 (m, 2H), 7.16 (dd, *J* = 10.5, 8.3 Hz, 1H), 5.85 (s, 1H), 5.27 (s, 1H) ppm; **^{13}C NMR** (100 MHz, $CDCl_3$) δ 150.81 (dd, *J* = 12.8, 8.6 Hz), 148.30 (dd, *J* = 12.8, 5.9 Hz), 147.47, 139.53 (dd, *J* = 5.7, 4.2 Hz), 138.91, 128.62, 128.22, 126.59, 121.93 (d, *J* = 19.8 Hz), 120.00 (d, *J* = 17.5 Hz), 117.14, 117.07 (d, *J* = 3.4, 3.8 Hz) ppm; **^{19}F NMR** (376 MHz, $CDCl_3$) δ -138.69, -136.47 ppm; **EI-MS** m/z (%): 294 (M^+); **HRMS** (EI): m/z Exact mass calcd for $C_{14}H_9F_2Br$ $[M]^+$: 293.9856, found: 293.9862.

2.2. Preparation of (hetero)aryl boronate esters **2**

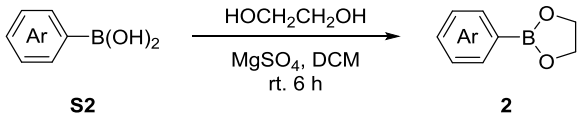

S2 **2**

Scheme S2. Synthesis of (hetero)aryl boronic acid glycol ester substrates **2**, related to **Scheme 2**.

To the stirring suspension of arylboronic acid **S2** (40 mmol) and $MgSO_4$ (60 mmol) in CH_2Cl_2 (80 mL) was added glycol (44 mmol) at room temperature dropwise. Then the resulting mixture was allowed to stir at room temperature for further 4 h. The white solid was filtered through a pad of Celite and the filtrate was concentrated under reduced pressure to afford the crude product as a solid. The crude was recrystallized with CH_2Cl_2-hexane mixed-solvent system to afford the pure product.

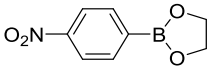

2-(4-nitrophenyl)-1,3,2-dioxaborolane (2i), pale yellow solid (87% yield); **^{1}H NMR** (400 MHz, $CDCl_3$) δ 8.22 (d, *J* = 8.6 Hz, 2H), 7.98 (d, *J* = 8.5 Hz, 2H), 4.44 (s, 4H) ppm; **^{13}C NMR** (100 MHz, $CDCl_3$) δ 150.10, 135.90, 122.70, 66.53 ppm; **EI-MS** m/z (%): 193 (M^+); **HRMS** (EI): m/z Exact mass calcd for $C_8H_8{}^{10}BO_4N$ $[M]^+$: 192.0583, found: 192.0591.

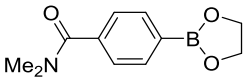

4-(1,3,2-dioxaborolan-2-yl)-*N*,*N*-dimethylbenzamide (2j), white solid (92% yield); **^{1}H NMR** (400 MHz, $CDCl_3$) δ 7.95-7.67 (m, 2H), 7.56-7.33 (m, 2H), 4.40 (s, 4H), 3.04 (br, 6H) ppm; **^{13}C NMR** (100 MHz, $CDCl_3$) δ 171.47, 139.16, 134.88, 126.35, 66.17, 39.50, 35.30 ppm; **EI-MS** m/z (%): 218 (M^+); **HRMS** (EI): m/z Exact mass calcd for $C_{11}H_{13}{}^{10}BO_3N$ $[M]^+$: 217.1025, found: 217.1032.

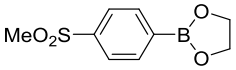

2-(4-(methylsulfonyl)phenyl)-1,3,2-dioxaborolane (2k), white solid (95% yield); **^{1}H NMR** (400 MHz, $CDCl_3$) δ 8.28-7.60 (m, 4H), 4.43 (s, 4H), 3.07 (s, 3H) ppm; **^{13}C NMR** (100 MHz, $CDCl_3$) δ 142.90, 135.74, 126.49, 66.43, 44.43 ppm; **EI-MS** m/z (%): 226 (M^+); **HRMS** (EI): m/z Exact mass calcd for $C_9H_{11}{}^{10}BO_4S$ $[M]^+$: 225.0507, found: 225.0513.

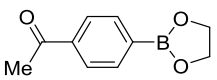

1-(4-(1,3,2-dioxaborolan-2-yl)phenyl)ethan-1-one (2m), white solid (88% yield); **^{1}H NMR** (400 MHz, $CDCl_3$) δ 7.92 (ddd, *J* = 13.4, 7.8, 3.6 Hz, 4H), 4.40 (s, 4H), 2.62 (s, 3H) ppm; **^{13}C NMR** (100 MHz, $CDCl_3$) δ 198.40, 139.17, 135.04, 127.42, 66.23, 26.77 ppm; **EI-MS** m/z (%): 190 (M^+); **HRMS** (EI): m/z Exact mass calcd for $C_{10}H_{11}{}^{10}BO_3$ $[M]^+$: 189.0838, found: 189.0836.

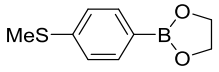

2-(4-(methylthio)phenyl)-1,3,2-dioxaborolane (2p), white solid (78% yield);**^{1}H NMR** (400 MHz, $CDCl_3$) δ 7.71 (d, *J* = 8.2 Hz, 2H), 7.24 (d, *J* = 8.3 Hz, 2H), 4.37 (s, 4H), 2.50 (s, 3H) ppm; **^{13}C NMR** (100 MHz, $CDCl_3$) δ 143.06, 135.27, 125.12, 66.15, 15.05 ppm; **EI-MS** m/z (%): 194 (M^+); **HRMS** (EI): m/z Exact mass calcd for $C_9H_{11}{}^{10}BO_2S$ $[M]^+$: 193.0609, found: 193.0611.

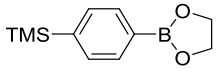

(4-(1,3,2-dioxaborolan-2-yl)phenyl)trimethylsilane (2r), colorless oil (97% yield); **^{1}H NMR** (400 MHz, $CDCl_3$) δ 7.78 (d, *J* = 7.9 Hz, 2H), 7.55 (d, *J* = 7.9 Hz, 2H), 4.37 (s, 3H), 0.27 (s, 9H) ppm; **^{13}C NMR** (100 MHz, $CDCl_3$) δ 144.67, 134.04, 132.87, 66.15, -1.12 ppm; **EI-MS** m/z (%): 220 (M^+); **HRMS** (EI): m/z Exact mass calcd for $C_{11}H_{17}{}^{10}BO_2Si$ $[M]^+$: 219.1127, found: 219.1136.

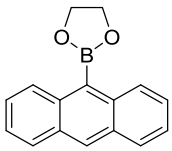

2-(anthracen-9-yl)-1,3,2-dioxaborolane (5d), pale yellow solid (85% yield); **^{1}H NMR** (400 MHz, $CDCl_3$) δ 8.50 (s, 1H), 8.44 (d, *J* = 8.6 Hz, 2H), 8.00 (d, *J* = 7.8 Hz, 2H), 7.52-7.42 (m, 4H), 4.63 (s, 4H) ppm; **^{13}C NMR** (100 MHz, $CDCl_3$) δ 136.18, 131.27, 130.04, 128.94, 128.73, 125.99, 125.12, 66.27 ppm; **EI-MS** m/z (%): 248 (M^+); **HRMS** (EI): m/z Exact mass calcd for $C_{16}H_{13}{}^{10}BO_2$ $[M]^+$: 247.1045, found: 247.1041.

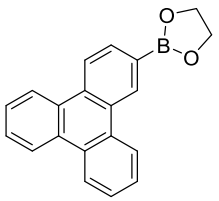

2-(triphenylen-2-yl)-1,3,2-dioxaborolane (5e), white solid (90% yield); **^{1}H NMR** (400 MHz, $CDCl_3$) δ 9.15 (d, *J* = 1.1 Hz, 1H), 8.81-8.73 (m, 1H), 8.71-8.60 (m, 4H), 8.05 (dd, *J* = 8.3, 1.3 Hz, 1H), 7.66 (qd, *J* = 4.1, 2.1 Hz, 4H), 4.47 (s, 4H) ppm; **^{13}C NMR** (100 MHz, $CDCl_3$) δ 132.79, 132.26, 130.79, 130.43, 129.91, 129.79, 129.64, 129.11, 127.80, 127.37, 127.32, 127.29, 123.78, 123.59, 123.39, 123.31, 122.71, 66.29 ppm; **EI-MS** m/z (%): 298 (M^+); **HRMS** (EI): m/z Exact mass calcd for $C_{20}H_{15}{}^{10}BO_2$ $[M]^+$: 297.1201, found: 297.1200.

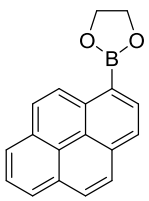

2-(pyren-1-yl)-1,3,2-dioxaborolane (5f), brown solid (80% yield); **^{1}H NMR** (400 MHz, $CDCl_3$) δ 9.05 (d, *J* = 9.2 Hz, 1H), 8.56 (d, *J* = 7.7 Hz, 1H), 8.27-8.10 (m, 5H), 8.07 (d, *J* = 8.9 Hz, 1H), 8.01 (t, *J* = 7.6 Hz, 1H), 4.56 (s, 4H) ppm; **^{13}C NMR** (100 MHz, $CDCl_3$) δ 136.63, 134.24, 133.81, 131.23, 130.85, 128.87, 128.07, 127.96, 127.59, 125.92, 125.62, 125.48, 124.70, 124.55, 124.30, 66.21 ppm; **EI-MS** m/z (%): 272 (M^+); **HRMS** (EI):

m/z Exact mass calcd for $C_{18}H_{13}{}^{10}BO_2$ $[M]^+$: 271.1045, found: 271.1046.

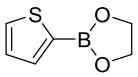

2-(thiophen-2-yl)-1,3,2-dioxaborolane (5i), white solid (80% yield); **^{1}H NMR** (400 MHz, $CDCl_3$) δ 7.67 (t, *J* = 4.4 Hz, 2H), 7.21 (dd, *J* = 4.5, 3.6 Hz, 1H), 4.38 (s, 4H) ppm; **^{13}C NMR** (100 MHz, $CDCl_3$) δ 137.64, 132.86, 128.49, 66.29 ppm; **EI-MS** m/z (%): 154 (M^+); **HRMS** (EI): m/z Exact mass calcd for $C_6H_7{}^{10}BO_2S$ $[M]^+$: 153.0296, found: 153.0289.

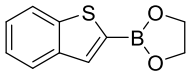

2-(benzo[b]thiophen-2-yl)-1,3,2-dioxaborolane (5k), white solid (90% yield); **^{1}H NMR** (400 MHz, $CDCl_3$) δ 7.94-7.84 (m, 3H), 7.43-7.30 (m, 2H), 4.42 (s, 4H) ppm; **^{13}C NMR** (100 MHz, $CDCl_3$) δ 143.88, 140.51, 134.96, 125.61, 124.62, 124.32, 122.67, 66.43 ppm; **EI-MS** m/z (%): 204 (M^+); **HRMS** (EI): m/z Exact mass calcd for $C_{10}H_9{}^{10}BO_2S_2$ $[M]^+$: 203.0453, found: 203.0455.

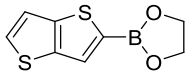

2-(thieno[3,2-b]thiophen-2-yl)-1,3,2-dioxaborolane (5l), gray solid (70% yield); **^{1}H NMR** (400 MHz, $CDCl_3$) δ 7.78 (s, 1H), 7.51 (d, *J* = 5.3 Hz, 1H), 7.29 (d, *J* = 5.3 Hz, 1H), 4.40 (s, 4H) ppm; **^{13}C NMR** (100 MHz, $CDCl_3$) δ 145.87, 140.96, 130.43, 129.39, 119.57, 66.34 ppm; **EI-MS** m/z (%): 210 (M^+); **HRMS** (EI): m/z Exact mass calcd for $C_8H_7{}^{10}BO_2S_2$ $[M]^+$: 209.0017, found: 209.0012.

3. General procedure for synthesis tri-aryl substituted olefins 3 and 6

3.1. Synthesis of compounds **3aa-3za**, **3ab-3ar**, **6aa-6af**, **6ai-6al**, **6ar**

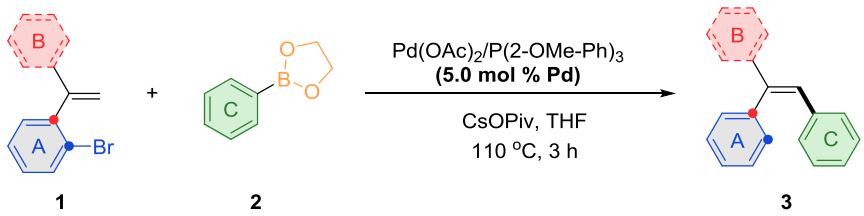

Scheme S3. Synthesis of compounds **3aa-3za**, **3ab-3ar**, **6aa-6af**, **6ai-6al**, **6ar**, related to **Scheme 2** and **Scheme 3**

To the suspension of *ortho*-vinyl arylbromides **1** (0.30 mmol), (hetero)arylboronates esters **2** (0.90 mmol), $Pd(OAc)_2$ (5 mol %), P(2-MeO-Ph)$_3$ (10 mol %) and CsOPiv (0.60 mmol) was added THF (3.0 mL) under argon atmosphere. The mixture was stirred at 110 ℃ for 3 h. After being cooled down to room temperature, the reaction was concentrated under reduced pressure. The residue was purified by flash chromatography on silica gel to afford pure product **3**.

3.2. Synthesis of compounds **6ag-6ah**, **6am-6aq**

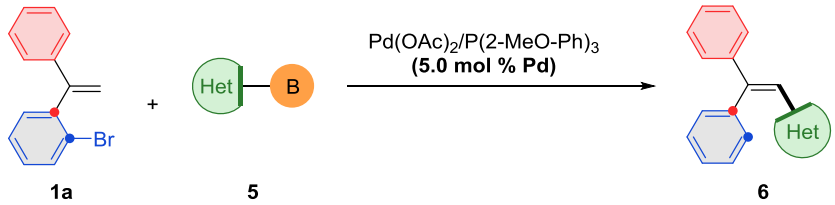

Scheme S4. Synthesis of compounds **6ag-6ah**, **6am-6aq**, related to **Scheme 3**

To the suspension of *ortho*-vinyl arylbromides **1** (0.30 mmol), (hetero)arylboronate esters **5** (0.90 mmol), $Pd(OAc)_2$ (5 mol %), P(2-MeO-Ph)$_3$ (10 mol %) and CsOPiv (0.60 mmol) was added THF (3.0 mL) under argon atmosphere. The mixture was stirred at 110 ℃ for 3 h. After being cooled down to room temperature, it was concentrated under reduced pressure and the residue was purified by flash chromatography on silica gel to afford pure product **6**.

3.3. Characterization data of Compounds **3aa-3za**, **3ab-3ar**, **6aa-6ar**, **4aa**

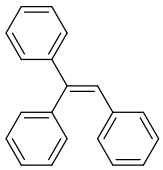

ethene-1,1,2-triyltribenzene (3aa), white solid (88% yield); **^{1}H NMR** (400 MHz, $CDCl_3$) δ 7.37-7.25 (m, 8H), 7.23-7.18 (m, 2H), 7.16-7.07 (m, 3H), 7.05-6.99 (m, 2H), 6.96 (s, 1H) ppm; **EI-MS** m/z (%): 256 (M^+). The data is consistent with the literature (Rao et al., 2018).

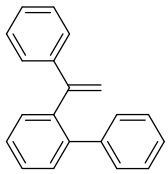

2-(1-phenylvinyl)-1,1'-biphenyl (4aa), Colorless oil; **^{1}H NMR** (400 MHz, $CDCl_3$) δ 7.42-7.29 (m, 4H), 7.27-7.18 (m, 2H), 7.18-7.01 (m, 8H), 5.56 (d, *J* = 1.3 Hz, 1H), 5.18 (d, *J* = 1.2 Hz, 1H) ppm; **EI-MS** m/z (%): 256 (M^+). The data is consistent with the literature (Wang et al., 2017).

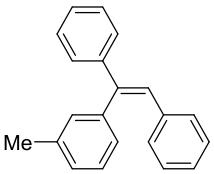

(*Z*)-(1-(m-tolyl)ethene-1,2-diyl)dibenzene (3ba), colorless oil (74% yield); **^{1}H NMR** (400 MHz, $CDCl_3$) δ 7.36-7.26 (m, 5H), 7.24-7.19 (m, 1H), 7.17-7.09 (m, 4H), 7.06-7.98 (m, 4H), 6.94 (s, 1H), 2.30 (s, 3H) ppm; **EI-MS** m/z (%): 270 (M^+). The data is consistent with the literature (Wen et al., 2017).

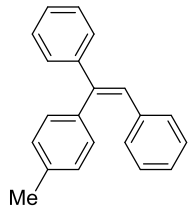

(*Z*)-(1-(p-tolyl)ethene-1,2-diyl)dibenzene (3ca), white solid (72% yield); **^{1}H NMR** (400 MHz, $CDCl_3$) δ 7.35-7.26 (m, 5H), 7.17-7.02 (m, 9H), 6.92 (s, 1H), 2.38 (s, 3H) ppm; **EI-MS** m/z (%): 270 (M^+). The data is consistent with the literature (Wen et al., 2017).

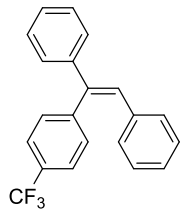

(*Z*)-(1-(4-(trifluoromethyl)phenyl)ethene-1,2-diyl)dibenzene (3da), white solid (78% yield); **^{1}H NMR** (400 MHz, $CDCl_3$) δ 7.57 (d, *J* = 8.1 Hz, 2H), 7.38-7.30 (m, 5H), 7.30-7.26 (m, 2H), 7.19-7.12 (m, 3H), 7.05-6.97 (m, 3H) ppm; **EI-MS** m/z (%): 324 (M^+). The data is consistent with the literature (Robbins and Hartwig, 2011).

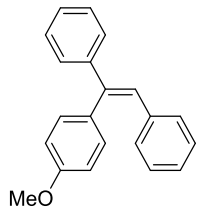

(*Z*)-(1-(4-methoxyphenyl)ethene-1,2-diyl)dibenzene (3ea), white solid (77% yield); **^{1}H NMR** (400 MHz, $CDCl_3$) δ 7.36-7.27 (m, 5H), 7.19-7.09 (m, 5H), 7.08-7.04 (m, 2H), 6.90 (s, 1H), 6.89-6.86 (m, 1H), 6.86-6.83 (m, 1H), 3.83 (s, 3H) ppm; **EI-MS** m/z (%): 286 (M^+). The data is consistent with the literature (Wen et al., 2017).

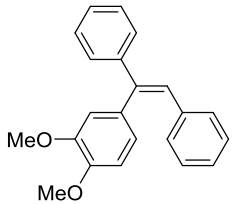

(*Z*)-(1-(3,4-dimethoxyphenyl)ethene-1,2-diyl)dibenzene (**3fa**), white solid (70% yield); ^{1}H NMR (400 MHz, $CDCl_3$) δ 7.39-7.26 (m, 5H), 7.21-7.09 (m, 3H), 7.07 (dd, *J* = 5.2, 3.1 Hz, 2H), 6.92 (s, 1H), 6.84 (d, *J* = 8.2 Hz, 1H), 6.75 (dd, *J* = 8.2, 1.9 Hz, 1H), 6.71 (d, *J* = 2.0 Hz, 1H), 3.91 (s, 3H), 3.68 (s, 3H) ppm; **^{13}C NMR** (100 MHz, $CDCl_3$) δ 149.05, 148.49, 143.67, 142.46, 137.72, 132.85, 129.63, 128.32, 128.13, 128.03, 127.81, 127.67, 126.82, 123.02, 113.68, 111.29, 55.94 ppm; **EI-MS** m/z (%): 316 (M^+); **HRMS** (EI): m/z Exact mass calcd for $C_{22}H_{20}O_2$ $[M]^+$: 316.1463, found: 316.1467.

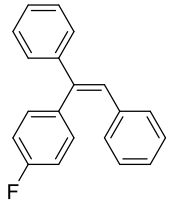

(*Z*)-(1-(4-fluorophenyl)ethene-1,2-diyl)dibenzene (3ga), white solid (85% yield); **^{1}H NMR** (400 MHz, $CDCl_3$) δ 7.33-7.28 (m, 5H), 7.19-7.11 (m, 5H), 7.05-6.99 (m, 4H), 6.96 (s, 1H) ppm; **EI-MS** m/z (%): 274 (M^+). The data is consistent with the literature (Wen et al., 2017).

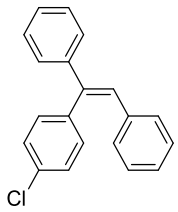

(*Z*)-(1-(4-chlorophenyl)ethene-1,2-diyl)dibenzene (3ha), white solid (85% yield); **^{1}H NMR** (400 MHz, $CDCl_3$) δ 7.35-7.26 (m, 7H), 7.20-7.10 (m, 5H), 7.07-7.01 (m, 2H), 6.96 (s, 1H) ppm; **EI-MS** m/z (%): 290 (M^+). The data is consistent with the literature (Robbins and Hartwig, 2011).

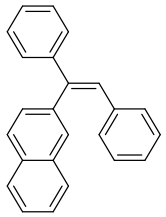

(*Z*)-2-(1,2-diphenylvinyl)naphthalene (3ia), white solid (40% yield); **^{1}H NMR** (400 MHz, $CDCl_3$) δ 7.85 (d, *J* = 7.7 Hz, 1H), 7.79 (d, *J* = 8.4 Hz, 1H), 7.75-7.66 (m, 2H), 7.52-7.42 (m, 2H), 7.38-7.27 (m, 6H), 7.12-7.02 (m, 6H) ppm; **^{13}C NMR** (100 MHz, $CDCl_3$) δ 143.78, 142.56, 138.10, 137.43, 133.77, 132.86, 129.72, 129.47, 128.83, 128.75, 128.37, 128.29, 128.24, 128.17, 127.95, 127.86, 127.71, 126.97, 126.16, 126.12 ppm; **EI-MS** m/z (%): 306 (M^+); **HRMS** (EI): m/z Exact mass calcd for $C_{24}H_{18}$ $[M]^+$: 306.1409, found: 306.1417.

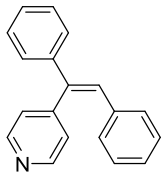

(*Z*)-4-(1,2-diphenylvinyl)pyridine (3ja), white solid (91% yield); **^{1}H NMR** (400 MHz, $CDCl_3$) δ 8.57 (d, *J* = 5.9 Hz, 2H), 7.33 (t, *J* = 5.7 Hz, 3H), 7.30-7.23 (m, 2H), 7.20-7.12 (m, 5H), 7.06-7.02 (m, 3H) ppm; **^{13}C NMR** (100 MHz, $CDCl_3$) δ 150.35, 148.84, 142.06, 140.15, 136.55, 130.09, 129.65, 128.61, 128.38, 128.16, 127.74, 127.57, 125.65 ppm; **EI-MS** m/z (%): 257 (M^+); **HRMS** (ESI): m/z Exact mass calcd for $C_{19}H_{16}N$ $[M+H]^+$: 258.1277, found: 258.1277.

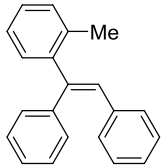

(*E*)-(1-(o-tolyl)ethene-1,2-diyl)dibenzene (3ka), white solid (97% yield); **^{1}H NMR** (400 MHz, $CDCl_3$) δ 7.28 (dd, *J* = 6.8, 2.0 Hz, 1H), 7.25-7.09 (m, 13H), 6.61 (s, 1H), 2.11 (s, 3H) ppm; **EI-MS** m/z (%): 270 (M^+). The data is consistent with the literature (Rao et al., 2018).

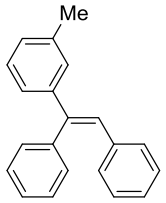

(*E*)-(1-(m-tolyl)ethene-1,2-diyl)dibenzene (3la), colorless oil (69% yield); **^{1}H NMR** (400 MHz, $CDCl_3$) δ 7.34 (dd, *J* = 5.0, 1.7 Hz, 3H), 7.25-7.19 (m, 3H), 7.18-7.09 (m, 6H), 7.06-7.00 (m, 2H), 6.96 (s, 1H), 2.35 (s, 3H) ppm; **EI-MS** m/z (%): 270 (M^+). The data is consistent with the literature (Kumar et al., 2016).

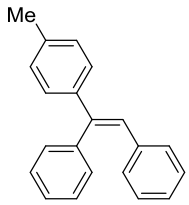

(*E*)-(1-(p-tolyl)ethene-1,2-diyl)dibenzene (3ma), white solid (60% yield); **^{1}H NMR** (400 MHz, $CDCl_3$) δ 7.36-7.28 (m, 3H), 7.24-7.16 (m, 4H), 7.12-7.08 (m, 5H), 7.04-6.98 (m, 2H), 6.93 (s, 1H), 2.34 (s, 3H) ppm; **EI-MS** m/z (%): 270 (M^+). The data is consistent with the literature (Rao et al., 2018).

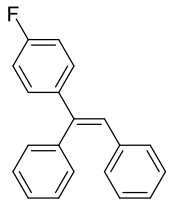

(*E*)-(1-(4-fluorophenyl)ethene-1,2-diyl)dibenzene (3na), white solid (68% yield); **^{1}H NMR** (400 MHz, $CDCl_3$) δ 7.38-7.22 (m, 5H), 7.21-7.08 (m, 5H), 7.07-6.94 (m, 4H), 6.90 (s, 1H) ppm; **EI-MS** m/z (%): 274 (M^+). The data is consistent with the literature (Rao et al., 2018).

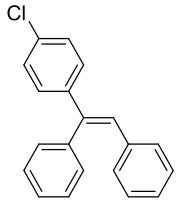

(*E*)-(1-(4-chlorophenyl)ethene-1,2-diyl)dibenzene (3oa), white solid (84% yield); **^{1}H NMR** (400 MHz, $CDCl_3$) δ 7.35-7.30 (m, 3H), 7.29-7.21 (m, 4H), 7.20-7.16 (m, 2H), 7.15-7.08 (m, 3H), 7.04-6.99 (m, 2H), 6.94 (s, 1H) ppm; **EI-MS** m/z (%): 290 (M^+). The data is consistent with the literature (Rao et al., 2018).

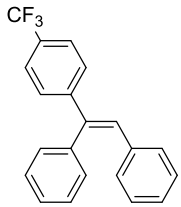

(*E*)-(1-(4-(trifluoromethyl)phenyl)ethene-1,2-diyl)dibenzene (3pa), white solid (89% yield); **^{1}H NMR** (400 MHz, $CDCl_3$) δ 7.56 (d, *J* = 8.3 Hz, 2H), 7.42 (d, *J* = 8.2 Hz, 2H), 7.38-7.32 (m, 3H), 7.21-7.18 (m, 2H), 7.16-7.11 (m, 3H), 7.06-7.02 (m, 2H), 7.01 (s, 1H) ppm; **EI-MS** m/z (%): 324 (M^+). The data is consistent with the literature (Rao et al., 2018).

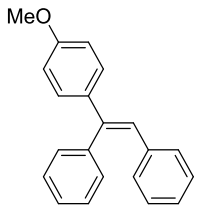

(*E*)-(1-(4-methoxyphenyl)ethene-1,2-diyl)dibenzene (3qa), colorless oil (70% yield); **^{1}H NMR** (400 MHz, $CDCl_3$) δ 7.36-7.29 (m, 3H), 7.29-7.23 (m, 2H), 7.23-7.17 (m, 2H), 7.15-7.06 (m, 3H), 7.04-6.97 (m, 2H), 6.89 (s, 1H), 6.87-6.82 (m, 2H), 3.81 (s, 3H) ppm; **EI-MS** m/z (%): 286 (M^+). The data is consistent with the literature (Wu et al., 2001).

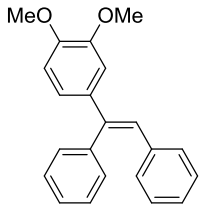

(*E*)-(1-(3,4-dimethoxyphenyl)ethene-1,2-diyl)dibenzene (**3ra**), white solid (60% yield); **^{1}H NMR** (400 MHz, $CDCl_3$) δ 7.35-7.28 (m, 3H), 7.23-7.19 (m, 2H), 7.16-7.07 (m, 3H), 7.05-6.97 (m, 2H), 6.90 (s, 2H), 6.86-6.77 (m, 2H), 3.89 (s, 3H), 3.83 (s, 3H) ppm; **^{13}C NMR** (100 MHz, $CDCl_3$) δ 148.92, 148.75, 142.49, 140.52, 137.64, 136.57, 130.57, 129.59, 128.71, 128.09, 127.57, 126.92, 126.67, 120.68, 110.85, 110.83, 56.08, 56.00 ppm; **EI-MS** m/z (%): 316 (M^+); **HRMS** (EI): m/z Exact mass calcd for $C_{22}H_{20}O_2$ $[M]^+$: 316.1463, found: 316.1474.

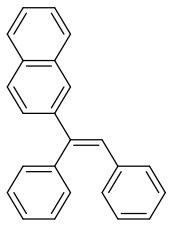

(*E*)-2-(1,2-diphenylvinyl)naphthalene (3sa), white solid (71% yield); **^{1}H NMR** (400 MHz, $CDCl_3$) δ 7.86-7.72 (m, 3H), 7.70 (s, 1H), 7.52 (dd, *J* = 8.6, 1.8 Hz, 1H), 7.48-7.41 (m, 2H), 7.39-7.33 (m, 3H), 7.30-7.22 (m, 3H), 7.18-7.09 (m, 4H), 7.09-7.02 (m, 2H) ppm; **^{13}C NMR** (100 MHz, $CDCl_3$) δ 142.69, 140.92, 140.44, 137.53, 133.43, 132.95, 130.63, 129.73, 128.84, 128.39, 128.13, 127.85, 127.67, 127.66, 126.98, 126.94, 126.30, 126.11, 125.74 ppm; **EI-MS** m/z (%): 306 (M^+); **HRMS** (EI): m/z Exact mass calcd for $C_{24}H_{18}$ $[M]^+$: 306.1409, found: 306.1402.

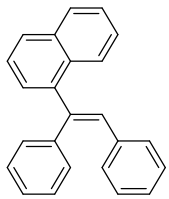

(*E*)-1-(1,2-diphenylvinyl)naphthalene (3ta), white solid (94% yield); **^{1}H NMR** (400 MHz, $CDCl_3$) δ 8.10 (d, *J* = 8.4 Hz, 1H), 7.83 (dd, *J* = 16.2, 7.9 Hz, 2H), 7.49-7.40 (m, 3H), 7.41-7.33 (m, 1H), 7.29-7.13 (m, 10H), 6.80 (s, 1H) ppm; **EI-MS** m/z (%): 306 (M^+). The data is consistent with the literature (Rao et al., 2018).

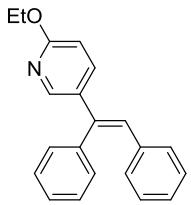

(*E*)-5-(1,2-diphenylvinyl)-2-ethoxypyridine (3ua), colorless oil (92% yield); **^{1}H NMR** (400 MHz, $CDCl_3$) δ 8.05 (d, *J* = 2.5 Hz, 1H), 7.41 (dd, *J* = 8.7, 2.5 Hz, 1H), 7.29-7.20 (m, 3H), 7.15-7.09 (m, 2H), 7.09-6.98 (m, 3H), 6.98-6.89 (m, 2H), 6.80 (s, 1H), 6.58 (d, *J* = 8.7 Hz, 1H), 4.29 (q, *J* = 7.1 Hz, 2H), 1.32 (t, *J* = 7.1 Hz, 3H) ppm; **^{13}C NMR** (100 MHz, $CDCl_3$) δ 163.43, 145.80, 139.79, 139.45, 137.86, 137.24, 132.48, 130.33, 129.61, 128.90, 128.13, 127.76, 127.28, 126.95, 110.50, 62.00, 14.83 ppm; **EI-MS** m/z (%): 301 (M^+); **HRMS** (EI): m/z Exact

mass calcd for $C_{21}H_{19}NO$ $[M]^+$: 301.1467, found: 301.1460.

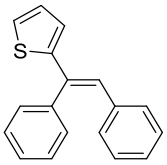

(*E*)-2-(1,2-diphenylvinyl)thiophene (3va), colorless oil (67% yield); **^{1}H NMR** (400 MHz, $CDCl_3$) δ 7.40-7.35 (m, 3H), 7.33-7.28 (m, 2H), 7.21 (d, *J* = 5.1 Hz, 1H), 7.09 (t, *J* = 5.8 Hz, 3H), 7.05 (s, 1H), 6.99-6.90 (m, 3H), 6.72 (d, *J* = 3.5 Hz, 1H) ppm; **^{13}C NMR** (100 MHz, $CDCl_3$) δ 148.05, 139.54, 136.74, 136.37, 130.02, 129.56, 128.92, 128.12, 127.97, 127.60, 126.95, 126.46, 126.23, 124.86 ppm; **EI-MS** m/z (%): 262 (M^+); **HRMS** (EI): m/z Exact mass calcd for $C_{18}H_{14}S$ $[M]^+$: 262.0816, found: 262.0821.

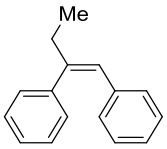

(*Z*)-but-1-ene-1,2-diyldibenzene (3wa), colorless oil (78% yield); **^{1}H NMR** (400 MHz, $CDCl_3$) δ 7.33-7.21 (m, 3H), 7.18-7.12 (m, 2H), 7.11-7.01 (m, 3H), 6.94-6.88 (m, 2H), 6.42 (s, 1H), 2.51 (qd, *J* = 7.4, 1.1 Hz, 2H), 1.07 (t, *J* = 7.4 Hz, 3H); **^{13}C NMR** (100 MHz, $CDCl_3$) δ 145.09, 141.62, 137.67, 129.11, 128.67, 128.60, 127.92, 126.93, 126.15, 125.18, 33.68, 13.04. **EI-MS (**m/z, %**)**: 208 (M^+); **HRMS** (EI): m/z Exact mass calcd for $C_{16}H_{16}$ $[M]^+$: 208.1252, found: 208.1253.

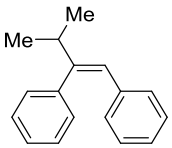

(*Z*)-(3-methylbut-1-ene-1,2-diyl)dibenzene (3xa), colorless oil (88% yield); **^{1}H NMR** (400 MHz, $CDCl_3$) δ 7.39-7.21 (m, 4H), 7.16-7.08 (m, 2H), 7.08-6.98 (m, 3H), 6.85 (d, *J* = 6.5 Hz, 2H), 6.40 (s, 1H), 3.12-2.44 (m, 1H), 1.11 (d, *J* = 6.8 Hz, 6H); **^{13}C NMR** (100 MHz, $CDCl_3$) δ 149.56, 141.36, 137.74, 129.12, 128.49, 127.89, 126.82, 126.11, 124.30, 37.52, 21.92; **EI-MS** m/z (%): 222 (M^+); **HRMS** (EI): m/z Exact mass calcd for $C_{17}H_{18}$ $[M]^+$: 222.1409, found: 222.1413.

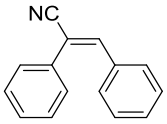

(*E*)-2,3-diphenylacrylonitrile (3ya), colorless oil (88% yield); **^{1}H NMR** (400 MHz, $CDCl_3$) δ 7.41-7.32 (m, 6H), 7.31-7.19 (m, 3H), 7.16 (d, *J* = 7.3 Hz, 2H); **EI-MS** m/z (%): 205 (M^+). The data is consistent with the literature (Wang et al., 2019).

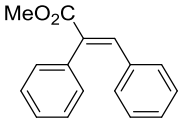

methyl (*E*)-2,3-diphenylacrylate (3za), colorless oil (81% yield); **^{1}H NMR** (400 MHz, $CDCl_3$) δ 7.85 (s, 1H), 7.41-7.34 (m, 3H), 7.24-7.10 (m, 5H), 7.03 (d, *J* = 7.2 Hz, 2H), 3.79 (s, 3H); **EI-MS** m/z (%): 238 (M^+). The

data is consistent with the literature (Tsoi et al., 2010).

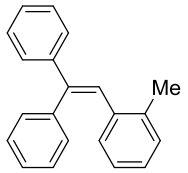

(2-(o-tolyl)ethene-1,1-diyl)dibenzene (3ab), white solid (60% yield); **^{1}H NMR** (400 MHz, $CDCl_3$) δ 7.38-7.28 (m, 5H), 7.23-7.18 (m, 3H), 7.15-7.07 (m, 3H), 7.06-7.00 (m, 1H), 6.97 (s, 1H), 6.90-6.79 (m, 2H), 2.33 (s, 3H) ppm; **EI-MS** m/z (%): 270 (M^+). The data is consistent with the literature (Shimasaki et al., 2009).

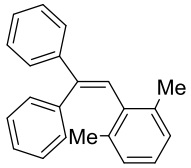

(2-(2,6-dimethylphenyl)ethene-1,1-diyl)dibenzene (3ac), white solid (44% yield); **^{1}H NMR** (400 MHz, $CDCl_3$) δ 7.43-7.31 (m, 5H), 7.18-7.08 (m, 3H), 7.07-6.99 (m, 1H), 6.99-6.90 (m, 4H), 6.83 (s, 1H), 2.12 (s, 6H) ppm; **^{13}C NMR** (100 MHz, $CDCl_3$) δ 144.47, 143.57, 140.36, 137.01, 136.28, 129.90, 128.56, 128.28, 127.81, 127.65, 127.55, 127.35, 127.31, 126.84, 20.70 ppm; **EI-MS** m/z (%): 284 (M^+); **HRMS** (EI): m/z Exact mass calcd for $C_{22}H_{20}$ $[M]^+$: 284.1565, found: 284.1572.

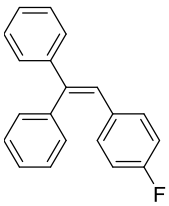

(2-(4-fluorophenyl)ethene-1,1-diyl)dibenzene (3ad), white solid (81% yield); **^{1}H NMR** (400 MHz, $CDCl_3$) δ 7.38-7.26 (m, 8H), 7.21-7.16 (m, 2H), 7.00-6.94 (m, 2H), 6.92 (s, 1H), 6.85-6.78 (m, 2H) ppm; **EI-MS** m/z (%): 274 (M^+). The data is consistent with the literature (Berthiol et al., 2003).

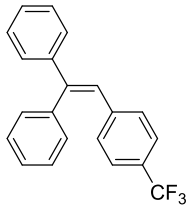

(2-(4-(trifluoromethyl)phenyl)ethene-1,1-diyl)dibenzene (3ae), white solid (76% yield); **^{1}H NMR** (400 MHz, $CDCl_3$) δ 7.38 (s, 1H), 7.37-7.28 (m, 9H), 7.21-7.15 (m, 2H), 7.10 (d, *J* = 8.2 Hz, 2H), 6.97 (s, 1H) ppm; **EI-MS** m/z (%): 324 (M^+). The data is consistent with the literature (Berthiol et al., 2003).

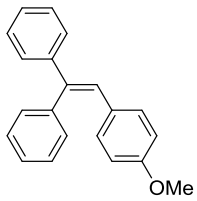

(2-(4-methoxyphenyl)ethene-1,1-diyl)dibenzene (3af), white solid (72% yield); **^{1}H NMR** (400 MHz, $CDCl_3$) δ 7.36-7.27 (m, 7H), 7.25-7.20 (m, 3H), 6.97-6.93 (m, 2H), 6.91 (s, 1H), 6.68-6.64 (m, 2H), 3.74 (s, 3H) ppm; **EI-MS** m/z (%): 286 (M^+). The data is consistent with the literature (Shimasaki et al., 2009).

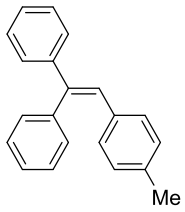

(2-(p-tolyl)ethene-1,1-diyl)dibenzene (3ag), white solid (79% yield); **^{1}H NMR** (400 MHz, $CDCl_3$) δ 7.37-7.26 (m, 8H), 7.23-7.18 (m, 2H), 6.97-6.88 (m, 5H), 2.26 (s, 3H) ppm; **EI-MS** m/z (%): 270 (M^+). The data is consistent with the literature (Shimasaki et al., 2009).

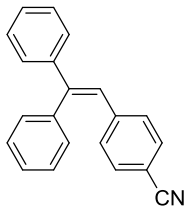

4-(2,2-diphenylvinyl)benzonitrile (3ah), white solid (83% yield); **^{1}H NMR** (400 MHz, $CDCl_3$) δ 7.39 (d, *J* = 8.3 Hz, 2H), 7.37-7.30 (m, 8H), 7.17 (s, 2H), 7.08 (d, *J* = 8.4 Hz, 2H), 6.94 (s, 1H) ppm; **EI-MS** m/z (%): 281 (M^+). The data is consistent with the literature (Rao et al., 2018).

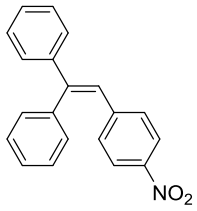

(2-(4-nitrophenyl)ethene-1,1-diyl)dibenzene (3ai), yellow solid (74% yield); **^{1}H NMR** (400 MHz, $CDCl_3$) δ 7.98 (d, *J* = 8.8 Hz, 2H), 7.40-7.30 (m, 8H), 7.20-7.15 (m, 2H), 7.13 (d, *J* = 8.8 Hz, 2H), 7.00 (s, 1H) ppm; **EI-MS** m/z (%): 301 (M^+). The data is consistent with the literature (Rao et al., 2018).

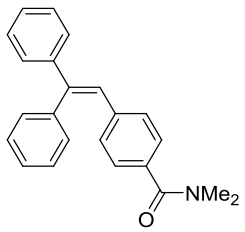

4-(2,2-diphenylvinyl)-N,N-dimethylbenzamide (3aj), colorless oil (74% yield); **^{1}H NMR** (400 MHz, $CDCl_3$) δ 7.36-7.28 (m, 8H), 7.22-7.16 (m, 4H), 7.04 (d, *J* = 8.1 Hz, 2H), 6.95 (s, 1H), 3.01 (s, 6H) ppm; **^{13}C NMR** (100 MHz, $CDCl_3$) δ 171.57, 144.01, 143.26, 140.11, 138.93, 134.29, 130.45, 129.49, 128.86, 128.38, 127.90, 127.80, 127.77, 127.36, 127.09 ppm; **EI-MS** m/z (%): 327 (M^+); **HRMS** (EI): m/z Exact mass calcd for $C_{23}H_{21}NO$ [M]+: 327.1623, found: 327.1621.

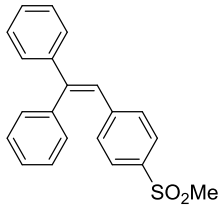

(2-(4-(methylsulfonyl)phenyl)ethene-1,1-diyl)dibenzene (3ak), white solid (99% yield); **^{1}H NMR** (400 MHz, $CDCl_3$) δ 7.68 (d, *J* = 8.5 Hz, 2H), 7.40-7.31 (m, 8H), 7.21-7.13 (m, 4H), 6.98 (s, 1H), 3.01 (s, 3H) ppm; **^{13}C NMR** (100 MHz, $CDCl_3$) δ 146.43, 143.15, 142.54, 139.41, 137.94, 130.20, 130.19, 129.00, 128.43, 128.39, 128.18, 127.85, 127.08, 125.99, 44.51 ppm; **EI-MS** m/z (%): 334 (M^+); **HRMS** (EI): m/z Exact mass calcd for $C_{21}H_{18}O_2S$ $[M]^+$: 334.1028, found: 334.1033.

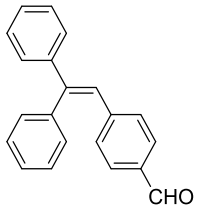

4-(2,2-diphenylvinyl)benzaldehyde (3al), white solid (77% yield); **^{1}H NMR** (400 MHz, $CDCl_3$) δ 9.89 (s, 1H), 7.64 (d, *J* = 8.2 Hz, 2H), 7.40-7.29 (m, 8H), 7.22-7.10 (m, 4H), 7.00 (s, 1H) ppm; **^{13}C NMR** (100 MHz, $CDCl_3$) δ 191.83, 146.06, 143.95, 142.87, 139.79, 134.48, 130.37, 130.10, 129.57, 128.95, 128.46, 128.32, 128.11, 127.94, 126.96 ppm; **EI-MS** m/z (%): 284 (M^+); **HRMS** (EI): m/z Exact mass calcd for $C_{21}H_{16}O$ $[M]^+$: 284.1201, found: 284.1207.

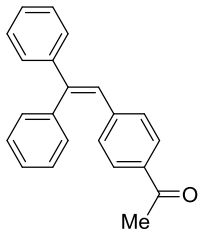

1-(4-(2,2-diphenylvinyl)phenyl)ethan-1-one (3am), white solid (84% yield); **^{1}H NMR** (400 MHz, $CDCl_3$) δ 7.72 (d, *J* = 8.4 Hz, 2H), 7.38-7.29 (m, 8H), 7.22-7.16 (m, 2H), 7.12-7.06 (m, 2H), 6.99 (s, 1H), 2.53 (s, 3H) ppm; **^{13}C NMR** (100 MHz, $CDCl_3$) δ 197.73, 145.36, 142.98, 142.47, 139.94, 135.11, 130.38, 129.70, 128.92, 128.43, 128.21, 128.18, 127.98, 127.88, 127.08, 26.69 ppm; **EI-MS** m/z (%): 298 (M^+); **HRMS** (EI): m/z Exact mass calcd for $C_{22}H_{18}O$ $[M]^+$: 298.1358, found: 298.1364.

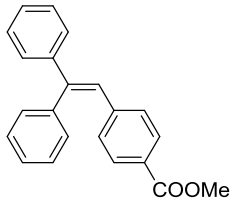

methyl 4-(2,2-diphenylvinyl)benzoate (3an), white solid (65% yield); **^{1}H NMR** (400 MHz, $CDCl_3$) δ 7.79 (d, *J* = 8.4 Hz, 2H), 7.36-7.28 (m, 8H), 7.20-7.16 (m, 2H), 7.07 (d, *J* = 8.3 Hz, 2H), 6.98 (s, 1H), 3.86 (s, 3H) ppm; **^{13}C NMR** (100 MHz, $CDCl_3$) δ 167.02, 145.15, 143.04, 142.27, 139.93, 130.40, 129.52, 129.37, 128.87, 128.42, 128.11, 128.07, 127.93, 127.88, 127.19, 52.14 ppm; **EI-MS** m/z (%): 314 (M^+); **HRMS** (EI): m/z Exact mass calcd for $C_{22}H_{18}O_2$ $[M]^+$: 314.1307, found: 314.1310.

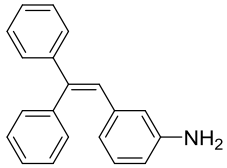

3-(2,2-diphenylvinyl)aniline (3ao), yellow oil (63% yield); **^{1}H NMR** (400 MHz, $CDCl_3$) δ 7.37-7.27 (m, 8H), 7.23-7.19 (m, 2H), 6.93 (t, *J* = 7.8 Hz, 1H), 6.88 (s, 1H), 6.45 (d, *J* = 7.8 Hz, 2H), 6.33 (s, 1H), 3.43 (br, 2H) ppm; **EI-MS** m/z (%): 271 (M^+). The data is consistent with the literature.

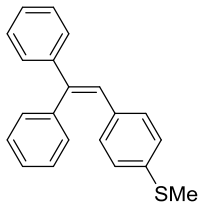

(4-(2,2-diphenylvinyl)phenyl)(methyl)sulfane (3ap), white solid (81% yield); **^{1}H NMR** (400 MHz, $CDCl_3$) δ 7.37-7.26 (m, 8H), 7.22-7.18 (m, 2H), 7.02-6.98 (m, 2H), 6.96-6.88 (m, 3H), 2.41 (s, 3H) ppm; **EI-MS** m/z (%): 302 (M^+). The data is consistent with the literature (Dai et al., 2014).

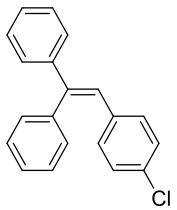

(2-(4-chlorophenyl)ethene-1,1-diyl)dibenzene (3aq), white solid (76% yield); **^{1}H NMR** (400 MHz, $CDCl_3$) δ 7.38-7.27 (m, 8H), 7.18 (dd, *J* = 6.6, 3.0 Hz, 2H), 7.10-7.07 (m, 2H), 6.95 (s, 1H), 6.92 (s, 1H), 6.90 (s, 1H) ppm; **EI-MS** m/z (%): 290 (M^+). The data is consistent with the literature (Wu et al., 2011).

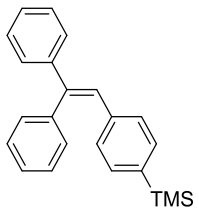

(4-(2,2-diphenylvinyl)phenyl)trimethylsilane (3ar), colorless oil (76% yield); **^{1}H NMR** (400 MHz, $CDCl_3$) δ 7.38-7.25 (m, 10H), 7.25-7.19 (m, 2H), 7.00 (d, *J* = 7.9 Hz, 2H), 6.95 (s, 1H), 0.21 (s, 9H) ppm; **^{13}C NMR** (100 MHz, $CDCl_3$) δ 143.56, 142.81, 140.59, 139.19, 137.77, 133.16, 130.42, 128.90, 128.85, 128.33, 128.29, 127.70, 127.64, 127.57, -1.01 ppm; **EI-MS** m/z (%): 328 (M^+); **HRMS** (EI): m/z Exact mass calcd for $C_{23}H_{24}Si$ $[M]^+$: 328.1647, found: 328.1654.

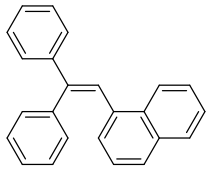

1-(2,2-diphenylvinyl)naphthalene (6aa), white solid (93% yield); **^{1}H NMR** (400 MHz, $CDCl_3$) δ 8.20-8.11 (m, 1H), 7.85-7.77 (m, 1H), 7.64 (d, *J* = 8.1 Hz, 1H), 7.51-7.44 (m, 3H), 7.44-7.40 (m, 2H), 7.39-7.30 (m, 3H), 7.19-7.11 (m, 4H), 7.10-7.06 (m, 2H), 7.06-7.02 (m, 1H) ppm; **EI-MS** m/z (%): 306 (M^+). The data is consistent with the literature (Shimasaki et al., 2009).

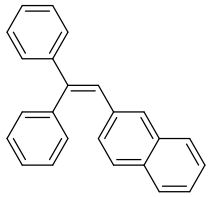

2-(2,2-diphenylvinyl)naphthalene (6ab), white solid (53% yield); **^{1}H NMR** (400 MHz, $CDCl_3$) δ 7.70 (dd, *J* = 6.0, 3.4 Hz, 1H), 7.63 (dd, *J* = 6.0, 3.3 Hz, 1H), 7.57 (s, 1H), 7.53 (d, *J* = 8.6 Hz, 1H), 7.44-7.29 (m, 9H), 7.27-7.21 (m, 3H), 7.13 (s, 1H), 7.05 (dd, *J* = 8.6, 1.4 Hz, 1H) ppm; **EI-MS** m/z (%): 306 (M^+). The data is consistent with the literature (Xiao et al., 2009).

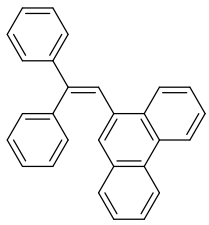

9-(2,2-diphenylvinyl)phenanthrene (**6ac**), white solid (79% yield); **^{1}H NMR** (400 MHz, $CDCl_3$) δ 8.71 (d, *J* = 8.0 Hz, 1H), 8.62 (d, *J* = 8.3 Hz, 1H), 8.23 (d, *J* = 7.5 Hz, 1H), 7.71-7.64 (m, 1H), 7.64-7.59 (m, 1H), 7.58-7.53 (m, 1H), 7.53-7.49 (m, 1H), 7.49-7.43 (m, 4H), 7.41-7.34 (m, 3H), 7.32 (s, 1H), 7.18-7.08 (m, 5H) ppm; **^{13}C NMR** (100 MHz, $CDCl_3$) δ 145.22, 143.46, 140.22, 133.91, 131.87, 131.73, 130.59, 130.42, 129.81, 128.75, 128.62, 128.44, 128.32, 128.24, 127.88, 127.28, 126.77, 126.62, 126.60, 126.50, 125.54, 123.12, 122.48 ppm; **EI-MS** m/z (%): 356 (M^+); **HRMS** (EI): m/z Exact mass calcd for $C_{28}H_{20}$ $[M]^+$: 356.1565, found: 356.1561.

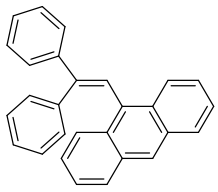

9-(2,2-diphenylvinyl)anthracene (**6ad**), canary solid (67% yield); **^{1}H NMR** (400 MHz, Tol) δ 8.27-8.17 (m, 2H), 8.05 (s, 1H), 7.75-7.66 (m, 2H), 7.52-7.43 (m, 3H), 7.26-7.13 (m, 7H), 6.97-6.89 (m, 2H), 6.63-6.52 (m, 3H) ppm; **^{13}C NMR** (100 MHz, Tol) δ 147.72, 143.44, 140.33, 133.02, 131.91, 130.06, 129.97, 129.03, 128.81, 128.64, 128.10, 127.85, 127.35, 126.98, 126.67, 125.65, 125.29, 125.26 ppm; **EI-MS** m/z (%):356 (M^+); **HRMS** (EI): m/z Exact mass calcd for $C_{28}H_{20}$ $[M]^+$: 356.1565, found: 356.1567.

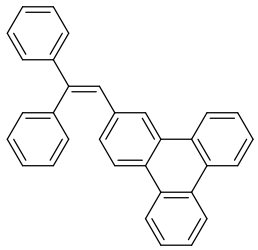

2-(2,2-diphenylvinyl)triphenylene (6ae), white solid (85% yield); **^{1}H NMR** (400 MHz, $CDCl_3$) δ 8.63-8.56 (m, 2H), 8.55-8.50 (m, 1H), 8.39 (d, *J* = 8.6 Hz, 1H), 8.31 (s, 1H), 8.05 (d, *J* = 8.1 Hz, 1H), 7.65-7.56 (m, 3H), 7.55-7.49 (m, 1H), 7.46-7.39 (m, 5H),7.38-7.28 (m, 6H), 7.23 (s, 1H) ppm; **^{13}C NMR** (100 MHz, $CDCl_3$) δ 143.33, 140.79, 136.10, 130.51, 129.95, 129.90, 129.85, 129.72, 129.44, 129.15, 128.94, 128.53, 128.44, 128.10, 127.80, 127.73, 127.31, 127.23, 127.17, 124.52, 123.43, 123.39, 123.35, 123.30, 123.03 ppm; **EI-MS** m/z (%): 406 (M^+); **HRMS** (EI): m/z Exact mass calcd for $C_{32}H_{22}$ $[M]^+$: 406.1722, found: 406.1724.

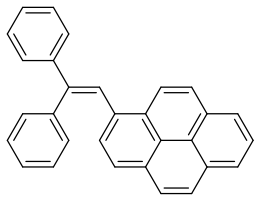

1-(2,2-diphenylvinyl)pyrene (6af), golden yellow solid (72% yield); **^{1}H NMR** (400 MHz, Tol) δ 8.22 (d, *J* = 9.2 Hz, 1H), 7.94-7.82 (m, 3H), 7.76-7.68 (m, 3H), 7.64 (d, *J* = 8.5 Hz, 2H), 7.57 (d, *J* = 8.0 Hz, 1H), 7.45 (dd, *J* = 7.9, 1.6 Hz, 2H), 7.22-7.16 (m, 3H), 7.15-7.11 (m, 2H), 6.95-6.85 (m, 3H) ppm; **^{13}C NMR** (100 MHz, Tol) δ 145.52, 144.11, 140.77, 133.32, 131.91, 131.61, 131.50, 130.81, 130.26, 128.77, 128.52, 128.06, 127.86, 127.59, 127.46, 127.16, 126.04, 125.51, 125.47, 124.72, 124.49 ppm; **EI-MS** m/z (%):380 (M^+); **HRMS** (EI): m/z Exact mass calcd for $C_{30}H_{20}$ $[M]^+$: 380.1565, found: 380.1562.

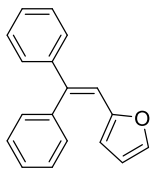

2-(2,2-diphenylvinyl)furan (6ag), red oil (66% yield); **^{1}H NMR** (400 MHz, $CDCl_3$) δ 7.46-7.38 (m, 3H), 7.34-7.28 (m, 4H), 7.28-7.23 (m, 3H), 7.16-7.13 (m, 2H), 6.88 (s, 1H), 5.61 (d, *J* = 1.1 Hz, 1H) ppm; **^{13}C NMR** (100 MHz, $CDCl_3$) δ 142.61, 142.56, 142.31, 141.01, 140.76, 130.04, 128.97, 128.36, 127.71, 127.34, 126.98, 123.56, 117.69, 110.18 ppm; **EI-MS** m/z (%): 246 (M^+); **HRMS** (EI): m/z Exact mass calcd for $C_{18}H_{14}O$ $[M]^+$: 246.1045, found: 246.1047.

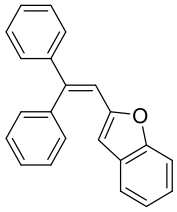

2-(2,2-diphenylvinyl)benzofuran (6ah), red oil (63% yield); **^{1}H NMR** (400 MHz, $CDCl_3$) δ 7.51-7.45 (m, 3H), 7.40-7.36 (m, 2H), 7.35-7.28 (m, 7H), 7.21-7.16 (m, 1H), 7.14-7.08 (m, 1H), 7.07 (s, 1H), 5.80 (s, 1H) ppm; **^{13}C NMR** (100 MHz, $CDCl_3$) δ 154.96, 154.10, 144.13, 141.57, 140.11, 129.68, 129.09, 129.05, 128.51, 128.16, 128.08, 127.31, 124.40, 122.83, 120.95, 116.29, 110.93, 105.36 ppm; **EI-MS** m/z (%): : 296 (M^+); **HRMS** (ESI): m/z Exact mass calcd for $C_{22}H_{17}O$ $[M+H]^+$: 297.1274, found: 297.1274.

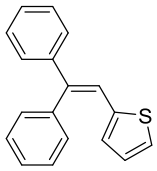

2-(2,2-diphenylvinyl)thiophene (6ai), colorless oil (76% yield); **^{1}H NMR** (400 MHz, $CDCl_3$) δ 7.51-7.44 (m, 3H), 7.37-7.27 (m, 6H), 7.27-7.23 (m, 2H), 7.04 (d, *J* = 5.0 Hz, 1H), 6.93 (d, *J* = 3.2 Hz, 1H), 6.87 (dd, *J* = 5.0, 3.7 Hz, 1H) ppm; **^{13}C NMR** (100 MHz, $CDCl_3$) δ 141.88, 141.46, 139.85, 139.54, 130.47, 129.45, 129.11, 128.43, 128.20, 127.49, 126.87, 126.41, 126.32, 121.01 ppm; **EI-MS** m/z (%): 262 (M^+); **HRMS** (EI): m/z Exact mass calcd for $C_{18}H_{14}S$ $[M]^+$: 262.0816, found: 262.0822.

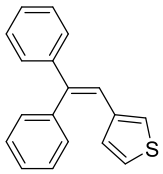

3-(2,2-diphenylvinyl)thiophene (6aj), colorless oil (67% yield); **^{1}H NMR** (400 MHz, $CDCl_3$) δ 7.45-7.36 (m, 3H), 7.35-7.21 (m, 7H), 7.06-7.00 (m, 2H), 6.87-6.81 (m, 1H), 6.53-6.47 (m, 1H) ppm; **^{13}C NMR** (100 MHz, $CDCl_3$) δ 142.75, 141.13, 140.81, 139.13, 130.19, 129.01, 128.39, 128.36, 127.70, 127.46, 127.27, 124.68, 124.62, 122.05 ppm; **EI-MS** m/z (%): 262 (M^+); **HRMS** (EI): m/z Exact mass calcd for $C_{18}H_{14}S$ $[M]^+$: 262.0816, found: 262.0822.

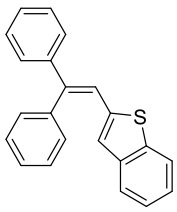

2-(2,2-diphenylvinyl)benzo[b]thiophene (6ak), white solid (78% yield); **^{1}H NMR** (400 MHz, $CDCl_3$) δ 7.63 (d, *J* = 7.5 Hz, 1H), 7.56 (d, *J* = 7.9 Hz, 1H), 7.52-7.46 (m, 3H), 7.39-7.15 (m, 11H) ppm; **^{13}C NMR** (100 MHz, $CDCl_3$) δ 142.34, 141.88, 141.52, 140.60, 138.93, 138.87, 130.73, 129.22, 128.51, 128.48, 127.88, 127.20, 126.08, 124.57, 124.30, 123.28, 122.05, 121.63 ppm; **EI-MS** m/z (%): 312 (M^+); **HRMS** (EI): m/z Exact mass calcd for $C_{22}H_{16}S$ $[M]^+$: 312.0973, found: 312.0976.

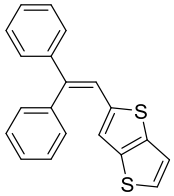

2-(2,2-diphenylvinyl)thieno[3,2-b]thiophene (6al), white solid (73% yield); **^{1}H NMR** (400 MHz, $CDCl_3$) δ 7.48 (dd, *J* = 4.9, 1.7 Hz, 3H), 7.31 (m, 7H), 7.26-7.20 (m, 2H), 7.08 (s, 1H), 6.99 (d, *J* = 5.2 Hz, 1H) ppm; **^{13}C NMR** (100 MHz, $CDCl_3$) δ 143.81, 141.77, 140.50, 140.19, 139.15, 138.48, 130.59, 129.41, 128.44, 128.40, 127.60, 127.50, 126.91, 121.68, 121.05, 119.57 ppm; **EI-MS** m/z (%): 318 (M^+); **HRMS** (EI): m/z Exact mass calcd for $C_{20}H_{14}S_2$ $[M]^+$: 318.0537, found: 318.0530.

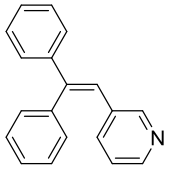

3-(2,2-diphenylvinyl)pyridine (6am), white solid (76% yield); **^{1}H NMR** (400 MHz, $CDCl_3$) δ 8.36 (d, *J* = 1.8 Hz, 1H), 8.32 (dd, *J* = 4.7, 1.3 Hz, 1H), 7.39-7.29 (m, 8H), 7.21-7.14 (m, 3H), 7.01 (dd, *J* = 7.9, 4.8 Hz, 1H), 6.93 (s, 1H) ppm; **EI-MS** m/z (%): 257 (M^+). The data is consistent with the literature (Shigeno et al., 2019).

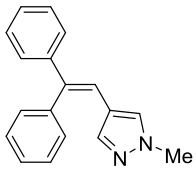

4-(2,2-diphenylvinyl)-1-methyl-1H-pyrazole (6an), red oil (65% yield); **^{1}H NMR** (400 MHz, $CDCl_3$) δ 7.54-7.37 (m, 3H), 7.37-7.15 (m, 7H), 7.02 (s, 1H), 6.89 (s, 1H), 6.57 (s, 1H), 3.72 (s, 3H) ppm; **^{13}C NMR** (100 MHz, $CDCl_3$) δ 142.14, 141.18, 139.76, 139.32, 129.78, 129.33, 129.24, 128.34, 127.68, 127.08, 126.63, 120.00, 117.68, 38.95 ppm; **EI-MS** m/z (%): 260 (M^+); **HRMS** (ESI): m/z Exact mass calcd for $C_{18}H_{17}N_2$ $[M+H]^+$: 261.1386, found: 261.1386.

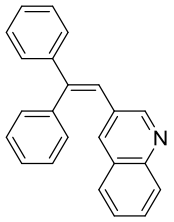

3-(2,2-diphenylvinyl)quinolone (6ao), white solid (97% yield); **^{1}H NMR** (400 MHz, $CDCl_3$) δ 8.59 (d, *J* = 2.1 Hz, 1H), 8.03 (d, *J* = 8.4 Hz, 1H), 7.69 (d, *J* = 1.9 Hz, 1H), 7.65-7.60 (m, 1H), 7.54 (d, *J* = 8.1 Hz, 1H), 7.50-7.42 (m, 1H), 7.41-7.30 (m, 7H), 7.28-7.19 (m, 3H), 7.10 (s, 1H) ppm; **EI-MS** m/z (%): 307 (M^+); **HRMS** (ESI): m/z Exact mass calcd for $C_{23}H_{18}N$ $[M+H]^+$: 308.1434, found: 308.1433.

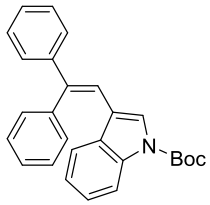

***tert*-butyl 3-(2,2-diphenylvinyl)-1H-indole-1-carboxylate (6ap)**, white solid (76% yield); **^{1}H NMR** (400 MHz, $CDCl_3$) δ 8.11 (d, J = 7.8 Hz, 1H), 7.66 (d, J = 7.7 Hz, 1H), 7.49-7.37 (m, 5H), 7.37-7.22 (m, 7H), 7.20 (s, 1H), 6.48 (s, 1H), 1.53 (s, 9H) ppm; **^{13}C NMR** (100 MHz, $CDCl_3$) δ 149.41, 142.27, 141.97, 141.33, 134.89, 130.58, 129.71, 129.31, 128.45, 127.79, 127.47, 127.00, 124.64, 124.18, 122.79, 118.73, 117.23, 116.99, 115.19, 83.50, 28.20 ppm; **ESI-MS (m/z)**: 396 $[M+H]^+$; **HRMS** (ESI): m/z Exact mass calcd for $C_{27}H_{26}O_2N$ $[M+H]^+$: 396.1958, found: 396.1958.

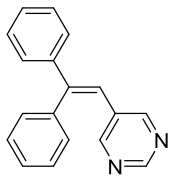

5-(2,2-diphenylvinyl)pyrimidine (6aq), white solid (87% yield); **^{1}H NMR** (400 MHz, $CDCl_3$) δ 8.90 (s, 1H), 8.32 (s, 2H), 7.42-7.30 (m, 8H), 7.18 (dd, *J* = 6.5, 3.0 Hz, 2H), 6.83 (s, 1H) ppm; **^{13}C NMR** (100 MHz, $CDCl_3$) δ 156.77, 156.04, 147.42, 141.90, 138.89, 131.57, 129.92, 129.33, 128.61, 128.52, 128.50, 127.71, 120.24 ppm; **EI-MS** m/z (%): 258 (M^+); **HRMS** (EI): m/z Exact mass calcd for $C_{18}H_{14}N_2$ $[M]^+$: 258.1157, found: 258.1154.

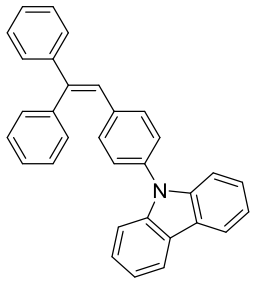

9-(4-(2,2-diphenylvinyl)phenyl)-9H-carbazole (6ar), white solid (83% yield); **^{1}H NMR** (400 MHz, $CDCl_3$) δ 8.09 (d, *J* = 7.7 Hz, 2H), 7.46-7.12 (m, 20H), 7.03 (s, 1H); **^{13}C NMR** (100 MHz, $CDCl_3$) δ 143.45, 143.28, 140.73, 140.26, 136.52, 136.06, 130.95, 130.42, 128.97, 128.41, 127.85, 127.83, 127.74, 127.20, 126.40, 125.98, 123.49, 120.37, 120.05, 109.96 ppm; **EI-MS** m/z (%): 421 (M^+); **HRMS** (EI): m/z Exact mass calcd for $C_{32}H_{23}N$ $[M]^+$: 421.1830, found: 421.1840.

4. General procedure for synthesis multi-aryl substituted 1,3-dienes **8**

4.1. Synthesis of 1,3-dienes **8**

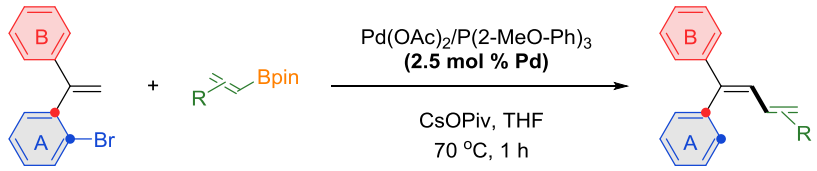

Scheme S5. Synthesis of 1,3-dienes **8**, related to **Scheme 4**

To the suspension of *ortho*-vinyl arylbromides **1** (0.30 mmol), vinylboronate ester **7** (0.60 mmol), $Pd(OAc)_2$ (2.5 mol %), $P(2\text{-MeO-Ph})_3$ (5.0 mol %) and CsOPiv (0.60 mmol) was added THF (3.0 mL) under argon atmosphere. The mixture was stirred at 70 ℃ for 1 h. After being cooled down to room temperature, it was concentrated under reduced pressure and the residue was purified by flash chromatography on silica gel to afford pure product **8**.

4.2. Characterization data of 1,3-dienes **8**

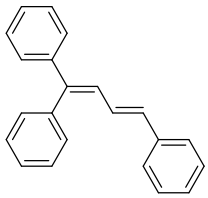

(*E*)-buta-1,3-diene-1,1,4-triyltribenzene (**8aa**), white solid (95% yield); **^{1}H NMR** (400 MHz, $CDCl_3$) δ 7.47-7.37 (m, 3H), 7.34-7.23 (m, 11H), 7.21-7.15 (m, 1H), 6.95-6.83 (m, 2H), 6.80-6.70 (m, 1H) ppm; **EI-MS** m/z (%): 282 (M^+). The data is consistent with the literature (Yang et al., 2013).

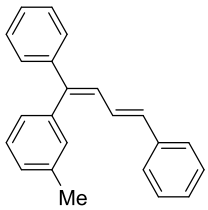

((1*Z*,3*E*)-1-(m-tolyl)buta-1,3-diene-1,4-diyl)dibenzene (8ba), white solid (98% yield); **^{1}H NMR** (400 MHz, $CDCl_3$) δ 7.35-7.22 (m, 10H), 7.21-7.15 (m, 2H), 7.12-7.04 (m, 2H), 6.95-6.83 (m, 2H), 6.78-6.67 (m, 1H), 2.38 (s, 3H) ppm; **^{13}C NMR** (100 MHz, $CDCl_3$) δ143.46, 142.50, 139.83, 137.98, 137.69, 133.81, 131.26, 128.70, 128.38, 128.34, 128.29, 128.22, 127.92, 127.73, 127.59, 127.55, 127.40, 126.60, 21.63 ppm; **EI-MS** m/z (%): 296 (M^+); **HRMS** (ESI): m/z Exact mass calcd for $C_{23}H_{21}$ $[M+H]^+$: 297.1638, found: 297.1638.

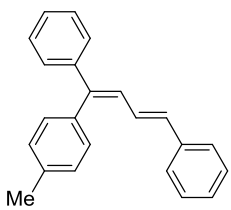

((1*Z*,3*E*)-1-(p-tolyl)buta-1,3-diene-1,4-diyl)dibenzene (**8ca**), white solid (99% yield); **^{1}H NMR** (400 MHz, $CDCl_3$) δ 7.34-7.14 (m, 14H), 6.94 (dd, *J* = 15.3, 10.9 Hz, 1H), 6.84 (d, *J* = 11.0 Hz, 1H), 6.72 (d, *J* = 15.3 Hz,

1H), 2.43 (s, 3H) ppm; **^{13}C NMR** (100 MHz, $CDCl_3$) δ 143.35, 142.70, 137.73, 137.35, 136.91, 133.74, 130.70, 129.07, 128.69, 128.31, 128.23, 127.83, 127.55, 127.54, 127.45, 126.58, 21.47 ppm; **EI-MS** m/z (%): 296 (M^+); **HRMS** (ESI): m/z Exact mass calcd for $C_{23}H_{21}$ $[M+H]^+$: 297.1638, found: 297.1638.

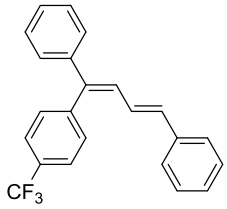

((1*Z*,3*E*)-1-(4-(trifluoromethyl)phenyl)buta-1,3-diene-1,4-diyl)dibenzene (**8da**), white solid (88% yield); **^{1}H NMR** (400 MHz, $CDCl_3$) δ 7.69 (d, *J* = 8.1 Hz, 2H), 7.41 (d, *J* = 8.0 Hz, 2H), 7.36-7.24 (m, 10H), 7.24-7.16 (m, 1H), 6.93 (dd, *J* = 7.8, 2.6 Hz, 1H), 6.84-6.74 (m, 2H) ppm; **^{13}C NMR** (100 MHz, $CDCl_3$) δ 143.76, 141.71, 141.55, 137.27, 135.30, 131.12, 129.73 (q, *J* = 270.7 Hz), 129.38, 128.80, 128.55, 128.01, 127.92, 127.66, 126.71, 126.29, 125.42 (q, *J* = 3.8 Hz), 124.39 (q, *J* = 32.2 Hz) ppm; **^{19}F NMR** (376 MHz, $CDCl_3$) δ -62.43 ppm; EI-MS m/z (%): 350(M^+); **HRMS** (EI): m/z Exact mass calcd for $C_{23}H_{17}F_3$ $[M]^+$: 350.1282, found: 350.1273.

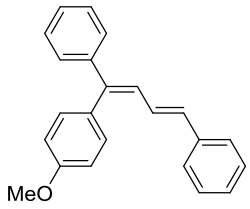

((1*Z*,3*E*)-1-(4-methoxyphenyl)buta-1,3-diene-1,4-diyl)dibenzene (**8ea**), white solid (90% yield); **^{1}H NMR** (400 MHz, $CDCl_3$) δ 7.35-7.23 (m, 9H), 7.23-7.15 (m, 3H), 6.99-6.89 (m, 3H), 6.82 (d, *J* = 11.0 Hz, 1H), 6.72 (d, *J* = 15.4 Hz, 1H), 3.87 (s, 3H) ppm; **^{13}C NMR** (100 MHz, $CDCl_3$) δ 159.15, 143.05, 142.81, 137.75, 133.59, 132.23, 132.01, 128.70, 128.32, 128.10, 127.87, 127.57, 127.54, 127.49, 126.54, 113.75, 55.42 ppm; EI-MS m/z (%): 312(M^+); **HRMS** (EI): m/z Exact mass calcd for $C_{23}H_{20}O$ $[M]^+$: 312.1514, found: 312.1509.

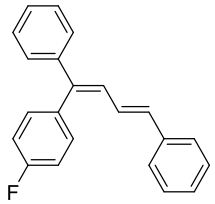

((1*Z*,3*E*)-1-(4-fluorophenyl)buta-1,3-diene-1,4-diyl)dibenzene (**8ga**), white solid (99% yield); **^{1}H NMR** (400 MHz, $CDCl_3$) δ 7.34-7.16 (m, 12H), 7.15-7.08 (m, 2H), 6.90-6.80 (m, 2H), 6.79-6.71 (m, 1H) ppm; **^{13}C NMR** (100 MHz, $CDCl_3$) δ 162.37 (d, *J* = 246.7 Hz), 142.25, 142.11, 137.51, 135.81 (d, *J* = 3.4 Hz), 134.33, 132.41 (d, *J* = 7.9 Hz), 128.76, 128.67, 128.44, 127.78, 127.75, 127.67, 126.90, 126.60, 115.41 (d, *J* = 21.3 Hz) ppm; **^{19}F NMR** (376 MHz, $CDCl_3$) δ -114.49 ppm; **EI-MS** m/z (%): 300 (M^+); **HRMS** (ESI): m/z Exact mass calcd for $C_{22}H_{18}F$ $[M+H]^+$: 301.1387, found: 301.1387.

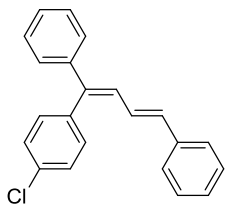

((1*Z*,3*E*)-1-(4-chlorophenyl)buta-1,3-diene-1,4-diyl)dibenzene (**8ha**), white solid (90% yield); **^{1}H NMR** (400 MHz, $CDCl_3$) δ 7.40 (d, *J* = 8.4 Hz, 2H), 7.34-7.24 (m, 9H), 7.21 (dd, *J* = 11.9, 5.3 Hz, 3H), 6.90-6.80 (m, 2H), 6.80-6.70 (m, 1H) ppm; **^{13}C NMR** (100 MHz, $CDCl_3$) δ 142.01, 141.88, 138.38, 137.43, 134.63, 133.55, 132.14, 128.85, 128.77, 128.68, 128.46, 127.85, 127.80, 127.69, 126.71, 126.64 ppm; **EI-MS** m/z (%): 316 (M^+); **HRMS** (ESI): m/z Exact mass calcd for $C_{22}H_{18}Cl$ $[M+H]^+$: 317.1092, found: 317.1090.

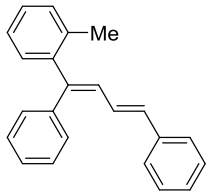

((1*E*,3*E*)-1-(o-tolyl)buta-1,3-diene-1,4-diyl)dibenzene (**8ka**), white solid (91% yield); **^{1}H NMR** (400 MHz, $CDCl_3$) δ 7.38-7.33 (m, 4H), 7.34-7.25 (m, 6H), 7.25-7.19 (m, 4H), 7.16-7.12 (m, 1H), 6.72 (d, *J* = 15.6 Hz, 1H), 6.50 (d, *J* = 11.1 Hz, 1H), 2.05 (s, 3H) ppm; **^{13}C NMR** (100 MHz, $CDCl_3$) δ 143.71, 143.53, 140.42, 137.65, 136.64, 134.24, 130.64, 130.56, 130.37, 130.04, 128.74, 128.26, 127.64, 127.62, 127.36, 126.63, 126.61, 125.75, 20.78 ppm; **EI-MS** m/z (%): 296 (M^+); **HRMS** (EI): m/z Exact mass calcd for $C_{23}H_{20}$ $[M]^+$: 296.1565, found: 296.1567.

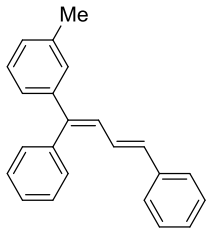

((1*E*,3*E*)-1-(m-tolyl)buta-1,3-diene-1,4-diyl)dibenzene (**8la**), white solid (86% yield); **^{1}H NMR** (400 MHz, $CDCl_3$) δ 7.46-7.34 (m, 3H), 7.33-7.23 (m, 6H), 7.22-7.15 (m, 2H), 7.14 (s, 1H), 7.11-7.04 (m, 2H), 6.94-6.82 (m, 2H), 6.78-6.67 (m, 1H), 2.32 (s, 3H) ppm; **^{13}C NMR** (100 MHz, $CDCl_3$) δ143.42, 142.44, 140.00, 137.90, 137.67, 133.84, 130.78, 128.70, 128.43, 128.37, 128.33, 128.31, 128.25, 127.59, 127.58, 127.31, 126.57, 125.03, 21.63 ppm; **EI-MS** m/z (%): 296 (M^+); **HRMS** (ESI): m/z Exact mass calcd for $C_{23}H_{21}$ $[M+H]^+$: 297.1638, found: 297.1637.

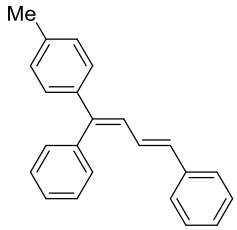

((1*E*,3*E*)-1-(p-tolyl)buta-1,3-diene-1,4-diyl)dibenzene (**8ma**), white solid (97% yield); **^{1}H NMR** (400 MHz, $CDCl_3$) δ 7.45-7.33 (m, 3H), 7.33-7.23 (m, 6H), 7.22-7.14 (m, 3H), 7.11 (d, *J* = 8.0 Hz, 2H), 6.94-6.80 (m, 2H), 6.76-6.66 (m, 1H), 2.34 (s, 3H) ppm; **^{13}C NMR** (100 MHz, $CDCl_3$) δ 143.25, 140.07, 139.61, 137.73, 137.52, 133.54, 130.77, 129.10, 128.69, 128.33, 127.64, 127.62, 127.56, 127.53, 127.38, 126.54, 21.30 ppm; **EI-MS** m/z (%): 296 (M^+); **HRMS** (ESI): m/z Exact mass calcd for $C_{23}H_{21}$ $[M+H]^+$: 297.1638, found: 297.1638.

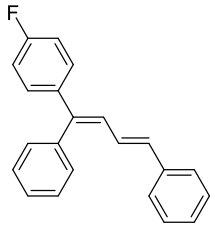

((1*E*,3*E*)-1-(4-fluorophenyl)buta-1,3-diene-1,4-diyl)dibenzene (**8na**), white solid (87% yield); **^{1}H NMR** (400 MHz, $CDCl_3$) δ 7.46-7.35 (m, 3H), 7.33-7.22 (m, 8H), 7.21-7.15 (m, 1H), 7.02-6.95 (m, 2H), 6.88 (dd, *J* = 15.1, 10.8 Hz, 1H), 6.80 (d, *J* = 10.8 Hz, 1H), 6.73 (d, *J* = 15.1 Hz, 1H) ppm; **^{13}C NMR** (100 MHz, $CDCl_3$) δ 162.48 (d, *J* = 247.3 Hz), 142.18, 139.74, 138.62 (d, *J* = 3.3 Hz), 137.55, 134.08, 130.53, 129.17 (d, *J* = 8.0 Hz), 128.56, 128.31, 128.06 (d, *J* = 1.5 Hz), 127.62, 127.69, 127.09, 126.59, 115.25 (d, *J* = 21.5 Hz) ppm; **^{19}F NMR** (376 MHz, $CDCl_3$) δ -114.82 ppm; **EI-MS** m/z (%): 300 (M^+); **HRMS** (ESI): m/z Exact mass calcd for $C_{22}H_{18}F$ $[M+H]^+$: 301.1387, found: 301.1387.

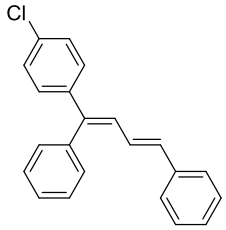

((1*E*,3*E*)-1-(4-chlorophenyl)buta-1,3-diene-1,4-diyl)dibenzene (**8oa**), white solid (89% yield); **^{1}H NMR** (400 MHz, $CDCl_3$) δ 7.46-7.38 (m, 3H), 7.34-7.17 (m, 11H), 6.92-6.81 (m, 2H), 6.80-6.72 (m, 1H) ppm; **^{13}C NMR** (100 MHz, $CDCl_3$) δ 142.00, 140.92, 139.46, 137.48, 134.53, 133.39, 130.69, 128.94, 128.74, 128.521, 128.515, 127.85, 127.80, 126.98, 126.65 ppm; **EI-MS** m/z (%): 316 (M^+); **HRMS** (ESI): m/z Exact mass calcd for $C_{22}H_{17}Cl$ $[M]^+$: 316.1013, found: 316.1013.

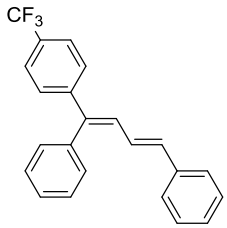

((1*E*,3*E*)-1-(4-(trifluoromethyl)phenyl)buta-1,3-diene-1,4-diyl)dibenzene (**8pa**), white solid (99% yield); **^{1}H NMR** (400 MHz, $CDCl_3$) δ 7.54 (d, *J* = 8.3 Hz, 2H), 7.49-7.36 (m, 5H), 7.36-7.24 (m, 6H), 7.23-7.18 (t, *J* = 7.0 Hz, 1H), 6.96-6.85 (m, 2H), 6.85-6.74 (m, 1H) ppm; **^{13}C NMR** (100 MHz, $CDCl_3$) δ 145.91, 141.75, 139.17, 137.30, 135.46, 130.68, 130.17, 129.30 (q, *J* = 30.1 Hz), 128.78, 128.62, 128.02, 127.99, 127.86, 126.76, 126.74, 125.31 (q, *J* = 3.8 Hz), 124.39 (q, *J* = 270.6 Hz) ppm; **^{19}F NMR** (376 MHz, $CDCl_3$) δ -62.47 ppm; **EI-MS** m/z (%): 350 (M^+); **HRMS** (ESI): m/z Exact mass calcd for $C_{23}H_{18}F_3$ $[M+H]^+$: 351.1355, found: 351.1355.

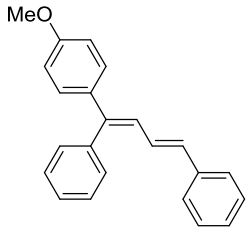

((1*E*,3*E*)-1-(4-methoxyphenyl)buta-1,3-diene-1,4-diyl)dibenzene (**8qa**), white solid (88% yield); **^{1}H NMR** (400 MHz, $CDCl_3$) δ 7.46-7.36 (m, 3H), 7.33-7.21 (m, 8H), 7.20-7.14 (m, 1H), 6.92-6.78 (m, 4H), 6.70 (d, *J* = 14.8 Hz, 1H), 3.81 (s, 3H) ppm; **^{13}C NMR** (100 MHz, $CDCl_3$) δ159.35, 142.91, 140.12, 137.79, 135.08, 133.09, 130.75, 128.91, 128.68, 128.34, 127.58, 127.46, 127.44, 126.82, 126.48, 113.78, 55.46 ppm; **EI-MS** m/z (%): 312 (M^+); **HRMS** (EI): m/z Exact mass calcd for $C_{23}H_{21}O$ $[M+H]^+$: 313,1587, found: 313.1587.

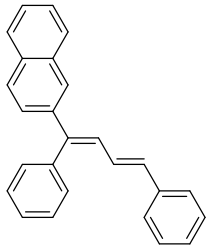

2-((1*E*,3*E*)-1,4-diphenylbuta-1,3-dien-1-yl)naphthalene (**8sa**), white solid (91% yield); **^{1}H NMR** (400 MHz, $CDCl_3$) δ 7.83-7.70 (m, 3H), 7.65 (s, 1H), 7.54 (dd, *J* = 8.6, 1.7 Hz, 1H), 7.49-7.37 (m, 5H), 7.36-7.24 (m, 6H), 7.22-7.16 (m, 1H), 7.03 (d, *J* = 10.9 Hz, 1H), 6.94 (dd, *J* = 15.1, 10.9 Hz, 1H), 6.79 (d, *J* = 15.1 Hz, 1H) ppm; **^{13}C NMR** (100 MHz, $CDCl_3$) δ 143.23, 139.88, 139.76, 137.63, 134.19, 133.48, 132.93, 130.87, 128.94, 128.73, 128.46, 128.39, 127.88, 127.73, 127.69, 127.66, 127.30, 127.10, 126.63, 126.32, 126.11, 125.56 ppm; EI-MS m/z (%): 332(M^+); **HRMS** (EI): m/z Exact mass calcd for $C_{26}H_{20}$ $[M]^+$: 332.1565, found: 332.1569.

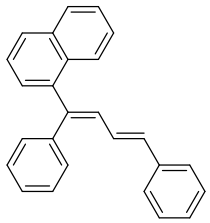

1-((1*E*,3*E*)-1,4-diphenylbuta-1,3-dien-1-yl)naphthalene (**8ta**), white solid (98% yield); **^{1}H NMR** (400 MHz, $CDCl_3$) δ 7.95 (d, *J* = 8.5 Hz, 1H), 7.83 (dd, *J* = 13.6, 8.1 Hz, 2H), 7.52-7.17 (m, 15H), 6.78-6.64 (m, 2H) ppm; **^{13}C NMR** (100 MHz, $CDCl_3$) δ 142.09, 141.77, 141.06, 137.61, 134.62, 134.09, 132.12, 132.03, 129.99, 128.77, 128.39, 128.06, 127.79, 127.75, 127.54, 126.68, 126.62, 126.42, 126.08, 125.76, 125.41 ppm; **EI-MS** m/z (%): 332 (M^+); **HRMS** (ESI): m/z Exact mass calcd for $C_{26}H_{21}$ $[M+H]^+$: 333.1638, found: 333.1638.

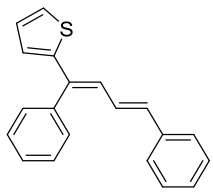

2-((1*E*,3*E*)-1,4-diphenylbuta-1,3-dien-1-yl)thiophene (**8va**), white solid (88% yield); **^{1}H NMR** (400 MHz, $CDCl_3$) δ 7.47-7.39 (m, 3H), 7.38-7.34 (m, 2H), 7.31-7.22 (m, 4H), 7.21-7.14 (m, 2H), 6.96-6.87 (m, 2H), 6.79-6.67 (m, 3H) ppm; **^{13}C NMR** (100 MHz, $CDCl_3$) δ 147.11, 138.86, 137.57, 137.11, 133.70, 130.34, 128.70, 128.43, 128.01, 127.71, 127.64, 127.10, 126.57, 126.55, 126.27, 124.89 ppm; **EI-MS** m/z (%): 288 (M^+); **HRMS** (ESI): m/z Exact mass calcd for $C_{20}H_{17}S$ $[M+H]^+$: 289.1045, found: 289.1045.

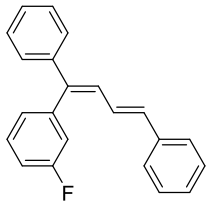

((1*Z*,3*E*)-1-(3-fluorophenyl)buta-1,3-diene-1,4-diyl)dibenzene (**8Aa**), white solid (97% yield); **^{1}H NMR** (400 MHz, $CDCl_3$) δ 7.41-7.35 (m, 1H), 7.34-7.16 (m, 10H), 7.11-7.04 (m, 2H), 7.02-6.97 (m, 1H), 6.90-6.81 (m, 2H), 6.80-6.71 (m, 1H) ppm; **^{13}C NMR** (100 MHz, $CDCl_3$) δ 162.90 (d, *J* = 246.4 Hz), 142.17 (d, *J* = 7.6 Hz), 141.80, 141.78, 137.41, 134.65, 129.89 (d, *J* = 8.4 Hz), 128.92, 128.75, 128.47, 127.86, 127.79, 127.61, 126.67, 126.56 (d, *J* = 2.9 Hz), 117.56 (d, *J* = 21.2 Hz), 114.61 (d, *J* = 21.0 Hz) ppm; **^{19}F NMR** (376 MHz, $CDCl_3$) δ -113.22 ppm; **EI-MS** m/z (%): 300 (M^+); **HRMS** (ESI): m/z Exact mass calcd for $C_{22}H_{18}F$ $[M+H]^+$: 301.1387, found: 301.1387.

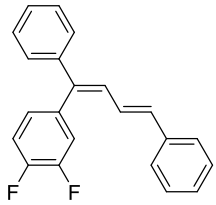

((1*Z*,3*E*)-1-(3,4-difluorophenyl)buta-1,3-diene-1,4-diyl)dibenzene (**8Ba**), white solid (91% yield); **^{1}H NMR** (400 MHz, $CDCl_3$) δ 7.37-7.17 (m, 11H), 7.14-7.05 (m, 1H), 7.05-6.99 (m, 1H), 6.91-6.72 (m, 3H) ppm; **^{13}C NMR** (100 MHz, $CDCl_3$) δ 150.22 (dd, *J* = 247,5, 40.0 Hz), 150.10 (dd, *J* = 248.0, 40.0 Hz), 141.67, 140.88, 137.30, 136.83 (dd, *J* = 5.7, 4.0 Hz), 135.07, 129.18, 128.81, 128.54, 127.99, 127.94, 127.59, 127.00 (dd, *J* = 6.1, 3.5 Hz), 126.68, 126.34, 119.59 (d, *J* = 16.9 Hz), 117.29 (d, *J* = 17.1 Hz) ppm; **^{19}F NMR** (376 MHz, $CDCl_3$) δ -137.72, -139.02 ppm; EI-MS m/z (%): 318(M^+); **HRMS** (EI): m/z Exact mass calcd for $C_{22}H_{16}F_2$ $[M]^+$: 318.1220, found: 318.1226.

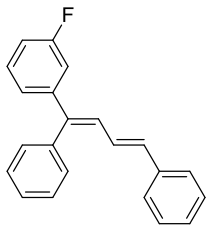

((1*E*,3*E*)-1-(3-fluorophenyl)buta-1,3-diene-1,4-diyl)dibenzene (**8Ca**), white solid (96% yield); **^{1}H NMR** (400 MHz, $CDCl_3$) δ 7.48-7.36 (m, 3H), 7.34-7.23 (m, 7H), 7.23-7.16 (m, 1H), 7.08 (d, *J* = 7.8 Hz, 1H), 7.03-6.91 (m, 2H), 6.91-6.82 (m, 2H), 6.80-6.71 (m, 1H) ppm; **^{13}C NMR** (100 MHz, $CDCl_3$) δ 162.99 (d, *J* = 245.0 Hz), 144.73 (d, *J* = 7.6 Hz), 142.00, 139.32, 137.43, 134.83, 130.69, 129.70 (d, *J* = 8.4 Hz), 129.26, 128.74, 128.52, 127.86, 126.88, 126.69, 123.32 (d, *J* = 2.7 Hz), 114.48 (d, *J* = 10.7 Hz), 114.27 (d, *J* = 9.9 Hz) ppm; **^{19}F NMR** (376 MHz, $CDCl_3$) δ -113.63 ppm; **EI-MS** m/z (%): 300 (M^+); **HRMS** (EI): m/z Exact mass calcd for $C_{22}H_{17}F$ $[M]^+$: 300.1314, found: 300.1318.

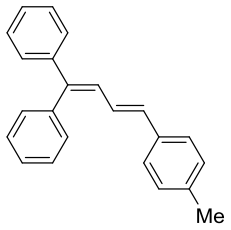

(*E*)-(4-(p-tolyl)buta-1,3-diene-1,1-diyl)dibenzene (**8ab**), white solid (95% yield); **^{1}H NMR** (400 MHz, $CDCl_3$) δ 7.45-7.34 (m, 3H), 7.33-7.23 (m, 7H), 7.22-7.18 (m, 2H), 7.07 (d, *J* = 8.0 Hz, 2H), 6.90-6.80 (m, 2H), 6.76-6.66 (m, 1H), 2.31 (s, 3H) ppm; **^{13}C NMR** (100 MHz, $CDCl_3$) δ 142.67, 142.53, 140.01, 137.59, 134.86, 134.06, 130.80, 129.43, 128.60, 128.35, 128.34, 127.71, 127.55, 127.48, 126.53, 126.33, 21.40 ppm; EI-MS m/z (%): 296(M^+); **HRMS** (EI): m/z Exact mass calcd for $C_{23}H_{20}$ $[M]^+$: 296.1565, found: 296.1566.

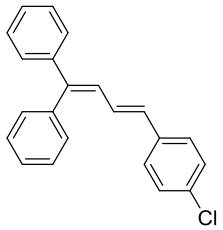

(*E*)-(4-(4-chlorophenyl)buta-1,3-diene-1,1-diyl)dibenzene (**8ac**), white solid (96% yield); **^{1}H NMR** (400 MHz, $CDCl_3$) δ 7.46-7.35 (m, 3H), 7.33-7.17 (m, 11H), 6.93-6.80 (m, 2H), 6.72-6.62 (m, 1H) ppm; **^{13}C NMR** (100 MHz, $CDCl_3$) δ 143.89, 142.28, 139.79, 136.14, 133.11, 132.55, 130.73, 128.86, 128.42, 128.39, 128.06, 127.79, 127.76, 127.74, 127.71 ppm; **EI-MS** m/z (%): 316 (M^+); **HRMS** (ESI): m/z Exact mass calcd for $C_{22}H_{18}Cl$ $[M+H]^+$: 317.1092, found: 317.1091.

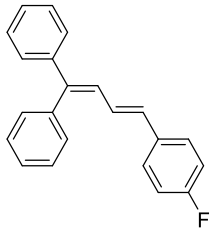

(*E*)-(4-(4-fluorophenyl)buta-1,3-diene-1,1-diyl)dibenzene (**8ad**), white solid (99% yield); **^{1}H NMR** (400 MHz, $CDCl_3$) δ 7.46-7.35 (m, 3H), 7.32-7.23 (m, 9H), 6.98-6.90 (m, 2H), 6.88-6.75 (m, 2H), 6.69 (d, *J* = 14.6 Hz, 1H) ppm; **^{13}C NMR** (100 MHz, $CDCl_3$) δ 162.36 (d, *J* = 247.5 Hz), 143.33 (d, *J* = 1.3 Hz), 142.36, 139.88, 133.83 (d, *J* = 3.4 Hz), 132.69, 130.74, 128.41, 128.38, 128.18, 128.10, 128.02, 127.72, 127.65 (d, *J* = 2.5 Hz), 126.98 (d, *J* = 2.4 Hz), 115.67 (d, *J* = 21.7 Hz) ppm; **^{19}F NMR** (376 MHz, $CDCl_3$) δ -114.17 ppm; **EI-MS** m/z (%): 300 (M^+); **HRMS** (ESI): m/z Exact mass calcd for $C_{22}H_{18}F$ $[M+H]^+$: 301.1387, found: 301.1388.

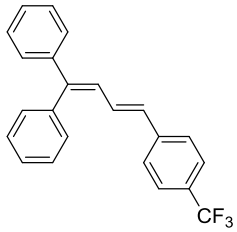

(*E*)-(4-(4-(trifluoromethyl)phenyl)buta-1,3-diene-1,1-diyl)dibenzene (**8ae**), white solid (96% yield); **^{1}H NMR**

(400 MHz, $CDCl_3$) δ 7.50 (d, *J* = 8.2 Hz, 2H), 7.47-7.35 (m, 5H), 7.34-7.24 (m, 7H), 6.96 (dd, *J* = 15.1, 11.0 Hz, 1H), 6.88 (d, *J* = 11.0 Hz, 1H), 6.74 (d, *J* = 15.1 Hz, 1H) ppm; **^{13}C NMR** (100 MHz, $CDCl_3$) δ 145.10, 142.13, 141.10, 139.63, 132.15, 130.73, 129.65, 129.12 (q, *J* = 32.3 Hz), 128.46, 128.43, 127.97, 127.91, 127.86, 127.76, 127.05 (q, *J* = 270.4 Hz), 126.59, 125.64 (q, *J* = 3.8 Hz) ppm; **^{19}F NMR** (376 MHz, $CDCl_3$) δ -62.51 ppm; EI-MS m/z (%): 350 (M^+); HRMS (ESI): m/z Exact mass calcd for $C_{23}H_{17}F_3$ $[M]^+$: 350.1277,found: 350.1277.

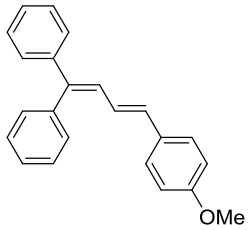

(*E*)-(4-(4-methoxyphenyl)buta-1,3-diene-1,1-diyl)dibenzene (**8af**), white solid (99% yield); **^{1}H NMR** (400 MHz, $CDCl_3$) δ 7.46-7.34 (m, 3H), 7.32-7.22 (m, 9H), 6.89-6.64 (m, 5H), 3.79 (s, 3H) ppm; **^{13}C NMR** (100 MHz, $CDCl_3$) δ 159.34, 142.56, 142.07, 140.07, 133.64, 130.80, 130.47, 128.67, 128.36, 128.33, 127.85, 127.64, 127.49, 127.39, 125.26, 114.17, 55.43 ppm; **EI-MS** m/z (%): 312 (M^+); HRMS (EI): m/z Exact mass calcd for $C_{23}H_{20}O$ $[M]^+$: 312.1514, found: 312.1516.

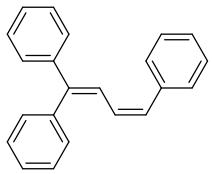

(*Z*)-buta-1,3-diene-1,1,4-triyltribenzene (**8ag**), white solid (73% yield); **^{1}H NMR** (400 MHz, $CDCl_3$) δ 7.43-7.34 (m, 7H), 7.32-7.22 (m, 8H), 7.17 (d, *J* = 11.4 Hz, 1H), 6.47 (d, *J* = 11.6 Hz, 1H), 6.31 (t, *J* = 11.4 Hz, 1H) ppm; **^{13}C NMR** (100 MHz, $CDCl_3$) δ 145.22, 142.45, 139.76, 137.76, 131.24, 130.76, 129.27, 128.47, 128.34, 128.27, 128.02, 127.73, 127.69, 127.23, 124.40 ppm; EI-MS m/z (%): 282(M^+); **HRMS** (EI): m/z Exact mass calcd for $C_{22}H_{18}$ $[M]^+$: 282.1409, found: 282.1406.

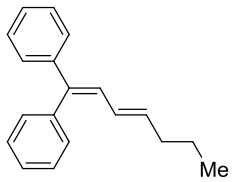

(*E*)-hepta-1,3-diene-1,1-diyldibenzene (8ah), colorless oil (83% yield); **^{1}H NMR** (400 MHz, $CDCl_3$) δ 7.42-7.30 (m, 3H), 7.30-7.18 (m, 7H), 6.67 (d, *J* = 11.0 Hz, 1H), 6.14 (dd, *J* = 15.1, 10.9 Hz, 1H), 5.96-5.84 (m, 1H), 2.04 (dd, *J* = 14.1, 7.0 Hz, 2H), 1.39 (dq, *J* = 14.7, 7.4 Hz, 2H), 0.89 (t, *J* = 7.4 Hz, 3H); **^{13}C NMR** (100 MHz, $CDCl_3$) δ 142.70, 140.28, 140.17, 137.30, 130.63, 128.56, 128.55, 128.27, 128.25, 127.52, 127.23, 127.14, 35.23, 22.72, 13.87; **EI-MS** m/z (%): 248 (M^+); HRMS (EI): m/z Exact mass calcd for $C_{19}H_{20}$ $[M]^+$: 248.1565, found: 248.1557.

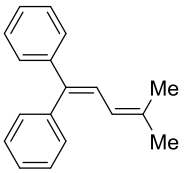

(4-methylpenta-1,3-diene-1,1-diyl)dibenzene (8ai), colorless oil (85% yield); **^{1}H NMR** (400 MHz, $CDCl_3$) δ 7.42-7.35 (m, 2H), 7.35-7.30 (m, 1H), 7.30-7.24 (m, 4H), 7.24-7.18 (m, 3H), 6.87 (d, *J* = 11.4 Hz, 1H), 5.92 (d, *J* = 11.4 Hz, 1H), 1.89 (s, 3H), 1.76 (s, 3H); **^{13}C NMR** (100 MHz, $CDCl_3$) δ 143.23, 140.32, 139.82, 137.90, 130.71, 128.25, 128.23, 127.56, 127.14, 127.03, 124.63, 123.28, 26.65, 18.78; EI-MS m/z (%): 234 (M^+); **HRMS** (EI): m/z Exact mass calcd for $C_{18}H_{18}$ $[M]^+$: 234.1409, found: 234.1402.

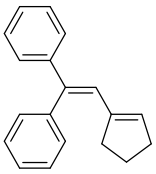

(2-(cyclopent-1-en-1-yl)ethene-1,1-diyl)dibenzene (8aj), colorless oil (49% yield); **^{1}H NMR** (400 MHz, $CDCl_3$) δ 7.38-7.30 (m, 3H), 7.29-7.22 (m, 4H), 7.22-7.16 (m, 3H), 6.88 (s, 1H), 5.86 (s, 1H), 2.35-2.25 (m, 2H), 1.85-1.74 (m, 2H), 1.74-1.65 (m, 2H); **^{13}C NMR** (100 MHz, $CDCl_3$) δ 143.18, 142.83, 140.98, 140.00, 135.50, 130.72, 128.21, 127.81, 127.27, 127.23, 127.05, 125.42, 33.55, 32.22, 24.44; EI-MS m/z (%):246(M^+); **HRMS** (EI): m/z Exact mass calcd for $C_{19}H_{18}$ $[M]^+$: 246.1409, found: 246.1414.

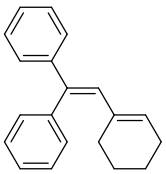

(2-(cyclohex-1-en-1-yl)ethene-1,1-diyl)dibenzene (8ak), colorless oil (53% yield); **^{1}H NMR** (400 MHz, $CDCl_3$) δ 7.35-7.28 (m, 3H), 7.28-7.17 (m, 7H), 6.55 (s, 1H), 5.85-5.76 (m, 1H), 2.14-2.06 (m, 2H), 1.70-1.60 (m, 2H), 1.52-1.46 (m, 2H), 1.45-1.39 (m, 2H); **^{13}C NMR** (100 MHz, $CDCl_3$) δ 144.08, 141.44, 138.66, 136.53, 132.38, 132.27, 130.64, 128.14, 127.91, 127.51, 127.06, 126.89, 28.25, 26.36, 23.10, 22.19; EI-MS m/z (%):260(M^+); **HRMS** (EI): m/z Exact mass calcd for $C_{20}H_{20}$ $[M]^+$: 260.1565, found: 260.1555.

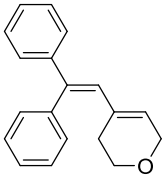

4-(2,2-diphenylvinyl)-3,6-dihydro-2H-pyran (8al), colorless oil (76% yield); **^{1}H NMR** (400 MHz, $CDCl_3$) δ 7.32 (m, 3H), 7.31-6.98 (m, 7H), 6.56 (s, 1H), 5.76 (s, 1H), 4.25-4.15 (br, 2H), 3.56 (t, *J* = 5.3 Hz, 2H), 1.78-1.70 (br, 2H); ^{13}C NMR (100 MHz, $CDCl_3$) δ 143.42, 140.80, 140.30, 134.10, 130.54, 130.00, 129.15, 128.23, 128.11, 127.52, 127.46, 127.31, 66.13, 64.38, 28.43; EI-MS m/z (%):262(M^+); **HRMS** (EI): m/z Exact

mass calcd for $C_{19}H_{18}O$ $[M]^+$: 262.1358, found: 262.1351.

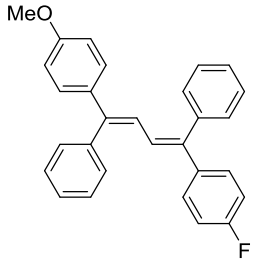

((*1E,3E*)-1-(4-fluorophenyl)-4-(4-methoxyphenyl)buta-1,3-diene-1,4-diyl)dibenzene (**8qm**), white solid (82% yield); **^{1}H NMR** (400 MHz, $CDCl_3$) δ 7.45-7.33 (m, 6H), 7.33-7.27 (m, 4H), 7.15-7.05 (m, 4H), 6.94-6.86 (m, 2H), 6.76 (d, *J* = 8.9 Hz, 2H), 6.68 (s, br, 2H), 3.77 (s, 3H) ppm; **^{13}C NMR** (100 MHz, $CDCl_3$) δ 162.31 (d, *J* = 247.1 Hz), 159.31, 143.87, 142.11, 140.17, 139.98, 138.90 (d, *J* = 3.3 Hz), 135.18, 130.78, 129.32 (d, *J* = 7.9 Hz), 129.01, 128.45, 128.37, 127.68, 127.64, 126.13, 126.11, 124.41, 115.12 (d, *J* = 21.4 Hz), 113.70, 55.42 ppm; **^{19}F NMR** (376 MHz, $CDCl_3$) δ -115.18 ppm; **EI-MS** m/z (%): 406 (M^+); **HRMS** (EI): m/z Exact mass calcd for $C_{29}H_{23}OF$ $[M]^+$: 406.1733, found: 406.1739.

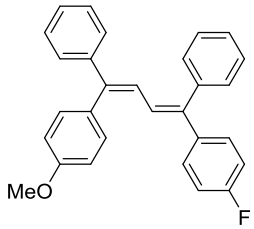

((*1E,3Z*)-1-(4-fluorophenyl)-4-(4-methoxyphenyl)buta-1,3-diene-1,4-diyl)dibenzene (**8em**), white solid (87% yield); **^{1}H NMR** (400 MHz, $CDCl_3$) δ 7.45-7.35 (m, 3H), 7.31-7.25 (m, 3H), 7.24-7.20 (m, 4H), 7.19-7.10 (m, 4H), 6.98-6.88 (m, 4H), 6.71 (dd, *J* = 11.4 Hz, 2H), 3.87 (s, 3H) ppm; **^{13}C NMR** (100 MHz, $CDCl_3$) δ 162.38 (d, *J* = 247.3 Hz), 159.17, 144.04, 142.94, 142.64, 139.92, 138.88 (d, *J* = 3.1 Hz), 132.29, 132.09, 130.74, 129.40 (d, *J* = 7.9 Hz), 128.45, 128.25, 128.00, 127.73, 127.53, 126.24, 125.71, 115.15 (d, *J* = 21.4 Hz), 113.75, 55.43. ppm; **^{19}F NMR** (376 MHz, $CDCl_3$) δ -115.06 ppm; **EI-MS** m/z (%): 406 (M^+); **HRMS** (EI): m/z Exact mass calcd for $C_{29}H_{23}OF$ $[M]^+$: 406.1733, found: 406.1740.

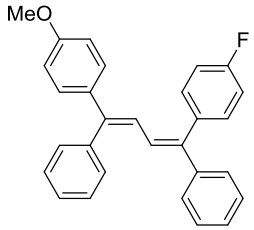

((*1Z,3E*)-1-(4-fluorophenyl)-4-(4-methoxyphenyl)buta-1,3-diene-1,4-diyl)dibenzene (**8qn**), white solid (78% yield); **^{1}H NMR** (400 MHz, $CDCl_3$) δ 7.44-7.34 (m, 3H), 7.33-7.26 (m, 4H), 7.23-7.18 (m, 3H), 7.16-7.07 (m, 6H), 6.81-6.76 (m, 2H), 6.74 (d, *J* = 11.5 Hz, 1H), 6.65 (d, *J* = 11.4 Hz, 1H), 3.78 (s, 3H) ppm; **^{13}C NMR** (100 MHz, $CDCl_3$) δ 162.30 (d, *J* = 246.5 Hz), 159.39, 144.16, 142.55, 142.04, 140.11, 136.05 (d, *J* = 3.4 Hz), 135.15,

132.50 (d, *J* = 8.0 Hz), 130.77, 129.01, 128.37, 128.33, 127.70, 127.67, 127.47, 126.62, 124.26, 115.38 (d, *J* = 21.3 Hz), 113.76, 55.43 ppm; **^{19}F NMR** (376 MHz, $CDCl_3$) δ -114.65 ppm; **EI-MS** m/z (%): 406 (M^+); **HRMS** (EI): m/z Exact mass calcd for $C_{29}H_{23}OF$ $[M]^+$: 406.1733, found: 406.1731.

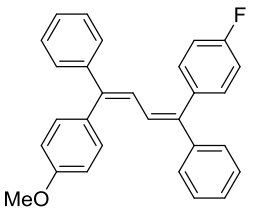

((*1Z,3Z*)-1-(4-fluorophenyl)-4-(4-methoxyphenyl)buta-1,3-diene-1,4-diyl)dibenzene (**8en**), white solid (75% yield); **^{1}H NMR** (400 MHz, $CDCl_3$) δ 7.32-7.20 (m, 10H), 7.20-7.14 (m, 4H), 7.13-7.05 (m, 2H), 6.96-6.91 (m, 2H), 6.81 (d, *J* = 11.4 Hz, 1H), 6.66 (d, *J* = 11.4 Hz, 1H), 3.86 (s, 1H) ppm; **^{13}C NMR** (100 MHz, $CDCl_3$) δ 162.32 (d, *J* = 246.6 Hz), 159.21, 144.33, 142.93, 142.58, 142.55, 136.01 (d, *J* = 3.4 Hz), 132.47 (d, *J* = 7.9 Hz), 132.24, 132.08, 128.35, 128.29, 127.99, 127.77, 127.61, 127.56, 126.72, 125.56, 115.38 (d, *J* = 21.2 Hz), 113.77, 55.42 ppm; **^{19}F NMR** (376 MHz, $CDCl_3$) δ -114.56 ppm; **EI-MS** m/z (%): 406 (M^+); **HRMS** (EI): m/z Exact mass calcd for $C_{29}H_{23}OF$ $[M]^+$: 406.1733, found: 406.1744.

5. Gram-scale reactions

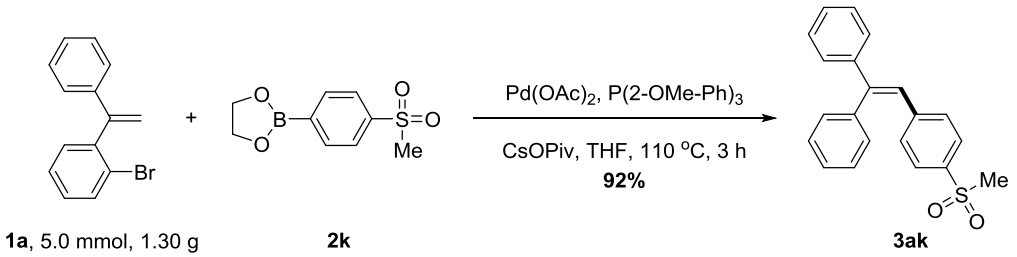

Scheme S6. Gram-scale reactions of **3ak**, related to **Scheme 5**

To the suspension of *ortho*-vinyl bromobenzene **1a** (1.30 g, 5.0 mmol), arylboronate ester **2k** (3.39 g, 15.0 mmol), $Pd(OAc)_2$ (56.0 mg, 0.25 mmol), $P(2\text{-MeO-Ph})_3$ (176.2 mg, 0.50 mmol) and CsOPiv (2.34 g, 10.0 mmol) was added THF (100 mL) under argon atmosphere. The mixture was stirred at 110 ℃ for 3 h. After being cooled down to room temperature, it was concentrated under reduced pressure and the residue was purified by flash chromatography on silica gel to afford pure product **3ak** with 92% yield.

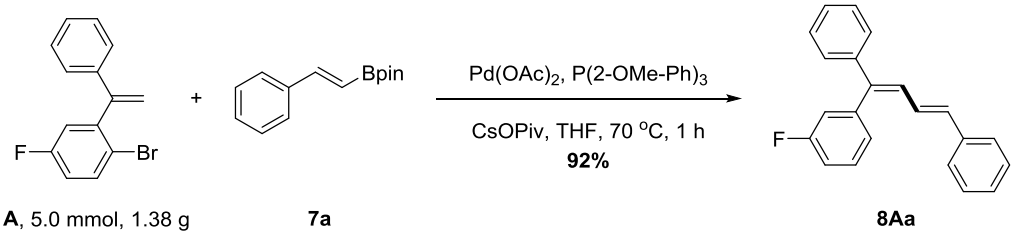

Scheme S7. Gram-scale reactions of **8Aa**, related to **Scheme 5**

To the suspension of *ortho*-vinyl bromobenzene **1A** (1.38 g, 5.0 mmol), vinylboronate ester **7a** (2.30 g, 10.0 mmol), $Pd(OAc)_2$ (28.0 mg, 0.125 mmol), P(2-MeO-Ph)$_3$ (88.1 mg, 0.25 mmol) and CsOPiv (2.34 g, 10.0 mmol) was added THF (100 mL) under argon atmosphere. The mixture was stirred at 70 ℃ for 1 h. After being cooled down to room temperature, it was concentrated under reduced pressure and the residue was purified by flash chromatography on silica gel to afford pure product **8Aa** with 92% yield.

6. Transformation of obtained products

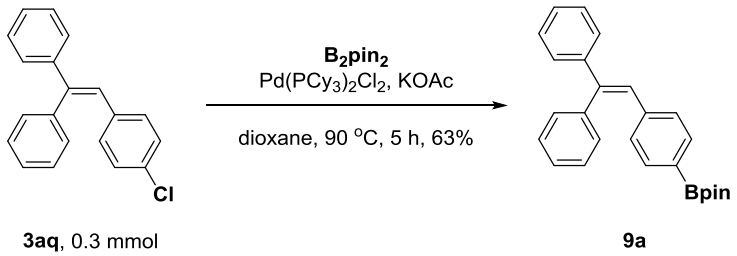

Scheme S8. Transformation of **3aq**, related to **Scheme 5**

2-(4-(2,2-diphenylvinyl)phenyl)-4,4,5,5-tetramethyl-1,3,2-dioxaborolane (**9a**) To the suspension of **3aq** (87 mg, 0.3 mmol), $Pd(PCy_3)_2Cl_2$ (11.1 mg, 5 mol %), KOAc (59 mg, 0.6 mmol) and B_2pin_2 (152.4 mg, 0.6 mmol) was added dioxane (3 mL) under argon atmosphere. The mixture was stirred at 90 ℃ for 5 h. After being cooled down to room temperature, it was concentrated under reduced pressure and the residue was purified by flash chromatography on silica gel to afford pure product **9a** with 63% yield as a while solid. **^{1}H NMR** (400 MHz, $CDCl_3$) δ 7.56 (d, *J* = 8.1 Hz, 2H), 7.36-7.26 (m, 8H), 7.22-7.15 (m, 2H), 7.01 (d, *J* = 8.0 Hz, 2H), 6.97 (s, 1H), 1.31 (s, 12H) ppm; **^{13}C NMR** (100 MHz, $CDCl_3$) δ 143.65, 143.41, 140.35, 140.33, 134.50, 130.48, 128.96, 128.76, 128.33, 128.26, 127.80, 127.76, 127.59, 83.82, 25.01 ppm; **EI-MS** m/z (%): 382 (M^+); **HRMS** (EI): m/z Exact mass calcd for $C_{26}H_{27}O_2{}^{10}B$ $[M]^+$: 381.2140, found: 381.2143.

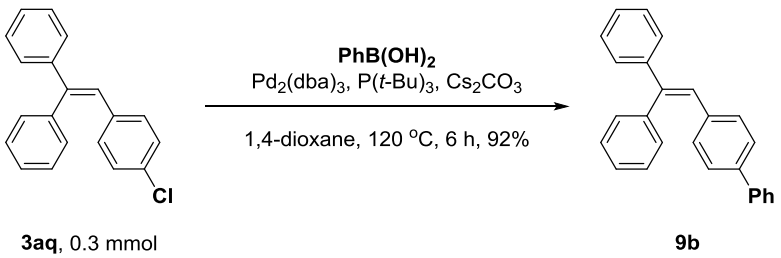

Scheme S9. Transformation of **3aq**, related to **Scheme 5**

4-(2,2-diphenylvinyl)-1,1'-biphenyl (**9b**) To the suspension of **3aq** (87 mg, 0.3 mmol), $Pd_2(dba)_3$ (6.9 mg, 2.5 mol %), Cs_2CO_3 (196 mg, 0.6 mmol), phenylboronic acid (110.0 mg, 0.9 mmol) and P^{t}Bu$_3$ (6.1 mg, 10 mol %) was added dioxane (3 mL) under argon atmosphere. The mixture was stirred at 120 ℃ for 6 h. After being cooled down to room temperature, it was concentrated under reduced pressure and the residue was purified by flash chromatography on silica gel to afford pure product **9b** with 92% yield as a while solid. **^{1}H NMR** (400 MHz, $CDCl_3$) δ 7.58-7.51 (m, 2H), 7.43-7.21 (m, 15H), 7.09 (d, *J* = 8.2 Hz, 2H), 7.00 (s, 1H) ppm; **EI-MS** m/z (%): 332 (M^+); The data is consistent with the literature (Doni et al., 2015).

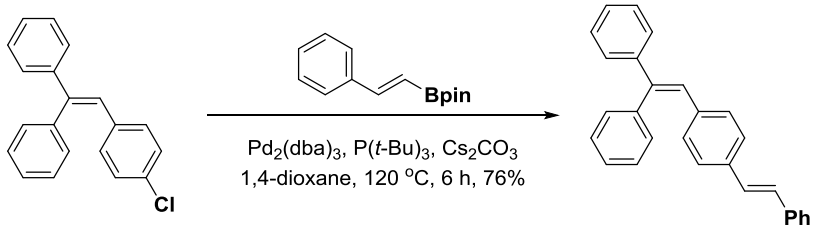

3aq, 0.3 mmol **9c**

Scheme S10. Transformation of **3aq**, related to **Scheme 5**

(*E*)-(2-(4-styrylphenyl)ethene-1,1-diyl)dibenzene (9c) To the suspension of **3aq** (87 mg, 0.3 mmol), $Pd_2(dba)_3$ (6.9 mg, 2.5 mol %), Cs_2CO_3 (196 mg, 0.6 mmol), trans-β-styrylboronic acid pinacol ester (207.0 mg, 0.9 mmol) and and P^tBu_3 (6.1 mg, 10 mol %) was added dioxane (3 mL) under argon atmosphere. The mixture was stirred at 120 ℃ for 6 h. After being cooled down to room temperature, it was concentrated under reduced pressure and the residue was purified by flash chromatography on silica gel to afford pure product **9b** with 92% yield as a while solid. **^{1}H NMR** (400 MHz, $CDCl_3$) δ 7.51-7.41 (m, 2H), 7.38-7.14 (m, 15H), 7.09-6.89 (m, 5H); **^{13}C NMR** (100 MHz, $CDCl_3$) δ 143.51, 142.76, 140.58, 137.49, 136.98, 135.87, 130.52, 130.02, 128.87, 128.81, 128.66, 128.41, 128.36, 127.94, 127.72, 127.67, 127.64, 126.60, 126.27 ppm; **EI-MS** m/z (%): 358 (M^+); **HRMS** (EI): m/z Exact mass calcd for $C_{28}H_{22}$ $[M]^+$: 358.1722, found: 358.1729.

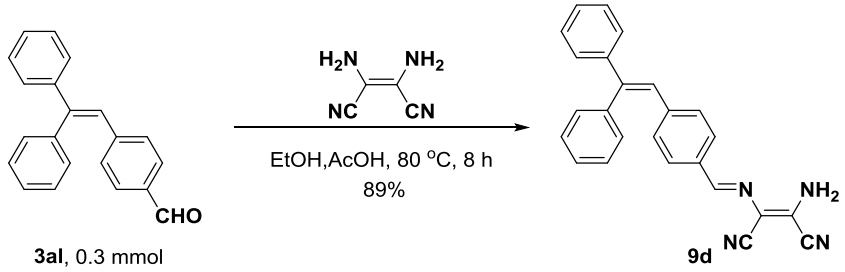

3al, 0.3 mmol **9d**

Scheme S11. Transformation of **3al**, related to **Scheme 5**

2-amino-3-(((E)-4-(2,2-diphenylvinyl)benzylidene)amino)maleonitrile (9d) A mixture of **3al** (85 mg, 0.3 mmol), 2,3-diaminomaleonitrile (35 mg, 0.3 mmol), AcOH (0.1 mL) in ethyl alcohol (1 mL) was heated at 85 °C for 8 h. After cooling down to the room temperature, the mixture was concentrated under reduced pressure. The residue was purified by recrystallization (CH_2Cl_2-hexane mixed-solvent system) to afford **9d** with 89% yield as a pale brown solid. **^{1}H NMR** (400 MHz, CD_2Cl_2) δ 8.30 (s, 1H), 7.60 (d, *J* = 8.4 Hz, 2H), 7.42-7.26 (m, 7H), 7.24-7.16 (m, 2H), 7.10 (d, *J* = 8.4 Hz, 2H), 7.01 (s, 1H), 5.32-5.30 (m, 1H), 5.24 (br, 2H); **^{13}C NMR** (100 MHz, CD_2Cl_2) δ 158.58, 145.49, 143.28, 142.24, 140.41, 133.51, 130.61, 130.41, 129.18, 129.14, 128.66, 128.39, 128.19, 128.05, 127.49, 124.90, 114.13, 112.76, 108.68 ppm; **EI-MS** m/z (%): 374 (M^+); **HRMS** (EI): m/z Exact mass calcd for $C_{25}H_{18}N_4$ $[M]^+$: 374.1531, found: 374.1533.

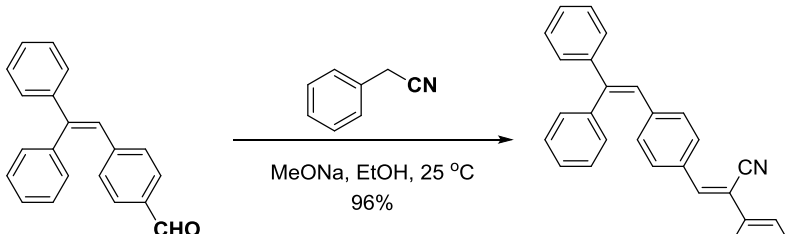

3al, 0.3 mmol **9e**

Scheme S12. Transformation of **3al**, related to **Scheme 5**

(*Z*)-3-(4-(2,2-diphenylvinyl)phenyl)-2-phenylacrylonitrile (9e) A mixture of **3al** (85 mg, 0.3 mmol), benzyl cyanide (39 mg, 0.33 mmol), MeONa (3.3 mg, 0.06 mmol) in ethyl alcohol (10 mL) was stirred at 25 ^{o}C for 8 h. The mixture was quenched with water and exacted with ethyl acetate. The combined organic phases were washed with brine, dried over $MgSO_4$ and concentrated under reduced pressure. The residue was purified by silica gel chromatography (hexane-ethyl acetate mixed-solvent system) to afford **9e** with 96% yield as a golden yellow solid. **^{1}H NMR** (400 MHz, $CDCl_3$) δ 7.71-7.66 (m, 2H), 7.66-7.60 (m, 2H), 7.48-7.28 (m, 12H), 7.24-7.19 (m, 2H), 7.13-7.05 (m, 2H), 6.98 (s, 1H) ppm; **EI-MS** m/z (%): 383 (M^+); The data is consistent with the literature (Wen et al., 2016).

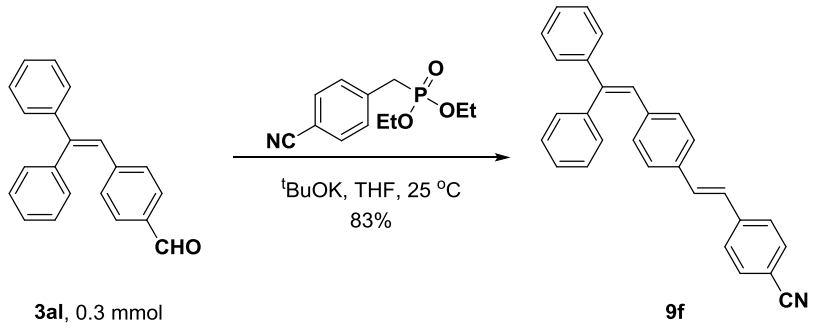

Scheme S13. Transformation of **3al**, related to **Scheme 5**

(*E*)-4-(4-(2,2-diphenylvinyl)styryl)benzonitrile (9f) A mixture of **3al** (85 mg, 0.3 mmol), diethyl (4-cyanobenzyl)phosphonate (114 mg, 0.45 mmol), ^{t}BuOK (67 mg, 0.6 mmol) in THF (6 mL) was stirred at 25 ^{o}C for 8 h. The mixture was quenched with water and exacted with ethyl acetate. The combined organic phases were washed with brine, dried over $MgSO_4$ and concentrated under reduced pressure. The residue was purified by silica gel chromatography (hexane-ethyl acetate mixed-solvent system) to afford **9f** with 83% yield as a pale yellow solid. **^{1}H NMR** (400 MHz, $CDCl_3$) δ 7.61 (d, *J* = 8.4 Hz, 2H), 7.57-7.49 (m, 2H), 7.38-7.27 (m, 10H), 7.25-7.19 (m, 2H), 7.15-6.95 (m, 5H) ppm; **EI-MS** m/z (%): 383 (M^+); The data is consistent with the literature (Wen et al., 2016).

7. Photophysical propertied of the prepared olefins and 1,3-dienes

Table S4. Photophysical propertied of the prepared olefins and 1,3-dienes, related to **Figure 3**.

Entry	Compounds	Geometry of double bonds	λ_{abs} (nm)	Solution (THF)		Solid	
				λ_{em} (nm)	Φ_f (%)	λ_{em} (nm)	Φ_f (%)
1	**3nh**	***E***	289	357, 374	1.3	431	12
2	**3ga**	***Z***	298	361, 374	0.9	430	0.1
3	**3ma**	***E***	298	359, 374	0.7	433	20.8
4	**3ca**	***Z***	306	359, 375	1.4	423	0.1
5	**8aa**	***3E***	337	406	0.6	419	23.0
6	**8ag**	***3Z***	324	397	0.3	423	3.1
7	**8na**	***1E***	337	397	1.0	417	41.5

8	**8ga**	***1Z***	337	400	0.4	431	12.0

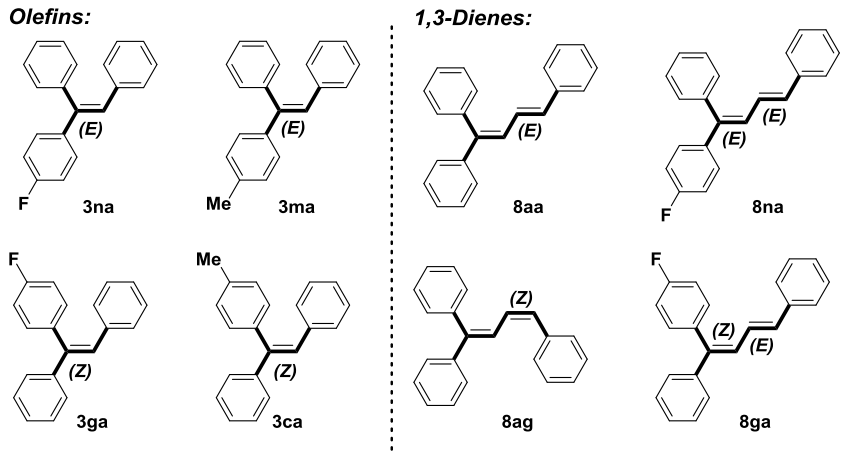

References

Bello, C. S. and Schmidt-Leithoff, J. (2012). Borylation of organo halides and triflates using tetrakis (dimethyl-amino) diboron. Tetrahedron Lett. *53*, 6230-6235.

Berthiol, F., Doucet, H. and Santelli, M. (2003). Synthesis of polysubstituted alkenes by heck vinylation or Suzuki cross-coupling reactions in the presence of a tetraphosphane-palladium catalyst. European J. Org. Chem. 1091-1096.

Burstein, C., Lehmann, C. W. and Glorius, F. (2005). Imidazo[1,5-a]pyridine-3-ylidenes—pyridine derived N-heterocyclic carbene ligands. Tetrahedron *61*, 6207-6217.

Carreira-Barral, I., Fernandez-Perez, I., Mato-Iglesias, M., de Blas, A., Platas-Iglesias, C. and Esteban-Gomez, D. (2018). Recognition of AMP, ADP and ATP through Cooperative Binding by Cu(II) and Zn(II) Complexes Containing Urea and/or Phenylboronic-Acid Moieties. Molecules *23*, 479-503.

Dai, W., Xiao, J., Jin, G., Wu, J. and Cao, S. (2014). Palladium- and Nickel-Catalyzed Kumada Cross-Coupling Reactions of gem-Difluoroalkenes and Monofluoroalkenes with Grignard Reagents. J. Org. Chem. *79*, 10537-10546.

Doni, E., Zhou, S. and Murphy, J. A. (2015). Electron transfer-induced coupling of haloarenes to styrenes and 1,1-diphenylethenes triggered by diketopiperazines and Potassium tert-butoxide. Molecules *20*, 1755-1774.

Gómez-Blanco, N., Fernández, J. J., Fernández, A., Vázquez-García, D., López-Torres, M., Rodríguez, A. and Vila, J. M. (2009). Synthesis and reactivity of new functionalized Pd(II) cyclometallated complexes with boronic esters. J. Organomet. Chem. *694*, 3597-3607.

Hu, T. J., Li, M. Y., Zhao, Q., Feng, C. G. and Lin, G. Q. (2018). Highly Stereoselective Synthesis of 1,3-Dienes through an Aryl to Vinyl 1,4-Palladium Migration/Heck Sequence. Angew. Chem. Int. Ed. *57*, 5871-5875.

Hu, T. J., Zhang, G., Chen, Y. H., Feng, C. G. and Lin, G. Q. (2016). Borylation of Olefin C-H Bond via Aryl to Vinyl Palladium 1,4-Migration. J. Am. Chem. Soc. *138*, 2897-2900.

Iwai, Y., Gligorich, K. M. and Sigman, M. S. (2008). Aerobic alcohol oxidation coupled to palladium-catalyzed alkene hydroarylation with boronic esters. Angew. Chem. Int. Ed. *47*, 3219-3222.

Kumar, N. Y., Bechtoldt, A., Raghuvanshi, K. and Ackermann, L. (2016). Ruthenium(II)-Catalyzed

Decarboxylative C-H Activation: Versatile Routes to meta-Alkenylated Arenes. Angew. Chem. Int. Ed. *55*, 6929-6932.

Ranjani, G. and Nagarajan, R. (2017). Insight into Copper Catalysis: In Situ Formed Nano Cu2O in Suzuki-Miyaura Cross-Coupling of Aryl/Indolyl Boronates. Org. Lett. *19*, 3974-3977.

Rao, S., Joy, M. N. and Prabhu, K. R. (2018). Employing Water as the Hydride Source in Synthesis: A Case Study of Diboron Mediated Alkyne Hydroarylation. J. Org. Chem. *83*, 13707-13715.

Robbins, D. W. and Hartwig, J. F. (2011). A Simple, Multidimensional Approach to High-Throughput Discovery of Catalytic Reactions. Sci. *333*, 1423-1427.

Rossi, R., Carpita, A., Ribecai, A. and Mannina, L. (2001). Stereocontrolled synthesis of carbon-carbon double bond locked analogues of strobilurins which are characterized by a trans-1,2-disubstituted cyclopropane ring. Tetrahedron *57*, 2847-2856.

Hayashi, R.; Shimizu, A.; Davies, J. A.; Ishizaki, Y.; Willis, C.; Yoshida, J.-i. (2018). Metal- and Oxidant-Free Alkenyl C-H/Aromatic C-H Cross-Coupling Using Electrochemically Generated Iodosulfonium Ions. Angew. Chem. Int. Ed. *57*, 12891-12895.

Shen, X., Liu, P., Liu, Y. and Dai, B. (2017). Synthesis of naphthyl-substituted terminal olefins via Pd-Catalyzed one-pot coupling of acetylnaphthalene, N -Tosylhydrazide with aryl halide. Tetrahedron *73*, 6558-6563.

Shigeno, M., Nakaji, K., Nozawa-Kumada, K. and Kondo, Y. (2019). Catalytic Amide-Base System of TMAF and N(TMS)3 for Deprotonative Coupling of Benzylic C(sp(3))-H Bonds with Carbonyls. Org. Lett. *21*, 2588-2592.

Shimasaki, T., Konno, Y., Tobisu, M. and Chatani, N. (2009). Nickel-Catalyzed Cross-Coupling Reaction of Alkenyl Methyl Ethers with Aryl Boronic Esters. Org. Lett. *11*, 4890-4892.

Stephen J. Baker, Y.-K. Z., Tsutomu Akama, Agnes Lau, Huchen Zhou, Vincent Hernandez, Weimin Mao, M. R. K. Alley, Virginia Sanders, and Jacob J. Plattner (2006). Discovery of a New Boron-Containing Antifungal Agent, 5-Fluoro-1,3-dihydro-1-hydroxy-2,1benzoxaborole (AN2690), for the Potential Treatment of Onychomycosis. J. Med. Chem. *49*, 4447-4450.

Tsoi, Y.-T., Zhou, Z., Chan, A. S. C. and Yu, W.-Y. (2010). Palladium-Catalyzed Oxidative Cross-Coupling Reaction of Arylboronic Acids with Diazoesters for Stereoselective Synthesis of (E)-alpha,beta-Diarylacrylates. Org. Lett. *12*, 4506-4509.

Wang, Z., He, X., Zhang, R., Zhang, G., Xu, G., Zhang, Q., Xiong, T. and Zhang, Q. (2017). Copper-Catalyzed Asymmetric Hydroboration of 1,1-Disubstituted Alkenes. Org. Lett. *19*, 3067-3070.

Wang, Z., Wang, X., Ura, Y. and Nishihara, Y. (2019). Nickel-Catalyzed Decarbonylative Cyanation of Acyl Chlorides. Org. Lett. *21*, 6779-6784.

Wei, D., Hu, T.-J., Feng, C.-G. and Lin, G.-Q. (2018). Synthesis of Substituted Naphthalenes by 1,4-Palladium Migration Involved Annulation with Internal Alkynes. Chin. J. Chem. *36*, 743-748.

Wei, D., Li, M. Y., Zhu, B. B., Yang, X. D., Zhang, F., Feng, C. G. and Lin, G. Q. (2019). Sequential Cross-Coupling/Annulation of *ortho*-Vinyl Bromobenzenes with Aromatic Bromides for the Synthesis of

Polycyclic Aromatic Compounds. Angew. Chem. Int. Ed. *58*, 16543-16547.

Wen, H., Zhang, L., Zhu, S., Liu, G. and Huang, Z. (2017). Stereoselective Synthesis of Trisubstituted Alkenes via Cobalt-Catalyzed Double Dehydrogenative Borylations of 1-Alkenes. ACS Catal. *7*, 6419-6425.

Wen, W., Shi, Z.-F., Cao, X.-P. and Xu, N.-S. (2016). Triphenylethylene-based fluorophores: Facile preparation and full-color emission in both solution and solid states. Dyes Pigm. *132*, 282-290.

Wong, K. T., Chien, Y. Y., Liao, Y. L., Lin, C. C., Chou, M. Y. and Leung, M. K. (2002). Efficient and convenient nonaqueous workup procedure for the preparation of arylboronic esters. J. Org. Chem. *67*, 1041-1044.

Wu, M. J., Wei, L. M., Lin, C. F., Leou, S. P. and Wei, L. L. (2001). Palladium-catalyzed reactions of aryl iodides with trimethylsilylacetylenes and disubstituted alkynes: the synthesis of diarylacetylenes and triarylethylenes. Tetrahedron *57*, 7839-7844.

Wu, S., Ma, H., Jia, X., Zhong, Y. and Lei, Z. (2011). Biopolymer-metal complex wool–Pd as a highly active heterogeneous catalyst for Heck reaction in aqueous media. Tetrahedron *67*, 250-256.

Xiao, Q., Ma, J., Yang, Y., Zhang, Y. and Wang, J. (2009). Pd-Catalyzed C=C Double-Bond Formation by Coupling of N-Tosylhydrazones with Benzyl Halides. Org. Lett. *11*, 4732-4735.

Yang, Q., Chai, H., Liu, T. and Yu, Z. (2013). Palladium-catalyzed cross-coupling of cyclopropylmethyl N-tosylhydrazones with aromatic bromides: an easy access to multisubstituted 1,3-butadienes. Tetrahedron Lett. *54*, 6485-6489.

Yu, J. Y., Shimizu, R. and Kuwano, R. (2010). Selective cine substitution of 1-arylethenyl acetates with arylboron reagents and a diene/rhodium catalyst. Angew. Chem. Int. Ed. *49*, 6396-6399.

Zhang, K., Sun, Q., Tang, L., Wang, Y., Fan, X., Liu, L., Xue, S. and Yang, W. (2018). Cyclic boron esterification: screening organic room temperature phosphorescent and mechanoluminescent materials. J. Mater. Chem. C. *6*, 8733-8737.

Zhou, Y. B., Wang, Y. Q., Ning, L. C., Ding, Z. C., Wang, W. L., Ding, C. K., Li, R. H., Chen, J. J., Lu, X., Ding, Y. J. and Zhan, Z. P. (2017). Conjugated Microporous Polymer as Heterogeneous Ligand for Highly Selective Oxidative Heck Reaction. J. Am. Chem. Soc. *139*, 3966-3969.